

**Towards Sequence-Selective DNA
Recognition with Designed Major
Groove Binders**

Dissertation

Wenbin Hu

Essen 2011

Towards Sequence-Selective DNA Recognition with Designed Major Groove Binders

Dissertation

zur Erlangung des akademischen Grades eines

Doktors der Naturwissenschaften

- Dr. rer. nat. –

vorgelegt von

Wenbin Hu

geboren in Peking, Volksrepublik China

Fakultät für Chemie, Institut für Organische Chemie

der

Universität Duisburg-Essen

Essen 2011

**Towards Sequence-Selective DNA
Recognition with Designed Major
Groove Binders**

Dissertation

Wenbin Hu

**In Partial Fulfillment of the
Requirements for the Degree
Doctor of Philosophy in Chemistry
(Dr. rer. nat.)**

**Faculty of Chemistry
University of Duisburg-Essen**

Essen 2011

Die vorliegende Arbeit wurde unter Leitung von Herrn Prof. Dr. Thomas Schrader in der Zeit von August 2007 bis April 2011 an der Fakultät für Chemie der Universität Duisburg-Essen durchgeführt.

Diese Arbeit wurde am 07. Juli 2011 eingereicht und am 29. August 2011 von der Fakultät für Chemie der Universität Duisburg-Essen als Dissertation angenommen.

Tag der Disputation: 26. September 2011

Prüfungsvorsitzende: PD. Dr. Ursula Telgheder

Erstgutachter: Prof. Dr. Thomas Schrader

Zweitgutachter: Prof. Dr. Carsten Schmuck

This work was performed during the period from August 2007 to April 2011 at the Department of Organic Chemistry, University of Duisburg-Essen, under the supervision of Prof. Dr. Thomas Schrader.

This dissertation was submitted on 7th July 2011 and was accepted on 29th August 2011 by the Faculty of Chemistry in the University of Duisburg-Essen in Germany. The oral defence was on 26th September 2011.

Chairwoman: PD. Dr. Ursula Telgheder

Reviewer: Prof. Dr. Thomas Schrader

Reviewer: Prof. Dr. Carsten Schmuck

Hiermit versichere ich, dass ich die vorliegende Arbeit mit dem Titel

„Towards Sequence-Selective DNA Recognition with Designed Major Groove Binders ”

selbst verfasst und keine außer den angegebenen Hilfsmitteln und Quellen benutzt habe, und dass die Arbeit in dieser oder ähnlicher Form noch bei keiner anderen Universität eingereicht wurde.

Essen, im Juli 2011

Wenbin Hu

This work was performed during the period from August 2007 to April 2011 at the Department of Organic Chemistry, University of Duisburg-Essen, under the supervision of Prof. Dr. Thomas Schrader.

I declare that this dissertation represents my own work, except where due acknowledgement is made.

Wenbin Hu

Acknowledgement

I have been lucky to carry out research within the Faculty of Chemistry, University of Duisburg-Essen. I wish to thank all the persons who provided invaluable support and encouragement. I would like to express my sincere gratitude to the numerous persons who have contributed to my work. In particular, I am deeply grateful to the following individuals:

Prof. Dr. Thomas Schrader for accepting and supporting me as a Ph.D. student, for providing this interesting project, for offering me valuable ideas and suggestions with his profound knowledge and rich research experiences and for his thoughtful supervision.

Prof. Dr. Carsten Schmuck for reviewing my thesis as well as for his advice and discussion.

Prof. Lars Baltzer, my M. Sc supervisor at Uppsala University, for introducing me to the field of bioorganic chemistry, for introducing me to Prof. Dr. Thomas Schrader's laboratory, for his kind consideration for my future as well as for standing behind me all the time.

Dr. Ivo Piantanida, Dr. Marijeta Kralj and Dr. Lidija Šuman in Ruđer Bošković Institute for the very pleasant cooperation and discussion.

Mr. Heinz Bandmann, Dr. Torsten Schaller, Prof. Dr. Heiko Ihmels, Dr. Thomas Paululat and Mrs. Sandra Uebach for NMR measurements; Mr. Werner Karow and Mr. Winfried van Hoof for MS measurements; Mrs Petra Schneider and Mrs. Christine Kallweit for CD measurements; Mrs. Ingeborg Reiter for her kind help; Mrs. Heike Wöll for the HPLC and Mr. Klaus Kowoski for ITC measurements.

All the former and present colleagues of our research group: Kai Bernitzki, Wei Sun, Caroline Blecking, Max Sena Peters, Som Dutt, Kirstin Wenck, Marc Blecking, Katrin Hochdörffer, Julia März-Berberich, Peter Talbiersky, Jolanta Polkowska, Thomas Gersthagen, Patrick Gilles, Marco Hellmert, Patricia Latza, Constanze Wilch and Eva Zeppenfeld for supporting and keeping a lively atmosphere in the laboratory.

All my friends in Germany as well as in Sweden for sharing good time together: Per Löwdin, Marita Wigren-Svensson, Wei Sun, Dongming He, Haofei Guo, Jun Wang, Zhaoqing Pei, Jing Lei, Qian Yang, Dongxu Yin, Qianqian Jiang, Junchen Wu, Hui Tong and Chuanzheng Zhou.

Last but not least, my parents for providing a happy home environment and for their endless love, understanding, encouragement and support from the beginning of my Ph.D. study in Germany.

To My Parents

Abstract

This thesis is mainly focused on the design, synthesis and DNA binding studies of aminobenzyl and guanidinium calix[4]arene dimers. The work consists of two parts.

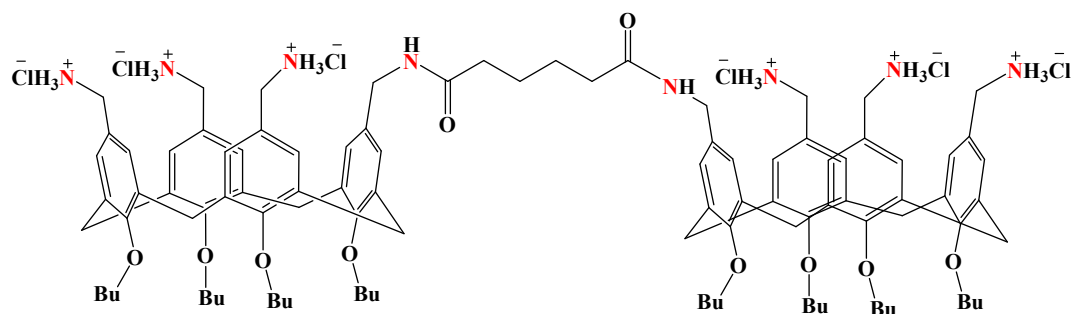
The first part of my Ph.D. work was focused on the synthesis and DNA binding studies of Dimer A and Dimer B. Structures of these molecules can be found on the next page. In order to broaden the scope of the investigation, the corresponding monomeric calixarenes (Monomer A and Monomer B) were also synthesized. Compared with anilino-calix[4]arenes (R. Zadnani, T. Schrader, *Angew. Chem. Int. Ed.* **2006**, *45*, 2703 –2706), these dimers and monomers are water-soluble, and bind to DNA with much higher affinity (binding constants: 10^6 – 10^8 M⁻¹ in 2 mM Hepes buffer with 150 mM NaCl).

When investigating the properties of new DNA binding molecules, one initial goal is to establish their mode of binding to DNA. Because direct structure information from a crystal or NMR structure was not yet available in my work, several other biophysical experiments have been designed and performed between calixarenes and different nucleic acids with varying base composition and conformation. The following results from established binding assays strongly support a major groove binding mode:

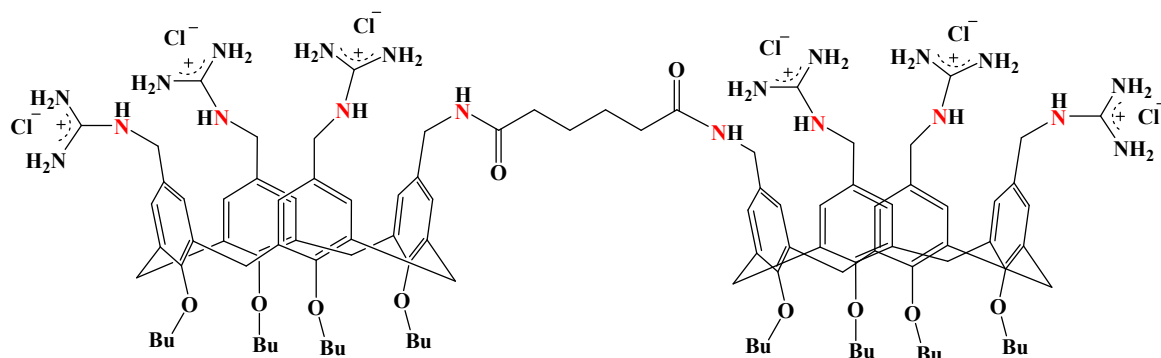
(1). The DAPI displacement assay indicates that the calixarene dimers and DAPI can simultaneously bind to poly (dAdT) – poly (dAdT). Because DAPI occupies the minor groove, the dimeric calixarenes should reside in the major groove.

(2). Ethidium bromide displacement assays, fluorescence titrations, and circular dichroism measurements indicate that calixarene dimers strongly prefer nucleic acids with a wide, shallow or even major groove; while low affinities are observed for nucleic acids with a narrow, deep or rugged major groove, which must be widened before complexation occurs. This characteristic also implies that the accessible area for our ligands is on the major groove side, contrary to the well-known slim oligoamide binders, which target the minor groove.

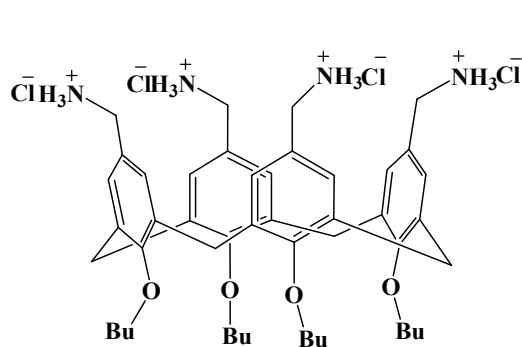
In line with these observations, it was noticed that changes in shape and width of the minor groove had no influence on the ligands' affinities.



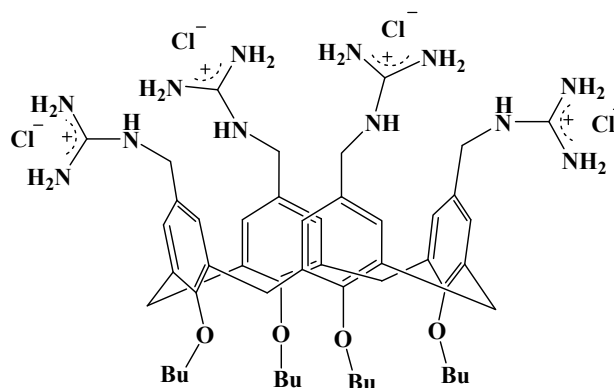
Dimer A



Dimer B



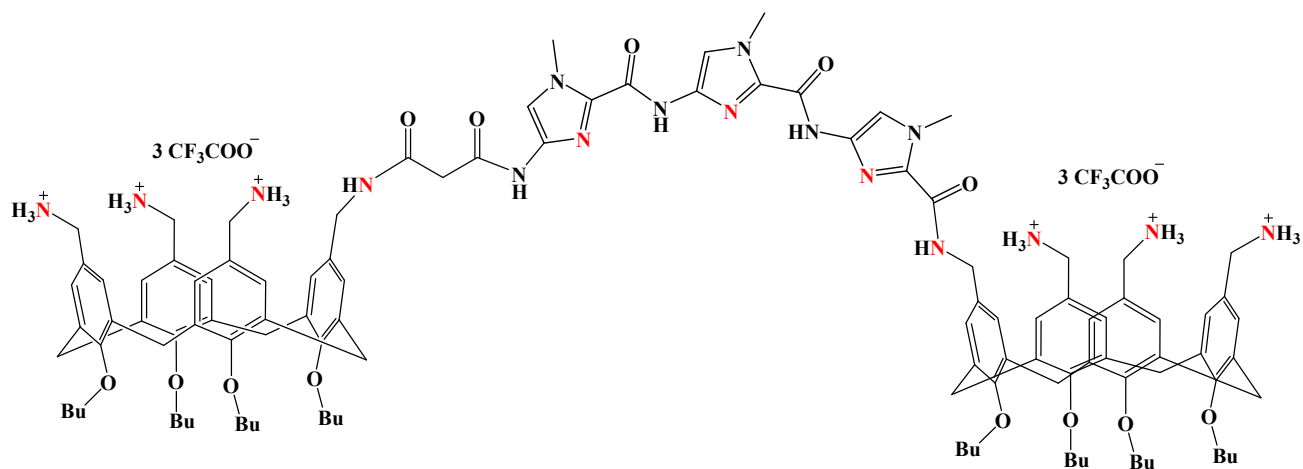
Monomer A



Monomer B

Unfortunately, Dimer A and Dimer B showed similar affinities for different DNA duplexes. Therefore, we planned to replace the simple alkyl bridge between both calixarenes by a fragment which should be able to bind specific sequences of DNA in the promoter region of each gene. Heterocyclic oligoamides were found out. They consist of *N*-methylpyrrole, 3-hydroxypyrrole and *N*-methyl imidazole amino acid building blocks (P. B. Dervan, *Bioorganic & Medicinal Chemistry* **2001**, *9*, 2215–2235.).

In the second part of my Ph.D. work, a calixarene dimer with a triimidazole bridge (Dimer C) was synthesized.



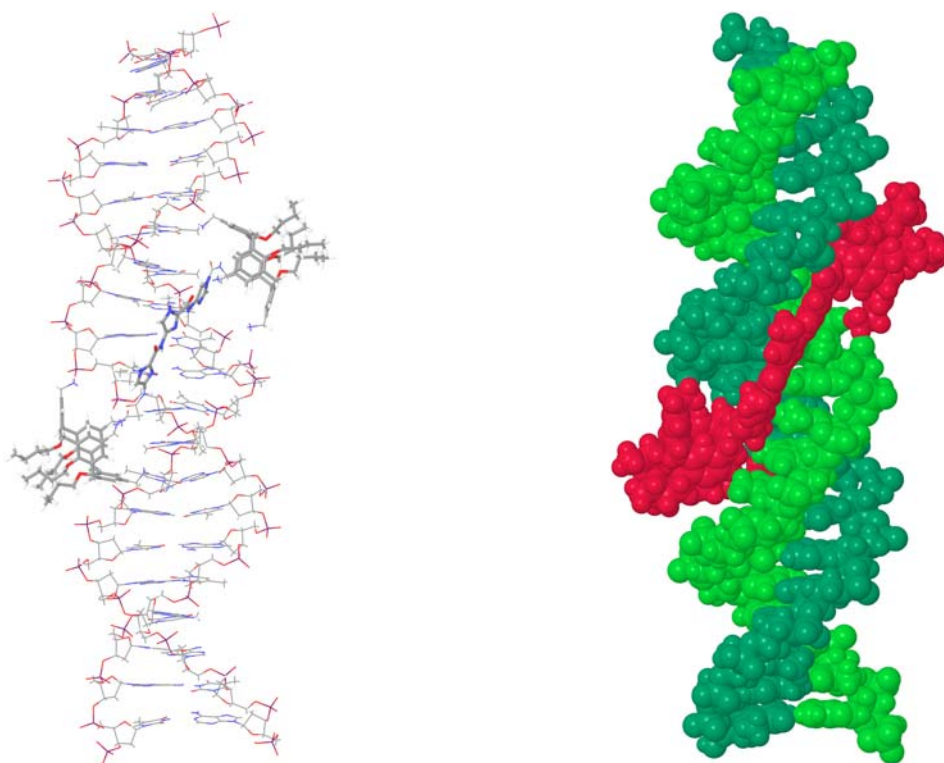
Dimer C

Because in minor grooves, *N*-methylimidazoles of polyamides could recognize the positive electrostatic potential of amino groups of guanine bases via hydrogen bonds, it was assumed that Dimer C, which contained a triimidazole bridge, could prefer a major groove with large positive potentials. Moreover, because the triimidazole bridge is slim, it was also assumed that Dimer C should prefer a narrow major groove, which could offer the appropriate shape for the bridge's recognition. In view of the above-mentioned assumptions, we found that the major groove of poly dG – poly dC fulfilled both requirements. Therefore, it was predicted that Dimer C should show the high affinity for poly dG – poly dC.

Ethidium bromide displacement assays, fluorescence titrations, and circular dichroism measurements imply that Dimer C is a major groove binder. Furthermore, as we expected, these experiments indicate that Dimer C showed stronger preference for this specific DNA duplex: poly dG – poly dC.

It was also observed that Dimer C frequently showed reduced affinity to other DNA duplexes. Probably, the decrease in affinity is related to their wider major grooves, in which the slim triimidazole bridge will not produce extensive close van der Waals contacts, and the whole ligand itself shows orientational disorder. Another explanation is the unfavorable electrostatic potentials, because these DNA duplexes have more neutral areas in major grooves than does poly dG – poly dC.

Herein, we present a proposed mechanism of DNA binding by Dimer C: the cationic moieties on the upper rim of the calixarenes form hydrogen bonds with nucleobases as well as phosphate groups of the nucleic acid, the butoxy tail is toward the free solution, and the triimidazole bridge binds along the major groove and recognizes the amino groups of nucleobases.



Keywords: major groove binding, dimeric calixarene, polyamide, sequence selectivity, binding affinity, minor groove binding, DAPI, ethidium bromide, circular dichroism spectroscopy, fluorescence titration

Contents

1	Introduction	1
1.1	Introduction to Nucleic acids	1
1.1.1	Composition of Nucleic acids	1
1.1.2	Structural and Conformational Properties of Nucleotides	2
1.1.3	Helical Structures of Nucleic Acids	5
1.2	Introduction to Regulation of Gene Expression.....	8
1.3	Binding of Small Molecules to DNA.....	10
1.3.1	Intercalation	10
1.3.2	Minor Groove Binding.....	12
1.3.3	Major Groove Binding	19
1.4	Calixarene	24
1.5	Objectives.....	29
1.6	Overview of the Thesis	32
2	Synthesis.....	33
2.1	Synthesis of Monomeric Calixarenes	33
2.1.1	Synthesis of Calix[4]arene	33
2.1.2	Lower Rim Etherifications of Calix[4]arene.....	35
2.1.3	Upper Rim Functionalizations	36
2.2	Synthesis of Dimeric Calixarenes	37
2.3	Synthesis of <i>N</i> -Protected <i>N</i> -methylimidazole Amino Acids.....	42
2.4	Synthesis of Spacers and Coupling Reactions	44
3	Methodology	53
3.1	Ethidium Bromide Displacement Assay	53
3.2	Circular Dichroism Spectroscopy	56
3.3	DAPI Displacement Assay.....	59
3.4	Fluorescence Titration Experiments	61
3.5	Isothermal Titration Calorimetry	67
3.6	The Assessment of Thermal Denaturation of DNA.....	69
3.7	Triple Helix-Forming Oligonucleotide Displacement Assay	71

4	Results and Discussion	73
4.1	The Mechanism of DNA Binding by Dimeric Calixarenes	73
4.1.1	DAPI Displacement Assay	77
4.1.2	Ethidium Bromide Displacement Assay	81
4.1.3	Circular Dichroism Spectroscopy	84
4.1.4	The Assessment of Thermal Denaturation of DNA	88
4.1.5	Fluorescence Titration Experiments	92
4.2	Sequence-Specific Major Groove Recognition with Dimer C	95
4.2.1	Ethidium Bromide Displacement Assay and Fluorescence Titrations	95
4.2.2	Circular Dichroism Spectroscopy	99
4.2.3	The Assessment of Thermal Denaturation of DNA	101
4.2.4	NMR Spectroscopy	102
4.3	Antiproliferative Effects of Various Calixarenes <i>in vitro</i>	104
5	Conclusions and Outlook	108
5.1	Conclusions	108
5.2	Outlook	111
6	Experiments	115
6.1	Chemicals and Equipments	115
6.2	DNA / RNA Binding Experiments	117
6.3	Synthesis	121
6.4	NMR and MS Spectra of Synthetic Compounds	157
6.5	Data of Fluorescence Titration Experiments	211
	Abbreviations	262
	References	264
	Curriculum Vitae	271
	List of Publications and Conferences	272

1. Introduction

Nucleic acids are biological polymers, which have essential roles in transmission, expression and conservation of genetic information. They are universal in living organisms and can be found in all cells. In nature, nucleic acids exist as deoxyribonucleic acid (DNA) and ribonucleic acid (RNA). The main role of DNA is storage and transmission of biological information, whereas RNA has a broader range of functions. Several different types of RNA have been found in cells. For example, messenger RNA (mRNA) is transcribed from DNA, and carries genetic information that will be translated in ribosomes to proteins ^[1]. During transcription, transcription factors perform their functions alone or with other proteins in a complex, by promoting (as an activator) or blocking (as a repressor) the recruitment of RNA polymerase to specific genes, and control the movement of genetic information from DNA to mRNA ^[2,3]. Consequently, a number of transcription factors unquestionably became the target sites in medicinal chemistry in the past ^[4,5]. With the completion of the Human Genome Project, the new challenge now is to develop new pharmaceutical interventions to regulate and manipulate genes and treat diseases at the DNA level ^[6,7,8,9,10]. The common method of this strategy is to identify pathogenicity genes and use artificial molecules to target them for silencing. This strategy was applied to my work: because the major groove is more informative than the minor groove, we planned to design and synthesize artificial major groove binders to target specific DNA sequences (for example, pathogenicity genes). They could block these sequences and perturb gene expression at the initiation of transcription.

1.1 Introduction to Nucleic acids

1.1.1 Composition of Nucleic acids

Nucleic acids are made from repeating units called nucleotides, each of which has three components ^[11]: a heterocyclic nitrogenous base, a 2'-deoxy-D-ribose (in DNA) or D-ribose (in RNA) sugar ring, and a phosphate group. The phosphate group connects two pentofuranose sugars to form a 3'→5' phosphate diester bond (Figure 1.1). The nucleobases in DNA are represented by purines [adenine (Ade) and guanine (Gua)] and pyrimidines

[cytosine (Cyt) and thymine (Thy)]. For RNA, the pyrimidine Uracil (Ura) takes place of thymine (Figure 1.2). Purines are linked at N9 to the C1' of the sugar and pyrimidines are linked at N1. The pentofuranose sugar and a heterocyclic aromatic nucleobase are attached through an *N*-glycosidic bond in β configuration to form a nucleoside.

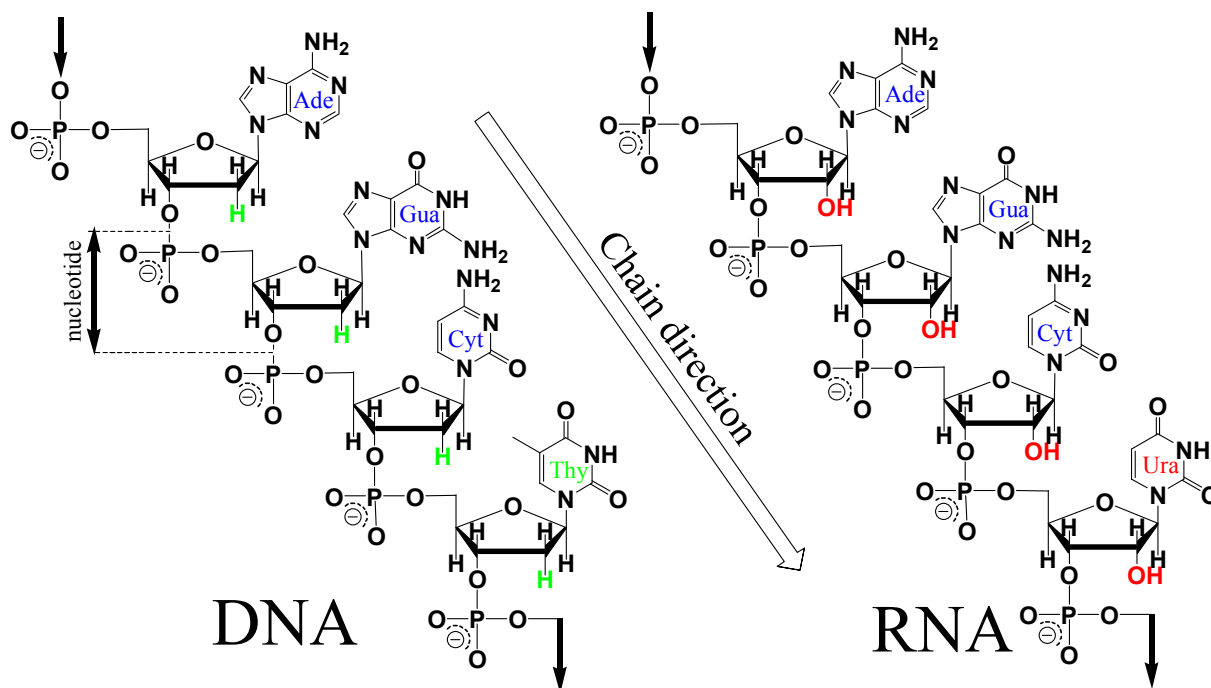


Figure 1.1. General structures of nucleic acids. The nucleotides are connected by the 3'→5' phosphate diester linkage. The chain direction is from 5' to 3' end as shown by arrow. The pentofuranose sugar and phosphate form the backbone to which bases (Ade, Gua, Cyt and Thy / Ura) are attached. Compared with deoxyribonucleic acid (DNA), in ribonucleic acid (RNA), the hydrogen attached to C2' is replaced by hydroxyl, and thymine by uracil.

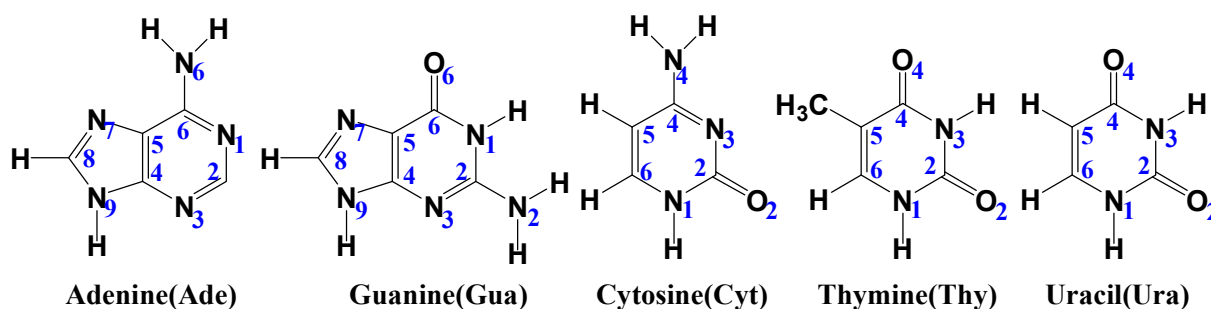


Figure 1.2. Chemical structures of nucleobases.

1.1.2 Structural and Conformational Properties of Nucleotides

1.1.2.1 Bases and Base Pairs

Purines and pyrimidines can form base pairs via hydrogen bonds. There are several different types of base pairs, for example, Watson-Crick base pairs ^[12], Hoogsteen base pairs ^[13], reversed Hoogsteen base pairs ^[14], and Wobble base pairs ^[15] and so on (Figure 1.3). In the canonical Watson-Crick DNA base pairing, adenine forms a base pair with thymine and guanine with cytosine. In RNA, thymine is replaced by uracil. Hoogsteen base pairing allows the third strand to occupy the major groove of the DNA double helix which are assembled in the Watson-Crick pattern to form triple-stranded helices, such as poly(dA)•2poly(dT) and poly(dG)•poly(dC)•poly(dC)⁺ ^[16,17,18,19]. Hoogsteen base pairing also allows the formation of G-quadruplex, which is the secondary structure of single stranded G-rich DNA and RNA. A wobble base pair is a non-Watson-Crick DNA base pair between two nucleotides in RNA molecules. There are four main wobble base pairs: guanine-uracil, inosine-uracil, inosine-adenine, and inosine-cytosine (G-U, I-U, I-A and I-C). They are fundamental in RNA secondary structures and are critical for proper translation of genetic codes. A complete graphic list of different base pairs can be found on page 120 of the text book ^[20].

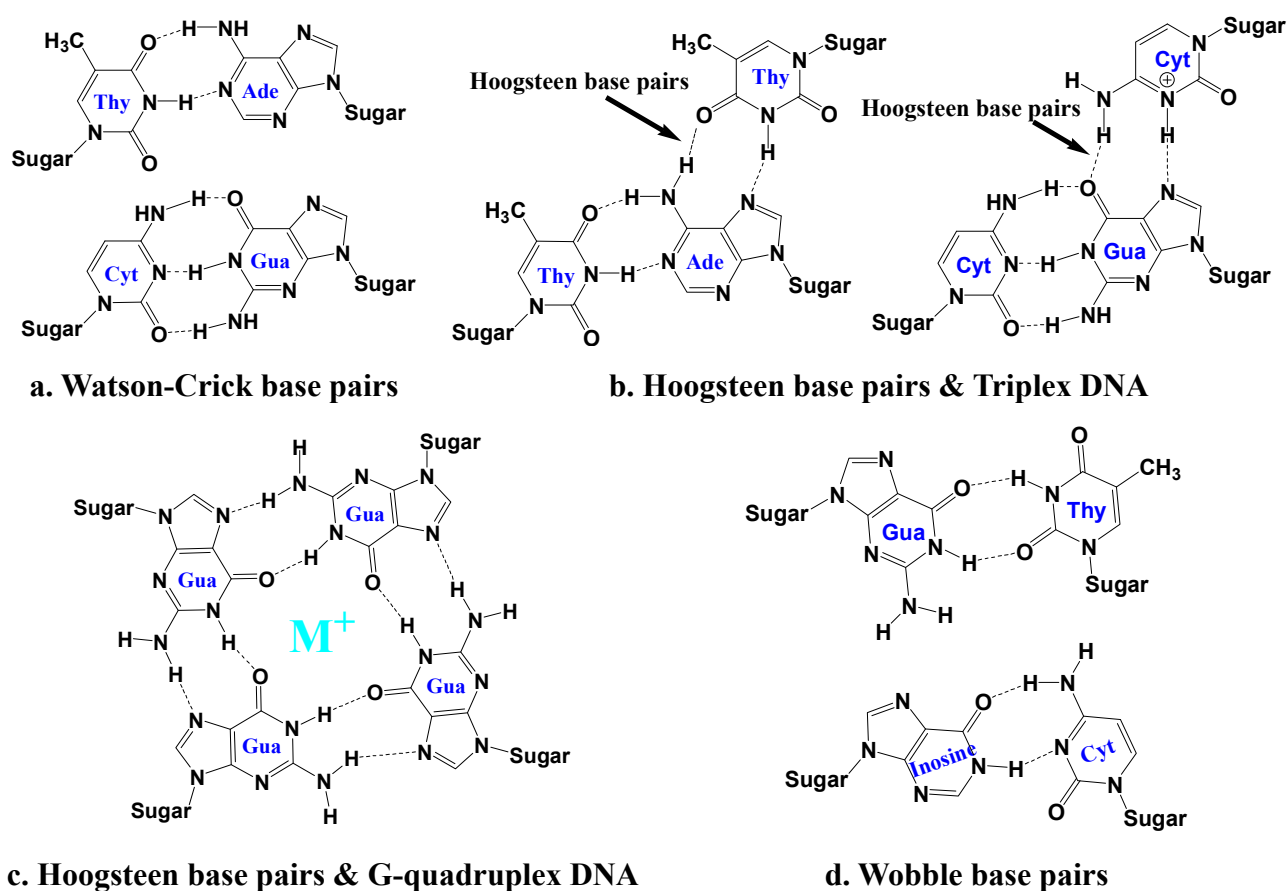


Figure 1.3. Some common types of base pairs

1.1.2.2 Sugar Conformations

A planar conformation for the pentafuranose sugar moiety of a nucleotide is energetically unfavorable because in this arrangement, all the substituents attached to carbon atoms are fully eclipsed. To reduce the non-bonded interaction between these substituents, the furanose ring could adopt preferably either the C3'-endo and C2'-exo conformation (the *North* or *N*-type conformation) or the C2'-endo and C3'-exo conformation (the *South* or *S*-type conformation) (Figure 1.4). The conformations of the pentofuranose sugars are not static and in solution they are involved in a dynamic two-state *North* \rightleftharpoons *South* equilibrium [21,22,23]. The deoxyribofuranosyl sugars of DNA are preferentially in the *South*-type form, whereas the ribofuranosyl sugars of RNA in the *North*-type form.

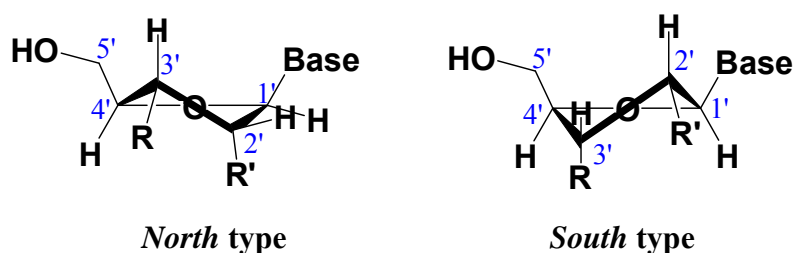


Figure 1.4 Definition of sugar puckering modes: *North* type (left) and *South* type (right)

In fact, the primary structure of DNA and RNA has a high degree of similarity, but the presence of 2'-OH in the ribose sugar differentiates RNA from DNA, and makes RNA structurally and functionally different from DNA. For example, DNA is double stranded but RNA, in most case, is a single-stranded molecule and consists of many types of secondary structures, for instant, hairpin loops, bulges, internal loops, junctions and so on [24]; the 2'-OH group of RNA can provide a scaffold for solvent or protein interactions [25], can mediate catalysis [26], can make RNA less stable than DNA [27] and can also stabilize RNA tertiary structures [28] and so on.

1.1.2.3 Phosphate Backbone Conformations

The conformation of the sugar phosphate backbone can be defined by torsion angles α , β , δ , ϵ ,

ζ (Figure 1.5). The sugar puckering mode is indicated by ζ : 74° to 95° corresponding to C3'-*endo* (*A*-DNA, *A*-RNA), and 134° to 158° corresponding to C2'-*endo* (*B*-DNA, *C*-DNA and *D*-DNA) [20]. The typical range of phosphate backbone torsions for *A* and *B* families of DNA and RNA can be found on page 230, reference 20. The torsion angles of the pentofuranose sugar ring are indicated by ν_0 to ν_4 . The torsion angle about a glycosidic bond is indicated by χ [O4'-C1'-N9-C4] for purines and [O4'-C1'-N1-C2] for pyrimidines. There are two main conformations: *syn* ($-90^\circ \leq \chi \leq 90^\circ$) and *anti* ($90^\circ \leq \chi \leq 180^\circ$). The *anti* conformation is usually more stable and more common, because there is no particular steric hindrance between the sugar and the nucleobase in the *anti* conformation.

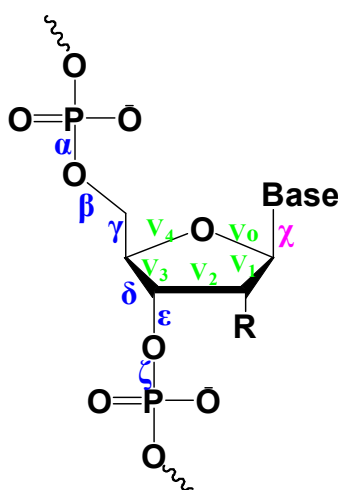


Figure 1.5 The definition of torsion angles for one nucleotide.

1.1.3 Helical Structures of Nucleic Acids

There are several types of double helix structures for DNA and RNA, depending on the sequence, relative humidity and salt concentration. *A*-form, *B*-form and *Z*-form [29] are the main three types of double helical structures. Nucleic acids also exist in other forms of duplexes, for example, *C*-form, *D*-form, *E*-form and *S*-form and so on. *A*-form, *B*-form and *C*-form are right handed, and *Z*-form is left handed. The RNA helix exists predominantly in *A*-form [20,30], and the DNA-RNA duplex adopts an intermediate conformation between *A* and *B* but closer globally to *A* than the *B* form [31]. *B*-form is the dominant form for DNA [32].

Table 1.1 Comparison of A form, B form and Z form of DNA ^[33,34,35,36]

	A form	B form	Z form
Helix sense	Right handed	Right handed	Left handed
Pitch (Å)	28.2	33.8	45
Base pairs per helical turn	11	10	6
Helix rise per base pair (Å)	2.56	3.38	3.7
Turn angle per base pair (°)	32.7	36.0	-33.0
Glycosidic bond conformation	<i>anti</i>	<i>anti</i>	C: <i>anti</i> , G: <i>syn</i>
Sugar pucker conformation	<i>C3'-endo</i>	<i>C2'-endo</i>	C: <i>C2'-endo</i> , G: <i>C2'-exo</i>
Diameter(Å)	26	20	18

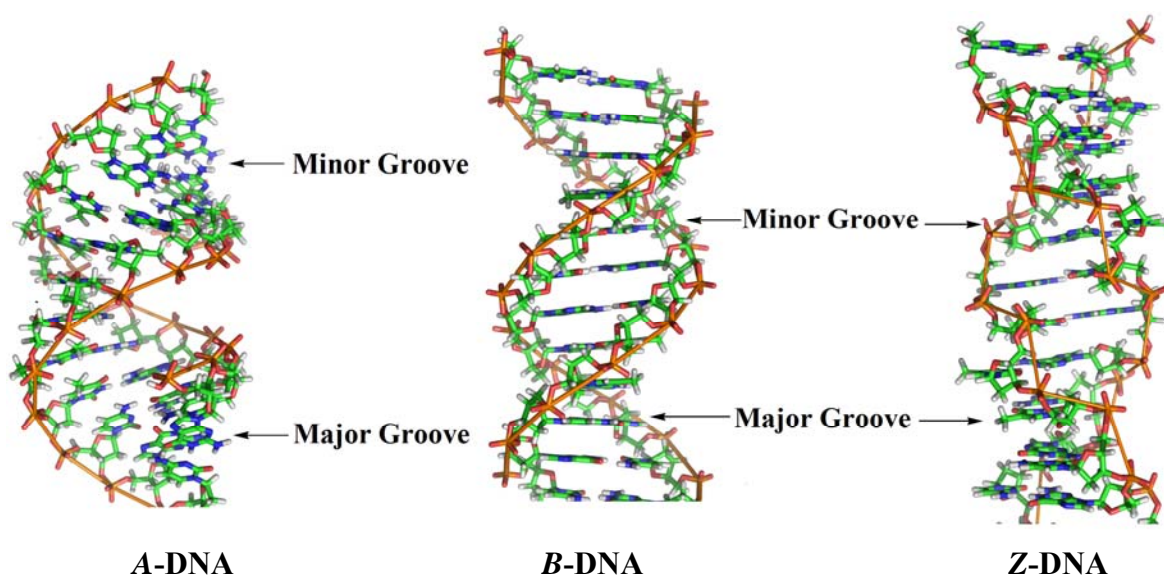


Figure 1.6 Helical Structures of A-DNA, B-DNA and Z-DNA.

In double helical structures, base pairs are usually not located at the center of the helix axis, but are displaced by distance D , and the two glycosidic bonds branch off from one side of the base pairs (figure 1.7a). The outer envelop of the double helix is not cylindrically smooth but can display two grooves of different widths and depths ^[20]. Any groove can be defined by two different regions ^[37]: the ‘bottom’ is formed by the edges of the nucleic base that faces into the groove, and the ‘walls’ are formed from the phosphate backbones of the nucleic acid. The minor groove is at the O₂ (pyrimidine) or N₃ (purine) side of the base pairs, and the major groove is on the opposite side. The pentafuranose sugar is on the minor groove side. Furthermore, A:T sequences produce steric hindrance within the major groove by the presence of the methyl group of thymine (figure 1.7b), and the minor groove of G:C is blocked by the guanine’s amino group (figure 1.7c). Generally speaking, B-DNA has a wide major groove

and a narrow minor groove; *A*-DNA or *A*-RNA has a shallow, wide minor groove and a narrow, deep major groove (Table 1.2). Table 1.3 lists the groove widths and groove depths of several selected nucleic acid sequences, which were studied in this work.

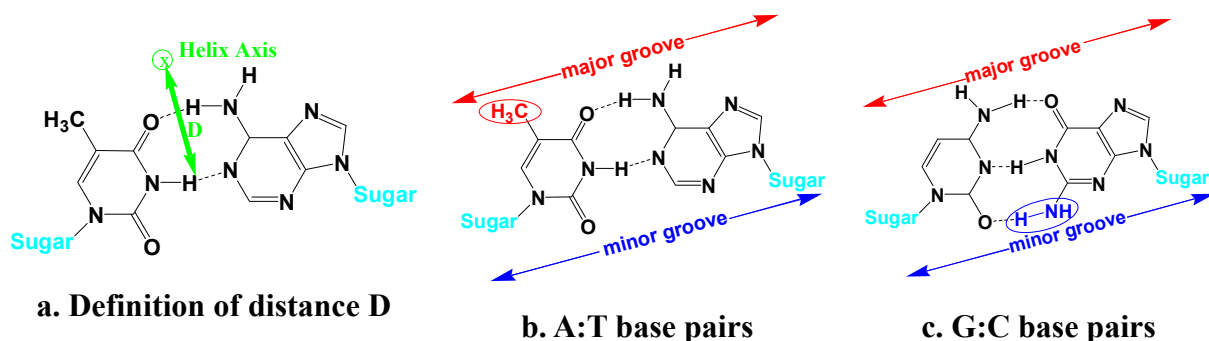


Figure 1.7 The major groove and the minor groove of double helical structures.

Table 1.2 Groove parameters of different forms of nucleic acids [20,38]

Structure type	Groove width ^a (Å)		Groove depth ^a (Å)	
	major	minor	major	minor
<i>A</i> -DNA	2.7	11.0	13.5	2.8
<i>A</i> -RNA	3.8	10.9	-	-
<i>B</i> -DNA	11.7	5.7	8.5	7.5
<i>C</i> -DNA	10.5	4.8	7.5	7.9
<i>D</i> -DNA	8.9	1.3	5.8	6.7
<i>Z</i> -DNA	2.0	8.8	13.8	3.7

a. Groove widths are defined to be the perpendicular separation of the two helices that connect the phosphorus atoms of each strand in least distance, reduced by 0.58 nm, the minimum diameter assumed for a phosphate group. Minor groove depth is defined as $r_{P-O2T} + 0.14$ nm. Major groove depth is defined to be $r_{P-N6A} + 0.14$ nm [reference 42, 20].

Table 1.3 Groove parameters of several nucleic acid sequences

Nucleic acids	Groove width(Å)		Groove depth(Å)	
	major	minor	major	minor
poly (dGdC) – poly (dGdC) [39]	13.5	9.5	10.0	7.2
poly (dG) – poly (dC) [30]	8.1	9.5	-	-
poly (dAdT) - poly (dAdT) [40]	11.23	6.30	-	-
poly dA - poly dT [41]	11.4	3.3	-	-
poly dA - poly dU [42]	13.5	3.0	9.3	7.4
poly A - poly U [38]	3.8	10.9	-	-

1.2 Introduction to Regulation of Gene Expression

Generally speaking, DNA stores genetic information. A segment of a DNA molecule that contains the information required for the synthesis of functional biological products, whether proteins or RNA, is referred to as a gene. After transcription and translation, genes can be expressed as proteins which are the physical manifestations of the abstract information recorded in the genes and help to carry out almost all biological activities. There are at least seven processes to control or regulate gene expression (Figure 1.8) ^[43]:

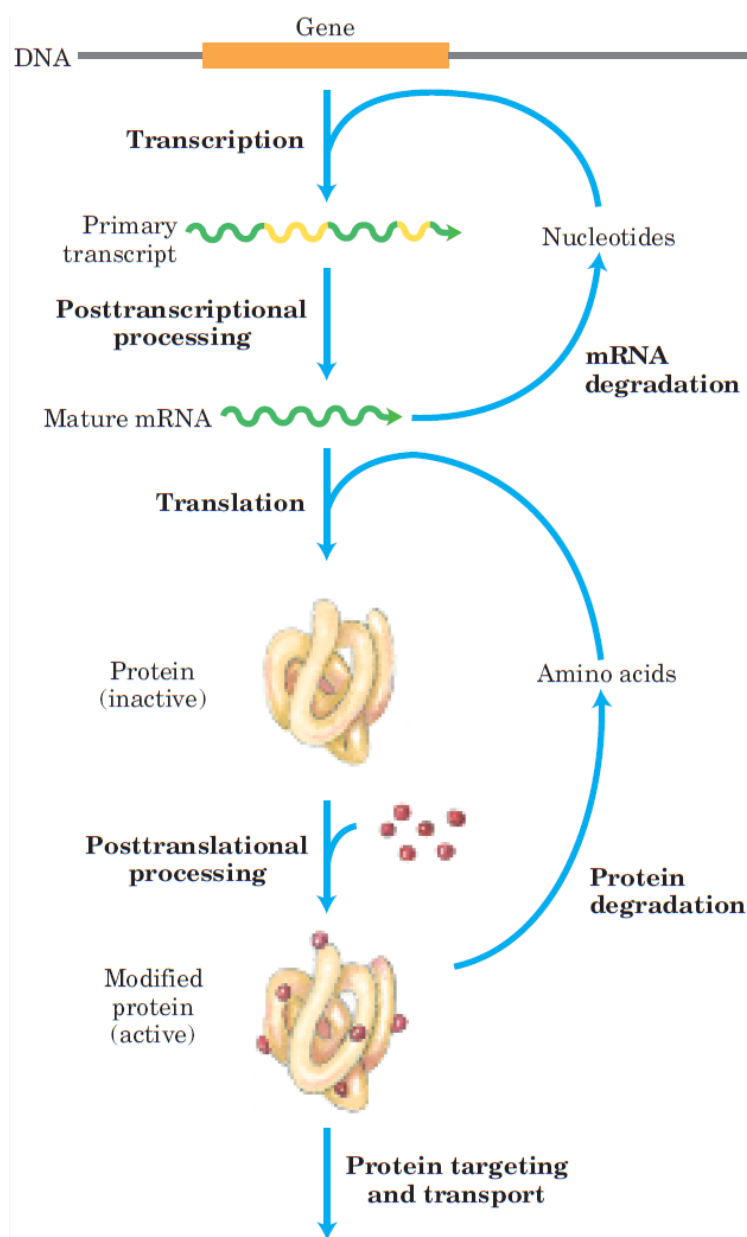


Figure 1.8 Seven processes that affect the gene expression ^[43].

(1). Transcription: Synthesis of the primary RNA transcript. (2). Posttranscriptional modification of mRNA. (3). mRNA degradation. (4). Translation: Protein synthesis. (5). Posttranslational modification of proteins. (6). Protein targeting and transport. (7). Protein degradation. Because in all biochemical processes, an efficient place for the regulation is at the beginning of the pathway, the initiation of transcription is probably the best place for gene regulation.

Interestingly, the interactions between proteins and DNA are the key to the regulation of transcription initiation. RNA polymerase binds to DNA at promoters, and requires transcription factors to form an active transcription complex. Generally speaking, these transcription factors are proteins. They not only could bind to RNA polymerases, but also may recognize other factors, or recognize DNA. Transcription factors usually contain DNA binding domains (DBD) ^[44,45] and trans-activating domains (TAD), and sometimes also contain signal sensing domains (SSD). DNA binding domains are known to interact specifically with either the major or the minor grooves of DNA. For example, helix-turn-helix domains (THT) ^[46], basic leucine zipper domains (bZIP) ^[47] and zinc finger domains ^[48] recognize major grooves of DNA; TATA box binding proteins (TBP) ^[49], integration host factors (IHF) ^[50], and HMG-Box domains ^[51] recognize minor grooves ^[52]. Transcription factors play an important role in the long-term regulation of cell growth ^[53], differentiation ^[54], and programmed cell death (apoptosis) ^[55]. There is growing evidence that transcription factors are closely associated with the development and maintenance of the diseased state at the genetic level ^[56]. Therefore, transcription factors became pharmaceutical target sites. Several transcription factors have been used in the treatment of diseases ^[57].

Small molecules can also bind to DNA in the place of transcription initiation. In general, there are three different binding modes between guest molecules and host DNA ^[58,59]: (1). minor or major groove binding (2). intercalation (3). external binding. These molecules can modulate transcription by any means, and therefore provide potential opportunities for the rational design of drugs. These molecules will probably become novel pharmaceutical interventions in the future.

1.3 Binding of Small Molecules to DNA

1.3.1 Intercalation

Intercalation is the reversible inclusion of a molecule (or a group) between two base pairs ^[60] (Figure 1.9). It is typically observed for cationic molecules having planar aromatic rings. The positive charge need not be part of the ring system, but rather could be on a substituent (Figure 1.10). Anthracyclines ^[61], berberine ^[62], ethidium bromide ^[63,64,65], proflavine ^[66], and thalidomide ^[67] etc. are typical intercalators. Some intercalators can inhibit DNA replication and have been used as antineoplastic agents. For example, doxorubicin ^[68] and daunorubicin ^[69] are used in the treatment of Hodgkin's lymphoma, and dactinomycin is used in the treatment of Wilm's tumour ^[70].



Figure 1.9 The intercalative mode of binding within DNA

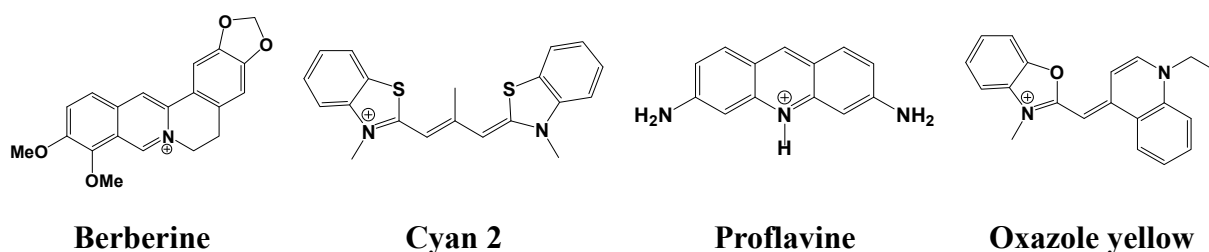


Figure 1.10 Several examples of intercalators

In the classical model of intercalation, the binding process consists of three steps ^[71]: The first step is a thermally activated local opening of DNA, creating a binding site for an intercalating molecule. The second step is the insertion of the intercalator into the binding site (a hydrophobic transfer process). The third step is the formation of molecular interactions (hydrogen bonds between the intercalator and surrounding base pairs). The intercalated site is

then slightly smaller in size than the preintercalation site required to accommodate the first intercalator. The important driving forces for these steps are dipole-dipole interactions and π stacking interactions of the guest molecule with the aromatic nucleic bases. Compared with groove binding, interaction has a significant effect on DNA structures, because the DNA must unwind to enable the intercalators to fit between the two base pairs [37,58,72]. This unwinding leads to the lengthening of the helix, and can cause DNA cleavage.

In addition, intercalators only show modest DNA sequence selectivity [73]. For example, the anthracycline drug daunomycin has been shown by footprinting studies that it prefers the triplet sequence 5'- pyrimidine - purine – purine [74,75]. A molecule which has site-specificity of three bases can only distinguish one out of 32 random sequences. In the context of the human genome, such a molecule will have ca. 100000000 unique binding sites [76]. Therefore, these agents cannot readily discriminate between different genes. Thus, their mode of action is inherently non-selective in terms of the genomes of normal versus abnormal cells [77].

Therefore, some intercalators are high toxicity chemicals, and most of intercalative drugs have strong side effects.

Interestingly, some intercalators (for instance, ethidium bromide, oxazole yellow [78], thiazole orange [79,80], etc.) have low fluorescence until they bind to DNA. They are used to detect DNA fragments. In addition, they can also be used for the high throughput fluorescent intercalator displacement (HT-FID) assay [81], which makes possible highly sensitive and even sequence specific detections of DNA. HT-FID assays are used to judge the DNA binding site-selectivities of low molecular weight molecules and other agents, and are also used for a single-stranded DNA molecule of interest to be screened against a large number of compounds to discover low molecular weight ligands with particular binding properties. Details of this part can be found in chapter 3.1 Ethidium Bromide Displacement Assay.

1.3.2 Minor Groove Binding

A minor groove binder (MGB) refers to a compound that binds selectively to the minor groove of *B*-DNA [82]. They typically contain aromatic rings and charged end groups. Compared with intercalation which requires a major deformation due to the formation of a binding cavity, minor groove binding does not require large conformational changes of DNA [83]. The interactions between MGB and DNA are the combination of ionic, hydrophobic, and hydrogen bond interactions [84,85]. Hydrogen bonding is very important, in that many MGBs can read DNA strand sequences through specific hydrogen bonds with those parts of DNA bases exposed at the ‘bottom’ of a minor groove (see below) [37]. The general mechanism of groove binding is shown in Figure 1.11 [71,86]. Conceptually, the binding process may be divided into at least two processes. First, the groove binder undergoes a hydrophobicity transfer from a solution into the DNA groove. If the groove binder is positively charged, this event will be accompanied by the release of condensed counter ions that surround the DNA (Figure 1.11a). Second, the groove binder will form specific molecular interactions with DNA, including van der Waals attractions and hydrogen bond interactions (Figure 1.11b).

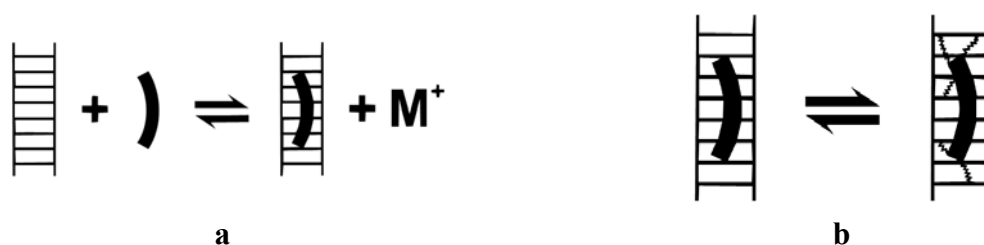


Figure 1.11 The mechanism of groove binding [71]

1.3.2.1 Classification of MGBs

There are three broad families of noncovalent minor groove binders that bind without a significant increase in the groove width from free DNA [87,88]. They are natural products or synthetic compounds based on natural products. The first family of the compounds is the analogues of the nature product, netropsin or distamycin (Figure 1.12a, b). The second family of the compounds is the analogues of CC-1065 and anthramycin (Figure 1.12c, d). They have more complex heterocyclic systems of cyclopropanopyrroles and pyrrolobenzodiazepines. The third family of the compounds is the benzheterocyclic-containing dyes, including

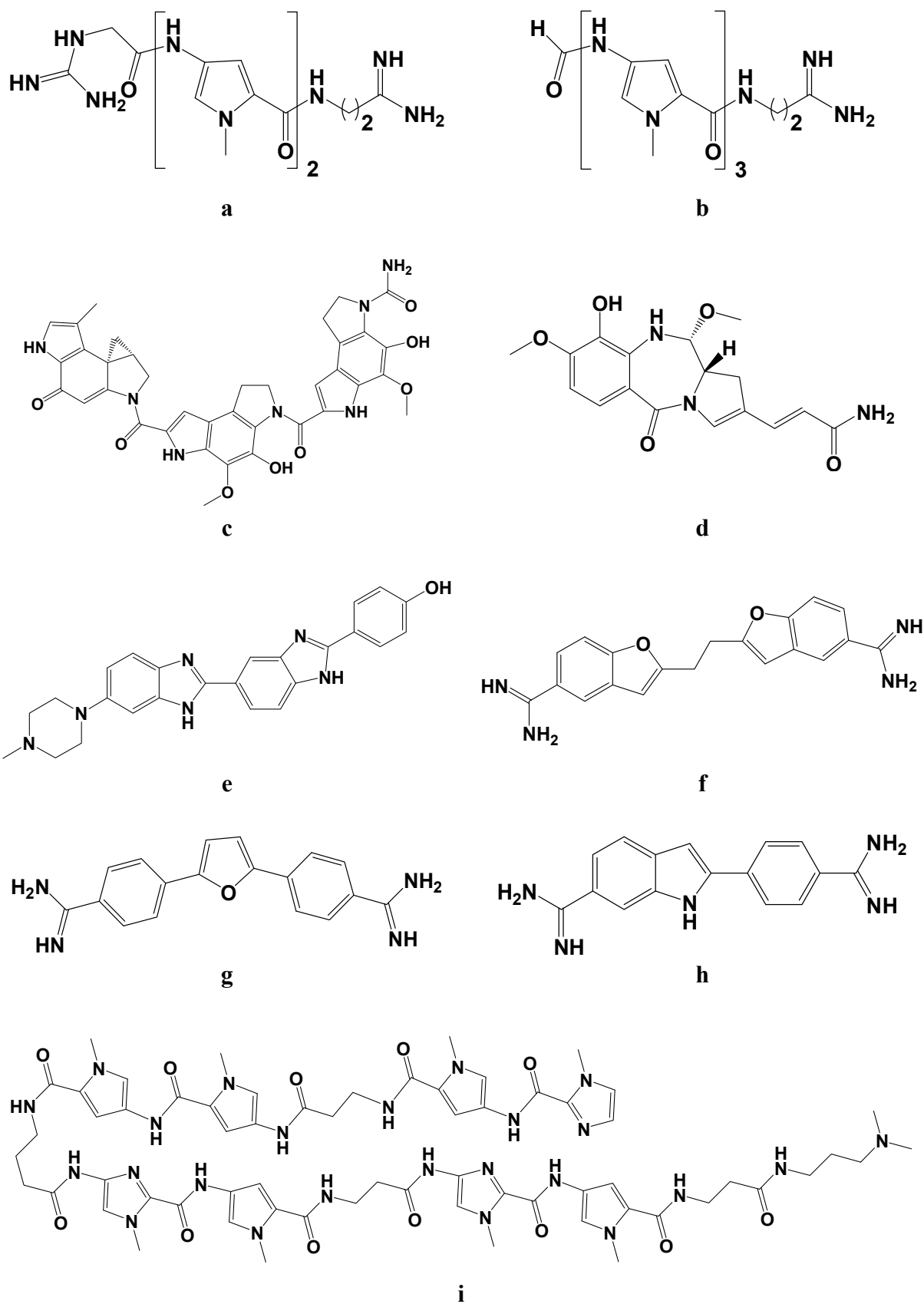


Figure 1.12 Different classes of MGBs

benzimidazoles (for example, Hoechst-33258, Figure 1.12e; DAPI, Figure 1.12h),

benzofurans (Figure 1.12f), bisarylfurans (Figure 1.12g) and so on. Structural derivatives of these families have been exploited, including the introduction of longer and branched alkyl groups in place of the *N*-methyl group, the variation of N- and C-terminal groups and the introduction of other aromatic or heteroaromatic amino acids.

Another type of the minor groove binder is the polyamide hairpin and related compounds (Figure 1.12i). They broaden minor grooves to accommodate side-by-side chains of the aromatic rings joined with amide bonds to give a high level of sequence selectivity^[89].

1.3.2.2 Sequence Selectivity of MGBs

Importantly, sequence selectivity of drug-DNA binding is generally higher for MGBs than for intercalators. These MGBs can bind specifically and selectively to a defined region of DNA with sufficient affinity to inhibit the normal functions of DNA, including replication, transcription and expression of specific genes. With the availability of the data in the Human Genome Project, it is possible to combine genomics and chemistry to develop specific disease agents that act at the DNA level. These MGBs have therapeutic potential in a wide range of applications, not least of which include anti-biotic, anti-viral and anti-cancer drugs.

Majority of MGBs bind to DNA and show higher affinity for A:T-rich sequences^[78,90,91]. There are two reasons. On the one hand, the minor groove with alternating A and T sequences is generally narrow (see table 1.3) and can be approximated by a single smooth curve, which allow favorable van der Waals interactions between the MGB and the DNA. Whereas, G:C-rich sequences have wider minor grooves, and also have the amino groups of guanine bases, which affect the groove geometry (Figure 1.13). These prevent groove-binding molecules from attaining the multiple close contacts with the floor in G:C sequences that are possible in the A:T regions^[92]. Interestingly, a highly structured network of water molecules has been observed in A:T regions^[93,94], so it is possible that displacement of water located in the minor groove (especially in A:T regions) by a minor groove binder contributes to the entropic changes^[95] (see below: Chapter 3.5 ITC Experiment).

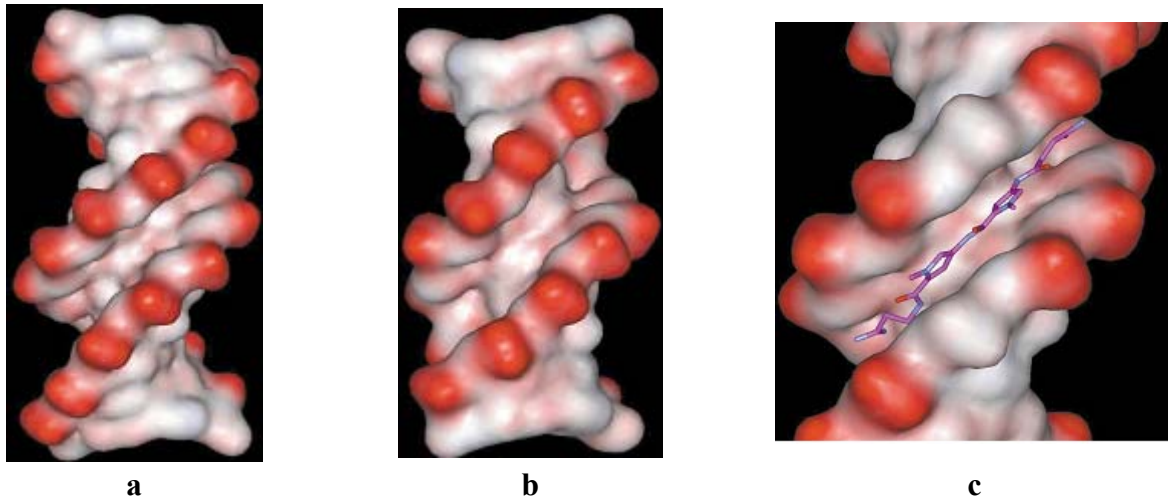


Figure 1.13 DNA minor grooves and minor groove binders [78,91,96]

- The dodecanucleotide d(CGCAAATTTGCG) has a narrow A:T minor groove at the center of the sequence.
- The sequence d(CCAGGCCTGG) has a wide G:C minor groove.
- The crystal structure of the netropsin complex with the dodecanucleotide d(CGCGAATTCGCG)

On the other hand, the distribution of electrostatic potential along a DNA sequence is also sequence-dependent. A:T base pairs have the greatest negative potential at the floor of the minor groove. But for G:C base pairs, they are not as negative as the A:T base pairs, due to the guanine 2-NH₂ (δ^+) in the minor groove of G:C base pairs (Figure 1.14) [97]. Almost all minor groove binders carry cationic charges and complement the potential in A:T regions.

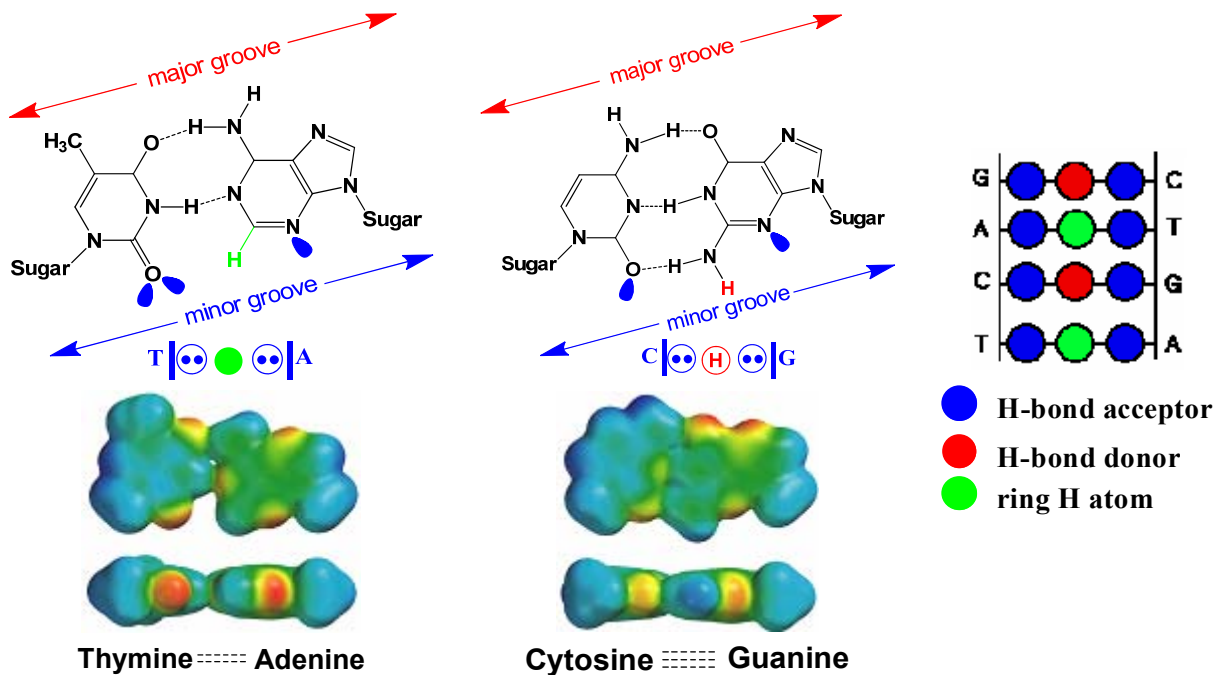


Figure 1.14 Donors & acceptors and electropotential surfaces in minor grooves [97]

In fact, hydrogen bonding to base edges in minor grooves provides the ability to discriminate between A:T and G:C base pairs, due to the differences in numbers of hydrogen bond donors and acceptors (Fig. 1.14).

1.3.2.3 The Development of Sequence-Specific MGBs ^[78,90]

In my opinion, the development of sequence-specific MGBs has gone through four stages:

- 1). The crystal structures of a netropsin complex with the dodecanucleotide duplex sequence d(CGCGAATTCGCG) ^[96] and a distamycin complex ^[98] with the sequence d(CGCAAATTTGCG) provided detail pictures of the interactions between these MGBs and A:T base pairs. It also provided an explanation for its A:T selectivity and a paradigm for other MGBs in this class (Figure 1.15 a). In the crystal structures, (i). Netropsin and distamycin fit into the 5'-AATT region of DNA. (ii). The walls of the minor groove are in close contact with pyrrole and amide groups. (iii). Hydrogen bonding to base edges provides selectivity for A:T base pair edges: each amide group forms a hydrogen bond to N₃ of adenine or O₂ of thymine, and the terminal guanidinium groups are also involved in hydrogen bonding to bases.
- 2). Based on the facts mentioned above, it was assumed that a modification of netropsin to produce a *N*-methylimidazole group taking place of a pyrrole ring could result in recognition of the minor groove exocyclic N₂ atom of guanine, i.e. active recognition of a G:C base pair. And then lexitropsins were synthesized ^[99]. Unfortunately, although they showed ability to recognize G:C base pairs, however, the A:T recognition was retained. In addition, they frequently show reduced affinity for the overall DNA ^[100,101].
- 3). After that, a surprising discovery was shown by NMR ^[102,103] and crystal ^[104] studies: distamycin and DNA can form a 2:1 complex (Figure 1.15 b). In these structures, (i). Two distamycin molecules bind in a side by side manner to the A:T tract, with high orientational and sequence specificity. (ii). Each distamycin molecule binds to one strand. (iii). The DNA is overall in the *B*-form, but the minor groove is widened by 2 Å compared to canonical *B*-DNA.
- 4). The 2:1 motif has led to a new and effective class of DNA sequence recognition molecules,

the polyamides (Figure 1.12 i). These molecules combined the precise hydrogen bonding to base pair edges shown by netropsin and distamycin (Figure 1.15a), with the enhanced groove width in G:C-containing sequences, which can accommodate dimeric molecules (Figure 1.15b). The dimeric molecule (the polyamide) can “read” one DNA duplex at a time rather than the two in a 1: 1 complex. Therefore, the polyamide shows much higher affinity (at least tenfold) for DNA compared to the monomer. In addition, the enhanced affinity is usually accompanied by a corresponding increase in sequence specificity.

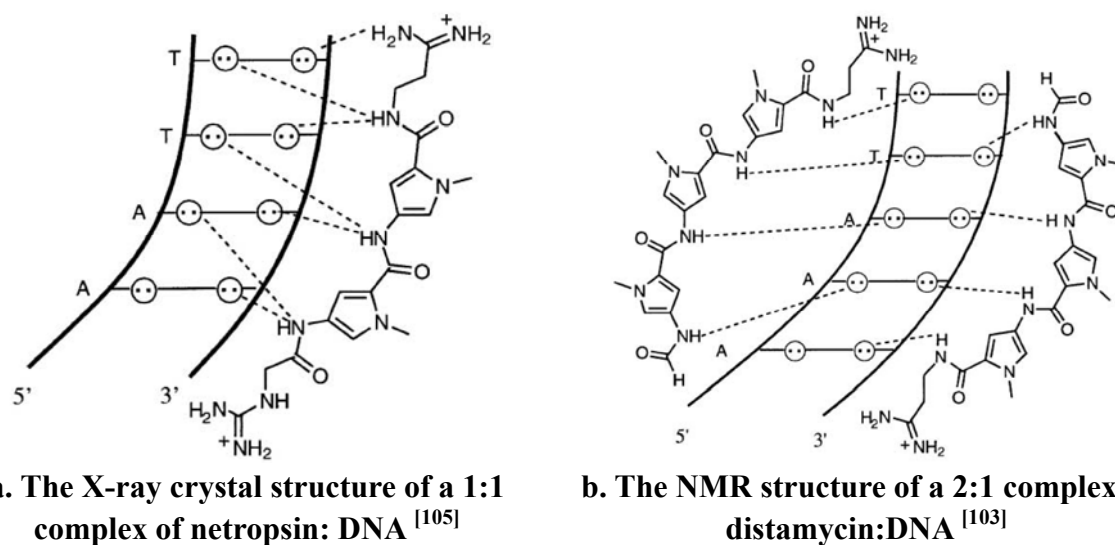


Figure 1.15

1.3.2.4 Sequence Specificity of Polyamides and Pairing Rules for Minor Groove Recognition ^[89]

For polyamides designed by Peter B Dervan, Im/Py recognizes G:C and disfavours C:G, A:T and T:A; Py/Im only favours C:G; Py/Py recognizes A:T and T:A; and Im/Im does not recognize any of the four, and thus is useful in correctly positioning a polyamide within a sequence (Figure 1.16).

However, the defect of the pairing code mentioned above is that Py/Py can not distinguish between A:T and T:A base pairs. 3-hydroxypyrrole (Hp) was then introduced to the recognition motifs ^[106], in that the 3-hydroxy group can form a specific hydrogen bond with the O₂ of thymine (Figure 1.17a), and the Hp-OH has a steric clash with the adenine of the T:A base pair (Figure 1.17b). The Hp/Py pair shows steric destabilization against T:A, but steric permissiveness at A:T.

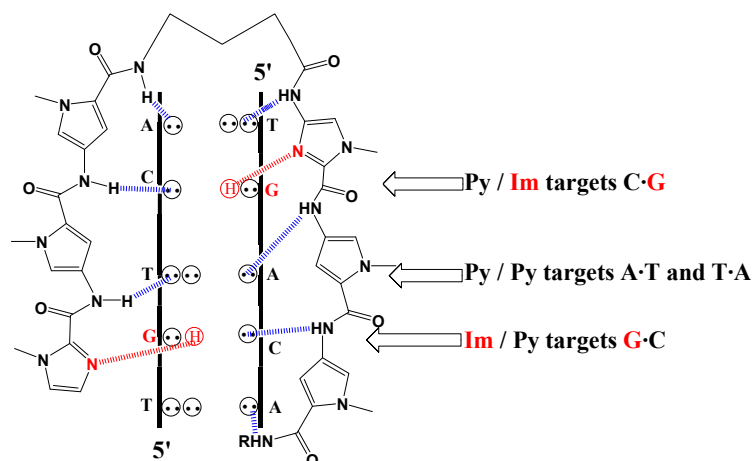


Figure 1.16. The hydrogen-bonding model of the hairpin motif

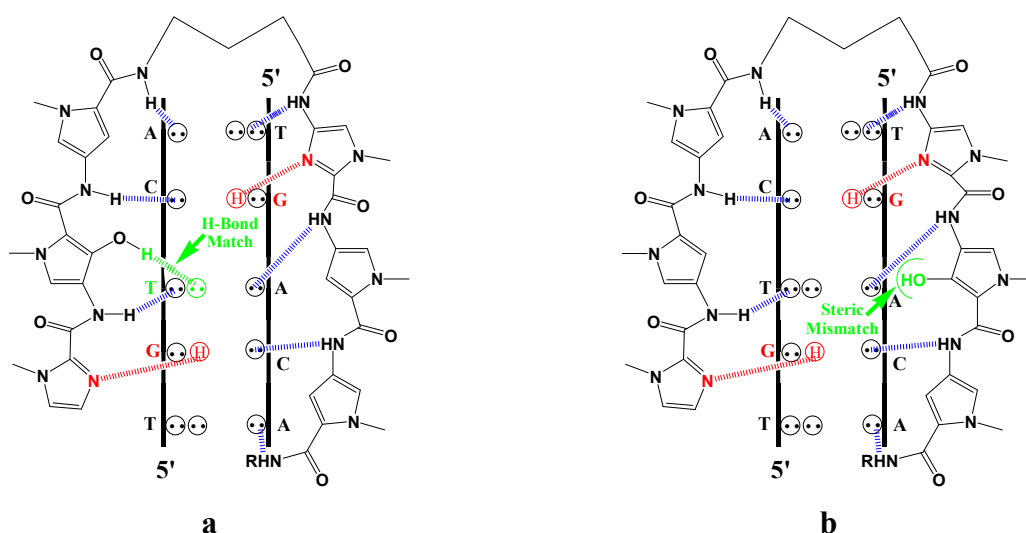


Figure 1.17 Models for Py/Hp binding A:T, but not T:A

Thus, four Watson–Crick base pairs can be unequivocally recognized by Hairpin-linked polyamides composed of Py, Im and Hp (table 1.4).

Table 1.4 Pairing rules for minor groove recognition

	C:G	G:C	T:A	A:T
Im/Py	-	+	-	-
Py/Im	+	-	-	-
Hp/Py	-	-	+	-
Py/Hp	-	-	-	+

Favored (+), disfavored (-)

1.3.3 Major Groove Binding

Because the minor groove is too narrow and backbones are on the minor groove side, relatively large molecules (for example, DNA binding proteins) often interact with the bases (the internal parts of the DNA molecule) on the major groove side ^[37]. In nature, most protein-DNA contacts occur in major grooves. Because the base pairs contain genetic information, and in major grooves, the four base pairs present four different edge patterns to amino acids approaching (Figure 1.18), the major groove is therefore more informative than the minor groove (the minor groove only has two distinct patterns, Figure 1.14).

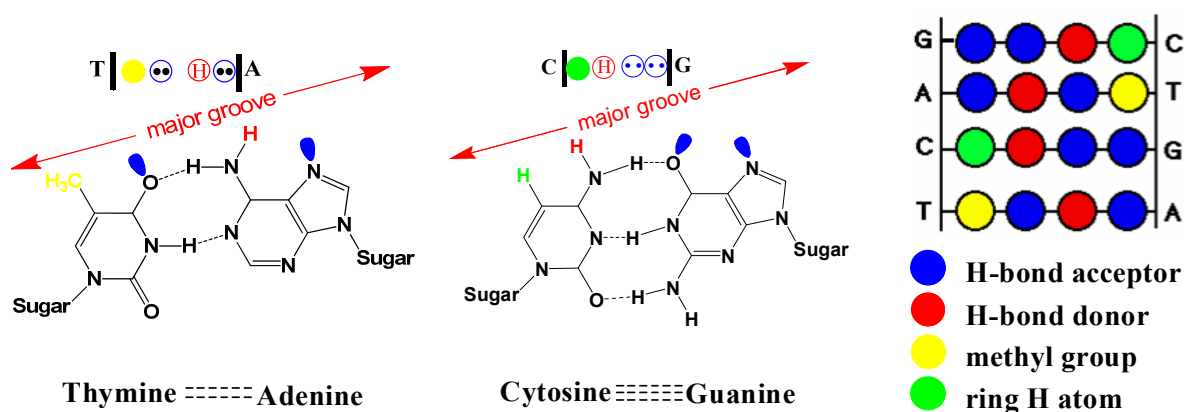


Figure 1.18 Steric geometries and donors & acceptors in the major groove

In a major groove, protein-nucleic acid interactions are sequence-specific recognition ^[107]. The sequence-specific recognition is closely related to the geometry (the shape) and the electrostatic potential of the major groove (Figure 1.18, Table 1.2 and Table 1.3).

The electrostatic potential is a key point to understand intermolecular association ^[108]. For nucleic acids, the first contributor to different electrostatic potentials is the intrinsic base pair potential. In major grooves, G:C base pairs [C-4-NH₂ (δ^+), G-6-CO (δ^-), and G-N7 (δ^-)] have a larger electrostatic potential gradient than T:A base pairs [T-4-CO (δ^-), A-6-NH₂ (δ^+), and A-N7 (δ^-)]. For example, dG₆-dC₆ and dA₆-dT₆ have dramatic differences between the potentials in major grooves. For dG₆-dC₆, one side of the major groove is negative, and the other side is positive. For dA₆-dT₆, there are no negative potentials at all. The second main

contributor is a nearest-neighbor interaction, which can either reinforce the intrinsic base pair potentials or decrease these potentials. For example, in major grooves, d(CGCGCG)-d(CGCGCG) has more neutral areas than does dG₆-dC₆ because the neighboring base pair potentials $\mp\pm\pm$ somewhat cancel each other. The electrostatic patterns of the major grooves of d(TATATA)-d(TATATA) and dA₆-dT₆ are more similar than those of d(CGCGCG)-d(CGCGCG) and dG₆-dC₆.

From the examples mentioned above, we know that in major grooves, G:C base pairs are more special than A:T base pairs. That is indeed the case. Although some amino acid side chains (for example, Asn and Gln) have hydrogen bonding complementarity to the major groove site of adenine ^[109] and A:T pair hydrogen bonding interactions are sources of major groove specificity ^[110], however, G:C base pairs are more important in major grooves: G:C base pairs confer greater specificity, and nature likely takes advantage of the greater potential specificity of G:C base pairs ^[109]. For example ^[110,111], there are more than twice as many G:C as A:T pairs in the known recognition sequences of restriction endonucleases; and for a lot of restriction endonucleases, adenine can replace thymine in the recognition pattern, but guanine can replace cytosine.

Zinc finger domains, helix-turn-helix domains and basic leucine zipper domains are typical major groove binders. They have been studied in detail and have been used to interpret sequence-specific recognition in major grooves between DNA binding proteins and double-stranded DNA (ds-DNA).

(1). Zinc finger domains ^[112,113,114]

This domain is common in eukaryotic DNA-binding proteins. It was originally found in the eukaryotic transcription factor TFIIIA. TFIIIA contains nine repeated modules. The general transcription factor Sp1 has a DNA-binding domain that consists of three zinc fingers, each of which contains two Cysteine and two Histidine residues. These four residues coordinate one Zn²⁺ ion. The C-terminal part of each finger forms α -helices that bind to the major groove of

DNA, and the N-terminal part forms β -sheets (Figure 1.19a). The three fingers line up in the same major groove of the DNA (Figure 1.19b). There are direct amino acid-base pair contacts as well as amino acid-DNA backbone contacts. The amino acids in the C-terminal side of each finger are responsible for recognizing specific target sites of DNA. The target bases all lie on one strand. Each finger interacts with three bases. In zinc finger domains, Arg (24, 18, 46, 74, 80) contacts with guanine; His (49) intercalates between guanine and thymine, forms a hydrogen bond with N7 with the guanine, and has van der Waals interactions with thymine.

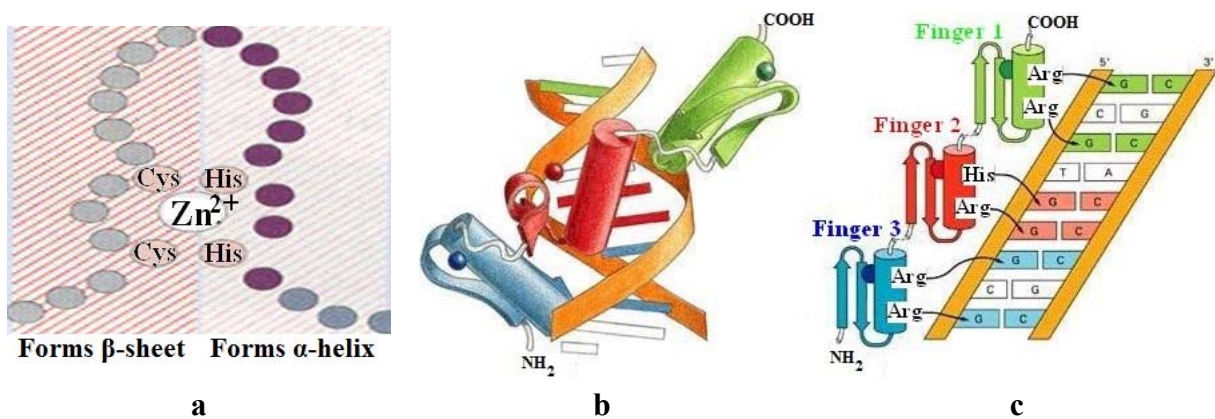
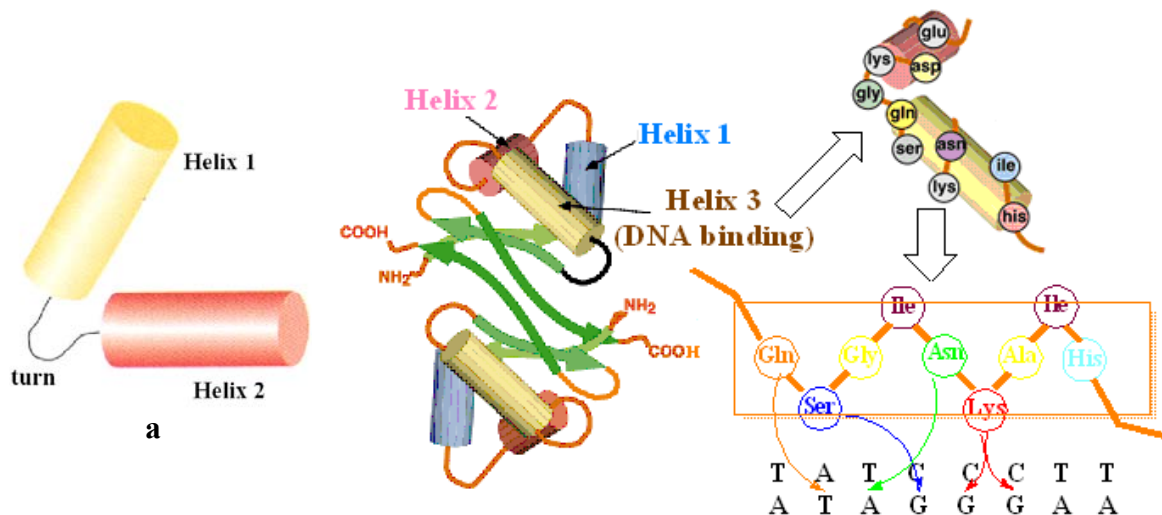


Figure 1.19 Zinc finger domains ^[114]

(2). Helix-turn-helix domains ^[114,115,116]

This motif was originally identified in bacterial proteins, and has been found in hundreds of DNA-binding proteins from both eucaryotes and prokaryotes. This motif has both the ability to bind DNA and to dimerize. It is constructed from two amphipathic α helices connected by a short extended chain of amino acids, which constitutes the "turn" (Figure 1.20a). HTH proteins can form both homodimers and heterodimers by means of interactions between the hydrophobic residues on the corresponding faces of the two helices. The dimer binds to DNA stronger than the monomer, and furthermore, by changing the relative positions of monomers, the dimer activity can be easily turned on and off. The carboxyl-terminal helix is called the recognition helix because it fits into the major groove of DNA. The amino acid side chains of the recognition helix are positioned to facilitate hydrogen bonding with the edges of base pairs in the specific DNA sequence to which the protein binds (Figure 1.20b).



b Helix turn helix motif of Cro repressor protein (phage Lambda)

Figure 1.20 Helix-turn-helix domains ^[114]

By analyzing several examples of the protein-DNA interactions, we can get some valuable conclusions:

- (1). The specificity of DNA-protein interactions depends upon certain amino acids in recognition domains that protrude into the groove of the DNA double helix and make specific contacts with functional groups of specific bases. Several studies proved that interactions between arginine-guanine, lysine-guanine and lysine-thymine in major grooves would be unusually strong. Ser also bind to guanine on the major groove side ^[115,20,110]. (Figure 1.21a-c)
- (2). Asn or Gln can interact with adenine (N6 and N7), guanine (O6 and N7), and backbones via hydrogen bonds ^[20]. (Figure 1.21 d-e)
- (3). The methyl groups of the some side chains (for example, Ala and Thr) can form a hydrophobic pocket to receive the methyl group of thymine.
- (4). Peptide backbone NH groups can form hydrogen bonds with the DNA phosphate groups. It is sequence unspecific interactions, but these interactions stabilize the appropriate DNA conformation and a large number of residues are distributed along the polypeptide chain. These unspecific interactions make the 'unit' which is responsible for differential binding to different DNA regions become really a specific binding domain. (Figure 1.21 f-h)
- (5). These interactions are electrostatic and topographic complementarity ^[108].

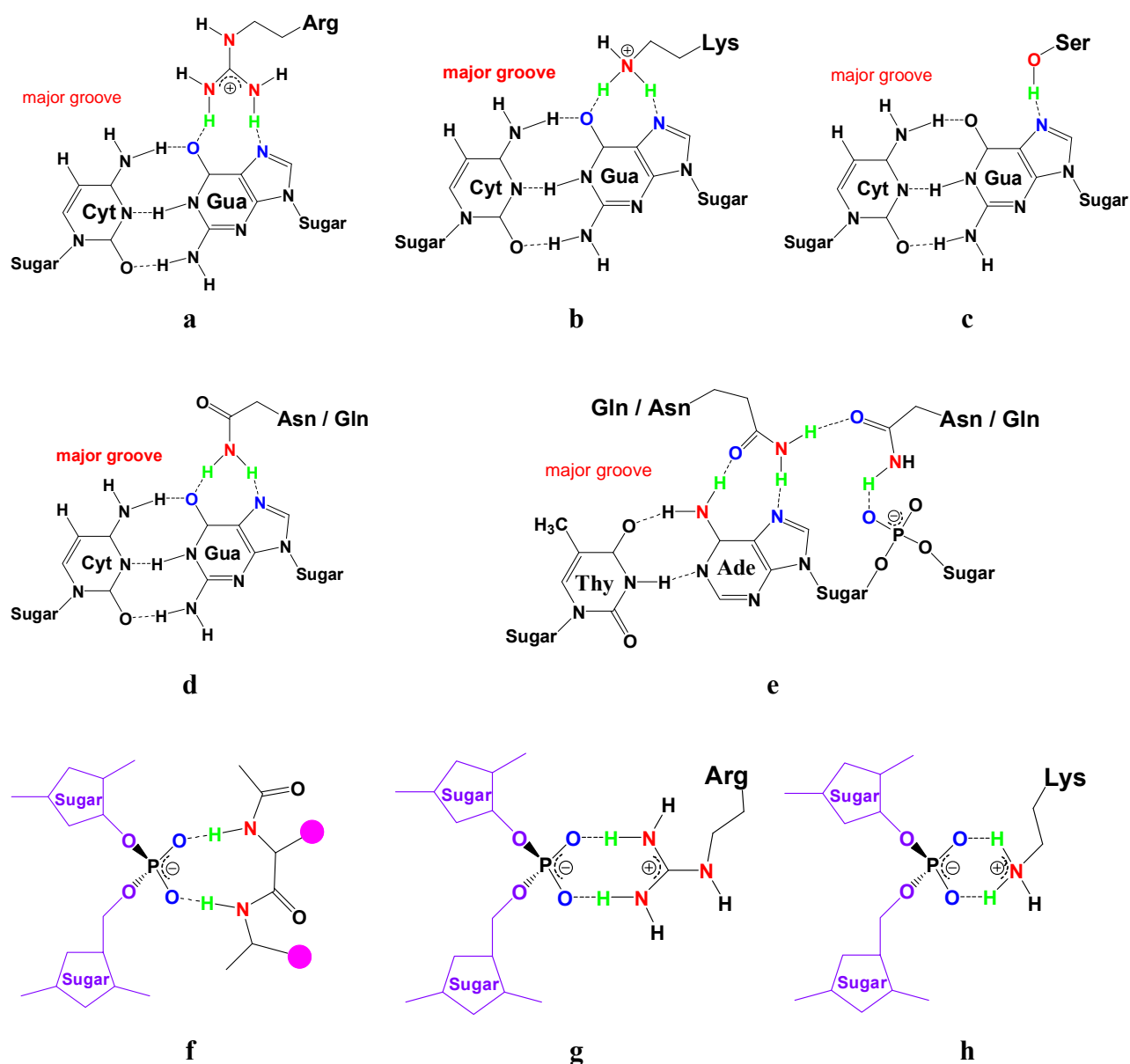


Figure 1.21 Examples of Protein-Nucleic Acid Interactions

Beside DNA binding proteins, several small molecules also bind to major grooves of DNA. For example, methyl green ^[117] [poly(dAdT)-poly(dAdT) and poly dA-poly dT], methylene blue ^[118] [poly dA-poly dT], APF [poly(dGdC)-poly(dGdC), also intercalation], and Hoechst 33258 ^[119] [poly(dGdC)-poly(dGdC), also intercalation]. Another major groove binder candidate, which was first synthesized and studied by the group Prof. Dr. Thomas Schrader, is the large calixarene dimer ^[120] .

1.4 Calixarene

Calixarenes are a readily available and important class of macrocycles in supramolecular chemistry. Compared with traditional molecular chemistry, which is focused on the covalent bond, supramolecular chemistry pays more attention to noncovalent interactions between molecules^[121]. These interactions are weaker and reversible^[122]. The driving forces for the formation of supramolecular structures include hydrophobic interactions, electrostatic interactions, hydrogen bond interactions, van der Waals interactions, cation – π interactions, π - π stacking interactions and so on. The total intermolecular force acting between two molecules is the sum of all the forces they exert on each other. Supramolecules can form some special structures, for example, self-assembly, folding, mechanically interlocked molecular architectures. Supramolecular chemistry is often related to several research areas, for instance, molecular recognition, host – guest chemistry, dynamic covalent chemistry^[123], etc. Because the noncovalent interactions are the basis of life, supramolecular chemistry becomes crucial to understanding, modeling and mimicking biological processes and biological systems, and it can broaden our horizons to develop new materials with special properties and functions.

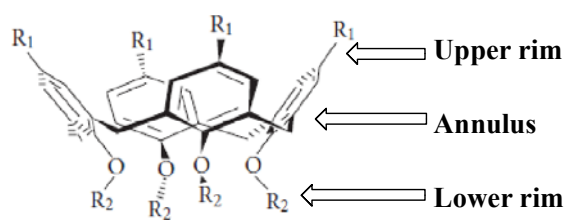
The design and synthesis of water-soluble synthetic macrocycles as artificial receptors and bio-mimetic models has been a major subject of supramolecular chemistry in recent years. Calixarenes are one of the most famous macrocyclic compounds. They were obtained by the oligomerization of phenol and formaldehyde, and consist of phenolic units arranged in cyclic arrays by the linking with methylene bridges *ortho* to the phenol groups^[124]. They can be defined with upper and lower rims and a central annulus (Figure 1.22a). Compared with other macrocycles (for example, cyclodextrins, crown ethers, cryptands, etc.), calixarenes have several special properties and advantages^[125], which can be involved in molecular recognition processes.

(1). They have different forms due to the flexibility in the rotation of Ar – CH₂ – Ar bonds^[126]. For example, the calix[4]arene macrocycle is in one of its four possible conformations: ‘cone’, ‘partial cone’, ‘1,2-alternate’, ‘1,3-alternate’ conformations (Figure 1.22). Calix[6]arenes can

exist in eight different ‘up-down’ conformations like calix[4]arenes. The core conformation is the most stable conformation amongst all the forms of calix[n]arenes.

(2). The larger and conformationally more mobile calix[6]- and -[8]arenes can adapt their conformations to the stereochemical request of the multivalent receptor entity through induced fit ^[130].

(3). The cavity with a size is suitable for inclusion of ions and small molecules ^[127].



a. Division of calixarene

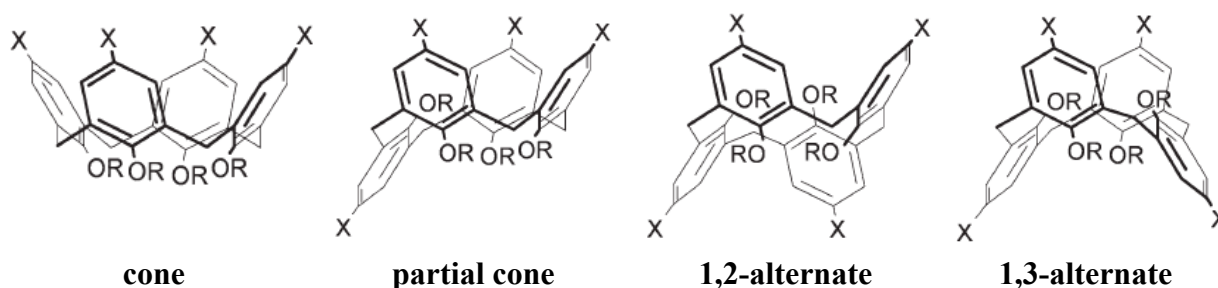


Figure 1.22 The division and four conformations of a calix[4]arene ^[128]

(4). It is possible to create ligands with binding sites or functional groups at the upper or lower rims of the present compounds, for example, –CHO, –COOH, –NH₂, –NCS, etc ^[129].

These modifications not only make calixarenes easily form complexes with a variety of guests, but also extend their use in the construction of large architectures, such as calixcrowns, calixcryptands, and calixspherands, calixcavitands, and calixcarcerands. Calixarenes can form dimers with the help of spacers. In this work, I exclusively focused attention on the calixarene dimers.

Compared with a calixarene monomer, the corresponding calixarene dimer is bigger and contains more binding sites (or functional groups), which make them useful building blocks

and carrier molecules. Furthermore, they can use the internal dynamics to arrange multiple and interconnected components to minimize free energy^[130]. In solution, they could form a tightly packed ball. Such intramolecular reorganizations may lead to shape and volume changes, the creation of internal microenvironments, the cooperative organization of the surface or inner functionalities, the concentration or the exclusion of substrates from the molecular “cavity” of calixarene dimers, and the formation of defined multimolecular assemblies.

The first work about DNA recognition with large calixarene dimers was published by the group Professor Dr. Thomas Schrader in 2006^[120]. Two different calixarene dimers connected by either a flexible aliphatic linker or a rigid aromatic linker were synthesized (Figure 1.23).

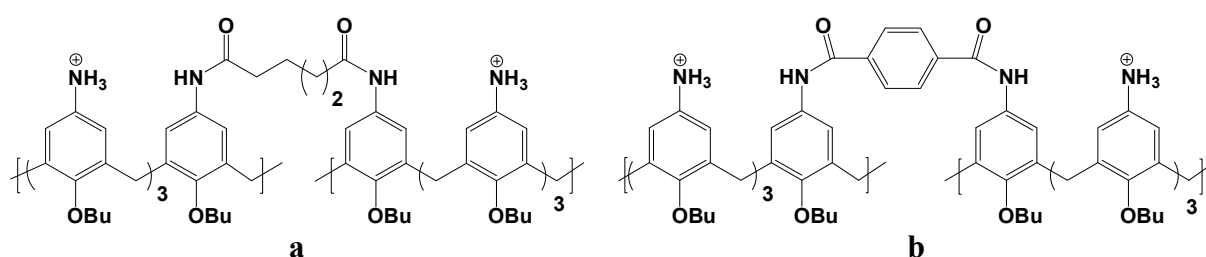


Figure 1.23 Calix[4]arene dimers a/b based on trifunctional anilinium building blocks

Because direct structure information from a crystal or NMR structure was not available, a number of DNA binding experiments were performed. The binding mode between the calixarene dimers and nucleic acids was established according to the following arguments:

- (1). The average size of these molecules is about 3 nm². The dimension excludes intercalation and minor groove binding.
- (2). ¹H NMR spectroscopy and fluorescence titrations indicate that there is no interaction between sugars and the dimers, and the binding of dimers with phosphate backbones is weak. These results exclude external binding.
- (3). The dimer showed efficient displacement of intercalated ethidium bromide, which can prove that the calixarene dimer does not attack the phosphodiester backbone by multiple salt bridges, but rather inserts into the groove.

(4). The UV absorption intensity strongly enhanced and the melting curves were inverted in the presence of the calixarene dimers. This is in perfect agreement with an insertion of the extended nonpolar calixarene dimer corpus into the groove accompanied by hydrogen bonding to the chromophores (nucleic bases) in Hoogsteen sites.

(5). As A:T pairs present methyl groups into the major groove but G:C pairs do not, pure (GC)_n DNA strands should be preferred for insertion into the calixarene dimer owing to additional hydrogen bond contacts. This sequence selectivity was indeed established with fluorescein-labeled dG₁₂-dC₁₂ and dA₁₂-dT₁₂ model DNA, which produced a pronounced difference in the K_D value of one order of magnitude. This experiment proved the major groove binding mode.

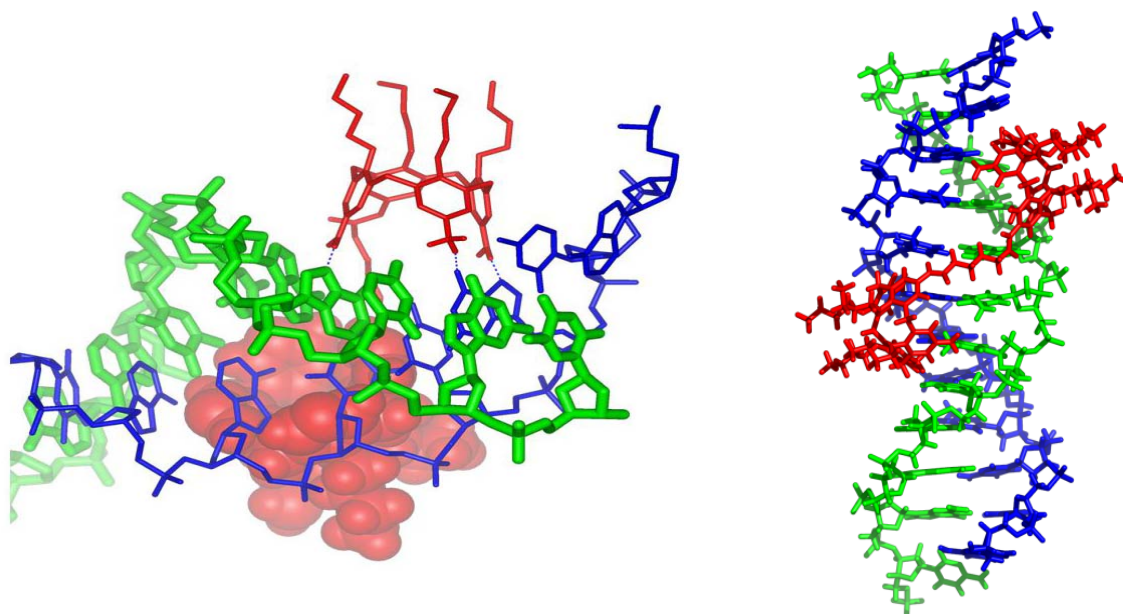


Figure 1.24 The mechanism of DNA binding by dimeric calixarenes.

The mechanism of DNA binding by dimeric calixarenes was presented: the ammonium groups of the calixarene units were deeply buried within the major groove, and contact to various nucleic bases with hydrogen bonds. The butoxy tail is toward the free solution. The adipic acid linker binds along the major groove (Figure 1.24).

After that, two different series of related compounds with varied bridging units were synthesized by the same group (Figure 1.25) [131]. In one series, the alkyl bridge between both calixarenes was varied in successive steps of C-2 ethylene units from 4 to 6 and 8 up to 10 carbon atoms (Dimer 1-4). In a second series, they introduced two full positive charges directly into the bridging alkyl chain or alternatively into its close vicinity (Dimer 5-6). All the calixarene dimers were subjected to a wide range of DNA or RNA binding experiments. We can get some valuable results.

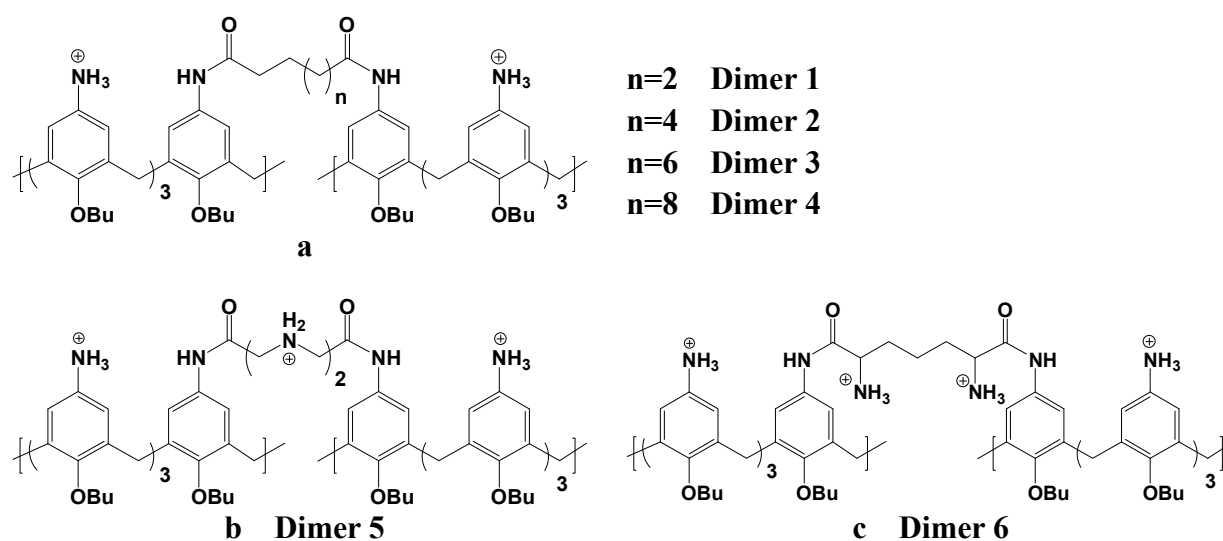


Figure 1.25 Calixarene dimers with different spacers

(1). Dimer 1, Dimer 2, Dimer 3 and Dimer 4 (Figure 1.24 a) can not dissolve in water, and have similar equilibrium binding affinities for DNA.

(2). Dimer 5 and Dimer 6 (Figure 1.25b, Figure 1.25c) exhibit higher equilibrium binding affinities (about one order of magnitude) for DNA, more efficient displacement of intercalated ethidium bromide, and significant stabilization in the DNA duplex.

Unfortunately, the two additional charges can not render the whole calixarene dimers water soluble, and the affinity is only at the micromolar level. In order to block pathogenicity genes, it is necessary to synthesize new calixarene dimers, which not only should be water-soluble but also should show much higher affinities for DNA.

1.5 Objectives

Objective 1: To synthesize water-soluble dimeric aminobenzyl calixarene (Dimer A) and its guanidinium counterpart (Dimer B) (Figure 1.26), and to observe whether they bind DNA with higher affinity, and to prove whether they are major groove binders.

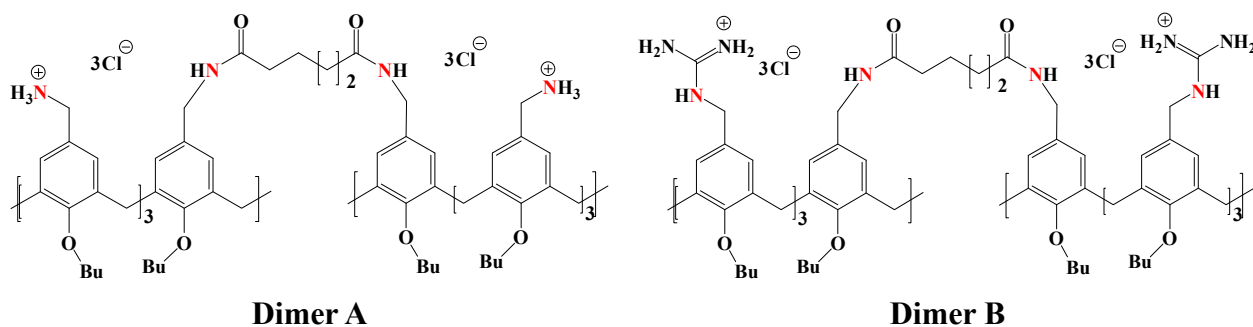


Figure 1.26 Structures of calixarene dimers

The design of Dimer A and Dimer B was based on the following experimental results:

- (1). Previous experimental results have been implied that anilino-calixarenes (Figure 1.23, Figure 1.25) could be major groove binders ^[120].
- (2). Compared with aniline analogues, benzylamine and its guanidinium counterpart have good solubility in water.
- (3). Benzylamine and its guanidinium counterpart have higher pK_a values than aniline analogues ($pK_a \approx 5$). Thus at physiological pH (7.3-7.4), benzylamine ($pK_a \approx 10$) and its guanidinium counterpart ($pK_a \approx 12$) are easily protonated. They can exhibit high affinities for nucleobases and phosphate backbones via hydrogen bond interactions and electrostatic interactions.
- (4). Benzylamine and its guanidinium counterpart can mimic lysine and arginine to interact with nucleobases via hydrogen bond interactions on the major groove side or to interact with phosphate backbones via electrostatic interactions (Figure 1.21 a, b, g, h).
- (5). The amides of Dimer A and Dimer B could mimic NH groups of peptide backbones to

form hydrogen bonds with the phosphate groups or the nucleobases on the major groove side (Figure 1.21 d, e and f).

In order to broaden the scope of the investigation, the corresponding monomeric calixarenes (Figure 1.27) were also synthesized. Because direct structure information from a crystal or NMR structure was not yet available in my work, several other biophysical experiments have been designed and performed between these calixarenes and different nucleic acids with varying base composition and conformation. These experiments include DAPI displacement assays, EtBr displacement assays, fluorescence titrations, CD measurements and so on.

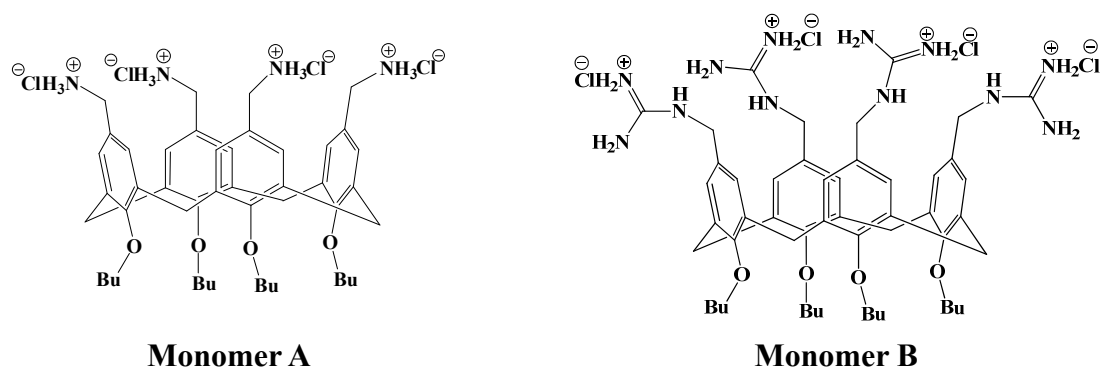
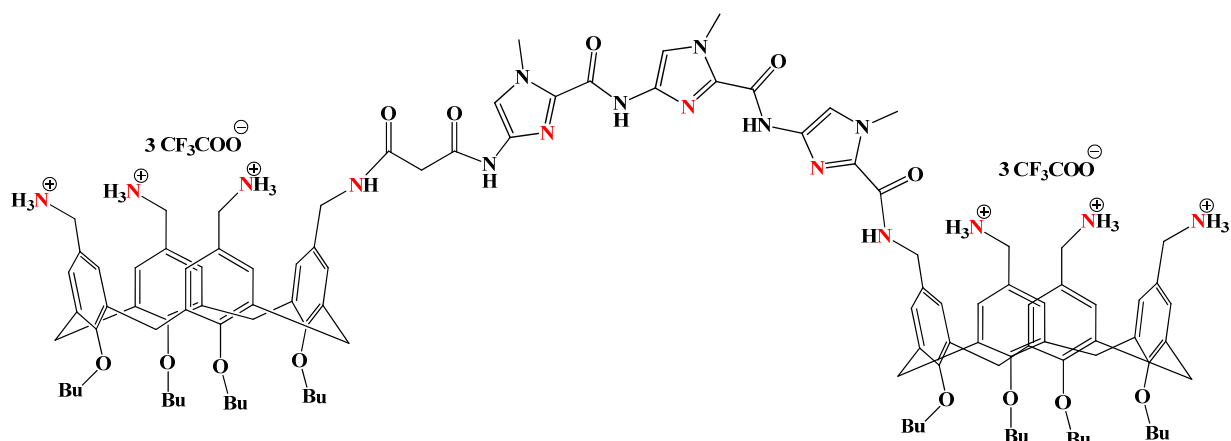


Figure 1.27 Structures of calixarene monomers

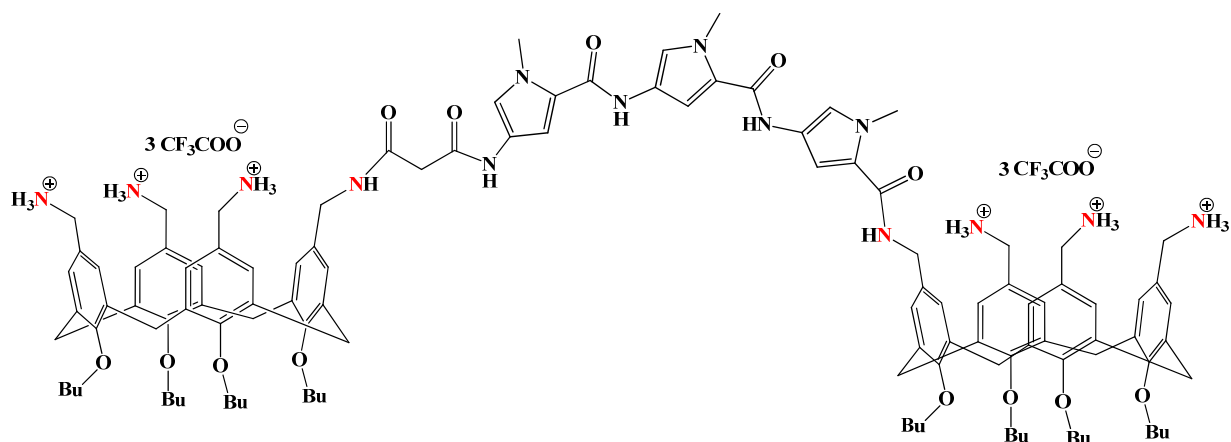
Although the experimental results indicate that they are water-soluble and they exhibit much high affinities for DNA, and the results also strongly support a major groove binding mode, however, these calixarenes (Dimer A, Dimer B, Monomer A and Monomer B) showed similar affinities for different DNA duplexes. Thus, it is urgent to design a new class of calixarene dimers, each of which can show stronger preference for only one specific DNA duplex.

Objective 2: To synthesize calixarene dimers containing heterocyclic oligoamide bridges (Figure 1.28), and to prove whether they are major groove binders, and furthermore, to observe whether they can recognize specific DNA sequences.

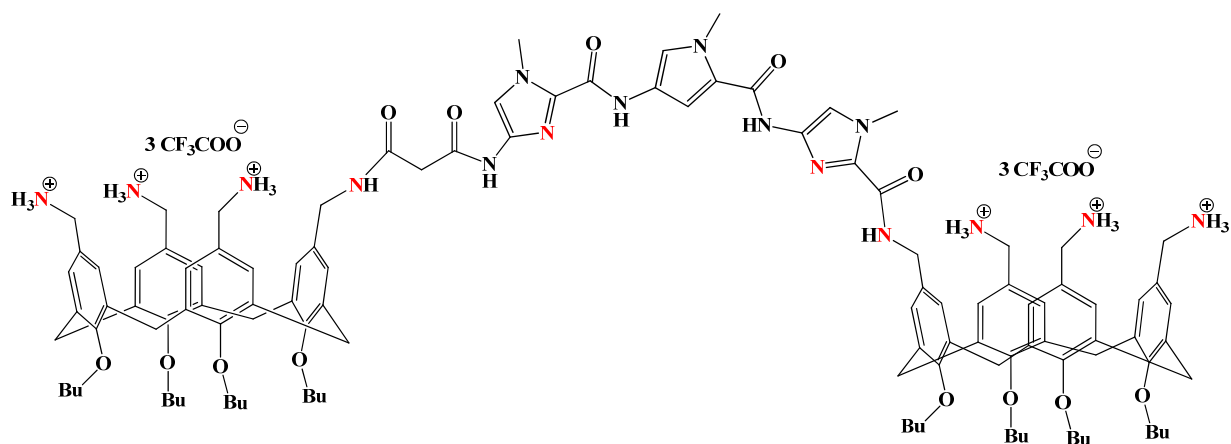
The heterocyclic oligoamides contain *N*-methylpyrrole, 3-hydroxypyrrole and *N*-methylimidazole amino acid building blocks. In this part, I synthesized the calixarene dimer with a triimidazole bridge (Dimer C).



Dimer C



Dimer D



Dimer E

The design of Dimer C-E was based on the following experimental results:

- (1). Dimer A and Monomer A are major groove binders.
- (2). The hydrogen bonding of polyamides^[89] to base edges in minor grooves provides the ability to discriminate between A:T and G:C base pairs, due to the differences in numbers of hydrogen bond donors and acceptors (Figure 1.16 and Table 1.4).

(3). Dimer A or Monomer A binds DNA with higher affinity, which can drive the oligoamide bridge (probably a minor groove binder) from a minor groove to a major groove.

(4). Because in major grooves, the four base pairs present four different edge patterns to amino acids approaching (Figure 1.18), the heterocyclic oligoamide bridges (amino acids) can specifically recognize different edge patterns in major grooves.

At the same time, we also want to know, *in vitro*, whether these calixarene dimers or monomers have biological activities, whether they can regulate gene expression, and whether they really bind to the major groove of promoters and block pathogenicity genes. In this thesis, recent studies on these topics will be reported.

1.6 Overview of the Thesis

This thesis presents the design, synthesis and DNA binding studies of aminobenzyl and guanidinium calix[4]arene dimers. The present work consists of three parts. The first part describes the synthesis of dimeric calixarenes in Chapter 2. In the second part (Chapter 3, 4 and 5) the bindings of these dimers with nucleic acids have been examined. Chapter 3 highlights the methodology and the basic theories and the most important experimental techniques that were used throughout the work. Chapter 4 addresses the results of DNA binding experiments, and the mechanism of DNA binding by dimeric calixarenes is elucidated. Then, the focus is shifted towards the proliferation study of living cells. Chapter 5 focuses on the conclusions of previous studies and discusses the work in the future. The last part of the thesis (Chapter 6) provides the experimental procedures, the spectra of NMR and MS, and the data of fluorescence titration experiments.

2. Synthesis

2.1 Synthesis of Monomeric Calixarenes

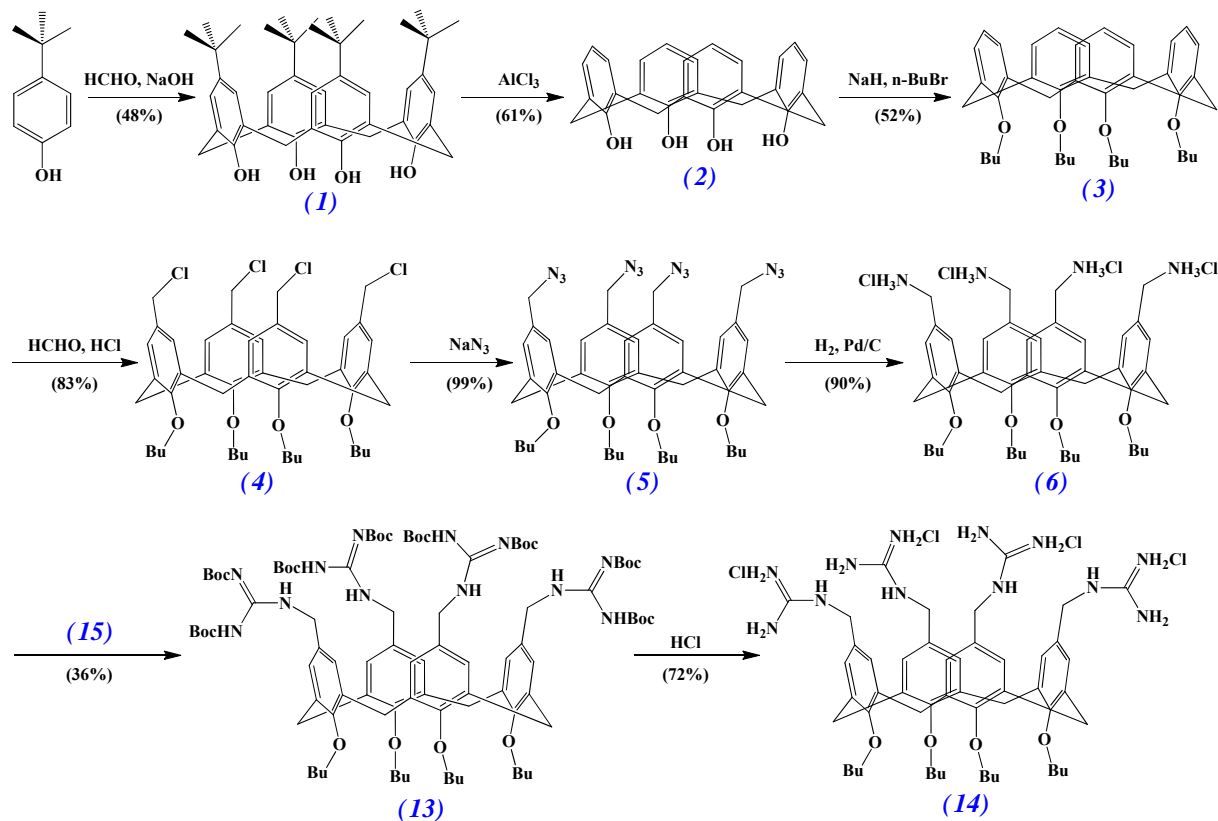


Figure 2.1 Synthesis of Monomer A (6) and Monomer B (14)

2.1.1 Synthesis of Calix[4]arene

Calixarenes are macrocyclic compounds, which are composed of phenolic units. The phenolic units are connected by methylene bridges to form a hydrophobic cavity. These molecules were generated from the base catalyzed reactions of *p*-alkylphenols with formaldehyde. It is necessary to use *p*-substituted phenols to avoid the formation of cross-linked networks when both *ortho* and *para* positions of phenols are available for condensation [132].

Because the base catalyzed synthesis is the most convenient and reliable, the mechanism of these reactions was studied (Figure 2.2) [133]. The first step is a nucleophilic addition reaction of the *ortho*-position of a phenoxide ion to the carbonyl group of formaldehyde and forms a

hydroxymethyl phenol. The second step is the formation of a quinomethidine intermediate. Then, the quinomethidine intermediate reacts with another phenolate anion to produce a diphenylmethane derivative and even more complicated liner oligomers (precursors).

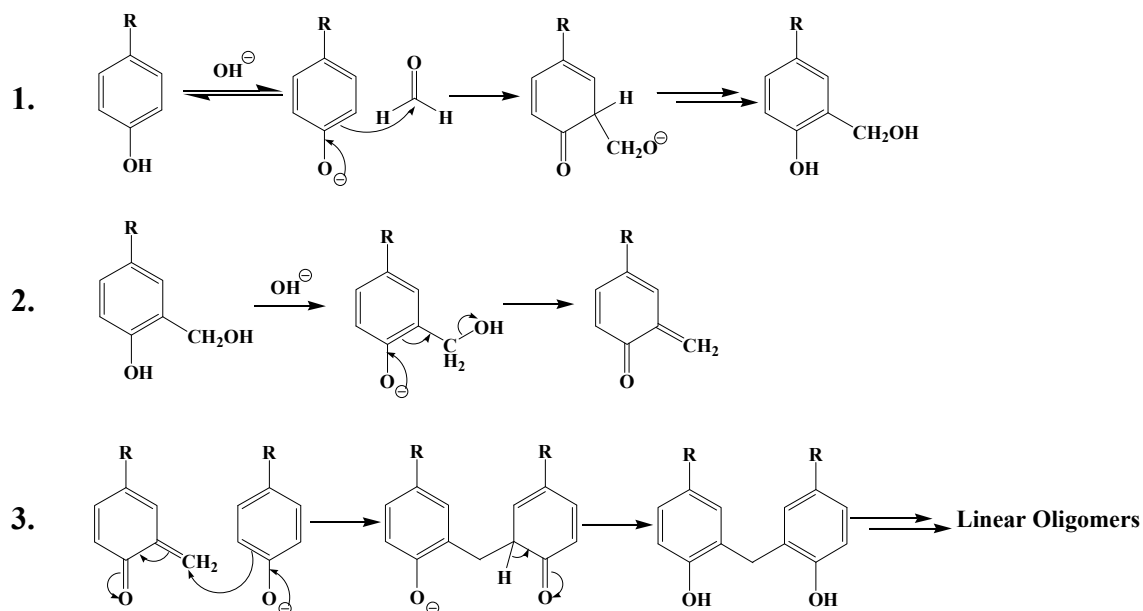


Figure 2.2 The mechanism of the base-induced condensation reaction

There are more than 36 noncyclic components in precursors ^[132]. How the cyclic oligomers are produced from the mixture and why the different liner oligomers can form a specific cyclic oligomer remain to be clarified. But the experimental results are quite definite:

(1). A mixture of *p-tert*-butylphenol (1 eq.), 37 % formaldehyde (1.25 eq.) and NaOH (0.045 eq.) is heated for 2 hours at 100-120 °C to produce the “precursor”. The “precursor” is then refluxed in diphenyl ether for 3-4 hours, cooled and added ethyl acetate to get tetra(*tert*-butyl)-tetrahydroxy-calix[4]arene (**I**) in 61 % yield ^[134].

(2). If this “precursor” is refluxed in xylene, the product collected is the octa(*tert*-butyl)-octahydroxy-calix[8]arene in 62-65 % yield ^[135].

(3). If the base is KOH (0.34 eq.), then reflux in xylene, the product is the hexa(*tert*-butyl)-hexahydroxy-calix[6]arene in 83-88 % yield ^[136].

(4). The base (or the cation) has a significant effect on the final product. For example, NaOH tends to give high yields of the cyclic octamer, while LiOH gives low yields; the larger radii alkali metal cation (K^+ , Rb^+ and Cs^+) produces the cyclic hexamer in high yields^[133,137].

Based on the observation and investigations of Gutsche and coworkers, it is suggested that the octamer is the kinetic controlled product, and the tetramer is the thermodynamic controlled product^[133,137,138]. It has been proven that after heating octa(*tert*-butyl)-octahydroxycalix[8]arene in diphenyl ether, the product was identified as tetra(*tert*-butyl)-tetrahydroxycalix[4]arene. It is thought that the cyclic octamer is generated in the beginning, and then undergoes some kind of transformation to yield the cyclic tetramer. There are two explanations. (1). The fragmentation recombination pathway^[139]: the cyclic octamer is completely broken into single aryl units and subsequent recombination produces two cyclic tetramers. (2). The molecular mitosis mechanism: the cyclic octamer divides into two cyclic tetramers. More mechanisms remain to be studied.

In order to introduce a functional group on the upper rim, it is necessary to remove the alkyl group (*tert*-butyl) by a retro Friedel-Craft alkylation reaction in the presence of a Lewis acid (for example, $AlCl_3$) and an acceptor solvent such as phenol^[140]. Thus, calix[4]arene (**2**) was synthesized in 61% yield.

2.1.2 Lower Rim Etherifications of Calix[4]arene

Calix[4]arenes contain free intraannular OH groups, and have four conformational isomers: cone, partial cone, 1,2-altemate, and 1,3-altemate because of the rotation of bonds of the Ar-CH₂-Ar groups. All the aryl units of calix[4]arenes can rotate independently in a 'lower rim through the annulus' mode, but not in an 'upper rim through the annulus' mode. The latter mode can be found in the rotation of aryl units in the larger cyclic oligomers. The rotation effect is considerably more pronounced in polar solvents^[133], such as acetone, acetonitrile and pyridine, than in non-polar solvents, such as chloroform and benzene. It may be explained in terms of the inversion barrier in which polar solvents are able to disrupt the intramolecular

hydrogen bonds that contribute in maintaining the calixarene in the cone conformation.

Because of the 'lower rim through the annulus' pathway, it is possible for the calix[4]arene to be locked in one of the four conformations by etherifications of the hydroxy groups. In fact, if the groups linked to the hydroxy groups are bulkier than an ethyl group, it is large enough to fix the conformations of calix[4]arenes^[141,142]. The result of the orientation depends on the bases^[143], counterions, solvents and reaction temperatures, and also depends on the *p*-substituents of the aromatic rings. For example, the treatment of calix[4]arenes with excess NaH in DMF (or DMF/THF) at room temperature followed by excess halogenides leads to the core conformation. 25, 26, 27, 28-tetra-*n*-butyl-calix[4]arene (**3**) was synthesised in 52% yield in this way. If Cs₂CO₃ is used at 80 °C, the main product of the etherification is 1,3-alternate conformers^[143,144].

2.1.3 Upper Rim Functionalizations

The upper rim functionalization originates from electrophilic substitution reactions of the *p*-H of the calixarenes. It has been proved that the calix[4]arene ethers have better behaviours of electrophilic substitutions than the *p*-H tetrahydroxy calix[4]arene. A set of upper rim modifications have been made, and can be divided into three classes:

(1). Anionic modifications: Sulfonic acid^[145], nitro^[146], phosphonic acid^[147], carboxyl moieties^[148], halogens derivatives^[149] and so on were introduced to the *p*-position of the calixarenes.

(2). Cationic modifications: It mainly focuses on the calixarenes containing tetraalkyl ammonium groups and primary amines^[150,151].

(3). Neutral modifications: In order to avoid unspecific bindings and prevent repulsions of ionic groups, calixarenes with sulfonamides^[152], hydroxyl groups containing amides^[153], sugars^[154], polyoxyethylenes^[155], polyalcohol residues^[156], etc. have been synthesized.

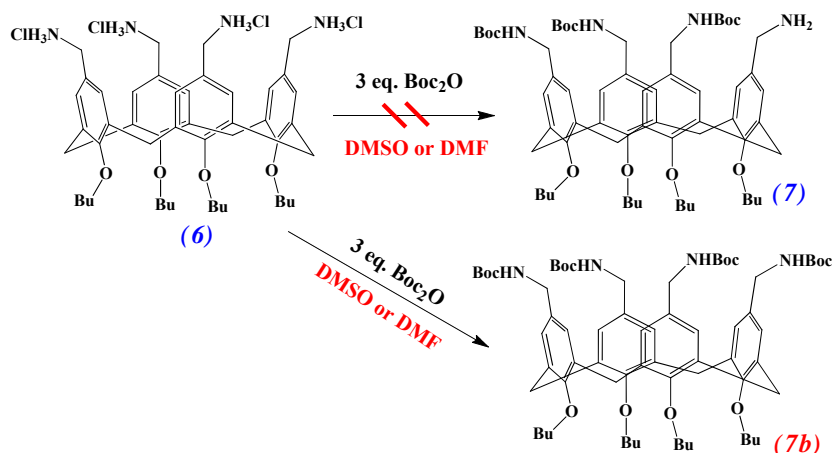
Our work was to synthesize calix[4]arenes with amino (aniline) or methyl amino (benzyl

amine) groups on the *p*-positions. The synthesis of aniline ^[120] started with the introduction of nitro groups to the *p*-positions. It was achieved by using nitric acid in acetic acid. The nitro groups were then reduced to amino groups by a Pd or Ni-catalyzed hydrogenation reaction. While the main synthetic route to 25,26,27,28-tetrabutoxy-5,11,17,23-tetrakis (aminomethyl) calix[4]arene tetrahydrochloride (**6**) started from 25,26,27,28-tetra-*n*-butyl-calix[4]arene (**3**) which was chloromethylated with formaldehyde and HCl to give 25,26,27,28-tetrabutoxy-5,11,17,23-tetrakis(chloromethyl) calix[4]arene (**4**) in 82% yield ^[149]. The reaction of (**4**) with sodium azide in DMF at 80 °C followed by the reduction reaction with hydrogen over Pd/C gave the aminobenzyl calix[4]arene (**6**) (Monomer A) ^[157]. In order to add guanidinium subunits to the benzylic tetramine, *N, N'*-bis-Boc-2-methyl-2-thiopseudourea (**15**) was synthesized ^[158] by stirring the solution of 2-methyl-2-thiopseudourea sulfate and di-*t*-butyldicarbonate at room temperature for 7 days. (**6**) was treated with (**15**) under the assistance of silver nitrate and triethylamine to provide 5,11,17,23-tetrakis{[2,3-bis(*tert*-butoxycarbonyl)guanidino]methyl}-25,26,27,28-tetrabutoxy calix[4]arene (**13**) as a white solid (Yield: 36%). 1M HCl was used to deprotect Boc groups of (**13**) to afford tetraguanidine monomer 25,26,27,28-tetrabutoxy-5,11,17,23-tetrakis[(guanidinium)methyl] calix[4]arene Tetrachloride (**14**) (Monomer B) in 72% yield ^[159,160]. Both monomers are stable at room temperature at least for two days. Both monomers display good solubility in aqueous solutions, Monomer A > 1 mM, Monomer B > 0.5 mM.

2.2 Synthesis of Dimeric Calixarenes

In my opinion, the most important step to the synthesis of aminobenzyl and guanidinium calix[4]arene dimers is the trifunctionalizations of the aminobenzyl calix[4]arene (**6**), i.e. the synthesis of (**7**) and (**10**). For the anilino-calix[4]arene series, tetraaniline was treated with exactly three equivalents of di-*tert*-butyl dicarbonate (Boc₂O) in dichloromethane, and from the mixture of 4-fold, 3-fold and 2-fold Boc-protected anilino-calix[4]arene. The desired compound was isolated by chromatographic separation in 65% yield ^[120,160]. Inspired by previous experiments, I carried out similar experiments. Because Monomer A (**6**) displays

poor solubility in dichloromethane, THF, acetone and acetonitrile, dipolar aprotic solvents, such as DMF and DMSO were used. At the same time, triethylamine was used to remove HCl of Monomer A. A series of experiments were performed at different temperatures (-60-20°C).



Unfortunately, the synthesis of (7) failed. Probably because the aminobenzyl group is too active (compared with the aniline group), the addition of 3 eq. Boc_2O always formed the 4-fold-Boc protected aminobenzyl calix[4]arene (7b),

and a few starting material (6) did not react with Boc_2O at all and remained in the solution.

In order to decrease the activity of the reactants, Boc_2O (an anhydride) was replaced by *tert*-butyl (2,5-dioxopyrrolidin-1-yl) carbonate (7c) (an active ester) (in Figure 2.3).

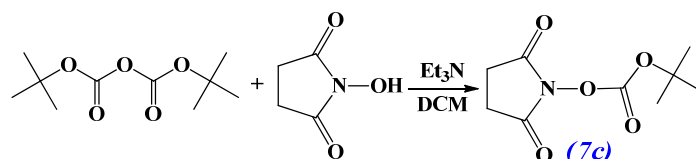


Figure 2.3 Synthesis of *tert*-butyl (2,5-dioxopyrrolidin-1-yl) carbonate (7c)

There are several characteristics for the NHS ester (7c) ^[161]: (1). The half life of (7c) in MeOH is over 20 hours, and in water the half life is over 5 hours. (2). Primary amines are the principal targets for NHS esters. (3). Phosphate, bicarbonate/carbonate, Hepes and borate buffers were often used for crosslinking. (4). NHS esters react rapidly with amino groups in the pH range 6-9. But the rate of hydrolysis of the NHS ester increases with increasing pH.

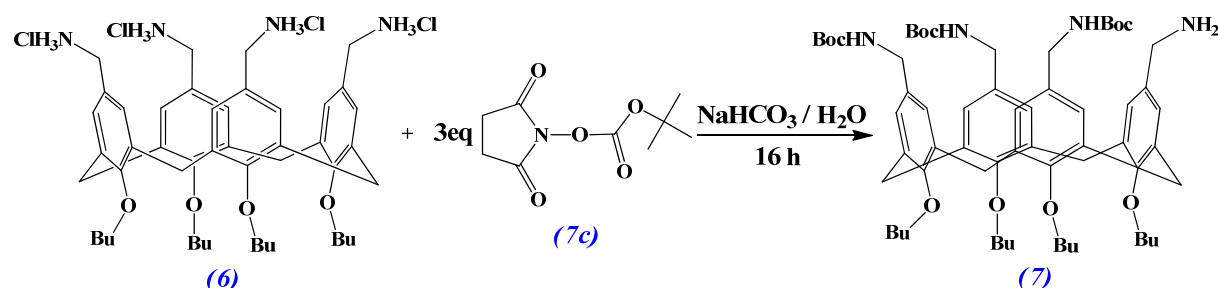


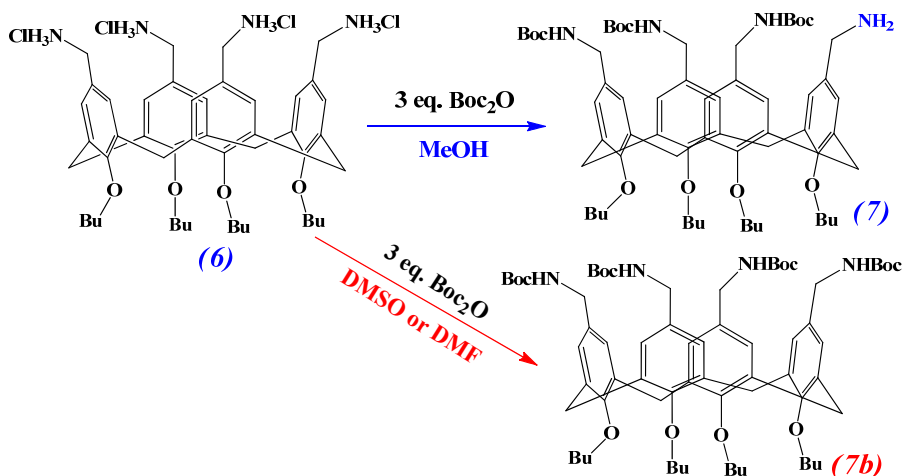
Figure 2.4 Synthesis of (7)

Based on the experimental facts mentioned above, a new synthetic scheme was designed for

the synthesis of (7) (in Figure 2.4): (6) (1 eq.) and (7c) (3 eq.) were dissolved in MeOH and were stirred at room temperature. The saturated NaHCO₃ (20 eq.) in aqueous solution was added dropwise to the mixture. The solution was stirred for 16 hour at room temperature.

After chromatographic separation, 5-(Aminomethyl)-25,26,27,28-tetrabutoxy-11,17,23-tris {[(*tert*butoxycarbonyl) amino]methyl}calix[4]arene (7) was synthesized in 25% yield. The base NaHCO₃ is very important. On the one hand, NaHCO₃ reacts with HCl of (6) to form free primary amines. On the other hand, NaHCO₃ can adjust solution to an alkaline pH level in order to increase the rate of the crosslinking. Furthermore, NaHCO₃ is weak alkali (pH: 7.5-8.5 in H₂O), so the rate of hydrolysis of the NHS ester decreased as low as possible.

By chance, a surprising phenomenon was observed: Monomer A (6) (1.0 g, 1.10 mmol) was dissolved in a mixture of anhydrous MeOH (10 mL) and Et₃N (1 mL). Di-*tert*-butylcarbonate (0.72 g, 3.30 mmol) was added to the solution. The mixture was stirred for 18 h at r.t. Subsequently, MeOH was removed in vacuo, and the residue was purified by flash column chromatography (SiO₂, DCM/MeOH, 100:1). (7) was synthesized in 21% yield.

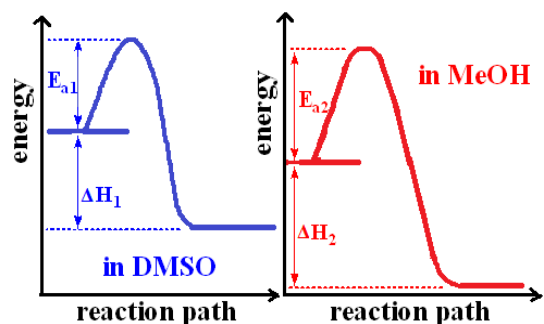


Apparently, the only difference between this procedure and previous one is the solvent: MeOH or DMF/DMSO. Because MeOH can react with Boc₂O under Et₃N catalysis to form an ester, therefore,

at the beginning DMF and DMSO were used. But the fact is that the reaction preferred to form amides instead of esters when MeOH was used. This can be explained by the fact that the nucleophilicity of amines is better than alcohols.

Another phenomenon should be paid more attention: in MeOH, (6) can form 4-fold, 3-fold, 2-fold and 1-fold Boc-protected aminobenzyl calix[4]arenes; while in DMF and DMSO, only the 4-fold Boc-protected aminobenzyl calix[4]arene (7b) was observed. It may be explained in

terms of solvation ^[162]. MeOH belongs to protic solvents. They possess a proton-donating function. They have both a large dipole moment and a capacity for hydrogen bonding.



$$E_{a2} > E_{a1}, \quad \Delta H_2 > \Delta H_1$$

Thus, MeOH can stabilize the substrate (free amines) via hydrogen bonds and increase activation energy. At the same time, MeOH can also stabilize the free amine of the 3-fold Boc-protected aminobenzyl calix[4]arene (**7**). In short, the protic solvent decreases the rate of the reaction and stabilizes the desired product (**7**). DMF and DMSO are dipolar aprotic solvents, which possess a large dipole moment and donor properties, but they have no acidic protons. Therefore, they can not stabilize the substrate and the product via hydrogen bonds, which leads to the 4-fold Boc-protected aminobenzyl calix[4]arene (**7b**).

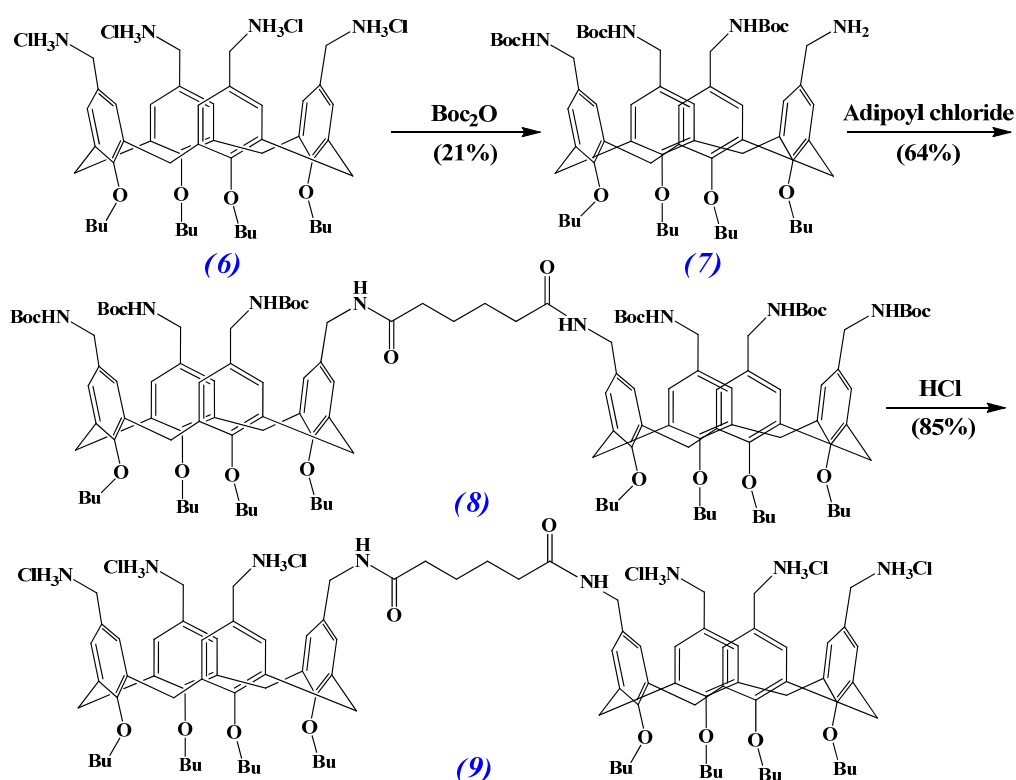


Figure 2.5 Synthesis of Dimer A (**9**)

The last two steps of the dimeric calixarene synthesis were the double peptide bond formation between the triBoc-protected calixarene's free benzylamino group and the adipic acid dichloride (Yield: 64%), and the final removal of all Boc groups by 1M HCl. The final product (**9**) was washed with acetone and was used without further purification (Yield: 85%).

In order to synthesize the guanidinium calix[4]arene dimer (Dimer B) (**12**), the six guanidine function groups were tried to be introduced at the dimer stage at the beginning. Unfortunately, although the NMR spectra seem to be right, MS spectra indicated that the six guanidine function groups were not completely introduced. It was also useless to increase reaction temperatures (from 20°C to 120°C). Thus, Monomer A (**6**) had to be trisguanidinylated to yield the desired protected trisguanidine monomer (**10**) (in Figure 2.6). The yield of this step is as low as 12%. Adipic acid dichloride was then directly used to acylate the free amine of (**10**) under Et₃N catalysis. The last reaction was the HCl treatment (1M) at ambient temperature. This resulted in complete cleavages of all the Boc groups. The final product (**12**) was also washed with acetone and was used without further purification (Yield: 85%).

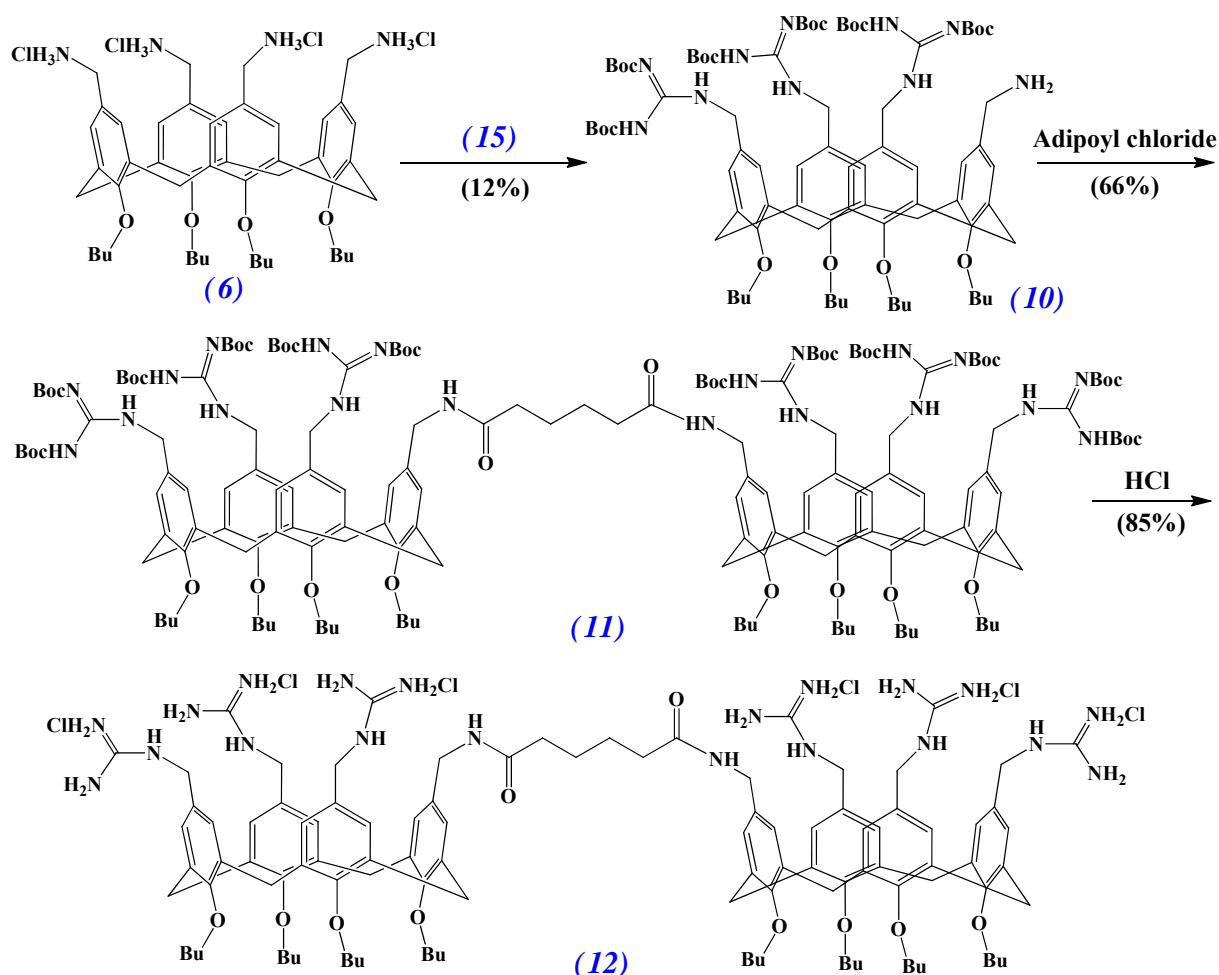


Figure 2.6 Synthesis of Dimer B (**12**)

2.3 Synthesis of *N*-Protected *N*-Methylimidazole Amino Acids

Because of the use of recombinant DNA techniques and the advent of automated solid-phase peptide synthesis, today, peptide and protein synthesis becomes more and more efficient and convenient.

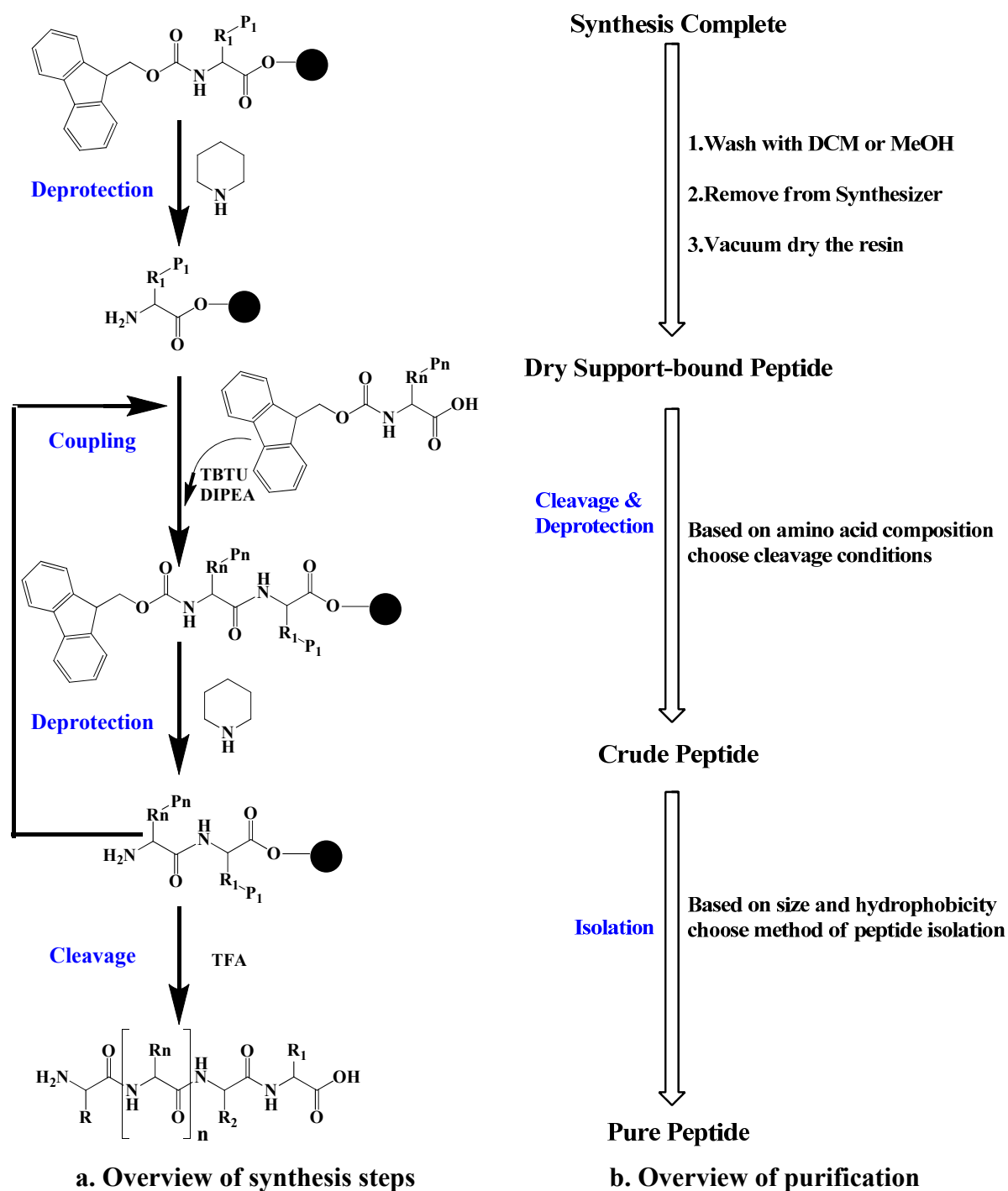


Figure 2.7 The solid-phase peptide synthesis

In the solid-phase peptide synthesis ^[163], the C terminal acid is attached to an insoluble polymeric support. A peptide is assembled by reacting the deblocked amino (N) - terminus, resulting in the formation of an amide bond. The process of deblocking the N-terminus, activating the carboxylic acid, and performing the coupling reaction with the next amino acid is repeated until the peptide of interest is complete. (Figure 2.7a) The solid phase allows convenient removal of soluble by-products and excess reagents without loss of peptide. High yields in each step (over 99%) enable sequences up to 100 amino acids to be synthesised. The peptide is then cleaved from the support. After deprotection, the crude peptide is purified by RP-HPLC or gel electrophoresis (Figure 2.7b).

Protecting groups are used for the amino groups of all amino acids. In general, they can be divided into four classes: alkoxycarbonyl-type (Urethane-Type) protecting groups, carboxamide-type protecting groups, sulfonamide and sulfenamide-type protecting groups, and alkyl-type protecting groups. Urethane-type amino-protecting groups were widely used, for example, the benzyloxycarbonyl group (Cbz or "Z"), the *tert*-butoxycarbonyl group (Boc), and the 9-fluorenylmethoxycarbonyl group (Fmoc) and so on. The Boc protecting group was used in my work (Figure 2.8).

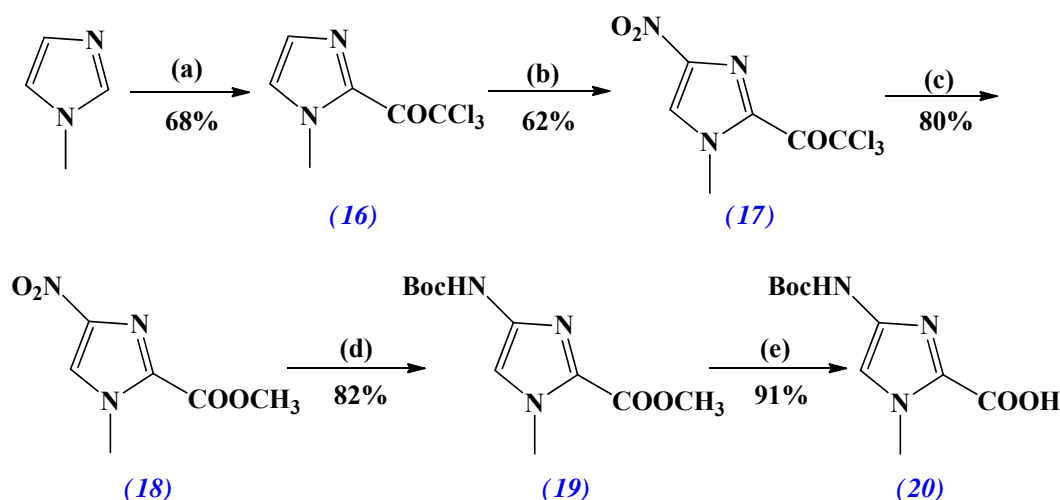


Figure 2.8 Synthesis of the *N*-protected *N*-methylimidazole Amino Acid building block

Reagents and conditions: (a) CCl_3COCl , CH_2Cl_2 , 12 h; (b) fuming HNO_3 , H_2SO_4 , Ac_2O , 0 °C to r.t., 24 h; (c) MeONa , MeOH , 3 h; (d) Boc_2O , 10% Pd/C , H_2 , MeOH , 28 h; (e) *t*-BuOK, H_2O , THF, r.t.

The synthesis of the *N*-methylimidazole amino acid building block (**20**)^[164,165,166] began with the synthesis of 2-trichloroacetyl-1-methylimidazole (**16**) as previously reported^[167]. The nitro derivative (**17**) was obtained by using HNO₃ and H₂SO₄. The nitro ester (**18**) was then synthesized through base hydrolysis of (**17**). One-pot catalytic reduction and Boc-protection gave the desired compound (**19**) in 82% yield for the two steps. Final hydrolysis by using *t*-BuOK in the mixture of THF and water produced the *N*-methylimidazole amino acid building block (**20**) in 91% yield. Compared with traditional scheme, where the nitration of ethyl 1-methylimidazole-2-carboxylate gave low yield (12%) in my work, this scheme could produce (**17**) in an improved yield (62%).

2.4 Synthesis of Spacers and Coupling Reactions

The formation of a peptide bond is a nucleophilic substitution reaction of an amino group (a nucleophile) and a carboxy group by forming a tetrahedral intermediate. In this process, carboxy components are first activated by the introduction of electron-accepting moieties to increase their electrophilicities. Several function groups which exert either an inductive (-I) effect or a mesomeric (-M) effect (or both) to decrease the electron density at the C=O group are widely used (see below). And then, the amino component attacks with its nitrogen lone pairs to the carboxy group to give a tetrahedral intermediate. Finally, the leaving group dissociates from the intermediate, and the peptide bond formation is then completed. In fact, the leaving group capacity (nucleofugicity) is another important factor which can influence the reaction rate and yield^[168].

There are a lot of reagents to activate carboxy groups, for example, acyl azides, anhydrides, carbodiimides, active esters, acyl halides, phosphonium reagents and uranium reagents^[168]. Among of these, carbodiimides (for example, DCC, DIC, EDCI, etc.), active esters (for example, NHS esters, OBt, etc.), phosphonium reagents (for example, BOP, PyBOP, PyBrOP, etc.) and uranium reagents (for example, HBTU, HATU, TBTU, etc.) are widely used in the solid-phase peptide synthesis. In fact, it was very important to choose proper coupling reagents to increase reaction rates and yields, and to reduce the formation of by-products.

According to previous reports ^[165,166,169], *N*-protected *N*-methylpyrrole amino acid building blocks were activated with DCC/DMAP, EDCI/DMAP or HBTU/DIEA. Coupling times were from 1 h to 60 h. The yield is as high as 99% for solid-phase peptide synthesis and the yield is higher than 50% for the liquid-phase synthesis. Unfortunately, if carbodiimides were used in my work for the coupling of *N*-protected *N*-methylimidazole amino acid building blocks (**20**), the yield was lower than 20%. In my opinion, there are two reasons: (1). The nucleophilicity of the amine of the *N*-methylimidazole amino acid building block (**20**) is weaker than the amine of the *N*-methylpyrrole amino acid building block. Therefore, the *N*-acylurea by-product formed (in Figure 2.8-2a). (2). The amine of the *N*-methylimidazole amino acid building block (**20**) can also react with carbodiimides and form a guanylidine moiety (in Figure 2.8-2b). The guanylidine moiety has been identified by MS.

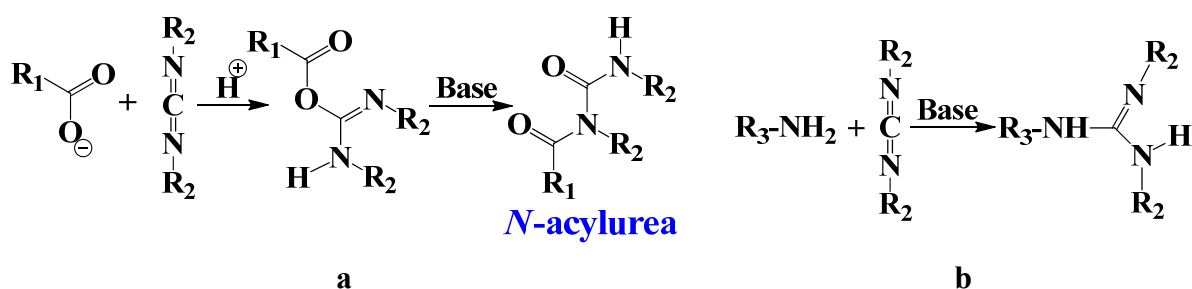


Figure 2.8-2 By-products of carbodiimide-mediated peptide couplings

Thus, uranium reagents ^[170,171,172] (for example, HBTU, HATU) were used in my work. These reagents were added in equal molar amounts to the carboxylic acid component of the coupling reaction. The activation time should be over 5 minutes, because HBTU and HATU can also react with the unprotected N-terminus of the peptide to form a guanylidine moiety that blocks further elongation of the peptide.

Figure 2.9 described the synthesis of the triimidazole spacer (**27**). The monoimidazole intermediate (**21**) was obtained from the *N*-protected *N*-methylimidazole amino acid building block (**20**) by coupling with the β-Alanine methyl ester hydrochloride. For the elongation of the spacer, it consists of two cycles of Boc deprotection (with TFA), followed by HBTU/DIEA coupling with (**20**). (**23**) was then equipped with the succinic acid monobenzyl ester (**24**). Final removes of the Cbz ester (by H₂/Pd) and the methyl ester (by base hydrolysis) gave the triimidazole spacer (**27**) with the end of α,ω-dicarboxylic acids.

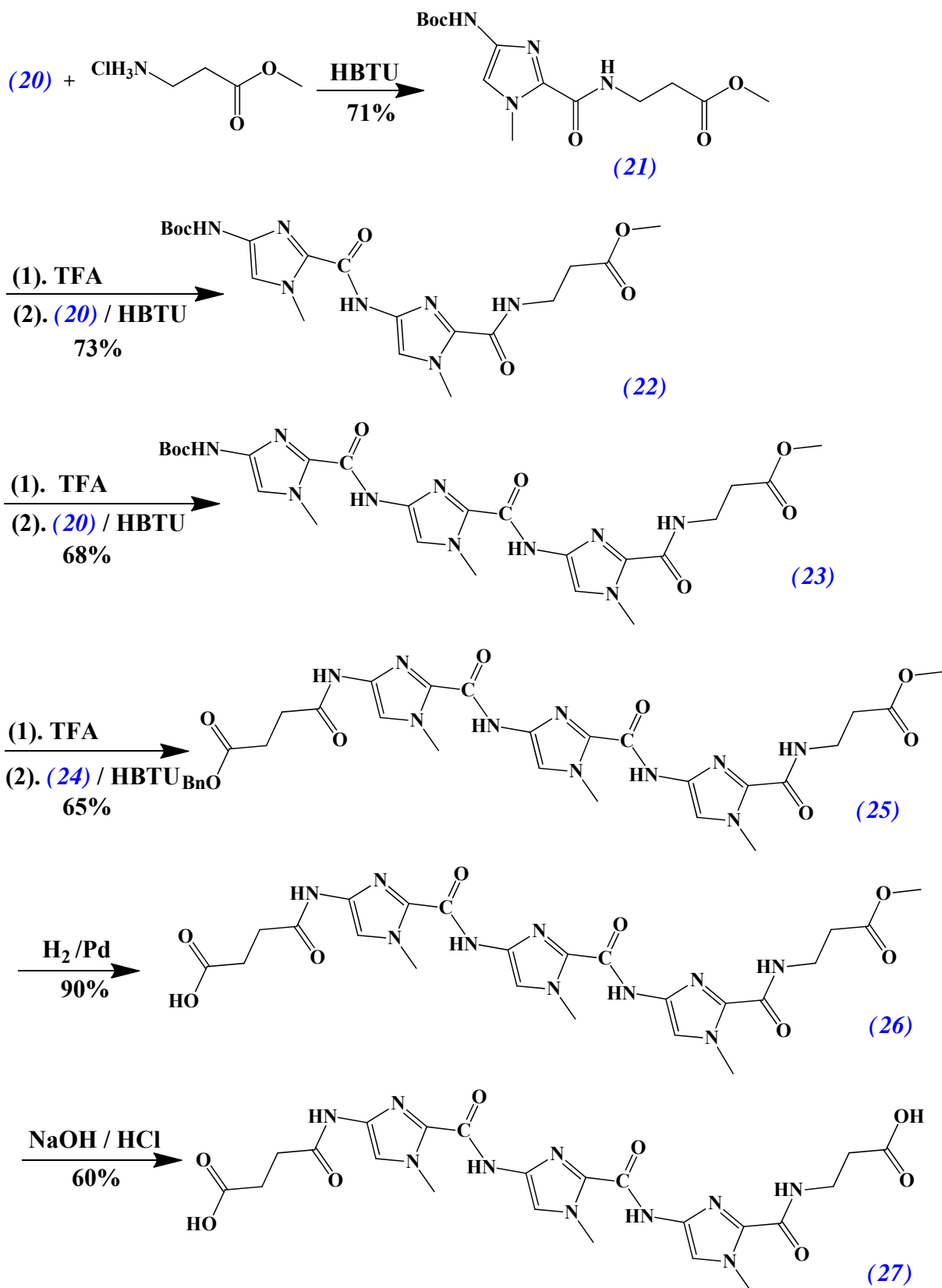


Figure 2.9 Synthesis of the triimidazole spacer (27)

Unfortunately, an intramolecular reaction was encountered during the attempted coupling of the carboxylic acid of linker (26) with the monoamine of (7) (Figure 2.10).

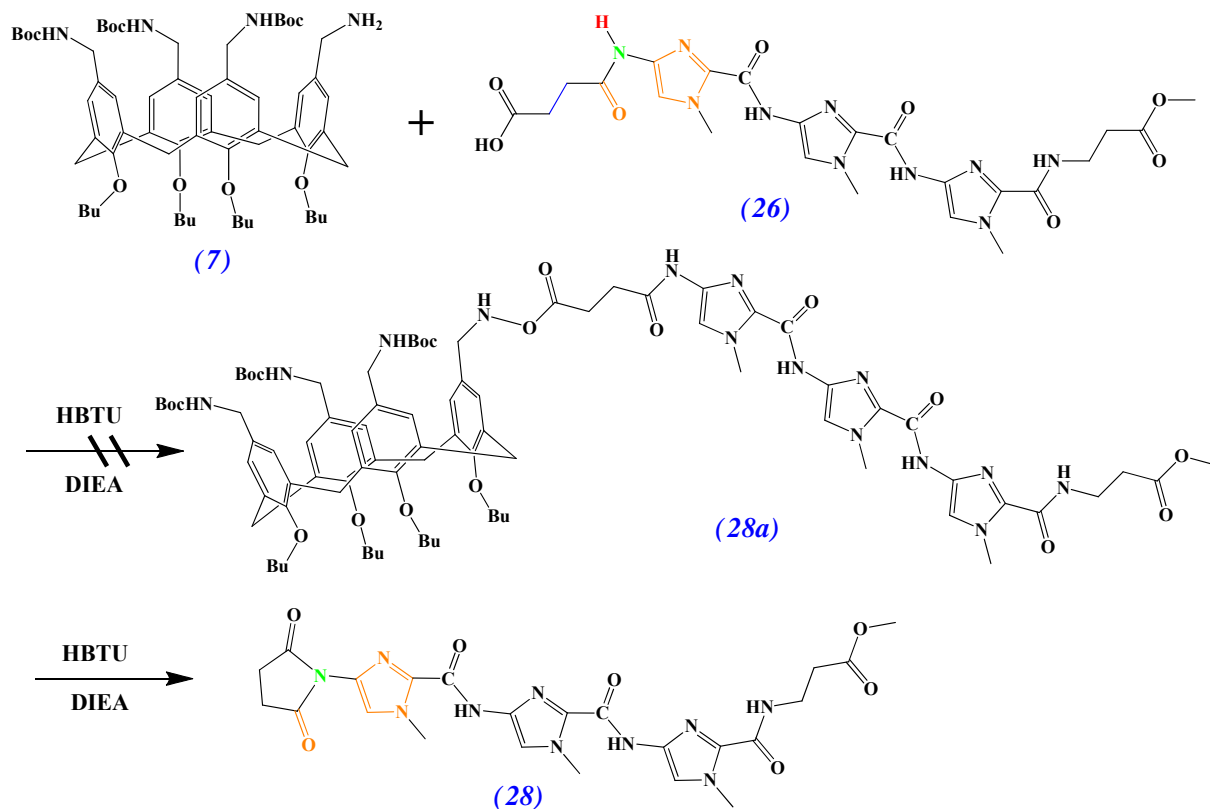


Figure 2.10 The intramolecular reaction of the spacer (27)

This intramolecular reaction originates from the proton of the amide (the color of this proton is red in figure 2.10 and figure 2.11). The nitrogen connects to a carbonyl group and an imidazole ring, both of which belong to electron withdrawing groups. They can decrease the electron density of the nitrogen. The proton connected to the nitrogen is acidic. A proposed mechanism is shown in Figure 2.11. Nucleophilic attack of the carboxylate (26) results in an O-acyluronium species (26a) that is further transformed into the HOBt active ester (26b) in the presence of HOBt. With the help of the base (DIEA), the nucleophilic attack from the electrons of the nitrogen to the HOBt active ester gave the pyrrolidine-2,5-dione analogue (28). (28) has been identified by NMR and MS.

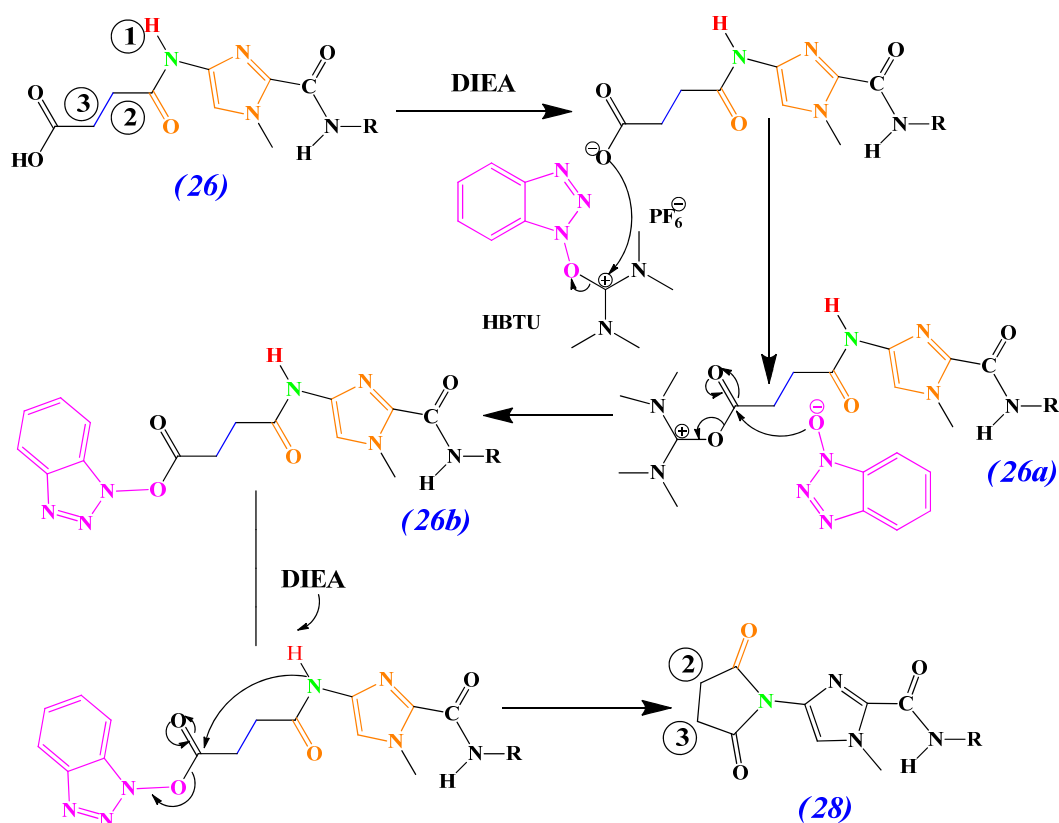


Figure 2.11 A proposed mechanism of the intramolecular reaction

	1H-NMR (300 MHz, DMSO <i>-d</i> ₆)			MS (ESI-TOF, pos. MeOH)			
	H-1	H-2	H-3	[M+Na] ⁺		[M+H] ⁺	
				calculation	found	calculation	found
(26)	10.42 ppm	2.60 ppm	2.60 ppm	C ₂₃ H ₂₈ N ₁₀ NaO ₈		C ₂₃ H ₂₉ N ₁₀ O ₈	
				<i>m/z</i> 595.1984	595.2010	<i>m/z</i> 573.2164	573.2188
(28)	×	2.83 ppm	2.83 ppm	C ₂₃ H ₂₆ N ₁₀ NaO ₇		C ₂₃ H ₂₇ N ₁₀ O ₇	
				<i>m/z</i> 577.1878	577.1879	<i>m/z</i> 555.2059	555.2048

In order to prevent the cyclization, two strategies were carried out:

(1). Strategy one ^[160]: The β-Alanine methyl ester was not used any more. The terminal carboxylic acid of the *N*-methylimidazole amino acid building block will directly couple to the triBoc-protected calixarene (7). At the same time, the succinic acid linker was replaced by a malonic acid linker or an isophthalic acid linker (figure 2.12). Thus, another two new spacers (33) and (34) were synthesized.

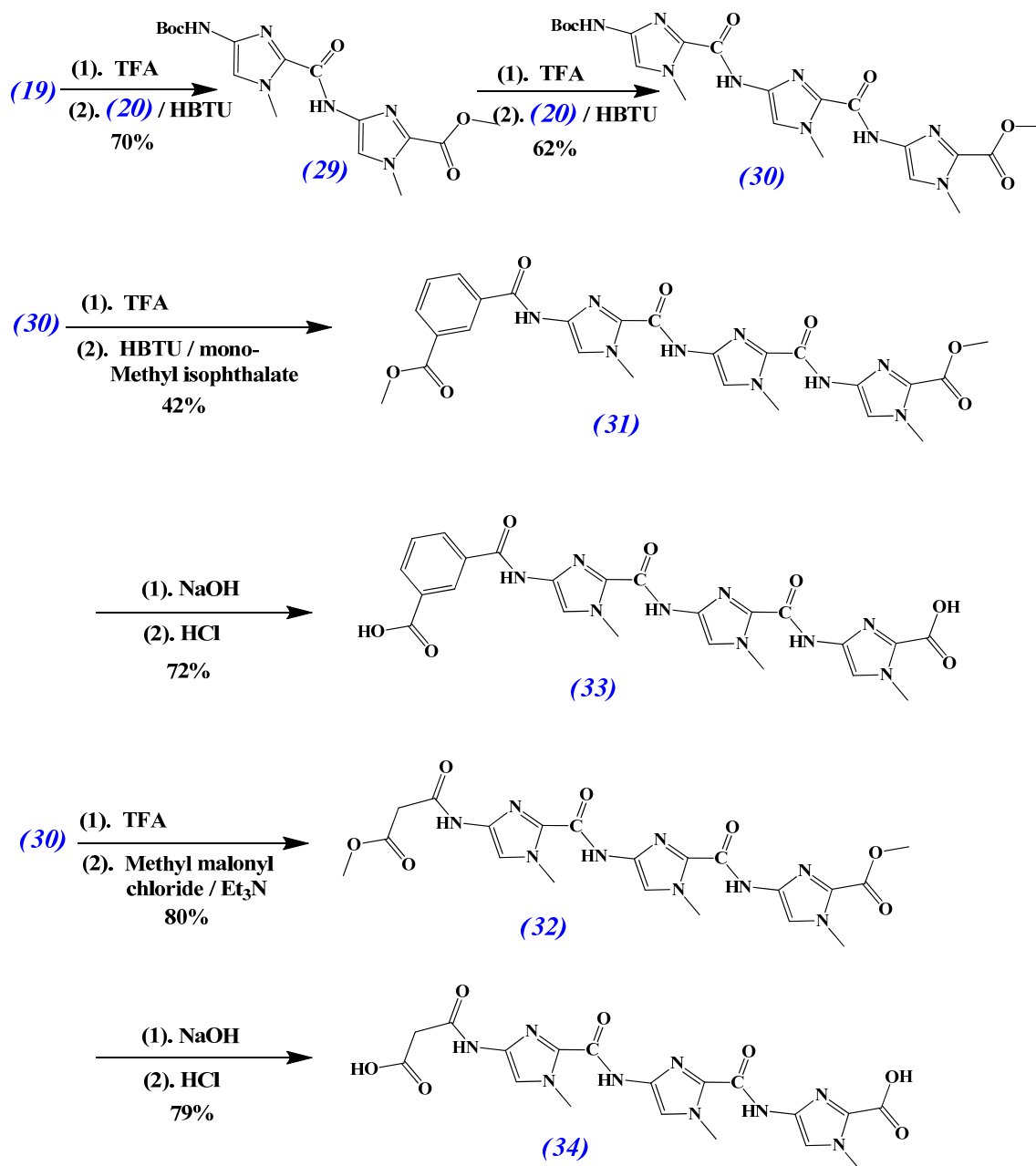


Figure 2.12 Synthesis of new triimidazole spacers (33) and (34)

The key step is the peptide bond formation between the free benzylamino group of the triBoc-protected calixarene (7) and the two terminal carboxylic acids of the new bridge (34). It was achieved by using the peptide coupling reagent HATU/DIEA (figure 2.13). There was no time for me to finish another coupling reaction of (7) and (33). The last reaction was the cleavage of all Boc groups with the treatment of TFA at ambient temperature. The final product (Dimer C, 40) was precipitated in chloroform to yield a white product which was used without further purification.

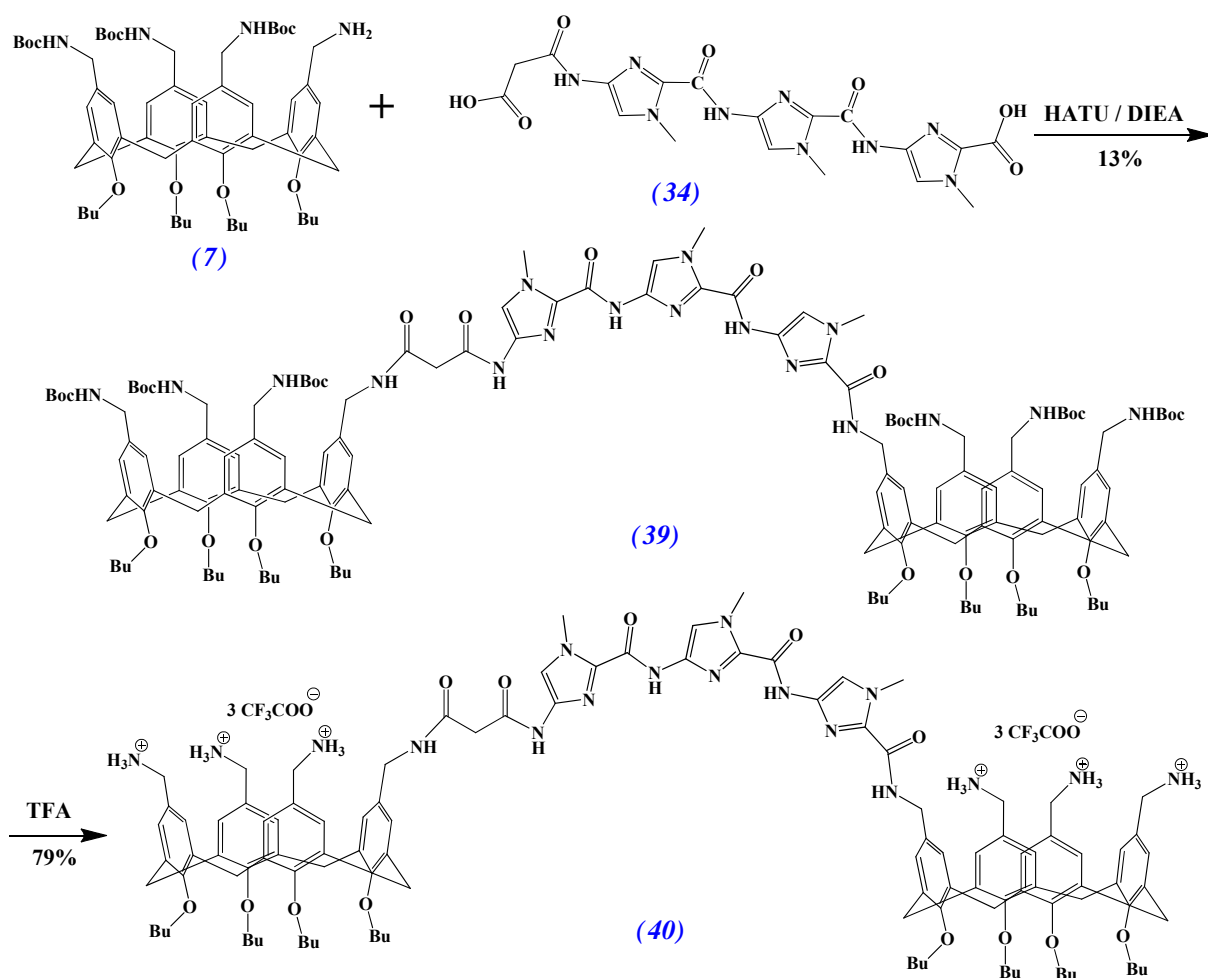


Figure 2.13 Synthesis of Dimer C (40)

Compared with Dimer A and Dimer B, Dimer C displays poor solubility in water. However, its complex with DNA exhibits good solubility in any aqueous buffer at physiological salt loads. Dimer C degrades in the presence of strong acid (for example, HCl), and should be stored in the freezer.

(2). Strategy two: β -Alanine methyl ester was replaced by ethylenediamine (Figure 2.14). After deprotection of the Boc group, the bridge C (36) was synthesized. It contains two terminal amines.

At the same time, the triBoc-protected calixarene (7) reacted with the succinic acid monobenzyl ester (24) and after deprotection of the Cbz group of (37), (38) provided the carboxyl-terminus (Figure 2.15). The new amide of (37) and (38) is a 'normal amide', because the nitrogen not only connects to a carbonyl group but also connects to a benzyl group which is an electron donating group. But, I did not have time to carry out the last two steps.

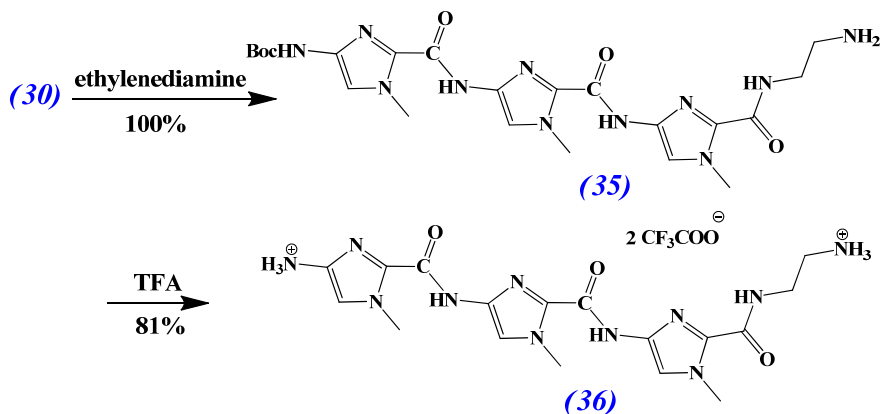


Figure 2.14 Synthesis of Bridge C (36)

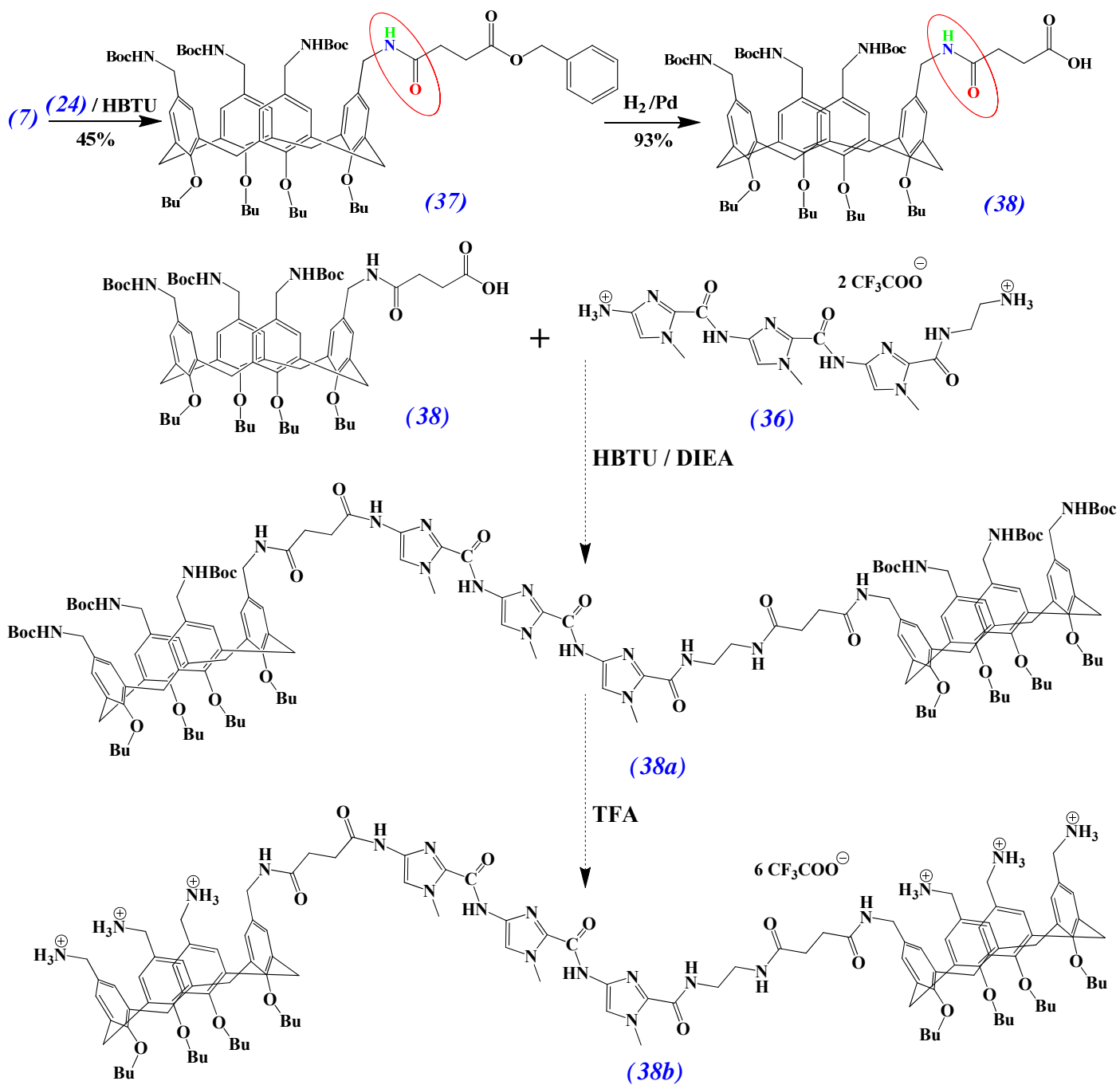


Figure 2.15 A proposed scheme of the synthesis of dimer 38b

(3). Strategy three: This strategy has been designed, but has not been carried out. All amide-NH groups of (25) will be protected to give (25a). In fact, the protection of amide-NH groups was received little attention at the beginning in this project. There are several protecting groups for the amide-NH^[173], for example, *N*-*t*-butylamide^[174] (*t*-Bu-NR₂CO-, which is cleaved with acid), *N*-pyrrolidinomethylamide^[175] (which is cleaved with the mixture of MeOH with 1% HCl or with MeOH:THF=1:9), *N*-*t*-butyldimethylsilylamide^[176] (TBDMS- NR₂CO-, which is cleaved with Me₃SiNa and THF) and so on. In all, these protecting groups should be introduced mildly, and should be stable in base condition (because NaOH will be used to remove Cbz and methyl groups of (25b)), and should be deprotected by acid, which is the same as the deprotection of Boc groups of (25c).

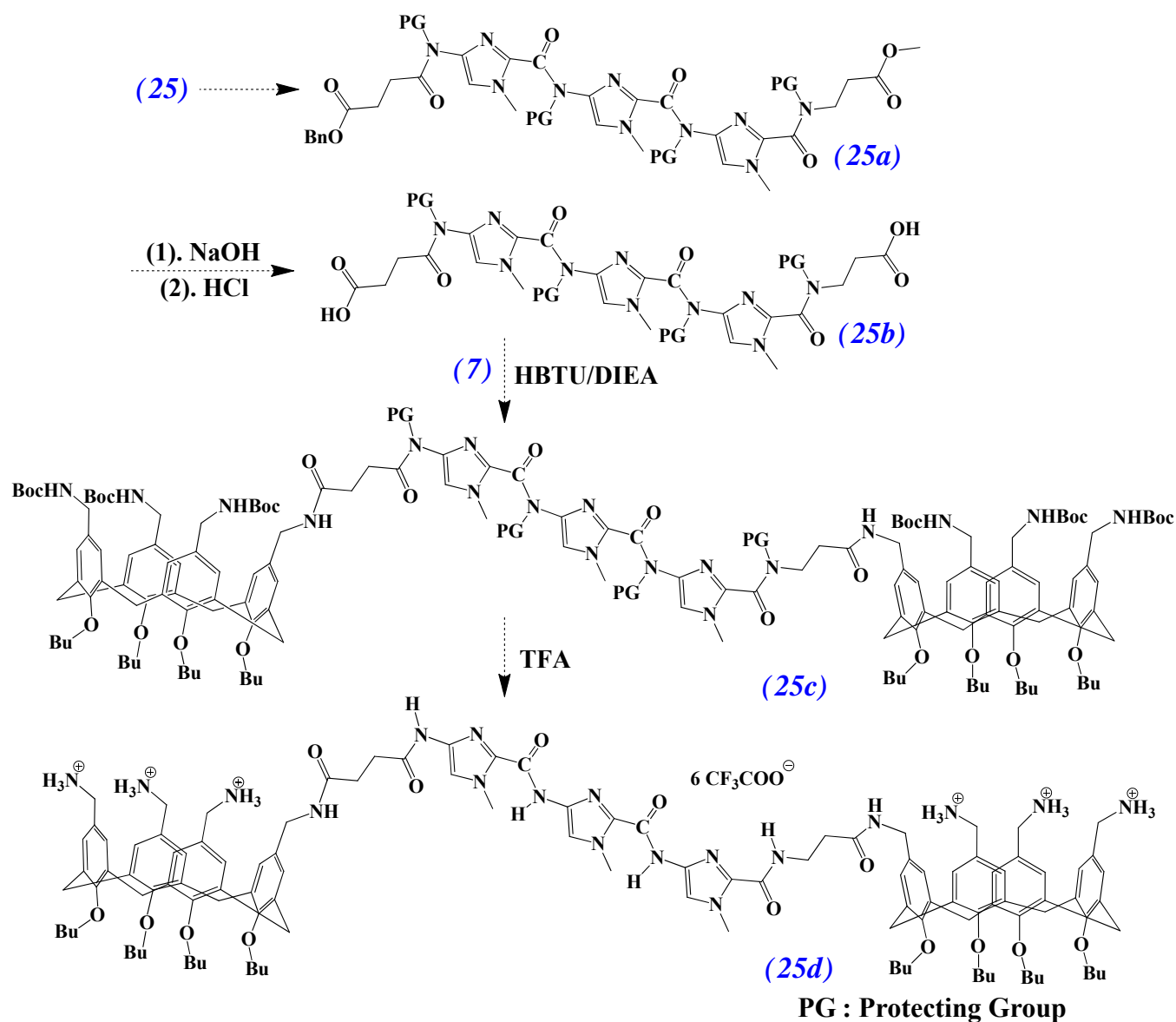


Figure 2.16 A proposed scheme of the synthesis of dimer 25d

3. Methodology

When investigating the properties of new DNA binding molecules, one initial goal is to establish their modes of binding to DNA. Until now, several methods have been used for an assessment of DNA-binding modes ^[177,178,179,180,181]. Among of these, there are two absolute methods: X-ray diffraction of crystals and NMR spectroscopy. Unfortunately, for my Ph.D. work, crystallization itself was a problem. Furthermore, the conformations of DNA or the ligand-DNA complex in aqueous solutions and crystals are different. NMR spectroscopy needs a large amount of material, high concentrations, long accumulation time, a single discrete structure, and a short DNA molecule ^[182,183,184]. However, in my work, the concentration of the DNA-dimer complex was too low (< 0.05 mM) in any aqueous buffer solution, the dimer aggregated itself at room temperature, and short DNA molecules have dangling ends that limit the stability of hybridization. In the absence of such high resolution data, the mode of binding must be inferred from the results of binding assays. Thus, a number of other methods were deployed to investigate their mode of binding to DNA, for example, ethidium bromide displacement assays, circular dichroism measurements, DAPI displacement assays, fluorescence titrations, isothermal titration calorimetry (ITC), the assessment of thermal denaturation of DNA, triple helix-forming oligonucleotide displacement assays and so on.

3.1 Ethidium Bromide Displacement Assay

Ethidium bromide (abbreviated as ‘EtBr’) is an intercalating agent which contains an extended electron deficient planar aromatic ring system. It resembles a DNA base pair. Due to its unique structure, it can nondestructively intercalate into DNA double strands and become the sandwiching between two adjacent base pairs ^[185] (Figure 3.1).

Upon binding, it extends and unwinds the deoxyribose–phosphate backbone, and then is stabilized by π – π stacking interactions with the planar aromatic bases, and lies in a plane perpendicular to the helix axis. In addition, the binding process is nondestructive and fully reversible. The DNA duplex structure is not destroyed by the process of its removal ^[186].

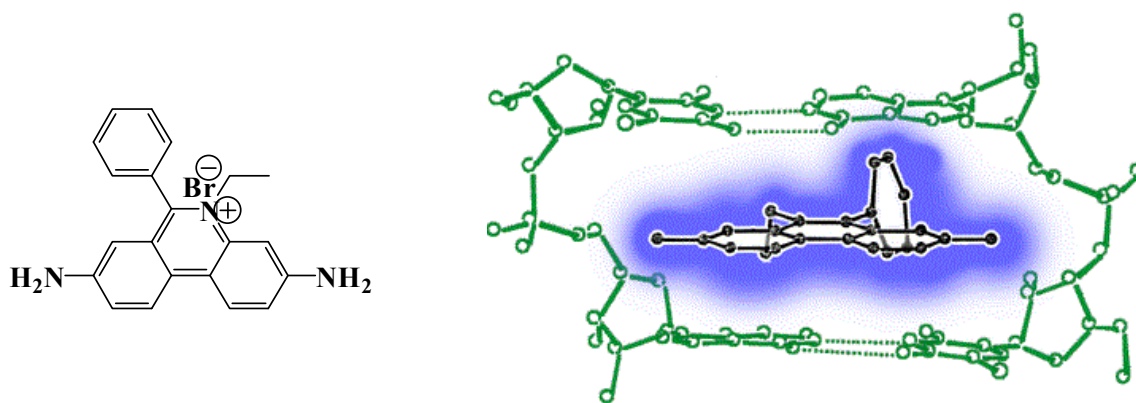


Figure 3.1 The structure of ethidium bromide and its intercalating into DNA strands ^[185]

When exposed to ultraviolet light, ethidium bromide will fluoresce with an orange color. In addition, it displays a striking fluorescence enhancement (almost 20-fold) after binding to DNA. It is generally agreed that the hydrophobic environment between the base pairs is responsible for the strong fluorescence enhancement. Proton transfer from the excited singlet state of EtBr to polar solvents (for example, water) is the process primarily responsible for the low fluorescence yield. If EtBr intercalates into two adjacent basepairs (a hydrophobic environment) of a DNA double helix, it must shed water molecules that were associated with it, and be far away from the solvent. Without water, which is a highly efficient fluorescent quencher, a large increase in fluorescence is observed ^[187]. The ethidium bromide – DNA complex can be detected by using excitation spectrum peaks at 300 nm or 520 nm and the emission peak at 600 nm.

Measurement of the ability of a drug to displace EtBr from DNA to solvent is established as a valid measurement of DNA binding ability for both intercalative and non-intercalative drugs. DNA molecules are treated with EtBr, yielding a fluorescence increase upon binding. Addition of a DNA binding compound results in decrease in fluorescence due to displacement of the bound intercalator, where the percent fluorescence decrease is directly related to the extent of binding. EtBr possesses relatively little sequence preference ^[188], although it displays a slight bias toward binding G:C-rich DNA tracts. The assay offers a qualitative comparison of binding affinities within a series of compounds with similar structures. It provides an indirect method of measuring the binding affinity (relative binding affinities) and stoichiometry of drugs. It also provides an indirect method of defining a compound's

sequence selectivity. Please Note: it can not provide a direct measure of the binding constant^[189]. On the one hand, the binding constant of EtBr to DNA is dependent on the molecular flexibility. DNA condensation might be expected to lower the affinity of EtBr for DNA. On the other hand, some molecules replace EtBr to solvent in the manner of a noncompetitive mode (in other word, binding to somewhere else also leads to displacing EtBr). For example, the binding of polyamines above a critical concentration induced DNA bending, which caused conformational changes of the double helix. The changes of the conformation facilitated the release of bound EtBr to solvent^[190]. So it is important to ensure that binding takes place exclusively at intercalation sites if the assay is used for determine binding constants.

There are two binding sites for EtBr^[63]: the primary site is intercalation between base pairs, and the secondary site is electrostatic interactions between the cationic EtBr and the anionic phosphate groups on the DNA surface. The secondary binding mode is most evident at low salt concentrations (below 10 mM) and high dye concentrations. The absorption spectrum is the same as that obtained on binding in the intercalation sites of DNA.

Base on the facts mentioned above, the assay was designed in this work^[120]:

(1). The direct excitation of EtBr was at 546 nm and the emission was at 590 nm, because there was no absorbance or fluorescence for our calixarenes at the critical wavelengths.

(2). Na⁺ was used to stabilize the intercalative architecture (the DNA–EtBr complex). There were three different aqueous buffer solutions in my work: (a). 2 mM of HEPES, and 9.4 mM of NaCl. The pH was adjusted to 7.1 with NaOH. (b). 2 mM of HEPES, and 150 mM of NaCl. pH = 7.1. (3). 20 mM sodium phosphate. pH = 7.0.

(3). EtBr was added to DNA to provide 1.26 eq. per base pair.

(4). Because of rapidly equilibrating, after stirring for 5 min and standing for 1 min the fluorescence was measured.

This assay provided very useful information in my work: (1). Whether the EtBr-displacing ligands can access to intercalation sites. (2). Whether the EtBr-displacing ligands bind the

intercalation sites with high affinities.

The shortcomings of the assay should also be paid attention. (1). The calixarenes are too large to be the intercalators to replace EtBr in a competitive mode. (2). The calixarenes may change the conformation of the double helix (This can be proved by CD measurements. See below) to make bound EtBr release to solvent. Therefore, the assay does not provide a direct measure of binding constants.

C_{50} values and CE_{50} values were used to evaluate displacement capacity ^[120]. They were also indirectly proportional to the apparent binding constant of the DNA ligands.

The C_{50} value is the ligand concentration required for 50% displacement of the ethidium bromide, i.e. for 50% fluorescence reduction.

The CE value (charge excess ratio of an EtBr-displacing ligand) was calculated as a ratio of positive charges in an EtBr-displacing ligand versus negative charges of DNA in the respective complex mixture.

The CE_{50} value is the CE at 50% of the original fluorescence emission intensity gained by intercalated ethidium bromide.

$$CE_{50} = \frac{C_{50} \cdot \text{positive ligand charges}}{[\text{DNA phosphates}]}$$

3.2 Circular Dichroism Spectroscopy

Linear polarized light can be viewed as a superposition of left circularly polarized light (LCP) and right circularly polarized light (RCP) with equal amplitude and phase ^[191]. A projection of any polarized light perpendicular to the propagation direction yields circularity and the projection of the combined amplitudes perpendicular to the propagation direction yields a line. When this linear polarized light passes through an optically active sample, the speed ($c_L \neq c_R$), the wavelength ($\lambda_L \neq \lambda_R$) and absorbance ($\epsilon_L \neq \epsilon_R$) of the right and left polarizations will be different. Thus, the projection of the resulting amplitude yields an ellipse instead of the usual

line. The occurrence of ellipticity is called circular dichroism (CD). The CD is a function of wavelength. The value which is presented must specify the wavelength at which it is measured.

For CD spectropolarimeters, ΔA is usually measured. ΔA (Delta Absorbance) is the difference between absorbance of left circularly polarized (LCP) and right circularly polarized (RCP) light: $\Delta A = A_L - A_R$. According to Beer's law: $\Delta A = (\epsilon_L - \epsilon_R) Cl$. ϵ_L and ϵ_R are the molar extinction coefficients for LCP and RCP light, C is the concentration, and l is the path length. By definition, $\Delta\epsilon = \epsilon_L - \epsilon_R$. Thus, $\Delta A = \Delta\epsilon Cl$

However, for CD spectropolarimeters, the value is usually reported in the form of molar ellipticity $[\theta]$ (instead of ΔA), which is defined by $\tan \theta = (E_R - E_L) / (E_R + E_L)$. E_R and E_L are the magnitudes of the electric field vectors of the right-circularly and left-circularly polarized light. After data processing, the formula can be expressed in this way: $\theta = 3298.2 \Delta\epsilon$. ($\Delta\epsilon$ is the function of ΔA , which is measured by the CD instrument.)

Compared with traditional optical rotatory dispersion (ORD) where the phase relationship between the circularly polarised wave changes and the resultant linearly polarised wave rotates, the polarization direction of CD does not change. Optical rotation and circular dichroism stem from the same quantum mechanical phenomena and one can be derived mathematically from the other by Kronig-Kramers transformation, but, CD is only observed at wavelengths where absorbances of light or light components of circularly polarized light are not zero, i.e. in or near the UV absorption bands of the molecule of interest, while ORD can be measured far from these bands. This is the advantage of CD. It makes CD clearly distinguish structural elements because their recorded bands (CD bands) also have UV absorption and do not overlap extensively at particular wavelengths with non-UV absorption function groups. In fact, this is also the fundamental for CD of nucleic acids.

Nucleic acid contains sugar-phosphate backbones and unsaturated benzenelike bases. Both phosphate groups and sugars have electronic transitions at high energy, and the wavelengths are shorter than 190 nm. The base contains π electrons, and a large number of π - π^* transitions (with high intensity) and n - π^* transitions (with low intensity) can be detected by ultraviolet

light and the wavelengths are within 180-300 nm range. The bases themselves have a plane of symmetry, so they have no optical activity. But the sugars are asymmetric and they can induce a CD in the absorption bands of the chromophoric bases. Therefore, this technique is often used to investigate the changes of nucleic acid secondary structures ^[192].

Because the theoretical description of CD spectra of DNA is very complex, CD is not able to provide structure information on the molecules at the atomic level. However, according to previous reports, we can find some valuable conclusions, which were directly used in my work ^[192,193,194].

- (1). The typical *B*-form has a positive band centered near 275 nm, a negative band centered near 240 nm, and a crossover around 258 nm which is the wavelength maximum for the normal absorption.
- (2). The *A*-form has a more intense positive CD in the long-wavelength region, and a reasonably intense negative at 210 nm.
- (3). (dG + dC) rich DNA fragments exhibit *A*-form features in aqueous solutions.
- (4). As (dA + dT) content increases, the negative band becomes deeper and conformational variability increases.
- (5). CD spectra not only depend on the secondary structures, but also depend on the sequences of nucleic acids.
- (6). High concentrations of methanol induce the 10.2 basepairs per turn *B*-form, but high concentrations of ethanol induce the *A*-form for sodium salts of DNA.

In fact, CD spectroscopy is largely used empirically in studies of DNA. It exhibits several special advantages in my work:

- (1). The concentrations of DNA samples can be very low (about 5 – 20 μM in terms of basepairs). This is advantageous in studies of calixarene – DNA samples of low solubility.
- (2). Polynucleotides can be studied by CD spectroscopy.

3.3 DAPI Displacement Assay

4',6-diamidino-2-phenylindole (abbreviated as 'DAPI') is a blue fluorescent probe, which appears to associate with 3-4 nearest-neighbor A:T base pairs in the minor groove of double stranded DNA (Figure 3.2). Due to the displacement of water molecules from both DAPI and the minor groove, the fluorescence of the DAPI-DNA complex is approximately 20-fold greater than in the unbound state. When bound to double stranded DNA, DAPI has an absorption maximum at the wavelength of 358 nm and the emission maximum is at 461 nm. DAPI as an intercalator also binds RNA, but the fluorescence enhancement is not so strong, and the emission of the DAPI-RNA complex shifts to around 500 nm ^[195,196,197,198].

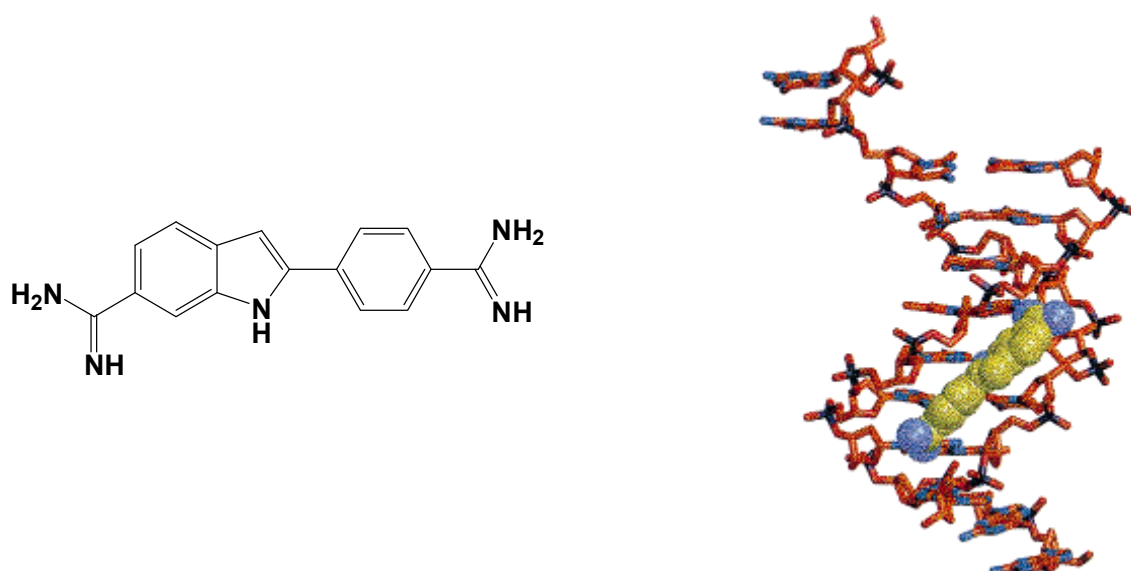


Figure 3.2 The structure of DAPI and stereoview of the d(GGCCAATTGG)-DAPI structure ^[199]

When DAPI binds AT-rich sequences, the conformation of the AT sequence is changed into stiffer *B*-form DNA. DAPI is edgewise inserted into the minor groove at an angle of approximately 45° to the helix axis ^[200]. DAPI itself is not chiral but acquires an induced circular dichroism (ICD) upon chiral perturbation through binding to the chiral DNA helix. The mechanism behind the induced CD is not clear in detail but it is believed to be primarily due to the effect of nondegenerate coupling between transitions of DAPI and transitions of the bases of the nucleic acid host.

According to the facts mentioned above, another two assays were designed. The two assays are based on the changes in the fluorescence ^[201] and the changes in CD upon DAPI-

displacing ligand binding. The binding of the DAPI-displacing ligand to the DAPI-poly (dAdT) complex results in displacement of the bound DAPI, producing a decrease in the observed fluorescence or CD (molar ellipticity). The percent fluorescence or CD (molar ellipticity) decrease is directly related to the extent of binding.

But, not only minor groove binders, but also major groove binders, intercalators, or even phosphate backbone binders can drive bound DAPI to solvent. All these binders can displace DAPI and decrease fluorescence emission of DAPI-poly(dAdT). In order to avoid the shortcomings, we planned to use CD to perform DAPI displacement assays. Compared with fluorescence techniques, circular dichroism can provide more specific information:

(1). Because the ICD at 370 nm comes from DAPI (the UV absorption band in this region comes from DAPI), the value of molar ellipticity in this region indicates whether DAPI remains to bind DNA (Figure 3.2B). (2). For DAPI-poly(dAdT) complex, the CD band at 265 nm is the sum of CD (DNA) and ICD of DAPI (Both DNA and DAPI have UV absorption bands in this region). The changes of CD at 265 nm not only describe whether DAPI remains to bind DNA, but also illustrate the conformational changes of DNA. The conformational changes of DNA are related to the binding between the DAPI-displacing ligand and the DAPI-poly(dAdT) complex. (3). The CD measurement records both CD and UV data at the same time. Therefore, it provides more information about the interaction of the DAPI-displacing ligands (calixarenes) and the DAPI-poly (dAdT) complex.

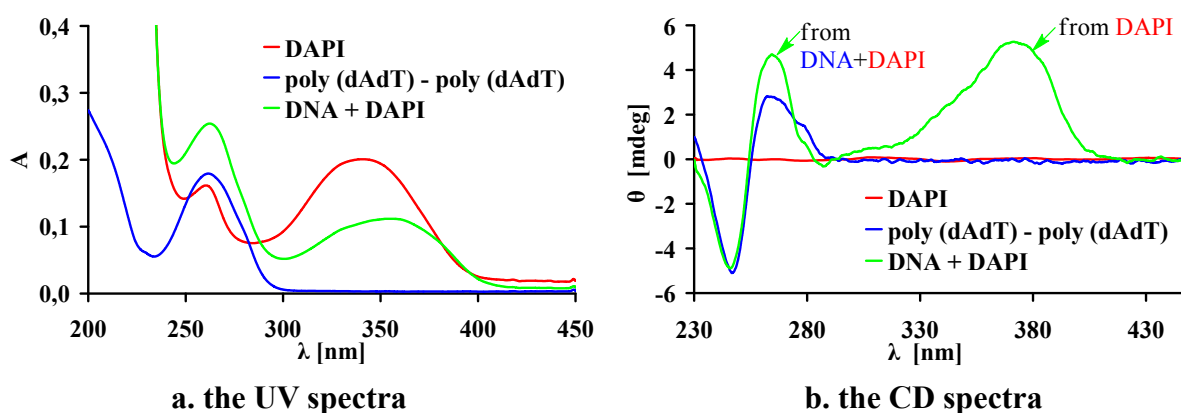


Figure 3.2B UV and CD spectra of DAPI, DNA and the complex

In this work, CD spectropolarimeters were used to perform DAPI displacement assays.

3.4 Fluorescence Titration Experiments

Fluorescence titration experiments have been developed to measure the association constants (K_a) of guests and hosts. In order to determine the binding constants, the following three tasks have to be carried out: (1). the titration of one binding partner into the other at specified concentration ranges to get a fluorescence titration curve. In this study, the fluorescence titration curve is a plot of the concentration ratio of calixarenes and nucleic acids with fluorophores vs. the changes of the fluorescence intensity obtained from fluorescence titration experiments. (2). the determination of the stoichiometry. (3). non-linear regression techniques for calculating K_a (1 : 1 complex stoichiometry).

3.4.1 The Definition of Binding Constants

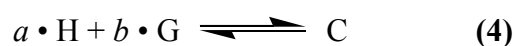
According to the definition of thermodynamics (1) and Gibbs free energy (2) ^[202], binding constants can be described in equation (3): the van't Hoff equation.

$$\Delta G = - RT \ln K \quad (1)$$

$$\Delta G = \Delta H - T\Delta S \quad (2)$$

$$\ln K = -\frac{\Delta H}{R} \cdot \frac{1}{T} + \frac{\Delta S}{R} \quad (3)$$

Our analysis to determine binding constants is based on the simple binding equilibrium model: equation (4) ^[203]



Definitions:

(a). the association equilibrium constant: K_a , equation (5).

Association equilibrium constants, binding constants, and stability constants are synonymous with each other.

(b). the dissociation equilibrium constant: K_d , equation (6)

$$K_a = \frac{[C]}{[H]^a \cdot [G]^b} \quad (5) \quad \text{H: the host; G: the guest; C: the complex}$$

$$K_d = \frac{[H]^a \cdot [G]^b}{[C]} \quad (6) \quad \text{a, b: stoichiometry}$$

$$K_d = \frac{1}{K_a} \quad (7) \quad \text{[H], [G], [C]: concentrations of the host, the guest, and the complex respectively at the final stage}$$

Equation (10) is derived from equations (5)–(9).

$$[H]_0 = [H] + a \cdot [C] \quad (8) \quad [H]_0: \text{the total concentration of the host molecule at the initial state}$$

$$[G]_0 = [G] + b \cdot [C] \quad (9) \quad [G]_0: \text{the total concentration of the guest molecule at the initial stage}$$

$$K_a = \frac{[C]}{([H]_0 - a \cdot [C])^a \cdot ([G]_0 - b \cdot [C])^b} \quad (10)$$

K_a , a , b are unknown, $[H]_0$ and $[G]_0$ can be set up as experimental conditions, and $[C]$ is related to the changes of fluorescence intensity. In order to calculate the binding constants, determination of stoichiometry (namely, a and b) has to be carried out.

3.4.2 The Determination of Stoichiometry

The Continuous Variation Method is adopted to determine the stoichiometry. The stoichiometry [$a / (a + b)$] is obtained from the x-coordinate at the maximum in Job's curve, where the y-axis is $[C]$ and the x-axis is:

$$x = \frac{[H]_0}{[H]_0 + [G]_0}$$

For example, when 1 : 1 complexation is predominant at equilibrium, the maximum appears $x = 0.5$ ($a = b = 1$). In the case of 1 : 2 complexation $x = 0.333$ gives the maximum.

Because the concentration of the complex ($[C]$) could not be measured directly, the $[C]$ (y-axis) would be replaced with a property proportional to $[C]$. For fluorescence titration experiments, $[C]$ is related to the changes of fluorescence intensity, and could be replaced by

the following equation:

$$y = \frac{[H]_0}{[H]_0 + [G]_0} \cdot \Delta \text{ fluorescence intensity}$$

For DNA experiments, a is equal to 1, and b is always integer larger than or equal to 1.

3.4.3 Calculation

In order to simplify the calculation, the association equilibrium constant was calculated by non-linear regression methods by a Sigma-Plot program for the host : guest = 1 : 1 complexation (equation 11)



The problem is $a = 1$, but $a \neq b$, $b > 1$ (equation 12)



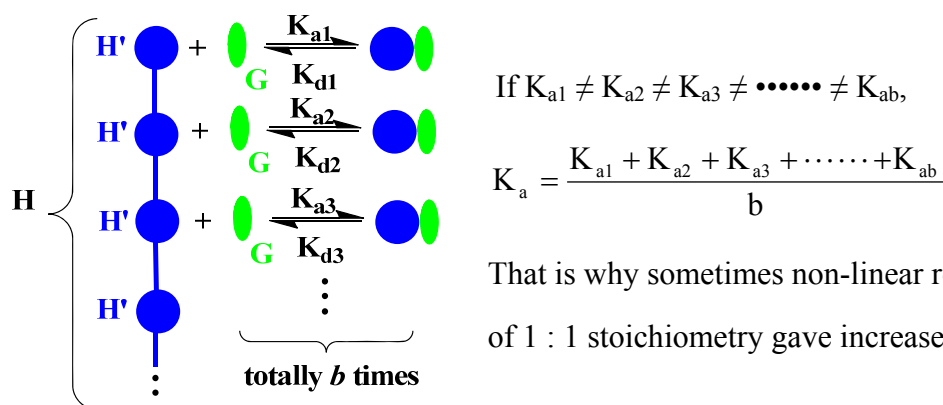
Therefore, we have to think about the way to set up the experimental conditions to fulfil the requirement of 1 : 1 complex stoichiometry.

We increase the concentration of $[H]_0$ b times, and get the new equation (13).

Please note: H' replaces H . The new equation is 1 : 1 binding mode^[204].



After calculation^[205], we get the binding constant. In this way, each guest molecule binds the host molecule with the same binding affinity, $K_{a1} = K_{a2} = K_{a3} = \dots = K_{ab}$.



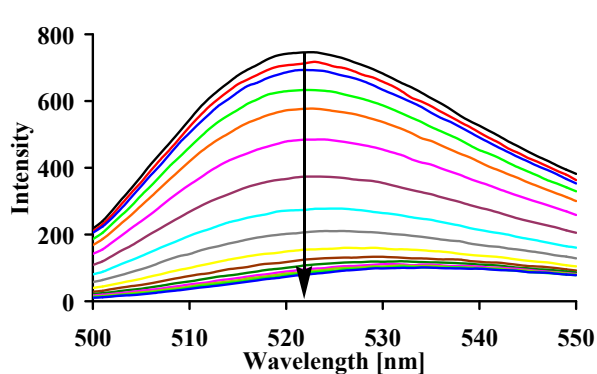
In several cases, the 1 : 2 or 2 : 1 complex was evaluated by a WinEQNMR program, where we can get a better fitting than the corrected 1 : 1 case and we can also get a better understanding about the binding events.

For example: **DNA:** (dGdC)₁₀-(dGdC)₁₀ **ligand:** Dimer C
 C_{FI-DNA}: 1.0×10⁻⁶M **C_{ligand}:** 1.0×10⁻³M
 Buffer: 2 mM of HEPES and 150 mM NaCl in water. pH=7.10

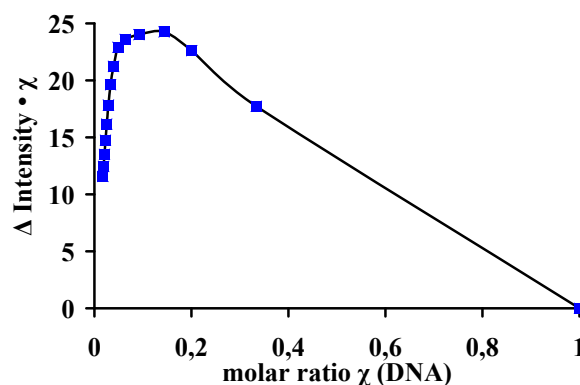
Addition ligand (μL)	Total volume (μL)	C _{FI-DNA} (mol/L)	C _{ligand} (mol/L)	ratio (C _{ligand} /C _{FI-DNA})	fluorescence emission	relative emission difference
0	500	1,00E-06	0,00E+00	0,00	941,984	0,000
1	501	1,00E-06	2,00E-06	2,00	888,886	53,098
2	502	1,00E-06	3,98E-06	3,98	829,280	112,704
3	503	1,00E-06	5,96E-06	5,96	773,019	168,965
5	505	1,00E-06	9,90E-06	9,90	680,197	261,787
7,5	507,5	1,00E-06	1,48E-05	14,78	569,613	372,371
10	510	1,00E-06	1,96E-05	19,61	469,962	472,022
12,5	512,5	1,00E-06	2,44E-05	24,39	402,901	539,083
15	515	1,00E-06	2,91E-05	29,13	350,799	591,185
17,5	517,5	1,00E-06	3,38E-05	33,82	321,183	620,801
20	520	1,00E-06	3,85E-05	38,46	303,755	638,229
22,5	522,5	1,00E-06	4,31E-05	43,06	292,366	649,618
25	525	1,00E-06	4,76E-05	47,62	284,672	657,312
27,5	527,5	1,00E-06	5,21E-05	52,13	280,287	661,697
30	530	1,00E-06	5,66E-05	56,60	275,396	666,588

After fluorescence titrations, we got fluorescence quenching and resulting titration curves (in Figure 6.1a). And then, [DNA]_{total}, [ligand]_{total} and relative emission differences can be calculated. The Continuous Variation Method was used to determine the stoichiometry (in Figure 6.1b). In Figure 6.1b,

$$x = \frac{[\text{DNA}]_{\text{total}}}{[\text{DNA}]_{\text{total}} + [\text{ligand}]_{\text{total}}} \quad \text{and} \quad y = \frac{[\text{DNA}]_{\text{total}}}{[\text{DNA}]_{\text{total}} + [\text{ligand}]_{\text{total}}} \cdot \Delta \text{ fluorescence intensity}$$



a. Fluorescence quenching curves

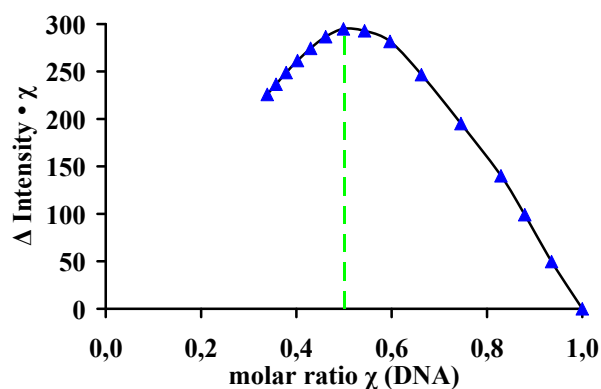


b. Job's plot for complexation of DNA and Dimer C

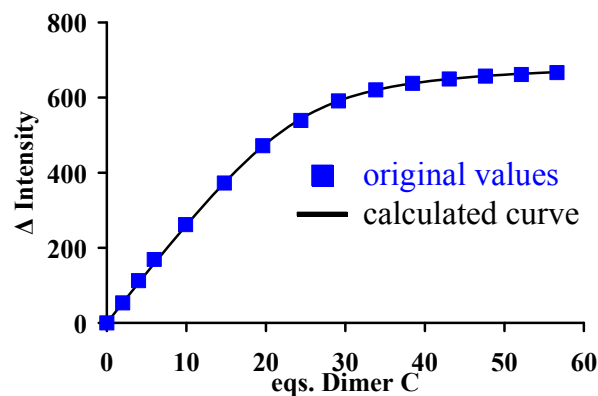
Figure 6.1

In Figure 6.1b, when $x = 0.05$, $y = [C]_{\max}$. It indicated that the binding mode was not 1 : 1 complexation. $[DNA]_{\text{total}}$ was then multiplied with a virtual correction factor, until the Job-Plot showed a 1 : 1 complex stoichiometry, i.e. $x = 0.5$, $y = [C]_{\max}$ (in Figure 6.2a). Herein, the virtual correction factor was equal to 24. Thus, the stoichiometry was 24:1.

Addition ligand (μL)	Total volume (mL)	$C_{\text{FI-DNA}}$ (mol/L)	C_{ligand} (mol/L)	ratio ($C_{\text{ligand}}/C_{\text{FI-DNA}}$)	fluorescence emission	relative emission difference
0	500	$24 \times 1,00\text{E-}06$	0,00E+00	0,00	941,984	0,000
1	501	$24 \times 1,00\text{E-}06$	2,00E-06	0,08	888,886	53,098
2	502	$24 \times 1,00\text{E-}06$	3,98E-06	0,16	829,280	112,704
3	503	$24 \times 1,00\text{E-}06$	5,96E-06	0,24	773,019	168,965
5	505	$24 \times 1,00\text{E-}06$	9,90E-06	0,41	680,197	261,787
7,5	507,5	$24 \times 1,00\text{E-}06$	1,48E-05	0,61	569,613	372,371
10	510	$24 \times 1,00\text{E-}06$	1,96E-05	0,80	469,962	472,022
12,5	512,5	$24 \times 1,00\text{E-}06$	2,44E-05	1,00	402,901	539,083
15	515	$24 \times 1,00\text{E-}06$	2,91E-05	1,19	350,799	591,185
17,5	517,5	$24 \times 1,00\text{E-}06$	3,38E-05	1,39	321,183	620,801
20	520	$24 \times 1,00\text{E-}06$	3,85E-05	1,58	303,755	638,229
22,5	522,5	$24 \times 1,00\text{E-}06$	4,31E-05	1,77	292,366	649,618
25	525	$24 \times 1,00\text{E-}06$	4,76E-05	1,95	284,672	657,312
27,5	527,5	$24 \times 1,00\text{E-}06$	5,21E-05	2,14	280,287	661,697
30	530	$24 \times 1,00\text{E-}06$	5,66E-05	2,32	275,396	666,588



a. Modified Job's plot for complexation of DNA and Dimer C by fluorescence titrations



b The graphical representation of the titration curve

Figure 6.2

The binding constant was calculated with the corrected concentrations of $[DNA]_{\text{total}}$ by non-linear regression methods by a Sigma-Plot program for the host : guest = 1 : 1 complexation. After calculation, the values of K_a , statistical errors and calculated relative emission differences were provided. We could compare the calculated values with the original values (relative emission differences) to evaluate the effect of the calculation (in Figure 6.2b).

3.4.4 Fluorescence Titration Curves and Binding Constants

Fluorescence titration curves ^[206] themselves can be used to evaluate the binding constants, because dissociation was shown in the neighborhood of the stoichiometric point. If the binding constant is high (the red curve in Figure 3.3), there will be no appreciable dissociation of the complex at or near the stoichiometric point. If the complex is moderately stable (the green curve and the orange curve in Figure 3.3), the plot consists of two straight-line portions with a central curved portion. If the binding constant is low, a large excess of ligands have to be used to drive the binding to completion, and there is no detectable break in the curve, from which to obtain the stoichiometry (the blue curves in Figure 3.3).

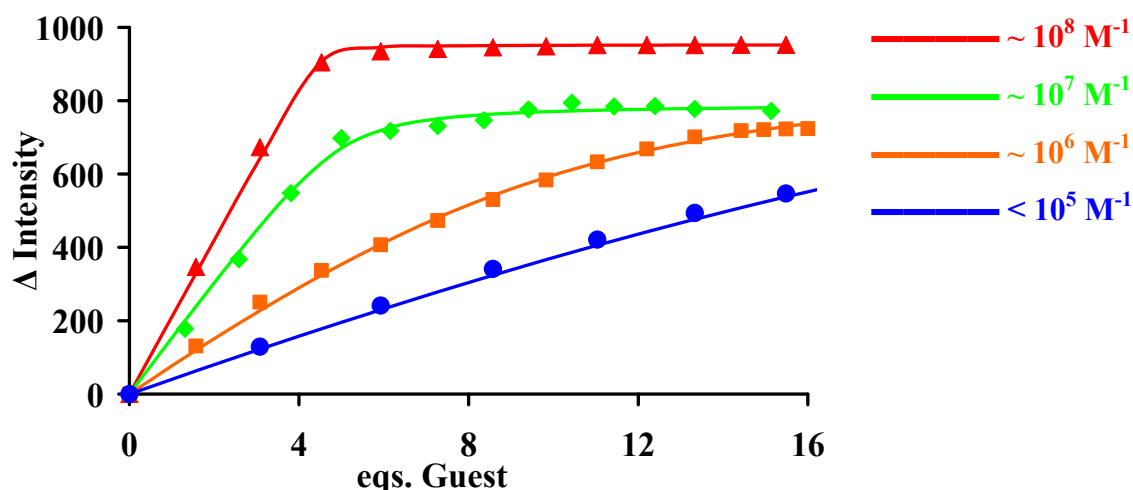


Figure 3.3 Fluorescence titration curves reflect the stability of the complex in the neighborhood of the stoichiometric point

In my work, fluorescence titration experiments have been used to measure the binding constants (affinity) between nucleic acids and calixarenes. The affinity includes three parts: electrostatic interactions, hydrophobic interactions and hydrogen bond interactions. The electrostatic interaction between DNA phosphate groups and the amino groups of calixarenes enhances the affinity but not the specificity of the binding. The specificity of the binding is determined by the non-electrostatic interaction, i.e. the hydrogen bond interactions between amino groups of calixarenes and DNA base pairs. In other word, high specificity does not demand high affinity ^[207]. In order to investigate the specificity of the binding, buffers with high concentration NaCl (150 mM) were used to decrease the electrostatic interactions.

Fluorescence titration experiments, ethidium bromide displacement assays, and CD measurements complement each other in my work. The fluorescence titration experiment was performed to determine the binding constants between calixarenes and DNA (the binding sites include nucleobases and phosphate backbones). The ethidium bromide displacement assay was performed to determine the relative binding affinities between calixarenes and intercalation sites (the binding site is the nucleobases). The CD experiment was performed to observe the conformational changes of the phosphate backbone (between 260nm and 300 nm). The binding site is phosphate backbones. The calixarene dimer sometimes showed similar affinities for different nucleic acids (measured by fluorescence titration experiments), but exhibited different EtBr displacement capacities, and induced different conformational changes of the phosphate backbones. These methods were combined together to infer DNA binding modes.

3.5 Isothermal Titration Calorimetry

When guest molecules bind nucleic acids, heat (ΔH) is either generated or absorbed, which can be measured directly by isothermal titration calorimetry (ITC) during the biomolecular binding event. The measurement of heat allows accurate determinations of binding constants (K_a), reaction stoichiometry (n), enthalpy (ΔH) and entropy (ΔS), thereby providing a complete thermodynamic profile of molecular interactions in a single experiment (in Figure 3.5b).

In the view of energetic profiles of protein–DNA systems, the research from Peter L. Privalov^[95] proved that: (1). There are no dramatic differences in the Gibbs free energies of protein binding to the major and minor grooves of DNA (the top panel of the Figure 3.4a). (2). The enthalpies of binding to minor grooves are always positive, but the enthalpies of binding to major grooves are invariably negative (the middle panel of the Figure 3.4a) (3). Because the Gibbs free energies of binding at 20 °C are similar, the enthalpy differences are essentially balanced by entropic factors. The entropic contribution (i.e. $T\Delta S$) of minor groove binding is significantly larger than that of major groove binding (the bottom panel of the Figure 3.4a).

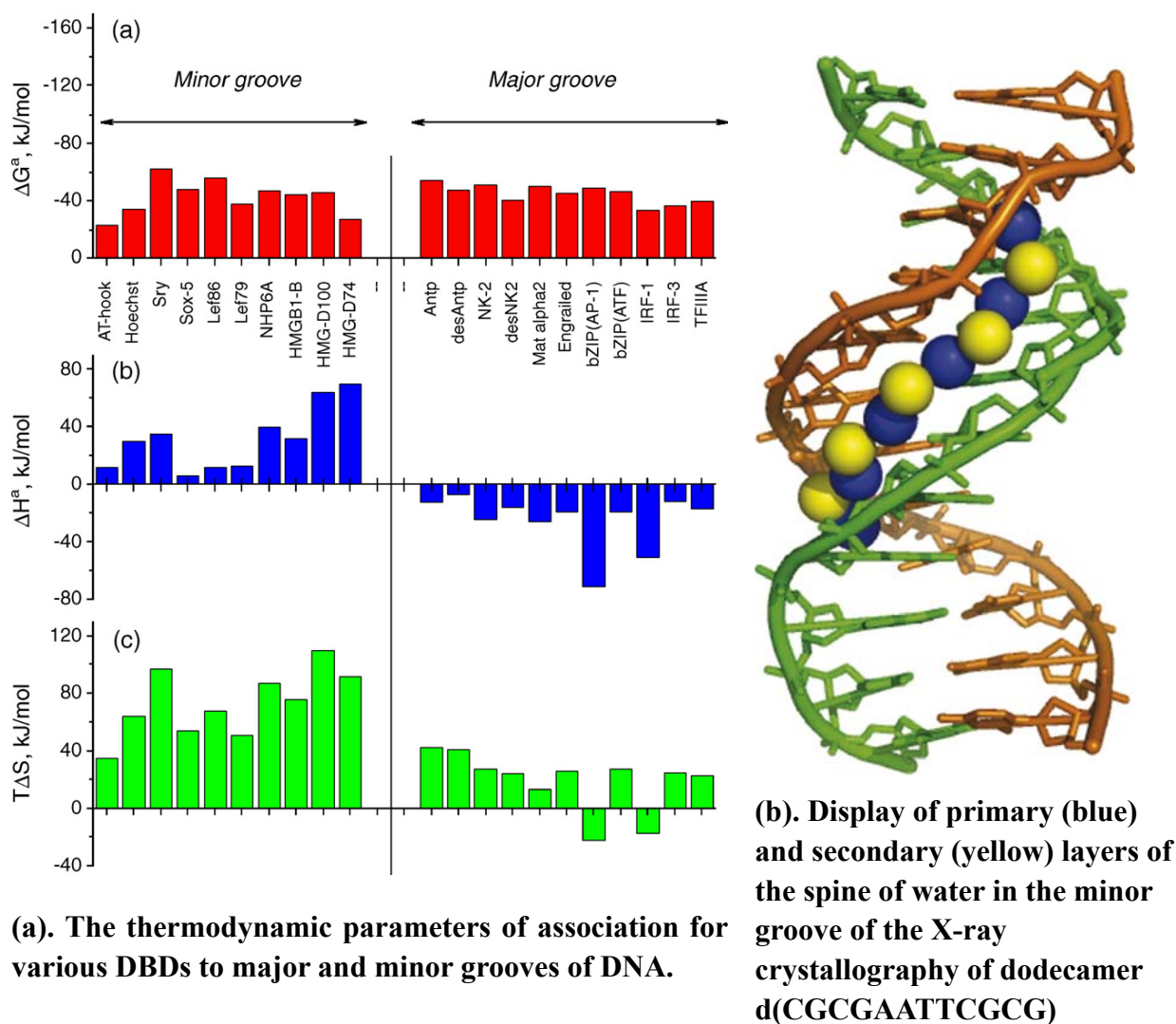
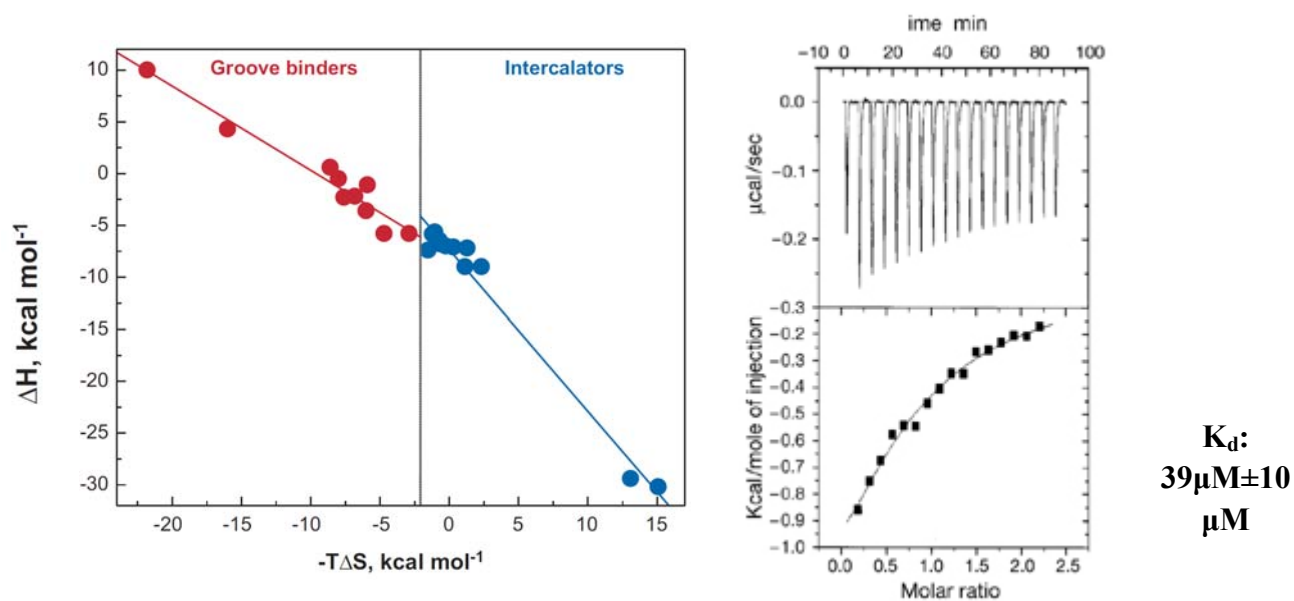


Figure 3.4 The different energetic profiles of minor groove binders and major groove binders [93,94,95]

Therefore, association with major grooves is primarily an enthalpy driven process, whereas binding to minor grooves is characterized by an unfavorable enthalpy that is compensated by favorable entropic contributions. These results mentioned above can be explained by the fact that the water hydrating in the minor groove of A:T-rich DNA is more ordered than the water hydrating in the major groove (Figure 3.4b). The removal of water results in a substantial positive contribution to the binding entropy. The removal of water hydrating in minor grooves is expected to require a greater enthalpy and thereby provide a larger entropy increase than removal of water hydrating in major grooves.

In contrast, the binding of intercalators is typically an enthalpy driven process [208]. For

intercalation, the DNA must undergo reorganization to accommodate a more rigid architecture, which is entropically less favourable. The entropic penalty must be overcome by enthalpy values (arising in part from van der Waals stacking interactions between the base pairs and the intercalated chromophores). Therefore, intercalators have large negative enthalpy, and near zero, or even large positive values for the $-T\Delta S$ (in Figure 3.5a).



a. The enthalpic and entropic contributions to DNA binding for groove binders and intercalators

b. The top panel shows the primary titration data, and the lower panel shows the binding isotherm constructed from the primary data.

K_d :
39 μM ± 10 μM

Figure 3.5 The different energetic profiles of groove binders and intercalators [208]

3.6 The Assessment of Thermal Denaturation of DNA

DNA denaturation, also called DNA melting, refers to the melting of the double stranded DNA to generate two single strands, through the breaking of hydrogen bonding between the bases in the duplex. This process can be monitored experimentally by observing the absorption of ultraviolet light at 260 nm, where the bases absorb light. As DNA is heated and the strands separate, the amount of light absorbed increases until all of the DNA is melted.

This is called the hypochromic effect. Under a given set of conditions, there is a midpoint of the melting curve, which is called melting temperature. The melting temperature or the melting point (T_m) is defined as the temperature at which half of the DNA strands are in the double-helical state and half are in the random coil state (Figure 3.6, *left*). The T_m value of a given piece of DNA depends on several factors, for example, the length of the DNA sequence (shorter pieces of DNA will tend to melt more easily than longer pieces), the base composition of the DNA (as G:C base pairs have three hydrogen bonds and A:T base pairs only have two, the higher is the percentage of G:C base pairs, the higher is the melting point of a DNA molecule), the topological condition of the DNA, and the composition of the buffer (Na^+ and K^+ can stabilize the duplex) and so on. The difference between the T_m of a nucleic acid and the T_m observed in the presence of a drug is termed ΔT_m .

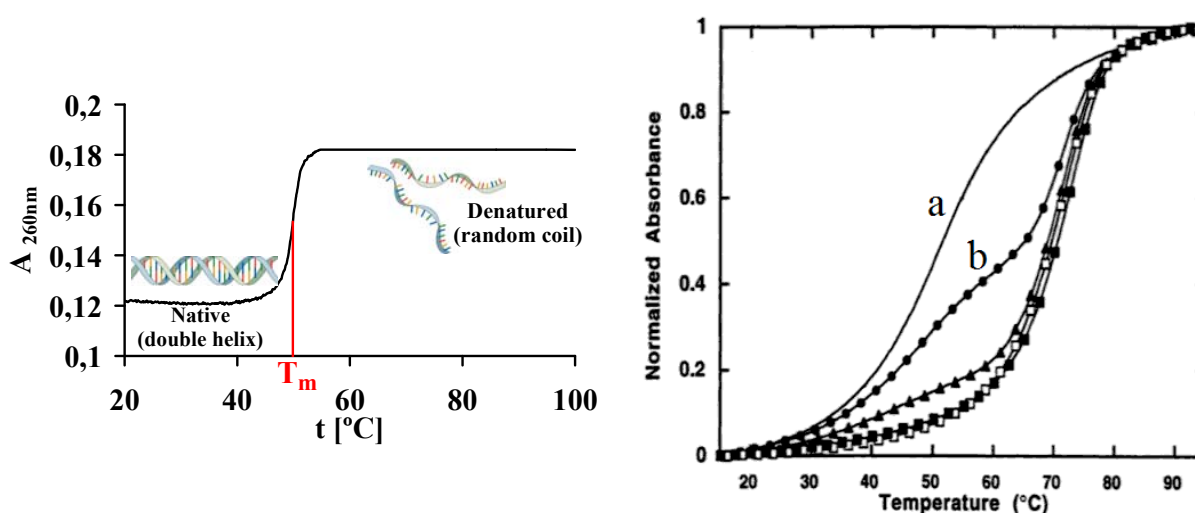


Figure 3.6 The melting curve of a nucleic acid (*left*) and the effects of drugs on melting curves (*right*)

Melting curves can provide binding information ^[209,210,211].

(1). The change in absorbance, termed hyperchromicity, is a physical property. An apparent decrease of hyperchromicity means a substantial fraction of the DNA was already dissociated into single strands prior to heating.

(2). ΔT_m is related to the affinity of binding of a drug to a nucleic acid. The increase of T_m indicates that the drug binds to the double strands with higher affinity than to the single

strands. If the drug binds to the single strands stronger than the double strands, T_m decreases.

(3). The change of the shape of a melting curve also indicates the interaction between the drug and the nucleic acid. For example, an increase in the breadth of the transition in the presence of drugs indicates the stronger binding of the drug to one specific region than other regions of nucleic acids (in Figure 3.6, *right*, curve **b**; curve **a** is a normal melting curve).

(4). Most of intercalators and groove binders can stabilize the double-stranded DNA better than the single-stranded DNA. T_m values increase.

3.7 Triple Helix-Forming Oligonucleotide Displacement Assay

An oligonucleotide can bind as a third strand of DNA in a sequence specific manner in the major groove in polypurine-polypyrimidine stretches in duplex DNA ^[212]. There are two basic manners. The first, a polypyrimidine oligonucleotide binds in a direction parallel to the purine strand in the duplex. The second, a polypurine strand binds anti-parallel to the purine strand. In all cases, the third strand binds in the major groove and recognizes the purine strand by establishing a pair of hydrogen bonds with the hydrogen bond donor and acceptor groups available on the major groove edge of purine bases (Figure 1.3b). Different base triplets can form through either Hoogsteen or reverse Hoogsteen hydrogen bond formation. Beside nucleotides, peptide nucleic acids (PNA), which is a mimic of nucleic acids where the natural sugar phosphate backbone has been replaced by achiral N-(2-aminoethyl) glycine units, also bind DNA on the major groove side ^[17,18]. In this thesis, triple helix-forming oligonucleotides (TFOs) specifically refer to nucleic acids.

Because the third strand of a triple helical DNA binds in the major groove, triple helix-forming oligonucleotide displacement assays have been designed to infer the DNA binding mode.

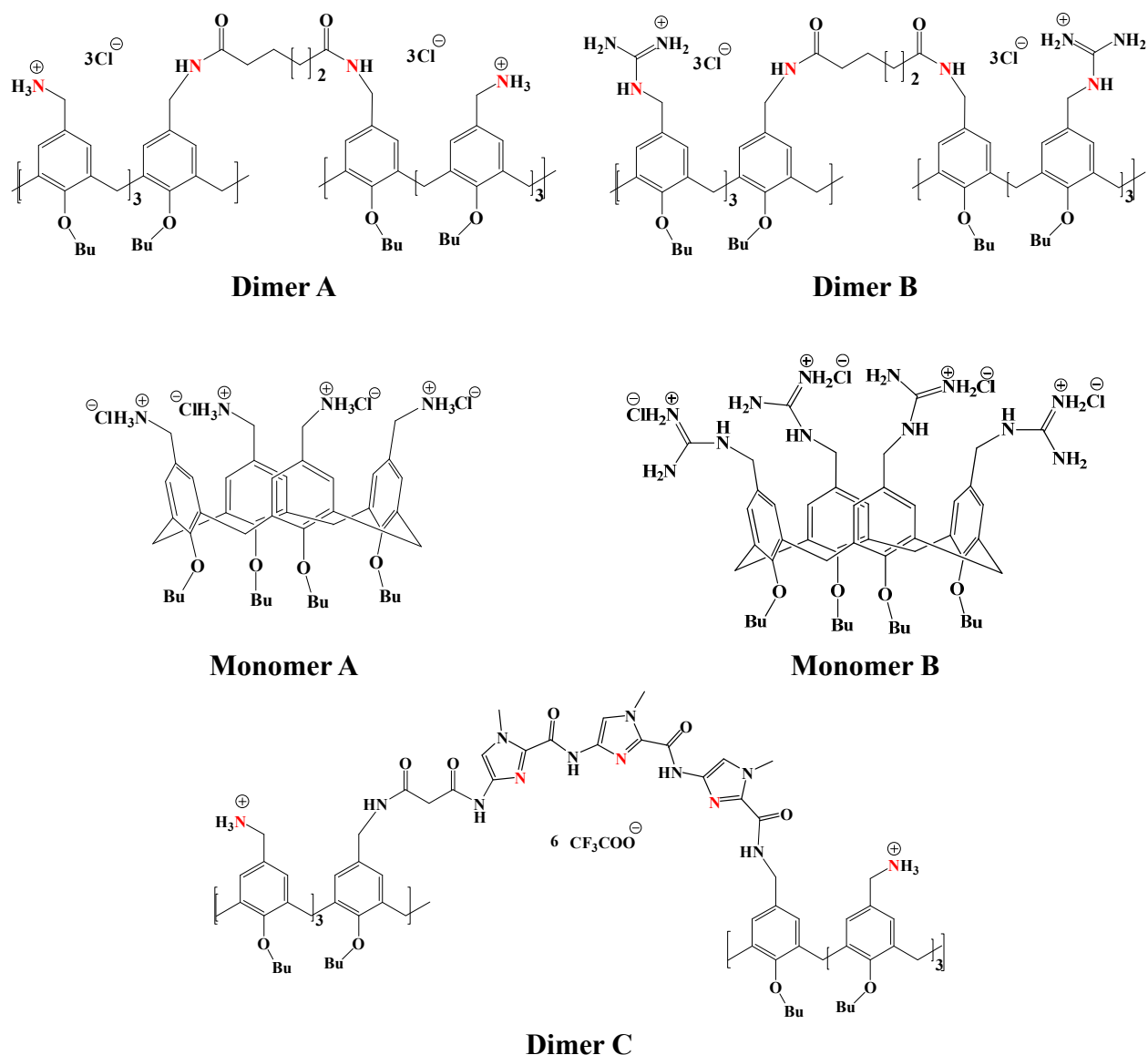
For example:

(1). The CD studies from Seog K. Kim ^[213] showed that the third strand in the triplex inhibited the formation of the TMPyP – double stranded DNA. Therefore, TMPyP stacking occurred in the major groove of both the d(A)₁₂-d(T)₁₂ and the d(G)₁₂-d(C)₁₂ duplexes. [TMPyP: *meso*-tetrakis(N-methylpyridium-4-yl)porphyrin]

(2). The melting curve studies from Dev P. Arya ^[119,214] showed that triplex melting was not observed for poly(dA)-2poly(dT) in the presence of the neomycin-Hoechst 33258 conjugate. This result suggested that the drug binding prevents the third strand polypyrimidine from binding in the major groove, and therefore indicated the major groove recognition of the neomycin-Hoechst 33258 conjugate.

(3). The linear dichroism studies from Bengt Nordén ^[117] showed that methyl green was found to be excluded from binding to the triple helical poly(dA)-2poly(dT) in which the major groove was filled by the third strand. Therefore, methyl green thus appeared to be a DNA major groove binding drug.

4. Results and Discussion



Structures of dimeric and monomeric calixarenes which were studied in this work

4.1 The Mechanism of DNA Binding by Dimeric Calixarenes

It was observed that in $\text{DMSO-}d_6$ and $\text{MeOD-}d_4$ all the calixarene characteristic signals (Dimer A, Dimer B, Monomer A and Monomer B) of NMR spectra were sharp at room temperature; but in D_2O the signals of Dimer A and Dimer B were much broader (Figure 4.1 a, c). As temperature increased, the signals of Dimer A and Dimer B became sharper and sharper

in D₂O. These clearly showed a dynamic effect, and indicated that the two molecules (Dimer A and Dimer B) formed self-aggregations. Compared with the two dimers, monomers did not show self aggregations (the NMR signals of Monomer A and Monomer B in D₂O were the same sharp as in DMSO-*d*₆ and MeOD-*d*₄, Figure 4.1 b, d).

In my opinion, the aggregation (Dimer A and Dimer B) should be due to the amphiphilic nature of the calixarenes. In addition, it is probably related to intramolecular reorganizations, because dimers may use internal dynamics to arrange the two monomer subunits to form a specific shape (for example, a tightly packed ball) through noncovalent interactions, which could minimize the free energy. This characteristic makes the properties of dimers (Dimer A and Dimer B) different from the properties of monomers (Monomer A and Monomer B).

Because of the amphiphilic property of the calixarenes, it would also be necessary to check whether these calixarenes were in the form of vesicles at lower concentrations, which were used for binding assays. Results: the UV/VIS absorbency values of studied compounds in aqueous buffer solutions were proportional to their concentrations up to 20 μM, while for the two dimers, deviations from a linear dependence between absorbance and the solution concentration were observed at higher concentrations. Therefore, there were no vesicles at low concentrations at room temperature. Temperature increase didn't influence UV-vis spectra significantly until 50°C, however at higher temperatures all spectra changed, probably because of the formation of precipitations.

Table 4.1. UV-Vis molar absorption coefficients of compounds at 20°C, pH=7.0 ^a

	λ_{\max} (nm)	$\epsilon (\times 10^3)$ (mmol ⁻¹ cm ²)
Dimer A	276	14.1
Monomer A	276	6.5
Dimer B	276	26.1
Monomer B	276	13.1

^a The buffer solution contained 20 mM sodium phosphate. The pH was adjusted to 7.00.

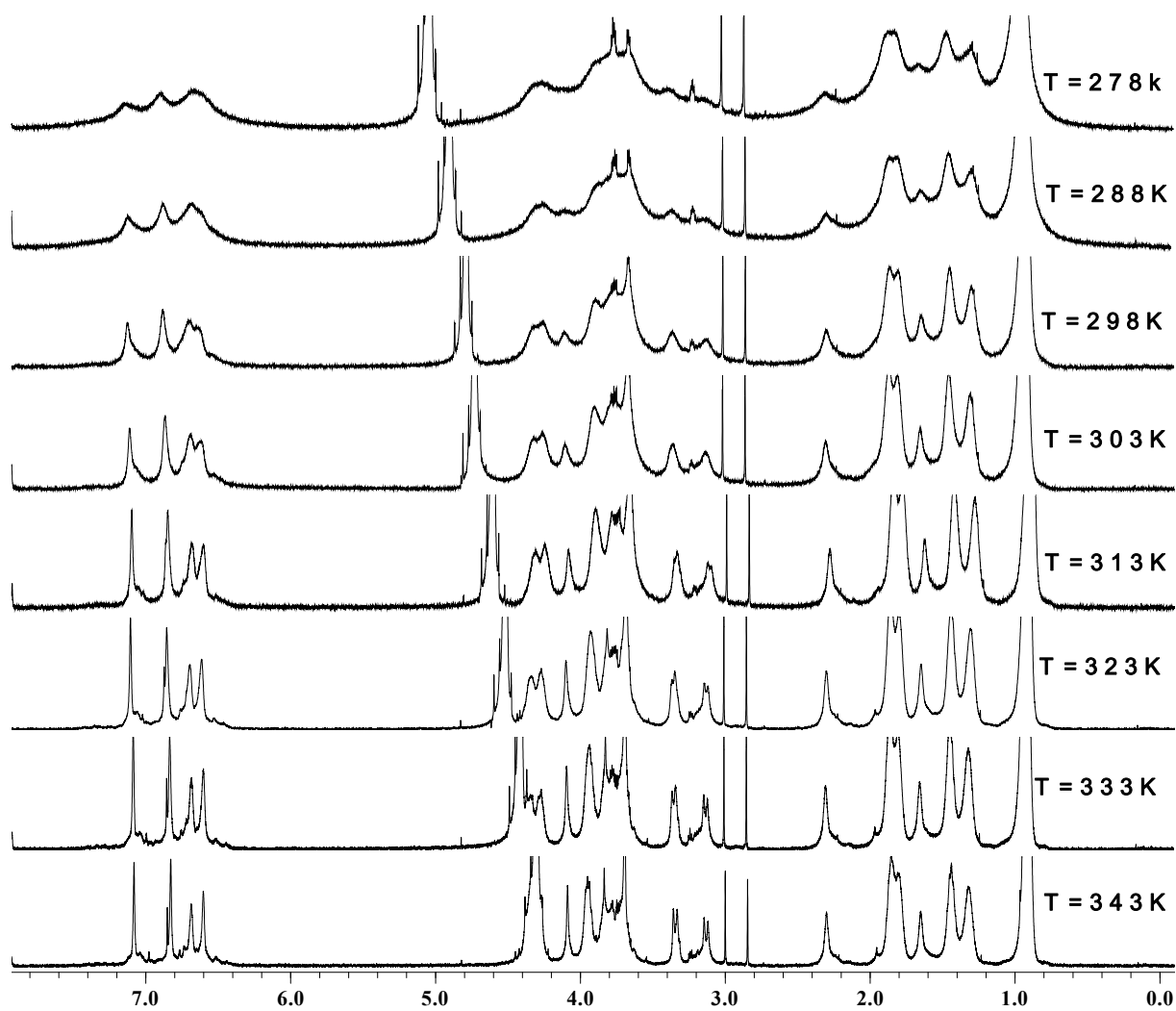


Figure 4.1a. $^1\text{H-NMR}$ spectra of Dimer A with different temperatures (500 MHz, D_2O)

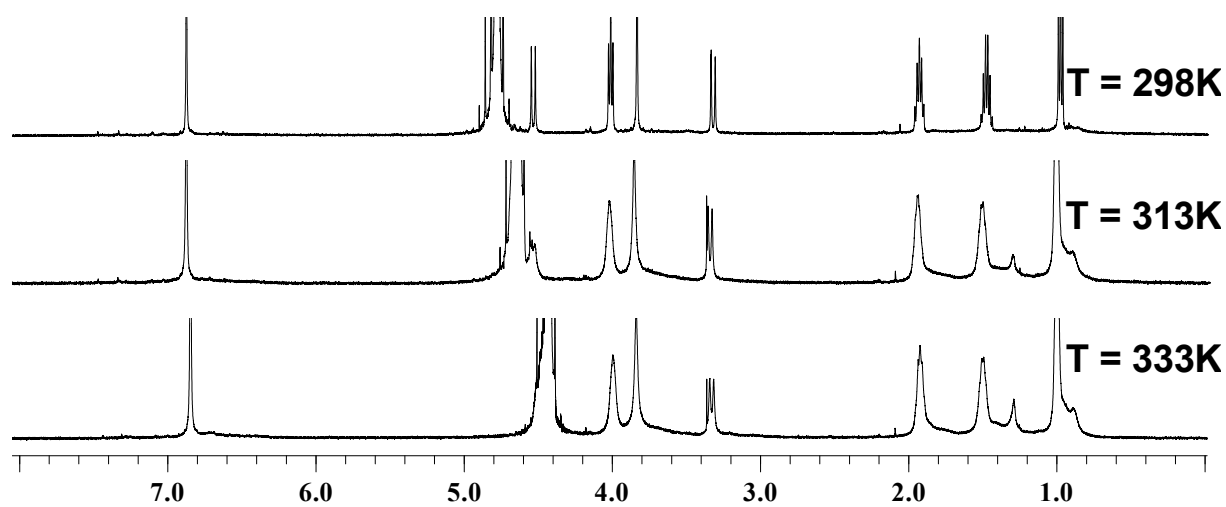


Figure 4.1b. $^1\text{H-NMR}$ spectra of Monomer A with different temperatures (500 MHz, D_2O)

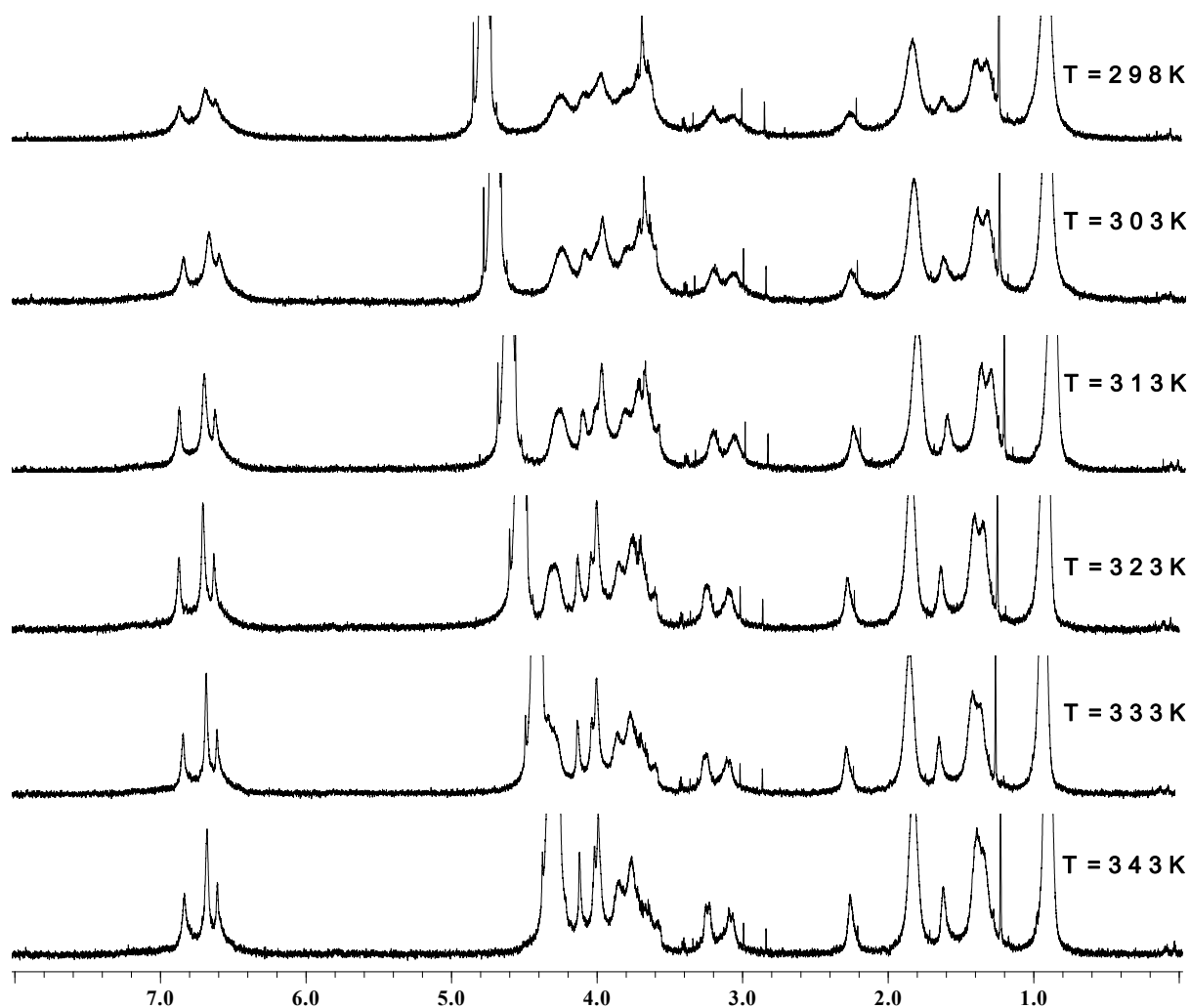


Figure 4.1c. $^1\text{H-NMR}$ spectra of Dimer B with different temperatures (500 MHz, D_2O)

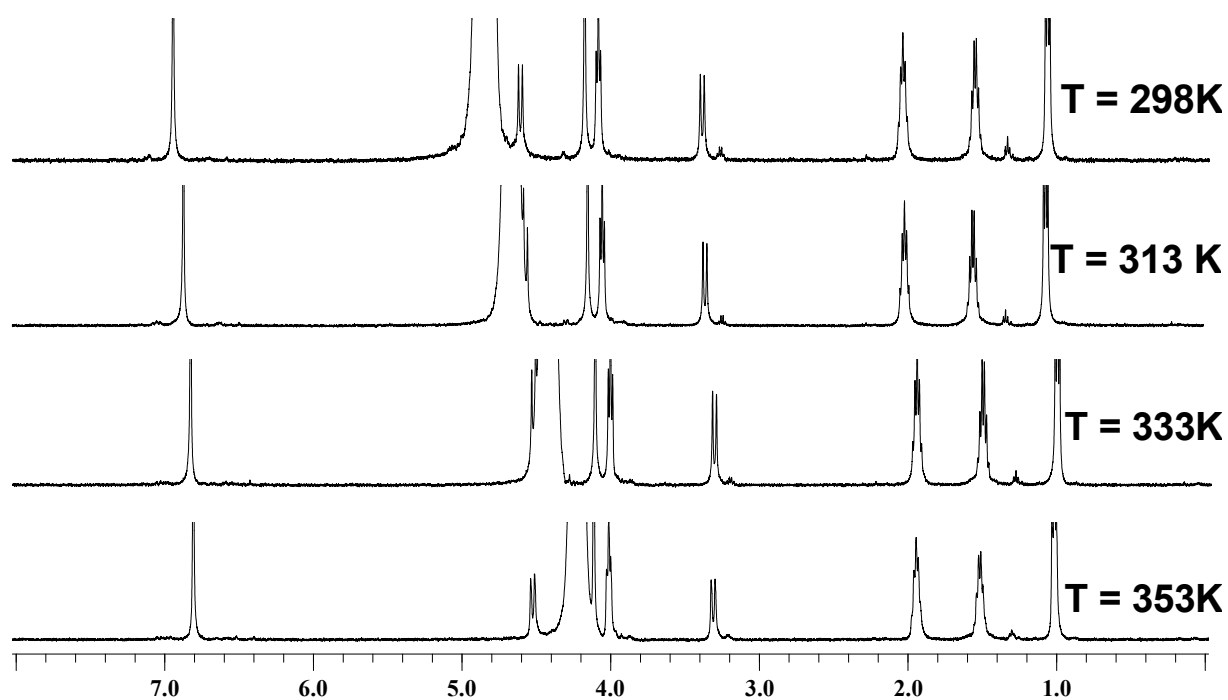


Figure 4.1d. $^1\text{H-NMR}$ spectra of Monomer B with different temperatures (500 MHz, D_2O)

4.1.1 DAPI Displacement Assay

4.1.1.1 Results (Figure 4.2 a-d)

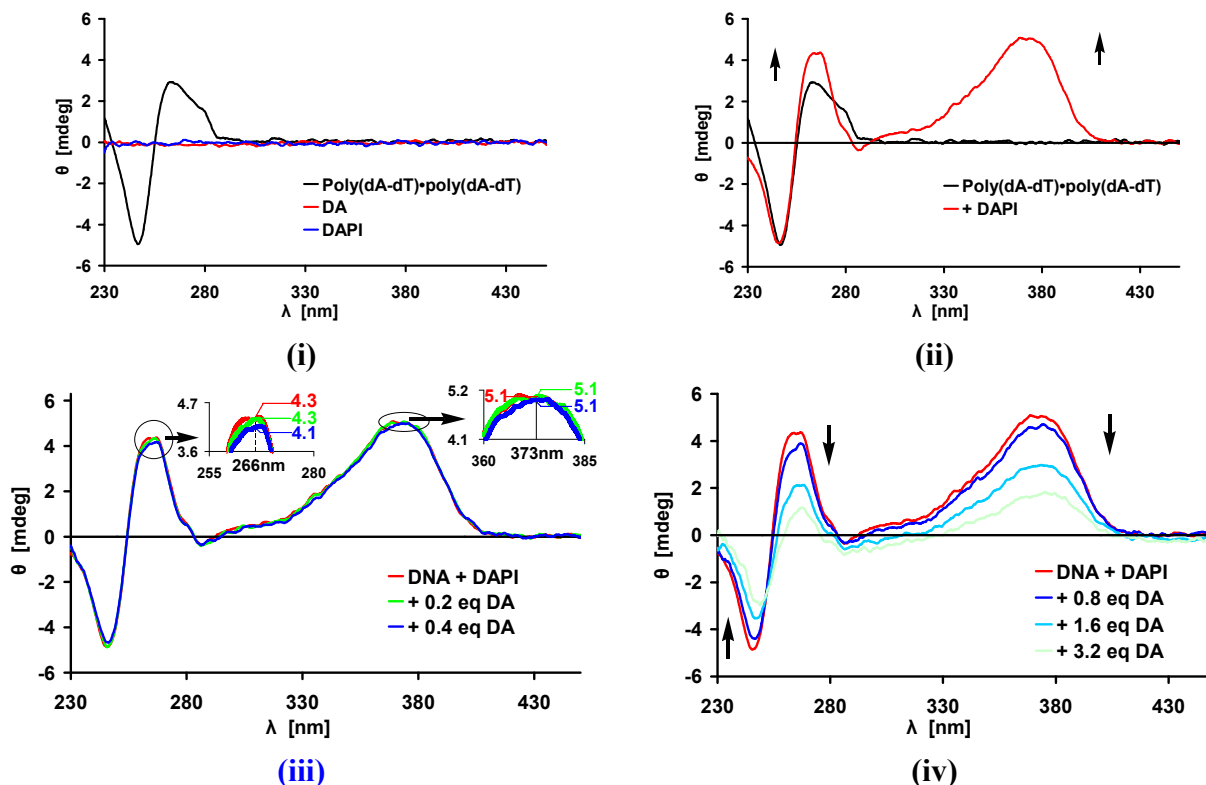


Figure 4.2a. DAPI Displacement of Dimer A (DA) Measured by CD Spectroscopy

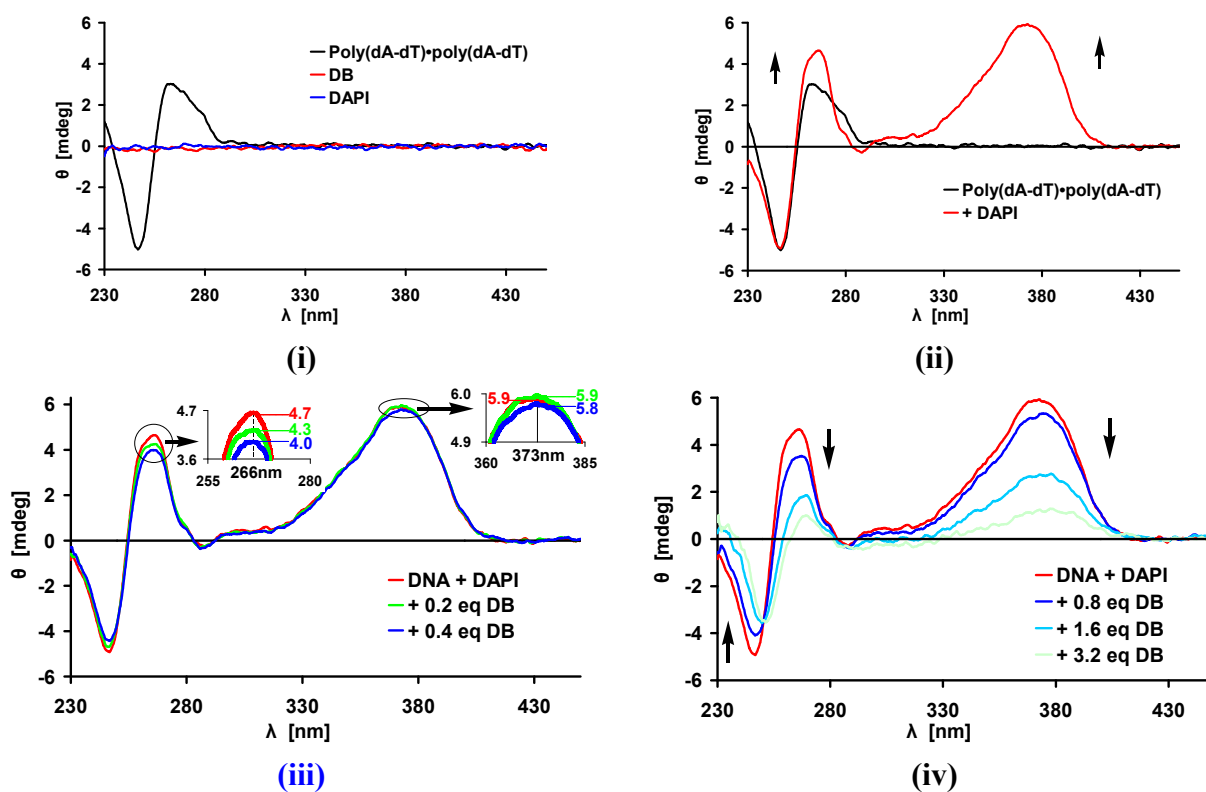


Figure 4.2b. DAPI Displacement of Dimer B (DB) Measured by CD Spectroscopy

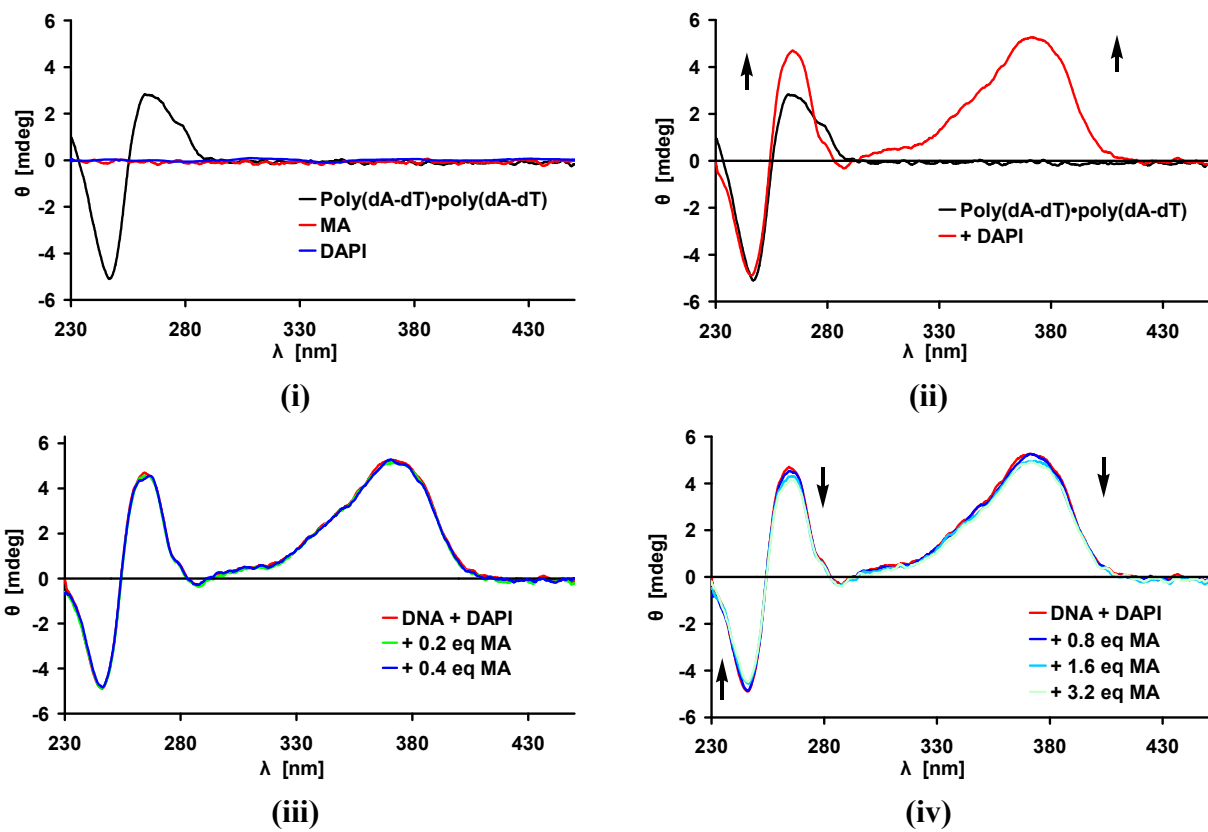


Figure 4.2c. DAPI Displacement of Monomer A (MA) Measured by CD Spectroscopy

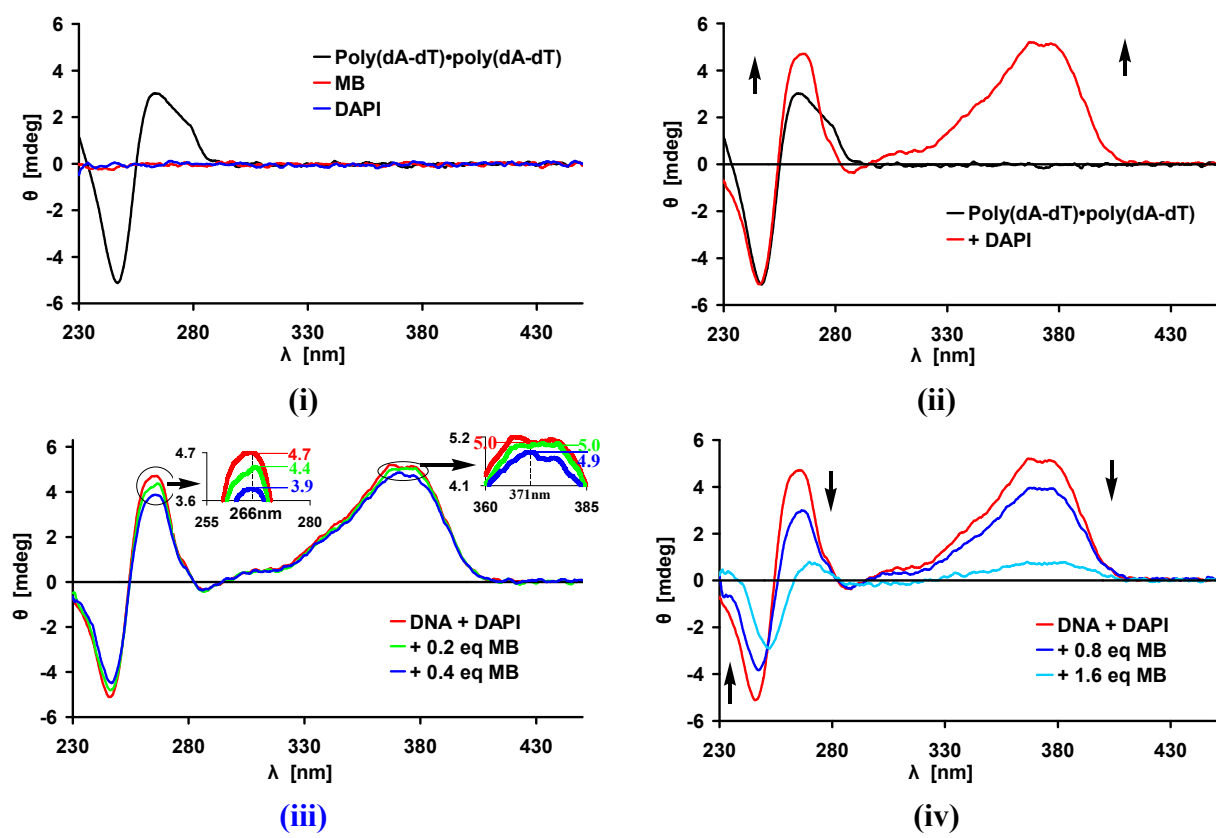


Figure 4.2d. DAPI Displacement of Monomer B (MB) Measured by CD Spectroscopy

For figure 4.2 a-d:

- (1). The buffer solution contained 20 mM sodium phosphate. The pH was adjusted to 7.00. DAPI displacement assays were measured at 20°C
- (2). (i) CD signature of the poly (dAdT) – poly (dAdT) (5 μM in basepairs) (ii) the induced CD band at 370 nm from added DAPI (0.6 eq. = 3 μM in basepairs); (iii) negligible changes on addition of the stoichiometric amount of calixarenes (0.4 eq. in basepairs); (iv) rapid dye displacement by excess calixarenes (except for Monomer A). All calixarene equivalents were calculated per basepairs.

4.1.1.2 Discussion

The discussions were based on the following facts:

- (1). DAPI binds to the minor groove of poly (dAdT) – poly (dAdT).
- (2). The induced CD band at 370 nm comes from DAPI, and the CD bands at 265nm and 245 nm come from DNA and DAPI.
- (3). Neither of calixarenes had CD bands over 230 nm, and therefore they could not interfere this assay by any means.
- (4). Compared with DAPI, calixarene dimers (Dimer A and Dimer B) and monomers (Monomer A and Monomer B) have higher affinities (K_a) for poly (dAdT) – poly (dAdT). The binding affinities have been measured by fluorescence titration experiments.

Table 4.2 Association constants between (dAdT)₁₀- (dAdT)₁₀ and calixarenes / DAPI ¹

	Dimer A	Dimer B	Monomer A	Monomer B	DAPI
K_a (M⁻¹) ²	5.6 e+5	2.3 e+6	2.9 e+6	7.3 e+6	1.3 e+5
Statistical error	24%	24%	20%	23%	8%
Stoichiometry ³	10:1	14:1	30:1	12:1	6:1
No. of data ⁴	No.2	No.5	No.8	No.11	No.13

1. The buffer solution contained 2 mM Hepes buffer with 150 mM NaCl in water. pH = 7.1.
2. 5.6 e+5 represents 5.6×10⁵.
3. Stoichiometry: [Guest] / [DNA duplex]
4. The fluorescence titration data were provided in Chapter 6.5.

Discussion:

CD experiments revealed that (1). in the beginning, stoichiometric amounts of the calixarene dimers were bound to the DNA-DAPI complex (Figure 4.2a iii, 4.2b iii). (2). if more than stoichiometric amounts of the calixarene dimers were added to the DNA-DAPI complex, the induced CD band declines and DAPI displacement begins (Figure 4.2a iv, 4.2b iv). This experiment suggests that the calixarene dimers and DAPI can *simultaneously* bind to poly (dAdT) – poly (dAdT) (Figure 4.2a iii, 4.2b iii). Because DAPI occupies the minor groove, the dimeric calixarenes should reside in the major groove.

(1). For the DNA-DAPI complex, the CD band at 265 nm is the sum of CD (DNA) and ICD of DAPI, and the CD band at 370 nm is only ICD of DAPI. Upon addition of Dimer A, Dimer B and Monomer B, the CD bands at 265 nm and 245nm decreased measurably even at $r=0.2$ and 0.4 , but, the ICD band of DAPI at 370 nm didn't change at all. Previous CD experiments of DNA with calixarenes showed a strong decrease in CD bands of poly (dAdT) – poly (dAdT) at 265 nm and 245nm (see below: circular dichroism measurements). Therefore, the changes at 265 nm and 245 nm in this assay most likely originate from the decrease of DNA bands due to the binding of calixarenes. There was no change at 370 nm, which pointed out that DAPI was not displaced. So, the assumption that Dimer A, Dimer B and Monomer B at low ratio bind to the major groove of poly (dAdT) – poly (dAdT) simultaneously with minor groove bound DAPI, could explain these results. For Monomer A, the displacement is not so obvious.

(2). Even if we assumed that the calixarenes bound to the minor groove of DNA, they should replace DAPI immediately, because their affinities for poly (dAdT) – poly (dAdT) are higher than DAPI's (table 4.2). But, this assumption was in contrast with the experimental results.

(3). Excess calixarenes dimers can pull DAPI out of its minor groove via a non-competitive binding mode and form a complex with the dye itself: additions of Dimer A or Dimer B resulted in a fluorescence increase of DAPI solution, but the addition of Monomer A or Monomer B didn't cause any fluorescence change of DAPI (Figure 4.2e).

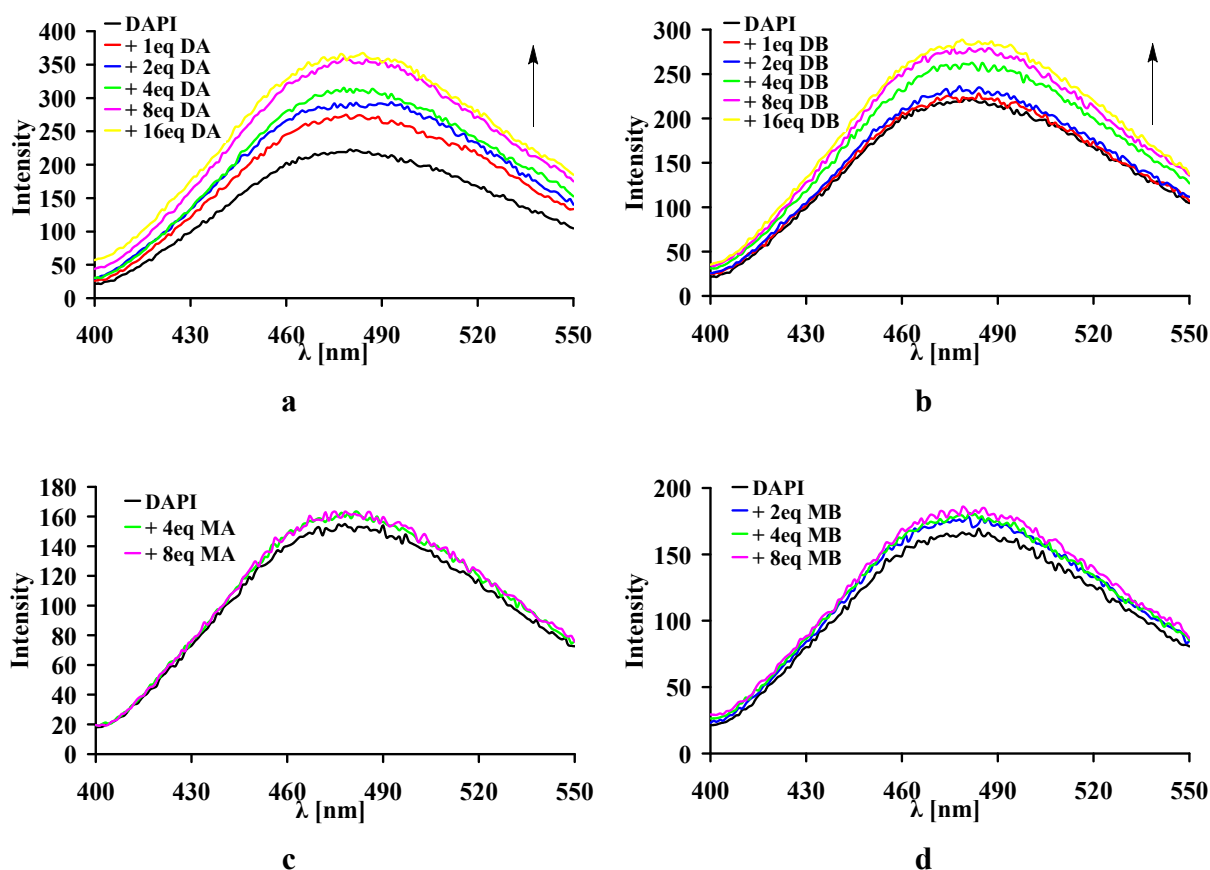


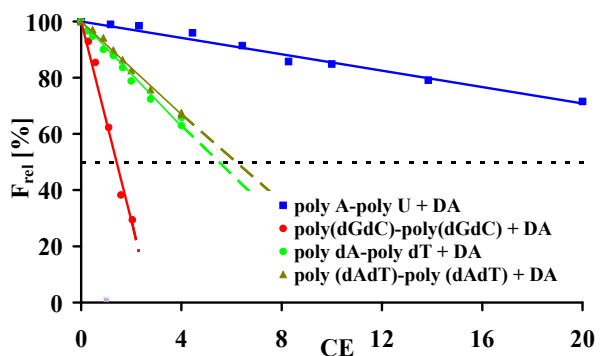
Figure 4.2e. Fluorescence titrations of DAPI with Dimer A (DA), Dimer B (DB), Monomer A (MA) and Monomer B (MB)

The buffer solution contained 20 mM sodium phosphate. The pH was adjusted to 7.00.

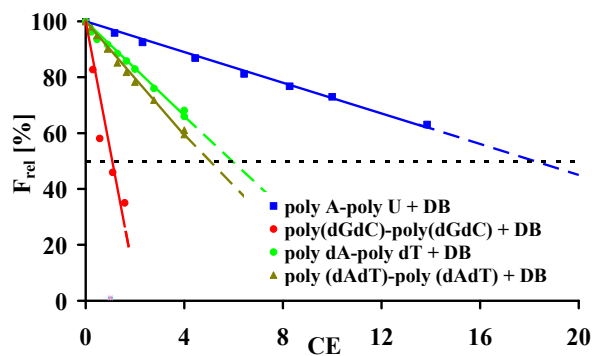
4.1.2 Ethidium Bromide Displacement Assay

4.1.2.1 Results (Figure 4.3 a-h)

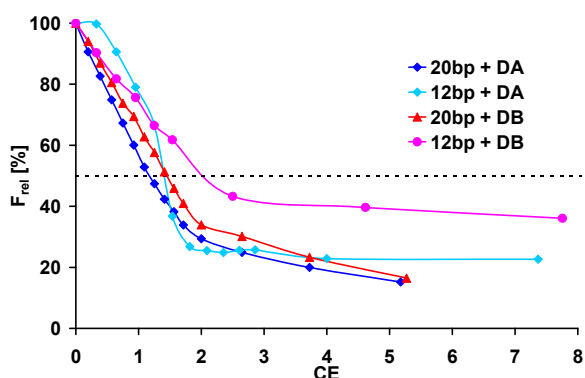
- (1). The buffer solution contained 20 mM sodium phosphate in water. pH = 7.1
- (2). The buffer solution contained 2 mM Hepes with 9.4 mM of NaCl in water. pH = 7.1
- (3). The buffer solution contained 2 mM Hepes with 9.4 mM of NaCl in methanol/water (1:1). pH = 7.1
- (4). The buffer solution contained 2 mM Hepes with 150 mM of NaCl in methanol/water (1:1). pH = 7.1



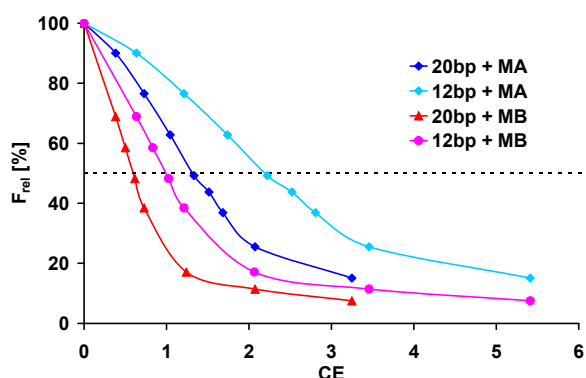
(a) H₂O buffer¹



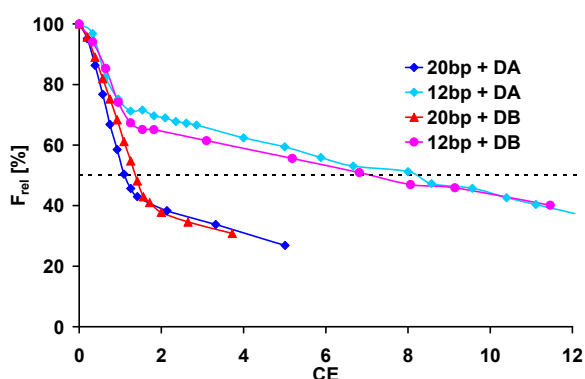
(b) H₂O buffer¹



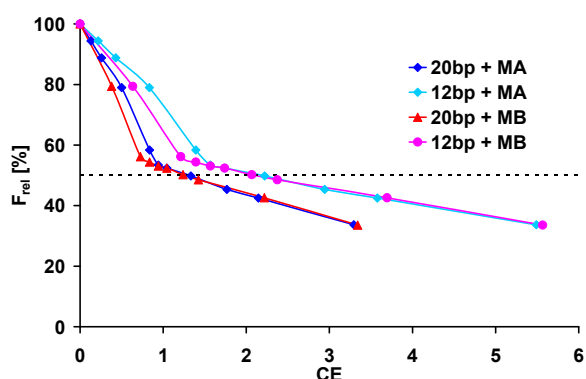
(c) H₂O buffer²



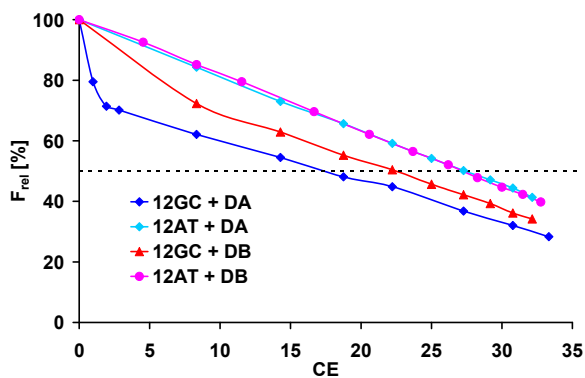
(d) H₂O buffer²



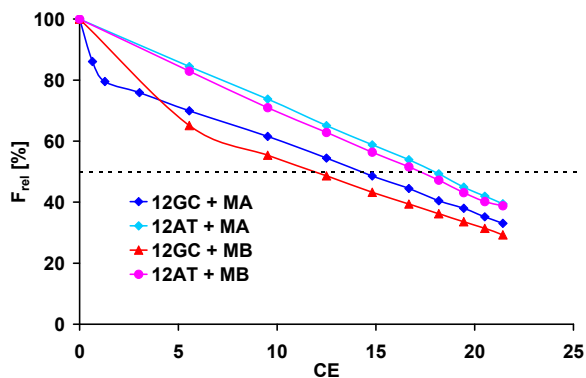
(e) MeOH:H₂O=1:1 buffer³



(f) MeOH:H₂O=1:1 buffer³



(g) MeOH:H₂O=1:1 buffer⁴



(h) MeOH:H₂O=1:1 buffer⁴

Figure 4.3 Ethidium bromide displacement curves for different nucleic acids by calixarenes

4.1.2.2 Discussion

1. Phosphate backbone binders exhibit high C_{50} and CE_{50} values. All calixarenes showed much lower C_{50} and CE_{50} values. This is the strong evidence for groove binding.

2. The bindings of calixarenes to nucleic acids can not cause entire release of EtBr, which excluded intercalation. Furthermore, each curve contains two parts: efficient displacement and weak displacement. The second part probably means that conformational changes of phosphate backbones make bound EtBr release to free solvent. Therefore, phosphate anion recognition may exist simultaneously.

3. It is important that, for polynucleotides, the best displacement was done with poly(dGdC) - poly(dGdC), followed by poly(dAdT)-poly(dAdT) and polydA-polydT, and the worst displacement was done on RNA (Figure 4.3a, 4.3b).

Table 4.3. Corresponding CE_{50} values for complexes between dimers and different polynucleotides

		poly(dGdC)- poly(dGdC)	poly (dAdT)- poly (dAdT)	poly dA- poly dT	poly A-polyU
Major Groove	Width(Å)	13.5	11.2	11.4	3.8
	shape	smooth curve	not smooth, because of the methyl group of thymine		smooth curve
CE_{50}	Dimer A	1.5	6.3	5.8	>30
	Dimer B	1.1	5.2	6.0	18.4
Minor groove	Width(Å)	9.5	6.3	3.3	10.9
	shape	not smooth, because of amino groups of guanine	smooth curve	smooth curve	smooth curve

Table 4.3 indicated that the nucleic acid with a wide and smooth major groove showed an efficient displacement (lower CE_{50} value); the nucleic acid with a narrow and rugged major groove showed a weak displacement. This characteristic implies that the accessible area for our ligands is on the major groove side.

4. Poly (dAdT) - poly (dAdT) and poly dA - poly dT have similar steric geometry of major grooves, but poly dA - poly dT contrasts itself from poly (dAdT) - poly (dAdT) in terms of a

very narrow minor groove. Table 4.3 indicated that the two different nucleic acids showed the similar CE_{50} values. It implies that changes in shape and width of the minor groove had no influence on the ligands' displacement capacity of EtBr. Thus, the minor groove binding is excluded.

4.1.3 Circular Dichroism Spectroscopy

4.1.3.1 Results (Figure 4.4 a-d)

4.1.3.2 Discussion

1. Because the calixarene monomers and dimers are achiral and hence CD silent, they could not interfere this assay by any means. Therefore, the changes of CD spectra showed the binding characteristics of calixarenes and nucleic acids.
2. In some experiments isoelliptic points were observed, strongly supporting the existence of only one type of complex geometry.
3. Addition of calixarenes invariably decreased molar ellipticities at all wavelengths of CD bands of polynucleotides. It pointed toward the decrease in helicity and the disruption of the DNA/RNA double helix, i.e. the decrease in twisting between the base pair layers, the lengthening of the DNA itself, the stiffening of the helix, and the decrease in mass per unit length.
4. It was observed that all calixarenes induced weak effects to the CD spectra (between 260nm and 300 nm) of ds-DNA, but induced the **strongest** effect to the CD spectra (between 260nm and 300 nm) of ds-RNA (poly A – poly U) (Figure 4.4 vi). Furthermore, CD maxima continuously shift during an RNA titration with calixarenes, and at the end the new CD spectrum closely resembled that of *B*-DNA.

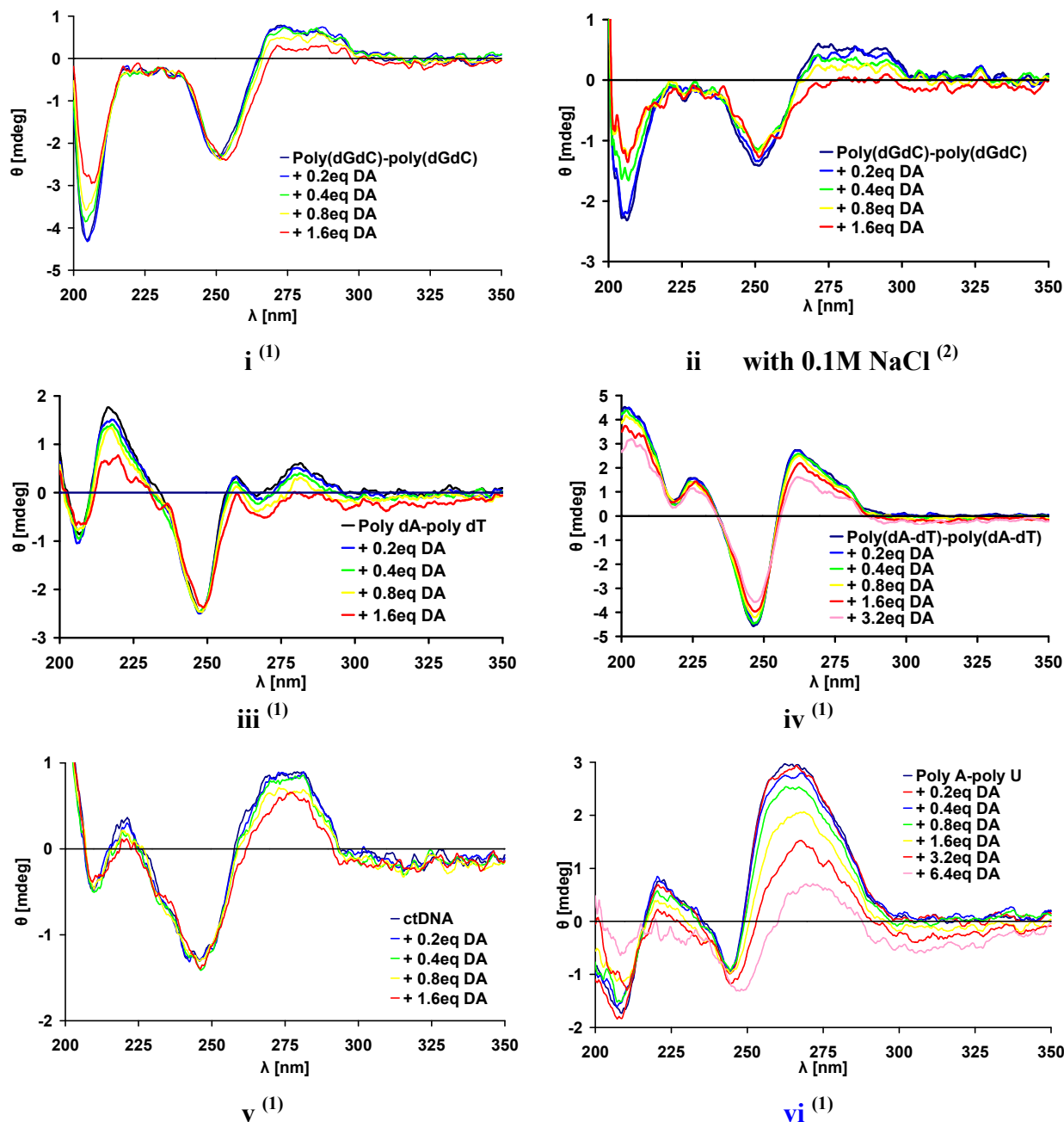


Figure 4.4 a. CD titration series for polynucleotides complexed by Dimer A (DA)

The CD spectrum between 260nm and 300 nm indicates the conformational changes of the phosphate backbone. The spectra above imply a major groove binding mode, because a superb fit into DNA's wide and shallow major groove induced a weaker effect to the phosphate backbone and an inaccessible binding to RNA's narrow and deep groove induced a stronger effect to the phosphate backbone. The deep and narrow major groove of the RNA duplex must first be widened by the calixarene to accommodate the sterically demanding calixarene guest itself [215,216,217,218].

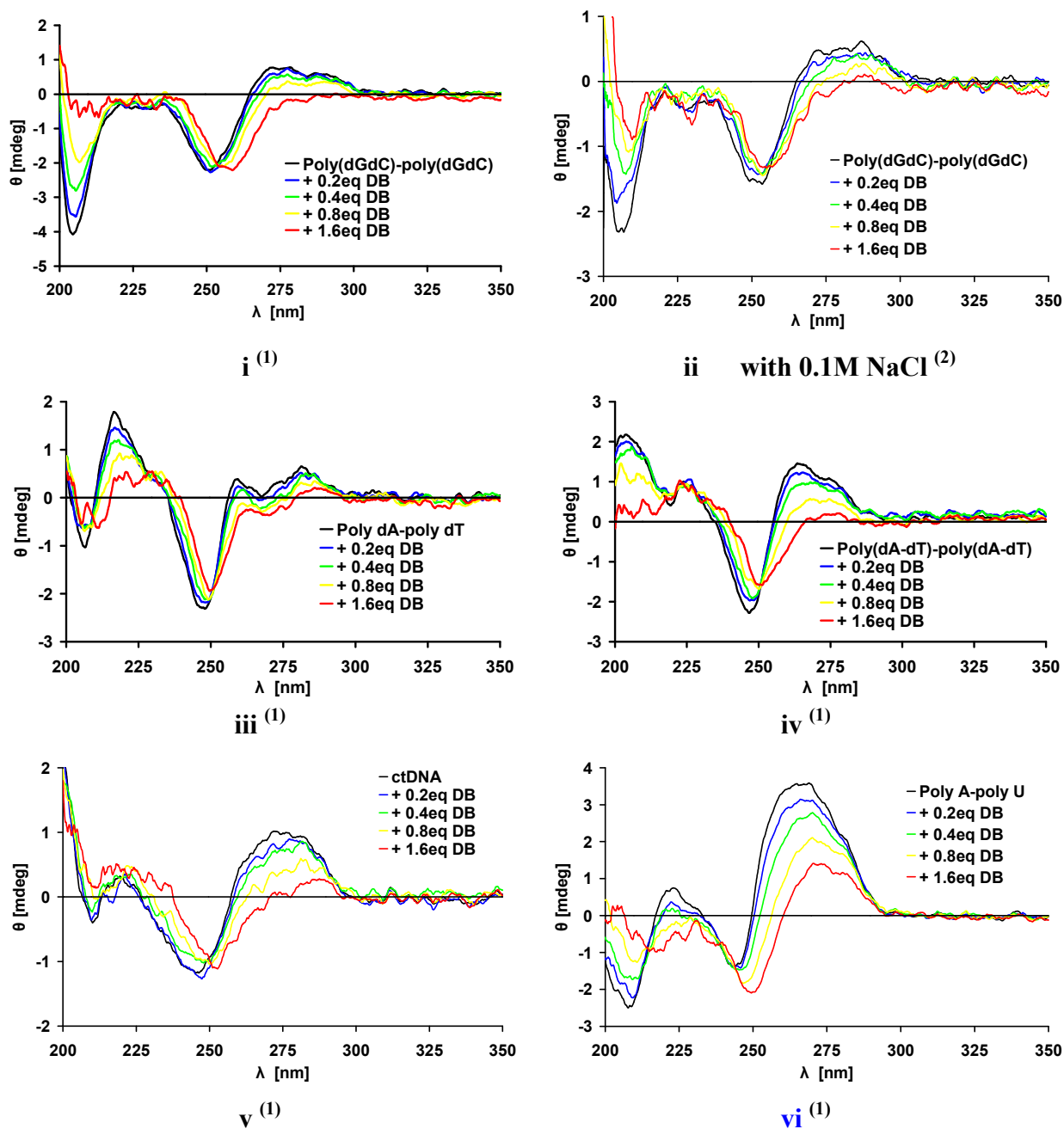


Figure 4.4 b. CD titration series for polynucleotides complexed by Dimer B (DB)

5. Amino analogues (Dimer A and Monomer A) induce significantly weaker changes in CD spectra than guanidinium analogues (Dimer B and Monomer B). That could be correlated to more possible binding interactions of the latter class of compounds.

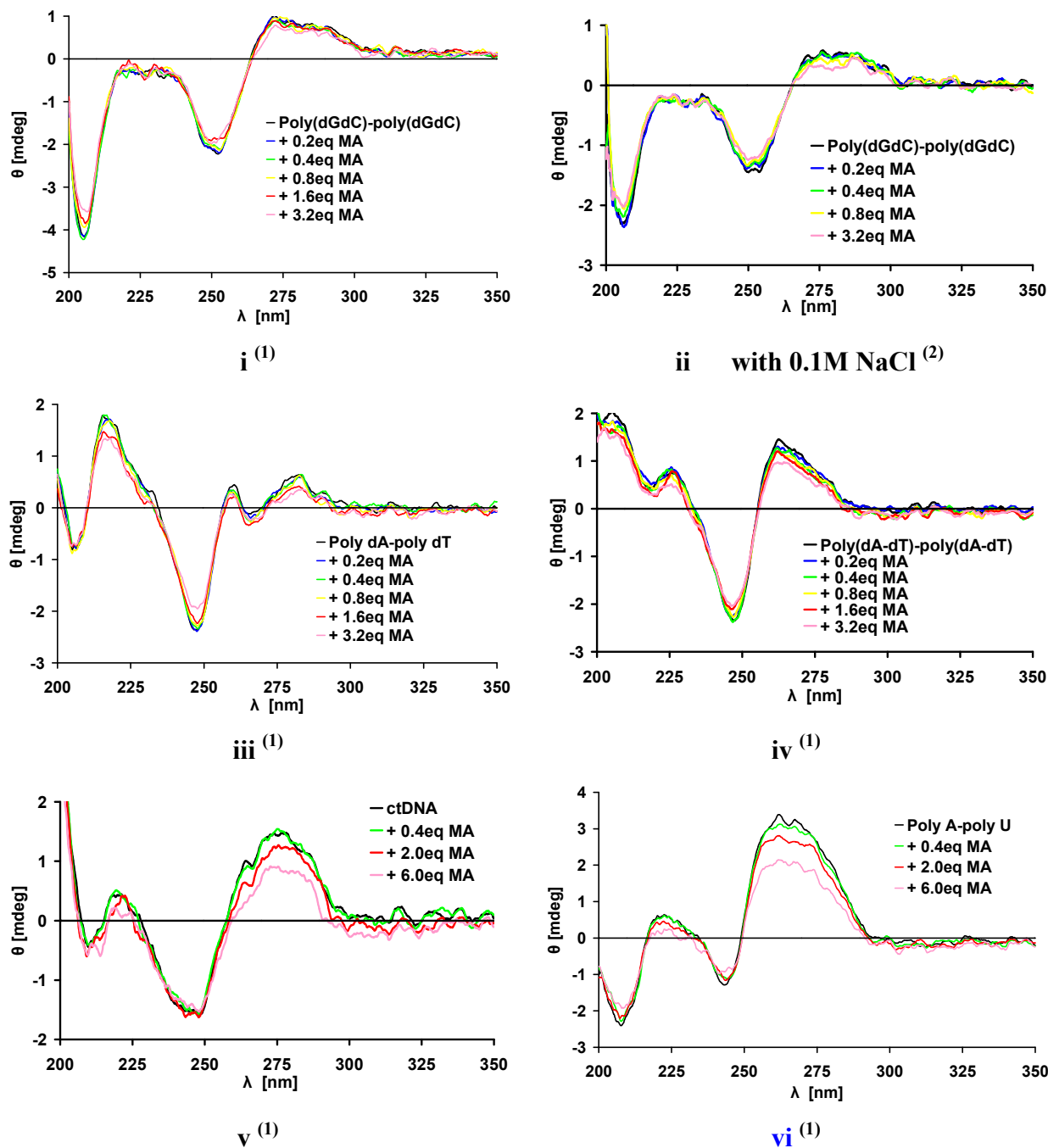


Figure 4.4 c. CD titration series for polynucleotides complexed by Monomer A (MA)

6. The increase of ionic strength (addition of 0.1M NaCl) had a little impact on the changes of poly(dGdC) – poly(dGdC) CD spectra (Figure 4.4 ii). It indicated that the interactions between calixarenes and polynucleotides are not dominated by electrostatic interactions but are more likely controlled by the hydrogen bonding pattern.

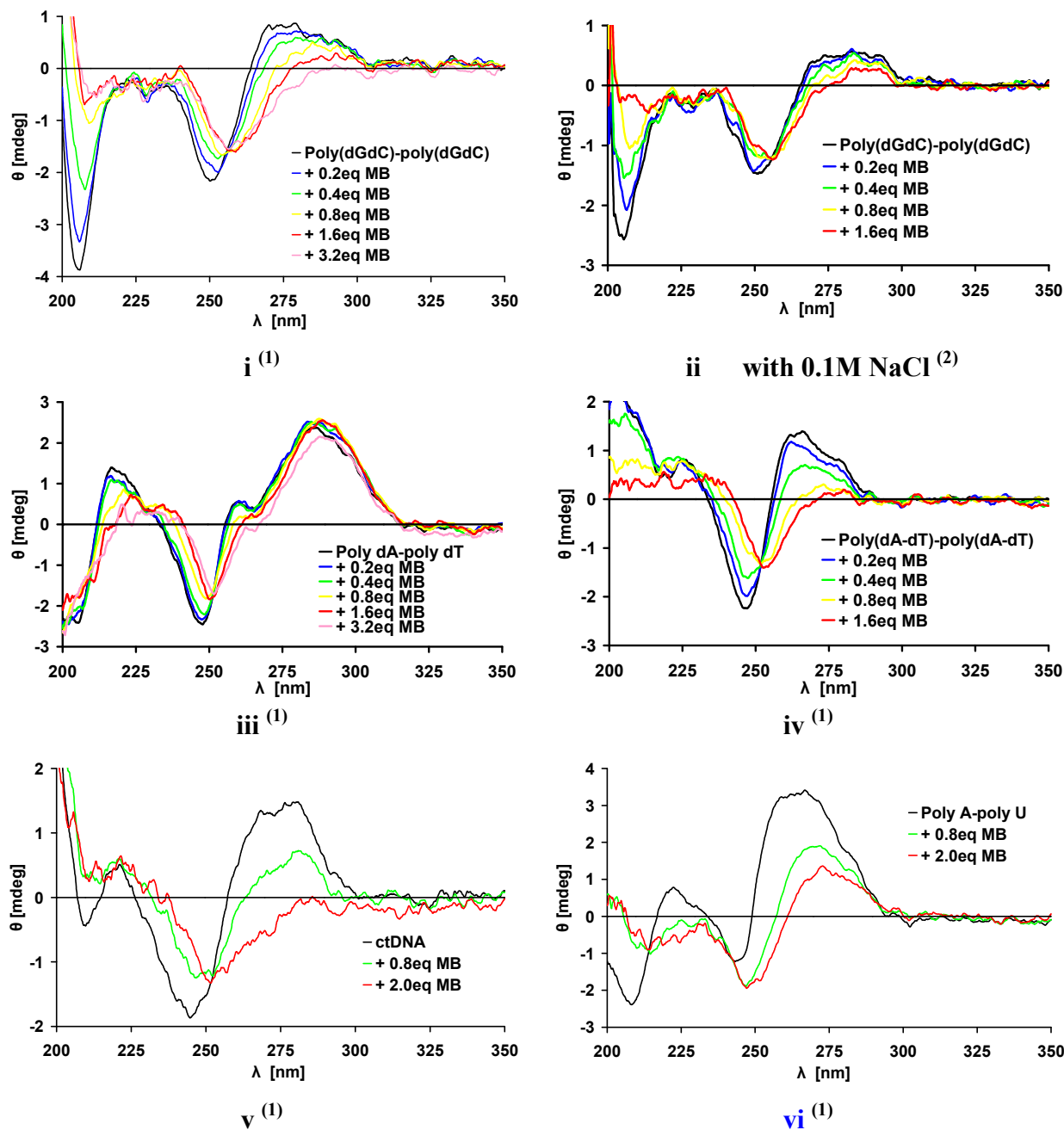


Figure 4.4 d. CD titration series for polynucleotides complexed by Monomer B (MB)

- (1). i, iii, iv, v, vi : The buffer solution contained 20 mM sodium phosphate. pH = 7.00
 (2). ii : The buffer solution contained 20 mM sodium phosphate with 0.1M NaCl in water.
 pH = 7.00

4.1.4 The Assessment of Thermal Denaturation of DNA

4.1.4.1 Results (Figure 4.5 a-d)

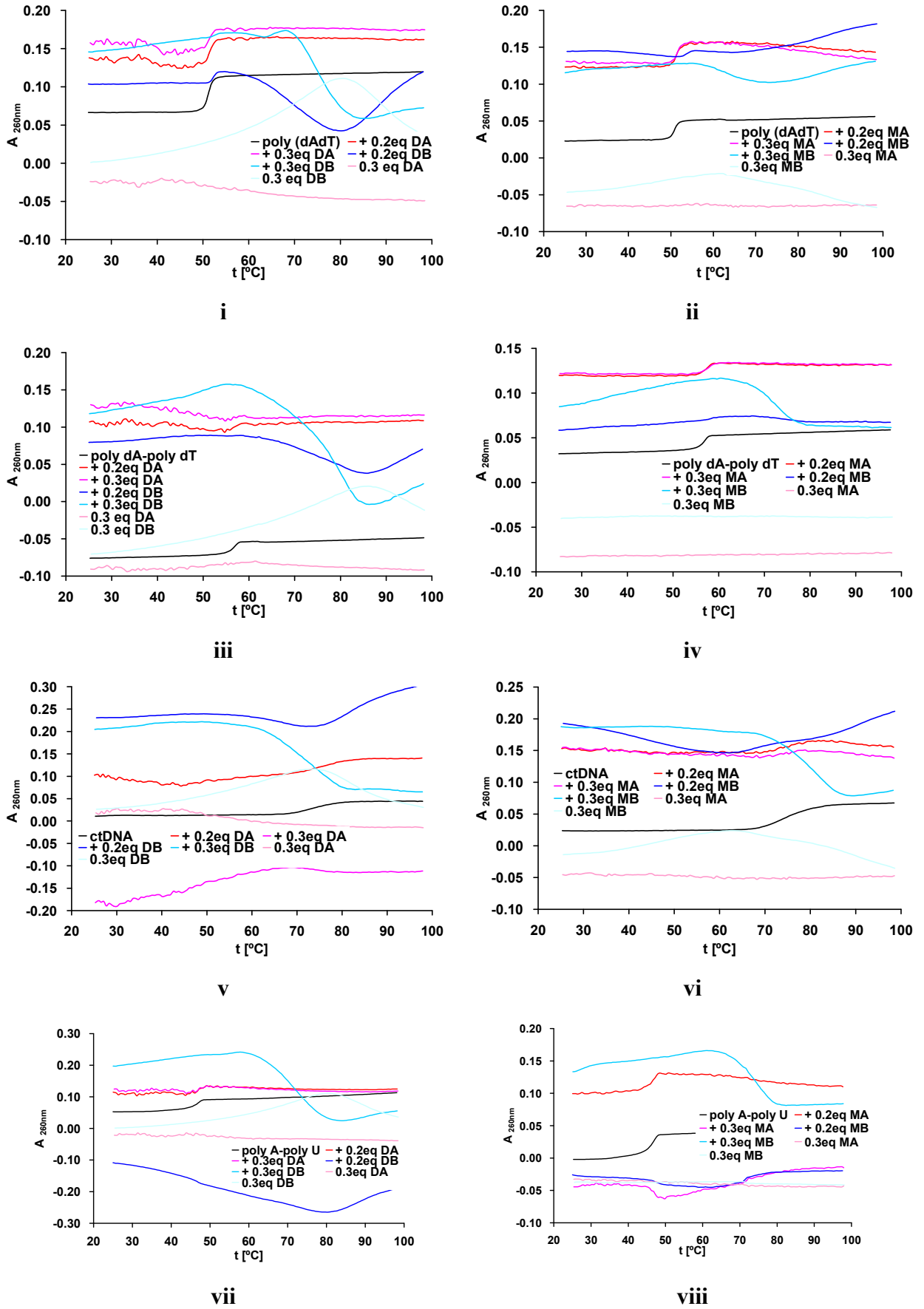


Figure 4.5a. UV-Vis melting curves for dimers and monomers with polynucleotides ¹

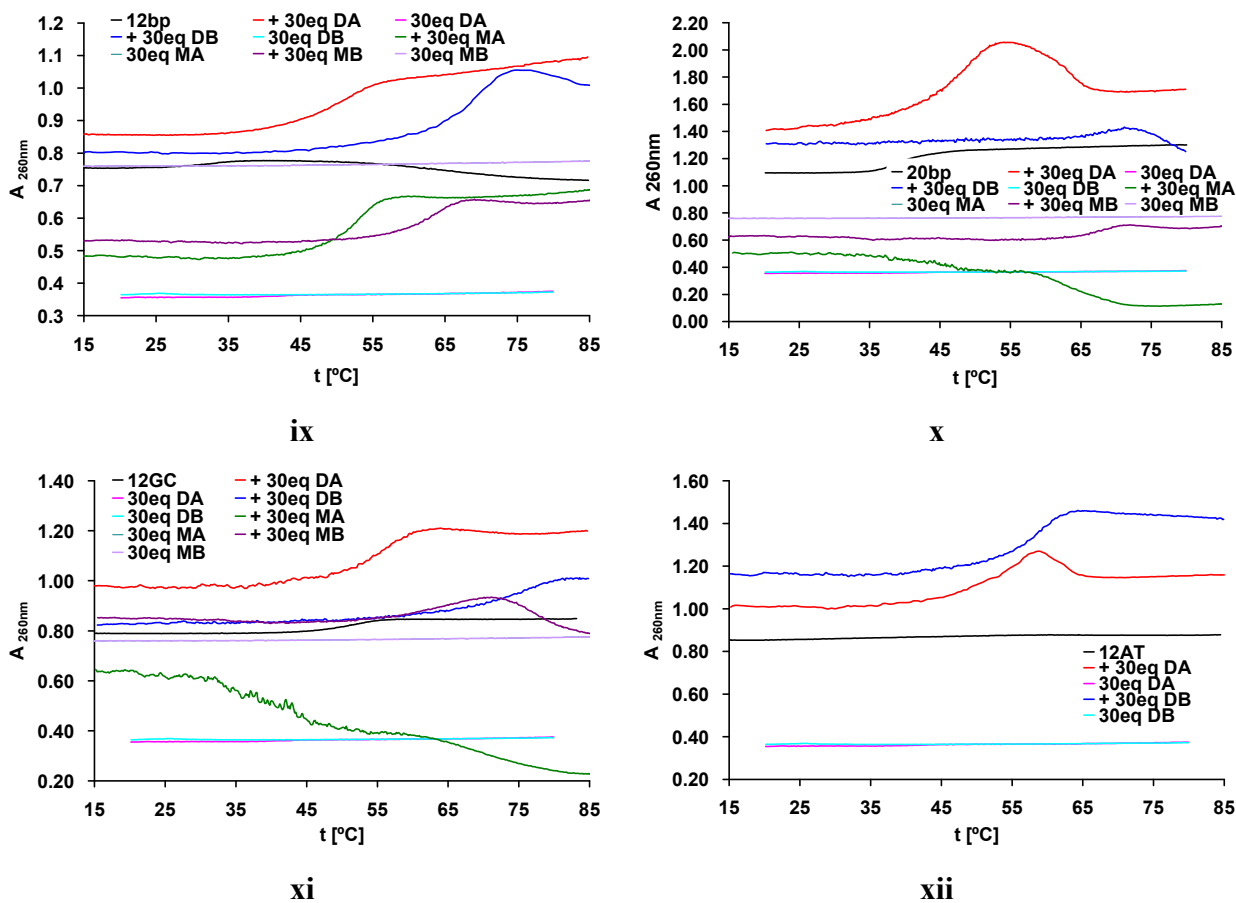


Figure 4.5b. UV-Vis melting curves for calixarenes with oligonucleotides in the H₂O buffer²

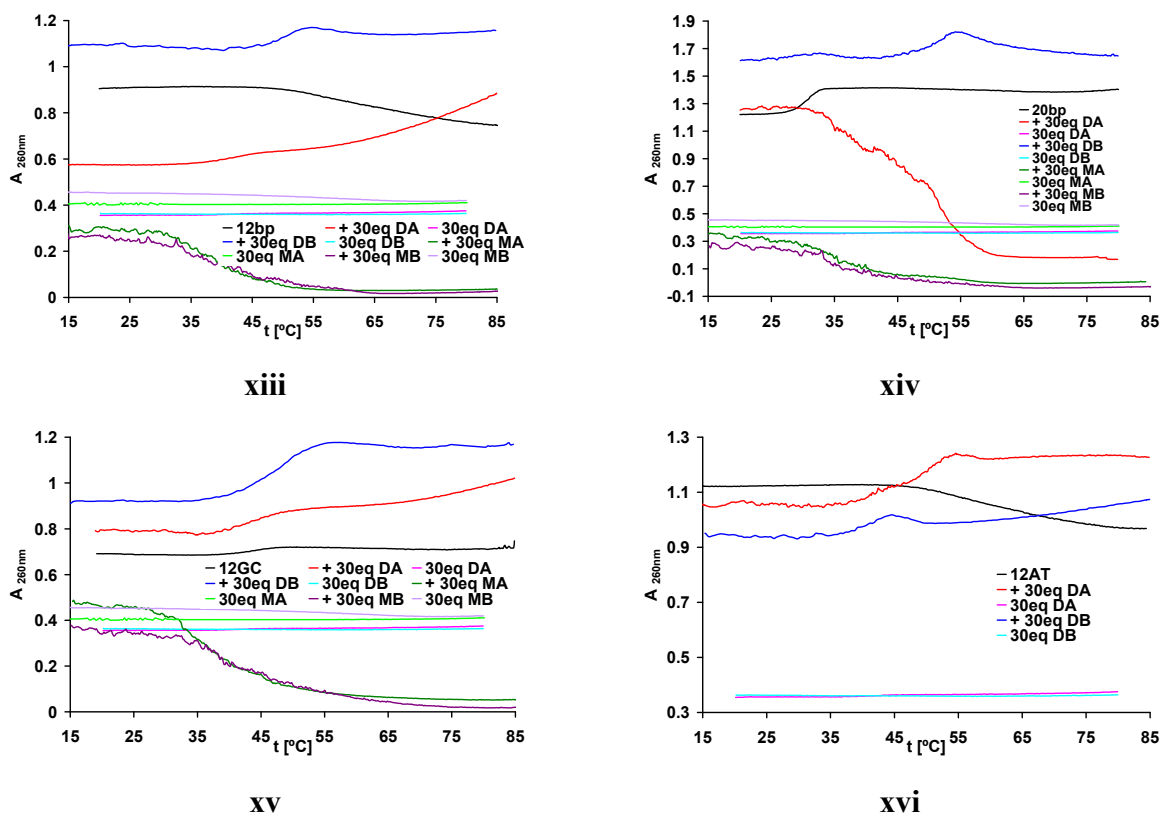


Figure 4.5c. UV-Vis melting curves for calixarenes with oligonucleotides in the MeOH/H₂O buffer³

1. The buffer solution contained 20 mM sodium phosphate. The pH was adjusted to 7.00.
2. The buffer solution contained 1 mM Hepes in water. pH = 7.1
3. The buffer solution contained 1 mM Hepes in methanol/water (1:1). pH = 7.1

4.1.4.2 Discussion

1. All studied compounds showed non-linear UV-Vis melting curves at $T > 50^{\circ}\text{C}$. It hampered the accurate experiments with nucleic acids which melt above mentioned temperatures.
2. Addition of 0.2 eq. or 0.3 eq. calixarenes (in terms of basepairs) could not stabilize polynucleotides ($\Delta T_m < 2^{\circ}\text{C}$) (Figure 4.5a). Furthermore, the hyperchromicity decreased. It means that a substantial fraction of the DNA was already dissociated into single strands prior to heating. This result is in line with the CD measurement, and indicates the decrease in helicity and the disruption of the DNA or RNA double helix.
3. For oligonucleotides (Figure 4.5b, 4.5c), addition of 30 eq. calixarenes (in terms of duplex DNA) could stabilize DNA (Table 4.4, Table 4.5). It is probably because electrostatic interactions and hydrogen bond interactions between calixarenes and oligonucleotides. There is another argument for strand end chelation.

Table 4.4. UV-vis Melting points and shifts induced by calixarenes in water ¹

Calixarenes	12 bp	dG ₁₂ -dC ₁₂	dA ₁₂ -dT ₁₂	20 bp
Dimer A	50°C (+14°C)	56°C (+08°C)	44°C (+6°C)	46°C (+11°C)
Dimer B	a	a	58°C (+20°C)	a
Monomer A	52°C (+16°C)	48°C (+0°C)	-	a
Monomer B	a	a	-	a

1. The buffer solution contained 1 mM Hepes in water. pH=7.1. In all cases 30 eq. calixarene.
 - a. UV spectra of DA, DB, MA and MB revealed decreasing extinction values with time at $T > 50^{\circ}\text{C}$, thus hampering accurate experiments with nucleotides which melt above this temperature.

Table 4.5. UV-vis Melting points and shifts induced by calixarenes in methanol/water ²

Calixarenes	12 bp	dG ₁₂ -dC ₁₂	dA ₁₂ -dT ₁₂	20 bp
Dimer A	42°C (+13°C)	44°C (+1°C)	47°C (+19°C)	47°C (+16°C)
Dimer B	50°C (+21°C)	48°C (+5°C)	42°C (+14°C)	51°C (+20°C)
Monomer A	39°C (+10°C)	39°C (-4°C)	-	35°C (+4°C)
Monomer B	39°C (+10°C)	44°C (+1°C)	-	35°C (+4°C)

2. 1 mM Hepes buffer in methanol/water (1:1), pH=7.1. In all cases 30 eq. calixarene.

4.1.5 Fluorescence Titration Experiments

4.1.5.1 Results (Table 4.6, Table 4.7)

Table 4.6 Association constants between various DNA/RNA strands and calixarenes ¹

	DNA/RNA	(dGdC) ₁₀ -(dGdC) ₁₀	(dAdT) ₁₀ -(dAdT) ₁₀	A ₂₀ - U ₂₀	12 bp	dG ₁₂ -dC ₁₂	dA ₁₂ -dT ₁₂	A ₁₂ -U ₁₂
DA²	K_a(M⁻¹)³	1.4 e+6	5.6 e+5	1.7 e+5	5.7 e+6	7.3 e+6	5.9 e+7	1.4 e+7
	Statistical error	23%	24%	22%	31%	30%	32%	22%
	Stoichiometry ⁴	11:1	10:1	23:1	10:1	5:1	9:1	41:1
	No. of data ⁵	No.1	No.2	No.3	No.15	No.16	No.17	No.18
DB	K_a(M⁻¹)	4.7 e+6	2.3 e+6	7.8 e+5	9.0 e+5	5.0 e+5	1.4 e+7	3.2 e+6
	Statistical error	22%	24%	8%	31%	39%	32%	24%
	Stoichiometry	12:1	14:1	15:1	23:1	7:1	11:1	13:1
	No. of data	No.4	No.5	No.6	No.19	No.20	No.21	No.22
MA	K_a(M⁻¹)	7.7 e+6	2.9 e+6	3.1 e+6	6.3 e+6	1.0 e+7	1.5 e+7	9.5 e+7
	Statistical error	25%	20%	24%	19%	15%	20%	10%
	Stoichiometry	10:1	30:1	10:1	4:1	14:1	18:1	3:1
	No. of data	No.7	No.8	No.9	No.23	No.24	No.25	No.26
MB	K_a(M⁻¹)	1.4 e+6	7.3 e+6	3.5 e+5	7.4 e+4	2.3 e+6	1.3 e+4	1.2 e+6
	Statistical error	18%	23%	18%	24%	35%	28%	25%
	Stoichiometry	24:1	12:1	23:1	78:1	61:1	67:1	90:1
	No. of data	No.10	No.11	No.12	No.27	No.28	No.29	No.30

1. The buffer solution contained 2 mM Hepes with 150 mM NaCl in water. pH = 7.1
2. DA: Dimer A, DB: Dimer B, MA: Monomer A, MB: Monomer B
3. 1.4 e+6 represents 1.4×10^6 .
3. Stoichiometry: [Guest] / [DNA duplex]
5. The fluorescence titration data were provided in Chapter 6.5.

Table 4.7 Association constants between various DNA/RNA strands and calixarenes⁶

	DNA/RNA	12 bp	dG ₁₂ -dC ₁₂	dA ₁₂ -dT ₁₂	A ₁₂ -U ₁₂
DA²	K_a(M⁻¹)	3.5 e+7	1.5 e+7	5.9 e+6	9.0 e+7
	Statistical error	15%	17%	4%	44%
	Stoichiometry	9:1	2:1	10:1	5:1
	No. of data ³	No.31	No.32	No.33	No.34
DB	K_a(M⁻¹)	9.1 e+6	3.1 e+6	1.0 e+7	1.2 e+7
	Statistical error	31%	9%	18%	11%
	Stoichiometry	11:1	2:1	12:1	6:1
	No. of data	No.35	No.36	No.37	No.38
MA	K_a(M⁻¹)	sigmoidal	×	×	×
	Statistical error				
	Stoichiometry				
	No. of data				
MB	K_a(M⁻¹)	sigmoidal	×	×	×
	Statistical error				
	Stoichiometry				
	No. of data				

6. The buffer solution contained 2 mM Hepes with 150 mM NaCl in MeOH/H₂O (1:1). pH = 7.1

4.1.5.2 Discussion

1. The titration of fluorescence-labeled nucleic acids with the calixarenes reveals strong binding. Compared with previous results^[120,131], benzyl series often display superior affinities over the anilino series (about 100 times).

2. For Dimer A and Dimer B, K_a values: $(dGdC)_{10}-(dGdC)_{10} > (dAdT)_{10}-(dAdT)_{10} > A_{20}-U_{20}$ (RNA), $dA_{12}-dT_{12} > A_{12}-U_{12}$ (RNA). It indicates that the nucleic acid with a wide and smooth major groove showed a higher binding affinity; the nucleic acid with a narrow and rugged major groove showed a lower binding affinity. Similar to EtBr displacement assays, this characteristic implies that the accessible area for our ligands is on the major groove side.

3. Obviously, the linear alignment of dimer molecules inside the major groove would produce much lower stoichiometries (the dimer : basepair $\approx 1 : 6$), but the stoichiometry values (the dimer : basepair) are about $0.6 : 1$. It indicates that the calixarene dimer with higher charges tends to form self-aggregate inside DNA's major groove, presumably with favorable van der Waals contacts between their butoxy tails and nonpolar arene faces.

4. With the increase of DNA length, affinities for each calixarene unit decreased. It pointed to a potential clamping effect on the loose strand ends.

4.2 Sequence-Specific Major Groove Recognition with Dimer C

4.2.1 Ethidium Bromide Displacement Assay and Fluorescence Titrations

4.2.1.1 Results (EtBr Displacement Assay: Figure 4.6, Fluorescence Titration: Table 4.8-4.9)

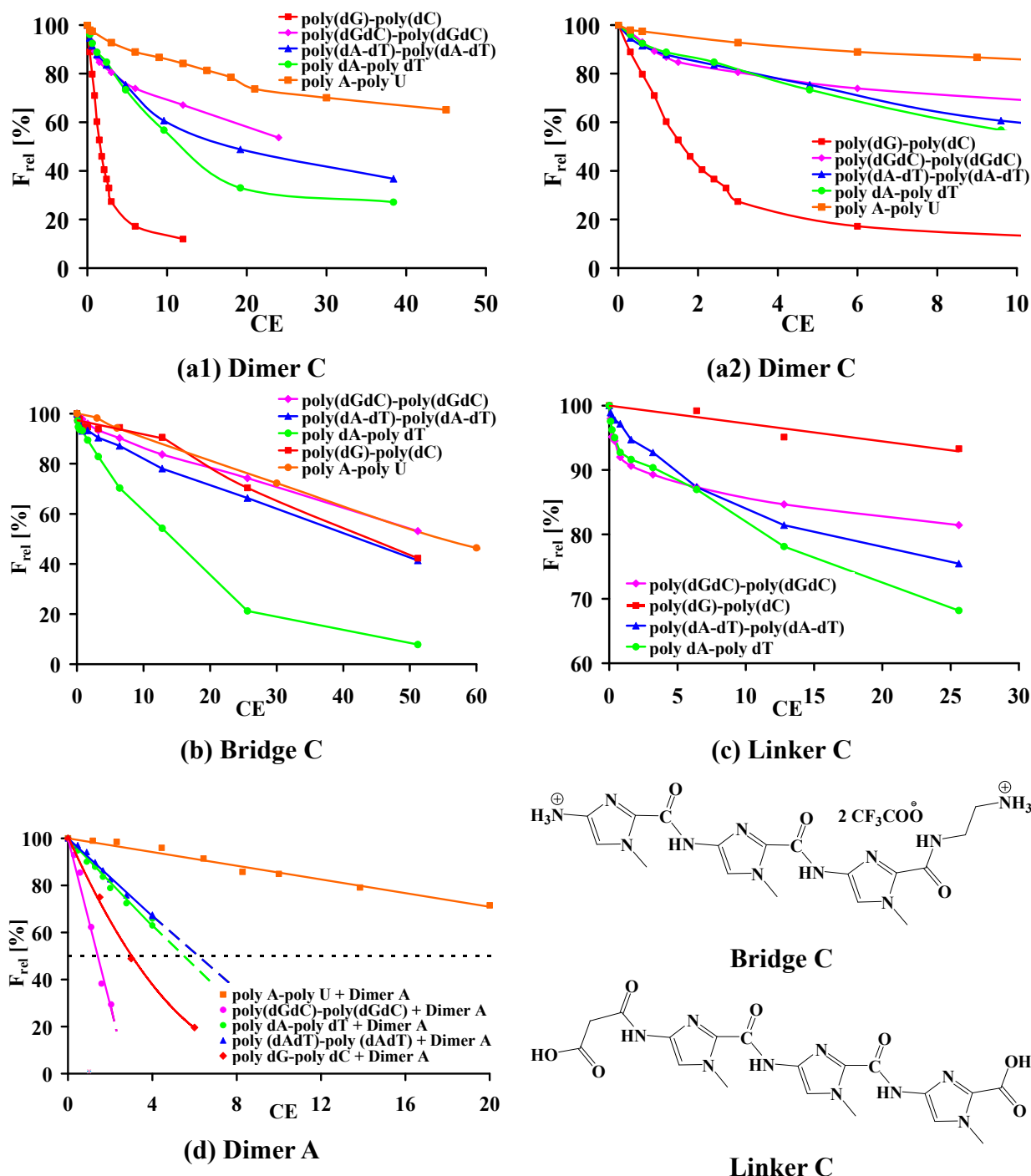


Figure 4.6 Ethidium bromide displacement curves for different nucleic acids by Dimer C (a1 and a2), Bridge C (b), Linker C (c) and Dimer A (d)

(1). The buffer solution contained 20 mM sodium phosphate. The pH was adjusted to 7.00.

Table 4.8 Association constants between various DNA strands and calixarenes / Bridge C ¹

	DNA/RNA	dG ₂₀ -dC ₂₀	(dGdC) ₁₀ - (dGdC) ₁₀	dA ₂₀ -dT ₂₀	(dAdT) ₁₀ - (dAdT) ₁₀
Dimer C	K_a(M⁻¹)²	3.7 e+7	6.4 e+5	4.8 e+5	1.2 e+7
	Statistical error	36%	7%	30%	38%
	Stoichiometry ³	15:1	24:1	10:1	14:1
	No. of data ⁴	No. 41	No. 39	No. 42	No. 40
Dimer A	K_a(M⁻¹)	1.5 e+6	1.4 e+6	1.1 e+6	5.6 e+5
	Statistical error	29%	23%	27%	24%
	Stoichiometry	28:1	11:1	29:1	10:1
	No. of data	No. 43	No.1	No. 44	No.2
Monomer A	K_a(M⁻¹)	×	7.7 e+6	×	2.9 e+6
	Statistical error		25%		20%
	Stoichiometry		10:1		30:1
	No. of data		No.7		No.8
Bridge C	K_a(M⁻¹)	The change of the fluorescence emission intensity was little.	1.1 e+5	3.8 e+4	3.3 e+4
	Statistical error		23%	7%	10%
	Stoichiometry		192:1	60:1	136:1
	No. of data		No. 49	No. 51	No. 50

1. The buffer solution contained 2 mM Hepes with 150 mM NaCl in water. pH = 7.1
2. 3.7 e+7 represents 3.7×10⁷.
3. Stoichiometry: [Guest] / [DNA duplex]
4. The fluorescence titration data were provided in Chapter 6.5.

Table 4.9 Association constants between various DNA strands and Dimer C ⁵

	DNA/RNA	dG ₂₀ -dC ₂₀	(dGdC) ₁₀ - (dGdC) ₁₀	dA ₂₀ -dT ₂₀	(dAdT) ₁₀ - (dAdT) ₁₀
Dimer C	K_a(M⁻¹)²	1.8 e+7	1.0 e+6	2.3 e+6	2.3 e+7
	Statistical error	29%	21%	24%	36%
	Stoichiometry ³	36:1	55:1	33:1	39:1
	No. of data ⁴	No. 47	No. 45	No. 48	No. 46

5. The buffer solution contained 20 mM sodium phosphate. The pH was adjusted to 7.00.

4.2.1.2 Discussion

1. Compared with Dimer A, Bridge C and Linker C showed higher CE_{50} values and lower association constants for all nucleic acids. Both experiments indicated that benzyl series calixarenes could drive the triimidazole bridge (probably a minor groove binder) to the major groove of DNA.

2. For Dimer C, the best displacement was done with polydG-polydC, followed by polydA-polydT, poly(dAdT)-poly(dAdT) and poly(dGdC)-poly(dGdC), and the worst displacement was done on RNA. In addition, K_a values: $dG_{20}-dC_{20} > (dAdT)_{10}-(dAdT)_{10} > dA_{20}-dT_{20}$. Figure 4.6a1 and Table 4.8 indicated that the nucleic acid with a wide and smooth major groove showed an efficient displacement (lower CE_{50} value) and high affinity; the nucleic acid with a narrow and rugged major groove showed a weak displacement and low affinity. These characteristics imply that the accessible area for Dimer C is on the major groove side. We interpret these results as compelling argument for the postulated major groove binding mechanism of Dimer C.

3. Obviously, the linear alignment of Dimer C inside the major groove would produce much lower stoichiometries (the dimer : basepair $\approx 1 : 6$), but stoichiometry values (the dimer : basepair) are about 0.8 : 1. It indicates that the Dimer C tends to form self-aggregate inside DNA's major groove, presumably with favorable van-der-Waals contacts between their butoxy tails and nonpolar arene faces.

4. Both experiments also indicated that Dimer C, which contained a triimidazole bridge, showed stronger preference for one specific DNA duplex: polydG-polydC. The specificity originates from the triimidazole bridge, and is also related to the special properties of the major groove of polydG-polydC:

(1). PolydG-polydC is similar to *A*-form. It has a wider minor groove (9.5Å) and a narrower major groove (8.1Å) (Table 1.3). The triimidazole bridge, which is slim, can fit into this narrow major groove superbly.

(2). The major groove of polydG-polydC can be approximated by a single smooth curve,

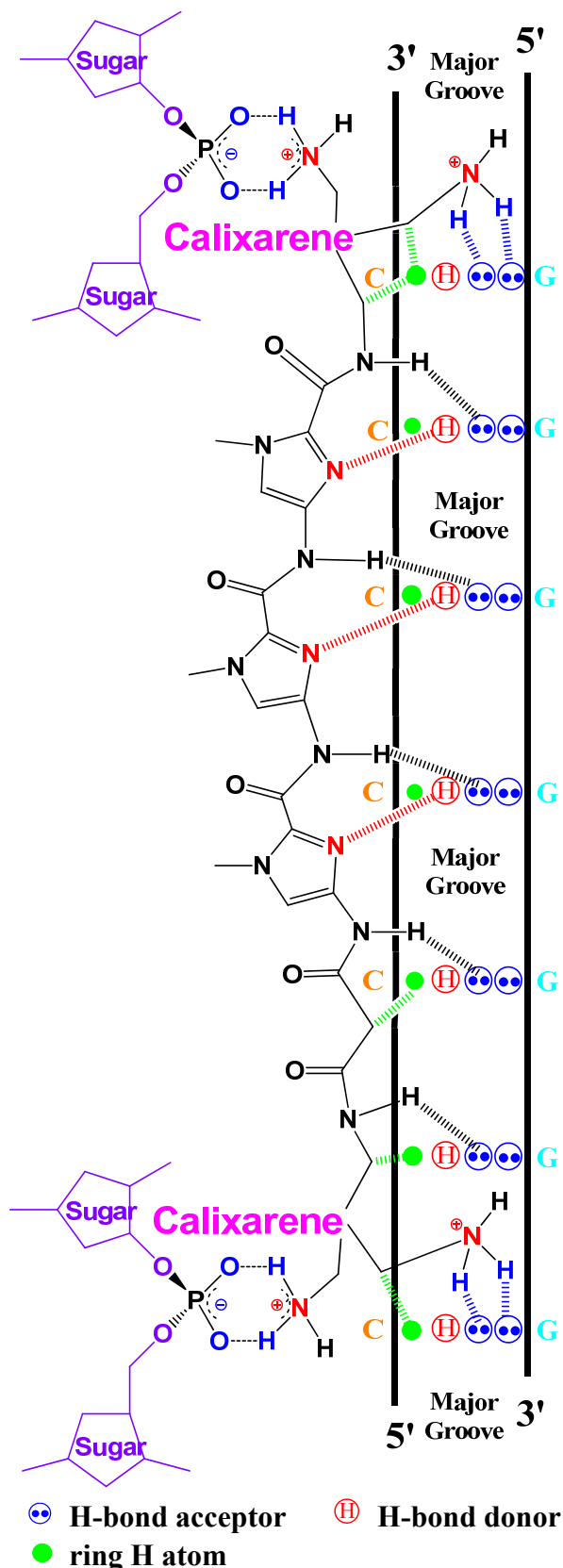


Figure 4.6a. A Proposed binding mechanism of Dimer C and polydG-polydC

which allow favorable van der Waals contacts between Dimer C and the functional groups of nucleobases. Whereas, A:T-rich sequences produce steric hindrance within the major groove by the presence of the methyl group of thymine, which affect the groove geometry. This prevents Dimer C from attaining the multiple close contacts with the floor in A:T sequences that are possible in G:C regions.

(3). In the major groove, G:C base pairs [C-4-NH₂ (δ^+), G-6-CO (δ^-), and G-N7 (δ^-)] have a larger electrostatic potential gradient than T:A base pairs [T-4-CO (δ^-), A-6-NH₂ (δ^+), and A-N7(δ^-)]. In addition, the nearest-neighbor interaction of polydG-polydC base pairs reinforces the intrinsic base pair potentials. For polydG-polydC, one side of the major groove is negative, and the other side is positive. The calixarene unit of Dimer C can carry cationic charges to complement the negative potential, and the nitrogen of the triimidazole bridge offers lone pair electrons to recognize the positive potential. Therefore, the electrostatic potential properties of this major groove lead to excellent recognition by Dimer C.

By contrast, in major grooves, poly(dGdC)-poly(dGdC) has more neutral areas than does

polydG-polydC because the neighboring base pair potentials $\mp\pm\pm$ somewhat cancel each other, and T:A base pairs also have more neutral areas than does polydG-polydC. The unfavorable electrostatic potentials lead to their poor recognitions by Dimer C.

5. Compared with Dimer A, Dimer C showed much higher CE_{50} values for polydA-polydT, poly(dAdT)-poly(dAdT) and poly(dGdC)-poly(dGdC), and lower association constants for dA₂₀-dT₂₀ and (dGdC)₁₀-(dGdC)₁₀. It indicated that Dimer C frequently showed reduced affinities to other DNA duplexes. The reduced affinities probably originate from the triimidazole bridge. Because the major groove of *B*-form DNA is wide, the slim triimidazole bridge will not produce extensive close van der Waals contacts with the floor of a wide major groove, and the whole ligand itself shows orientational disorder. Another explanation is the unfavorable electrostatic potentials, because these DNA duplexes have more neutral areas in major grooves than does poly dG - poly dC.

6. For Dimer C, with the increase of ionic strength (addition of 150 mM NaCl), the binding affinities decreased about 2-3 times (table 4.8, table 4.9). The ionic strength had a little impact on the binding affinities. It indicated that the interactions between Dimer C and DNA are not dominated by electrostatic interactions but are more likely controlled by the hydrogen bonding pattern.

4.2.2 Circular Dichroism Spectroscopy

4.2.2.1 Results (Figure 4.7)

4.2.2.2 Discussion

1. It was observed that Dimer C induced very weak effects to the CD spectra (between 260nm and 300 nm) of poly(dGdC)-poly(dGdC), poly(dAdT)-poly(dAdT) and polydA-polydT, but induced stronger effects to the CD spectra of poly dG – poly d C (*A*-form DNA) and poly A – poly U (*A*-form RNA).

The CD spectrum between 260nm and 300 nm indicates the conformational changes of the

phosphate backbone. These spectra imply a major groove binding mode, because a superb fit into DNA's wide and shallow major groove induced a weaker effect to the phosphate backbone and an inaccessible binding to RNA's narrow and deep groove induced a stronger effect to the phosphate backbone. The deep and narrow major groove of the RNA duplex must first be widened by Dimer C to accommodate the sterically demanding calixarene guest itself [219,220,221,222].

2. Addition of Dimer C invariably decreased molar ellipticities at all wavelengths of CD bands of polynucleotides. It pointed toward the decrease in helicity and the disruption of the DNA/RNA double helix.

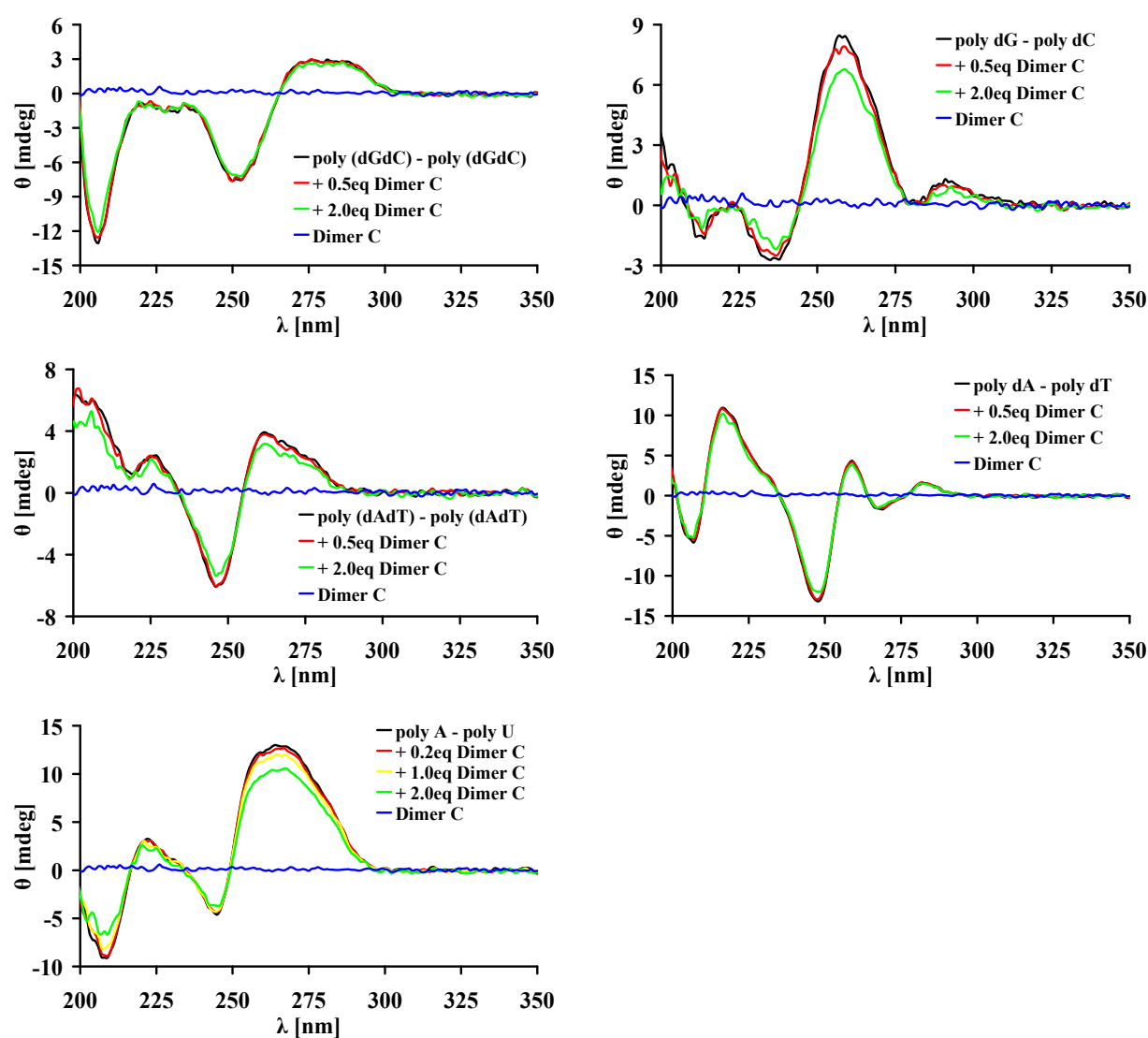


Figure 4.7 CD titration series for polynucleotides complexed by Dimer C

The buffer solution contained 20 mM sodium phosphate. The pH was adjusted to 7.00.

4.2.3 The Assessment of Thermal Denaturation of DNA

4.2.3.1 Results (Figure 4.8)

4.2.2.3 Discussion

1. Addition of 0.2 eq. – 1.6 eq. Dimer C (in terms of basepairs) could not stabilize both polynucleotides and oligonucleotides ($\Delta T_m < 2\text{ }^\circ\text{C}$) (Figure 4.8).

2. With the increase of the concentration of Dimer C, the hyperchromicity decreased. It indicates that the binding of Dimer C to the nucleic acid duplex is very strong, and it also means that a substantial fraction of the DNA was already dissociated into single strands prior to heating. This result is in line with the CD measurements, and indicates the decrease in helicity and the disruption of the nucleic acid double helix.

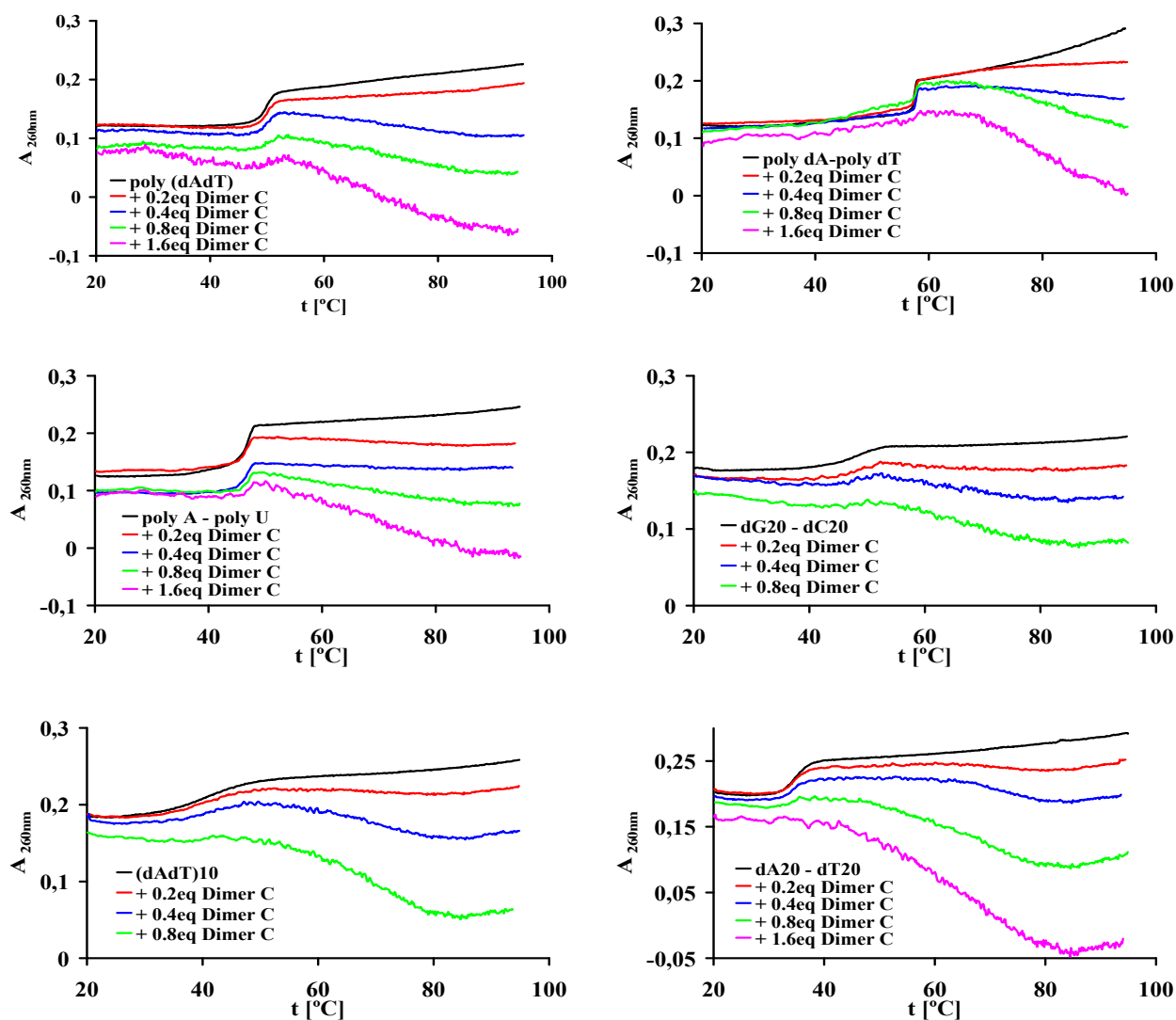


Figure 4.8 UV-Vis melting curves for Dimer C with nucleic acids

The buffer solution contained 20 mM sodium phosphate. The pH was adjusted to 7.00.

4.2.4 NMR Spectroscopy

The advancement of NMR instrumentation and methodology has made solution NMR spectroscopy an increasingly powerful tool for investigations of biomolecular structure and dynamics under physiological conditions, and also allows for studies of ligand binding and reaction mechanisms in solution ^[223]. However, the inherent sensitivity limitation of NMR requires the complex samples of biomolecules and ligands to be stable at high concentrations (> 50 μ M for structural studies) for an extended period (typically over a couple of days). Unfortunately, in my work, the DNA-calixarene complex has low solubility in any H₂O buffer solution. Therefore, it is impossible to investigate the NMR signals of any complex.

For NMR experiments, the Dickerson dodecamer d(CGCGAATTCGCG) was used. NMR samples for observation of the imino proton spectrum were prepared by dissolving 0.12 μ mol DNA in 0.6 ml H₂O buffer consisting of 20 mM sodium phosphate (pH = 7.0, Fluka, Product Number: 82591). The samples were lyophilized to dryness and redissolved in 0.6 ml of the mixture (H₂O : DMSO-*d*6 = 80 : 20). The assignment of protons and phosphates can be found in the references ^[182, 183, 184].



In figure 4.8b, it was observed that with the addition of Dimer C, the NMR signals of the Dickerson dodecamer became weaker and weaker. In addition, the signals of Dimer C can not be found. It was also observed that precipitations of the DNA-Dimer C complex formed in NMR tubes (in figure 4.8c). These figures indicated that the solubility of the DNA-Dimer C complex was too low to be investigated by NMR spectroscopy.

Figure 4.8 c

In my work, preparation of a concentrated and stable DNA-Dimer complex sample was a difficult task. In my opinion, there are three reasons. (1). The dimers (Dimer A, Dimer B and Dimer C) aggregate at higher concentrations in any H₂O buffer solution at r.t. (2). The DNA-Dimer complex formed precipitations at higher concentrations in any buffer solution. (3). Probably, the DNA-Dimer complex is sometimes subject to spontaneous degradation. Thus, preparation of well-behaved, non-aggregated samples at sufficiently high concentrations remains a serious challenge for structural and dynamic studies by NMR in our work.

[DNA] : [Dimer C]

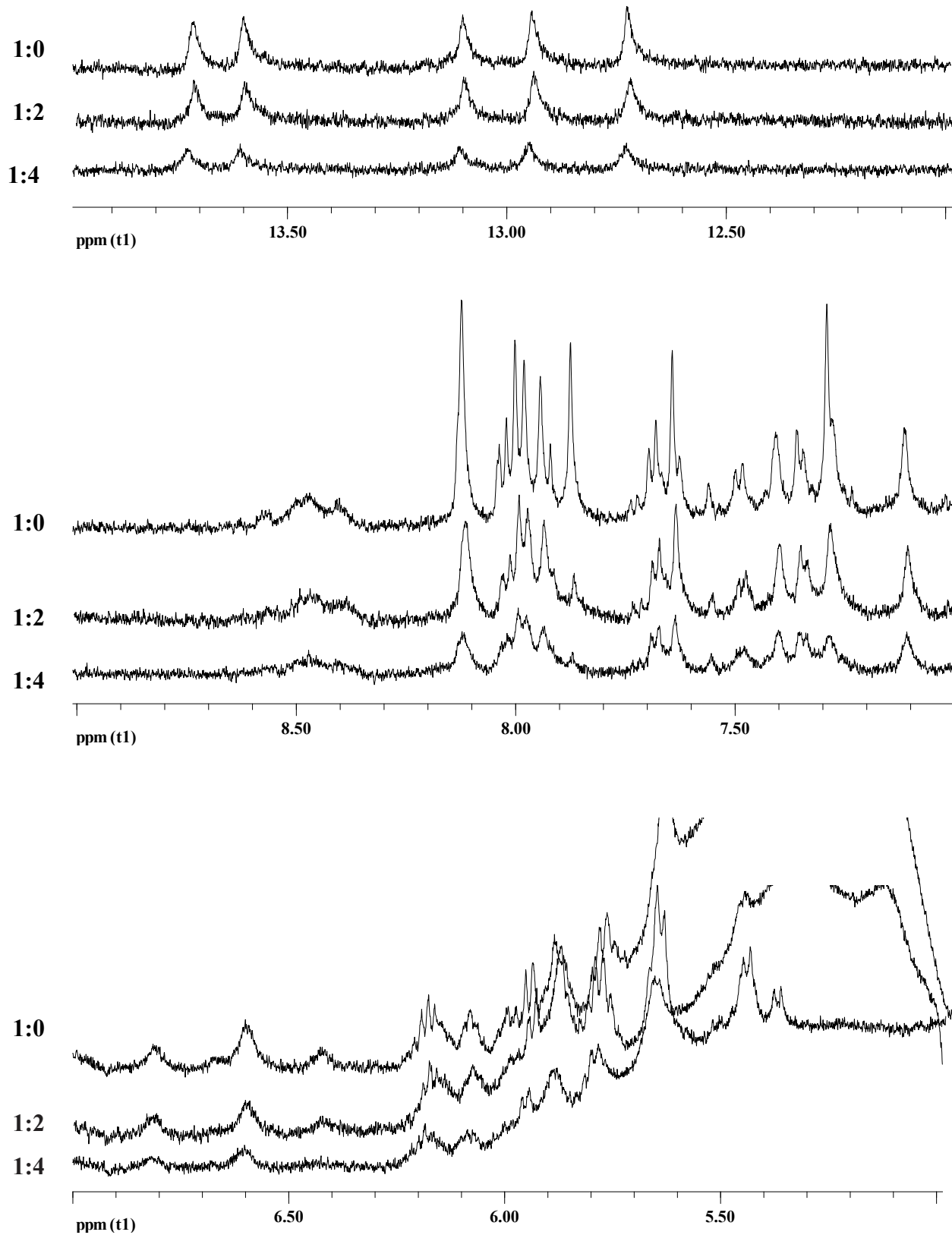


Figure 4.8b. ¹H-NMR spectra (500 MHz, 25 °C)

I declare that the proliferation experiments were performed by Marijeta Kralj, Lidija Šuman, and Ivo Piantanida in the Laboratory of Experimental Therapy, Division of Molecular Medicine, Ruđer Bošković Institute, Bijenička 54, 10000 Zagreb, Croatia. In this part, I only synthesized and purified the following studied molecules: Dimer A, Dimer B, Monomer A and Monomer B.

4.3 Antiproliferative Effects of Various Calixarenes *in vitro*

In order to investigate the effects of these calixarenes on proliferation of living cells, four different human tumor cell lines were cultivated: MCF-7 (breast carcinoma), SW 620 (colon carcinoma), HCT 116 (colon carcinoma) and H 460 (lung carcinoma). After 72 hours of incubation, the cell growth rate was evaluated by performing the MTT assay, which detects the dehydrogenase activity in viable cells. The MTT cell proliferation assay measures the reduction of a tetrazolium component (MTT) into an insoluble formazan product by the mitochondria of viable cells. The insoluble formazan product was dissolved in DMSO, and quantified by microplate readers at 570 nm. The absorbance is directly proportional to the cell viability. PG value (the percentage of growth) is used to evaluate the cell viability.

$$(1). \text{ If } \text{mean OD}_{\text{test}} - \text{mean OD}_{\text{tzero}} \geq 0 \quad \text{PG} = \frac{100 \times (\text{mean OD}_{\text{test}} - \text{mean OD}_{\text{tzero}})}{\text{mean OD}_{\text{ctrl}} - \text{mean OD}_{\text{tzero}}}$$

$$(2). \text{ If } \text{mean OD}_{\text{test}} - \text{mean OD}_{\text{tzero}} < 0 \quad \text{PG} = \frac{100 \times (\text{mean OD}_{\text{test}} - \text{mean OD}_{\text{tzero}})}{\text{mean OD}_{\text{tzero}}}$$

Mean OD_{tzero} = the average of optical density measurements before exposure of cells to the test compound.

Mean OD_{test} = the average of optical density measurements after the desired period of time.

Mean OD_{ctrl} = the average of optical density measurements after the desired period of time with no exposure of cells to the test compound.

The GI₅₀ measures the growth inhibitory power of the test agent and represents the concentration that causes 50% growth inhibition, and can be defined as PG values of 50 in this work. If antiproliferative activities are rather high, GI₅₀ values should be very low.

4.3.1 Results (Table 4.10, Figure 4.9, 4.10)

Table 4.10 GI₅₀ values (μM) of calixarenes on human tumor cell lines

Compound ID (LET) ^b	Compound ID	GI ₅₀ ^a (μM)			
		Cell lines			
		HCT 116	SW 620	MCF-7	H 460
852	Monomer B	2 ± 0.5	2 ± 0.04	1.5 ± 0.2	1.5 ± 0.1
853	Dimer A	3 ± 0.1	4 ± 4	5 ± 0.4	2 ± 1
854	Monomer A	2 ± 0.1	2 ± 0.01	2 ± 0.5	1.6 ± 0.04
855	Dimer B	14 ± 1	9 ± 4	3 ± 0.4	4 ± 0.03

a. GI₅₀; the concentration that causes 50% growth inhibition

b. LET; Laboratory of Experimental Therapy

Figure 4.9 Dose-response profiles for compounds 852-855 tested *in vitro*

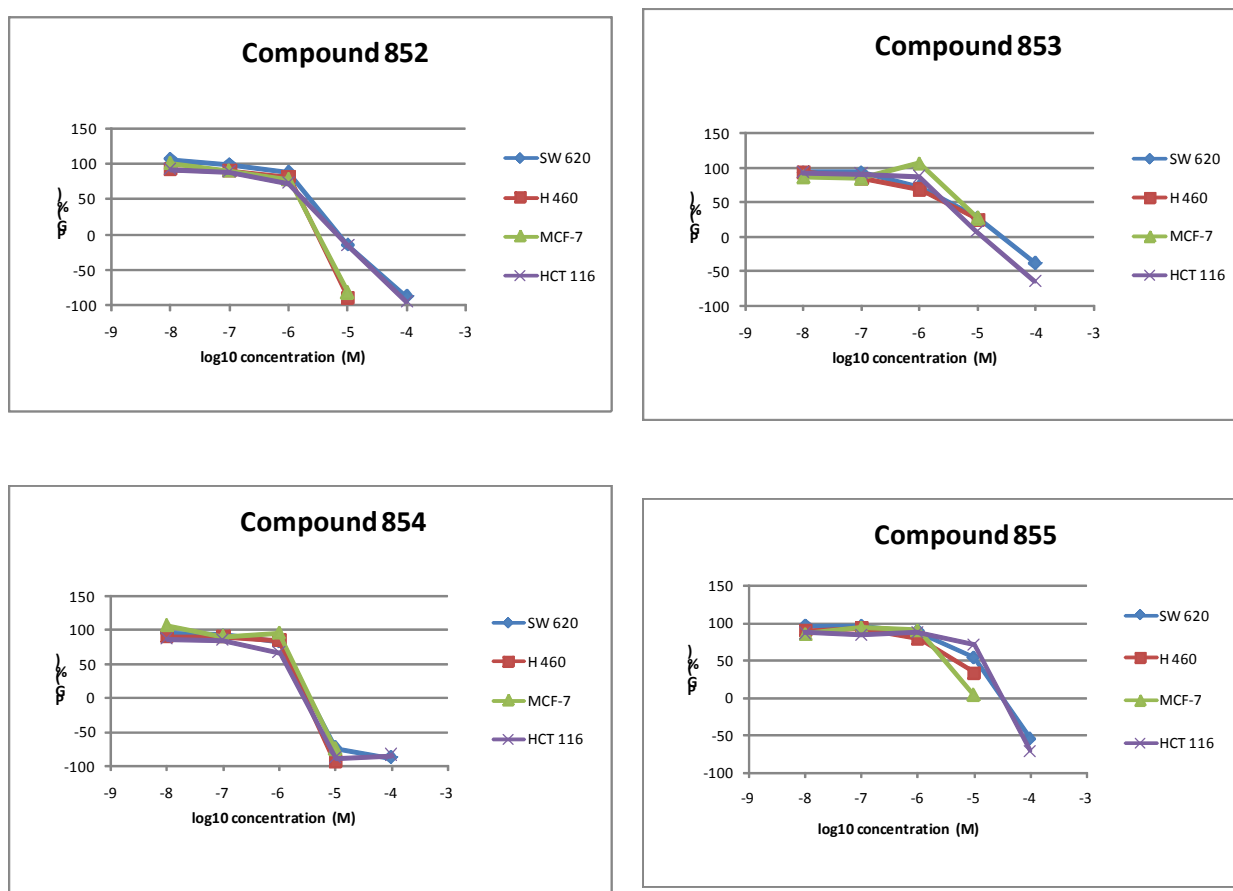
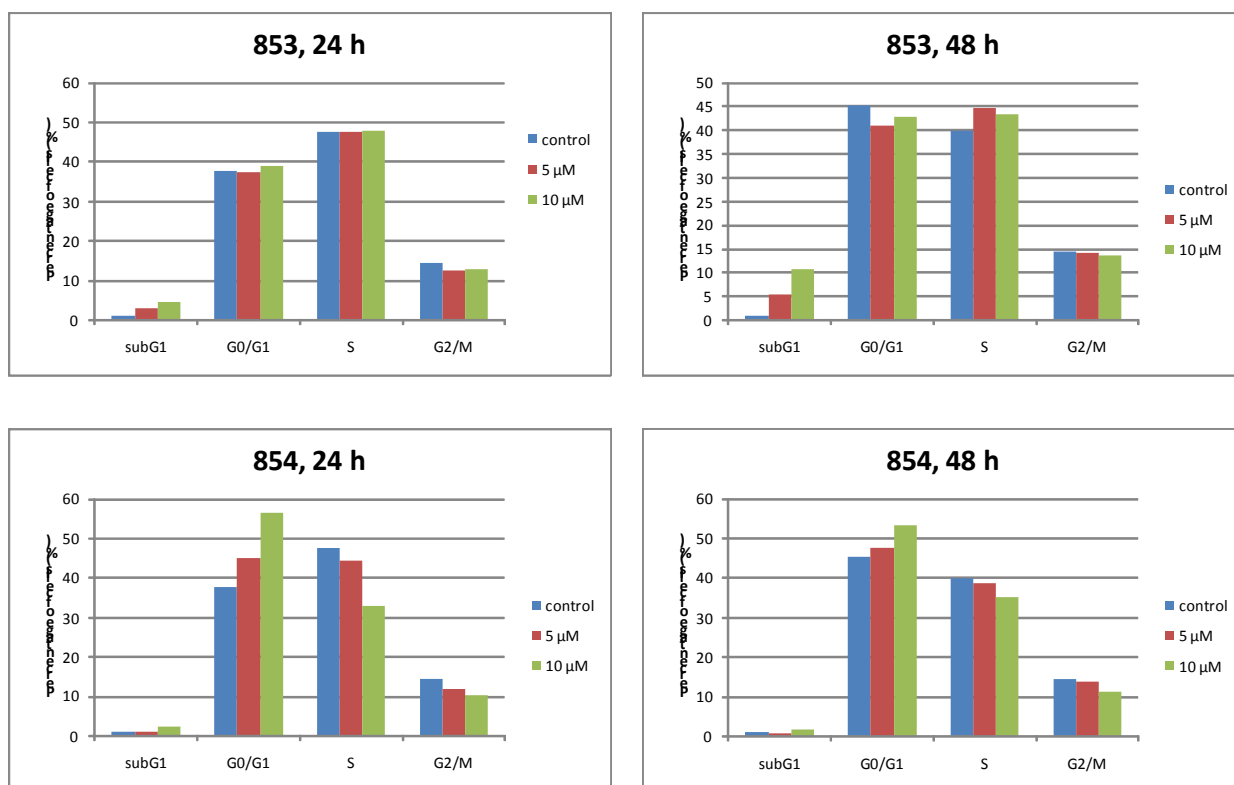


Figure 4.10 Preliminary testing of 853 & 854 for the potential disturbances of tumor cell cycle



4.3.2 Discussion

1. Compared with anilino series, benzyl series (Dimer A, Dimer B, Monomer A and Monomer B) have rather high antiproliferative activities, probably because the much higher pK_a values of the latter bears highly positive charges at experimental conditions ($pH = 7$).
2. The cell growth inhibition might originate from DNA complexation inside the tumor cells. However, more and more evidence showed that the cationic calixarenes could not pass the cell membranes. On the one hand, the studied molecules have a large size. On the other hand, as amphiphilic molecules, the dimeric (and monomeric) calixarenes may self-assemble inside the cell membrane, where the lipophilic part of calixarenes (-O-Bu tails) could be oriented inside a membrane and the positively charged side towards aqueous solutions (in the direction of both inside and outside of the cell). This architecture could alter membrane potential as well as ion flux across the double layer, and leads to the cell apoptosis.

3. The cell cycle analysis (Figure 4.10) indicated that there was no DNA damage during apoptosis. It means that the target of studied compounds is not DNA.

(1). Dimer A (**853**) did not induce any specific cell cycle disturbance, but induces time-dependent cell death (as evidenced by subG1 percentage of cells) at both concentrations (5 μ M and 10 μ M)

(2). Monomer A (**854**) induced strong delay of cell cycle progression from G1 phase to S (DNA synthesis) phase. The strong accumulation of cells in G1 cell cycle phase leads to the drastic reduction of cells in S phase. In G1 phase, Monomer A interacts with the target in the cell. During G1 phase, new organelles are being synthesized, so the cell requires both structural proteins and enzymes, resulting in great amount of protein synthesis and a high metabolic rate in the cell. Monomer A probably interferes with the protein synthesis.

In all, the mechanism of the action is sophisticated, and more specific experiments should be performed in the future.

5. Conclusions and Outlook

5.1 Conclusions

1. Compared with dimeric anilino-calix[4]arenes, dimeric aminobenzyl calixarene Dimer A and its guanidinium counterpart Dimer B are water-soluble, and bind to DNA with much higher affinity (binding constants: 10^6 – 10^8 M⁻¹ in 2 mM Hepes buffer with 150 mM NaCl). Although direct structure information from a crystal or NMR structure was not yet available, the following results from established binding assays strongly support a major groove binding mode:

(1). The DAPI displacement assay indicates that the calixarene dimers and DAPI can simultaneously bind to poly (dAdT) – poly (dAdT). Because DAPI occupies the minor groove, the dimeric calixarenes must reside in the major groove.

(2). Ethidium bromide displacement assays, fluorescence titrations, and circular dichroism measurements indicate that calixarene dimers strongly prefer nucleic acids with a wide, shallow or even major groove; while low affinities are observed for nucleic acids with a narrow, deep or rugged major groove, which must be widened before complexation occurs. This characteristic also implies that the accessible area for our ligands is on the major groove side, contrary to the well-known slim oligoamide binders, which target the minor groove.

Binding Properties of Dimer A and Dimer B with Different Nucleic Acids

	poly(dGdC)- poly(dGdC)	poly (dAdT)- poly (dAdT)	poly dA- poly dT	poly A-polyU
Major Groove Width	wide 13.5 Å	medium 11.2 Å	11.4 Å	narrow 3.8 Å
Major Groove Shape	smooth curve	not smooth , because of methyl group of thymine		smooth curve
EtBr Displacement Assays	efficient displacement	medium		weak displacement
Binding Constants	high	medium		low
CD Spectra	no induced conformational changes (<i>B</i> -DNA remains <i>B</i> -DNA)			shift from <i>A</i> -form to <i>B</i> -form

In line with these observations, it was noticed that changes in shape and width of the minor groove had no influence on the ligands' affinities.

2. Because in minor grooves, *N*-methylimidazoles of polyamides could recognize the positive electrostatic potential of amino groups of guanine bases via hydrogen bonds, it was assumed that Dimer C, which contained a triimidazole bridge, could prefer a major groove with large positive potentials. Moreover, because the triimidazole bridge is slim, it was also assumed that Dimer C should prefer a narrow major groove, which could offer the appropriate shape for the bridge's recognition. In view of the above-mentioned assumptions, we found that the major groove of poly dG – poly dC fulfilled both requirements. Therefore, it was predicted that Dimer C should show the high affinity for poly dG – poly dC.

Ethidium bromide displacement assays, fluorescence titrations, and circular dichroism measurements imply that Dimer C is a major groove binder. Furthermore, as we expected, these experiments indicate that Dimer C showed stronger preference for this specific DNA duplex: poly dG - poly dC.

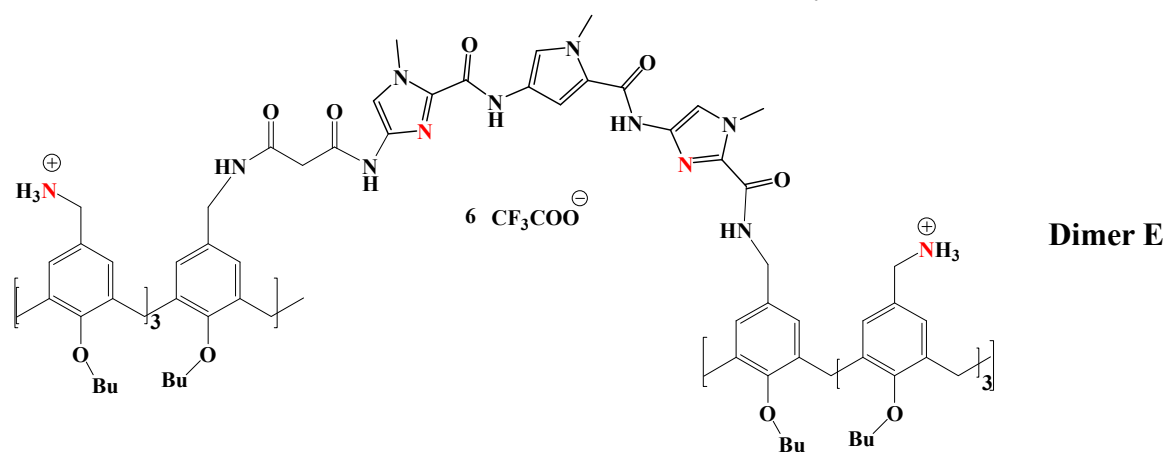
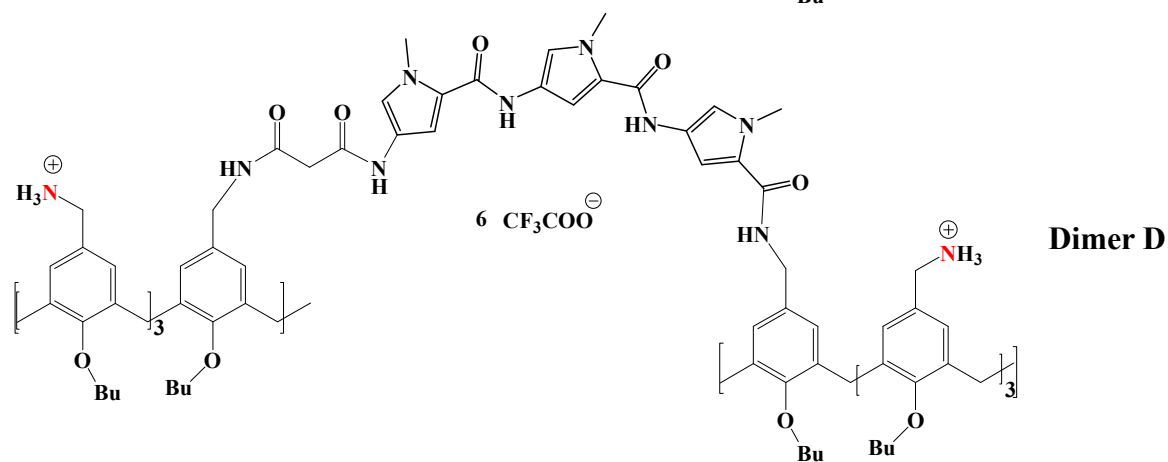
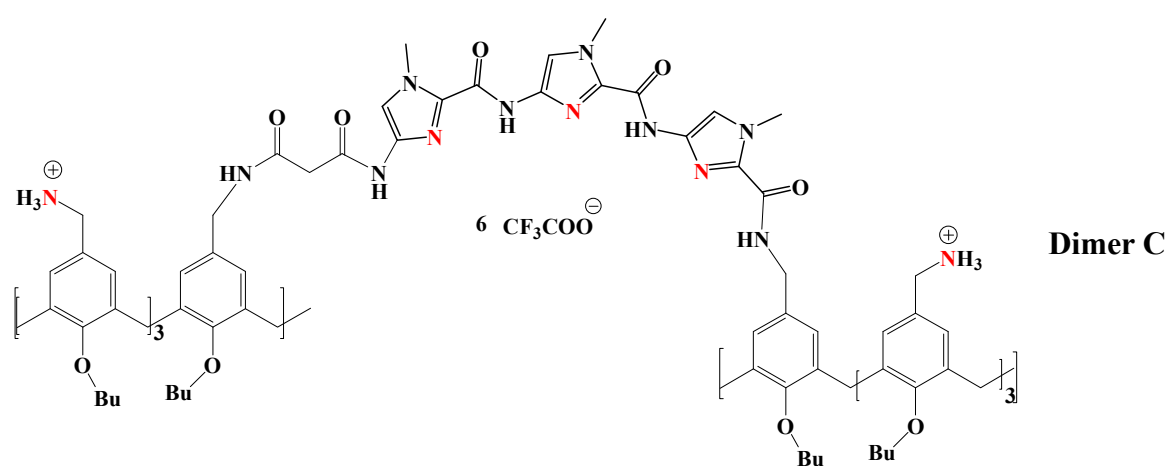
It was also observed that Dimer C frequently showed reduced affinity to other DNA duplexes. Probably, the decrease in affinity is related to their wider major grooves, in which the slim triimidazole bridge will not produce extensive close van der Waals contacts, and the whole ligand itself shows orientational disorder. Another explanation is the unfavorable electrostatic potentials, because these DNA duplexes have more neutral areas in major grooves than does poly dG - poly dC.

Herein, we present the mechanism of DNA binding by Dimer C: the cationic moieties on the upper rim of the calixarenes form hydrogen bonds with nucleobases as well as phosphate groups of the nucleic acid, the butoxy tail is toward the free solution, and the triimidazole bridge binds along the major groove and recognizes the amino groups of nucleobases.

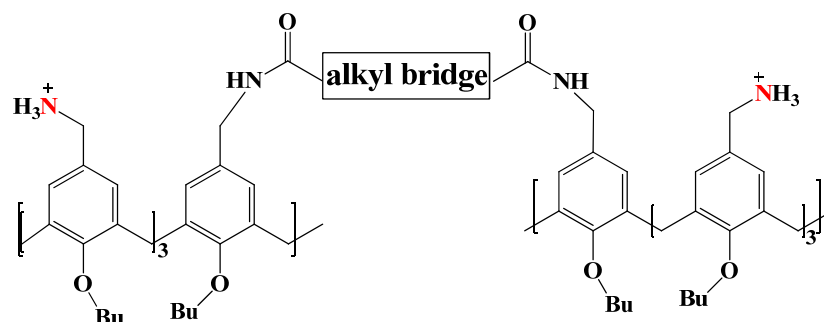
3. Dimer A, Dimer B, Monomer A and Monomer B have rather high antiproliferative activities. The cell cycle analysis indicates that Dimer A induces time-dependent cell death, and Monomer A induced strong delay of cell cycle progression from G1 phase to S phase. There was no evidence that the apoptosis was the consequence of DNA damage. Therefore, the target of the studied molecules is probably not DNA. Because the size of studied molecules is large and the calixarene head groups are known to interact with various metal cations and anions, it is assumed that as amphiphilic molecules, the dimeric and monomeric calixarenes may self-assemble inside the cell membrane, and alter membrane potential as well as ion flux across the double layer. More specific experiments should be performed to interpret the mechanism of the antiproliferative activity.

5.2 Outlook

1. In the future, we intend to synthesize the analogues of Dimer C, i.e. dimeric aminobenzyl calix[4]arenes connected by different linear heterocyclic oligomers, for example, Dimer D, Dimer E, etc. and assay their DNA-binding properties (especially binding affinities and sequence specificities) by a series of biophysical studies.

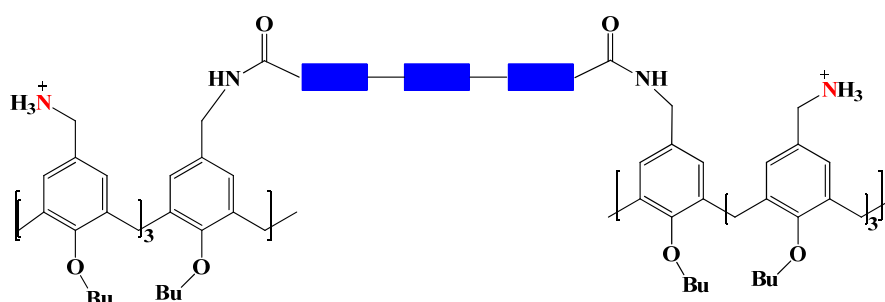


2. Inspired by the hairpin binding motif^[89], which results from covalent linkages between two antiparallel polyamide strands, we plan to design and synthesize calix[4]arene dimers with cyclic polyamide bridges (the third generation calix[4]arene dimers). These dimers with large dimensional bridges could superbly fit into DNA's wide major groove and recognize different hydrogen bond profiles, and probably they will show improved affinities and specificities.



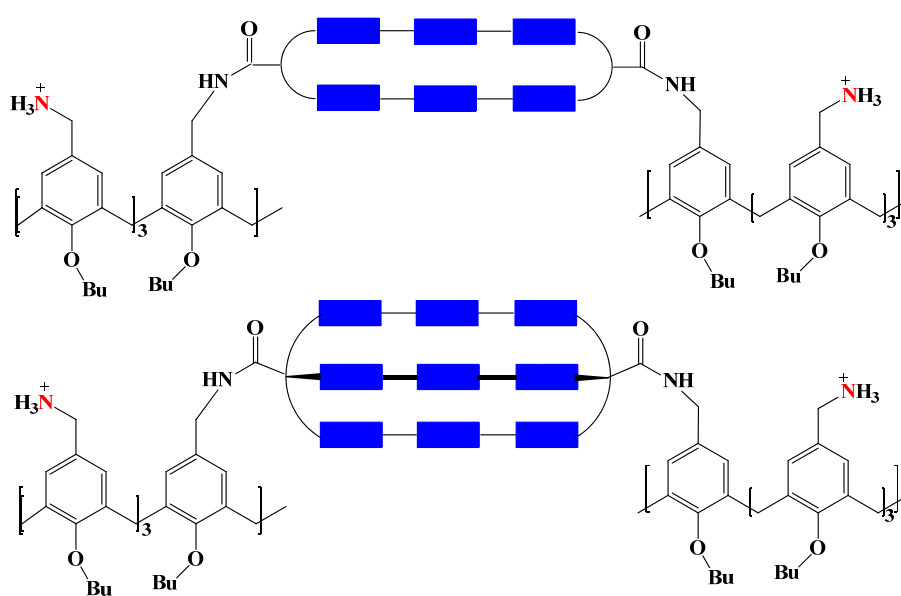
Dimeric Calix[4]arenes with Alkyl Bridges

The first generation



Dimeric Calix[4]arenes with Single Linear Polyamide Bridges

The second generation



Dimeric Calix[4]arenes with Cyclic Polyamide Bridges

The third generation

 : *N*-Methylpyrrole or *N*-Methylimidazole or 3-hydroxypyrrole Amino Acid

3. We will explore pairing rules for major groove recognition (for example, Figure 5.2), and discuss the scope and limitations of the pairing rules.

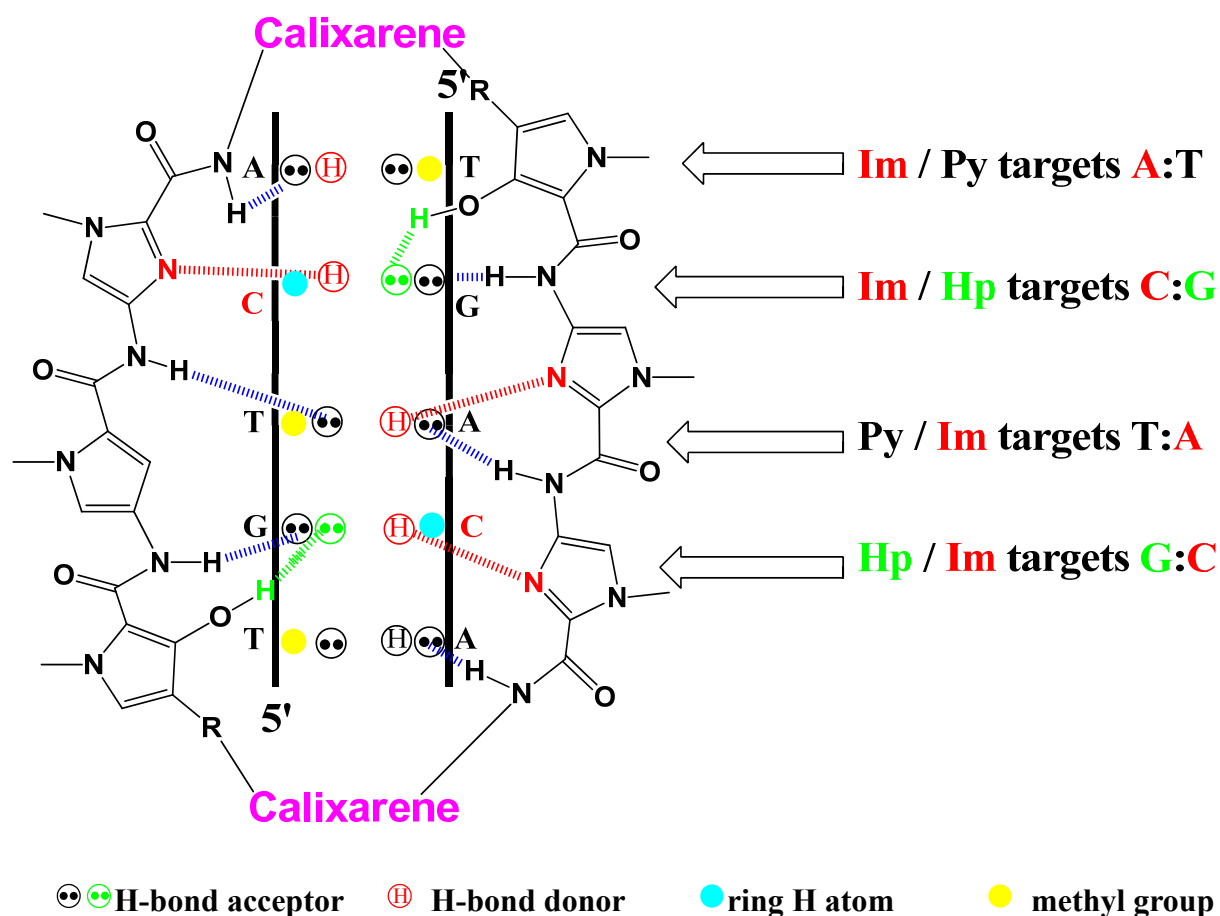


Figure 5.2. A Proposed Major Groove Alphabet

4. The ultimate goal behind this work is to design dimeric calixarene drugs capable of recognizing a specific sequence in DNA. It may be possible for them to control gene expression by blocking a specific promoter sequence, for example, to block a specific oncogene, inhibit the expression of this oncogene and thereby control the development of tumor cells. Specificity for much longer sequences is required in order to have site uniqueness at the genome level. It has been estimated that the minimum nucleotide binding site for the polyamide bridge is about 20 bases long. Thus, it is necessary to carry out solid-phase peptide synthesis to complete the synthesis of the macrocyclic polyamide bridges.

6. Experiments

6.1 Chemicals and Equipments

Chemicals. All the commercial chemicals were purchased from Sigma -Aldrich, Acros Organics, Merck and Fluka. All reagents were purchased at the highest commercial grade and were used without further purification.

Solvents. All the technical level organic solvents were distilled before use. Dry solvents were prepared with standard methods ^[224,225].

Nucleic Acids: Oligonucleotides used in the work were purchased from Metabion international AG. Polynucleotides were purchased from Aldrich.

Chromatography. Thin layer chromatography (TLC) with Merck silica-gel 60 F254 plates were used to monitor reactions. The detection was performed under 254 nm UV light. The eluting solvent and R_f value depend on the substance ^[226]. Flash chromatography was performed with silica gel 60 (200-400 mesh) from Merck. Yields referred to chromatographically and spectroscopically pure compounds unless otherwise noted. HPLC was performed by a Merck–Hitachi system with an L-7150 analytical pump, a K-1800 preparative pump, an L-7400 or K-2501 UV detector and an L-7614 solvent degasser.

NMR Spectroscopy. NMR spectra were recorded at 300 K on Bruker AMX 300 or Bruker DRX 500. The signals of some commonly used deuterated solvents were reported in the literature ^[227] and were used for calibrations. Chemical shifts were reported in ppm relative to tetramethylsilane. Multiplicities were indicated by s (singlet), d (doublet), t (triplet), m (multiplet) and br (broad). The unit of the coupling constant is herz (Hz). ¹³C spectra were broadband decoupled and calibrated on the particular solvent signal.

UV-Vis Spectroscopy. UV-Vis experiments were performed on a V-550 spectrometer from

Jasco with a Peltier thermostatted single cell holder with a stirring unit. Helma cuvettes with 2 mm inner diameter were used for the experiments.

Fluorescence Spectroscopy. Fluorescence experiments were performed at 25 °C on a Jasco FP-6500 spectrofluorometer with a stirring unit and a Haake water-temperating unit.

Mass Spectroscopy. High-resolution electron spray ionisation (ESI) mass spectra were recorded on a Bruker BioTOF III spectrometer.

Molecular Modeling. Force-field calculations were carried out with the program MacroModel 9.7 using the OPLS 2005 force-field and the GB/SA solvation model for water. Monte-Carlo simulations were conducted using 1000 starting structures and up to 2500 minimization steps without any constraint.

kept at room temperature overnight. The concentrations of polynucleotides were calculated in basepairs, and stoichiometries or equivalents of ligands were related to basepairs accordingly. The phosphate concentration of polynucleotides was then determined spectroscopically. This was also the base concentration, which was multiplied by 2 to furnish the nucleic acid concentration in base pairs.

poly dA - poly dT	$\lambda = 260 \text{ nm}$	$\epsilon = 6000 \text{ L mol}^{-1} \text{ cm}^{-1}$
poly (dAdT) - poly (dAdT)	$\lambda = 260 \text{ nm}$	$\epsilon = 6000 \text{ L mol}^{-1} \text{ cm}^{-1}$
poly A - poly U	$\lambda = 260 \text{ nm}$	$\epsilon = 6300 \text{ L mol}^{-1} \text{ cm}^{-1}$
poly(dGdC) - poly(dGdC)	$\lambda = 253 \text{ nm}$	$\epsilon = 7400 \text{ L mol}^{-1} \text{ cm}^{-1}$
poly dG – poly dC	$\lambda = 253 \text{ nm}$	$\epsilon = 7400 \text{ L mol}^{-1} \text{ cm}^{-1}$

6.2.2 Ethidium Bromide Displacement

A Jasco FP-6500 spectrofluorimeter was used to record the data. The samples were excited at a wavelength of 546 nm and the change of the emission intensity around 595 nm was recorded. Ethidium bromide was dissolved in buffers to provide 1.26 eq. per base pair. Short oligonucleotides were used in 1 μM duplex concentration [i.e., 12 μM (12 mer) or 20 μM (20 mer) in basepairs]. After stirring for 5 min and standing for 1 min the fluorescence was measured. For the graph, the relative decrease in fluorescence emission intensity of the intercalated dye EB is plotted against the ligand concentration corrected for its charge excess (CE value).

6.2.3 Circular Dichroism Spectroscopy

CD spectra were recorded on a Jasco J815 spectrometer, in all cases using quartz cuvettes (1 cm). The measurements were performed in the aqueous buffer consisting of 20 mM sodium phosphate (pH = 7.0, Fluka, Product Number: 82591). Under the experimental conditions used, the absorbance and fluorescence intensities of the studied compounds were proportional to their concentrations while none of studied compounds showed a CD spectrum. The samples containing DNA (5 μM in basepairs for Dimer A, Dimer B, Monomer A and Monomer B; 20 μM in basepairs for Dimer C) or its complex with calixarenes were scanned from 200 to 350 nm at a constant temperature of 20 °C. Eq. calixarene are also calculated per basepair.

6.2.4 DAPI Displacement

CD spectra were recorded on a Jasco J815 spectrometer, in all cases using quartz cuvettes (1 cm). The measurements were performed in the aqueous buffer consisting of 20 mM sodium phosphate (pH = 7.0, Fluka, Product Number: 82591). Under the experimental conditions used, the absorbance and fluorescence intensities of the studied compounds were proportional to their concentrations while none of studied compounds showed a CD spectrum. Poly (dAdT) - poly (dAdT) was purchased from Aldrich. The samples containing poly (dAdT) - poly (dAdT) (5 μ M in basepairs), DAPI (3 μ M = 0.6 eq. per base pair) or its complex with calixarenes were scanned from 230 to 450nm at a constant temperature of 20 °C. Eq. calixarene are also calculated per basepair.

6.2.5 UV-vis Melting Curves

The profiles of UV absorbance versus temperature were measured using a JASCO V-550 UV-vis spectrophotometer by monitoring the sample absorption at 260 nm. The sample cell was equipped with a Peltier type cell holder (ETC-273T) and the profiles of UV-vis absorption versus temperature were recorded. The concentration of oligonucleotides in each sample was 1 μ M (in duplex DNA) in buffer solutions. The concentration of polynucleotides in each sample was 10 μ M (in basepairs) in buffer solutions. The experiments were carried out by increasing the temperature at a rate of 1.0 °C / min from 20 to 95 °C and the temperature was recorded every minute (equal to each additional 1.0 °C).

6.2.6 Fluorescence Titration Experiments

Fluorescence titrations were performed with 5'-Fluorescein-labeled DNA or RNA of varying sequences. The guests were dissolved in HEPES-buffered solutions (pH = 7.1). For convenience, the host compounds were diluted in the DNA or RNA solutions, so that there was no change in the DNA or RNA concentration throughout the entire titration. A Jasco FP-6500 spectrofluorimeter was used to record the data. The samples were excited at a

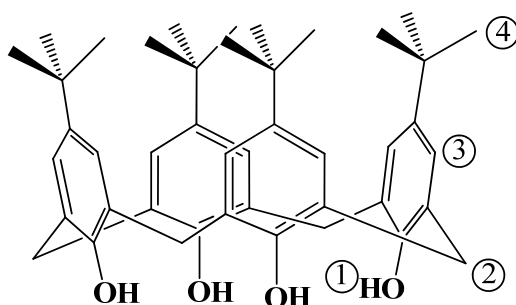
wavelength of 488 nm and the change of the emission intensity around 520 nm was recorded. 700 μ l of these solutions were filled into cuvettes and up to 500 μ l of the ligand solutions were added stepwise. The change of the emission intensity was measured at a constant temperature of 20 °C. The binding isotherms were fitted by standard nonlinear regression methods.

6.2.7 Preparation of NMR Samples

NMR samples for observation of the imino proton spectrum were prepared by dissolving 1.2 μ mol of the DNA in 0.6 ml of the aqueous buffer consisting of 20 mM sodium phosphate (pH = 7.0, Fluka, Product Number: 82591). The samples were lyophilized to dryness and redissolved in 0.6 ml of the mixture ($\text{H}_2\text{O} : \text{D}_2\text{O} = 95 : 5$). For non-exchangeable proton spectra these samples were repeatedly lyophilized to dryness in the NMR tube and redissolved in 99.996% D_2O .

6.3 Synthesis

p-*tert*-butylcalix[4]arene (1) ^[134]



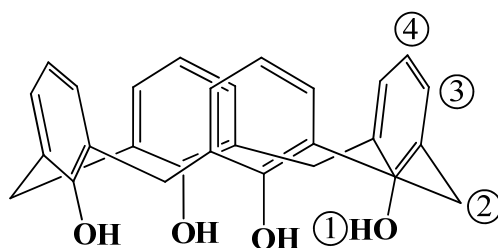
A mixture of 10 g (0.067 mol) of *p*-*tert*-butylphenol, 6.2 mL (0.083 mol) of 37% formaldehyde solution and 0.12 g (0.003 mol) of sodium hydroxide in 0.3 mL of water was placed in a 500 mL flask, stirred for 15 min at room temperature, and then heated for 2 hours at 111°C. The reaction mixture was cooled to room temperature. 80 mL of warm diphenyl ether was added to the flask. The contents of the flask were stirred and heated at 111°C while a stream of nitrogen was blown rapidly over the reaction mixture to facilitate the removal of the water as it was evolved. Then the content of the flask was heated at reflux for 2 hours and cooled to room temperature. The product was precipitated by the addition of 150 mL of ethyl acetate. The solid was washed twice with 50 mL ethyl acetate, twice with 50 mL acetic acid, twice with 50 mL water, and twice with 50 mL acetone to yield 5.1 g (48%) of crude product.

¹H-NMR (300 MHz, C₆D₆): δ (ppm) = 1.08 (s, 36H, H-4), 3.30 (bs, 4H, H-2), 4.34 (bs, 4H, H-2), 6.95 (s, 8H, H-3), 10.37 (s, 4H, H-1).

¹³C-NMR (75 MHz, C₆D₆): δ (ppm) = 147.12, 144.42, 127.41, 126.11, 33.93, 32.69, 31.40.

MS (ESI-TOF, pos. toluene): [M+Na]⁺ calc. for C₄₄H₅₆NaO₄ *m/z* 671.4071, found *m/z* 671.4132.

calix[4]arene (2) ^[228]



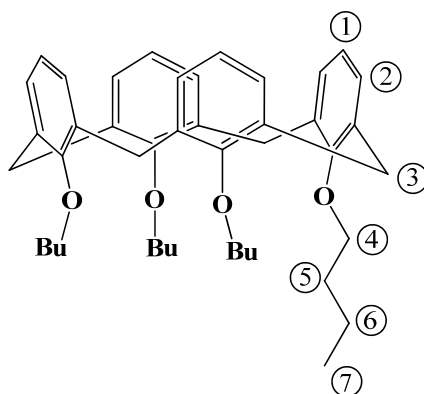
3.0 g (4.63 mmol) of *p-tert*-butylcalix[4]arene was dissolved in 50 mL of anhydrous toluene at 80°C, and was cooled to 50°C. 3.0 g (22.5 mmol) of AlCl₃ was added. The solution was vigorously stirred for 2 hours at 50°C, and was cooled to 5°C. The reaction was quenched using 1M HCl. The toluene phase was evaporated, and the solid in the flask was washed twice with 50 mL water and twice with 10 mL acetone to yield 1.2 g (61%) of product.

¹H-NMR (300 MHz, DMSO-*d*₆): δ (ppm) = 3.87 (bs, 8H, H-2), 6.64 (t, 4H, H-4), 7.11 (d, 8H, *J* = 7.54, H-3), 9.80 (bs, 4H, H-1).

¹³C-NMR (75 MHz, DMSO-*d*₆): δ (ppm) = 149.41, 128.65, 128.59, 121.10, 30.58.

MS (ESI-TOF, pos. toluene): [M+Na]⁺ calc. for C₂₈H₂₄NaO₄ *m/z* 447.1567, found *m/z* 447.1628; [M+H]⁺ calc. for C₂₈H₂₅O₄ *m/z* 425.1747, found *m/z* 425.1810.

25,26,27,28-tetra-O-ⁿbutyl-calix[4]arene (3) ^[228]



20 mL of anhydrous DMF was added to 100 mL round bottom flask containing 0.88 g (2.07

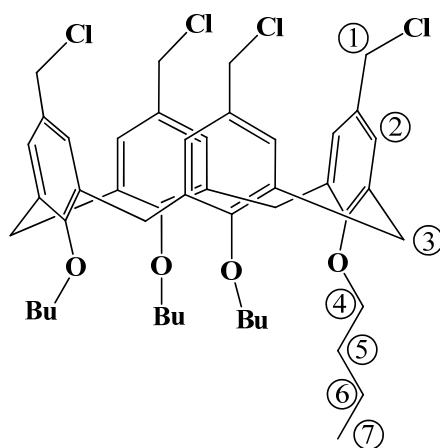
mmol) of calix[4]arene at 80°C. 0.34 g (8.5 mmol) of NaH (60% dispersion in mineral oil) were added slowly to the flask followed by 1.1 mL of 1-bromobutane (10.2 mmol). The solution was stirred for 1 hour at 80°C and cooled to room temperature. DMF is removed in vacuo. The residue was washed with 150 mL of *n*-hexane. The organic layer was evaporated to dryness to yield 0.7 g (52%) of product.

¹H-NMR (300 MHz, CDCl₃): δ (ppm) = 6.55-6.65 (m, 12H, H-1, H-2), 4.47 (d, 4H, *J* = 13.29, H-3), 3.91 (t, 8H, *J* = 7.50, H-4), 3.17 (d, 4H, H-3), 1.92 (quintet, 8H, H-5), 1.46 (sextet, 8H, H-6), 1.02 (t, 12H, H-7).

¹³C-NMR (75 MHz, CDCl₃): δ (ppm) = 156.57, 135.14, 128.09, 121.86, 74.81, 32.31, 22.70, 19.36, 14.08.

MS (ESI-TOF, pos. CH₂Cl₂): [M+Na]⁺ calc. for C₄₄H₅₆NaO₄ *m/z* 671.4071, found *m/z* 671.4148.

25,26,27,28-Tetrabutoxy-5,11,17,23-tetrakis(chloromethyl)calix[4]arene (4) ^[149]



25,26,27,28-tetra-*O*-ⁿbutyl-calix[4]arene (12.11 g, 18.5 mmol) and paraformaldehyde (36.0 g) were suspended in dioxane (500 mL). After addition of acetic acid (86 mL), phosphoric acid (200 mL), and concentrated HCl (250 mL), the reaction mixture was heated at 80°C for 6 days. After cooling, the mixture was diluted with ice-water and extracted with chloroform. The organic layer was washed twice with water and dried over MgSO₄. The solution was

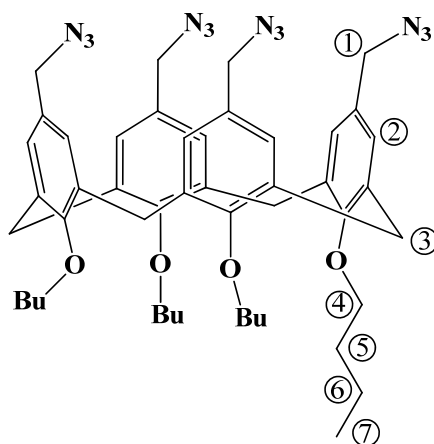
evaporated to dryness, and the residue was recrystallized from hexane. Yield: 83%

¹H-NMR (300 MHz, CDCl₃): δ (ppm) = 6.65 (s, 8H, H-2), 4.41 (d, 4H, *J* = 13.28, H-3), 4.3 (s, 8H, H-1), 3.88 (t, 8H, *J* = 7.48, H-4), 3.15 (d, 4H, H-3), 1.89 (quintet, 8H, H-5), 1.42 (sextet, 8H, H-6), 1.00 (t, 12H, H-7).

¹³C-NMR (75 MHz, CDCl₃): δ (ppm) = 156.72, 135.09, 130.84, 128.52, 75.02, 46.58, 32.15, 30.80, 19.24, 13.99.

MS (ESI-TOF, pos. CH₂Cl₂): [M+Na]⁺ calc. for C₄₈H₆₀Cl₄NaO₄ *m/z* 865.3118, found *m/z* 865.3169.

25,26,27,28-Tetrabutoxy-5,11,17,23-tetrakis(azidomethyl)calix[4]arene (5) ^[157]



25,26,27,28-Tetrabutoxy-5,11,17,23-tetrakis(chloromethyl)calix[4]arene (0.4214 g, 0.5 mmol) and sodium azide (0.325 g, 5 mmol) were stirred for 18 h at 60°C in DMF (30 mL). Subsequently DMF is removed in vacuo. The residue was washed with 100 mL of *n*-hexane. The organic layer was evaporated to dryness to yield 0.43 g (99%) of product.

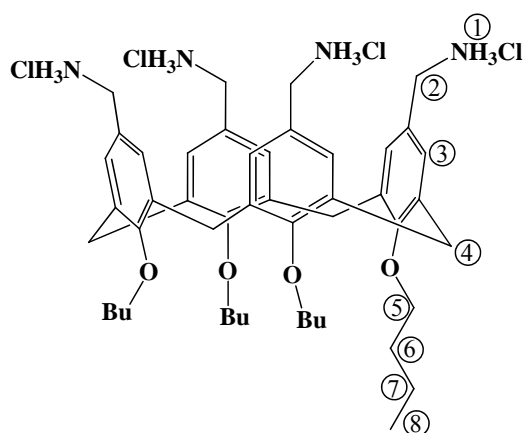
¹H-NMR (300 MHz, CDCl₃): δ (ppm) = 6.61 (s, 8H, H-2), 4.45 (d, 4H, *J* = 13.21, H-3), 3.95 (s, 8H, H-1), 3.90 (t, 8H, *J* = 7.48, H-4), 3.17 (d, 4H, H-3), 1.91 (quintet, 8H, H-5), 1.44 (sextet, 8H, H-6), 1.01 (t, 12H, H-7).

¹³C-NMR (75 MHz, CDCl₃): δ (ppm) = 156.57, 135.18, 128.63, 128.52, 75.06, 54.22, 32.24,

30.80, 19.29, 14.03.

MS (ESI-TOF, pos. CH₂Cl₂): [M+Na]⁺ calc. for C₄₈H₆₀N₁₂NaO₄ *m/z* 891.4753, found *m/z* 891.4810.

25,26,27,28-Tetrabutoxy-5,11,17,23-tetrakis(aminomethyl)calix[4]arene tetrahydrochloride (6) ^[157]



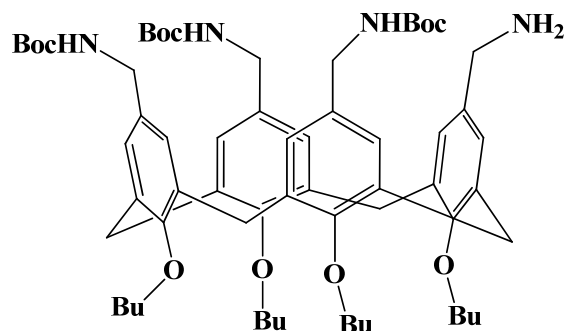
25,26,27,28-Tetrabutoxy-5,11,17,23-tetrakis(aminomethyl)calix[4]arene (1.0 g, 1.15 mmol) were dissolved in methanol (100 mL) and Pd/C (0.10 g, 10 weight-%) was added. After addition of 1 M hydrochloric acid (15 mL) the hydrogenation was carried out for 24 h. The catalyst was filtered off over Celite and the solution was evaporated to dryness. The residue was washed with acetone to yield 0.8 g (90%) of product.

¹H-NMR (300 MHz, DMSO-*d*₆): δ (ppm) = 8.47 (bs, 12H, H-1), 7.17 (s, 8H, H-3), 4.36 (d, 4H, *J* = 12.45, H-4), 3.82 (t, 8H, *J* = 7.36, H-5), 3.75 (m, 8H, H-2), 3.20 (d, 4H, H-4), 1.93 (quintet, 8H, H-6), 1.43 (sextet, 8H, H-7), 0.98 (t, 12H, H-8).

¹³C-NMR (75 MHz, DMSO-*d*₆): δ (ppm) = 156.57, 135.18, 128.63, 128.52, 75.06, 54.22, 32.24, 30.80, 19.29, 14.03.

MS (ESI-TOF, pos. MeOH, free base): [M+Na]⁺ calc. for C₄₈H₆₈N₄NaO₄ *m/z* 787.5133, found *m/z* 787.5178; [M+H]⁺ calc. for C₄₈H₆₉N₄O₄ *m/z* 765.5313, found *m/z* 765.5378.

5-(Aminomethyl)-25,26,27,28-tetrabutoxy-11,17,23-tris{[(*tert*-butoxycarbonyl)amino]methyl}calix[4]arene (7)



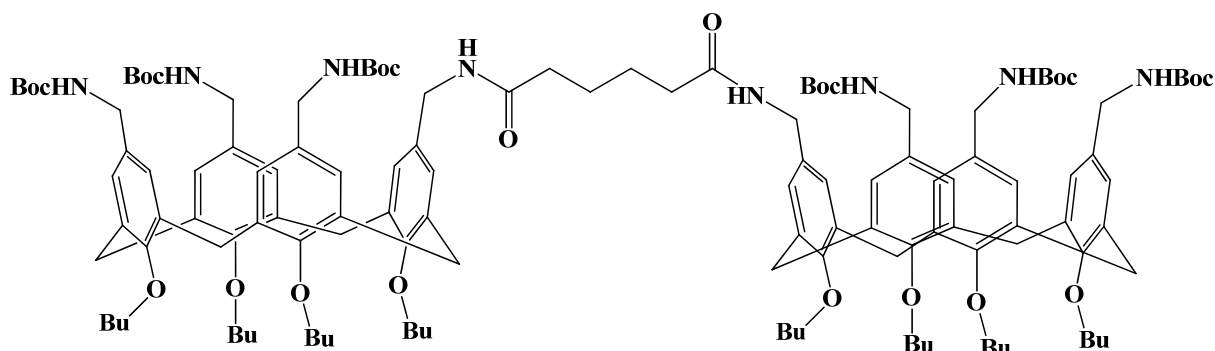
25,26,27,28-Tetrabutoxy-5,11,17,23-tetrakis(aminomethyl)calix[4]arene tetrahydrochloride (1.0 g, 1.10 mmol) was dissolved in a mixture of anhydrous MeOH (10 mL) and Et₃N (1 mL). Di-*tert*-butylcarbonate (0.72 g, 3.30 mmol) was added to the solution. The mixture was stirred for 18 h at r.t. Subsequently, MeOH was removed in vacuo, and the residue was purified by flash column chromatography (SiO₂, DCM/MeOH, 100:1). Yield: 0.25 g (21%)

¹H-NMR (300 MHz, CDCl₃): δ (ppm) = 6.60 (s, 2H, Ar-H), 6.55 (s, 2H, Ar-H), 6.50 (s, 2H, Ar-H), 6.48 (s, 2H, Ar-H), 4.39 (d, 2H, *J* = 13.09, Ar-CH₂-Ar), 4.38 (d, 2H, *J* = 13.07, Ar-CH₂-Ar), 4.01 (bs, 4H, Ar-CH₂-N), 3.92 (bs, 2H, Ar-CH₂-N), 3.87 (m, 4H, *J* = 7.37, Ar-O-CH₂-), 3.82 (m, 4H, Ar-O-CH₂-), 3.72 (t, 2H, *J* = 4.79, Ar-CH₂-N), 3.09 (d, 2H, Ar-CH₂-Ar), 3.08 (d, 2H, Ar-CH₂-Ar), 1.87 (m, 8H, Ar-O-CH₂-CH₂-), 1.43-1.45 (m, 35H, Ar-O-CH₂-CH₂-CH₂-, -C(CH₃)₃), 0.98 (t, 12H, Ar-O-CH₂-CH₂-CH₂-CH₃).

¹³C-NMR (75 MHz, CDCl₃): δ (ppm) = 156.18, 156.01, 155.85, 155.44, 135.39, 135.24, 134.91, 134.80, 132.15, 132.10, 127.43, 127.41, 126.90, 126.87, 75.09, 75.05, 75.00, 72.32, 32.37, 32.32, 32.25, 31.09, 28.57, 28.49, 19.45, 19.38, 14.16, 14.14.

MS (ESI-TOF, pos. CH₂Cl₂): [M+Na]⁺ calc. for C₆₃H₉₂N₄NaO₁₀ *m/z* 1087.6706, found *m/z* 1087.6785; [M+H]⁺ calc. for C₆₃H₉₃N₄O₁₀ *m/z* 1065.6886, found *m/z* 1065.6972.

***N,N'*-Bis[(25,26,27,28-tetrabutoxy-11,17,23-tris{[(*tert*-butoxycarbonyl)amino]methyl}]calix[4]aren-5-yl)methyl]hexanediamide (8)**



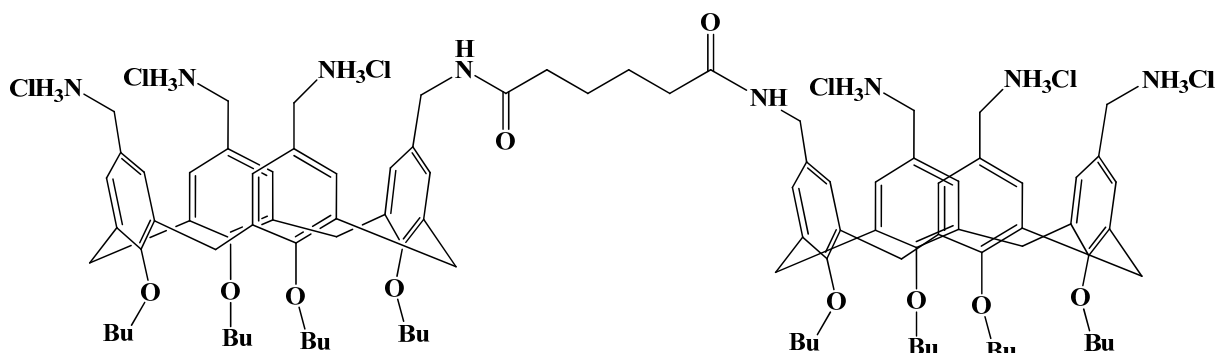
5-(Aminomethyl)-25,26,27,28-tetrabutoxy-11,17,23-tris{[(*tert*-butoxycarbonyl)amino]methyl}calix[4]arene (250 mg, 0.235 mmol) was dissolved in the mixture of anhydrous CH_2Cl_2 (10 mL) and Et_3N (1 mL). Adipic acid dichloride (21.5 mg, 0.117 mmol) was added to the solution. The reaction mixture was stirred for 1 h at r.t. and subsequently evaporated to dryness. The resulting residue was purified by flash column chromatography (SiO_2 , $\text{CH}_2\text{Cl}_2/\text{MeOH}$, 100:1). Yield: 0.17 g (64 %).

$^1\text{H-NMR}$ (300 MHz, CDCl_3): δ (ppm) = 6.49-6.53 (m, 16H, Ar-H), 4.38 (d, 8H, $J = 13.20$, Ar- CH_2 -Ar), 4.37 (d, 8H, $J = 12.96$, Ar- CH_2 -Ar), 4.11 (bs, 4H, Ar- CH_2 -N), 3.96 (bs, 12H, Ar- CH_2 -N), 3.84 (m, 16H, Ar-O- CH_2 -), 3.08 (d, 16H, Ar- CH_2 -Ar), 2.27 (m, 4H, N-CO- CH_2 -), 1.86 (m, 16H, Ar-O- CH_2 - CH_2 -), 1.73 (m, 4H, N-CO- CH_2 - CH_2 -), 1.44-1.46 (m, 70H, Ar-O- CH_2 - CH_2 - CH_2 -, $-\text{C}(\text{CH}_3)_3$), 0.98 (t, 12H, Ar-O- CH_2 - CH_2 - CH_2 - CH_3).

$^{13}\text{C-NMR}$ (75 MHz, CDCl_3): δ (ppm) = 172.91, 156.09, 156.02, 155.93, 135.12, 132.13, 127.28, 79.30, 79.25, 75.04, 70.30, 68.78, 64.28, 54.83, 53.53, 50.83, 44.33, 42.84, 36.25, 32.33, 31.12, 31.07, 29.80, 28.58, 27.44, 25.55, 19.44, 14.17.

MS (ESI-TOF, pos. CH_2Cl_2): $[\text{M}+\text{Na}]^+$ calc. for $\text{C}_{132}\text{H}_{190}\text{N}_8\text{NaO}_{22}$ m/z 2263.3920, found m/z 2263.3994; $[\text{M}+\text{H}]^+$ calc. for $\text{C}_{132}\text{H}_{191}\text{N}_8\text{O}_{22}$ m/z 2241.4100, found m/z 2241.4260.

***N,N'*-Bis{[11,17,23-tris(aminomethyl)-25,26,27,28-tetrabutoxycalix[4]aren-5-yl]methyl} hexanediamide Hexahydrochloride (9)**



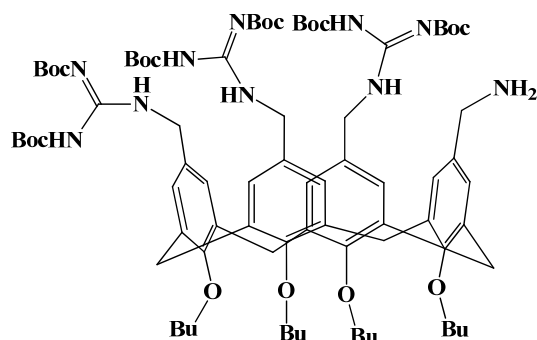
N,N'-Bis[(25,26,27,28-tetrabutoxy-11,17,23-tris{[(*tert*-butoxycarbonyl)amino]methyl})calix[4]aren-5-yl)methyl]hexanediamide (0.17 g, 0.1mmol) was dissolved in anhydrous MeOH (10 mL). To this solution was added 1 M HCl (1 mL). The resulting solution was stirred for 16 h at r.t. and subsequently evaporated to dryness. The solid was washed with acetone to yield 0.12 g (85%) of product.

¹H-NMR (300 MHz, DMSO-*d*₆): δ (ppm) = 8.39 (bs, 18H, Benzal-NH₃Cl), 7.18 (s, 4H, Ar-H), 7.08 (s, 4H, Ar-H), 7.01 (s, 4H, Ar-H), 6.75 (s, 4H, Ar-H), 4.40 (d, 4H, *J* = 12.25, Ar-CH₂-Ar), 4.37 (d, 4H, *J* = 12.27, Ar-CH₂-Ar), 3.96 (bs, 4H, Ar-CH₂-N), 3.87 (bs, 16H, Ar-O-CH₂-), 3.78 (m, 12H, Ar-CH₂-N), 3.24 (d, 4H, Ar-CH₂-Ar), 3.19 (d, 4H, Ar-CH₂-Ar), 2.21(m, 4H, N-CO-CH₂-), 1.92 (m, 16H, Ar-O-CH₂-CH₂-), 1.47 (m, 20H, N-CO-CH₂-CH₂-, Ar-O-CH₂-CH₂-CH₂-), 1.02 (t, 24H, Ar-O-CH₂-CH₂-CH₂-CH₃)

¹³C-NMR (75 MHz, DMSO-*d*₆): δ (ppm) = 172.11, 155.98, 155.71, 154.43, 134.80, 134.64, 134.19, 133.68, 133.05, 129.40, 129.22, 127.88, 127.76, 127.31, 74.86, 74.70, 41.72, 35.09, 31.86, 31.79, 29.94, 25.16, 18.82, 18.76, 13.91.

MS (ESI-TOF, pos. MeOH, free base): [M+H]⁺ calc. for C₁₀₂H₁₄₃N₈O₁₀ *m/z* 1641.0954, found *m/z* 1641.1108.

5-(Aminomethyl)-11,17,23-tris{[2,3-bis(*tert*-butoxycarbonyl)guanidino]methyl}-25,26,27,28-tetrabutoxycalix[4]arene (10)



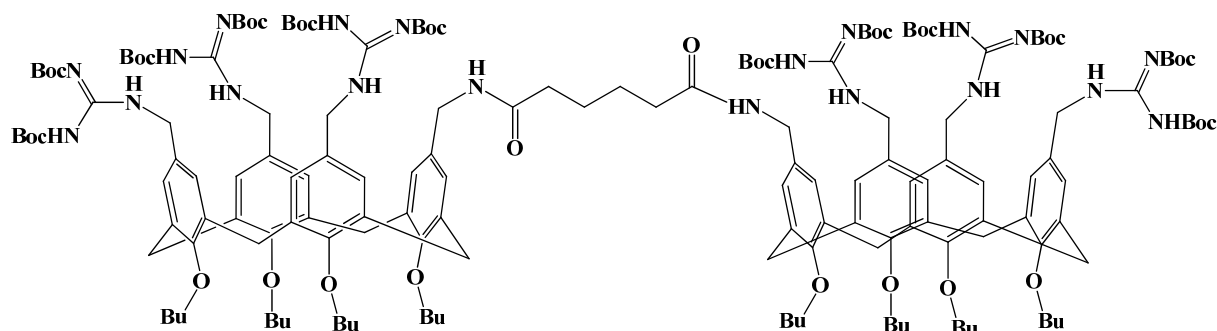
25,26,27,28-Tetrabutoxy-5,11,17,23-tetrakis(aminomethyl)calix[4]arene tetrahydrochloride (0.091 g, 0.1 mmol) was dissolved in the mixture of anhydrous MeOH (10 mL) and Et₃N (1 mL). *N,N'*-bis-Boc-2-methyl-2-thiopseudourea (0.087 g, 0.3 mmol) was added to the solution followed by AgNO₃ (0.11 g, 0.65 mmol). The mixture was stirred for 24 h at r.t. The catalyst was filtered off over celite and the solution was evaporated to dryness. The residue was purified by flash column chromatography (SiO₂, DCM/cyclohexane, 80:20). Yield: 0.018 g (12%)

¹H-NMR (300 MHz, CDCl₃): δ (ppm) = 11.52 (s, 2H, Boc-NH-), 11.48 (s, 1H, Boc-NH-), 11.44 (s, 1H, Boc-NH-), 8.76 (s, 1H, Benzal-NH), 8.47 (s, 2H, Benzal-NH), 8.05 (s, 1H, Benzal-NH), 6.87 (s, 2H, Ar-H), 6.84 (s, 2H, Ar-H), 6.30 (s, 2H, Ar-H), 6.26 (s, 2H, Ar-H), 4.45 (d, 4H, $J = 13.08$, Ar-CH₂-Ar), 4.01 (m, 2H, Ar-CH₂-N), 3.73 (m, 6H, Ar-CH₂-N, Ar-O-CH₂-), 3.62 (m, 8H, Ar-CH₂-N, Ar-O-CH₂-), 3.10 (d, 4H, Ar-CH₂-Ar), 1.89 (m, 8H, Ar-O-CH₂-CH₂-), 1.46-1.51 (m, 62H, Ar-O-CH₂-CH₂-CH₂-CH₃, -C(CH₃)₃), 0.98 (m, 12H, Ar-O-CH₂-CH₂-CH₂-CH₃).

¹³C-NMR (75 MHz, CDCl₃): δ (ppm) = 163.77, 163.62, 156.24, 155.92, 155.53, 153.47, 153.26, 153.08, 137.02, 136.48, 136.18, 134.18, 133.68, 130.51, 130.05, 83.54, 83.02, 82.86, 79.49, 79.25, 79.14, 75.20, 75.17, 75.02, 72.51, 69.12, 61.98, 53.55, 45.05, 40.46, 29.14, 28.89, 28.54, 28.45, 28.20, 27.74, 27.69, 27.48, 19.66, 19.26, 14.75, 14.65, 13.65.

MS (ESI-TOF, pos. CH₂Cl₂): [M+Na]⁺ calc. for C₈₁H₁₂₂N₁₀NaO₁₆ m/z 1513.8932, found m/z 1513.8998; [M+H]⁺ calc. for C₈₁H₁₂₃N₁₀O₁₆ m/z 1491.9113, found m/z 1491.9163.

***N,N'*-Bis(11,17,23-Tris{[2,3-bis(*tert*-butoxycarbonyl)guanidino]methyl}-25,26,27,28-tetrabutoxycalix[4]aren-5-ylmethyl}hexanediamide (II)**



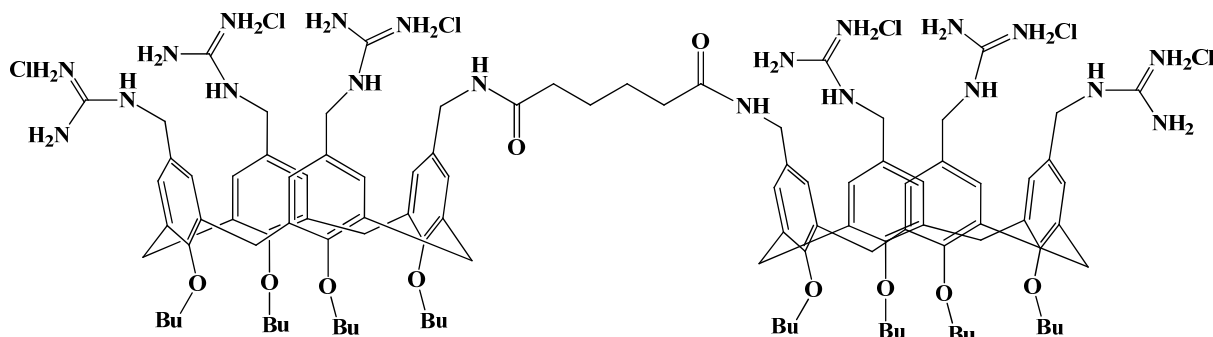
5-(Aminomethyl)-11,17,23-tris{[2,3-bis(*tert*-butoxycarbonyl)guanidino]methyl}-25,26,27,28-tetrabutoxycalix[4]arene (0.018 g, 0.012 mmol) was dissolved in the mixture of anhydrous CH_2Cl_2 (10 mL) and Et_3N (1 mL). Adipic acid dichloride (1.1 mg, 0.006 mmol) was added to the solution. The reaction mixture was stirred for 1 h at r.t. and subsequently evaporated to dryness. The resulting residue was purified by flash column chromatography (SiO_2 , DCM/cyclohexane, 20:80). Yield: 0.012 g (66 %).

$^1\text{H-NMR}$ (300 MHz, CDCl_3): δ (ppm) = 11.48 (s, 4H, Boc-NH-), 11.46 (s, 2H, Boc-NH-), 8.44 (s, 2H, Benzal-NH), 8.35 (s, 2H, Benzal-NH), 8.29 (s, 2H, Benzal-NH), 8.20 (s, 2H, Benzal-NH), 6.64 (s, 8H, Ar-H), 6.49 (s, 4H, Ar-H), 6.42 (s, 4H, Ar-H), 4.38 (m, 8H, $J = 12.50$, Ar- CH_2 -Ar), 4.11 (m, 4H, Ar- CH_2 -N), 3.90 (m, 8H, Ar- CH_2 -N), 3.85 (m, 8H, Ar-O- CH_2 -), 3.76 (m, 8H, Ar-O- CH_2 -), 3.62 (m, 4H, Ar- CH_2 -N), 3.09 (m, 8H, Ar- CH_2 -Ar), 2.20 (m, 4H, N-CO- CH_2 -), 1.86 (m, 16H, Ar-O- CH_2 - CH_2 -), 1.65 (m, 4H, N-CO- CH_2 - CH_2 -), 1.45-1.50 (m, 124H, Ar-O- CH_2 - CH_2 - CH_2 -, $-\text{C}(\text{CH}_3)_3$), 0.98 (m, 24H, Ar-O- CH_2 - CH_2 - CH_2 - CH_3).

$^{13}\text{C-NMR}$ (75 MHz, CDCl_3): δ (ppm) = 163.69, 155.75, 153.18, 135.47, 135.09, 134.51, 130.41, 130.03, 130.00, 129.09, 129.05, 129.01, 128.94, 128.90, 128.84, 128.34, 82.96, 79.16, 29.15, 28.91, 28.48, 28.20, 27.73, 27.48, 14.73, 14.65, 13.68, 13.62.

MS (ESI-TOF, pos. CH_2Cl_2): $[\text{M}+2\text{Na}]^{2+}$ calc. for $\text{C}_{168}\text{H}_{250}\text{N}_{20}\text{Na}_2\text{O}_{34}$ m/z 1569.4132, found m/z 1569.4113; $[\text{M}+2\text{H}]^{2+}$ calc. for $\text{C}_{168}\text{H}_{252}\text{N}_{20}\text{O}_{34}$ m/z 1547.4313, found m/z 1547.4319.

***N,N'*-Bis({25,26,27,28-Tetrabutoxy 11,17,23-tris[(guanidinium)methyl]calix[4]arene-5-yl}methyl)hexanediamide Hexachloride (12)**



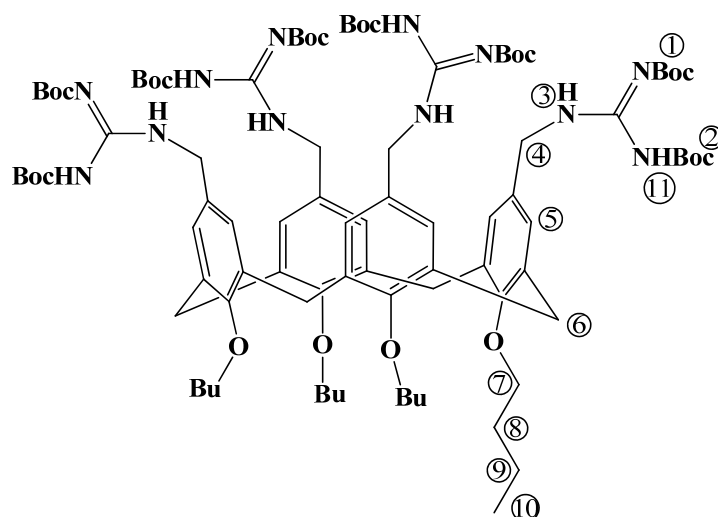
N,N'-Bis(11,17,23-Tris{[2,3-bis(tert-butoxycarbonyl)guanidino]methyl}-25,26,27,28-tetrabutoxycalix[4]aren-5-ylmethyl}hexanediamide (0.012 g, 0.004 mmol) was dissolved in anhydrous MeOH (10 mL). To this solution was added 1 M HCl (1 mL). The resulting solution was stirred for 16 h at r.t. and subsequently evaporated to dryness. The solid was washed with acetone to yield 0.007 g (85%) of product.

¹H-NMR (300 MHz, DMSO-*d*₆): δ (ppm) = 7.84 (bs, 2H, CNH₂Cl), 7.00-7.50 (bs, 8H, Benzal-NH), 6.71 (s, 4H, Ar-H), 6.70 (s, 4H, Ar-H), 6.66 (s, 4H, Ar-H), 6.60 (s, 4H, Ar-H), 4.31 (m, 8H, Ar-CH₂-Ar), 4.05 (m, 16H, Ar-CH₂-N), 3.80 (m, 16H, Ar-O-CH₂-), 3.10 (m, 8H, Ar-CH₂-Ar), 2.13 (m, 4H, N-CO-CH₂-), 1.86 (m, 16H, Ar-O-CH₂-CH₂-), 1.36-1.52 (m, 20H, N-CO-CH₂-CH₂-, Ar-O-CH₂-CH₂-CH₂-), 0.95 (m, 24H, Ar-O-CH₂-CH₂-CH₂-CH₃).

¹³C-NMR (125.6 MHz, CD₃OD): 159.32, 158.55, 158.50, 157.81, 157.51, 156.81, 137.08, 136.91, 136.42, 135.90, 133.34, 130.88, 129.14, 129.07, 128.95, 128.70, 76.27, 73.78, 70.62, 46.13, 43.90, 43.05, 36.89, 33.71, 33.67, 33.61, 32.04, 31.97, 28.38, 26.75, 20.74, 20.69, 20.62, 14.65, 14.63, 14.60.

MS (ESI-TOF, pos. MeOH, free base): [M+3H]³⁺ calc. for C₁₀₈H₁₅₇N₂₀O₁₀ *m/z* 631.4125, found *m/z* 631.4155.

5,11,17,23-Tetrakis{[2,3-bis(*tert*-butoxycarbonyl)guanidino]methyl}-25,26,27,28-tetrabutoxycalix[4]arene (13)



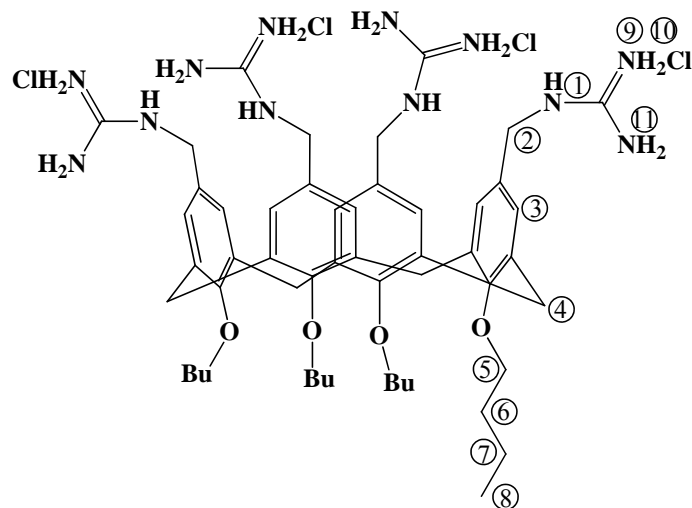
25,26,27,28-Tetrabutoxy-5,11,17,23-tetrakis(aminomethyl)calix[4]arene tetrahydrochloride (0.091 g, 0.1 mmol) was dissolved in the mixture of anhydrous MeOH (10 mL) and Et₃N (1 mL). *N,N'*-bis-Boc-2-methyl-2-thiopseudourea (0.17 g, 0.59 mmol) was added to the solution followed by AgNO₃ (0.11 g, 0.65 mmol). The mixture was stirred for 24 h at r.t. The catalyst was filtered off over celite and the solution was evaporated to dryness. The residue was purified by flash column chromatography (SiO₂, DCM/cyclohexane, 70:30). Yield: 0.062 g (36%)

¹H-NMR (300 MHz, CDCl₃): δ (ppm) = 11.45 (s, 4H, H-11), 8.26 (t, 4H, *J* = 4.62, H-3), 6.59 (s, 8H, H-5), 4.38 (d, 4H, *J* = 12.99, H-6), 4.27 (d, 4H, H-4), 3.85 (t, 8H, *J* = 7.55, H-7), 3.10 (d, 4H, H-6), 1.89 (quintet, 8H, H-8), 1.45-1.48 (m, 80H, H-9, H-1, H-2), 0.98 (t, 12H, H-10).

¹³C-NMR (75 MHz, CDCl₃): δ (ppm) = 163.68, 156.00, 155.66, 153.10, 135.01, 130.56, 127.88, 82.78, 81.96, 75.07, 44.96, 32.31, 28.41, 28.15, 26.96, 19.40, 14.14.

MS (ESI-TOF, pos. CH₂Cl₂): [M+Na]⁺ calc. for C₉₂H₁₄₀N₁₂NaO₂₀ *m/z* 1756.0199, found *m/z* 1756.0345; [M+H]⁺ calc. for C₉₂H₁₄₁N₁₂O₂₀ *m/z* 1734.0380, found *m/z* 1734.0510.

**25,26,27,28-Tetrabutoxy-5,11,17,23-tetrakis[(guanidinium)methyl]calix[4]arene
Tetrachloride (14)**



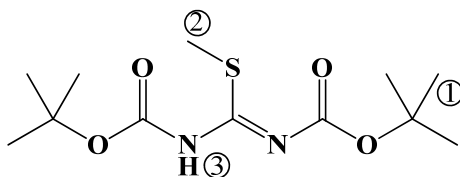
5,11,17,23-Tetrakis{[2,3-bis(*tert*-butoxycarbonyl)guanidino]methyl}-25,26,27,28-tetrabutoxycalix[4]arene (0.062 g, 0.036 mmol) was dissolved in anhydrous MeOH (10 mL). To this solution was added 1 M HCl (1 mL). The resulting solution was stirred for 16 h at r.t. and subsequently evaporated to dryness. The solid was washed with acetone to yield 0.028 g (72%) of product.

¹H-NMR (300 MHz, DMSO-*d*₆): δ (ppm) = 7.90 (t, 4H, J = 5.41, H-1), 7.02-7.36 (bs, 16H, H-9, H-10, H-11), 6.69 (s, 8H, H-3), 4.32 (d, 4H, J = 12.91, H-4), 4.08 (d, 4H, H-2), 3.80 (t, 8H, J = 7.22, H-5), 3.15 (d, 4H, H-4), 1.85 (quintet, 8H, H-6), 1.41 (sextet, 8H, H-7), 0.96 (t, 12H, H-8).

¹³C-NMR (75 MHz, DMSO-*d*₆): δ (ppm) = 156.66, 155.50, 134.50, 130.17, 127.58, 74.54, 44.03, 31.77, 30.12, 18.81, 13.87.

MS (ESI-TOF, pos. MeOH, free base): $[M+H]^+$ calc. for C₅₂H₇₇N₁₂O₄ m/z 933.6185, found m/z 933.6296.

***N, N'*-bis-Boc-2-methyl-2-thiopseudourea (15)** ^[158]



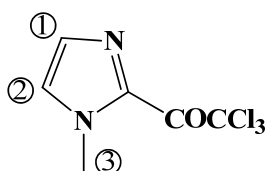
A mixture of di-*tert*-butyl dicarbonate (10 g, 45.82 mmol) and 2-methyl-2-thiopseudourea sulphate (2.0 g, 9.0 mmol) in 100 mL of 1:1 CH₂Cl₂ and saturated NaHCO₃ were stirred for 2 weeks at room temperature. Afterwards it was extracted with dichloromethane (100 mL) and purified by flash column chromatography (n-hexane: ethyl acetate 80:20) gave a white product. Yield: 78 %

¹H-NMR (300 MHz, CDCl₃): δ (ppm) = 1.51 (s, 18 H, H-1), 2.39 (s, 3 H, H-2), 11.59 (s, 1H, H-3).

¹³C-NMR (75 MHz, CDCl₃): δ (ppm) = 161.26, 151.30, 149.19, 83.92, 81.48, 28.57, 14.93.

MS (ESI-TOF, pos. CH₂Cl₂): [M+Na]⁺ calc. for C₁₂H₂₂N₂NaO₄S *m/z* 313.1192, found *m/z* 313.1230.

2-Trichloroacety-1-methylimidazole (16) ^[164]



N-Methylimidazole (50 g, 0.60 mol) in DCM (500 mL) was added dropwise to trichloroacetyl chloride (110 g, 0.60 mol) in CH₂Cl₂ (500 mL) over a period of 12 h. The mixture was then stirred for 12 h and cooled to 0 °C, and Et₃N (85 mL, 0.60 mol) was added dropwise over 10 h. The solvent was evaporated and the residue purified by flash chromatography (silica gel,

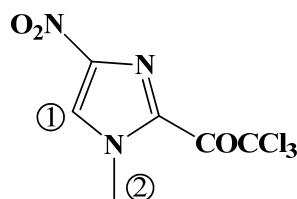
1:1 ethyl acetate/cyclohexane) to yield 94.6g, 68% as a white solid.

¹H-NMR (300 MHz, CDCl₃): δ (ppm) = 7.26 (s, 1H, H-1), 7.08 (s, 1H, H-2), 3.98 (s, 3H, H-3).

¹³C-NMR (75 MHz, CDCl₃): δ (ppm) = 172.45, 136.35, 130.97, 128.78, 95.03, 77.26, 37.36.

MS (ESI-TOF, pos. CH₂Cl₂): [M+H]⁺ calc. for C₆H₆Cl₃N₂O *m/z* 226.9540, found *m/z* 226.9555.

4-Nitro-2-trichloroacetyl-1-methylimidazole (17) ^[164]



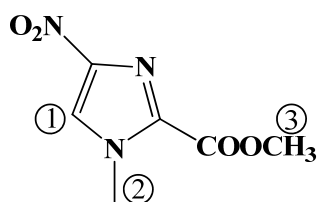
To acetic anhydride (100 mL) at 0 °C was added dropwise fuming HNO₃ (15 mL), followed by H₂SO₄ (0.10 mL). 2-trichloroacetyl-1-methylimidazole (15.0 g, 0.066 mol) was added slowly, and the solution was warmed slowly to room temperature and stirred overnight. The mixture was diluted with ice-water and extracted with chloroform. The organic layer was washed with NaHCO₃ (sat.) and dried (MgSO₄) and concentrated. The residue was purified by flash chromatography (silica gel, 1:1 ethyl acetate/cyclohexane) to yield 11.2 g, 62% as a white solid.

¹H-NMR (300 MHz, CDCl₃): δ (ppm) = 7.96 (s, 1H, H-1), 4.16 (s, 3H, H-2).

¹³C-NMR (75 MHz, CDCl₃): δ (ppm) = 172.96, 133.73, 130.68, 126.12, 93.62, 38.44.

MS (ESI-TOF, pos. CH₂Cl₂): [M+H]⁺ calc. for C₆H₅Cl₃N₃O₃ *m/z* 271.9391, found *m/z* 271.9399.

Methyl 1-Methyl-4-nitroimidazole-2-carboxylate (**18**) ^[164]



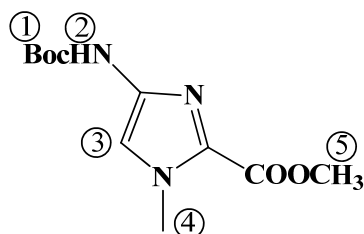
To 4-nitro-2-trichloroacety-1-methylimidazole (5.4 g, 0.02 mol) in anhydrous methanol (200 mL) was added sodium methoxide (4.32 g, 0.08 mol) and the solution stirred for 6 h. The reaction was quenched by the addition of HCl (pH=7.0). The solvent was evaporated. Water and DCM was added. The organic layer was dried by MgSO₄, and the residue was purified by flash chromatography (silica gel, 1:1 ethyl acetate/cyclohexane) to yield 3.0 g (80%) as a white solid.

¹H-NMR (300 MHz, DMSO-*d*₆): δ (ppm) = 8.60 (s, 1H, H-1), 3.97 (s, 3H, H-3), 3.86 (s, 3H, H-2).

¹³C-NMR (75 MHz, DMSO-*d*₆): δ (ppm) = 158.13, 144.88, 134.68, 126.77, 52.57, 36.70.

MS (ESI-TOF, pos. CH₂Cl₂): [M+Na]⁺ calc. for C₆H₇N₃NaO₄ *m/z* 208.0329, found *m/z* 208.0344; [M+H]⁺ calc. for C₆H₈N₃O₄ *m/z* 186.0509, found *m/z* 186.0528.

Methyl 4-[(*tert*-Butoxycarbonyl)amino]-1-methylimidazole-2-carboxylate (**19**) ^[164]



To methyl 1-methyl-4-nitroimidazole-2-carboxylate (1.85 g, 0.01 mol) in anhydrous methanol (100 mL) was added *tert*-butyl dicarbonate (6.5 g, 0.03 mol) followed by 10% Pd/C (0.10 g),

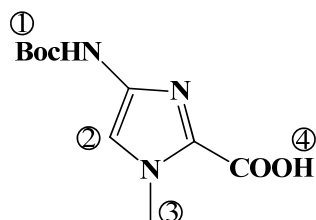
and the mixture was stirred under a hydrogen atmosphere for 24 h. H₂ was removed. The catalyst was filtered off over Celite and the solvent was evaporated. Water and DCM was added. The organic layer was dried by MgSO₄ and the residue was purified by flash chromatography (silica gel, 1:1 ethyl acetate/cyclohexane) to yield 2.1 g (82%) as a white solid.

¹H-NMR (300 MHz, CDCl₃): δ (ppm) = 7.23 (s, 1H, H-2), 6.85 (s, 1H, H-3), 3.97 (s, 3H, H-5), 3.92 (s, 3H, H-4), 1.50 (s, 9H, H-1).

¹³C-NMR (75 MHz, CDCl₃): δ (ppm) = 159.31, 152.64, 149.72, 137.99, 113.33, 81.08, 52.35, 35.98, 28.41.

MS (ESI-TOF, pos. CH₂Cl₂): [M+Na]⁺ calc. for C₁₁H₁₇N₃NaO₄ *m/z* 278.1111, found *m/z* 278.1124; [M+H]⁺ calc. for C₁₁H₁₈N₃O₄ *m/z* 256.1292, found *m/z* 256.1306.

4-[(*tert*-Butoxycarbonyl)amino]-1-methylimidazole-2-carboxylic Acid (20) ^[164]



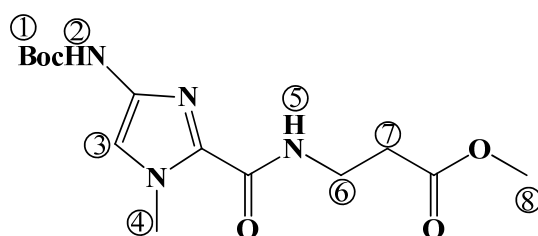
To sodium *tert*-butoxide (9.6 g, 0.1 mol) in dry THF (60 mL) at 0 °C was added water (100 mL) and the solution stirred for one hour. Methyl 4-[(*tert*-Butoxycarbonyl)amino]-1-methylimidazole-2-carboxylate (2.6 g, 0.01 mol) was added and the mixture stirred at room temperature for 3 h. It was then diluted with cold water and ethyl acetate, the layers were separated. The aqueous layer was acidified by HCl. The aqueous layer was extracted with ethyl acetate, dried (MgSO₄), and concentrated to yield 2.2 g (91%) as a white solid.

¹H-NMR (300 MHz, CDCl₃): δ (ppm) = 10.92 (s, 1H, H-4), 7.18 (s, 1H, H-2), 4.14 (s, 3H, H-3), 1.54 (s, 9H, H-1).

¹³C-NMR (75 MHz, CDCl₃): δ (ppm) = 159.72, 152.78, 133.90, 132.83, 109.28, 81.53, 35.57, 28.23.

MS (ESI-TOF, pos. CH₂Cl₂): [M+Na]⁺ calc. for C₁₀H₁₅N₃NaO₄ *m/z* 264.0955, found *m/z* 264.0991; [M+H]⁺ calc. for C₁₀H₁₅N₃O₄ *m/z* 241.1057, found *m/z* 241.1007.

3-[(4-*tert*-Butoxycarbonylamino-1-methyl-1*H*-imidazole-2-carbonyl)-amino]-propionic acid methyl ester (21) ^[165]



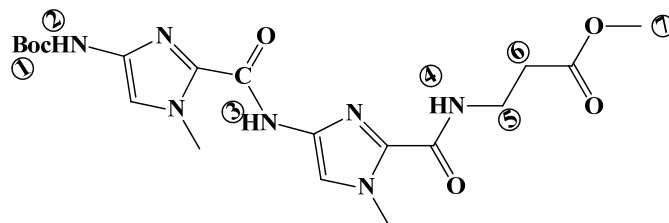
4-[(*tert*-Butoxycarbonyl)amino]-1-methylimidazole-2-carboxylic Acid (2.41 g, 0.01 mol) was dissolved in 20 mL of anhydrous DMF. HBTU (3.79 g, 0.01 mol) was added followed by DIEA (10 mL) and the solution stirred for 10 min. β-Alanine methyl ester hydrochloride (1.40 g, 0.01 mol) was added to the solution. The mixture stirred at room temperature for 18 h. DMF was removed in vacuo. The residue was purified by flash chromatography (silica gel, 1:1 ethyl acetate/cyclohexane) to yield 2.3 g (71%) as a white solid.

¹H-NMR (300 MHz, CDCl₃): δ (ppm) = 7.63 (bs, 1H, H-5), 7.19 (s, 1H, H-2), 7.08 (s, 1H, H-3), 3.97 (s, 3H, H-8), 3.68 (s, 3H, H-4), 3.62 (q, 2H, H-6), 2.60 (t, 2H, *J* = 6.38, H-7), 1.49 (s, 9H, H-1).

¹³C-NMR (75 MHz, CDCl₃): δ (ppm) = 172.62, 158.94, 152.66, 136.53, 133.79, 112.01, 80.93, 51.95, 35.66, 34.63, 34.04, 28.39.

MS (ESI-TOF, pos. CH₂Cl₂): [M+Na]⁺ calc. for C₁₄H₂₂N₄NaO₅ *m/z* 349.1482, found *m/z* 349.1514.

3-({4-[4-*tert*-Butoxycarbonylamino-1-methyl-1*H*-imidazole-2-carbonyl]-amino]-1-methyl-1-*H*-imidazole-2-carbonyl)-amino)-propionic acid methyl ester (22) ^[165]



2 mL of the mixture (80% TFA/DCM/0.4 M PhSH) was added to (**21**) (2.3 g, 7 mmol), and the reaction mixture was stirred for 10 min. The solvent was removed in vacuo.

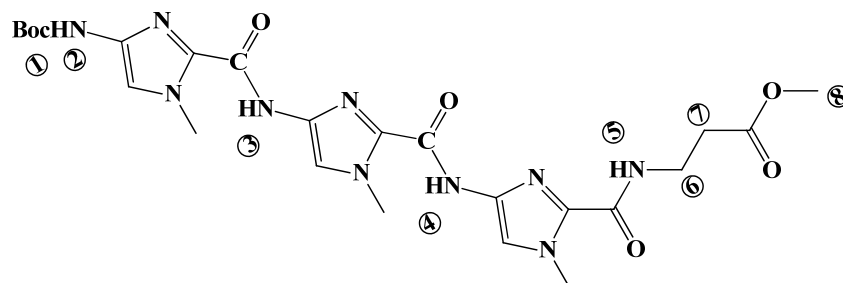
Separately, (**20**) (1.68 g, 7 mmol) was dissolved in 20 mL anhydrous DMF. HBTU (2.6 g, 7 mmol) was added followed by DIEA (10 mL). The reaction mixture was stirred for 10 min and immediately added to the deprotected compound. The mixture was stirred at room temperature for 18 h. DMF was removed in vacuo. The residue was purified by flash chromatography (silica gel, 1:1 ethyl acetate/cyclohexane) to yield 2.3 g (73%) as a white solid.

¹H-NMR (300 MHz, CDCl₃): δ (ppm) = 9.45 (s, 1H, H-3), 7.69 (t, 1H, $J = 6.29$, H-4), 7.40 (m, 2H, H-2, Im-H), 7.16 (s, 1H, Im-H), 4.01 (s, 3H, Im-CH₃), 4.00 (s, 3H, Im-CH₃), 3.69 (s, 3H, H-7), 3.65 (q, 2H, H-5), 2.62 (t, 2H, $J = 6.23$, H-6), 1.50 (s, 9H, H-1).

¹³C-NMR (75 MHz, CDCl₃): δ (ppm) = 172.68, 159.10, 156.00, 152.75, 137.07, 135.44, 134.26, 113.87, 112.79, 80.99, 51.99, 35.75, 35.68, 34.69, 34.03, 28.41.

MS (ESI-TOF, pos. CH₂Cl₂): [M+Na]⁺ calc. for C₁₉H₂₇N₇NaO₆ m/z 472.1915, found m/z 472.1946; [M+H]⁺ calc. for C₁₉H₂₈N₇O₆ m/z 450.2096, found m/z 450.2129.

3-[[4-({4-[(4-*tert*-Butoxycarbonylamino-1-methyl-1*H*-imidazole-2-carbonyl)-amino]-1-methyl-1*H*-imidazole-2-carbonyl}-amino)-1-methyl-1*H*-imidazole-2-carbonyl]-amino]-propionic acid methyl ester (23) ^[165]



2 mL of the mixture (TFA : DCM = 4 : 1) was added to (22) (2.3 g, 5.12 mmol), and the reaction mixture was stirred for 10 min. The solvent was removed in vacuo.

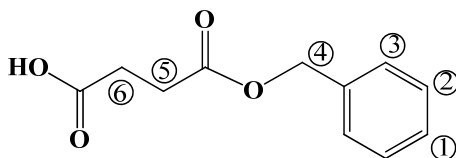
Separately, (20) (1.23 g, 5.12 mmol) was dissolved in 20 mL anhydrous DMF. HBTU (1.94 g, 5.12 mmol) was added followed by DIEA (10 mL). The reaction mixture was stirred for 10 min and immediately added to the deprotected compound. The mixture was stirred at room temperature for 18 h. DMF was removed in vacuo. The residue was purified by flash chromatography (silica gel, 1:1 ethyl acetate/cyclohexane) to yield 2.0 g (68%) as a white solid.

¹H-NMR (300 MHz, CDCl₃): δ (ppm) = 9.40 (s, 1H, H-3), 9.38 (s, 1H, H-4), 7.47 (s, 1H, H-2), 7.41 (s, 1H, Im-H), 7.18 (bs, 2H, Im-H), 4.05 (s, 3H, Im-CH₃), 4.04 (s, 3H, Im-CH₃), 4.02 (s, 3H, Im-CH₃), 3.72 (s, 3H, H-8), 3.67 (q, 2H, H-6), 2.64 (t, 2H, $J = 6.22$, H-7), 1.52 (s, 9H, H-1).

¹³C-NMR (75 MHz, CDCl₃): δ (ppm) = 172.60, 159.18, 156.13, 156.01, 152.80, 137.24, 135.84, 135.46, 134.33, 133.78, 133.36, 125.59, 114.59, 113.90, 112.79, 80.87, 51.96, 35.71, 35.67, 34.72, 34.05, 28.40.

MS (ESI-TOF, pos. CH₂Cl₂): $[M+Na]^+$ calc. for C₂₄H₃₂N₁₀NaO₇ m/z 595.2348, found m/z 595.2384; $[M+H]^+$ calc. for C₂₄H₃₃N₁₀O₇ m/z 573.2528, found m/z 573.2560.

Succinic acid monobenzyl ester (24)



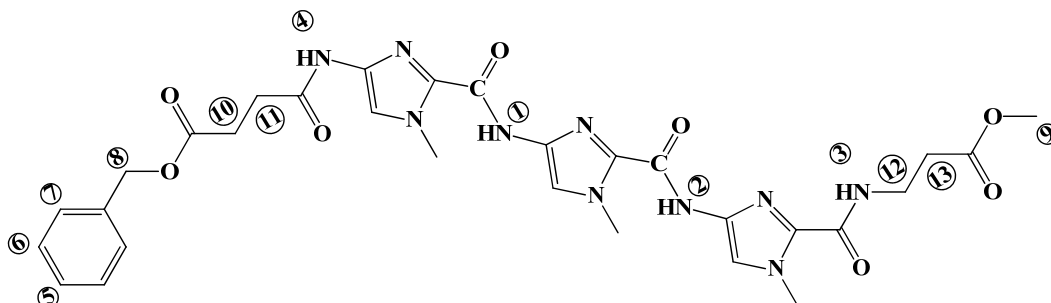
To succinyl chloride (1.55 g, 0.01 mol) in anhydrous DCM (100 mL) at -20 °C was added benzyl alcohol (1.08 g, 0.01 mol) and the reaction mixture was warmed slowly to room temperature and stirred for 3 days. Water (100 mL) was added followed by NaHCO₃ (1.68 g, 0.02 mol). The mixture was stirred at room temperature for 3 h. The layers were separated. The organic layer was dried by MgSO₄. The residue was purified by flash chromatography (silica gel, 1:1 ethyl acetate/cyclohexane) to yield 0.35 g (17%) as a white solid.

¹H-NMR (300 MHz, CDCl₃): δ (ppm) = 7.23-7.28 (m, 5H, H-1, H-2, H-3), 5.06 (s, 2H, H-4), 2.57-2.64 (m, 4H, H-5, H-6).

¹³C-NMR (75 MHz, CDCl₃): δ (ppm) = 177.83, 172.10, 135.82, 128.72, 128.44, 128.35, 66.80, 29.04, 28.98.

MS (ESI-TOF, pos. CH₂Cl₂): [M+Na]⁺ calc. for C₁₁H₁₂NaO₄ *m/z* 231.0628, found *m/z* 231.0653.

N-(2-{2-[2-(2-Methoxycarbonyl-ethylcarbamoyl)-1-methyl-1*H*-imidazol-4-ylcarbamoyl]-1-methyl-1*H*-imidazol-4-ylcarbamoyl}-1-methyl-1*H*-imidazol-4-yl)-succinamic acid benzyl ester (25)



2 mL of the mixture (TFA : DCM = 4 : 1) was added to (**23**) (0.98 g, 1.48 mmol), and the reaction mixture was stirred for 10 min. The solvent was removed in vacuo.

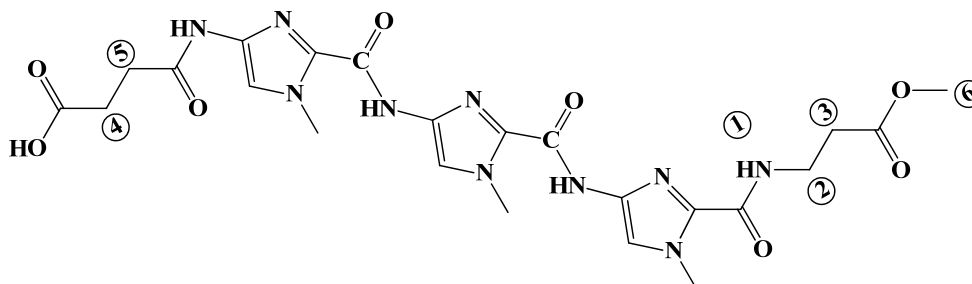
Separately, (**24**) (0.308 g, 1.48 mmol) was dissolved in 20 mL anhydrous DMF. HBTU (0.56 g, 1.48 mmol) was added followed by DIEA (10 mL). The reaction mixture was stirred for 10 min and immediately added to the deprotected compound. The mixture was stirred at room temperature for 18 h. DMF was removed in vacuo. The residue was purified by flash chromatography (silica gel, 1:1 ethyl acetate/cyclohexane) to yield 0.64 g (65%) as a white solid.

¹H-NMR (300 MHz, CDCl₃): δ (ppm) = 9.62 (bs, 2H, H-1, H-2), 8.90 (s, 1H, H-4), 7.81 (t, 1H, $J = 6.09$, H-3), 7.39 (s, 1H, Im-H), 7.37 (s, 1H, Im-H), 7.36 (s, 1H, Im-H), 7.26 (m, 5H, H-5, H-6, H-7), 5.05 (s, 2H, H-8), 3.95 (s, 3H, Im-CH₃), 3.94 (s, 3H, Im-CH₃), 3.93 (s, 3H, Im-CH₃), 3.61 (q, 2H, H-12), 3.60 (s, 3H, H-9), 2.72 (t, 2H, $J = 4.67$, H-11), 2.69 (t, 2H, H-10), 2.57 (t, 2H, $J = 6.34$, H-13).

¹³C-NMR (75 MHz, CDCl₃): δ (ppm) = 172.77, 172.69, 169.43, 158.65, 156.02, 155.78, 136.04, 135.83, 135.71, 134.75, 134.02, 133.66, 132.97, 128.68, 128.39, 128.29, 114.94, 114.90, 114.03, 66.77, 52.00, 35.94, 35.85, 34.94, 33.92, 30.93, 29.41.

MS (ESI-TOF, pos. CH₂Cl₂): [M+Na]⁺ calc. for C₃₀H₃₄N₁₀NaO₈ m/z 685.2453, found m/z 685.2504; [M+H]⁺ calc. for C₃₀H₃₅N₁₀O₈ m/z 663.2634, found m/z 663.2679.

N-(2-{2-[2-(2-Methoxycarbonyl-ethylcarbamoyl)-1-methyl-1*H*-imidazol-4-ylcarbamoyl]-1-methyl-1*H*-imidazol-4-ylcarbamoyl}-1-methyl-1*H*-imidazol-4-yl)-succinamic acid (26)



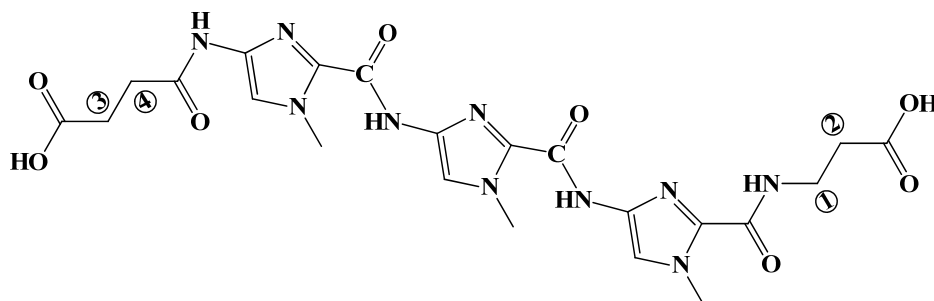
(25) (0.3 g, 0.36 mmol) were dissolved in 20 mL of the mixture (THF : H₂O = 4 : 1) and Pd/C (0.03 g, 10 weight-%) was added. The hydrogenation was then carried out for 24 h. The catalyst was filtered off over Celite and the solution was evaporated to dryness. The residue was washed with DCM to yield 0.185 g (90%) as a white solid.

¹H-NMR (300 MHz, DMSO-*d*₆): δ (ppm) = 10.40 (s, 1H, Im-NH-CO), 9.66 (s, 1H, Im-NH-CO), 9.62 (s, 1H, Im-NH-CO), 8.24 (t, 1H, *J* = 5.51, H-1), 7.63 (s, 1H, Im-H), 7.52 (s, 1H, Im-H), 7.49 (s, 1H, Im-H), 4.00 (s, 3H, Im-CH₃), 3.95 (s, 3H, Im-CH₃), 3.95 (s, 3H, Im-CH₃), 3.61 (s, 3H, H-6), 3.45 (q, 2H, H-2), 2.52-2.60 (m, 6H, H-3, H-4, H-5).

¹³C-NMR (75 MHz, DMSO-*d*₆): δ (ppm) = 173.70, 171.84, 169.01, 158.36, 155.51, 155.37, 136.45, 135.06, 134.55, 134.12, 133.27, 132.72, 114.68, 114.53, 114.10, 51.40, 35.21, 35.08, 34.98, 34.46, 33.49, 29.95, 28.78.

MS (ESI-TOF, pos. MeOH): [M+Na]⁺ calc. for C₂₃H₂₈N₁₀NaO₈ *m/z* 595.1984, found *m/z* 595.2010; [M+H]⁺ calc. for C₂₃H₂₉N₁₀O₈ *m/z* 573.2164, found *m/z* 573.2188.

N-(2-{2-[2-(2-Carboxy-ethylcarbamoyl)-1-methyl-1*H*-imidazol-4-ylcarbamoyl]-1-methyl-1*H*-imidazol-4-ylcarbamoyl]-1-methyl-1*H*-imidazol-4-yl)-succinamic acid (27)



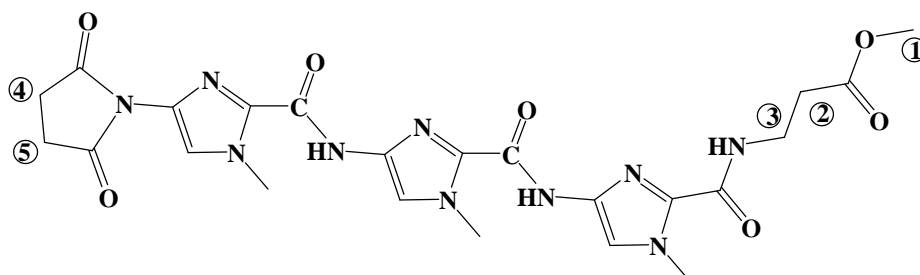
To sodium *tert*-butoxide (0.1 g, 0.001 mol) in dry THF (10 mL) at 0 °C was added water (10 mL) and the solution was stirred for one hour. **(26)** (0.64 g, 1 mmol) was added and the mixture was stirred at room temperature for 3 h. The reaction was cooled and quenched by the addition of HCl. The solvent was removed in vacuo. The product was extracted with methanol. Yield: 0.32 g (60%)

¹H-NMR (300 MHz, D₂O): δ (ppm) = 7.16 (s, 1H, Im-H), 7.00 (s, 1H, Im-H), 6.95 (s, 1H, Im-H), 3.81 (s, 3H, Im-CH₃), 3.80 (s, 3H, Im-CH₃), 3.78 (s, 3H, Im-CH₃), 3.33 (t, 2H, *J* = 7.31, H-1), 2.38-2.44 (m, 6H, H-2, H-3, H-4).

¹³C-NMR (75 MHz, D₂O): δ (ppm) = 180.85, 180.13, 172.27, 159.16, 155.23, 155.08, 135.43, 135.07, 134.75, 133.63, 132.67, 132.58, 114.98, 114.40, 114.04, 37.42, 36.73, 36.39, 35.70, 35.49, 32.43, 31.96.

MS (ESI-TOF, pos. CH₂Cl₂): [M+Na]⁺ calc. for C₂₂H₂₆N₁₀NaO₈ *m/z* 581.1827, found *m/z* 581.1848; [M+H]⁺ calc. for C₂₂H₂₇N₁₀O₈ *m/z* 559.2008, found *m/z* 559.2017.

3-({4-[4-{[4-(2,5-Dioxo-pyrrolidin-1-yl)-1-methyl-1*H*-imidazole-2-carbonyl]-amino}-1-methyl-1*H*-imidazole-2-carbonyl]-amino}-1-methyl-1*H*-imidazole-2-carbonyl)-amino)-propionic acid methyl ester (28)



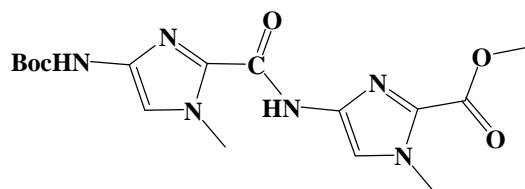
(26) (57.3 mg, 0.1 mmol) was dissolved in 20 mL anhydrous DMF. HBTU (38.0 mg, 0.1 mmol) was added followed by DIEA (10 mL). The reaction mixture was stirred for 10 min and immediately added to (7) (107 mg, 0.1 mmol). The mixture was stirred at room temperature for 18 h. DMF was removed in vacuo. The residue was purified by flash chromatography (silica gel, 1:1 ethyl acetate/cyclohexane) to yield 42.1 mg (74%) as a white solid.

¹H-NMR (300 MHz, DMSO-*d*₆): δ (ppm) = 10.09 (s, 1H, Im-NH-CO), 9.81 (s, 1H, Im-NH-CO), 8.32 (t, 1H, *J* = 5.51, Im-CO-NH), 7.64 (s, 1H, Im-H), 7.52 (s, 1H, Im-H), 7.52 (s, 1H, Im-H), 4.05 (s, 3H, Im-CH₃), 4.02 (s, 3H, Im-CH₃), 3.96 (s, 3H, Im-CH₃), 3.62 (s, 3H, H-1), 3.46 (q, 2H, H-3), 2.83 (m, 4H, H-4, H-5), 2.59 (t, 2H, H-2).

¹³C-NMR (125.6 MHz, DMSO-*d*₆): δ (ppm) = 176.58, 171.84, 158.42, 155.49, 155.44, 155.35, 136.03, 134.99, 134.64, 134.50, 134.12, 134.08, 133.36, 128.75, 123.00, 51.44, 45.67, 35.58, 35.23, 35.10, 34.50, 33.51, 28.38.

MS (ESI-TOF, pos. MeOH): [M+Na]⁺ calc. for C₂₃H₂₆N₁₀NaO₇ *m/z* 577.1878, found *m/z* 577.1879; [M+H]⁺ calc. for C₂₃H₂₇N₁₀O₇ *m/z* 555.2059, found *m/z* 555.2048.

4-[(4-*tert*-Butoxycarbonylamino-1-methyl-1*H*-imidazole-2-carbonyl)-amino]-1-methyl-1*H*-imidazole-2-carboxylic acid methyl ester (29) ^[165]



2 mL of the mixture (TFA : DCM = 4 : 1) was added to methyl 4-[(*tert*-butoxycarbonyl)amino]-1-methylimidazole-2-carboxylate (**19**) (2.55 g, 10 mmol), and the reaction mixture was stirred for 10 min. The solvent was removed in vacuo.

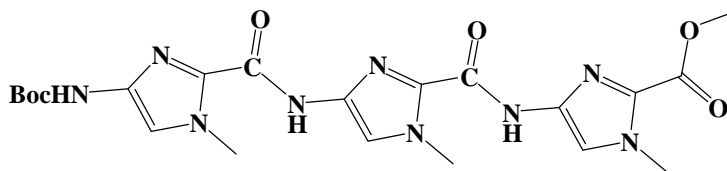
Separately, 4-[(*tert*-Butoxycarbonyl)amino]-1-methylimidazole-2-carboxylic Acid (**20**) (2.40 g, 10 mmol) was dissolved in 20 ml anhydrous DMF. HBTU (3.79 g, 10 mmol) was added followed by DIEA (10 mL). The reaction mixture was stirred for 10 min and immediately added to the deprotected compound. The mixture was stirred at room temperature for 18 h. DMF was removed in vacuo. The residue was purified by flash chromatography (silica gel, 1:1 ethyl acetate/cyclohexane) to yield 2.65 g (70%) as a white solid.

¹H-NMR (300 MHz, CDCl₃): δ (ppm) = 7.57 (s, 1H, Im-NH), 7.17 (s, 1H, Im-H), 6.87 (s, 1H, Im-H), 4.04 (s, 3H, Im-CH₃), 4.02 (s, 3H, Im-CH₃), 3.96 (s, 3H, Im-COOCH₃), 1.52 (s, 9H, -C(CH₃)₃).

¹³C-NMR (75 MHz, CDCl₃): δ (ppm) = 159.15, 156.17, 152.62, 137.19, 136.83, 133.09, 131.66, 114.99, 112.75, 80.83, 52.40, 35.98, 35.56, 28.33.

MS (ESI-TOF, pos. CH₂Cl₂): [M+Na]⁺ calc. for C₁₆H₂₂N₆NaO₅ m/z 401.1544, found m/z 401.1582; [M+H]⁺ calc. for C₁₆H₂₃N₆O₅ m/z 379.1724, found m/z 379.1755.

4-({4-[4-*tert*-Butoxycarbonylamino-1-methyl-1*H*-imidazole-2-carbonyl]-amino]-1-methyl-1*H*-imidazole-2-carbonyl}-amino)-1-methyl-1*H*-imidazole-2-carboxylic acid methyl ester (30) ^[165]



2 mL of the mixture (TFA : DCM = 4 : 1) was added to (**29**) (2.65 g, 7 mmol), and the reaction mixture was stirred for 10 min. The solvent was removed in vacuo.

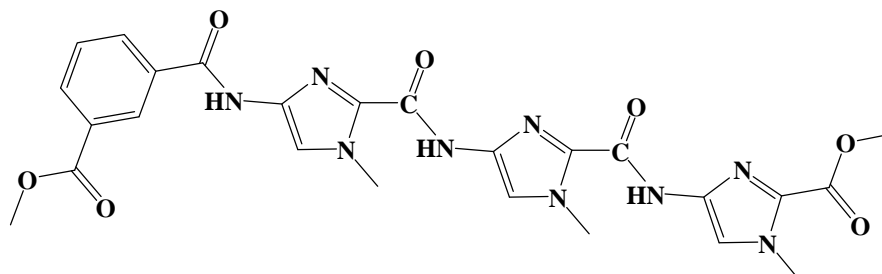
Separately, 4-[(*tert*-butoxycarbonyl)amino]-1-methylimidazole-2-carboxylic Acid (**20**) (2.40 g, 10 mmol) was dissolved in 20 mL anhydrous DMF. HBTU (3.79 g, 10 mmol) was added followed by DIEA (10 mL). The reaction mixture was stirred for 10 min and immediately added to the deprotected compound. The mixture was stirred at room temperature for 18 h. DMF was removed in vacuo. The residue was purified by flash chromatography (silica gel, 1:1 ethyl acetate/cyclohexane) to yield 2.18 g (62%) as a white solid.

¹H-NMR (300 MHz, CDCl₃): δ (ppm) = 9.62 (s, 1H, Im-NH), 9.32 (s, 1H, Im-NH), 7.58 (s, 1H, Im-H), 7.45 (s, 1H, Im-H), 7.16 (s, 1H, Im-H), 4.04 (s, 3H, Im-CH₃), 4.01 (s, 3H, Im-CH₃), 4.00 (s, 3H, Im-CH₃), 3.90 (s, 3H, Im-COOCH₃), 1.50 (s, 9H, -C(CH₃)₃).

¹³C-NMR (75 MHz, CDCl₃): δ (ppm) = 159.10, 156.14, 156.00, 152.74, 137.16, 136.71, 135.96, 133.41, 133.17, 131.67, 115.06, 114.59, 112.87, 80.94, 52.45, 36.12, 35.75, 35.68, 28.41.

MS (ESI-TOF, pos. CH₂Cl₂): [M+Na]⁺ calc. for C₂₁H₂₇N₉NaO₆ *m/z* 524.1977, found *m/z* 524.2023; [M+H]⁺ calc. for C₂₁H₂₈N₉O₆ *m/z* 502.2157, found *m/z* 502.2200.

4-[(4-{[4-(3-Methoxycarbonyl-benzoylamino)-1-methyl-1*H*-imidazole-2-carbonyl]-amino}-1-methyl-1*H*-imidazole-2-carbonyl)-amino]-1-methyl-1*H*-imidazole-2-carboxylic acid methyl ester (31)



2 mL of the mixture (TFA : DCM = 4 : 1) was added to (**30**) (1.00 g, 2 mmol), and the reaction mixture was stirred for 10 min. The solvent was removed in vacuo.

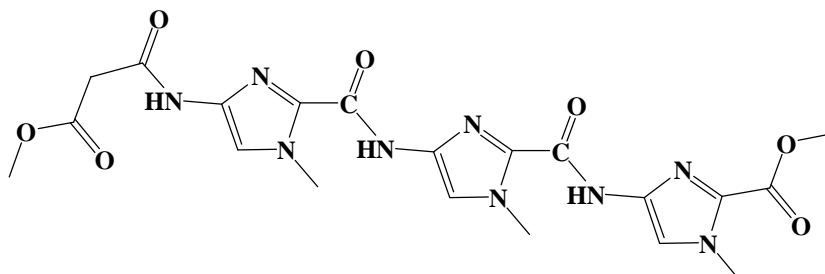
Separately, mono-methyl isophthalate (0.36 g, 2 mmol) was dissolved in 20 mL anhydrous DMF. HBTU (0.76 g, 2 mmol) was added followed by DIEA (10 mL). The reaction mixture was stirred for 10 min and immediately added to the deprotected compound. The mixture was stirred at room temperature for 18 h. DMF was removed in vacuo. The residue was purified by flash chromatography (silica gel, 1:1 ethyl acetate/cyclohexane) to yield 0.47 g (42%) as a white solid.

¹H-NMR (300 MHz, DMSO-*d*₆): δ (ppm) = 11.25 (s, 1H, Im-NH), 10.08 (s, 1H, Im-NH), 9.59 (s, 1H, Im-NH), 8.31 (m, 1H, benzene-H), 8.15 (m, 3H, benzene-H), 7.74 (s, 1H, Im-H), 7.74 (s, 1H, Im-H), 7.66 (s, 1H, Im-H), 4.03 (s, 3H, Im-CH₃), 3.94 (s, 3H, Im-CH₃), 3.91 (s, 3H, Im-CH₃), 3.88 (s, 3H, Im-COOCH₃), 3.81 (s, 3H, benzene -COOCH₃).

¹³C-NMR (75 MHz, DMSO-*d*₆): δ (ppm) = 165.71, 163.18, 158.69, 155.63, 155.30, 136.40, 136.20, 135.00, 134.05, 133.72, 133.37, 133.16, 133.10, 132.21, 131.19, 129.86, 129.71, 129.33, 129.00, 128.56, 52.33, 51.83, 35.60, 35.24, 35.08.

MS (ESI-TOF, pos. CH₂Cl₂): [M+Na]⁺ calc. for C₂₅H₂₅N₉NaO₇ *m/z* 586.1769, found *m/z* 586.1773; [M+H]⁺ calc. for C₂₅H₂₆N₉O₇ *m/z* 564.1950, found *m/z* 564.1911.

4-[(4-{[4-(2-Methoxycarbonyl-acetylamino)-1-methyl-1*H*-imidazole-2-carbonyl]-amino}-1-methyl-1*H*-imidazole-2-carbonyl)-amino]-1-methyl-1*H*-imidazole-2-carboxylic acid methyl ester (32)



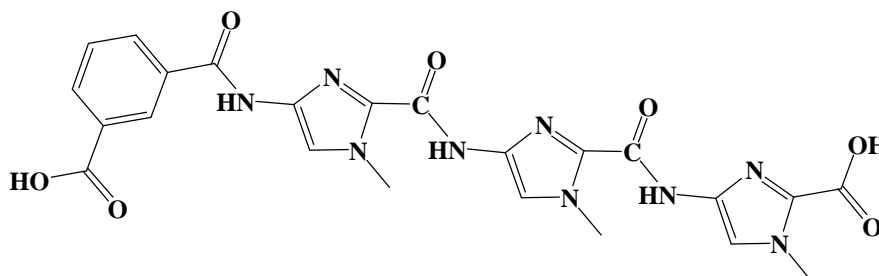
2 mL of the mixture (TFA : DCM = 4 : 1) was added to **(30)** (1.00 g, 2 mmol), and the reaction mixture was stirred for 10 min. The solvent was removed in vacuo and then the residue was dissolved in 20 mL anhydrous DCM. Et₃N (10 mL) was added to the solution. Methyl malonyl chloride (0.27 g, 2 mmol) was added to the deprotected compound. The mixture was stirred at room temperature for 18 h. DCM was removed in vacuo. The residue was purified by flash chromatography (silica gel, 1:1 ethyl acetate/cyclohexane) to yield 0.80 g (80%) as a white solid.

¹H-NMR (300 MHz, CDCl₃): δ (ppm) = 9.78 (s, 1H, Im-NH), 9.39 (s, 1H, Im-NH), 9.28 (s, 1H, Im-NH), 7.68 (s, 1H, Im-H), 7.50 (s, 1H, Im-H), 7.46 (s, 1H, Im-H), 4.06 (s, 6H, Im-CH₃), 4.06 (s, 3H, Im-CH₃), 3.99 (s, 3H, Im-COOCH₃), 3.83 (s, 3H, -CH₂-COOCH₃), 3.55 (s, 2H, -CH₂-COOCH₃).

¹³C-NMR (75 MHz, CDCl₃): δ (ppm) = 169.24, 162.32, 159.25, 156.20, 155.97, 136.77, 135.91, 135.86, 133.54, 133.38, 131.70, 115.17, 114.66, 52.84, 52.43, 41.47, 36.12, 35.80, 29.82.

MS (ESI-TOF, pos. CH₂Cl₂): [M+Na]⁺ calc. for C₂₀H₂₃N₉NaO₇ m/z 524.1613, found m/z 524.1680.

4-[(4-{[4-(3-Carboxy-benzoylamino)-1-methyl-1H-imidazole-2-carbonyl]-amino}-1-methyl-1H-imidazole-2-carbonyl)-amino]-1-methyl-1H-imidazole-2-carboxylic acid (33)



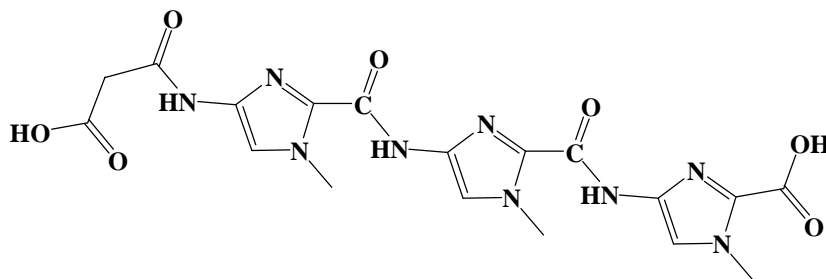
To sodium hydroxide (0.1 g, 2.5 mmol) in dry THF (10 mL) at 0 °C was added water (10 mL) and the solution was stirred for one hour. (**31**) (0.47 g, 0.83 mmol) was added and the mixture was stirred at room temperature for 3 h. The reaction was cooled and quenched by the addition of HCl. The solvent was removed in vacuo. The residue was washed with acetone to yield 0.32 g (72%) as a white solid.

¹H-NMR (300 MHz, DMSO-*d*₆): δ (ppm) = 11.20 (s, 1H, Im-NH), 10.01 (s, 1H, Im-NH), 9.67 (s, 1H, Im-NH), 8.26 (d, 1H, benzene-H), 8.12 (d, 1H, benzene-H), 7.74 (s, 1H, benzene-H), 7.63-7.66 (m, 4H, Im-H, benzene-H), 4.04 (s, 3H, Im-CH₃), 4.01 (s, 3H, Im-CH₃), 3.94 (s, 3H, Im-CH₃).

¹³C-NMR (125.6 MHz, DMSO-*d*₆): δ (ppm) = 166.79, 163.43, 159.80, 155.62, 155.41, 136.48, 135.74, 135.06, 133.99, 133.46, 133.16, 132.31, 132.20, 131.79, 131.08, 128.84, 128.82, 115.73, 115.26, 114.47, 35.67, 35.25, 35.10.

MS (ESI-TOF, pos. DMSO): [M+Na]⁺ calc. for C₂₃H₂₁N₉NaO₇ *m/z* 558.1456, found *m/z* 558.1472; [M+H]⁺ calc. for C₂₃H₂₂N₉O₇ *m/z* 536.1637, found *m/z* 536.1670.

4-[(4-{[4-(2-Carboxy-acetyl-amino)-1-methyl-1*H*-imidazole-2-carbonyl]-amino}-1-methyl-1*H*-imidazole-2-carbonyl)-amino]-1-methyl-1*H*-imidazole-2-carboxylic acid (34)



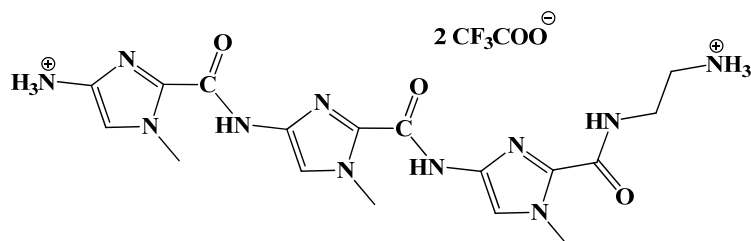
To sodium hydroxide (0.1 g, 2.5 mmol) in dry THF (10 mL) at 0 °C was added water (10 mL) and the solution was stirred for one hour. (32) (0.40 g, 0.80 mmol) was added and the mixture was stirred at room temperature for 3 h. The reaction was cooled and quenched by the addition of HCl. The solvent was removed in vacuo. The residue was washed with acetone to yield 0.30 g (79%) as a white solid.

¹H-NMR (300 MHz, DMSO-*d*₆): δ (ppm) = 10.62 (s, 1H, Im-NH), 10.05 (s, 1H, Im-NH), 9.62 (s, 1H, Im-NH), 7.66 (s, 1H, Im-H), 7.64 (s, 1H, Im-H), 7.52 (s, 1H, Im-H), 4.02 (s, 3H, Im-CH₃), 4.01 (s, 3H, Im-CH₃), 3.98 (s, 3H, Im-CH₃), 3.94 (s, 2H, -CH₂-COOH).

¹³C-NMR (125.6 MHz, DMSO-*d*₆): δ (ppm) = 169.29, 163.49, 159.73, 155.56, 155.44, 136.12, 135.70, 135.04, 133.36, 132.88, 132.30, 115.15, 114.72, 114.65, 42.64, 35.31, 35.23, 35.07.

MS (ESI-TOF, pos. DMSO): [M+Na]⁺ calc. for C₁₈H₁₇N₉NaO₇ *m/z* 494.1154, found *m/z* 494.1182.

(2-[[4-({4-[(4-Amino-1-methyl-1*H*-imidazole-2-carbonyl)-amino]-1-methyl-1*H*-imidazole-2-carbonyl]-amino)-1-methyl-1*H*-imidazole-2-carbonyl]-amino]-ethyl)-amine di(trifluoroacetate) (36)



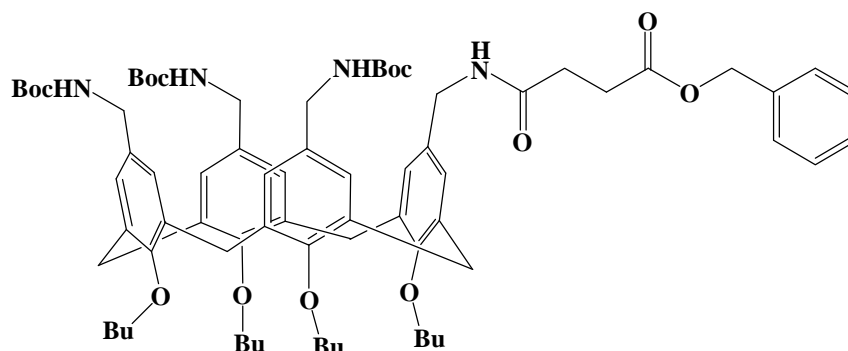
(30) (0.1 g, 0.2 mmol) was dissolved in ethylenediamine (1 mL). The mixture was stirred for 18 h at 80 °C. Subsequently, ethylenediamine was removed in vacuo. The residue was dissolved in anhydrous DCM (8 mL). To this solution was added 2 mL TFA. The reaction mixture was stirred for 16 h at r.t. and subsequently evaporated to dryness. The solid was washed with acetone to yield 0.07 g (81%) as a white solid.

¹H-NMR (300 MHz, CD₃OD): δ (ppm) = 7.40 (s, 1H, Im-H), 7.36 (s, 1H, Im-H), 4.89 (s, 1H, Im-H), 3.98 (s, 3H, Im-CH₃), 3.95 (s, 3H, Im-CH₃), 3.94 (s, 3H, Im-CH₃), 3.57 (t, 2H, Im-CONH-CH₂-), 3.12 (t, 2H, Im-CONH-CH₂-CH₂-).

¹³C-NMR (75 MHz, CD₃OD): δ (ppm) = 161.88, 157.45, 157.12, 137.24, 137.17, 135.50, 135.44, 135.10, 120.39, 116.42, 116.09, 115.65, 41.07, 38.09, 38.00, 36.23, 36.07.

MS (ESI-TOF, pos. MeOH): [M+H]⁺ calc. for C₁₇H₂₄N₁₁O₃ *m/z* 430.2058, found *m/z* 430.2097.

Succinic acid monobenzyl ester 4-{5,11,17-tris[(*tert*-butoxycarbonyl)-aminomethyl]-25,26,27,28-tetrabutoxycalix[4]arene-23-yl-methyl} amide (37)



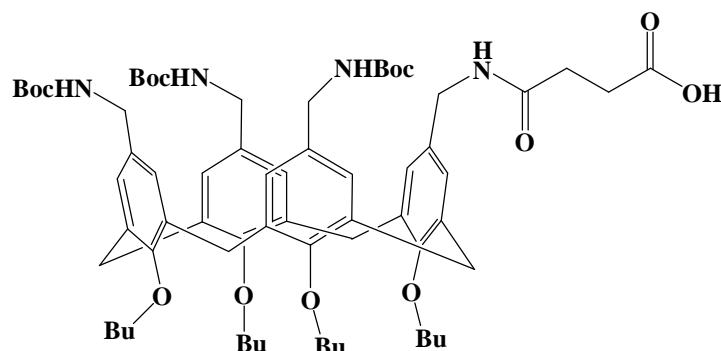
(24) (0.021 g, 0.1 mmol) was dissolved in 2 mL anhydrous DMF. HBTU (0.038 g, 0.1 mmol) was added followed by DIEA (1 mL). The reaction mixture was stirred for 10 min and immediately added to (7) (0.107 g, 0.1 mmol). The mixture was stirred at room temperature for 18 h. DMF was removed in vacuo. The residue was purified by flash chromatography (silica gel, 1:1 ethyl acetate/cyclohexane) to yield 0.056 g (45%) as a white solid.

¹H-NMR (300 MHz, CDCl₃): δ (ppm) = 7.23-7.28 (m, 5H, Ar-H of Cbz), 6.37-6.54 (m, 8H, Ar-H), 5.06 (s, 2H, CH₂ of Cbz), 4.30 (m, 4H, Ar-CH₂-Ar), 3.92-4.02 (m, 8H, Ar-CH₂-N), 3.76 (m, 8H, Ar-O-CH₂-), 3.00 (m, 4H, Ar-CH₂-Ar), 2.67 (t, 2H, -NHCO-CH₂-), 2.47 (t, 2H, -NHCO-CH₂-CH₂-COO-), 1.79 (m, 8H, Ar-O-CH₂-CH₂-), 1.37 (m, 35H, Ar-O-CH₂-CH₂-CH₂-, -C(CH₃)₃), 0.90 (m, 12H, Ar-O-CH₂-CH₂-CH₂-CH₃).

¹³C-NMR (75 MHz, CDCl₃): δ (ppm) = 173.05, 156.14, 156.09, 136.03, 135.32, 132.15, 132.03, 131.71, 128.64, 128.30, 127.36, 79.43, 79.31, 75.03, 66.58, 44.32, 42.91, 32.39, 32.31, 31.14, 31.06, 30.86, 29.73, 28.57, 19.43, 14.17.

MS (ESI-TOF, pos. CH₂Cl₂): [M+Na]⁺ calc. for C₇₄H₁₀₂N₄NaO₁₃ *m/z* 1277.7336, found *m/z* 1277.7458.

Succinic acid 4-{5,11,17-tris[*tert*-butoxycarbonyl]-aminomethyl}-25,26,27,28-tetrabutoxycalix[4]arene-23-yl-methyl} amide (38)



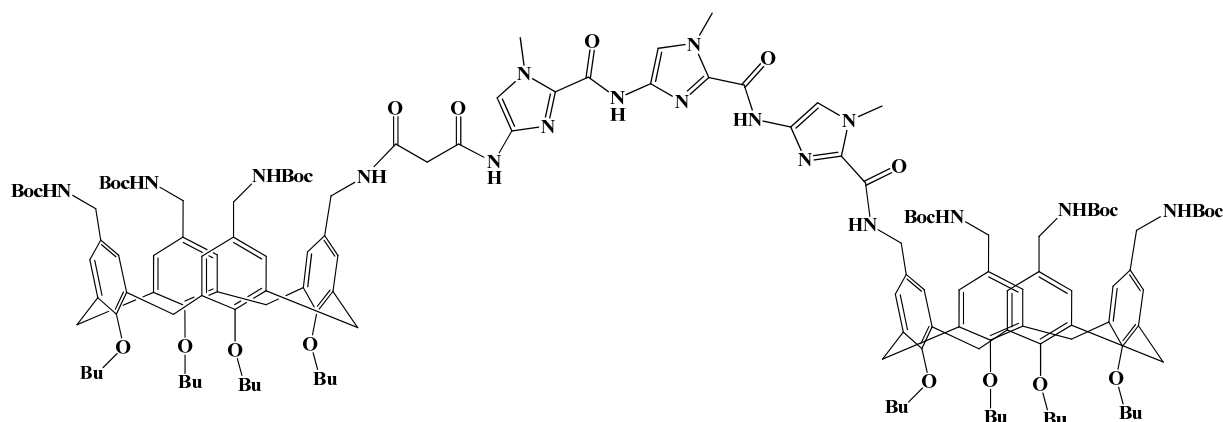
(37) (0.056 g, 0.045 mmol) were dissolved in 20 mL of the mixture (THF : H₂O = 4 : 1) and Pd/C (0.006 g, 10 weight-%) was added. The hydrogenation was then carried out for 24 h. The catalyst was filtered off over Celite and the solution was evaporated to dryness. The residue was washed with DCM to yield 0.048 g (93%) as a white solid.

¹H-NMR (300 MHz, DMSO-*d*₆): δ (ppm) = 8.09 (t, 1H, Ar-CH₂-NH-), 7.05-7.07 (m, 2H, Ar-CH₂-NH-), 6.57 (m, 8H, Ar-H), 4.31 (m, 4H, Ar-CH₂-Ar), 3.79-3.91 (m, 8H, Ar-CH₂-N), 3.79 (m, 8H, Ar-O-CH₂-), 3.10 (m, 4H, Ar-CH₂-Ar), 2.30-2.38 (m, 4H, -NHCO-CH₂-CH₂-COO-), 1.85 (m, 8H, Ar-O-CH₂-CH₂-), 1.37 (m, 35H, Ar-O-CH₂-CH₂-CH₂-, -C(CH₃)₃), 0.95 (m, 12H, Ar-O-CH₂-CH₂-CH₂-CH₃).

¹³C-NMR (75 MHz, DMSO-*d*₆): δ (ppm) = 174.20, 170.88, 162.13, 155.59, 154.85, 134.23, 134.19, 134.05, 133.17, 132.36, 127.21, 127.04, 126.99, 126.87, 126.84, 77.52, 74.41, 60.77, 57.03, 31.74, 30.35, 28.23, 18.81, 13.85.

MS (ESI-TOF, pos. CH₂Cl₂): [M+Na]⁺ calc. for C₆₇H₉₆N₄NaO₁₃ *m/z* 1187.6866, found *m/z* 1187.6963.

4-[(4-[4-(2-Carboxy-acetyl-amino)-1-methyl-1*H*-imidazole-2-carbonyl]-amino]-1-methyl-1*H*-imidazole-2-carbonyl)-amino]-1-methyl-1*H*-imidazole-2-carboxylic acid *N,N'*-Bis-{5,11,17-tris[(*tert*-butoxycarbonyl)-aminomethyl]-25,26,27,28-tetrabutoxy calix[4]arene-23-yl-methyl} diamide (39**)**



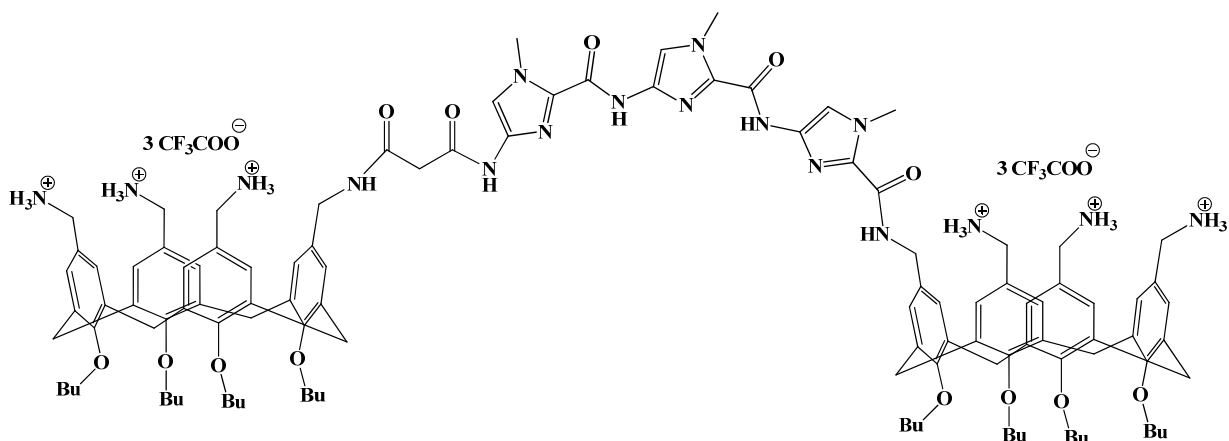
(**34**) (0.047 g, 0.1 mmol) was dissolved in 2 mL anhydrous DMF. HATU (0.076 g, 0.2 mmol) was added followed by DIEA (1 mL). The reaction mixture was stirred for 10 min and immediately added to (**7**) (0.214 g, 0.2 mmol). The mixture was stirred at room temperature for 18 h. DMF was removed in vacuo. The residue was purified by flash chromatography (silica gel, 3:2 ethyl acetate/cyclohexane) and then by preparative TLC (silica gel, 1:4 ethyl acetate/cyclohexane) to yield 0.034 g (13%) as a white solid.

¹H-NMR (300 MHz, DMSO-*d*₆): δ (ppm) = 10.54 (s, 1H, Im-NH), 9.72 (m, 2H, Im-NH), 8.40 (t, 1H, Ar-CH₂-NH-), 8.25 (t, 1H, Ar-CH₂-NH-), 7.62 (s, 1H, Im-H), 7.52 (s, 1H, Im-H), 7.51 (s, 1H, Im-H), 7.01 (m, 6H, Ar-CH₂-NH-), 6.54-6.63 (m, 16H, Ar-H), 4.30 (m, 8H, Ar-CH₂-Ar), 4.00 (s, 3H, Im-CH₃), 3.96 (s, 3H, Im-CH₃), 3.94 (s, 3H, Im-CH₃), 3.78 (m, 32H, Ar-O-CH₂-, Ar-CH₂-N), 3.50 (s, 2H, -NHCO-CH₂-CONH-), 3.10 (m, 8H, Ar-CH₂-Ar), 1.83 (m, 16H, Ar-O-CH₂-CH₂-), 1.36 (m, 70H, Ar-O-CH₂-CH₂-CH₂-, -C(CH₃)₃), 0.93 (m, 24H, Ar-O-CH₂-CH₂-CH₂-CH₃).

¹³C-NMR (125.6 MHz, DMSO-*d*₆): δ (ppm) = 155.61, 155.59, 155.55, 155.38, 155.19, 154.95, 154.93, 154.89, 154.80, 136.09, 135.09, 134.60, 134.44, 134.42, 134.29, 134.27, 134.22, 134.14, 134.11, 134.09, 134.02, 133.96, 133.92, 133.26, 133.18, 133.15, 133.12, 133.07, 133.04, 132.87, 127.44, 127.42, 127.17, 127.10, 127.08, 127.04, 127.02, 126.99, 126.95, 126.91, 126.87, 126.84, 126.82, 126.76, 77.53, 74.40, 53.30, 45.37, 35.23, 35.11, 35.05, 31.74, 30.36, 30.34, 30.27, 28.23, 18.83, 13.86.

MS (ESI-TOF, pos. CH₂Cl₂): [M+2Na]²⁺ calc. for C₁₄₄H₁₉₉N₁₇Na₂O₂₅ *m/z* 1306.7320, found *m/z* 1306.7379.

4-[(4-{[4-(2-Carboxy-acetyl-amino)-1-methyl-1*H*-imidazole-2-carbonyl]-amino}-1-methyl-1*H*-imidazole-2-carbonyl)-amino]-1-methyl-1*H*-imidazole-2-carboxylic acid *N,N'*-Bis-{5,11,17-tris-(aminomethyl)-25,26,27,28-tetrabutoxycalix[4]arene -23-yl-methyl} diamide hexakis(trifluoroacetate) (40**)**



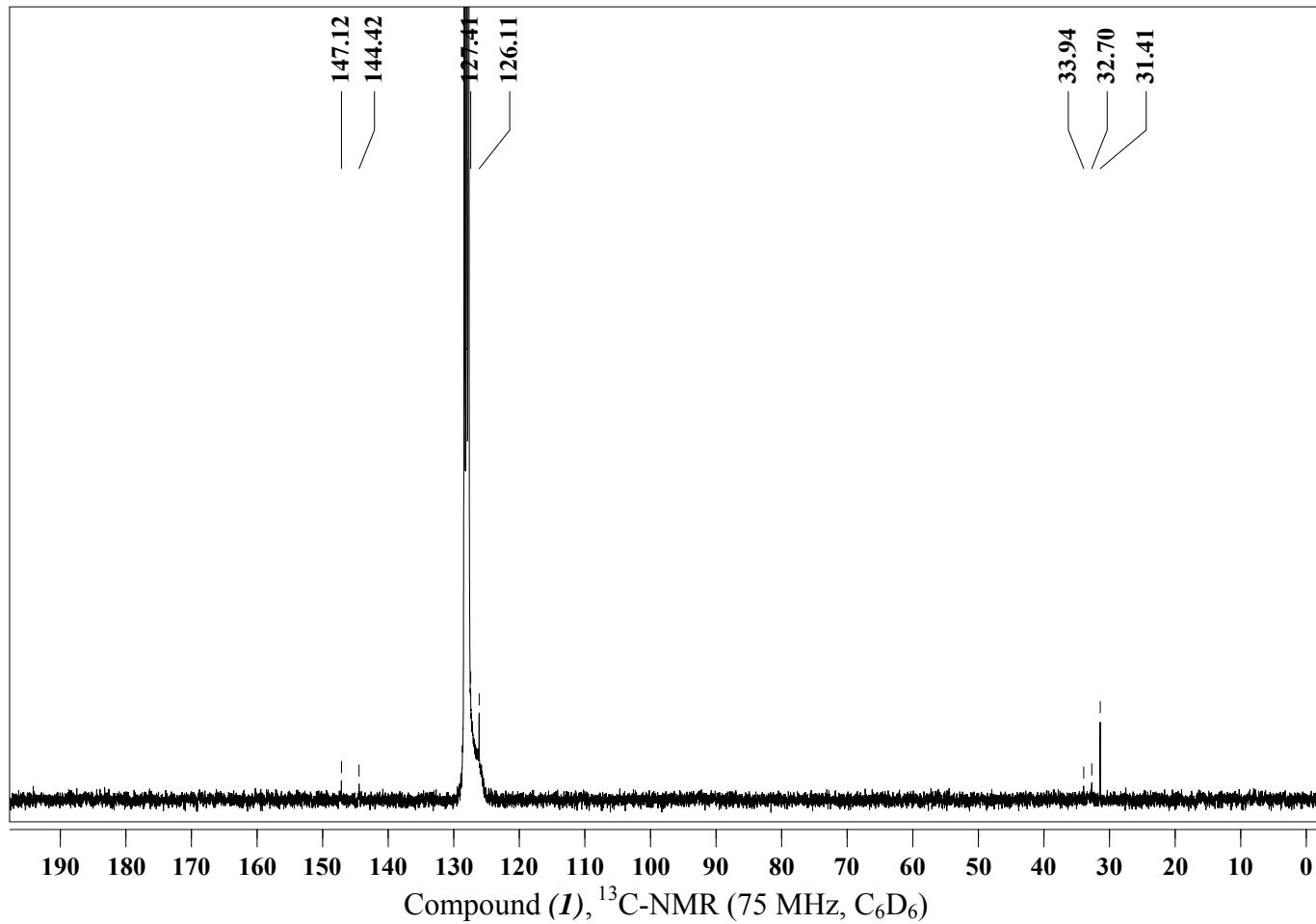
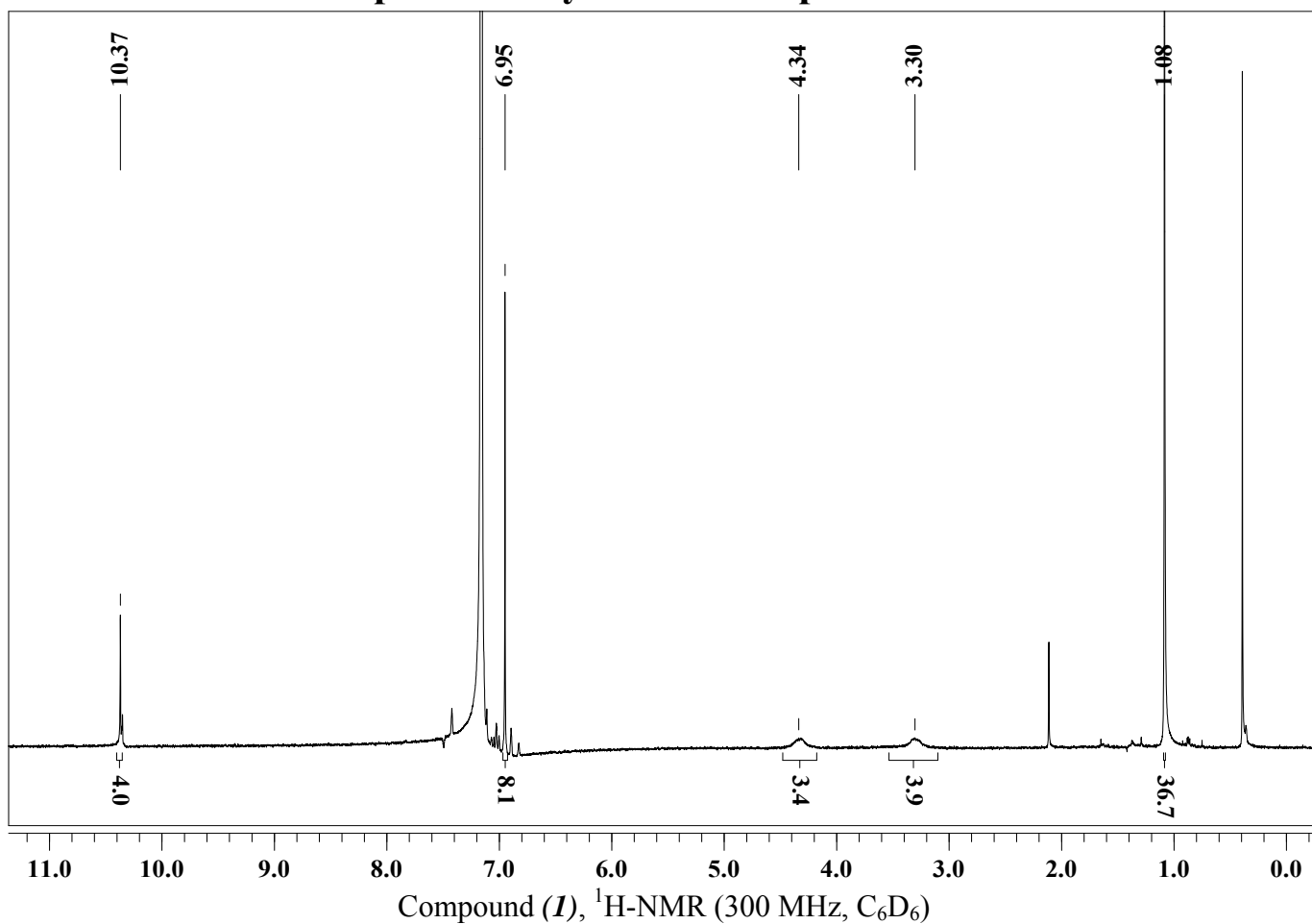
(**39**) (0.013 g, 0.05 mmol) was dissolved in DCM (8 mL). To this solution was added 2 mL TFA. The mixture was stirred for 15 min at r.t. and subsequently was evaporated to dryness. The solid was washed with CHCl₃ to yield 0.011 g (79%) as a white solid.

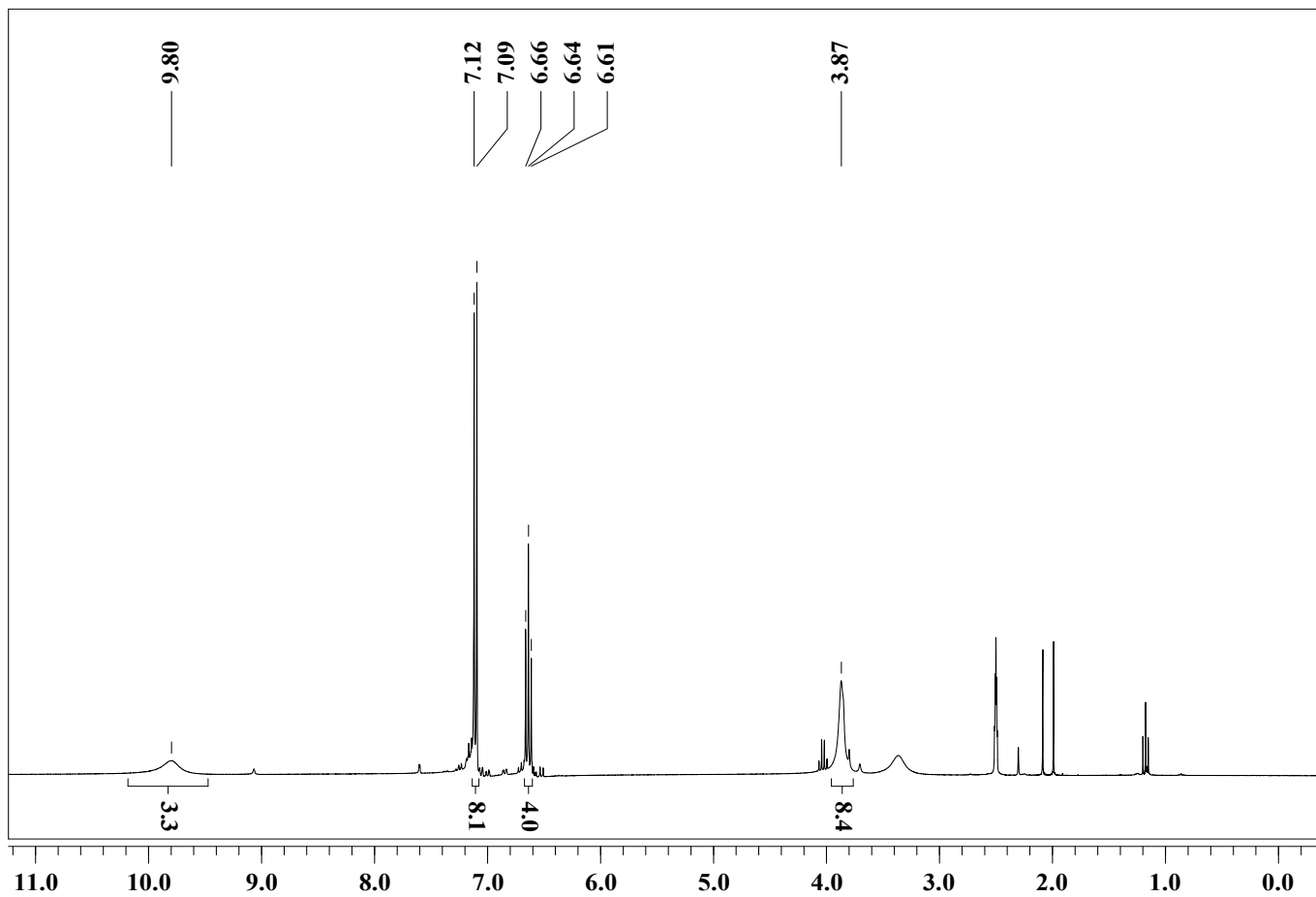
¹H-NMR (500 MHz, DMSO-*d*₆): δ (ppm) = 10.58 (s, 1H, Im-NH), 9.80 (s, 1H, Im-NH), 9.75 (s, 1H, Im-NH), 8.09 (m, 18H, Ar-CH₂-NH₃), 7.65 (s, 1H, Im-H), 7.55 (s, 1H, Im-H), 7.54 (s, 1H, Im-H), 6.64-6.93 (m, 16H, Ar-H), 4.36 (m, 8H, Ar-CH₂-Ar), 4.01 (s, 3H, Im-CH₃), 3.98 (s, 3H, Im-CH₃), 3.97 (s, 3H, Im-CH₃), 3.69-3.84 (m, 32H, Ar-O-CH₂-, Ar-CH₂-N), 3.50 (s, 2H, -NHCO-CH₂-CONH-), 3.17 (m, 8H, Ar-CH₂-Ar), 1.87 (m, 16H, Ar-O-CH₂-CH₂-), 1.42 (m, 16H, Ar-O-CH₂-CH₂-CH₂-), 0.97 (m, 24H, Ar-O-CH₂-CH₂-CH₂-CH₃).

¹³C-NMR (125.6 MHz, DMSO-*d*₆): δ (ppm) = 158.21, 156.45, 156.25, 155.67, 154.99, 136.37, 136.23, 136.08, 135.87, 135.66, 135.55, 135.36, 135.29, 135.24, 135.19, 135.14, 135.11, 134.92, 134.79, 134.72, 134.65, 134.51, 134.46, 134.39, 134.29, 134.25, 134.03, 133.97, 133.85, 133.43, 133.38, 133.29, 133.07, 132.50, 132.15, 129.21, 129.17, 129.14, 127.58, 127.53, 127.49, 127.43, 74.68, 74.60, 69.79, 42.07, 35.29, 35.17, 35.09, 31.82, 31.79, 31.75, 30.18, 30.10, 18.84, 18.77, 13.88.

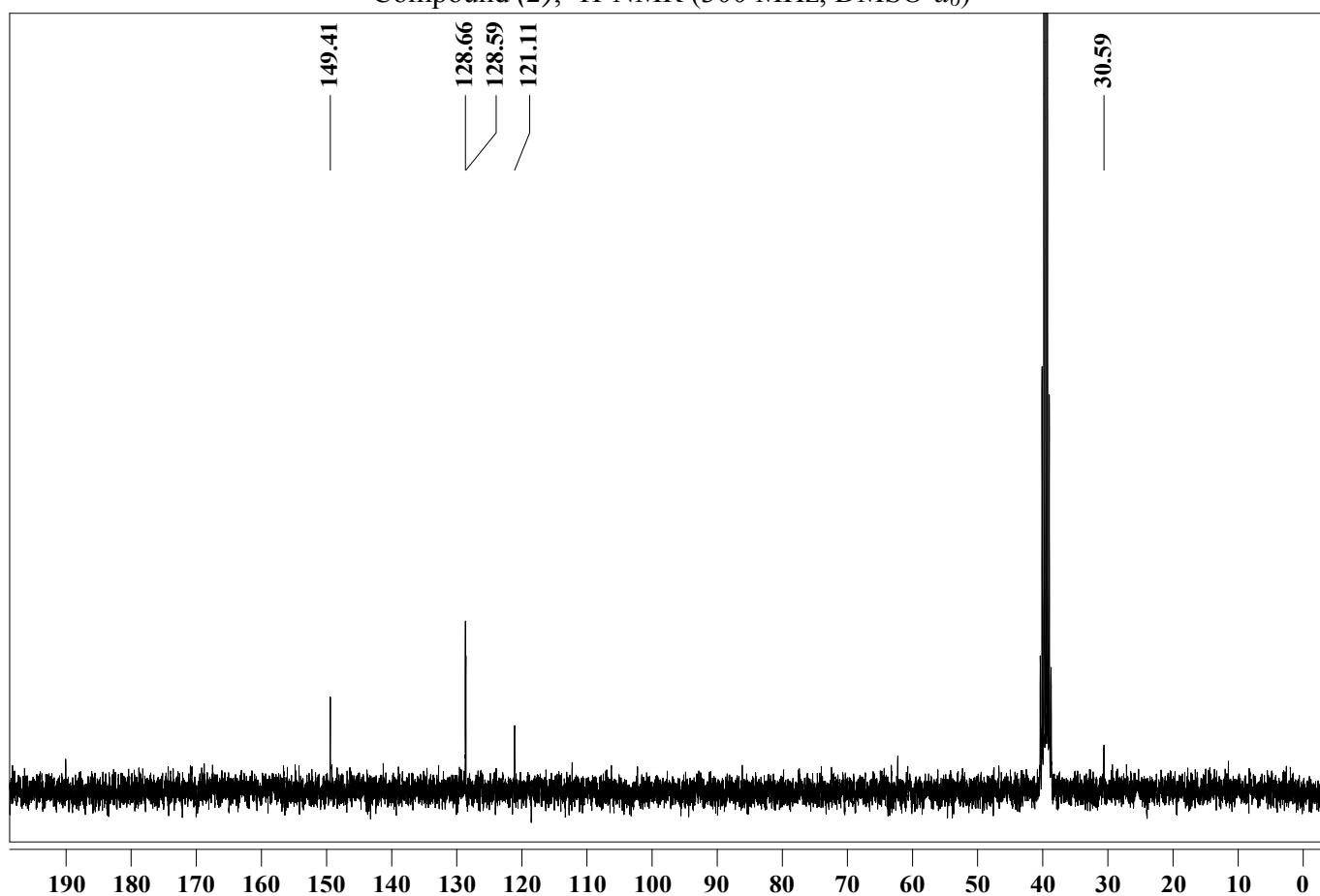
MS (ESI-TOF, pos. CH₂Cl₂, free base): [M+2H]²⁺ calc. for C₁₁₄H₁₅₃N₁₇O₁₃ *m/z* 984.5927, found *m/z* 984.5879.

6.4 NMR and MS Spectra of Synthetic Compounds

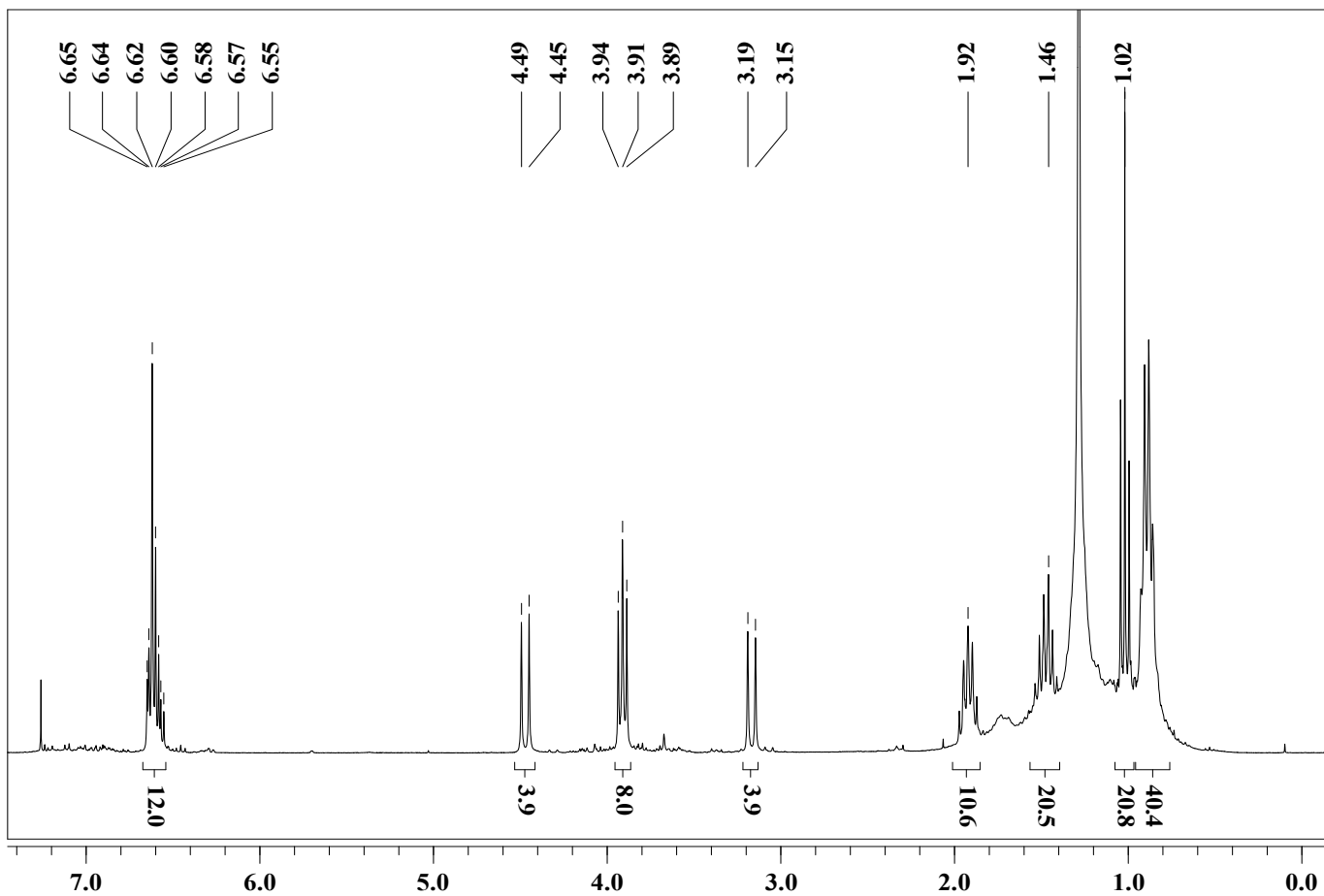




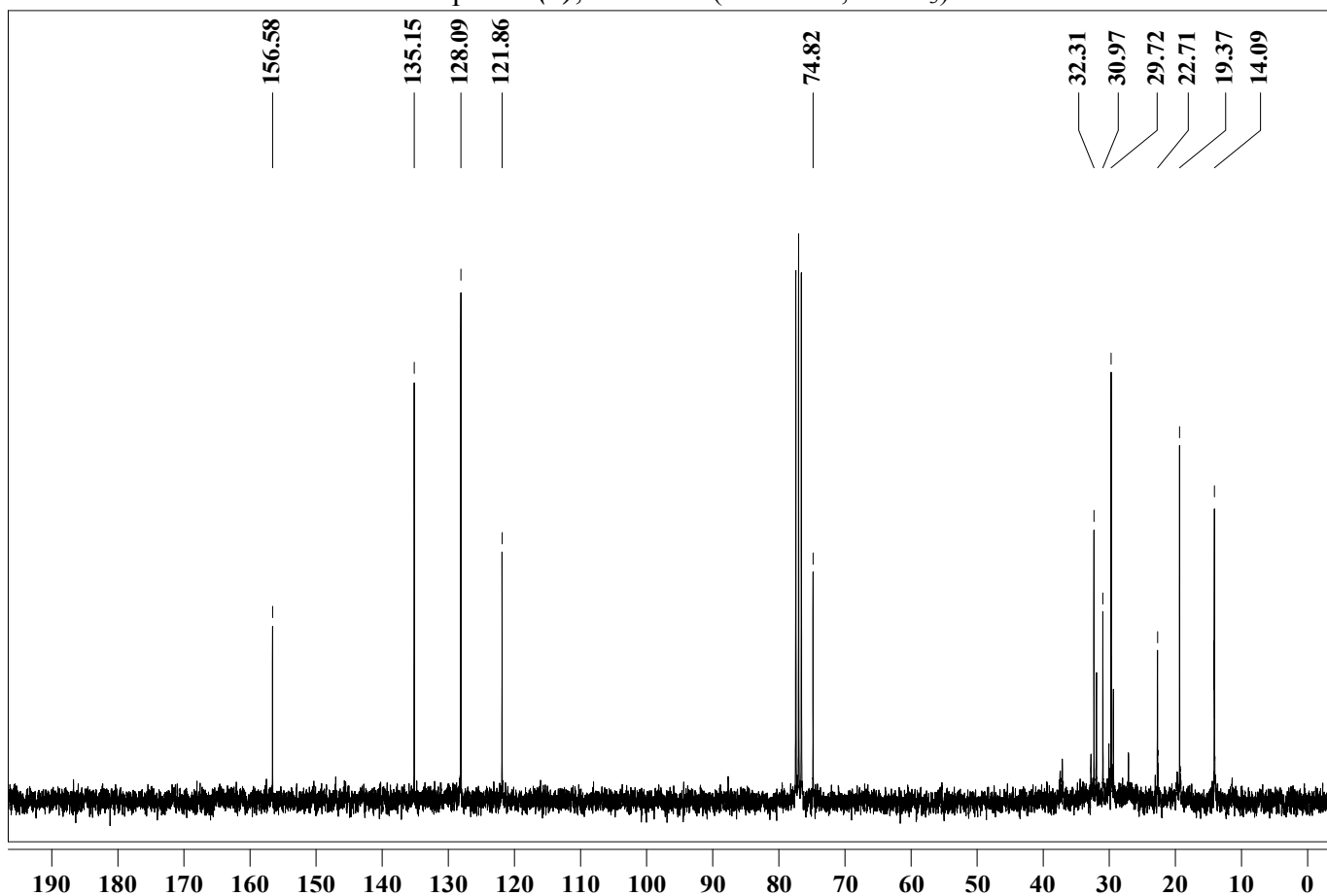
Compound (2), ¹H-NMR (300 MHz, DMSO-*d*₆)



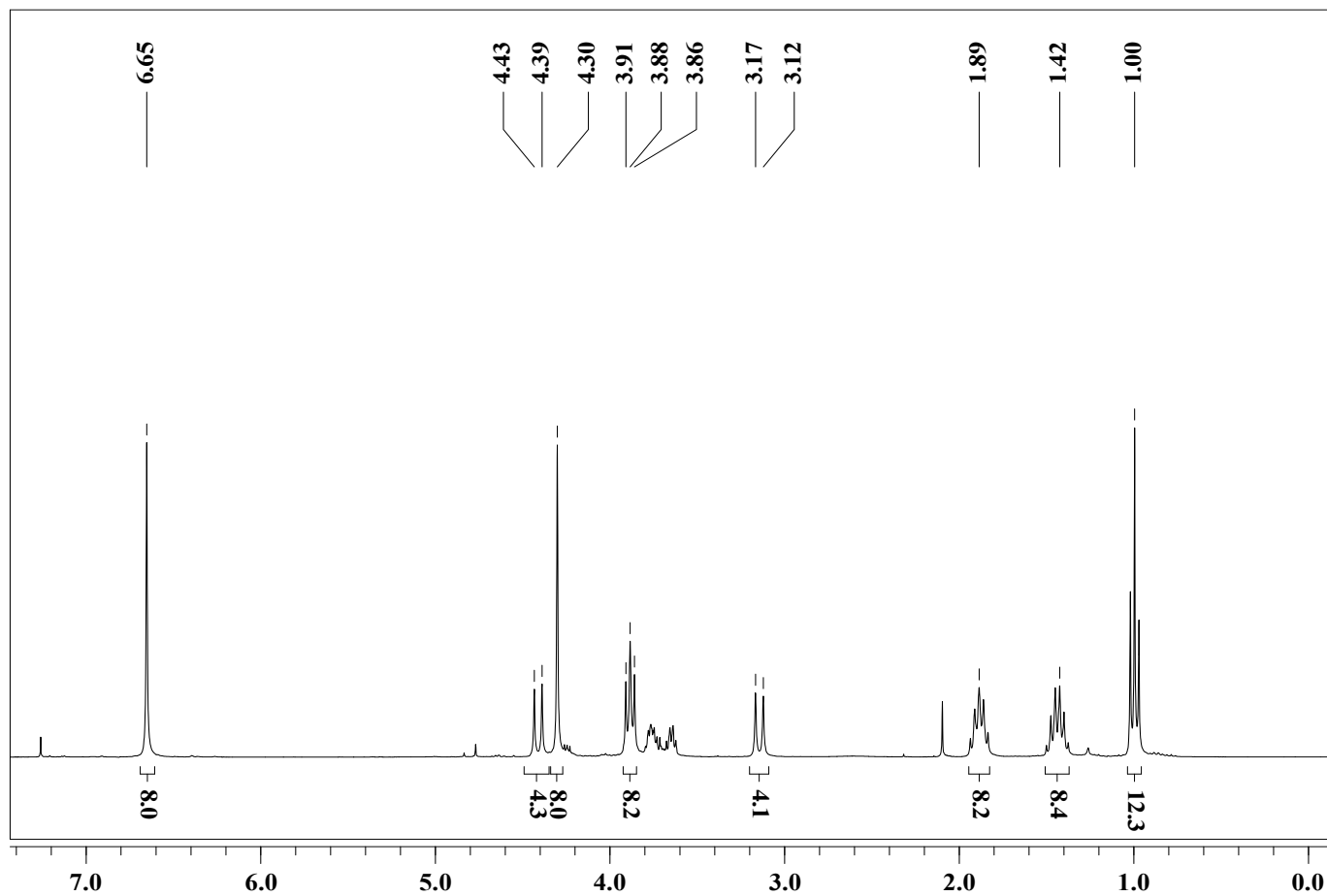
Compound (2), ¹³C-NMR (75 MHz, DMSO-*d*₆)



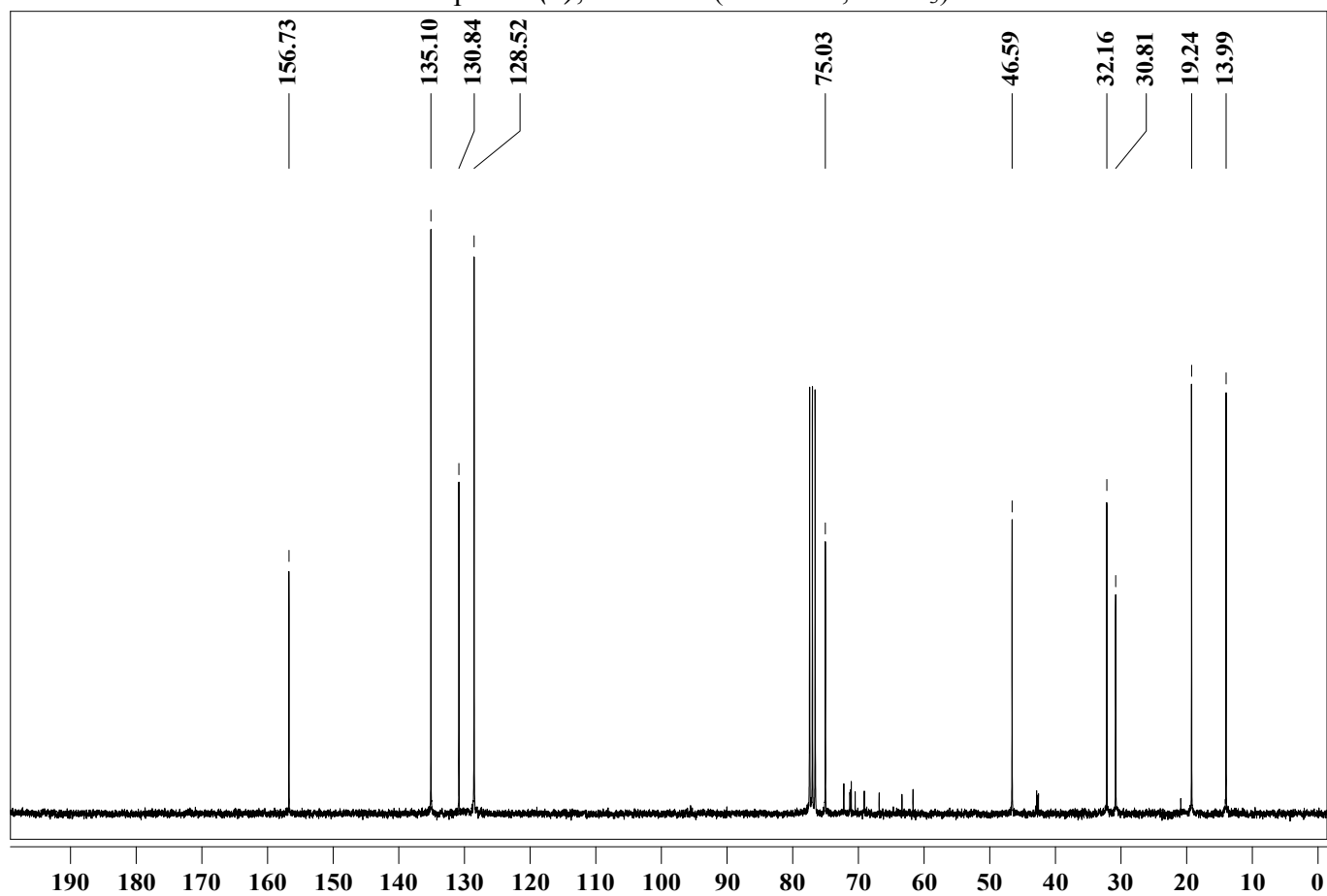
Compound (3), $^1\text{H-NMR}$ (300 MHz, CDCl_3)



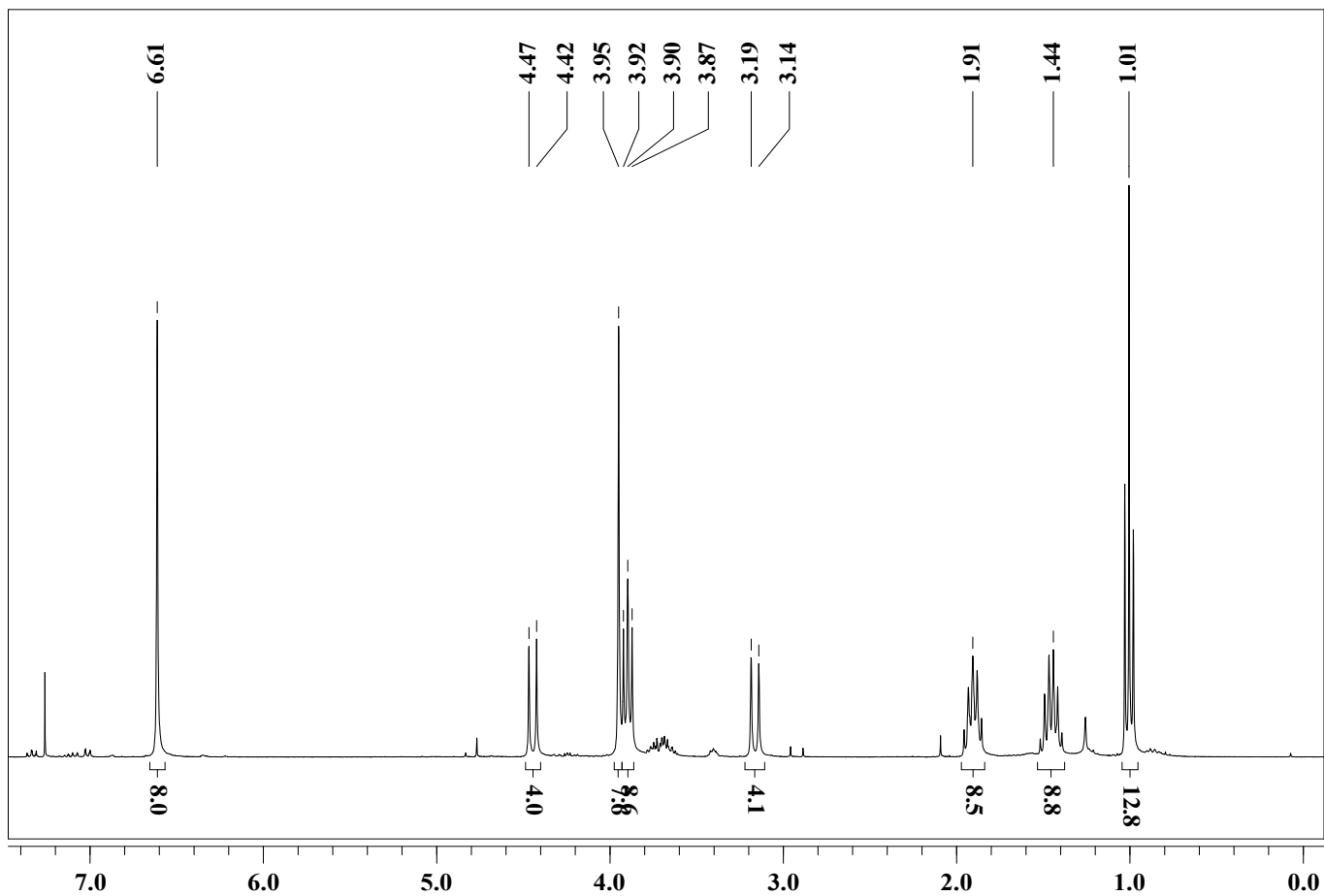
Compound (3), $^{13}\text{C-NMR}$ (75 MHz, CDCl_3)



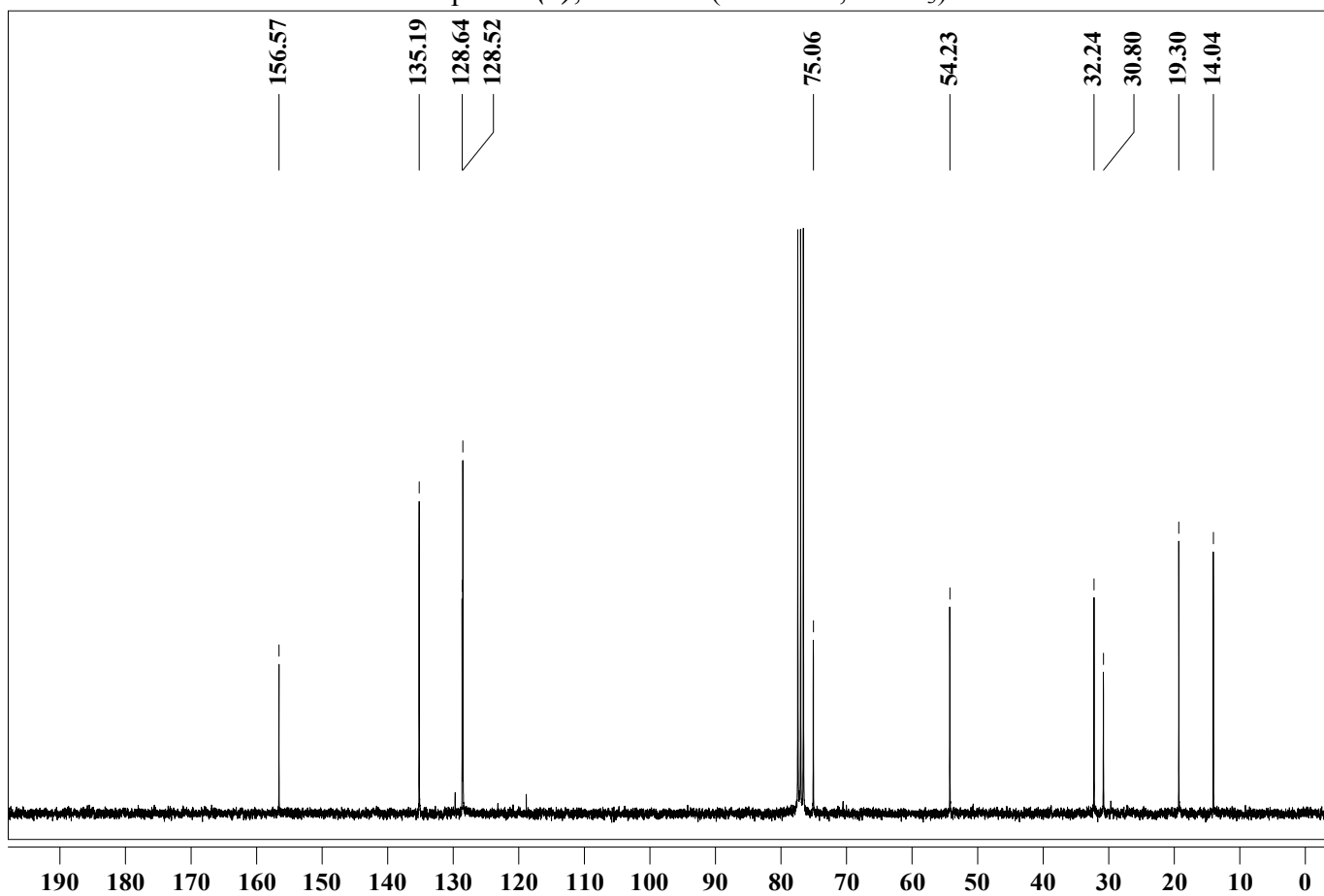
Compound (4), ¹H-NMR (300 MHz, CDCl₃)



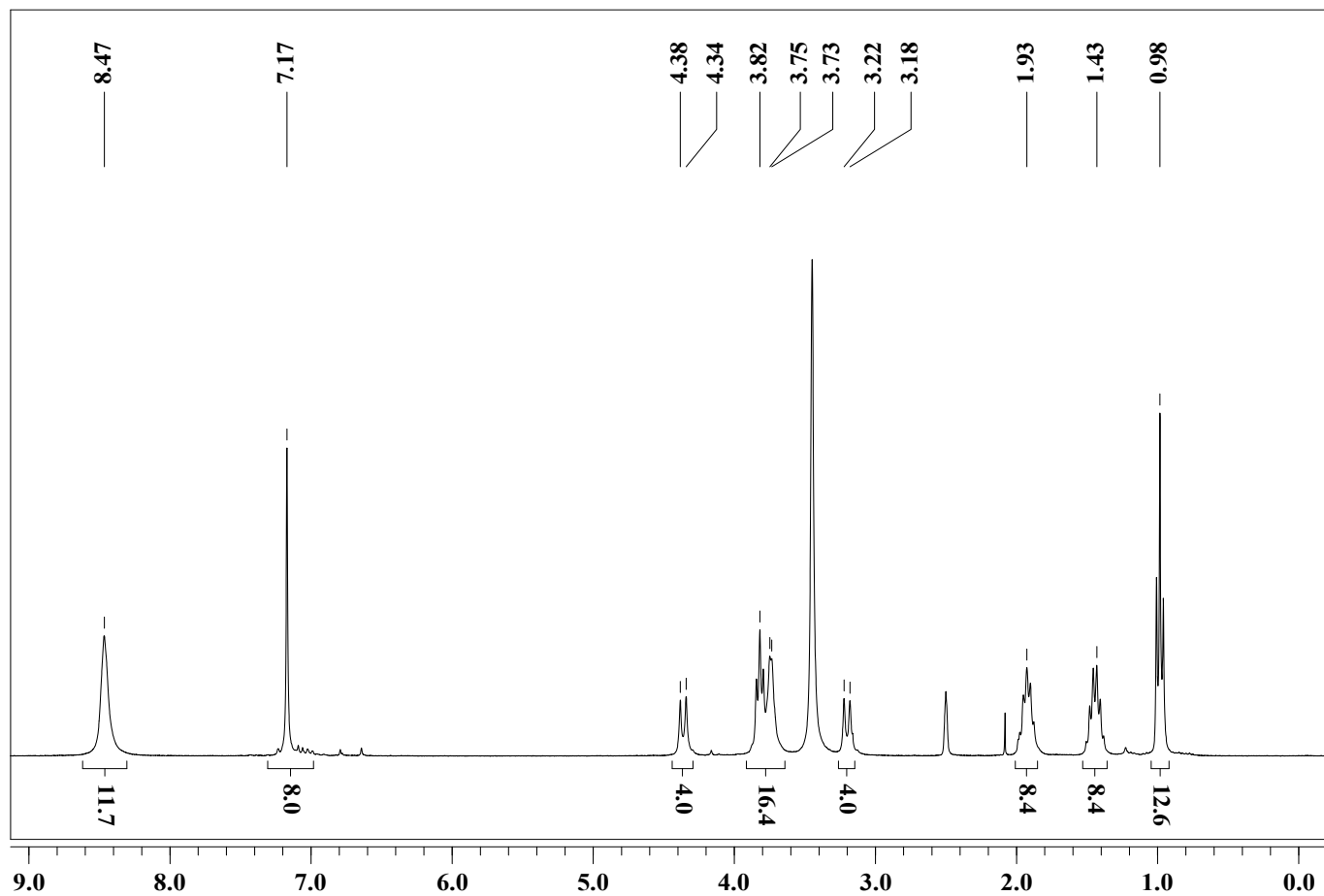
Compound (4), ¹³C-NMR (75 MHz, CDCl₃)



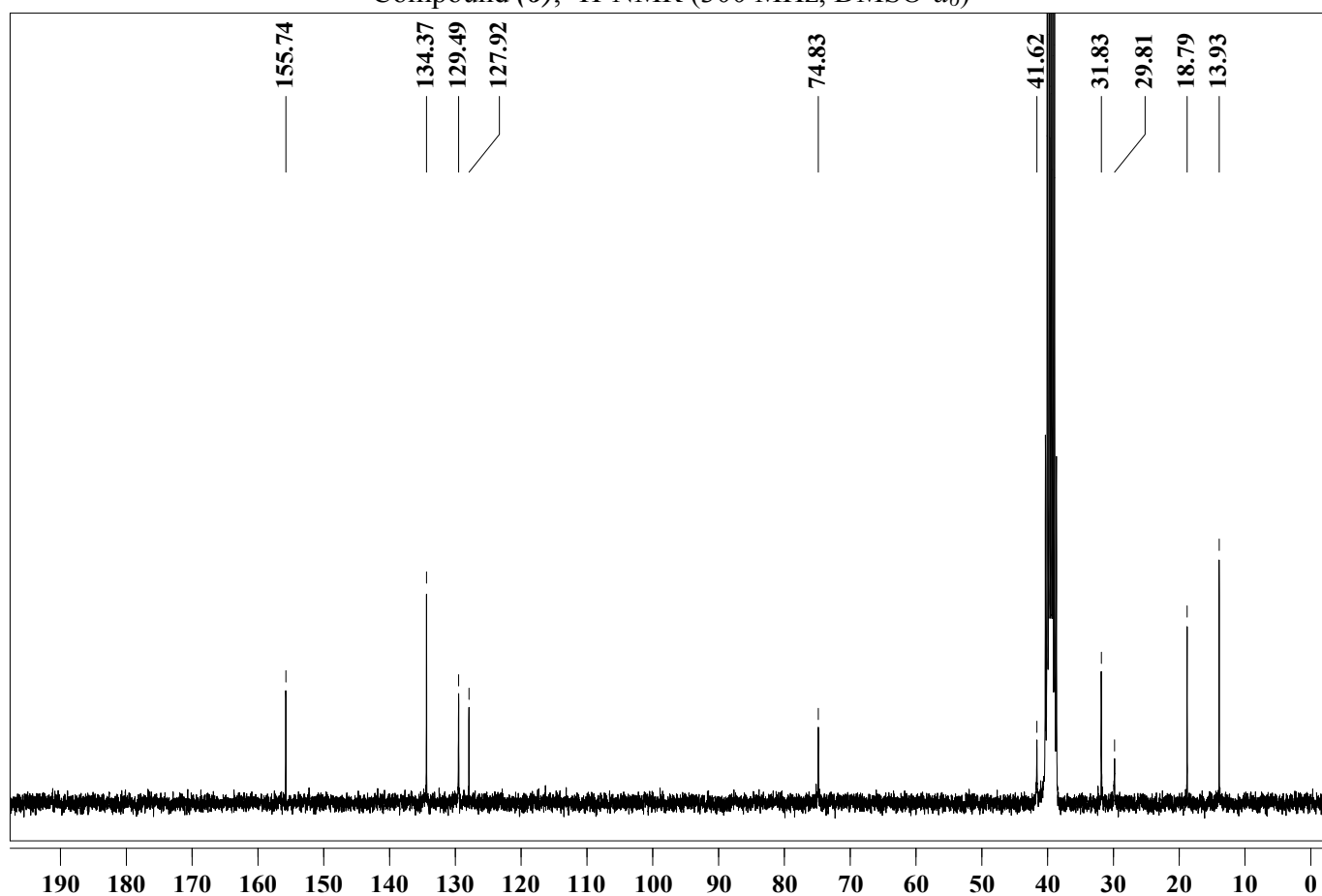
Compound (5), ¹H-NMR (300 MHz, CDCl₃)



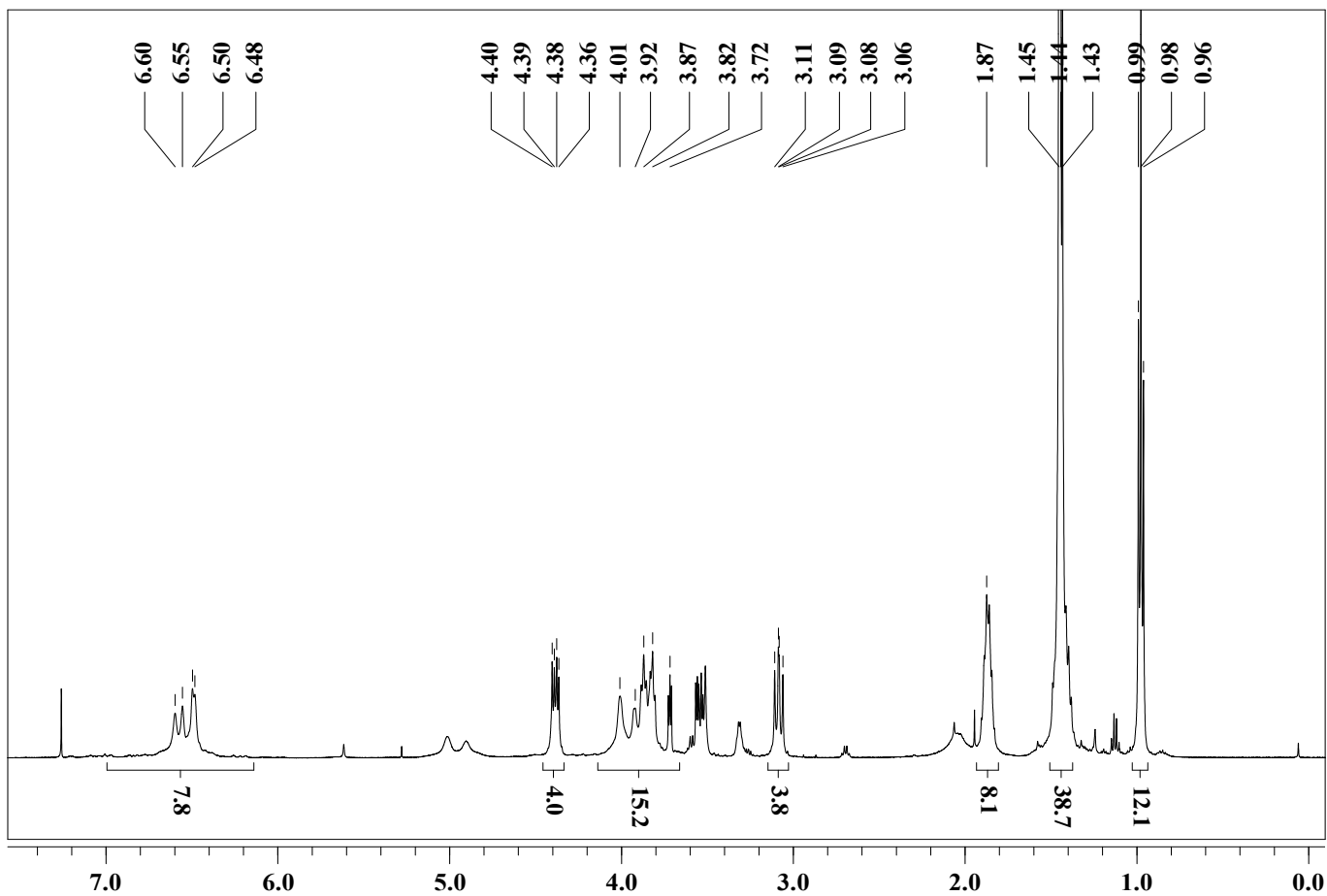
Compound (5), ¹³C-NMR (75 MHz, CDCl₃)



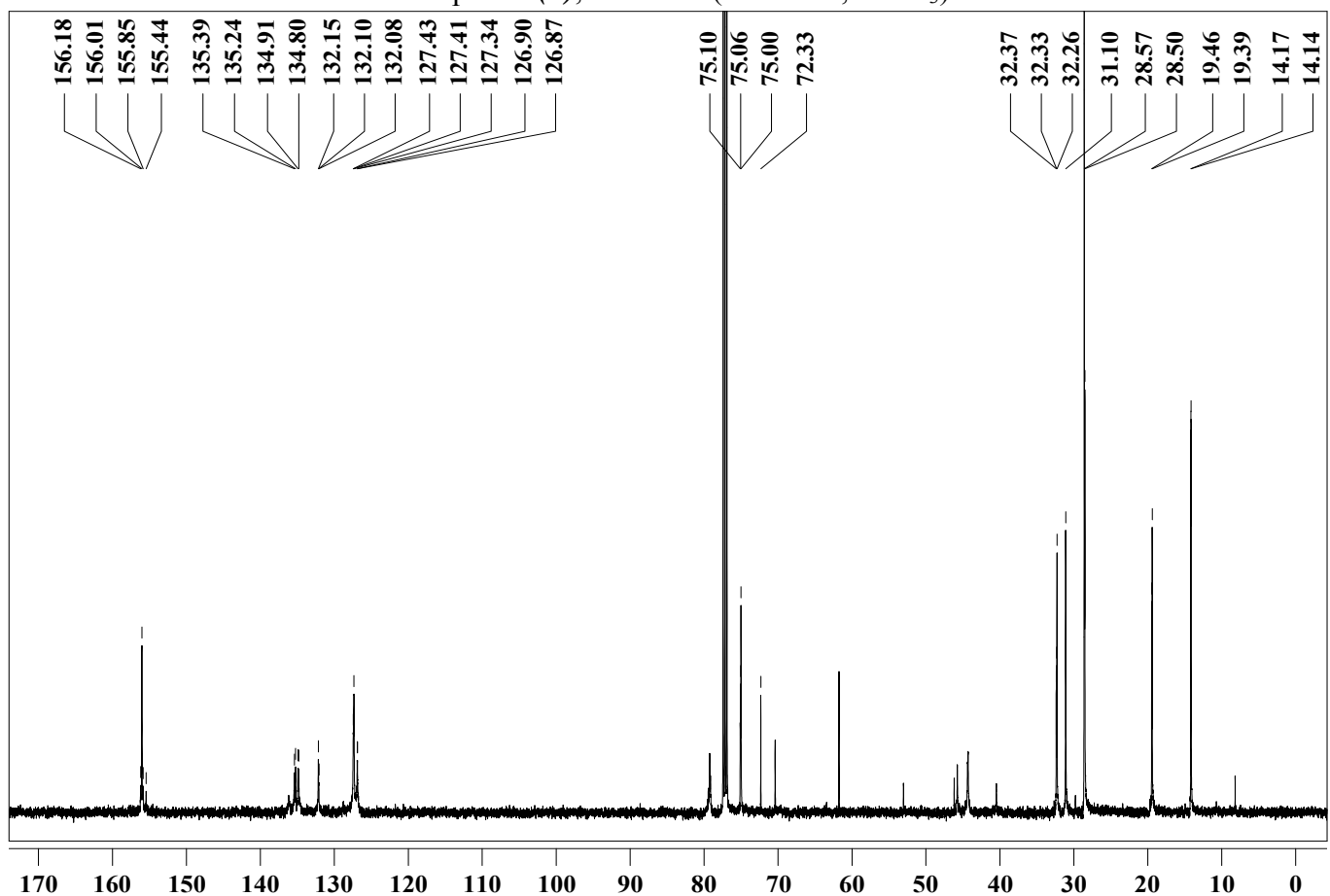
Compound (6), $^1\text{H-NMR}$ (300 MHz, $\text{DMSO-}d_6$)



Compound (6), $^{13}\text{C-NMR}$ (75 MHz, $\text{DMSO-}d_6$)



Compound (7), $^1\text{H-NMR}$ (300 MHz, CDCl_3)

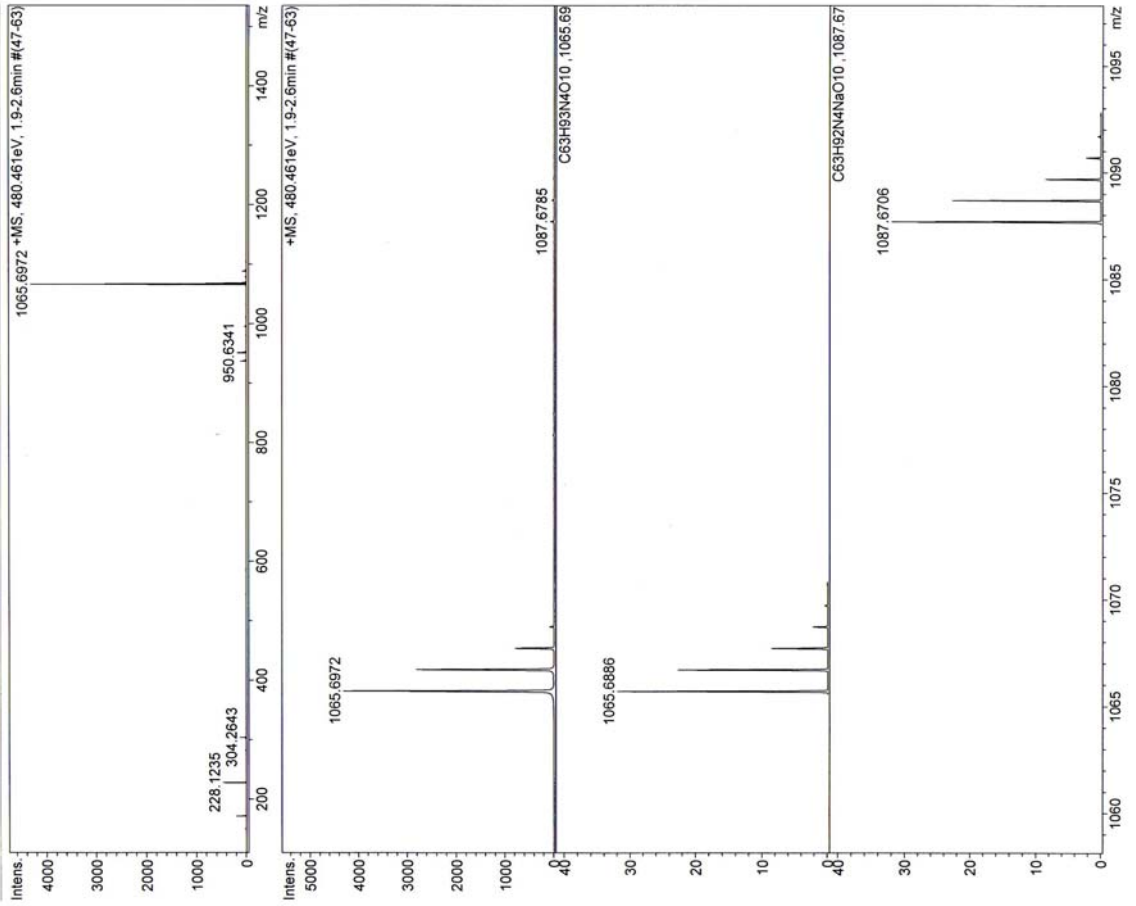


Compound (7), $^{13}\text{C-NMR}$ (75 MHz, CDCl_3)

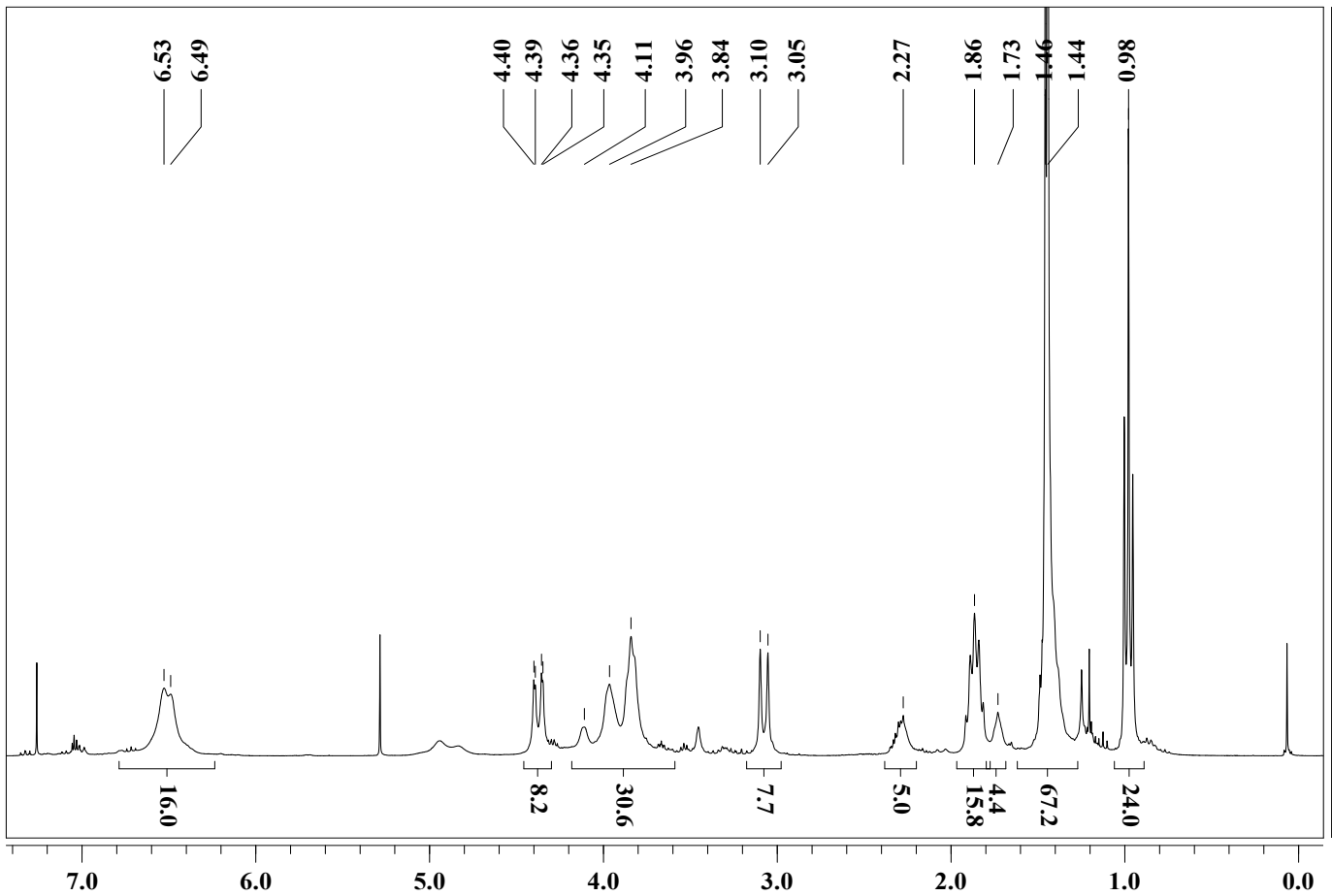
MS-Analyse: ESI-TOF

Analysis Name: E:\MS-Daten\HuWenbin\071213-Hu007-pos_01_9593.d\071213-Hu007-pos_01_9593.ser
Method: methodname
Operator: van Hoof
Acquisition Date: 12/13/2007 1:56:10 PM
Instrument: Bruker BioTOF III

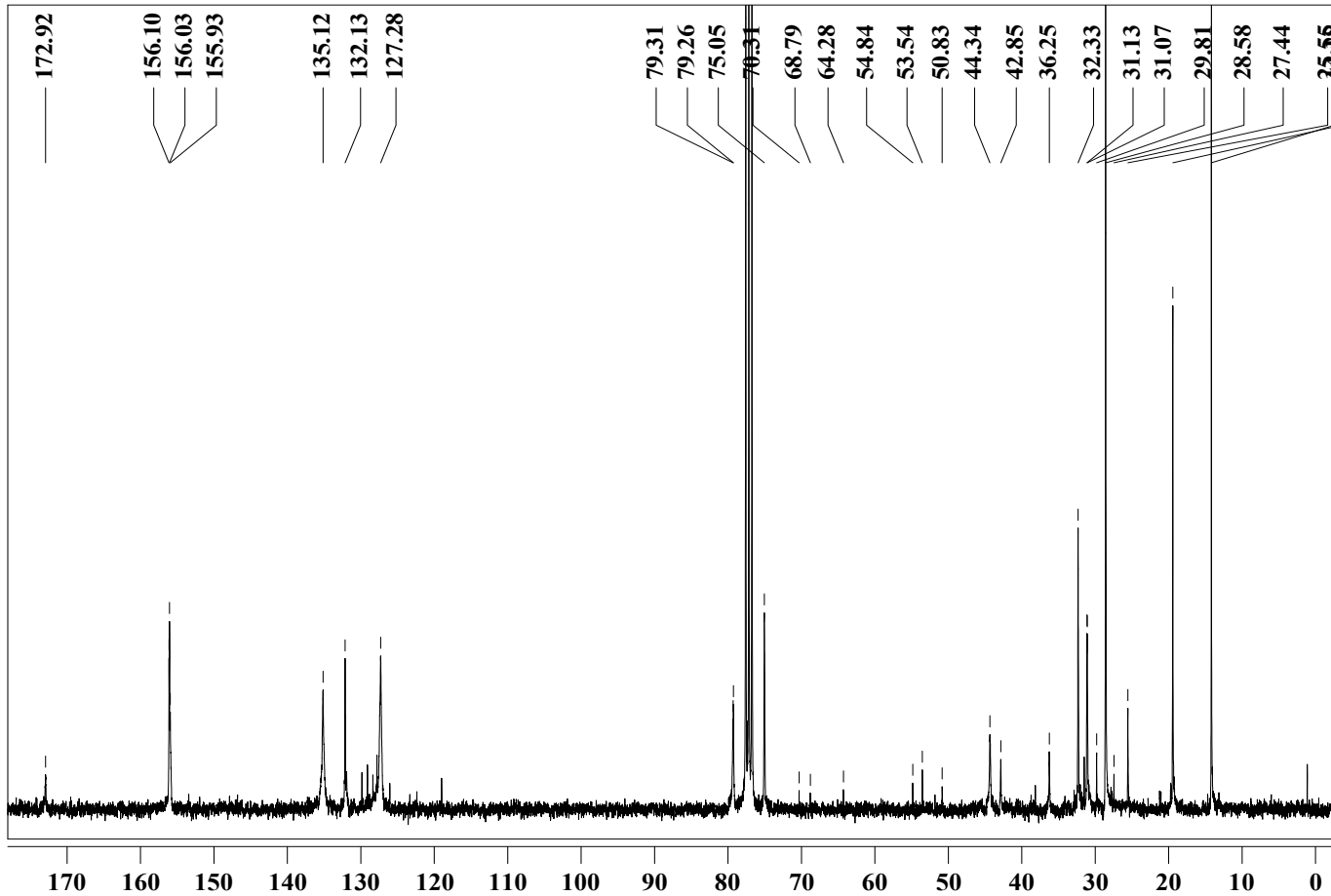
Comment: comment



Compound (7), MS (ESI-TOF, pos. CH₂Cl₂)



Compound (8), ¹H-NMR (300 MHz, CDCl₃)

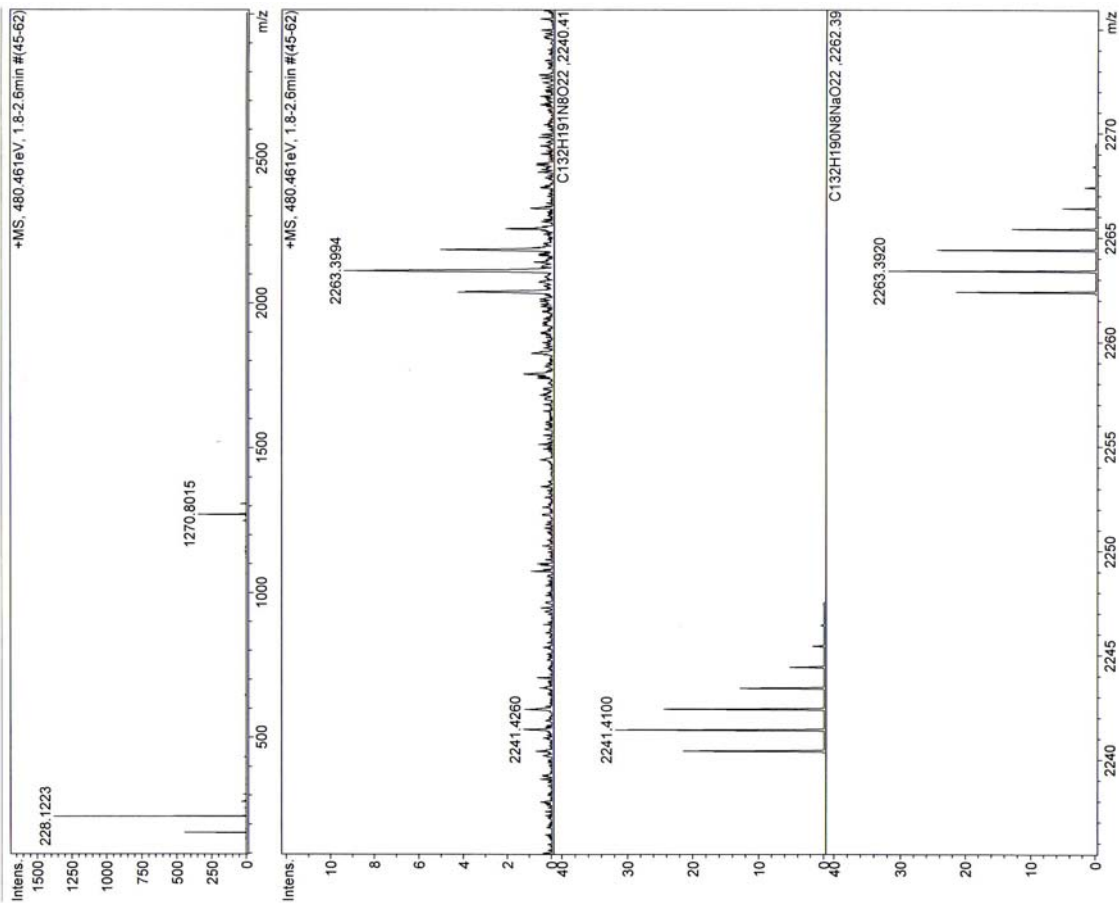


Compound (8), $^{13}\text{C-NMR}$ (75 MHz, CDCl_3)

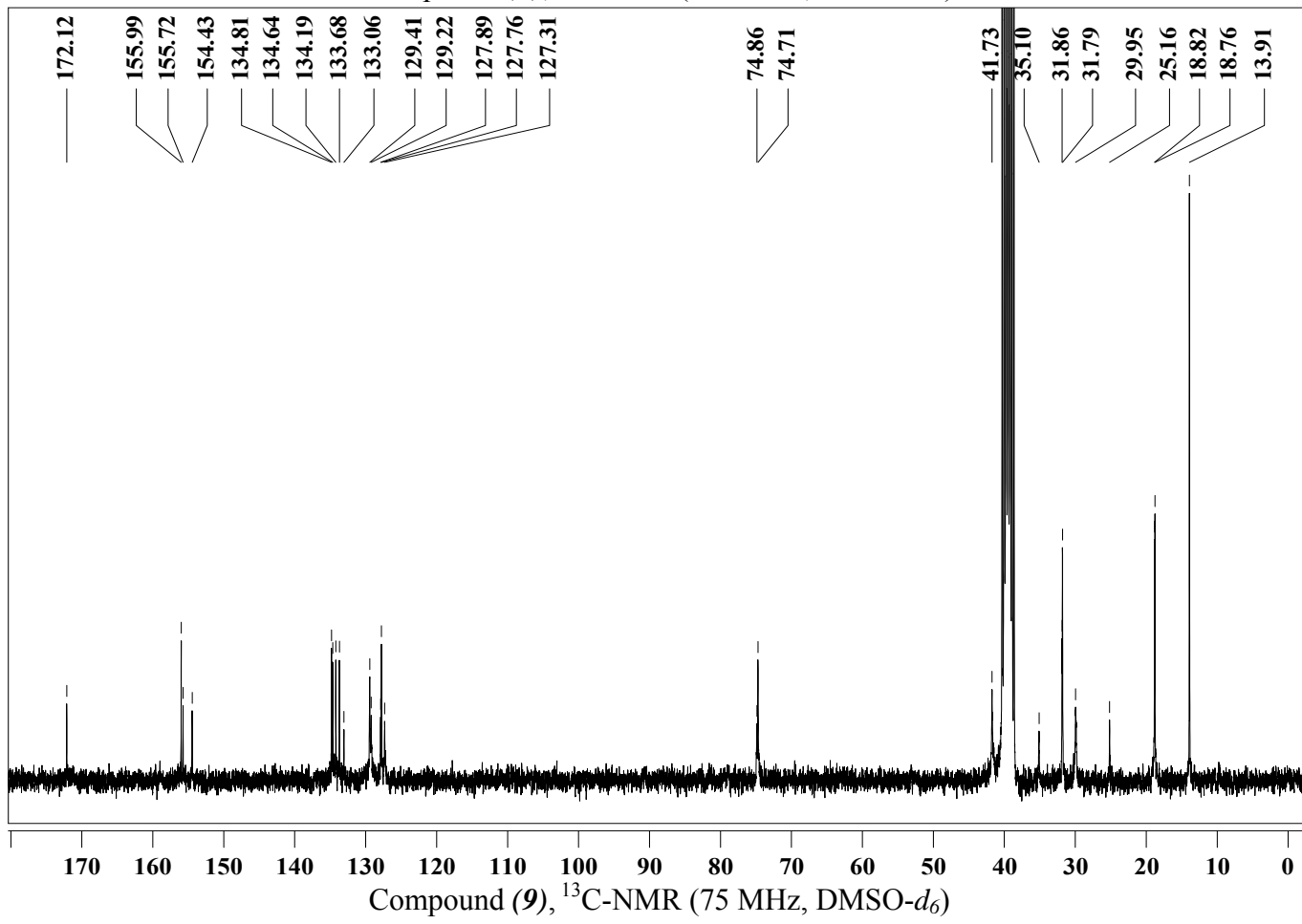
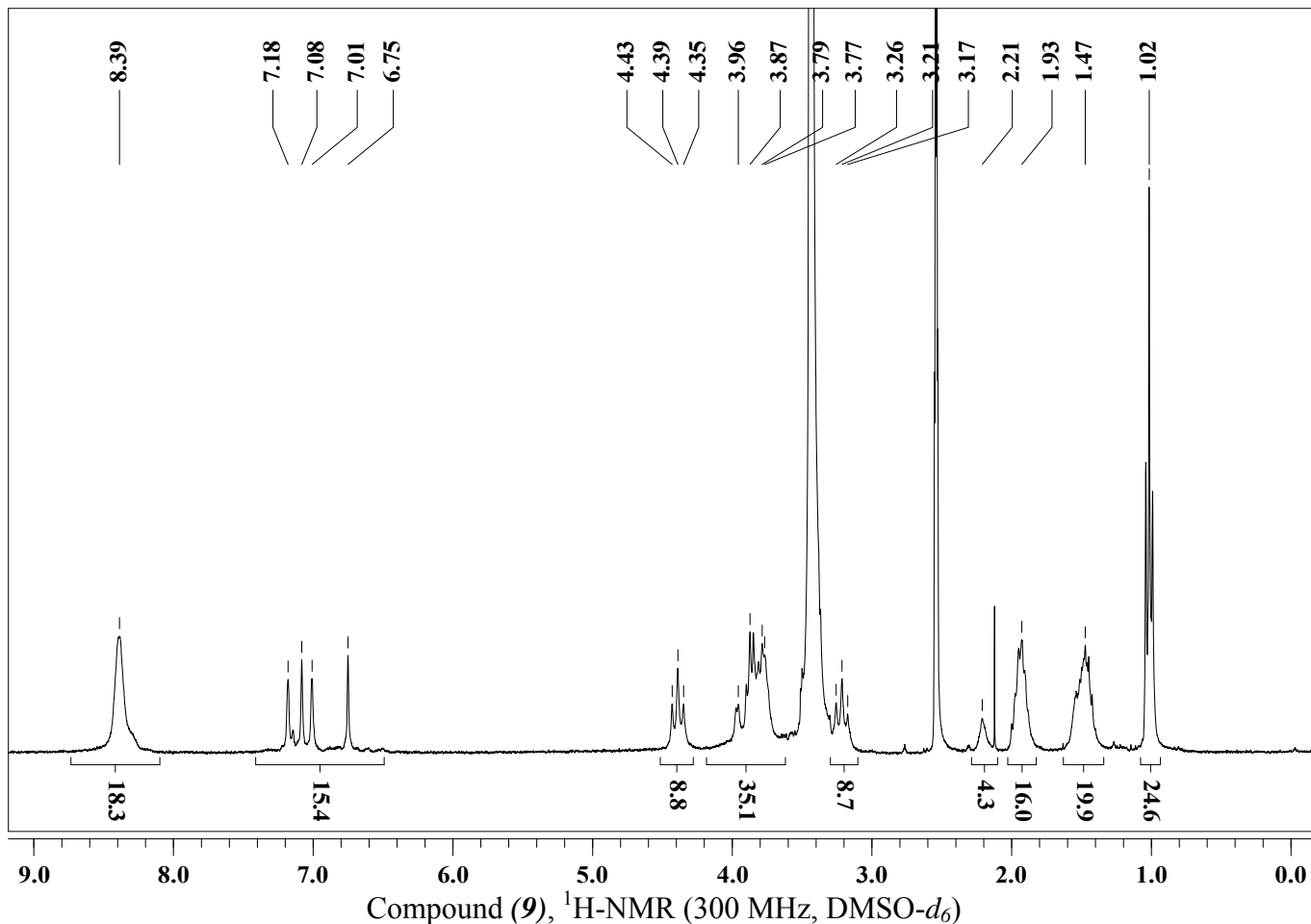
MS-Analyse: ESI-TOF

Analysis Name: E:\MS-Daten\HuWenbin\071213-Hu008-pos_01_9594.d\071213-Hu008-pos_01_9594.ser
Method: methodname
Operator: van Hoof
Acquisition Date: 12/13/2007 2:00:17 PM
Instrument: Bruker BioTOF III

Comment: comment



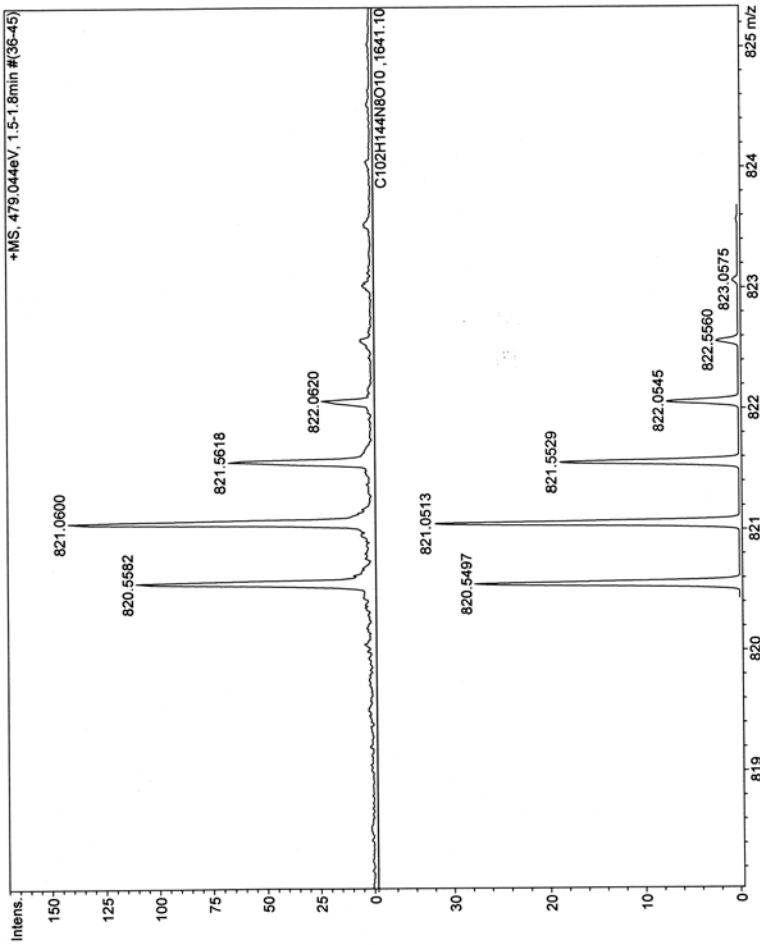
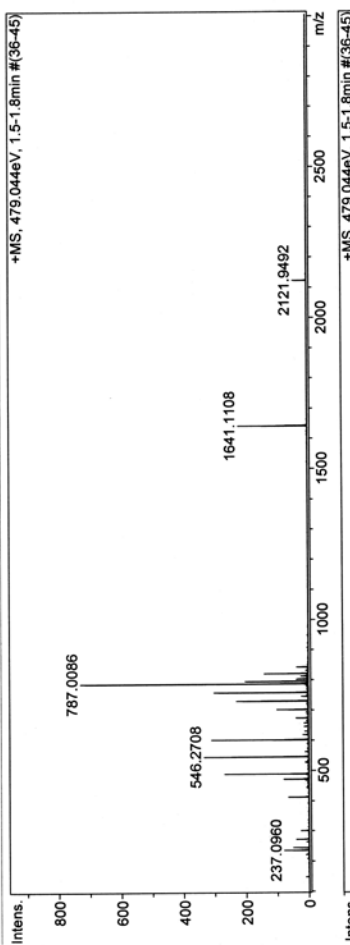
Compound (8), MS (ESI-TOF, pos. CH_2Cl_2)



MS-Analyse: ESI-TOF

Analysis Name: E:\MS-Daten\HuWenbin\091104-009-1-091103-pos_01_1641
Method: ~~file~~fcname Karow
Acquisition Date: 11/4/2009 9:57:43 AM Instrument: Bruker BioTOF III

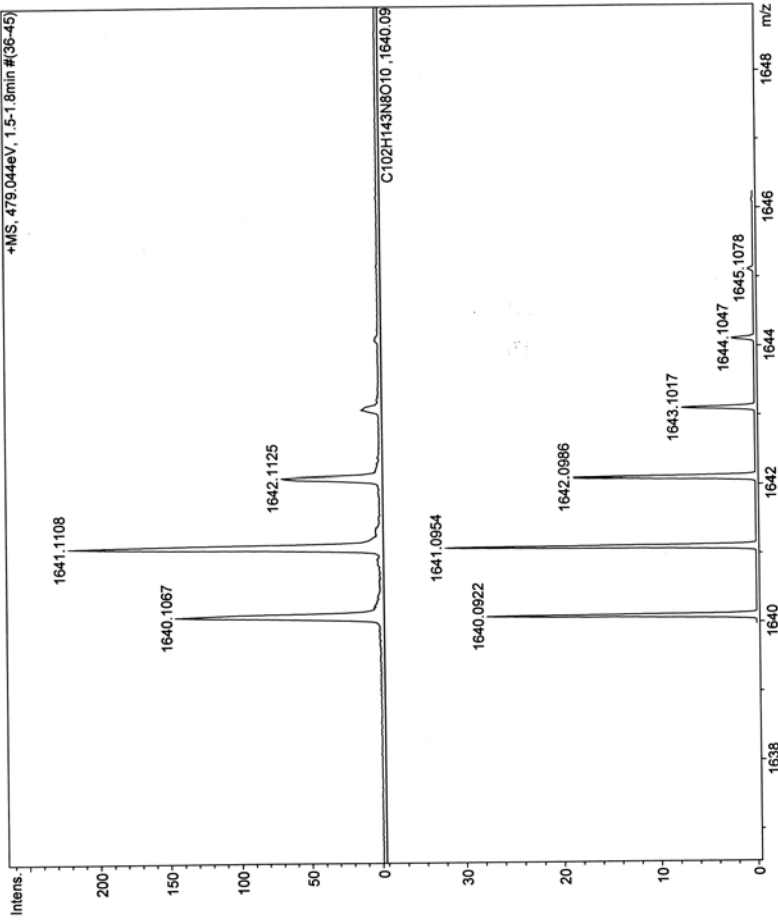
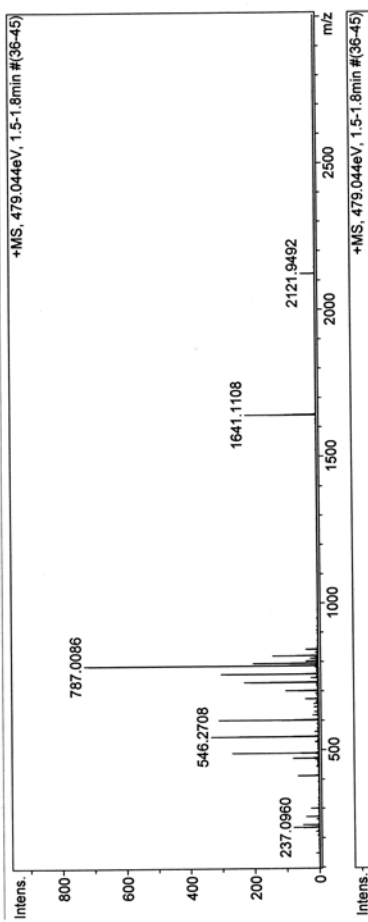
Comment: comment



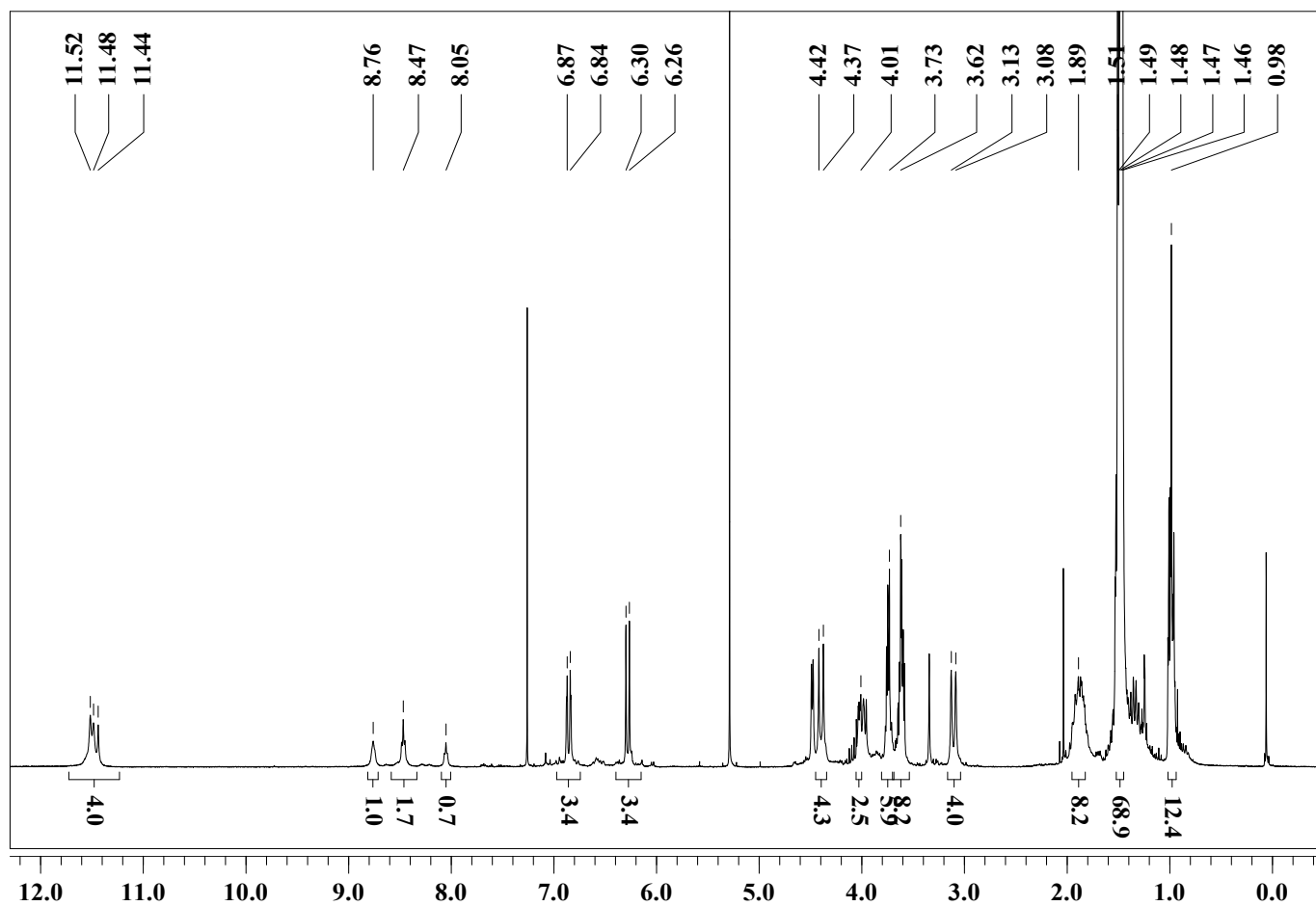
MS-Analyse: ESI-TOF

Analysis Name: E:\MS-Daten\HuWenbin\091104-009-1-091103-pos_01_16417.d\091104-009-1-091103-pos_01_1641
Method: ~~file~~fcname Karow
Acquisition Date: 11/4/2009 9:57:43 AM Instrument: Bruker BioTOF III

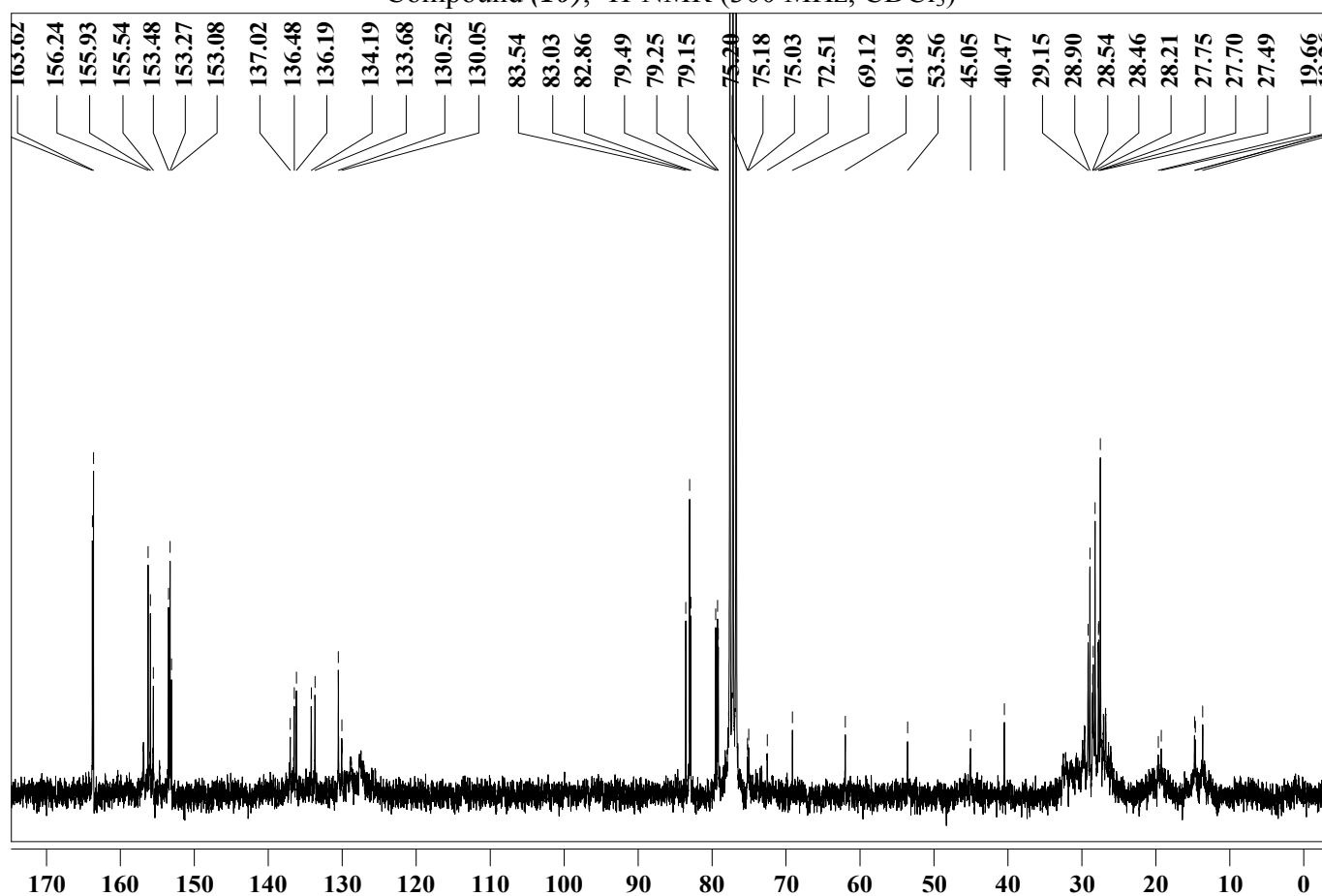
Comment: comment



Compound (9), MS (ESI-TOF, pos. MeOH, free base)



Compound (10), $^1\text{H-NMR}$ (300 MHz, CDCl_3)

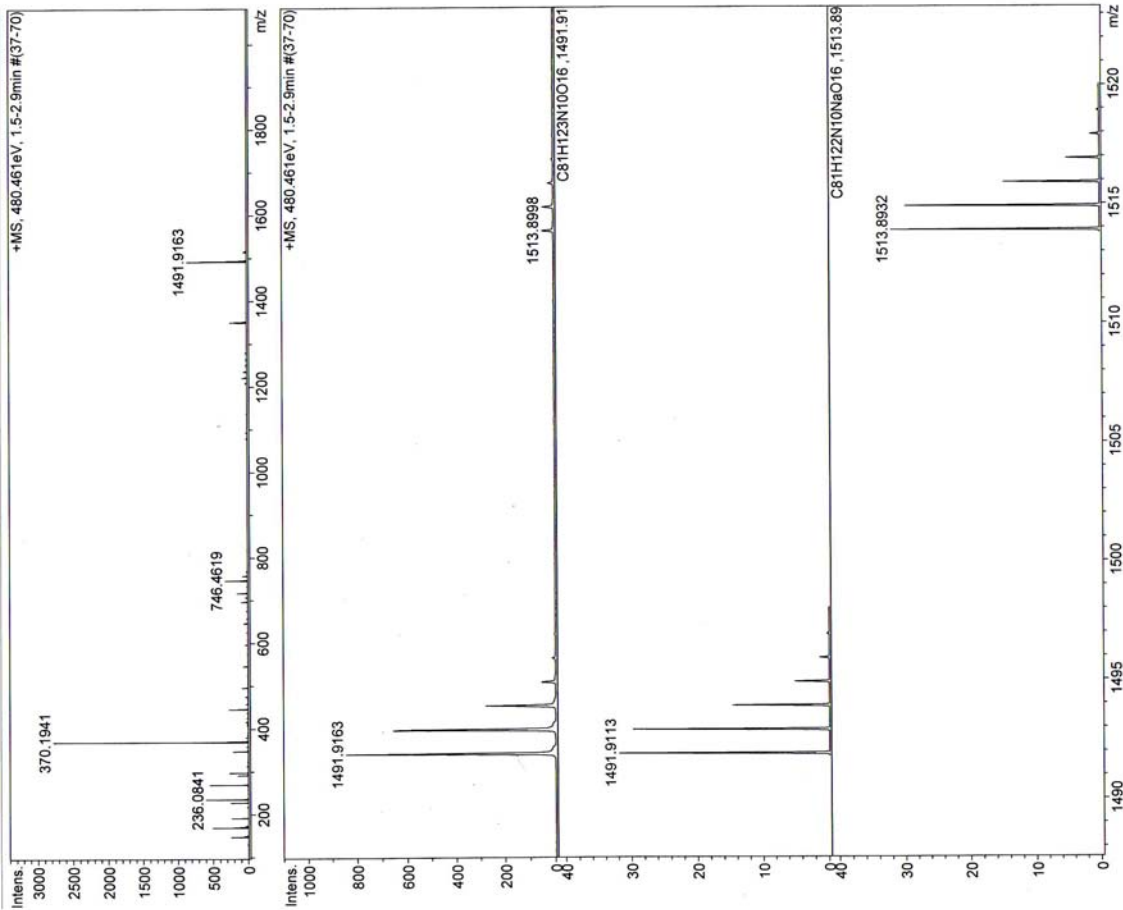


Compound (10), $^{13}\text{C-NMR}$ (75 MHz, CDCl_3)

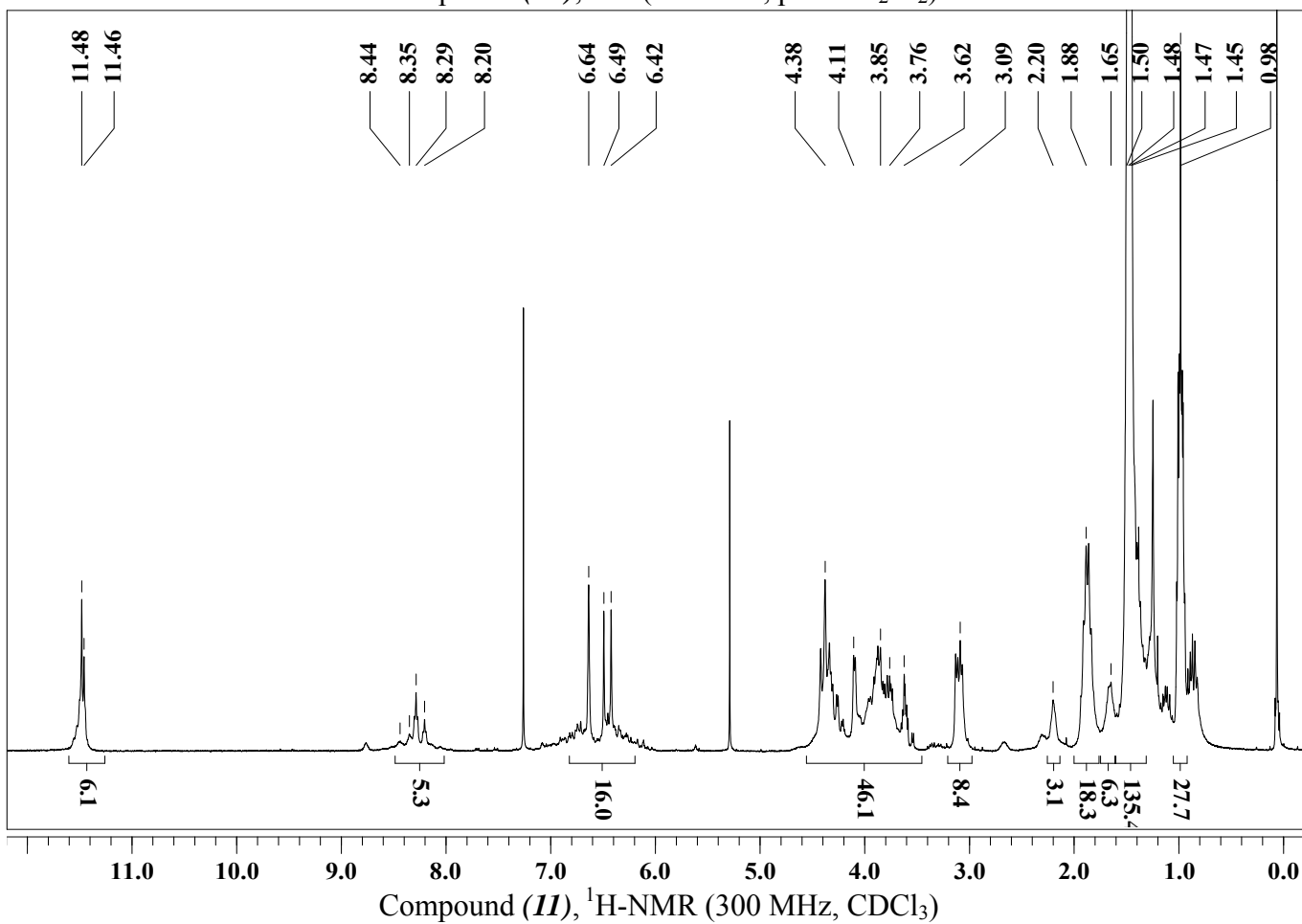
MS-Analyse: ESI-TOF

Analysis Name: E:\MS-Daten\HuWenbin\080402-Hu024-080331-pos_01_10301.d\080402-Hu024-080331-pos_01_103
Method: ~~file~~ name
Acquisition Date: 4/2/2008 11:57:46 AM
Operator: van Hoof
Instrument: Bruker BioTOF III

Comment: comment



Compound (**10**), MS (ESI-TOF, pos. CH₂Cl₂)

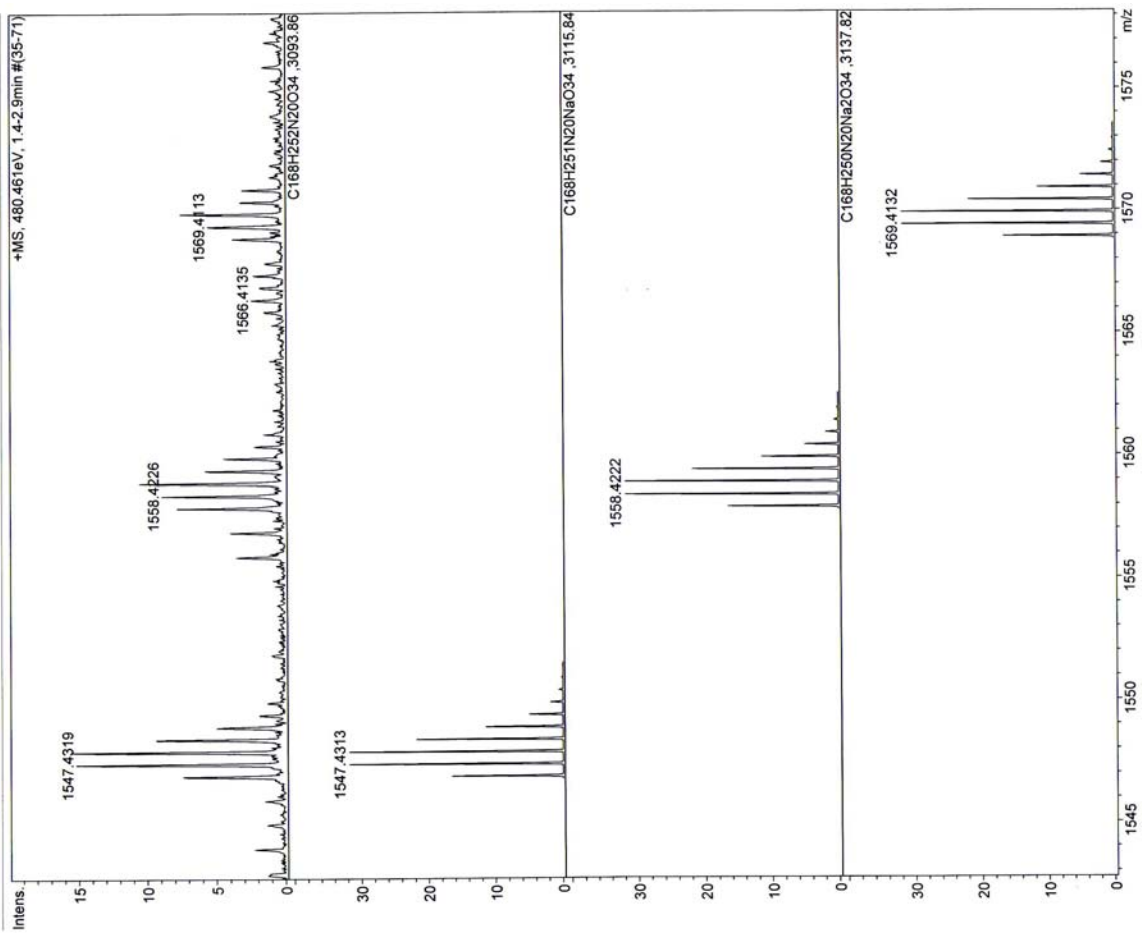


Compound (**11**), ¹H-NMR (300 MHz, CDCl₃)

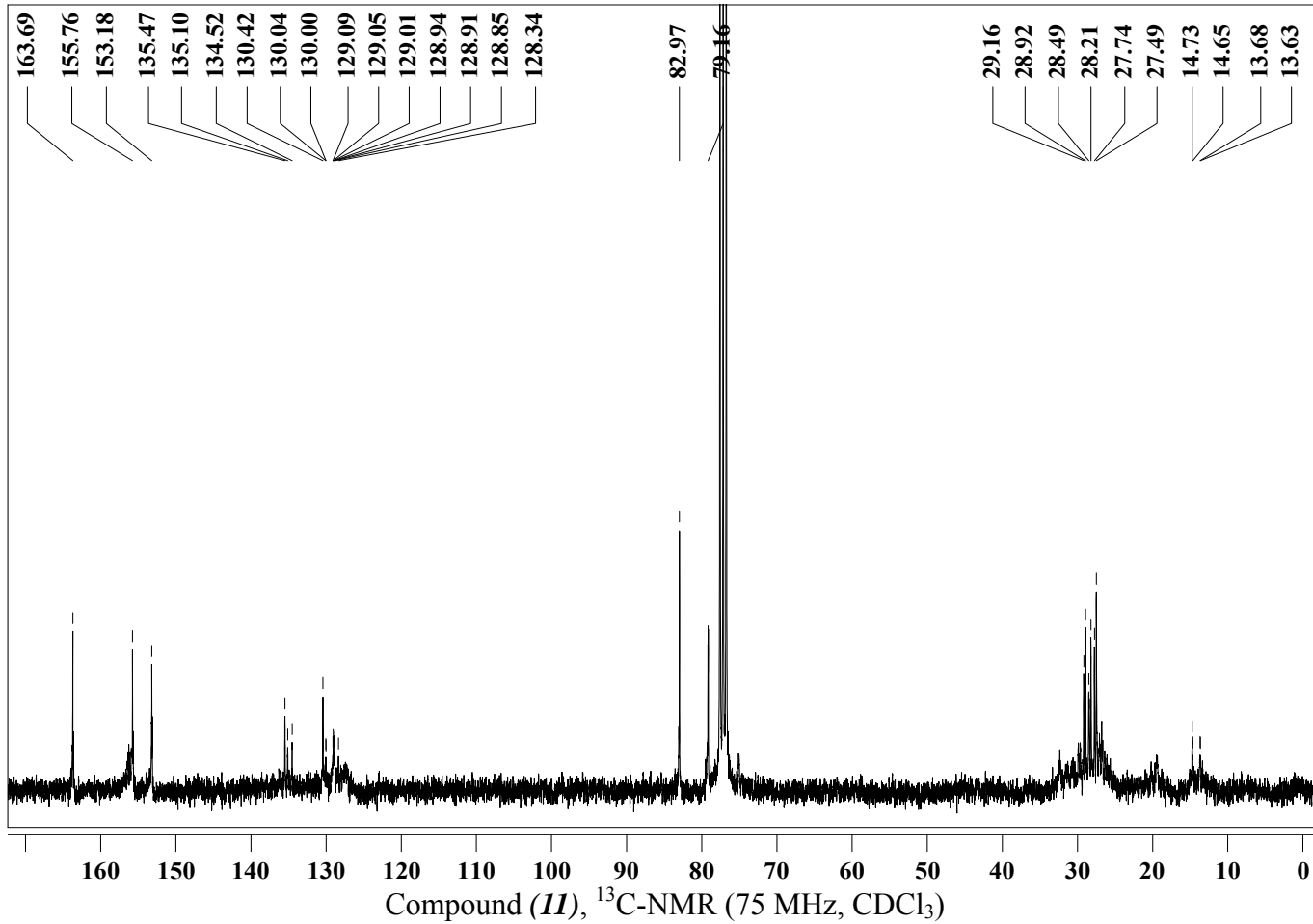
MS-Analyse: ESI-TOF

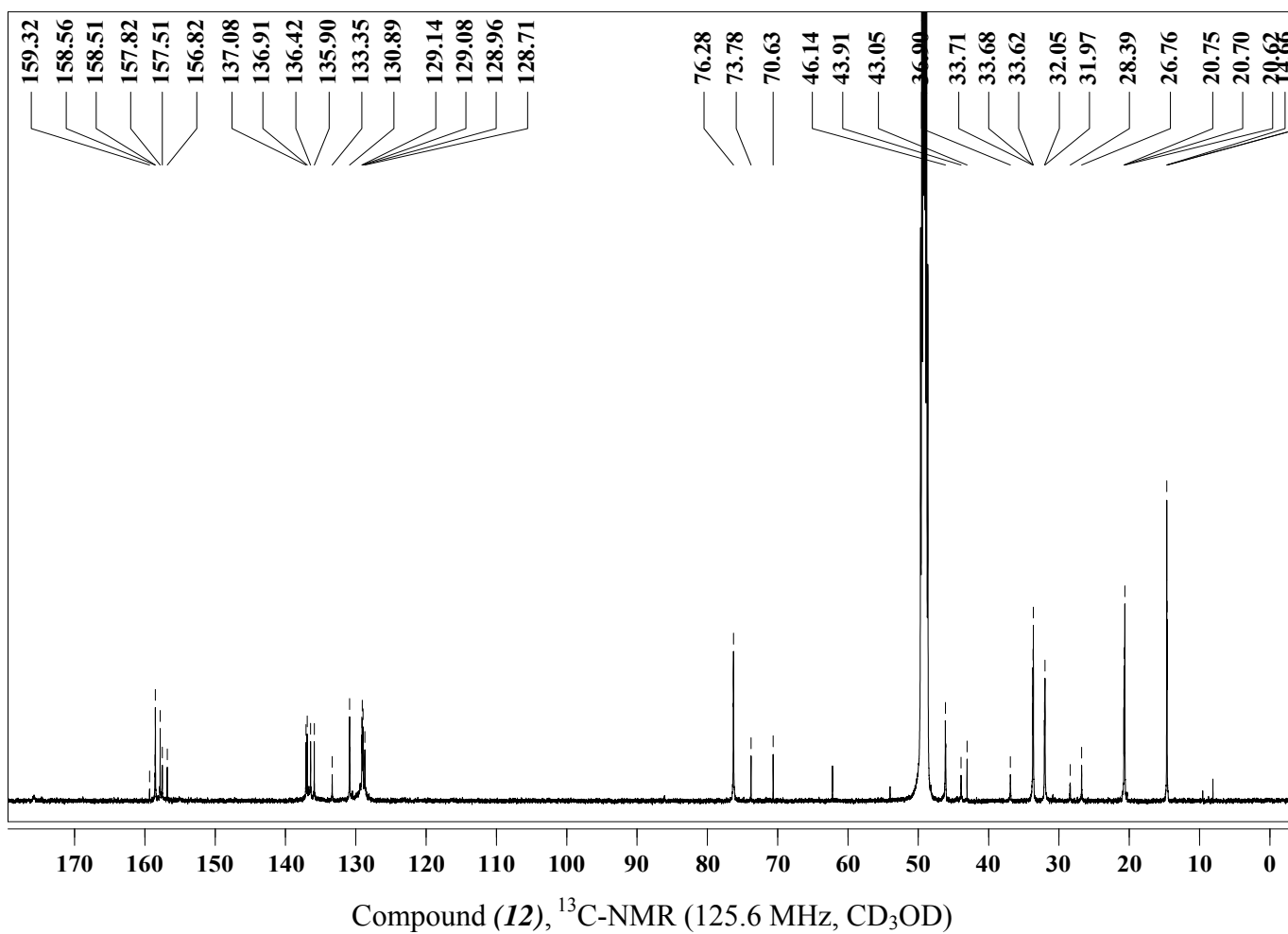
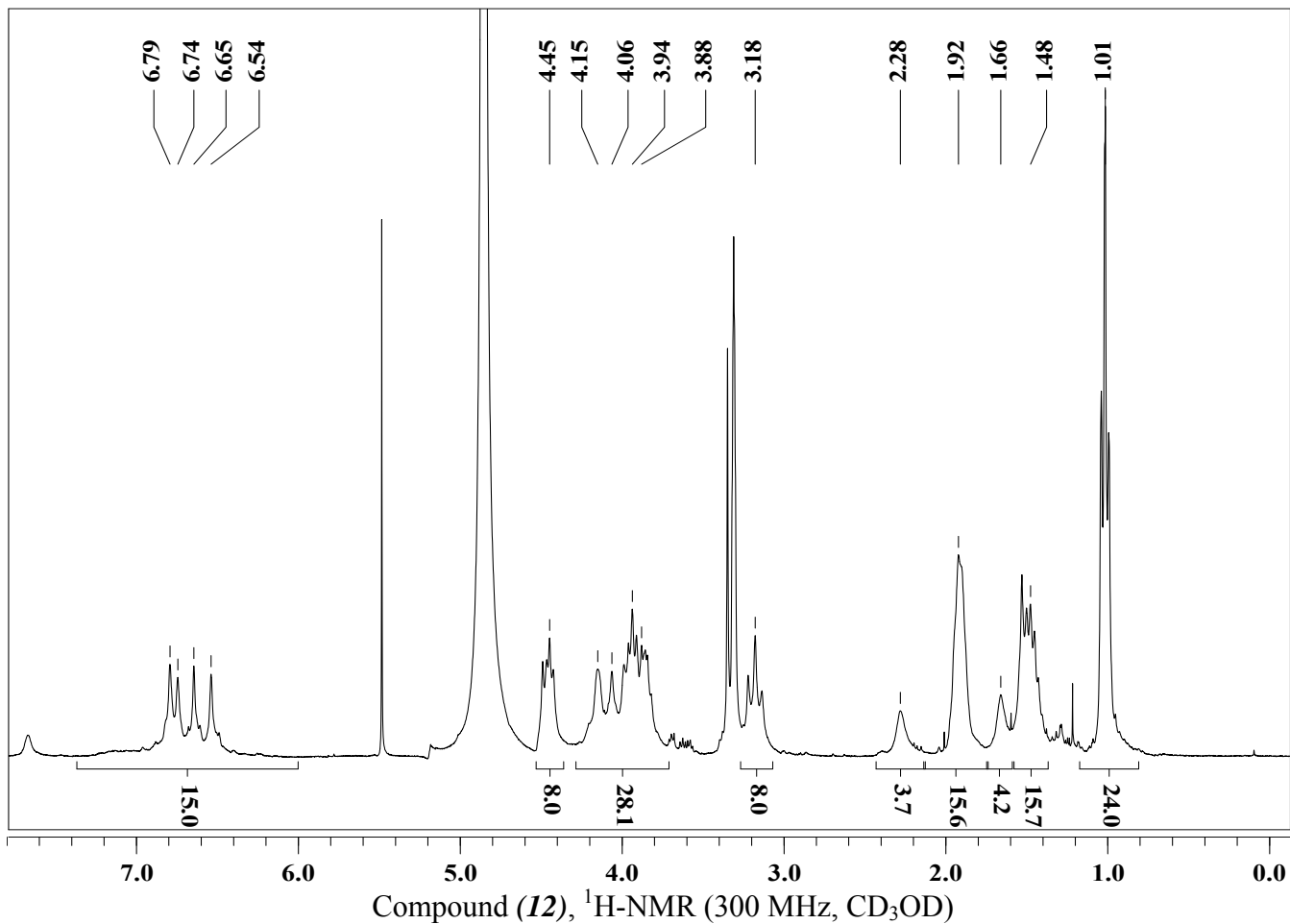
Analysis Name: E:\MS-Daten\HuWenbin\080415-Hu014-080415-pos_01_10393.d\080415-Hu014-080415-pos_01_103
Reference: van Hoof
Operator: van Hoof
Instrument: Bruker BioTOF III
Acquisition Date: 4/15/2008 9:34:12 AM

Comment: comment



Compound (II), MS (ESI-TOF, pos. CH₂Cl₂)

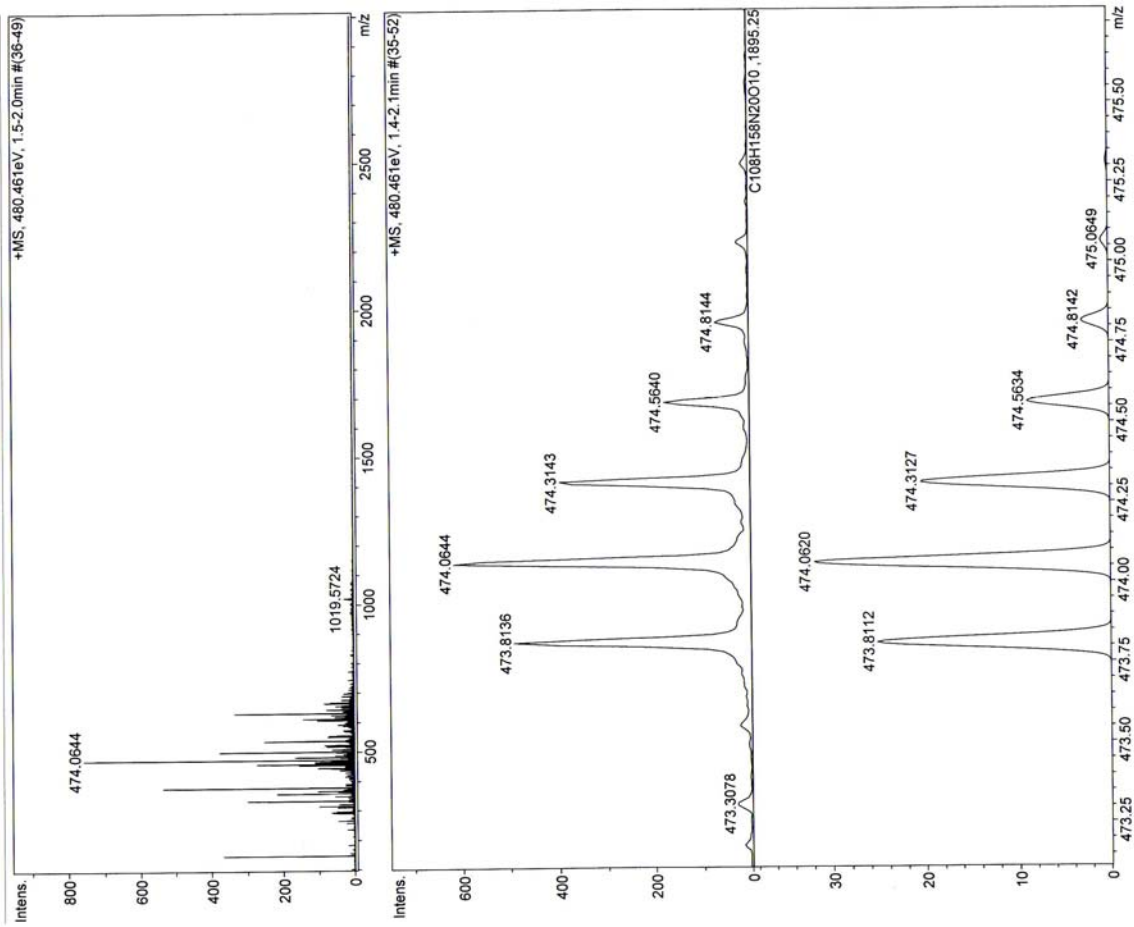




MS-Analyse: ESI-TOF

Analysis Name: E:\MS-Daten\HuWenbin\080416-Hu015-2-080416-pos_01_10401.d\080416-Hu015-2-080416-pos_01_10401.d
 Method: f0416_080416.ms
 Acquisition Date: 4/16/2008 2:03:16 PM
 Operator: Karow
 Instrument: Bruker BioTOF III

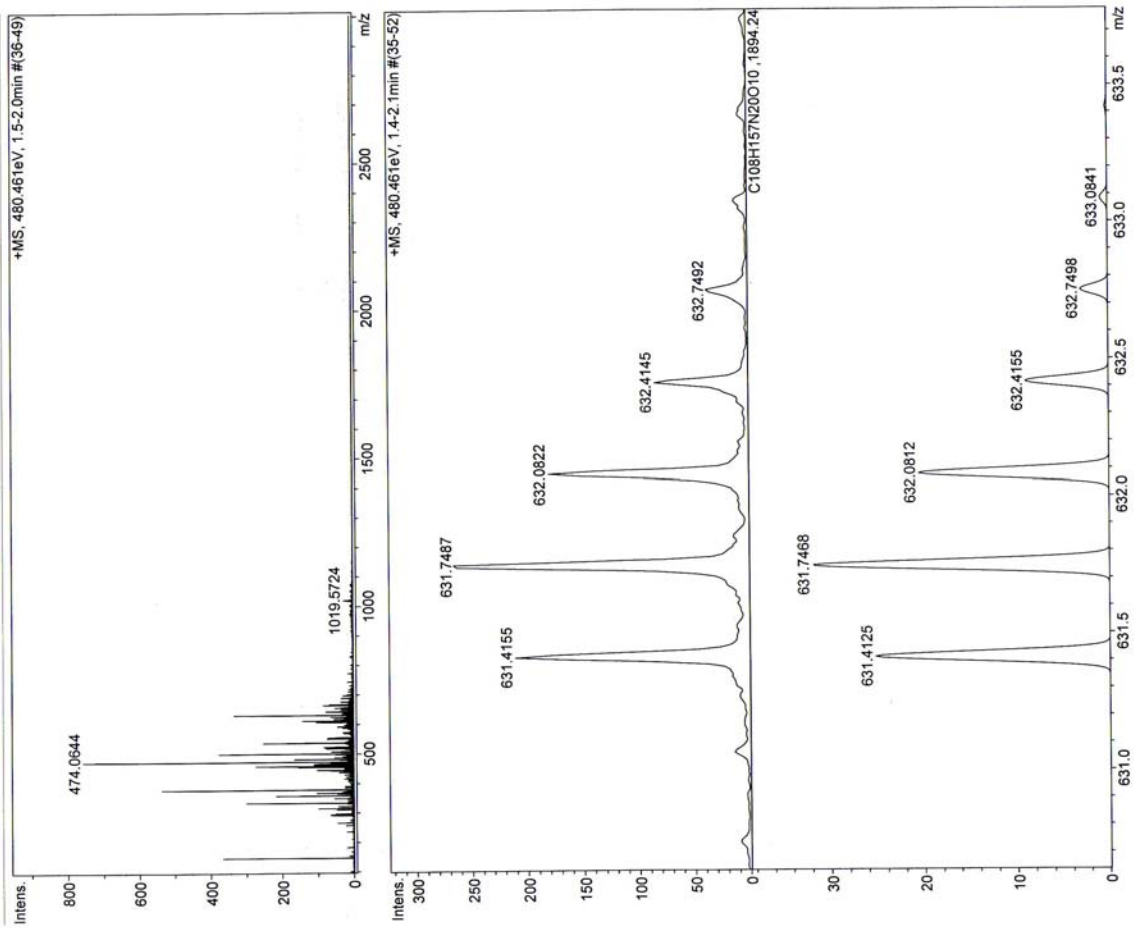
Comment: comment



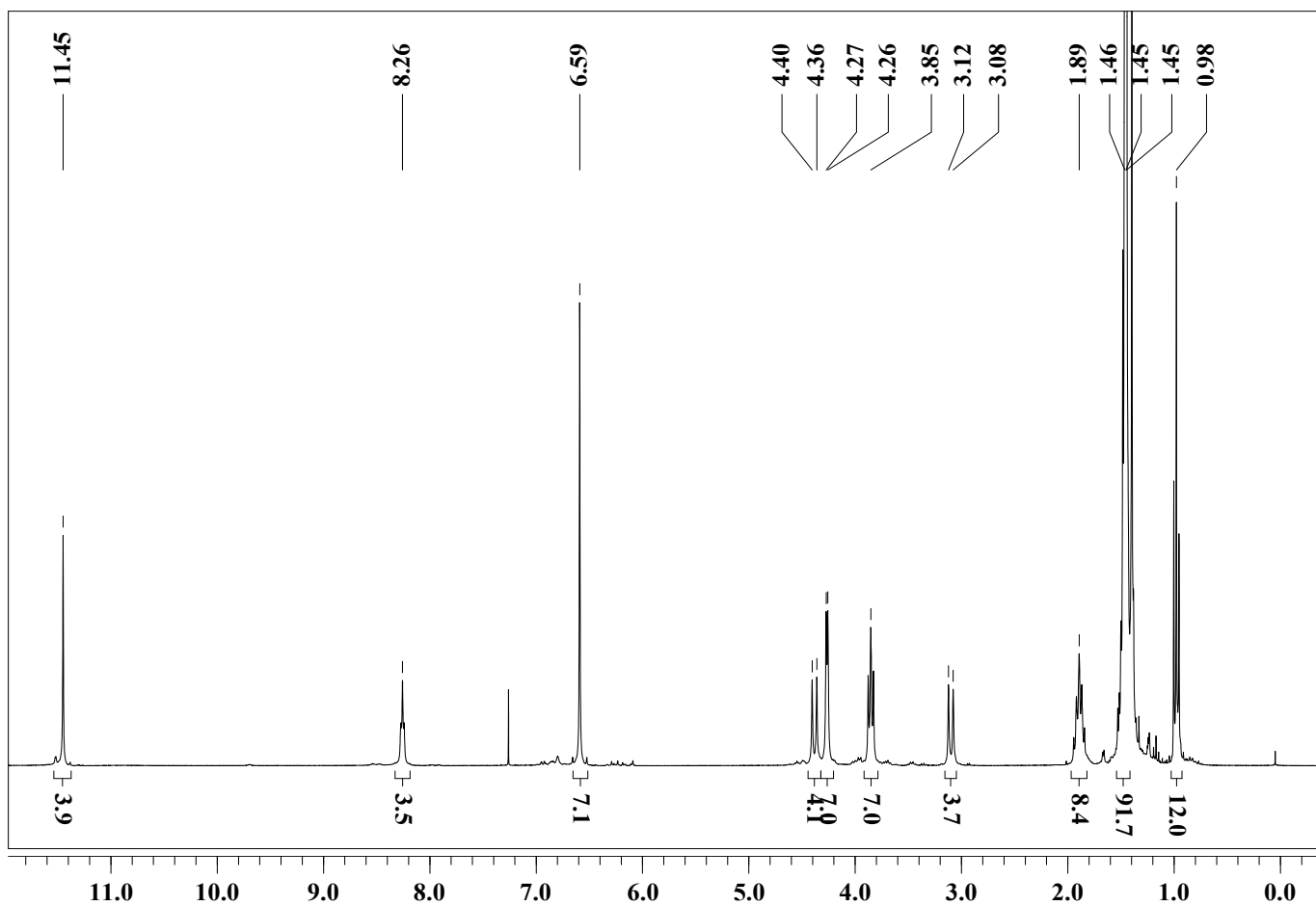
MS-Analyse: ESI-TOF

Analysis Name: E:\MS-Daten\HuWenbin\080416-Hu015-2-080416-pos_01_10401.d\080416-Hu015-2-080416-pos_01_10401.d
 Method: f0416_080416.ms
 Acquisition Date: 4/16/2008 2:03:16 PM
 Operator: Karow
 Instrument: Bruker BioTOF III

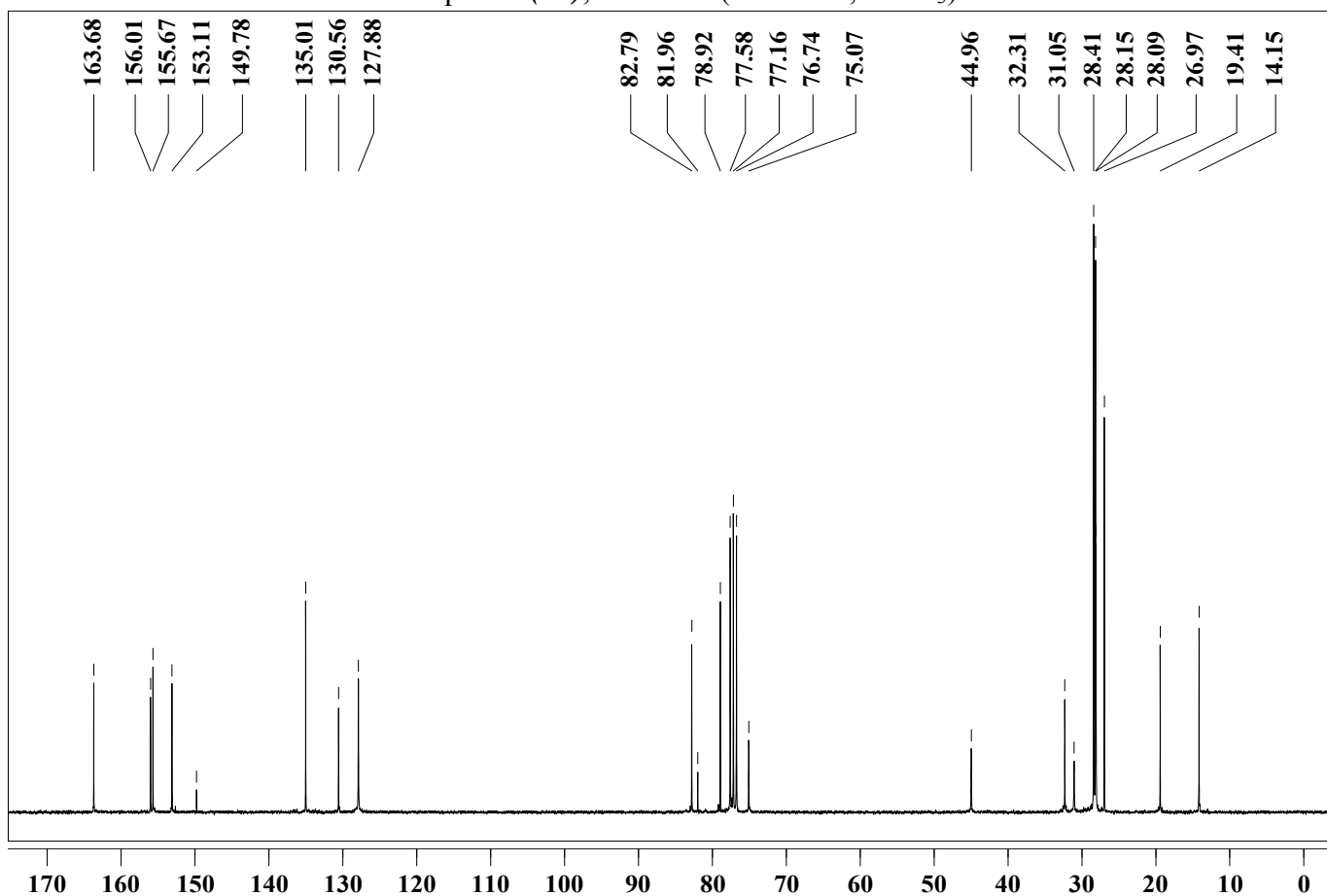
Comment: comment



Compound (12), MS (ESI-TOF, pos. MeOH, free base)



Compound (13), ¹H-NMR (300 MHz, CDCl₃)

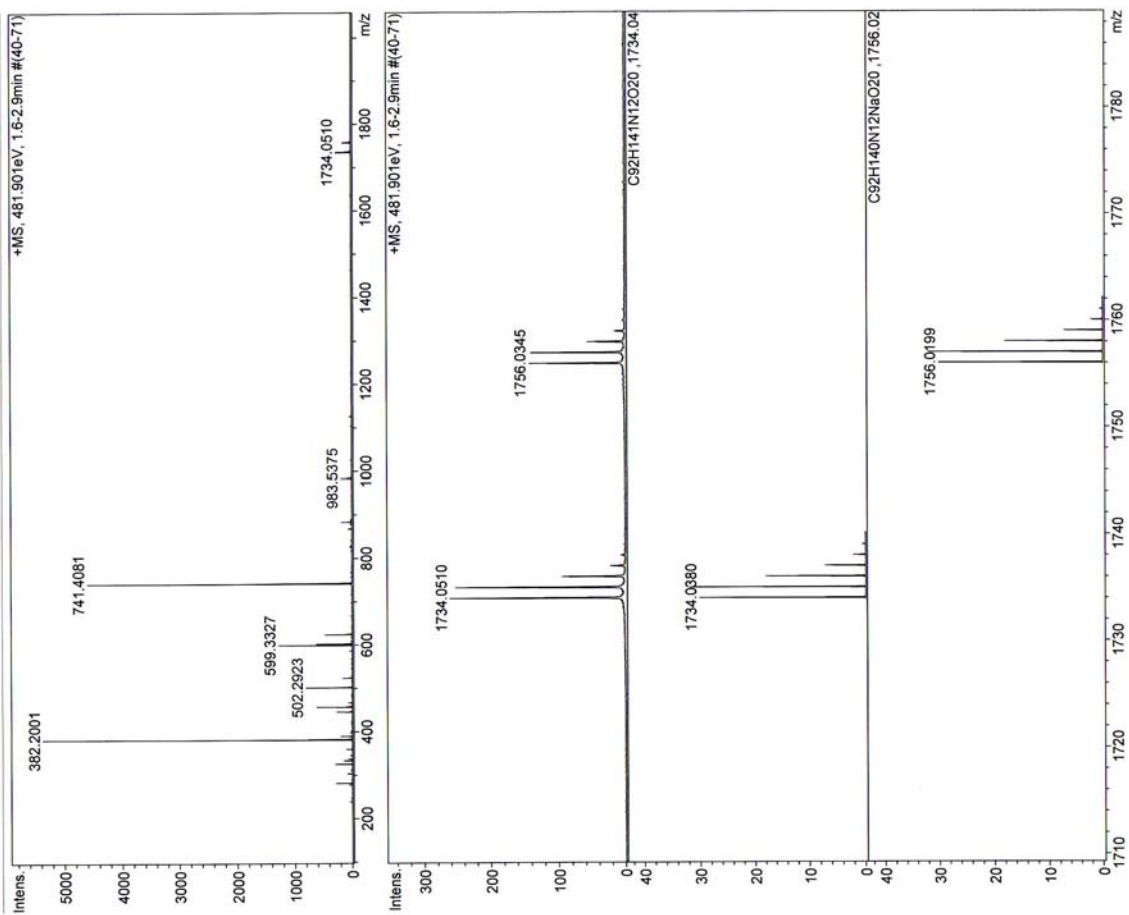


Compound (13), ¹³C-NMR (75 MHz, CDCl₃)

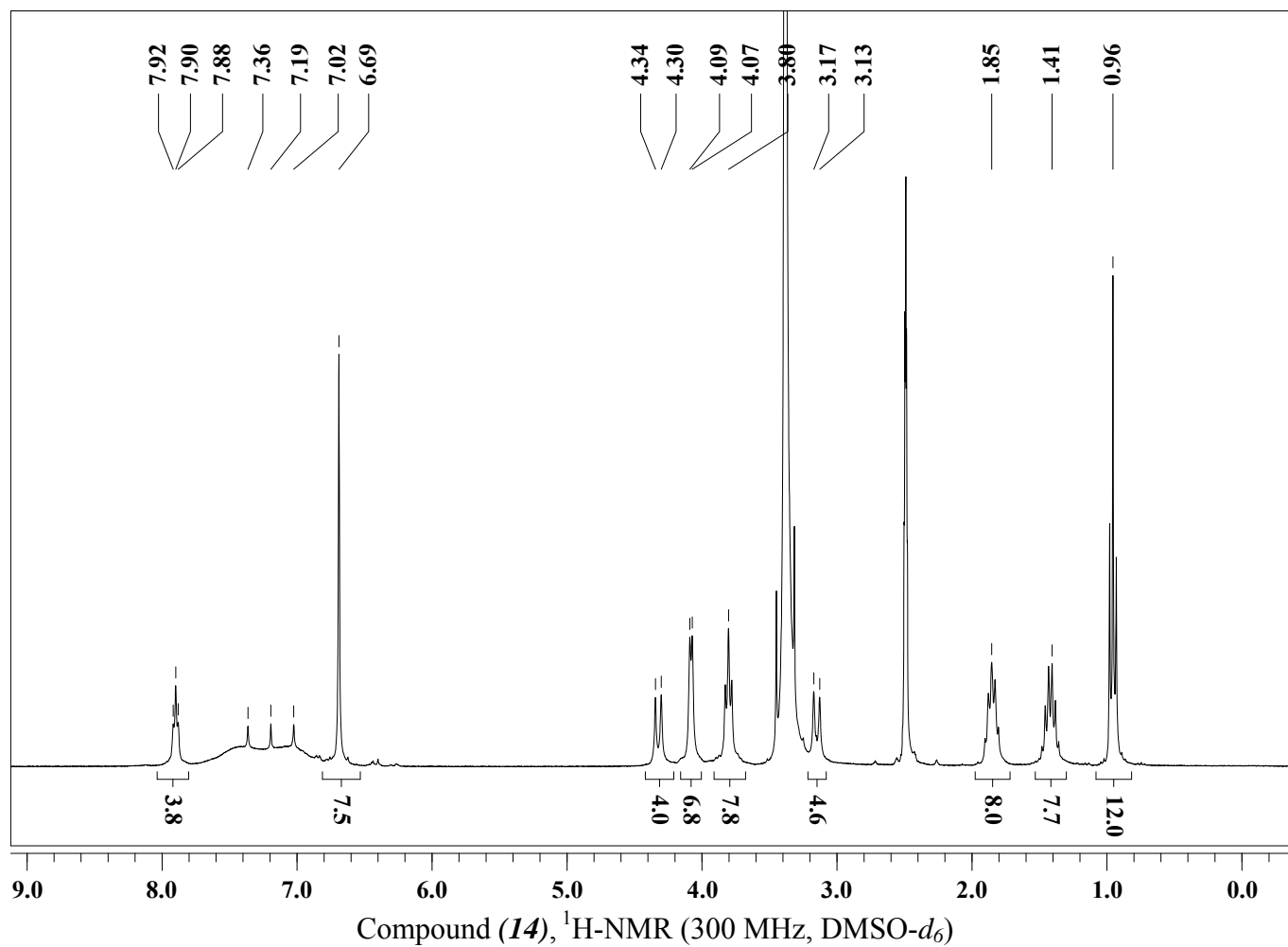
MS-Analyse: ESI-TOF

Analysis Name: E:\MS-Daten\HuWenbin\080624-Hu015boc-pos_01_10917.d\080624-Hu015boc-pos_01_10917.ser
Method: methodname
Operator: Karow
Acquisition Date: 6/24/2008 11:36:15 AM
Instrument: Bruker BioTOF III

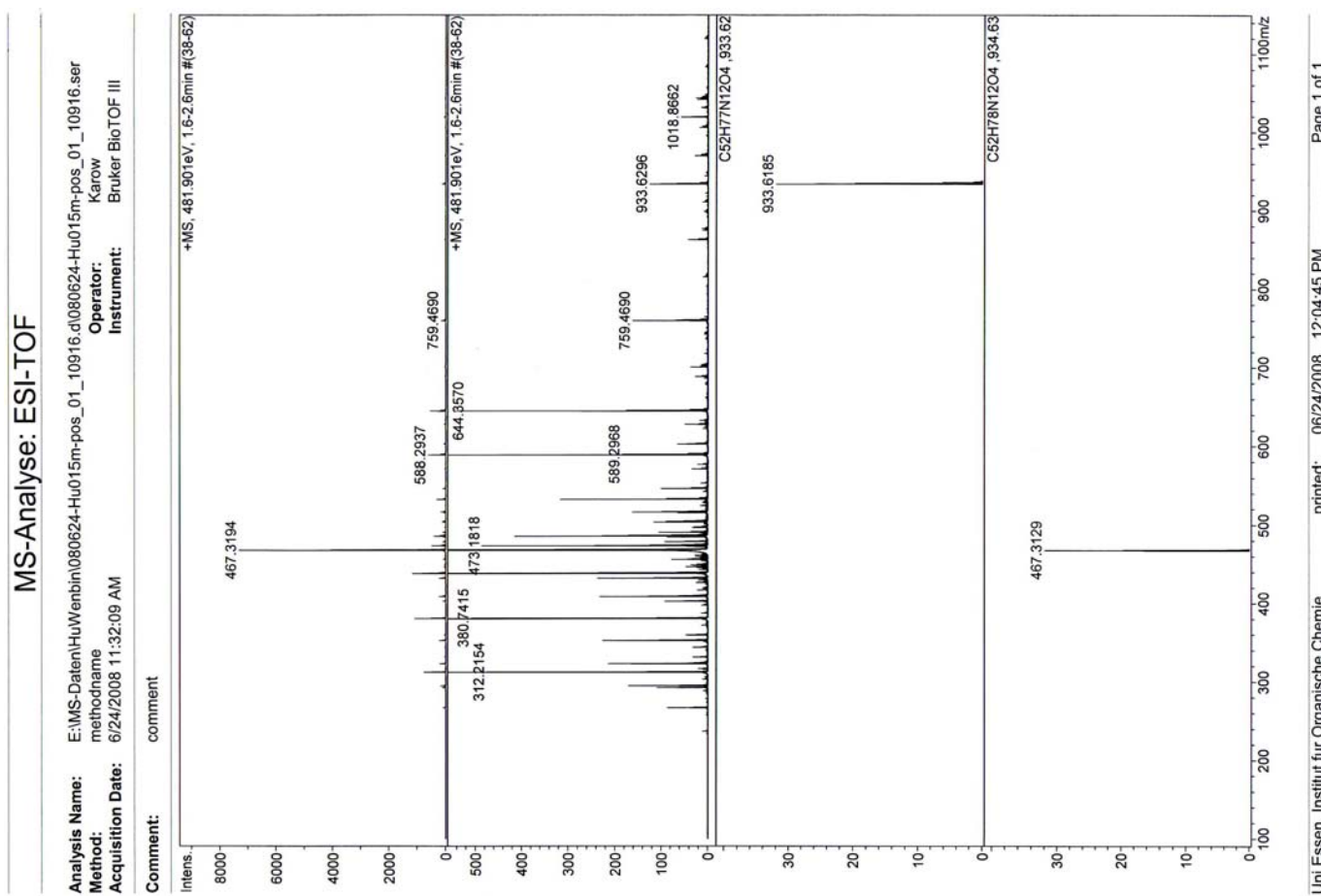
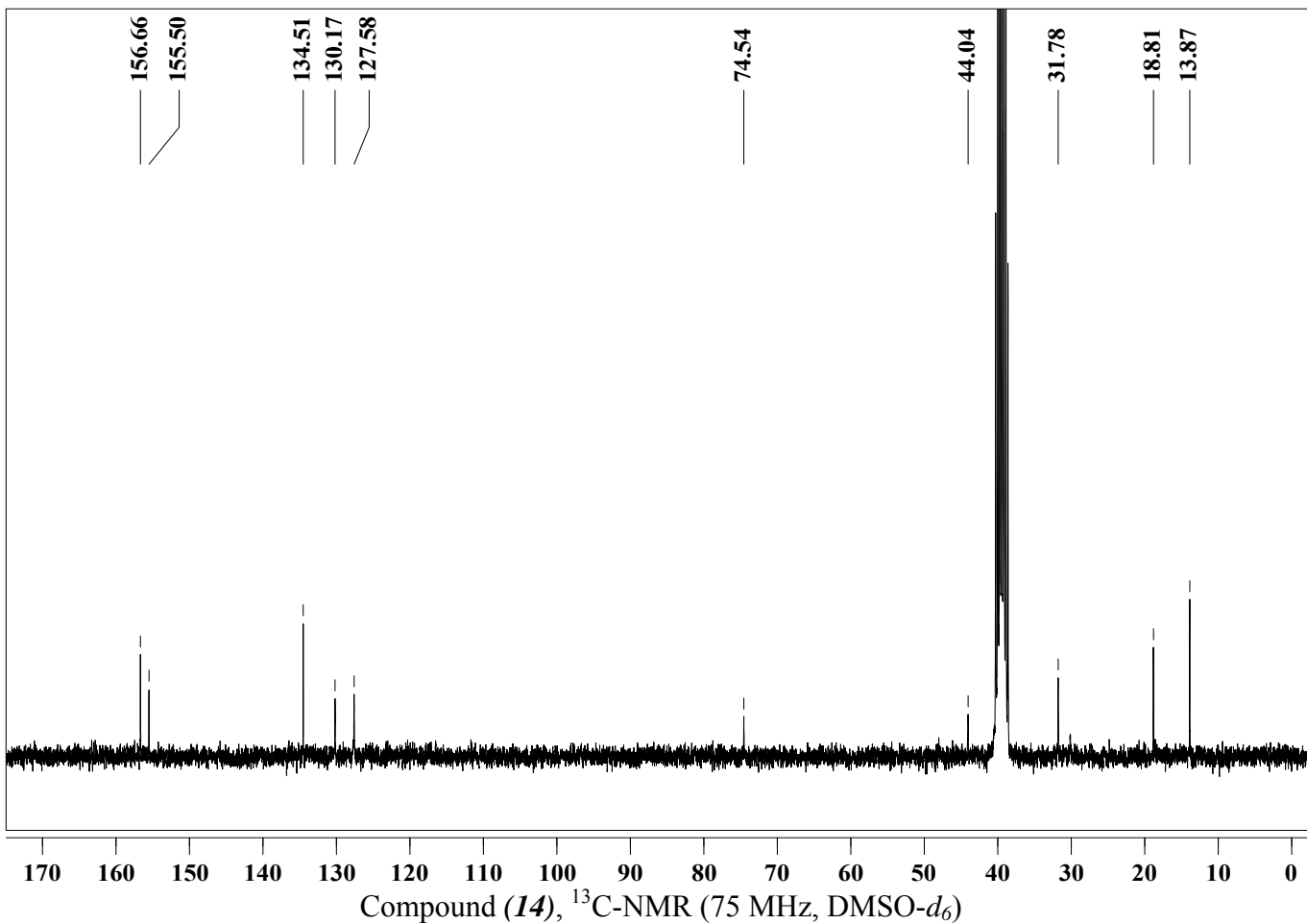
Comment: comment

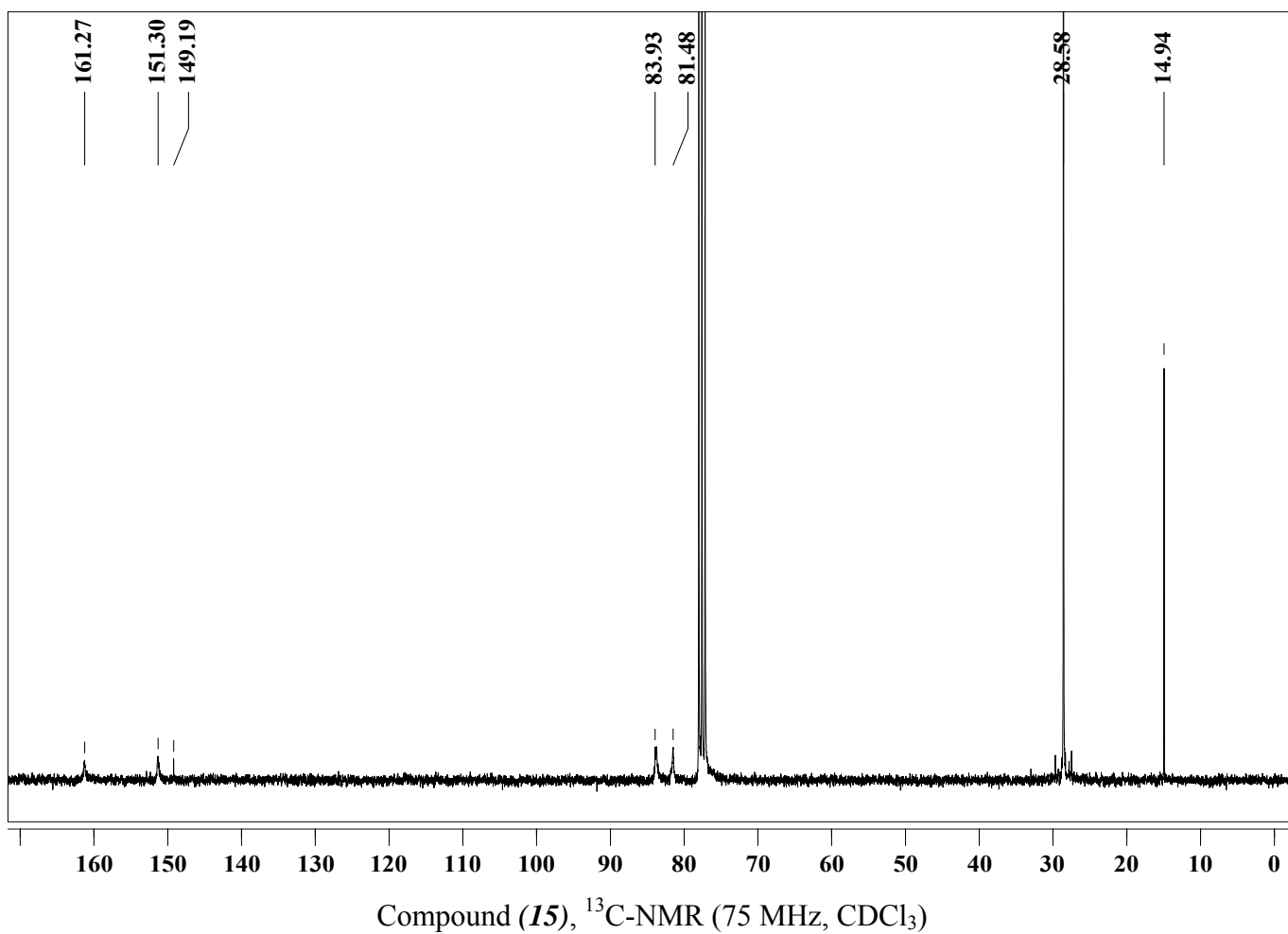
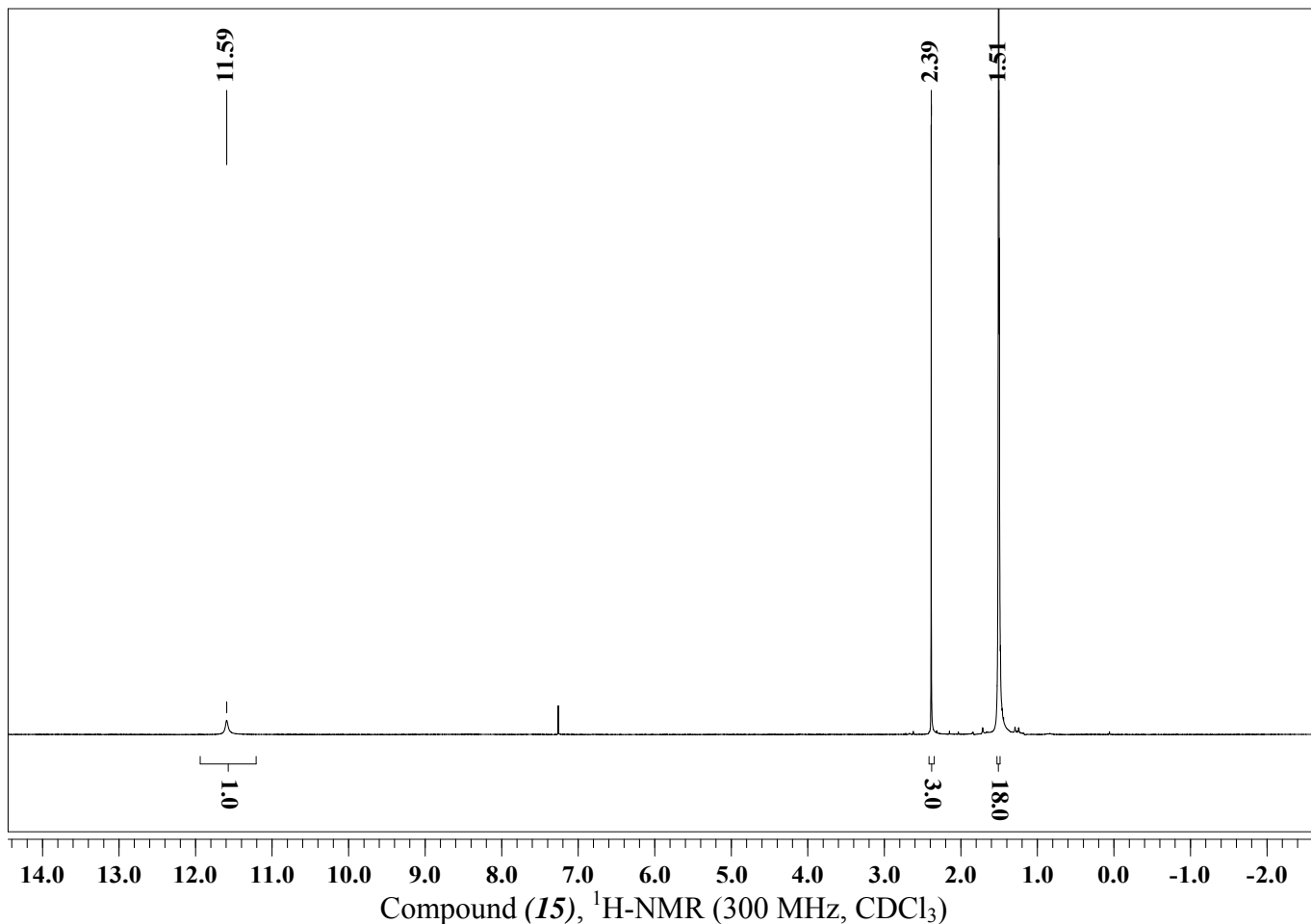


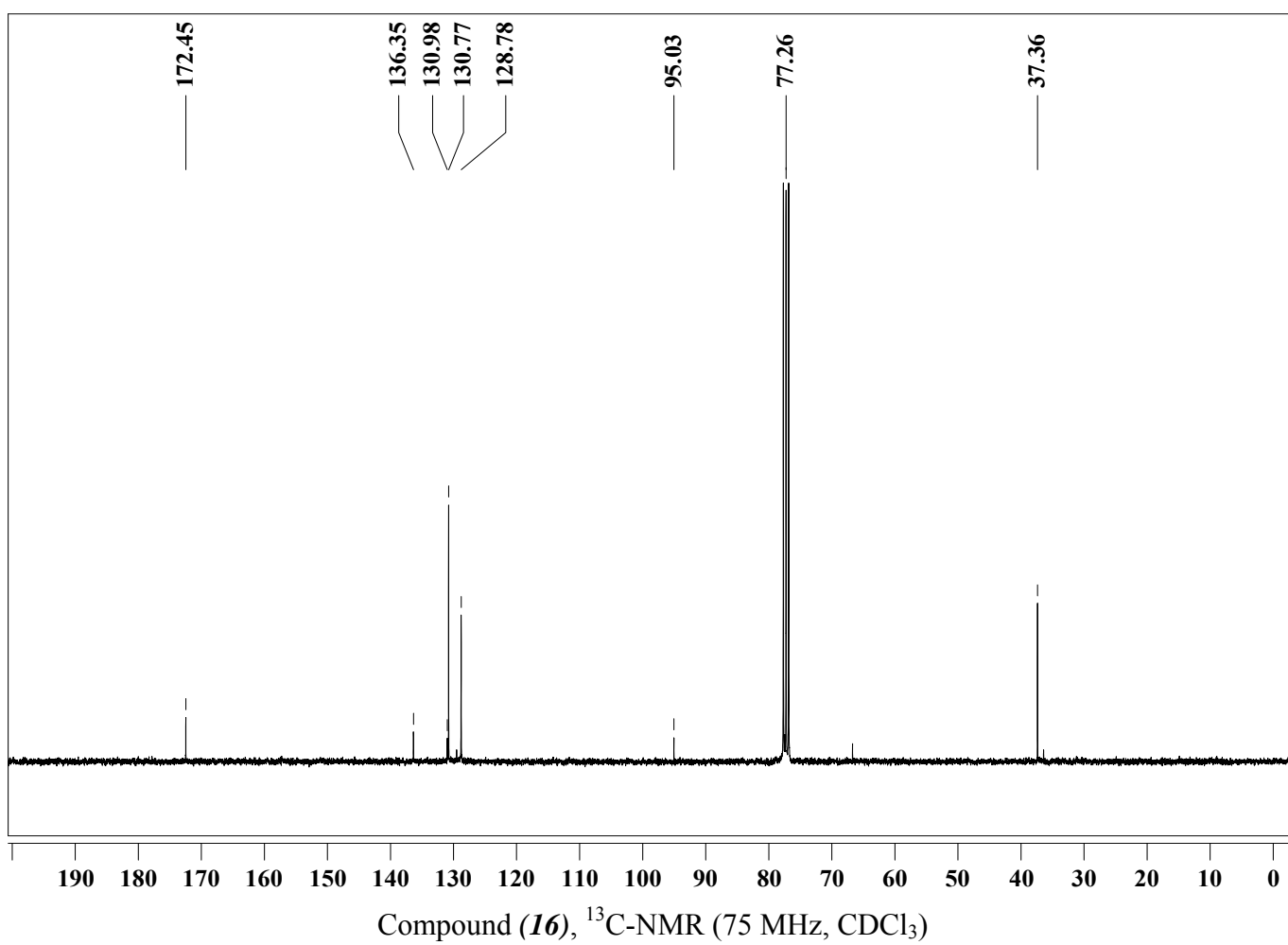
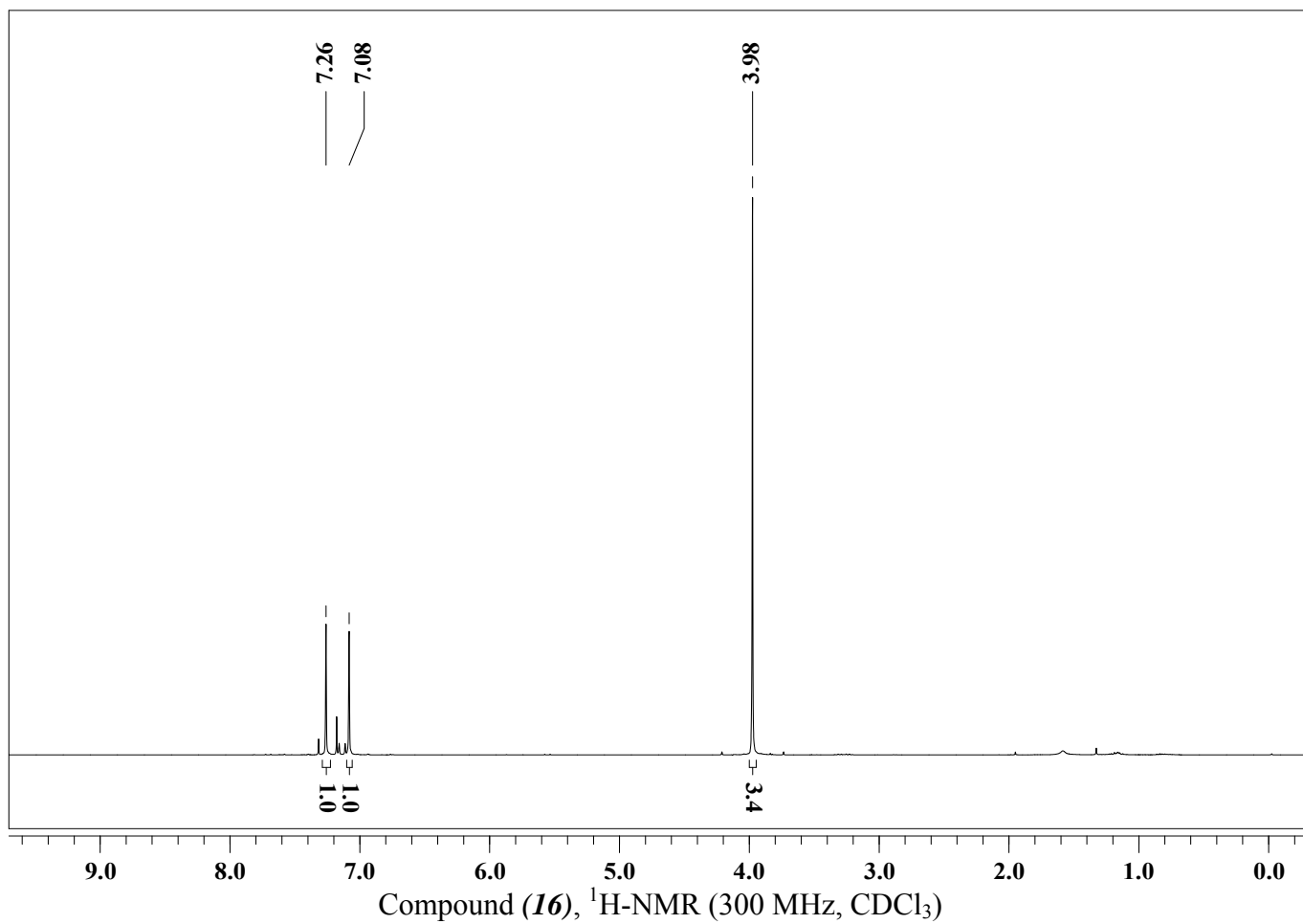
Compound (**13**), MS (ESI-TOF, pos. CH₂Cl₂)

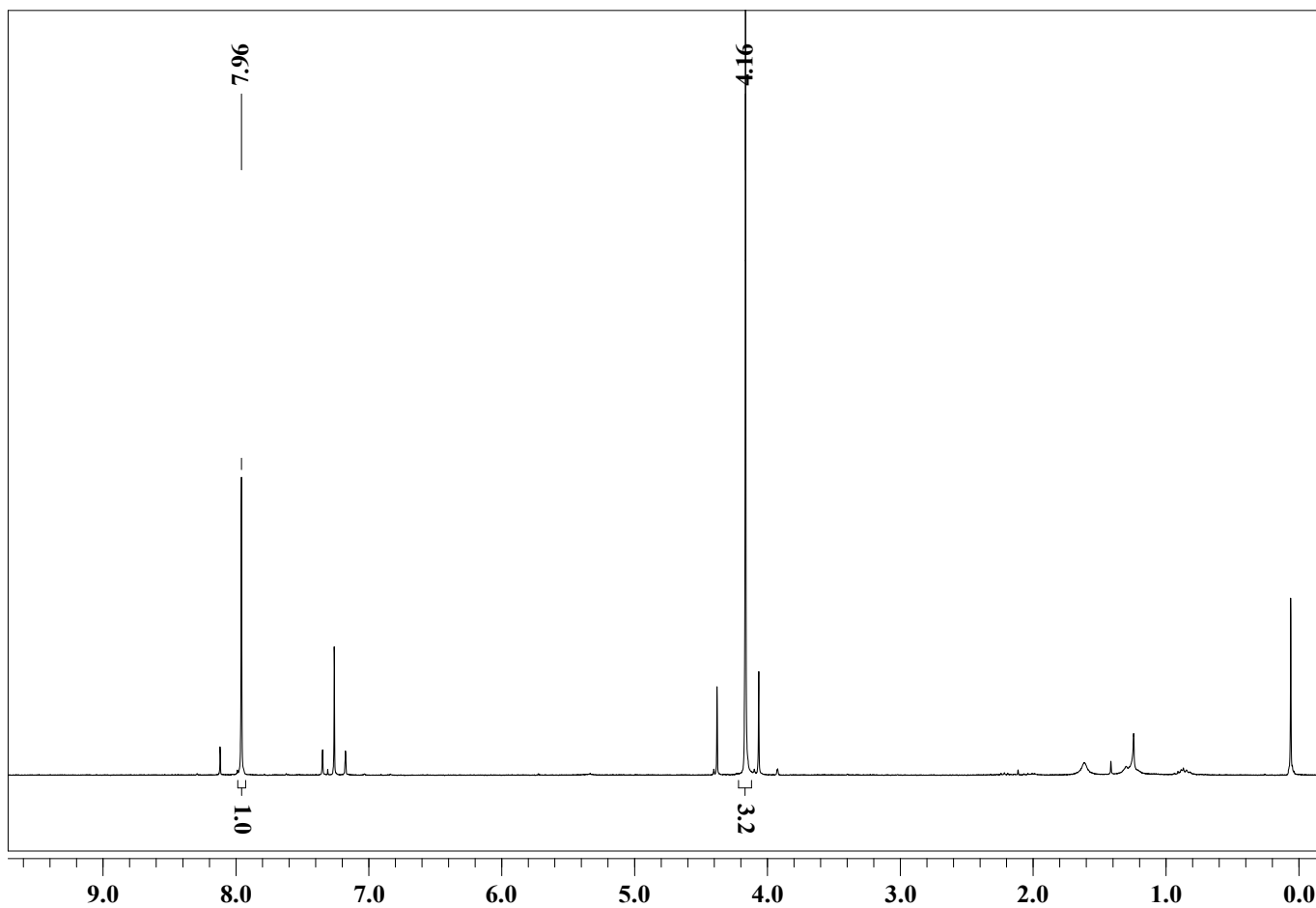


Compound (**14**), ¹H-NMR (300 MHz, DMSO-*d*₆)

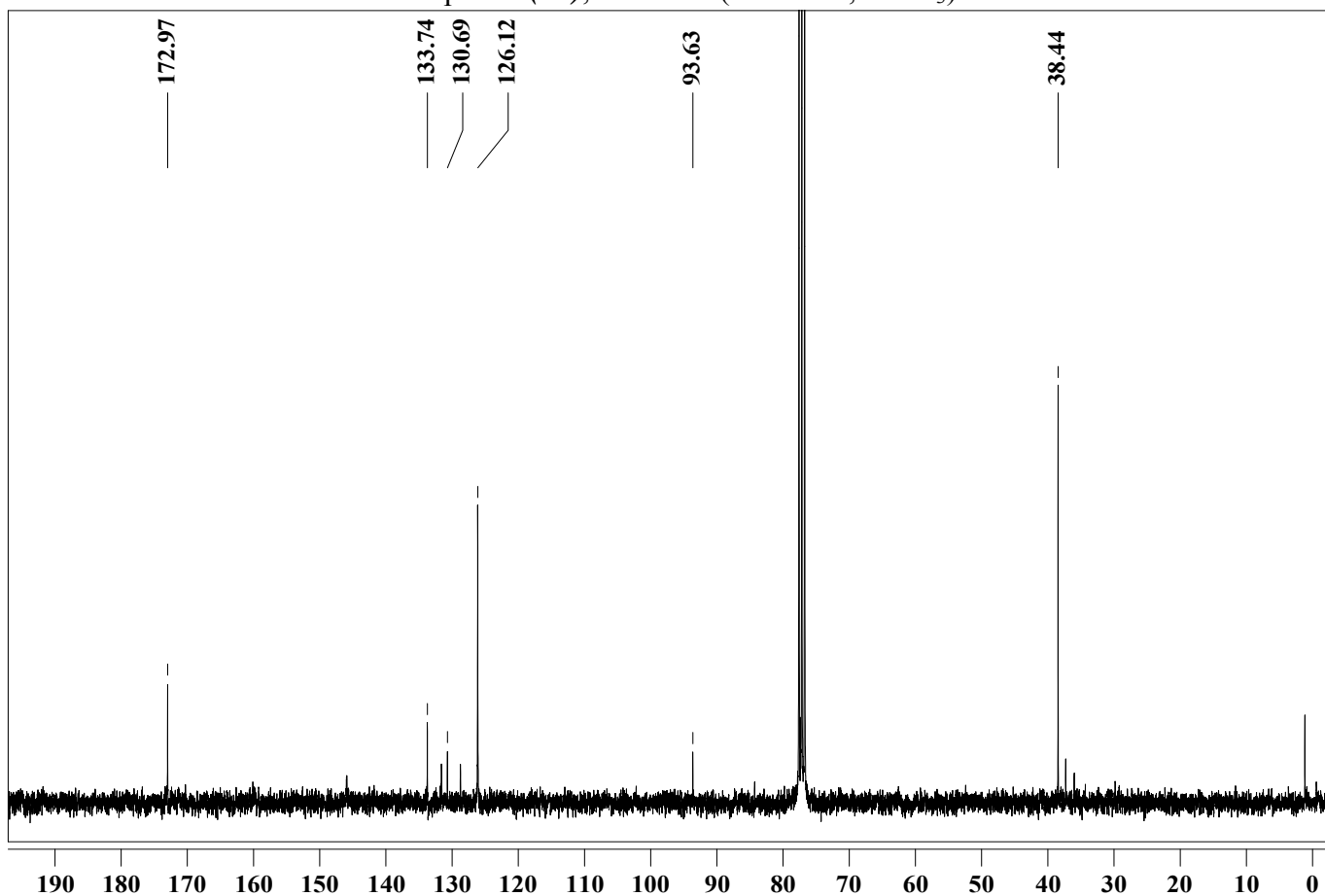




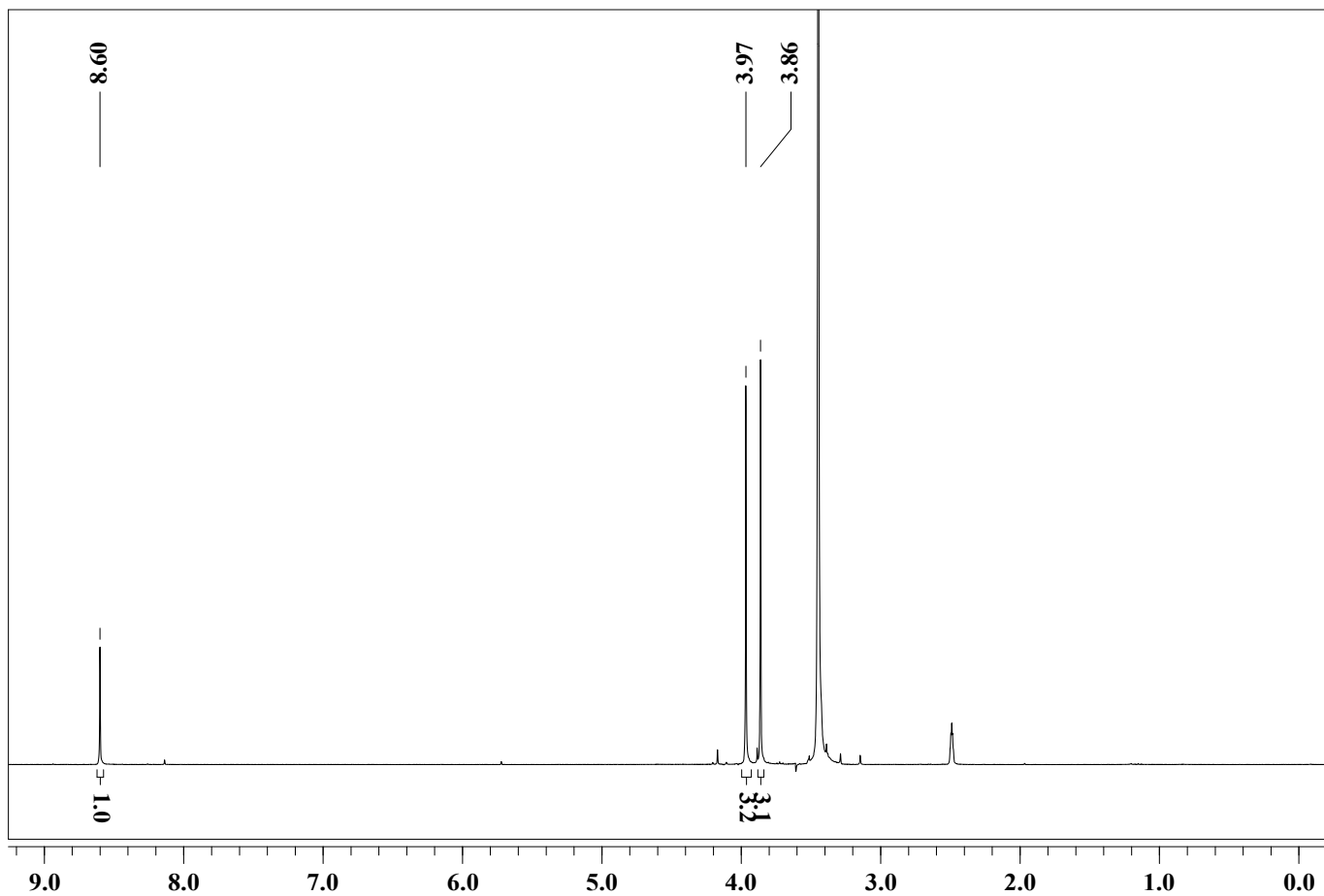




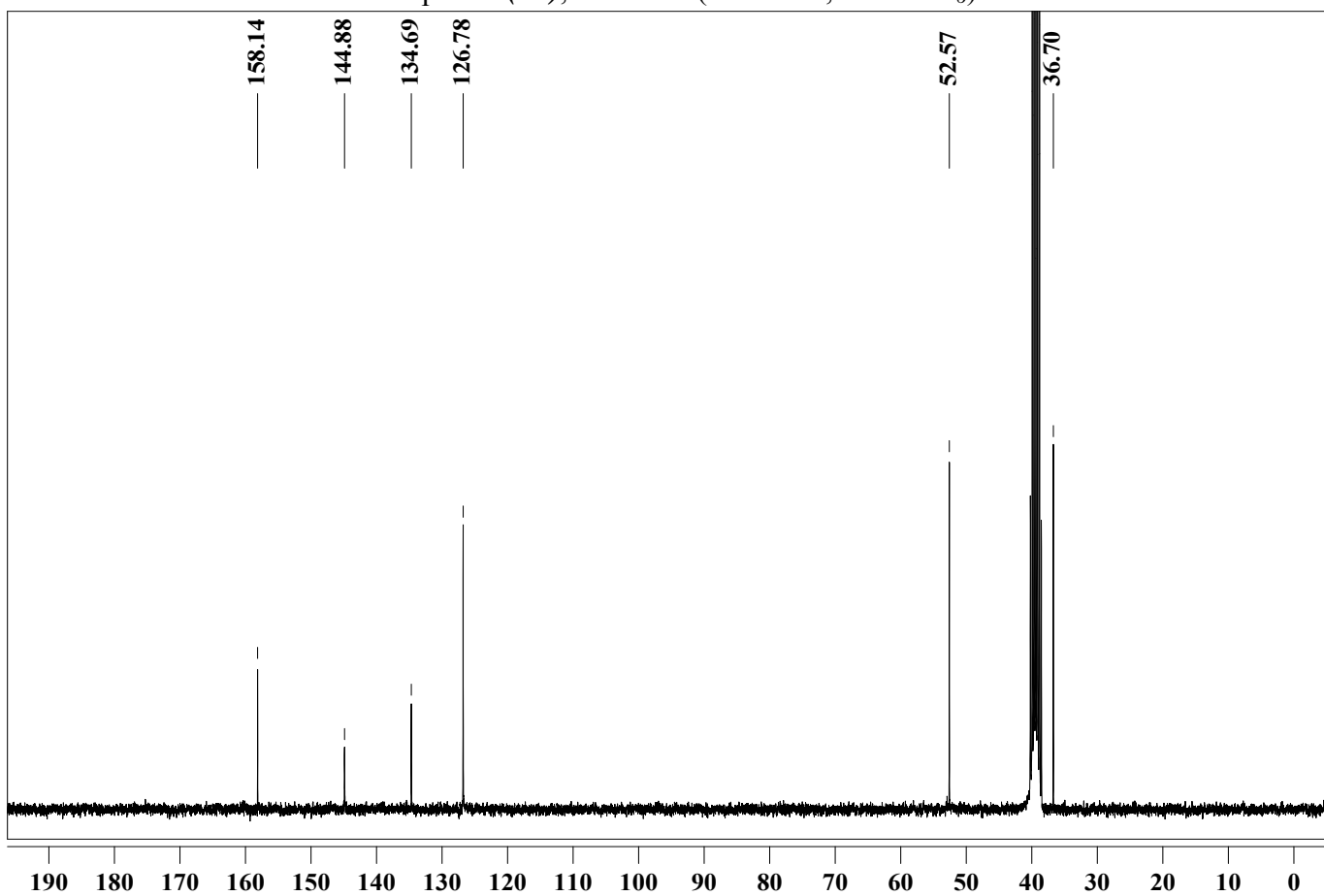
Compound (17), $^1\text{H-NMR}$ (300 MHz, CDCl_3)



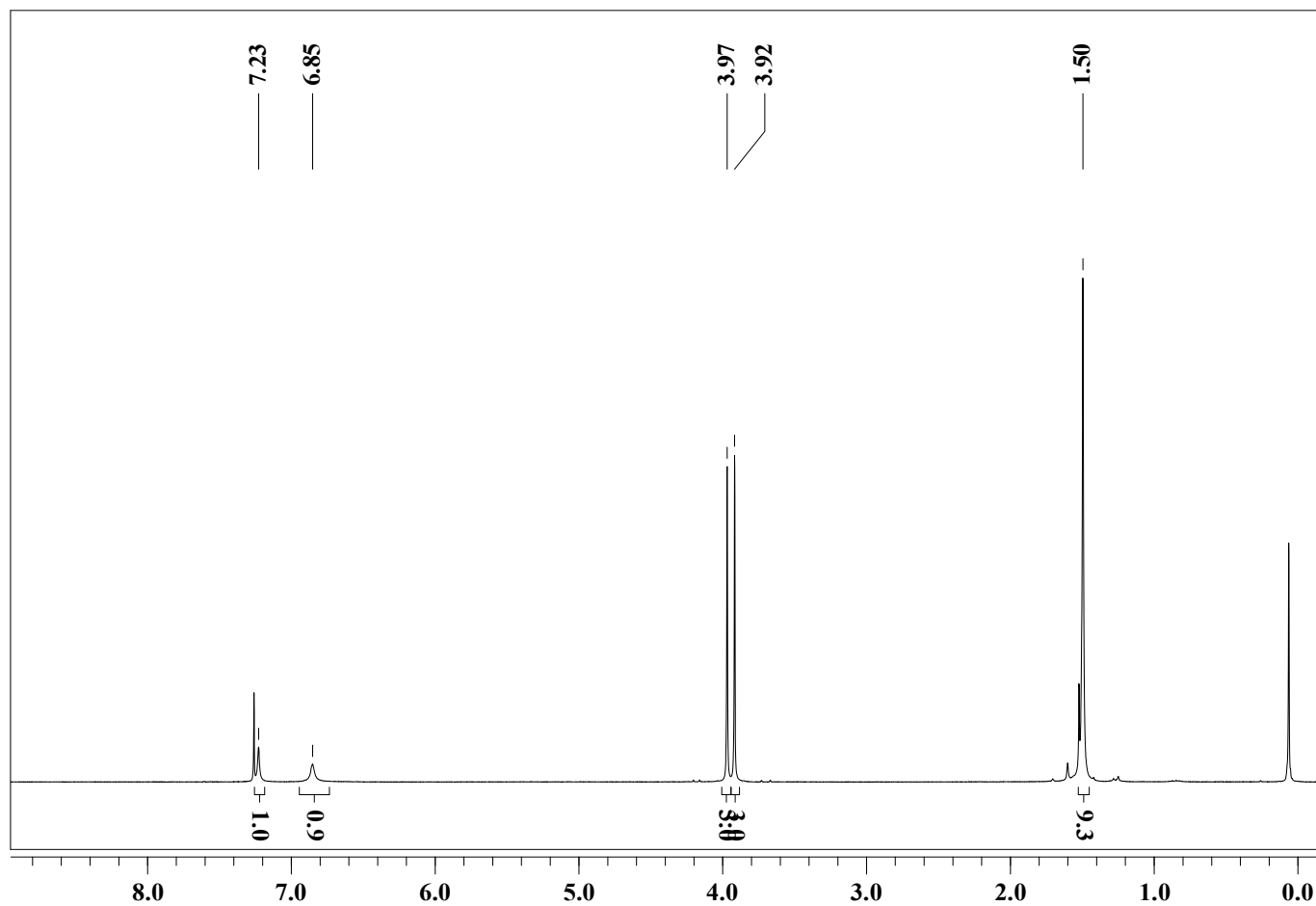
Compound (17), $^{13}\text{C-NMR}$ (75 MHz, CDCl_3)



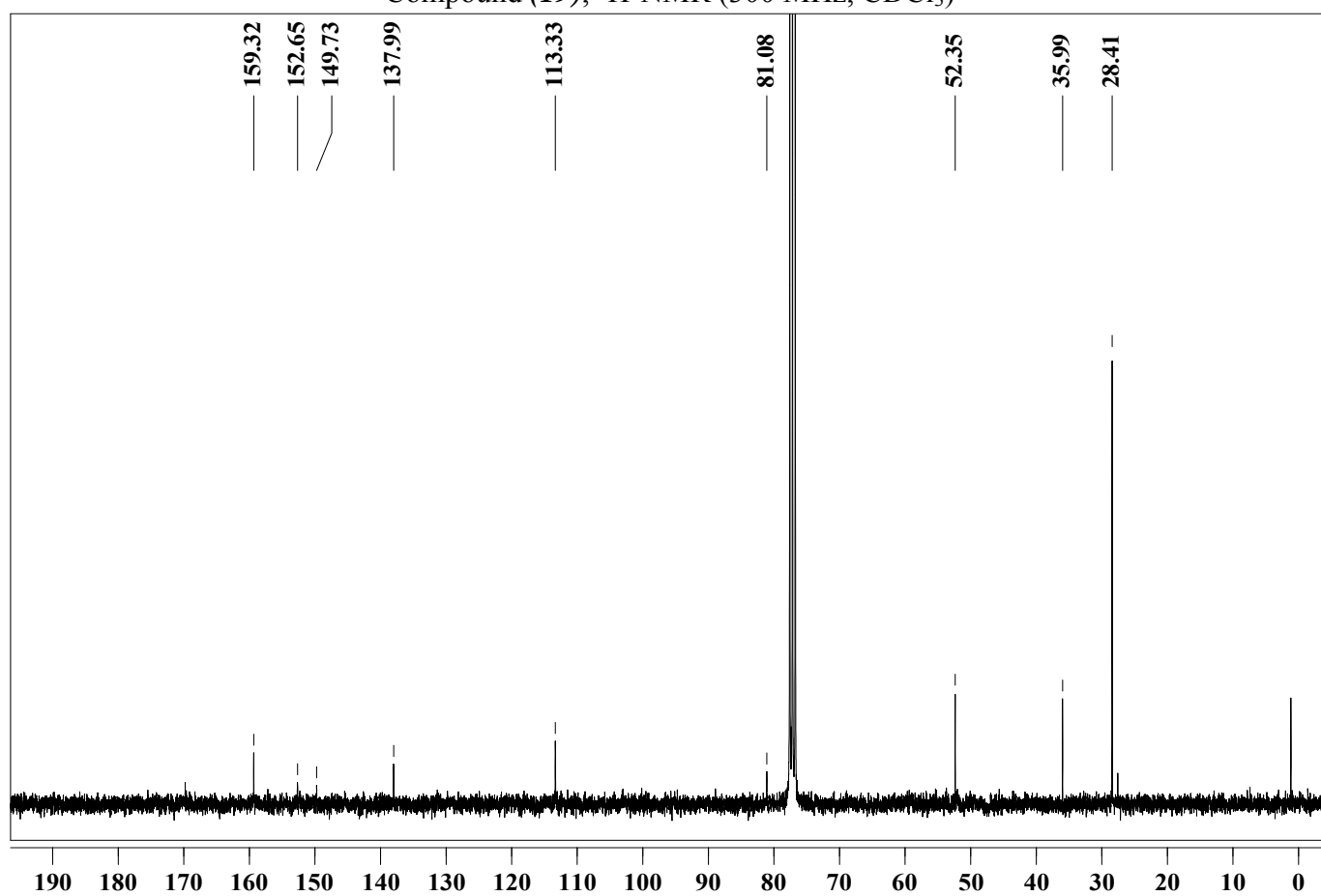
Compound (**18**), $^1\text{H-NMR}$ (300 MHz, $\text{DMSO-}d_6$)



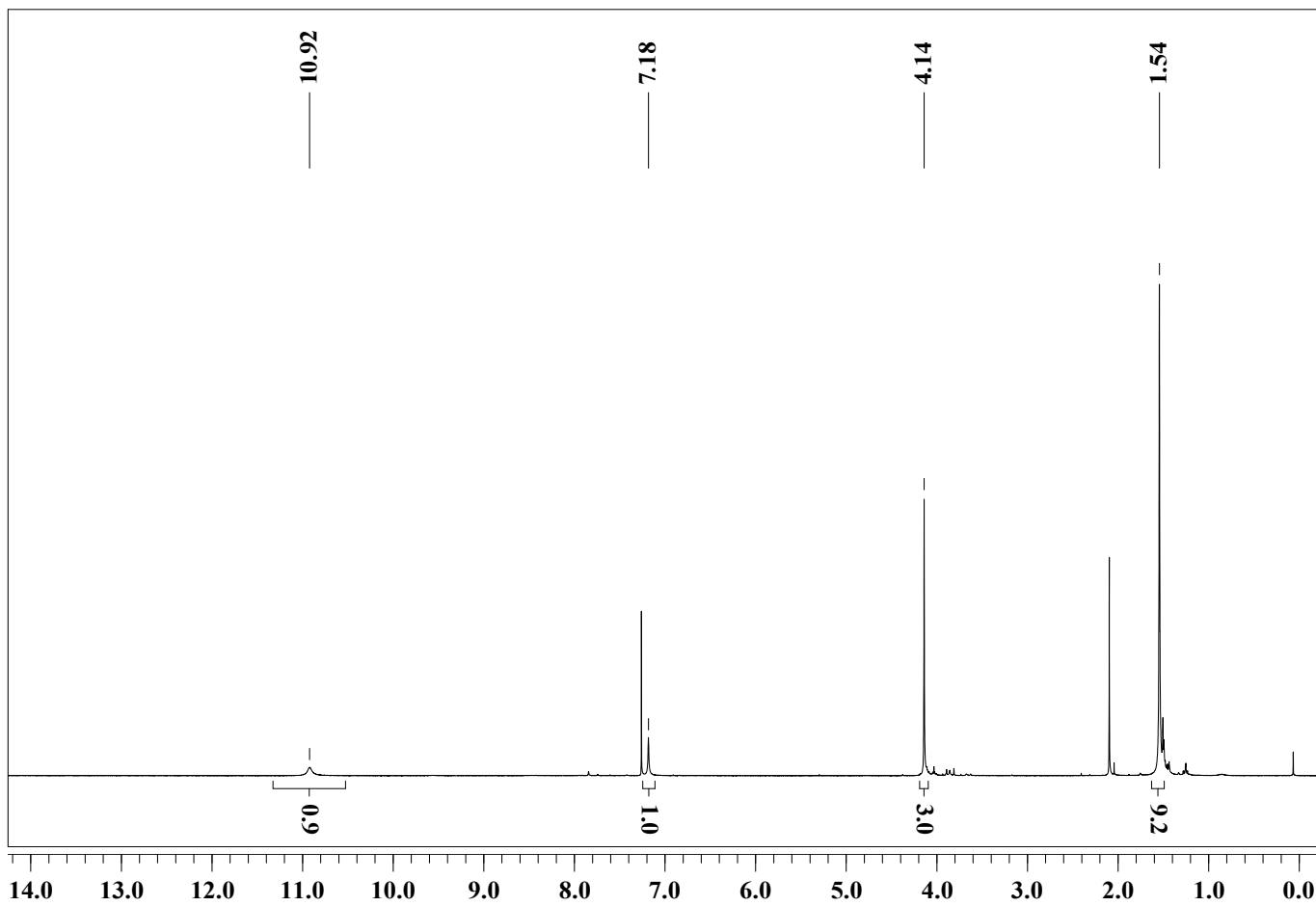
Compound (**18**), $^{13}\text{C-NMR}$ (75 MHz, $\text{DMSO-}d_6$)



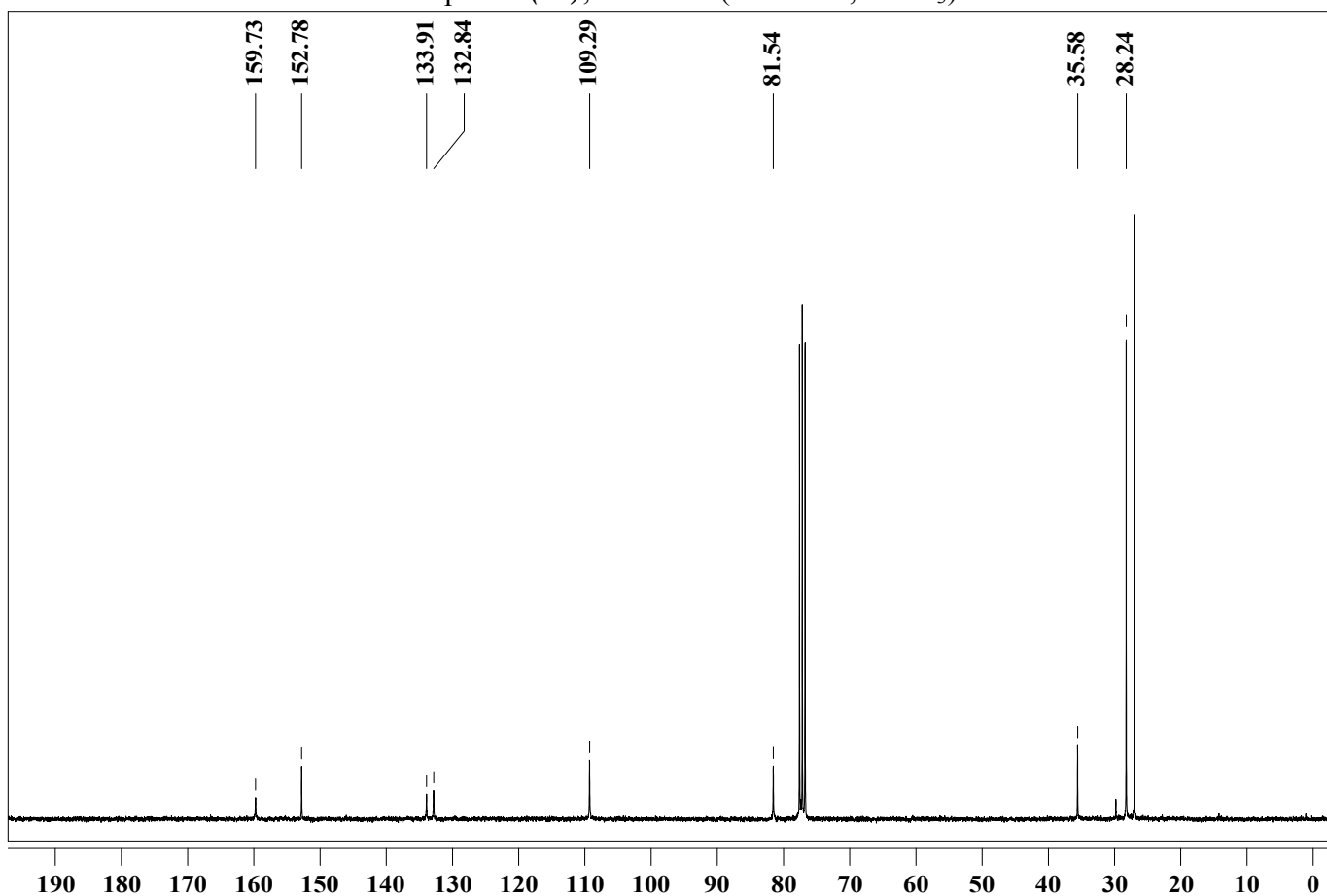
Compound (19), $^1\text{H-NMR}$ (300 MHz, CDCl_3)



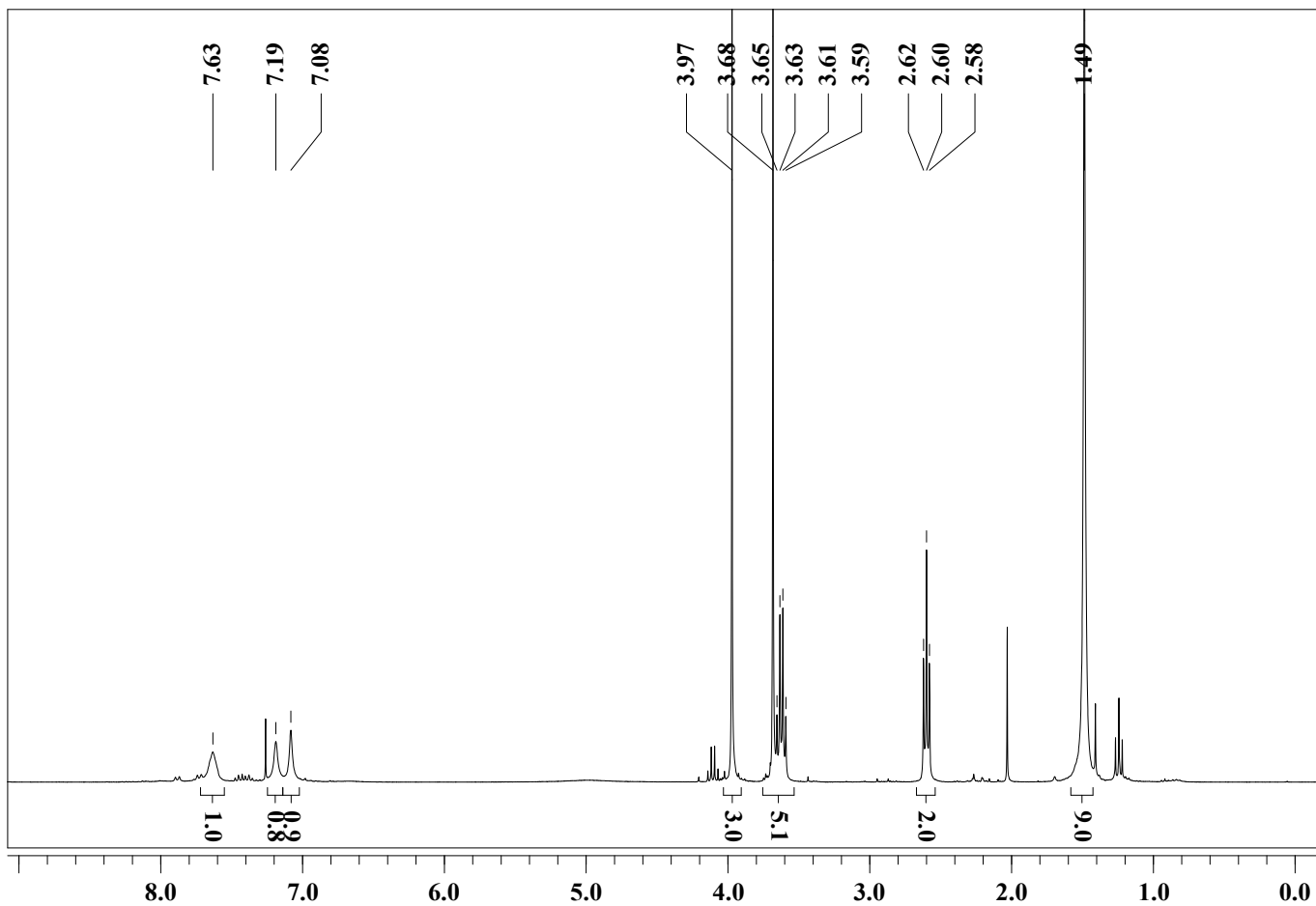
Compound (19), $^{13}\text{C-NMR}$ (75 MHz, CDCl_3)



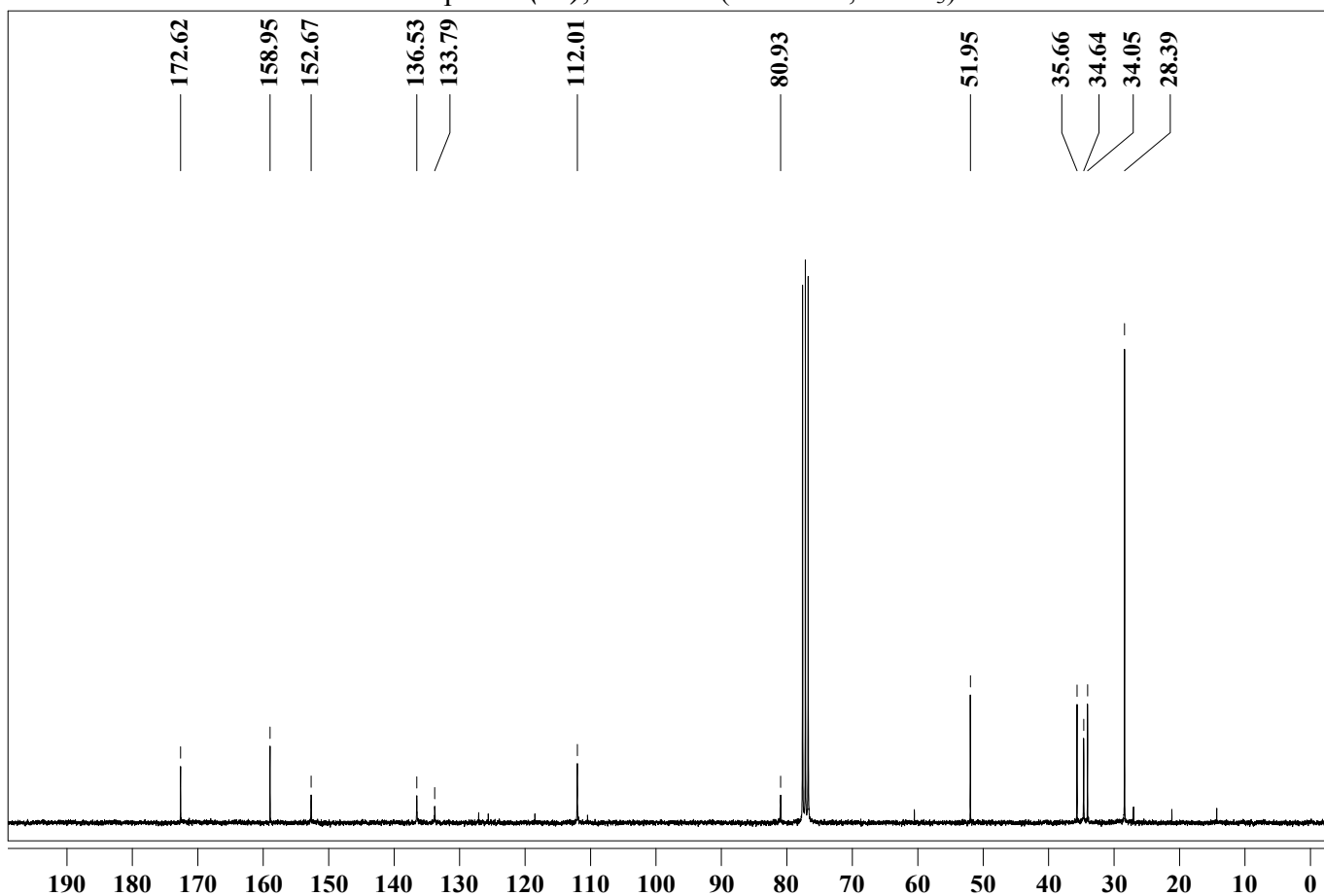
Compound (20), $^1\text{H-NMR}$ (300 MHz, CDCl_3)



Compound (20), $^{13}\text{C-NMR}$ (75 MHz, CDCl_3)



Compound (21), ¹H-NMR (300 MHz, CDCl₃)

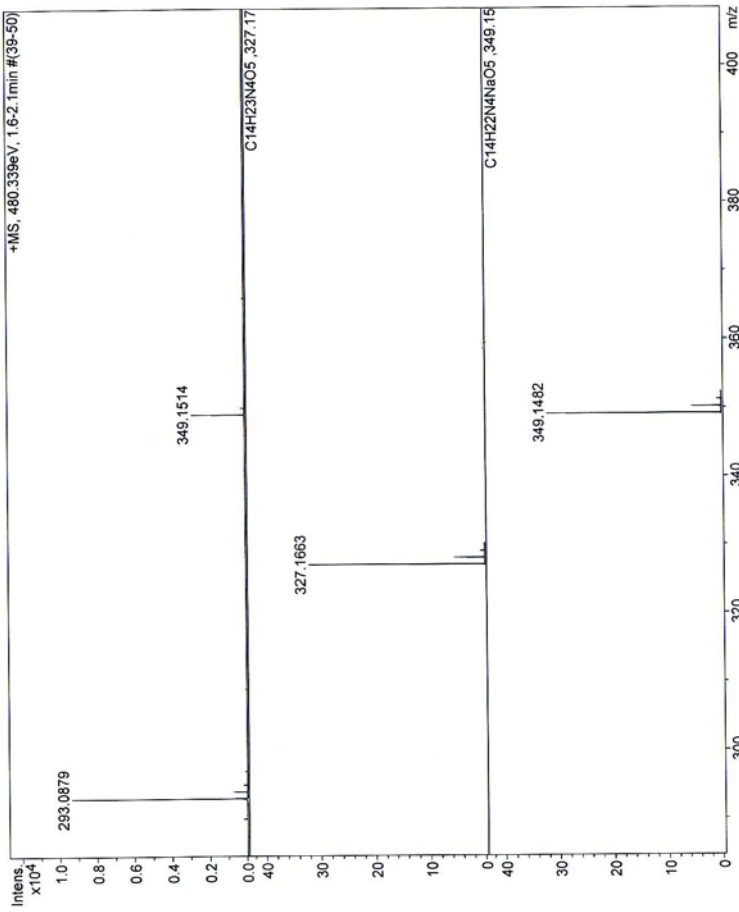
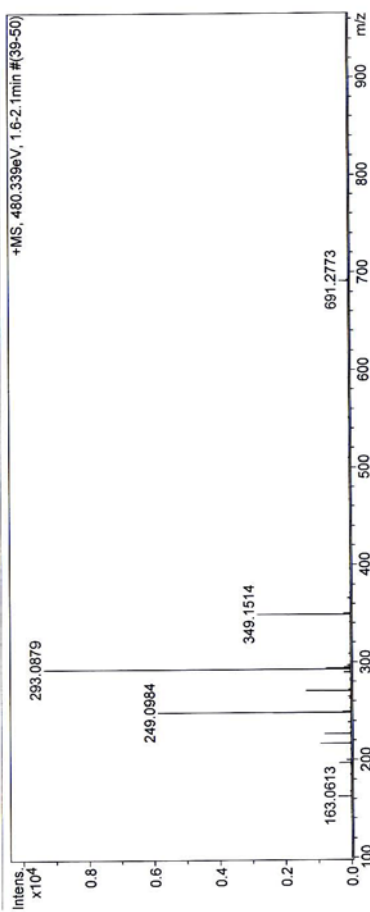


Compound (21), ¹³C-NMR (75 MHz, CDCl₃)

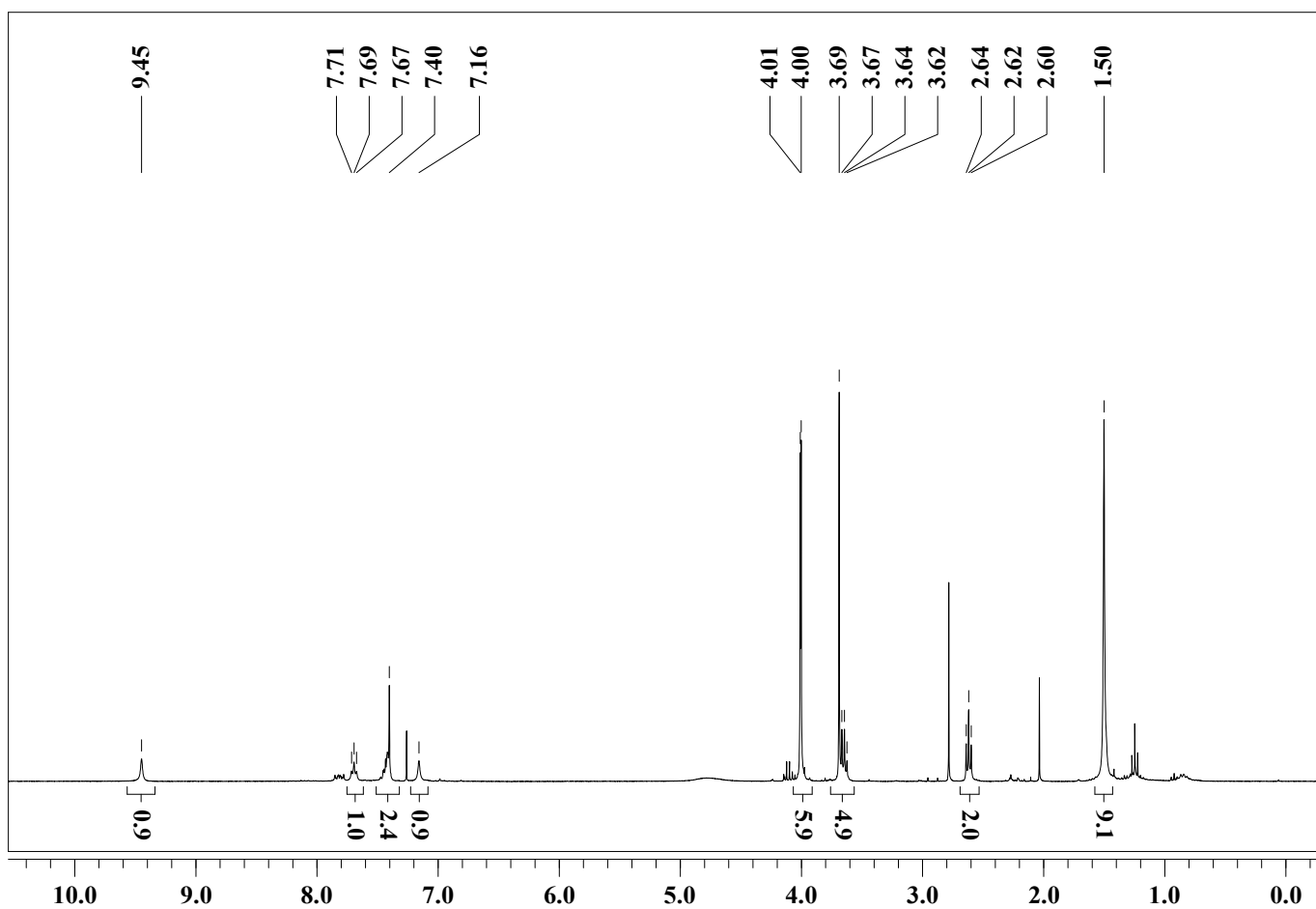
MS-Analyse: ESI-TOF

Analysis Name: E:\MS-Daten\HuWenbin\090505-L1-090504-pos_01_14151.d\090505-L1-090504-pos_01_14151.ser
Method: methodname
Acquisition Date: 5/5/2009 1:22:46 PM
Operator: Karow
Instrument: Bruker BioTOF III

Comment: comment



Compound (21), MS (ESI-TOF, pos. CH₂Cl₂)

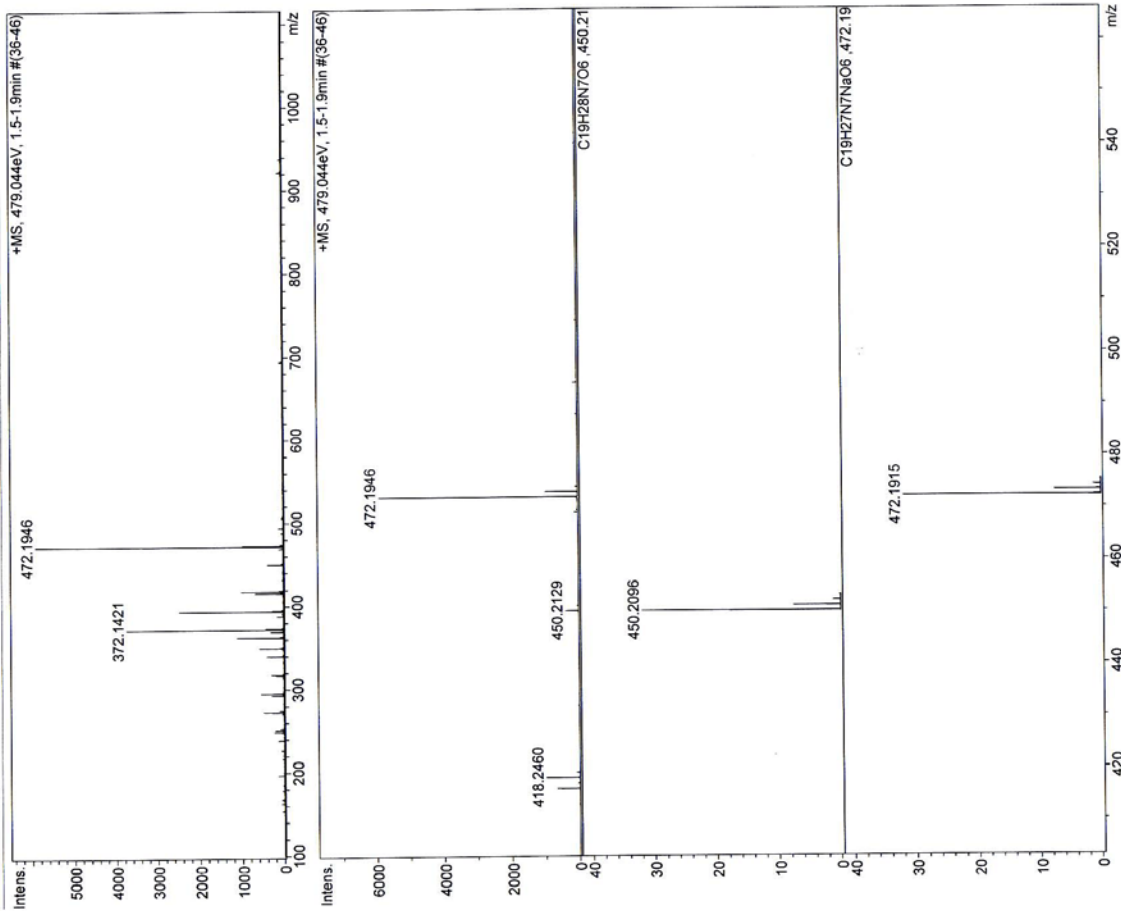


Compound (22), ¹H-NMR (300 MHz, CDCl₃)

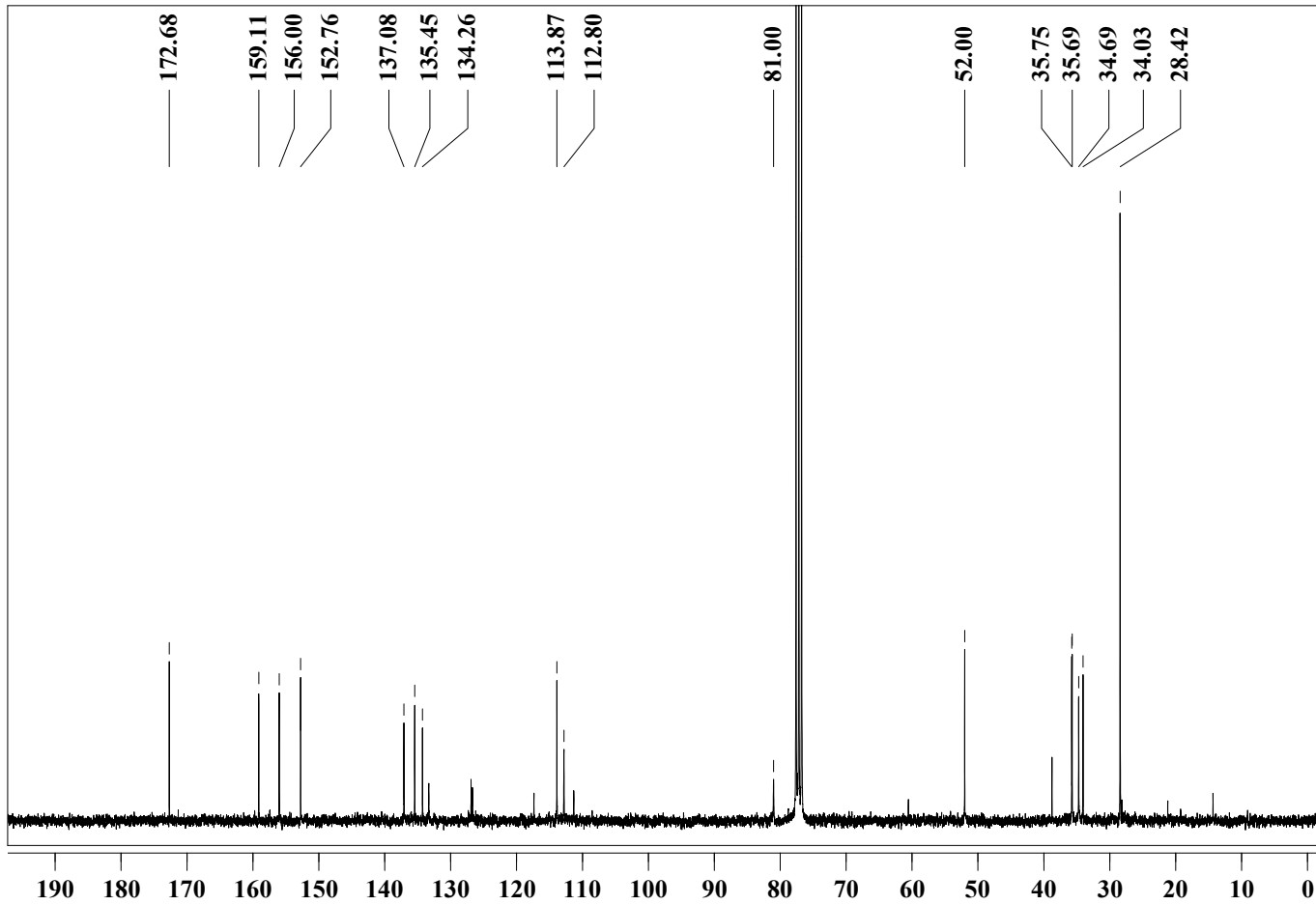
MS-Analyse: ESI-TOF

Analysis Name: E:\MS-Daten\HuWenbin\090917-M1-090917-pos_01_15837 ser
 Method: methodname
 Acquisition Date: 9/17/2009 12:55:36 PM
 Operator: Karow
 Instrument: Bruker BioTOF III

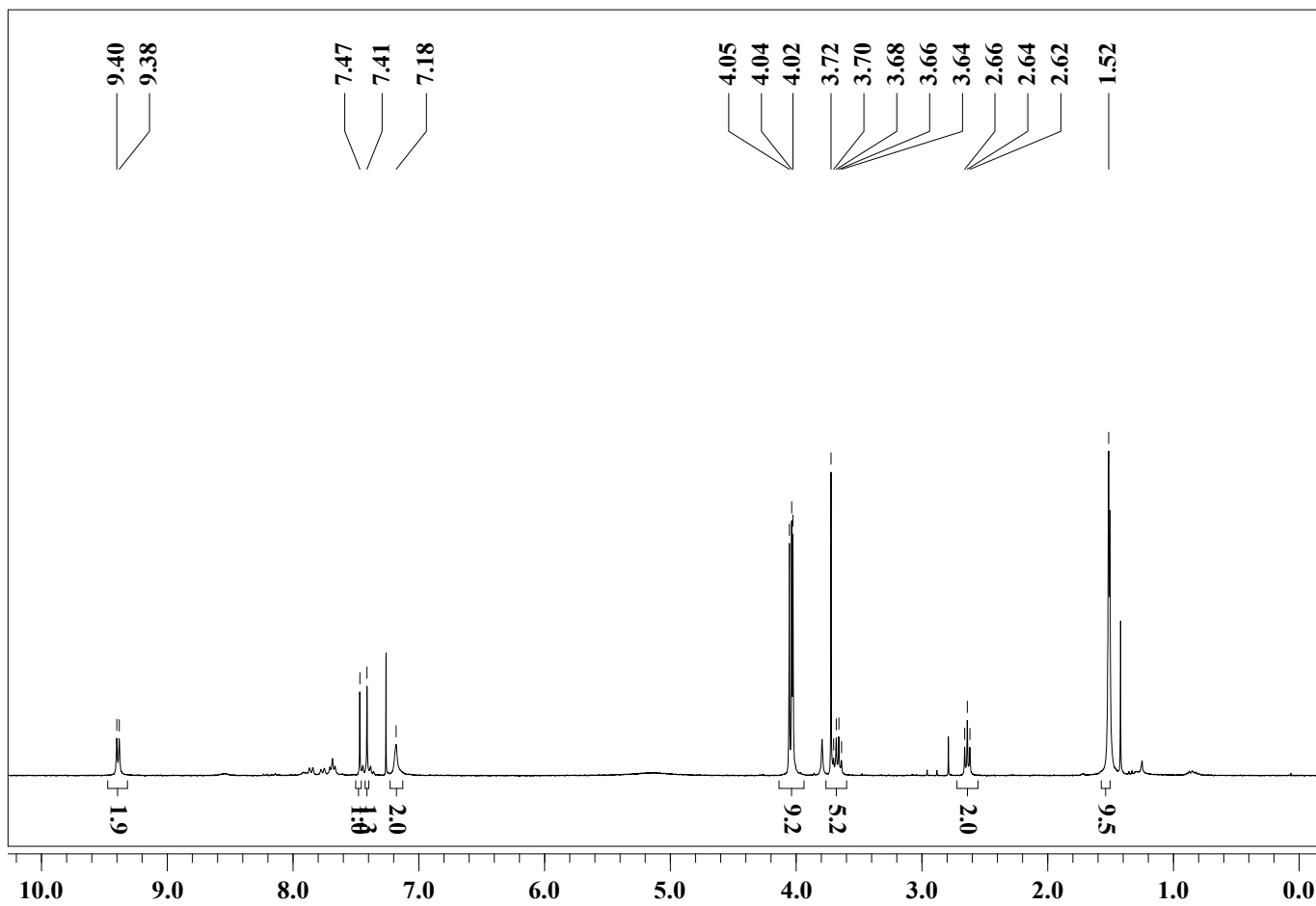
Comment:



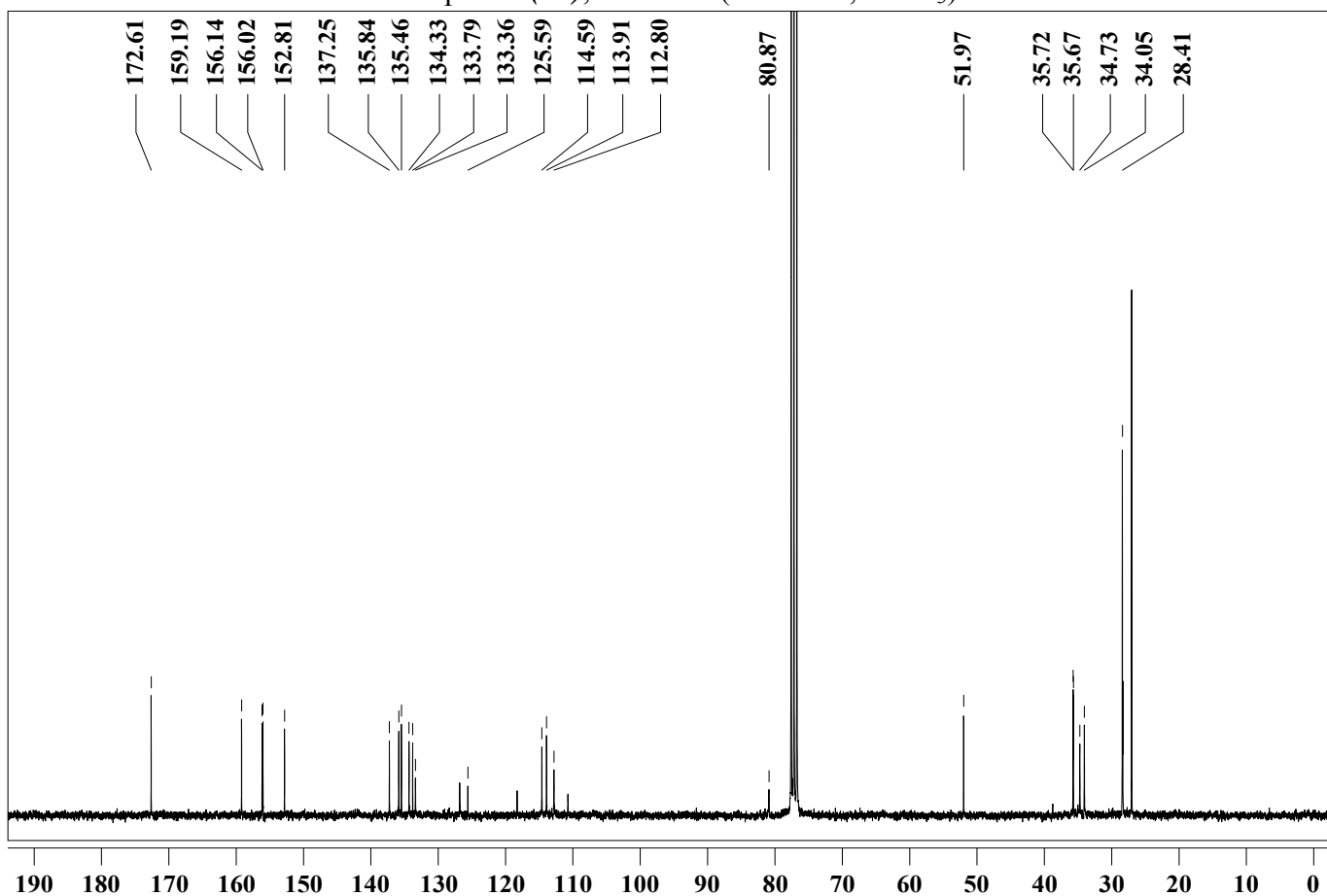
Compound (22), MS (ESI-TOF, pos. CH₂Cl₂)



Compound (22), ¹³C-NMR (75 MHz, CDCl₃)



Compound (23), $^1\text{H-NMR}$ (300 MHz, CDCl_3)

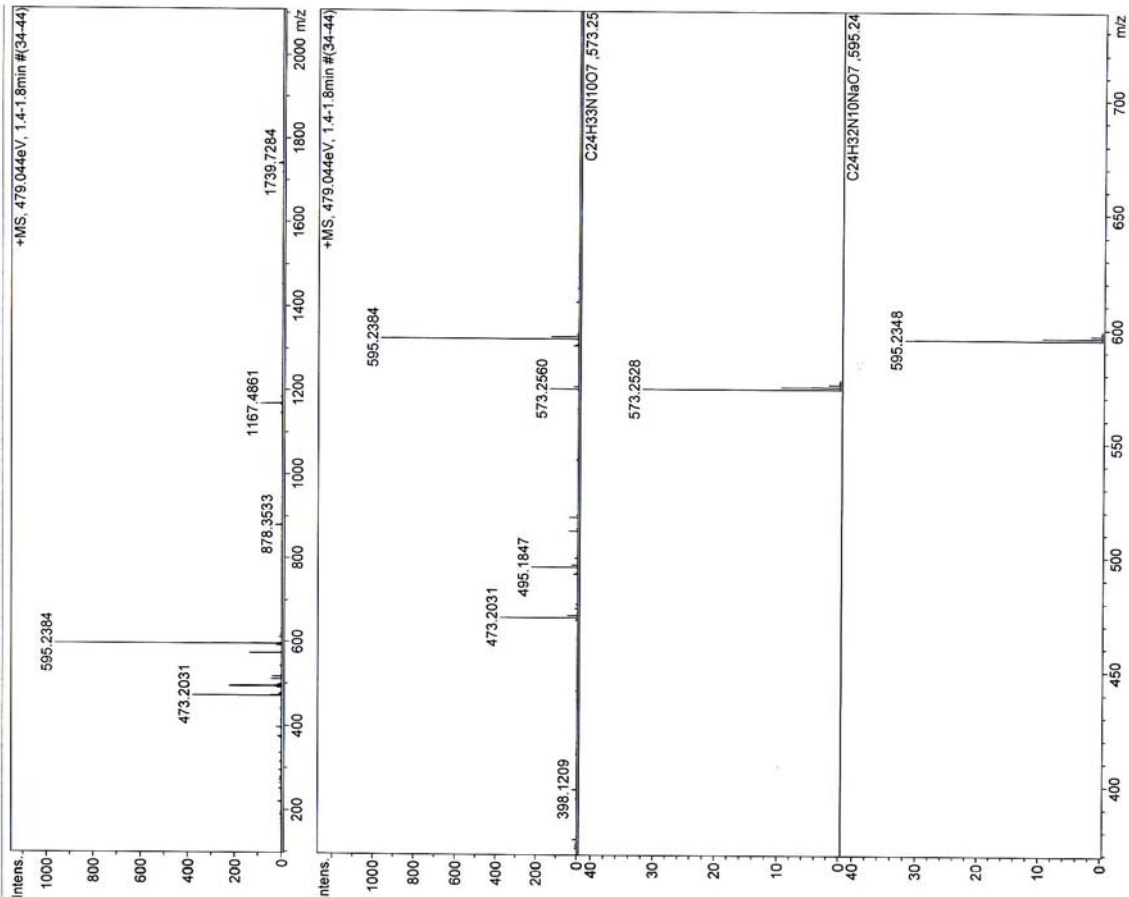


Compound (23), $^{13}\text{C-NMR}$ (75 MHz, CDCl_3)

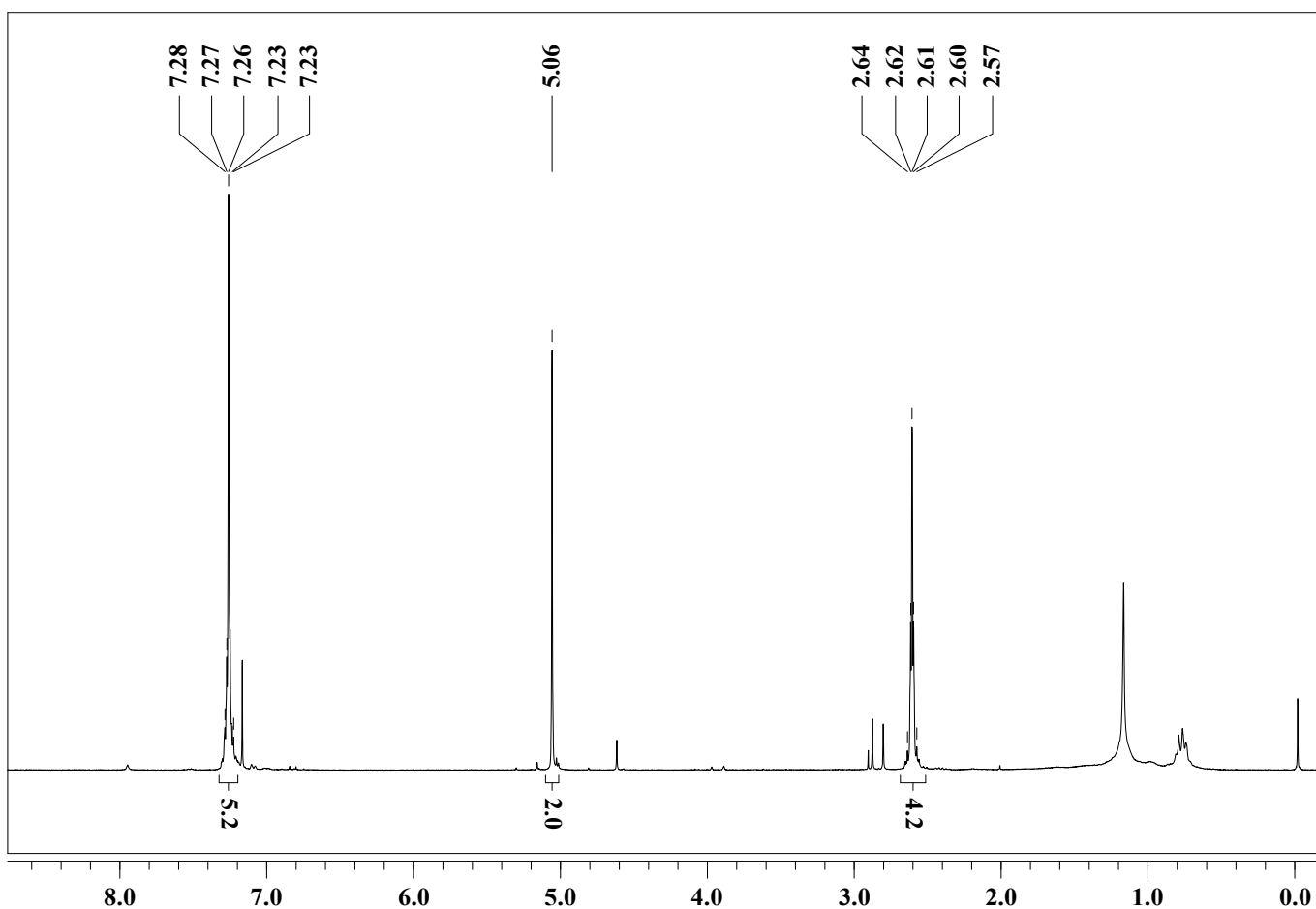
MS-Analyse: ESI-TOF

Analysis Name: E:\MS-Daten\HuWenbin\091007-N1-091007-pos_01_16017_d1091007-N1-091007-pos_01_16017.ser
 Method: methodname Operator: Karow
 Acquisition Date: 10/7/2009 11:39:37 AM Instrument: Bruker BioTOF III

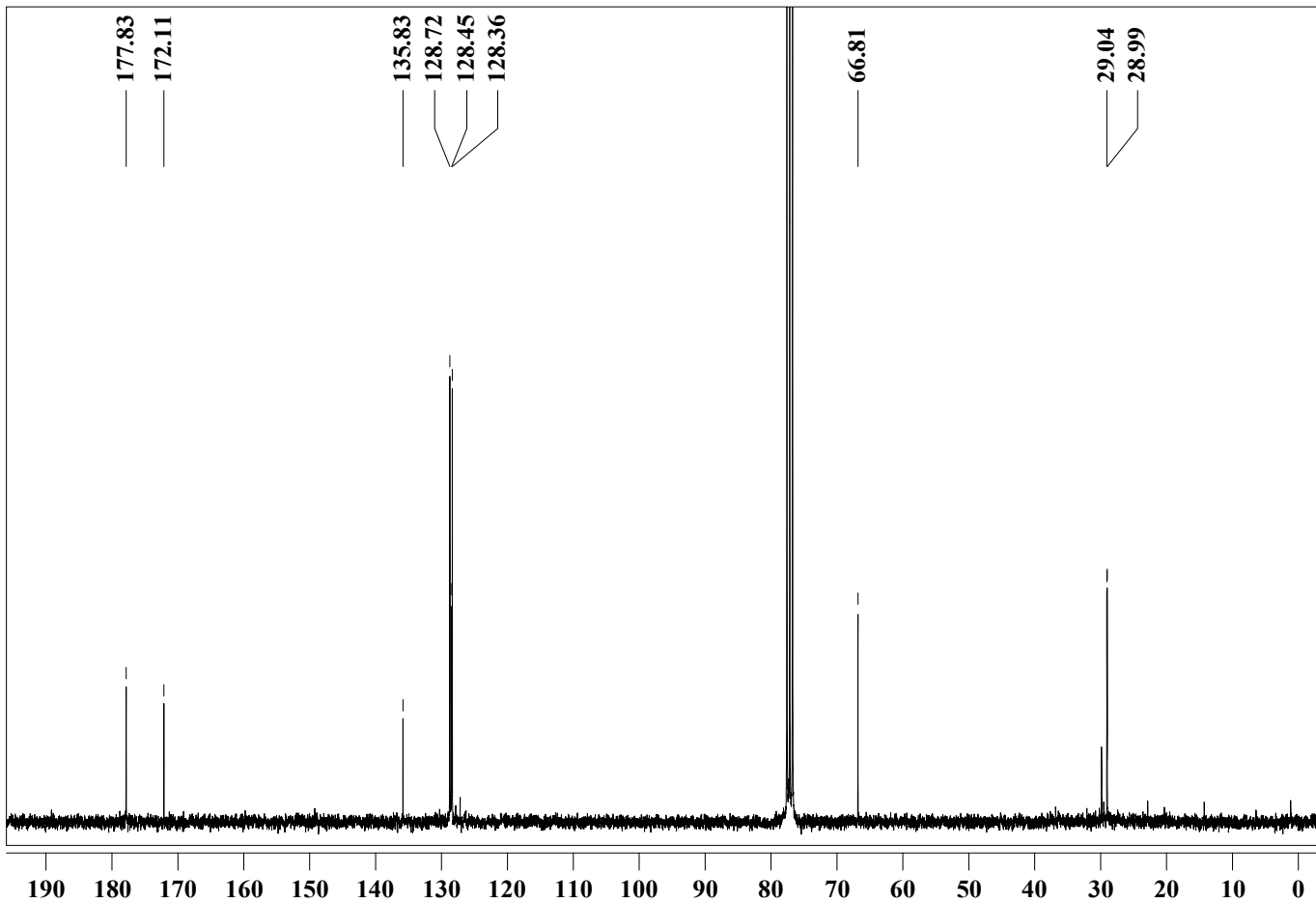
Comment: comment



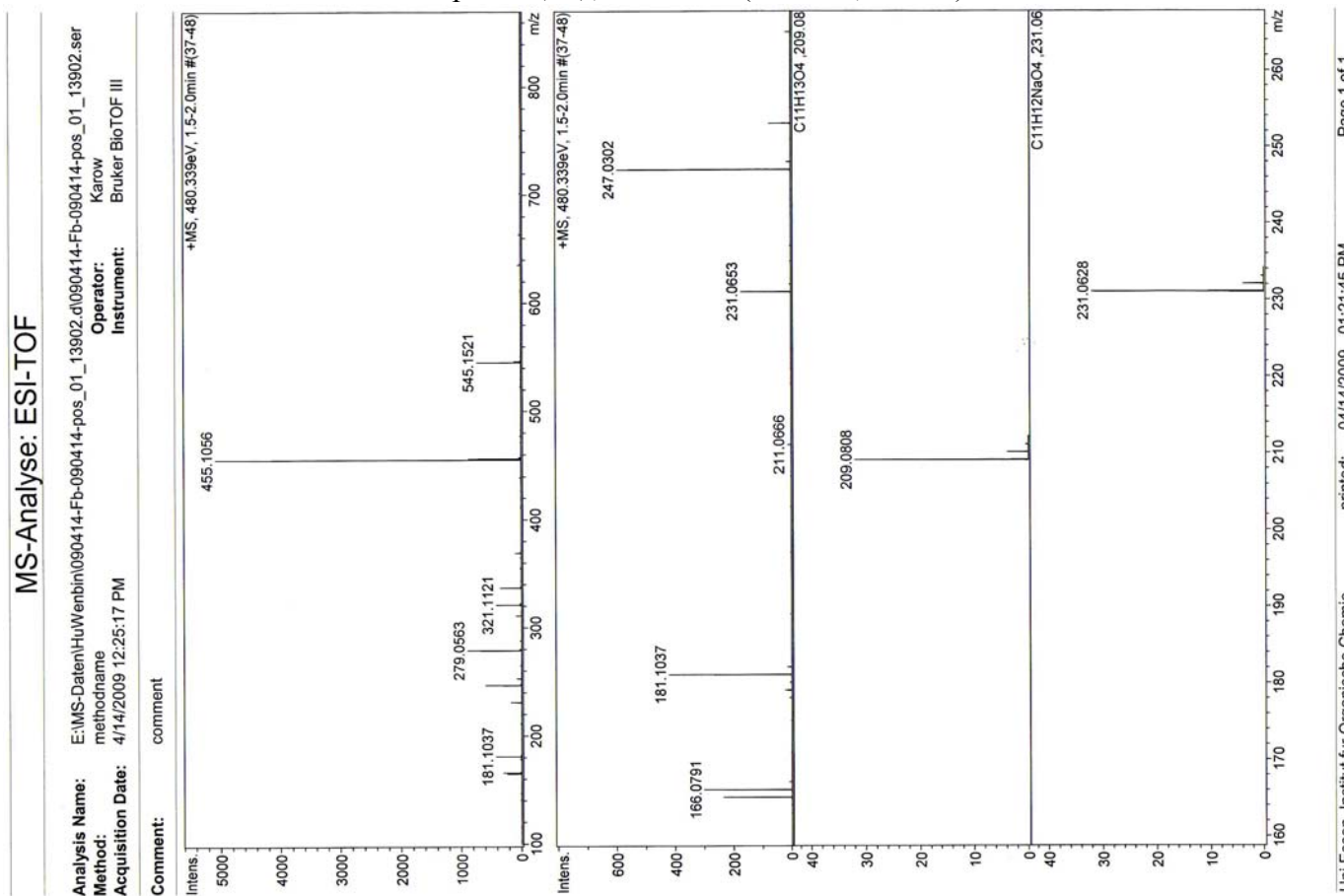
Compound (23), MS (ESI-TOF, pos. CH₂Cl₂)



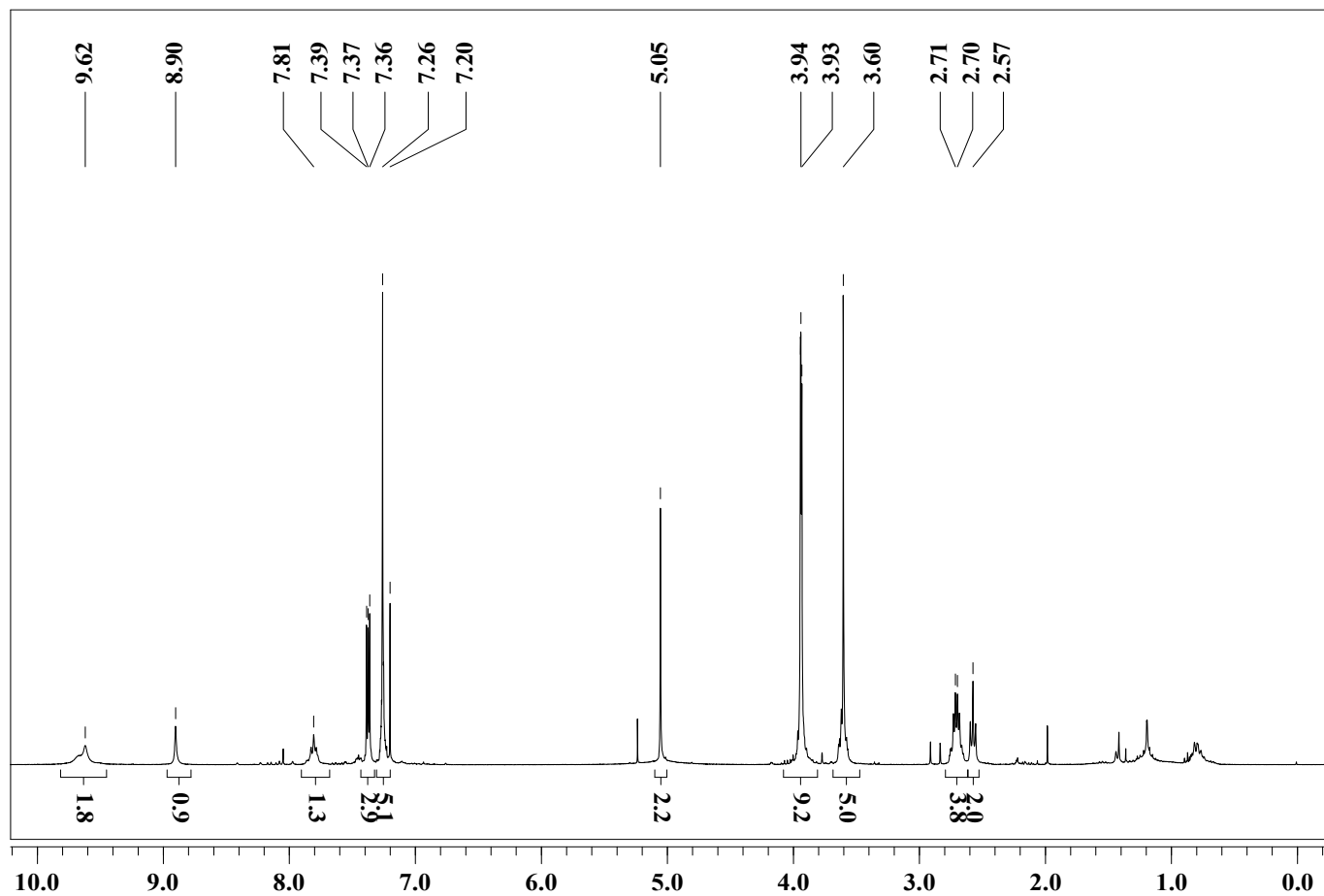
Compound (24), ¹H-NMR (300 MHz, CDCl₃)



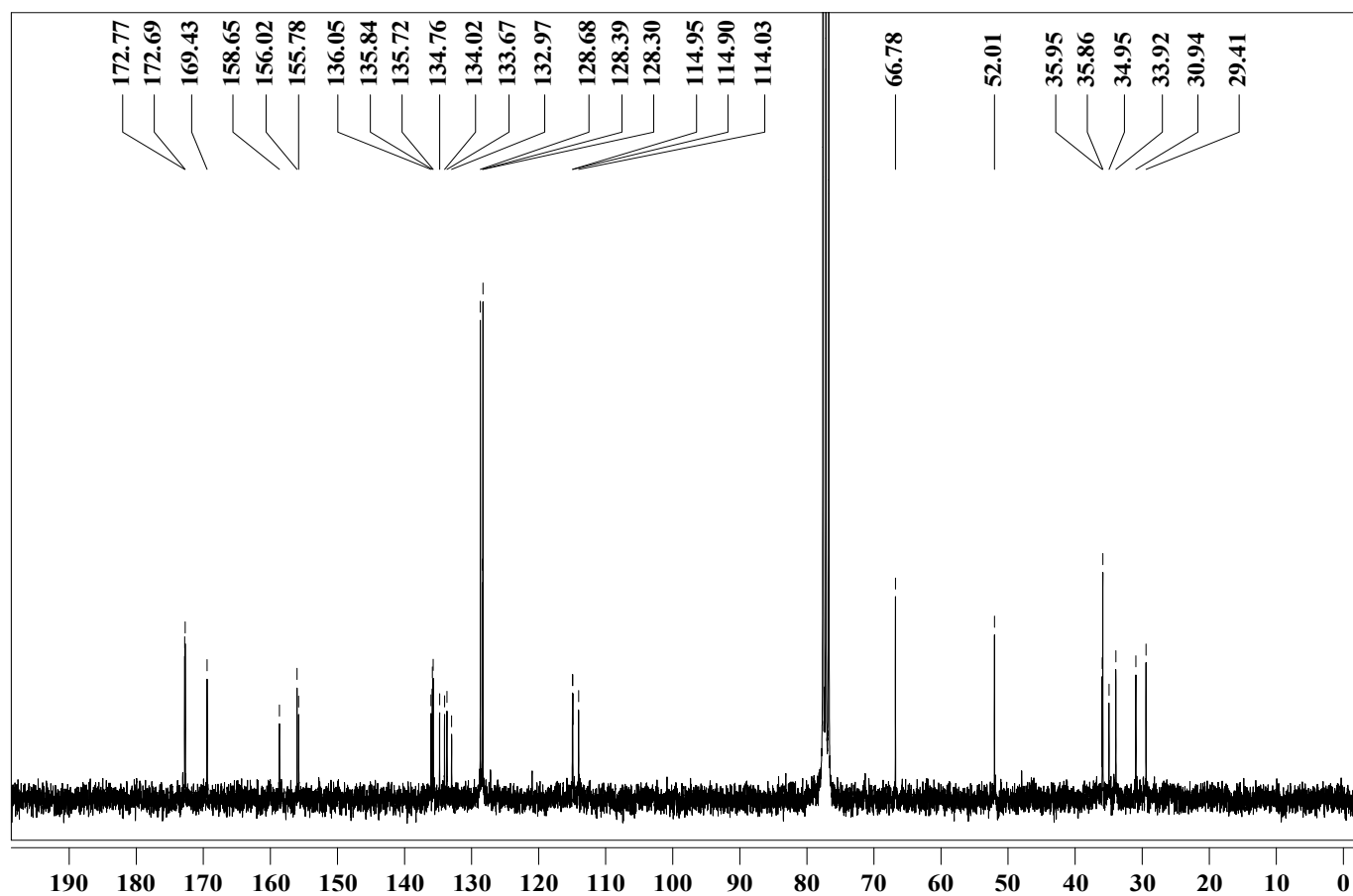
Compound (24), ^{13}C -NMR (75 MHz, CDCl_3)



Compound (24), MS (ESI-TOF, pos. CH_2Cl_2)



Compound (25), $^1\text{H-NMR}$ (300 MHz, CDCl_3)

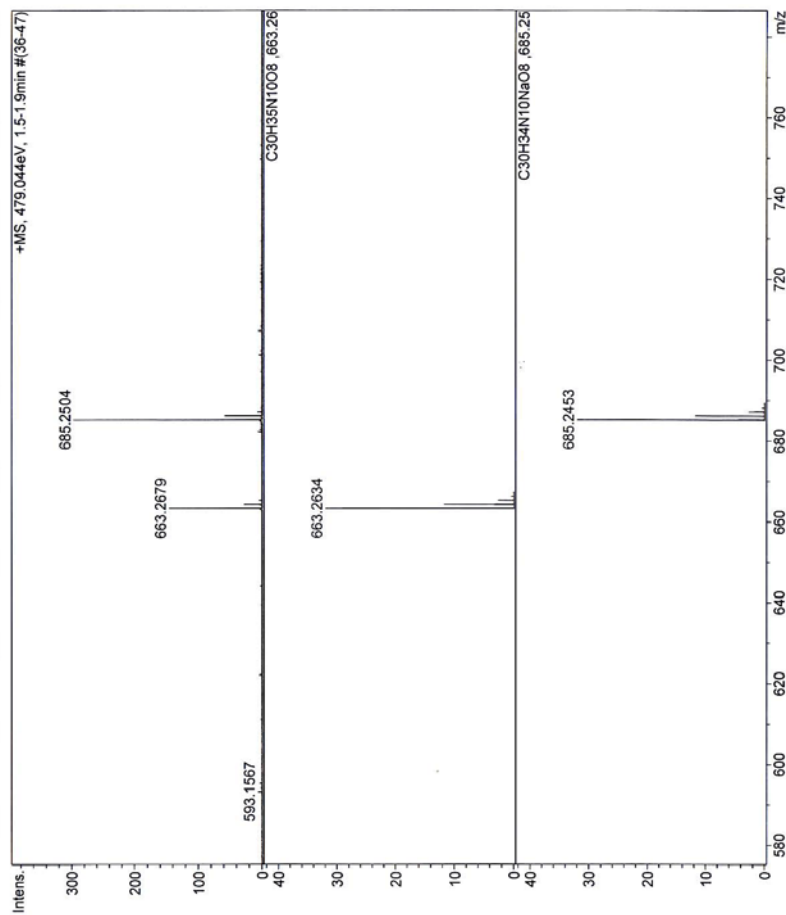
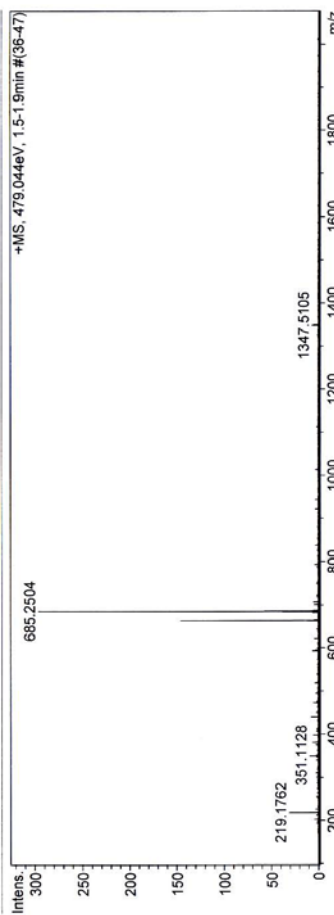


Compound (25), $^{13}\text{C-NMR}$ (75 MHz, CDCl_3)

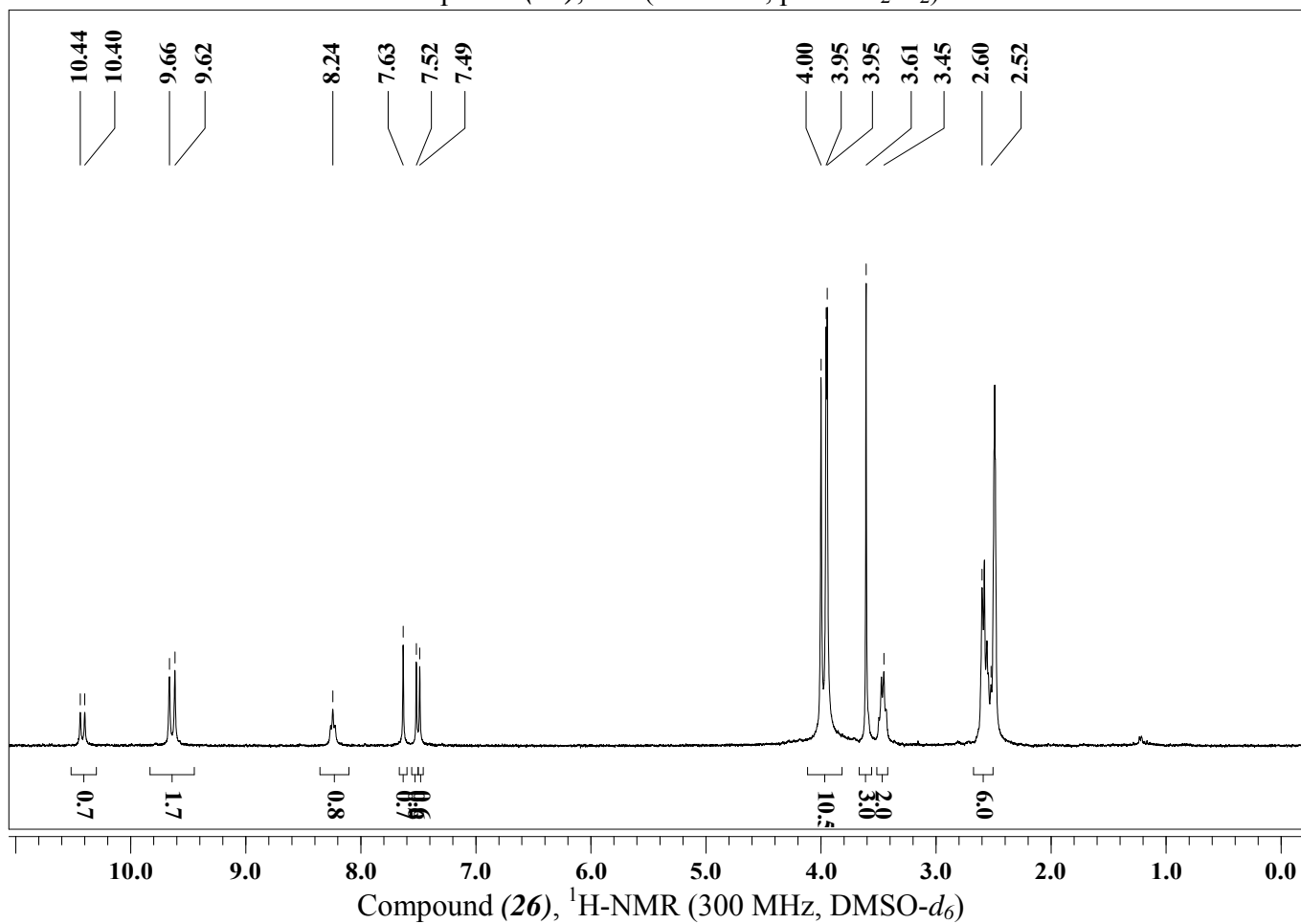
MS-Analyse: ESI-TOF

Analysis Name: E:\MS-Daten\HuWenbin\091012-01-091012-pos_01_16072.d\091012-pos_01_16072.ser
Method: methodname
Operator: Karow
Acquisition Date: 10/12/2009 11:42:09 AM
Instrument: Bruker BioTOF III

Comment: comment



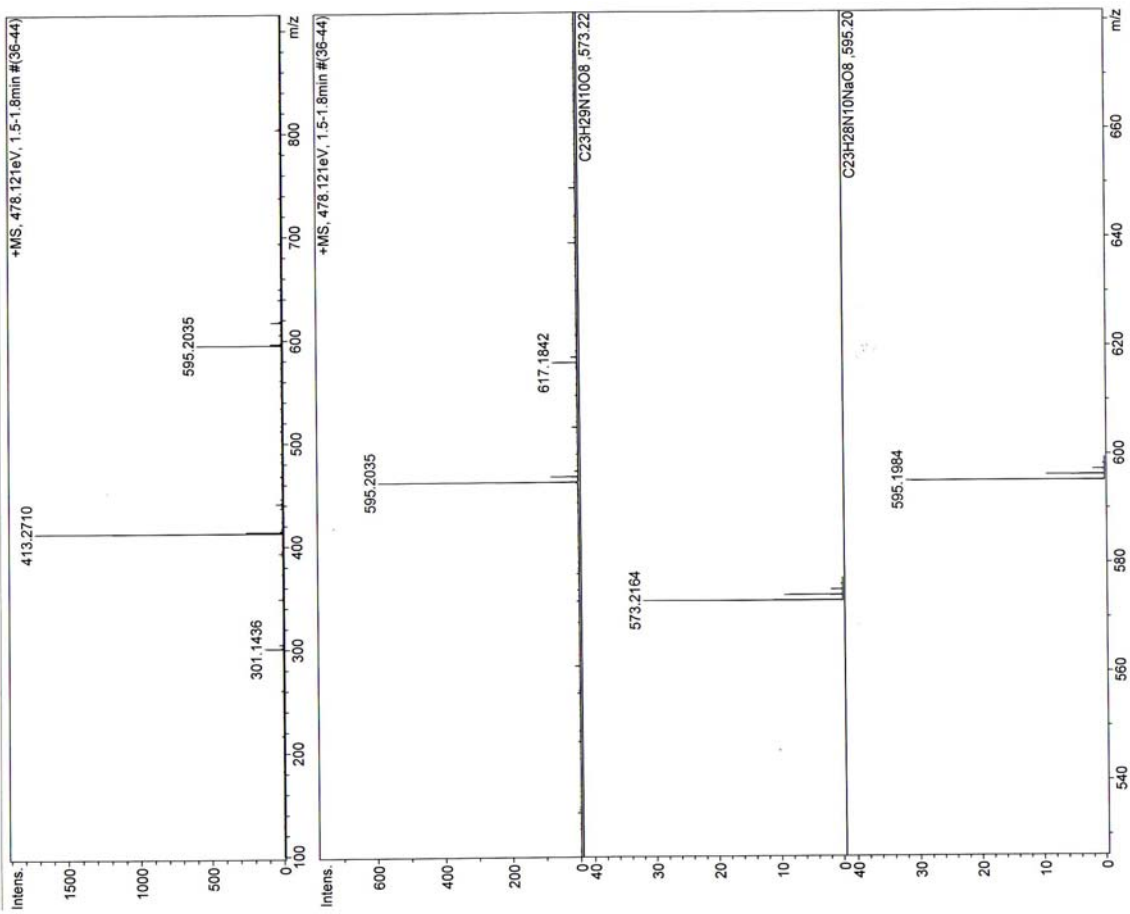
Compound (25), MS (ESI-TOF, pos. CH₂Cl₂)



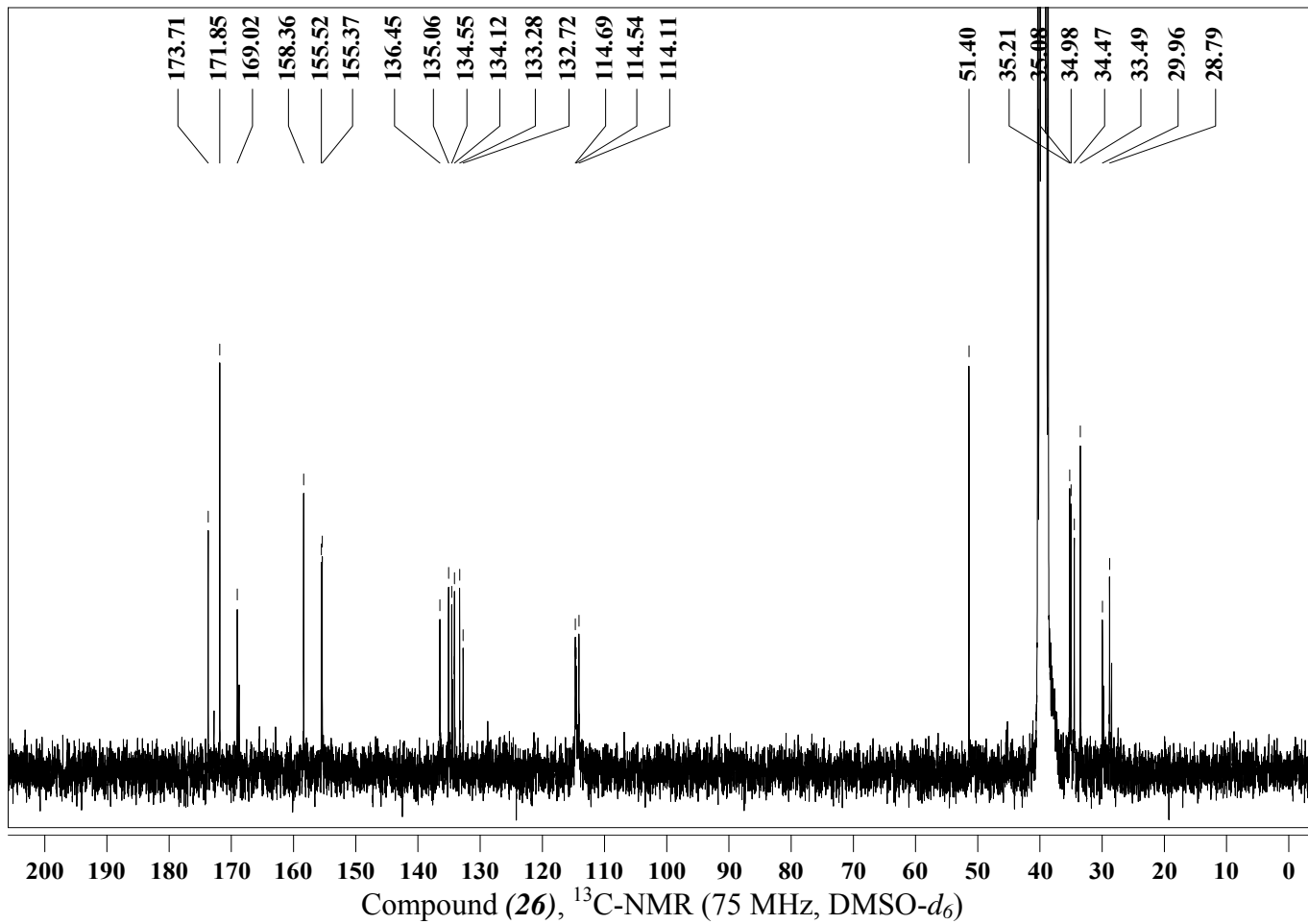
MS-Analyse: ESI-TOF

Analysis Name: E:\MS-Daten\HuWenbin\100615-Q-1-100615-pos_01_19320.se
Method: methodname
Acquisition Date: 6/15/2010 11:13:53 AM
Operator: Karow
Instrument: Bruker BioTOF III

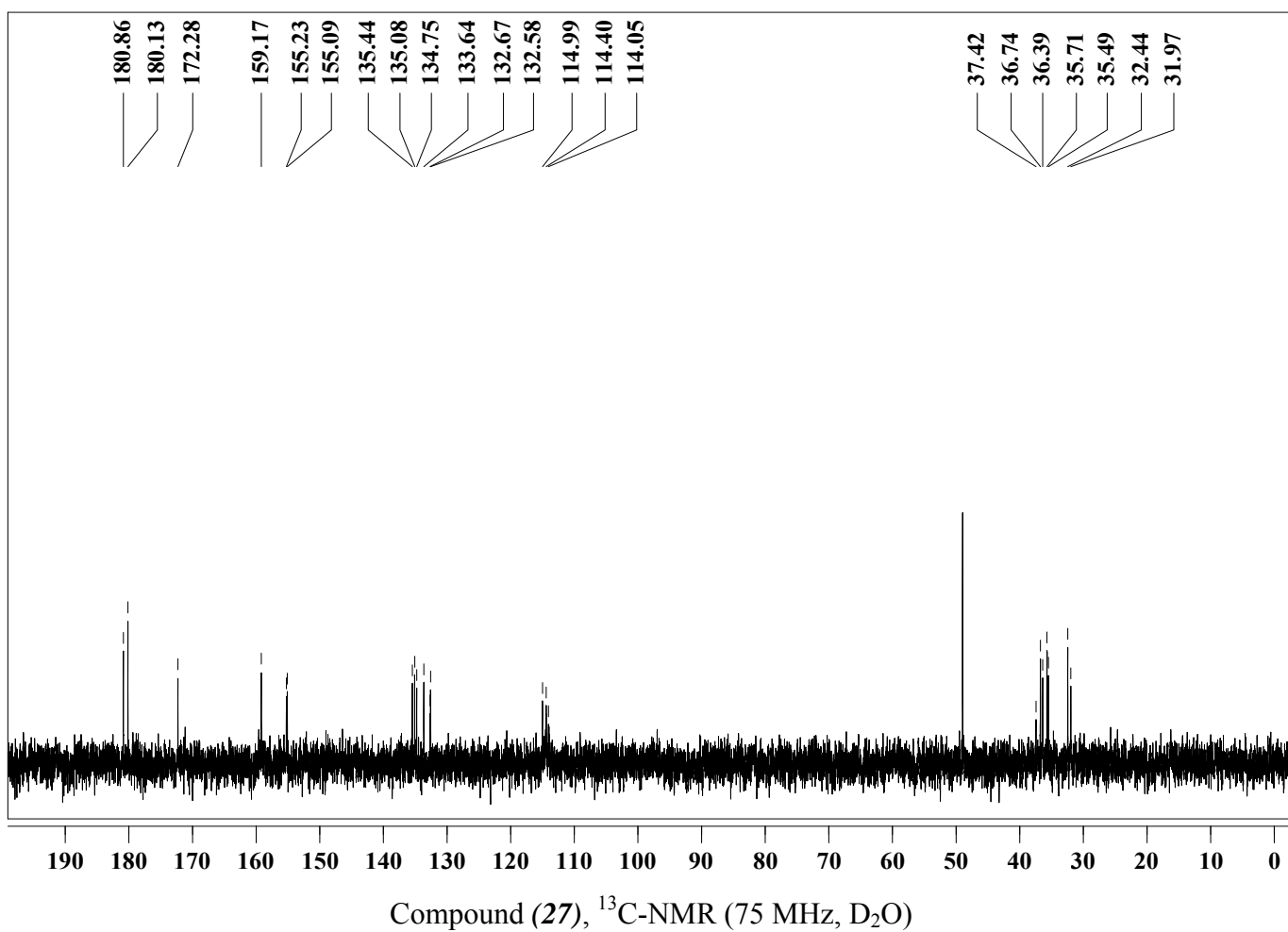
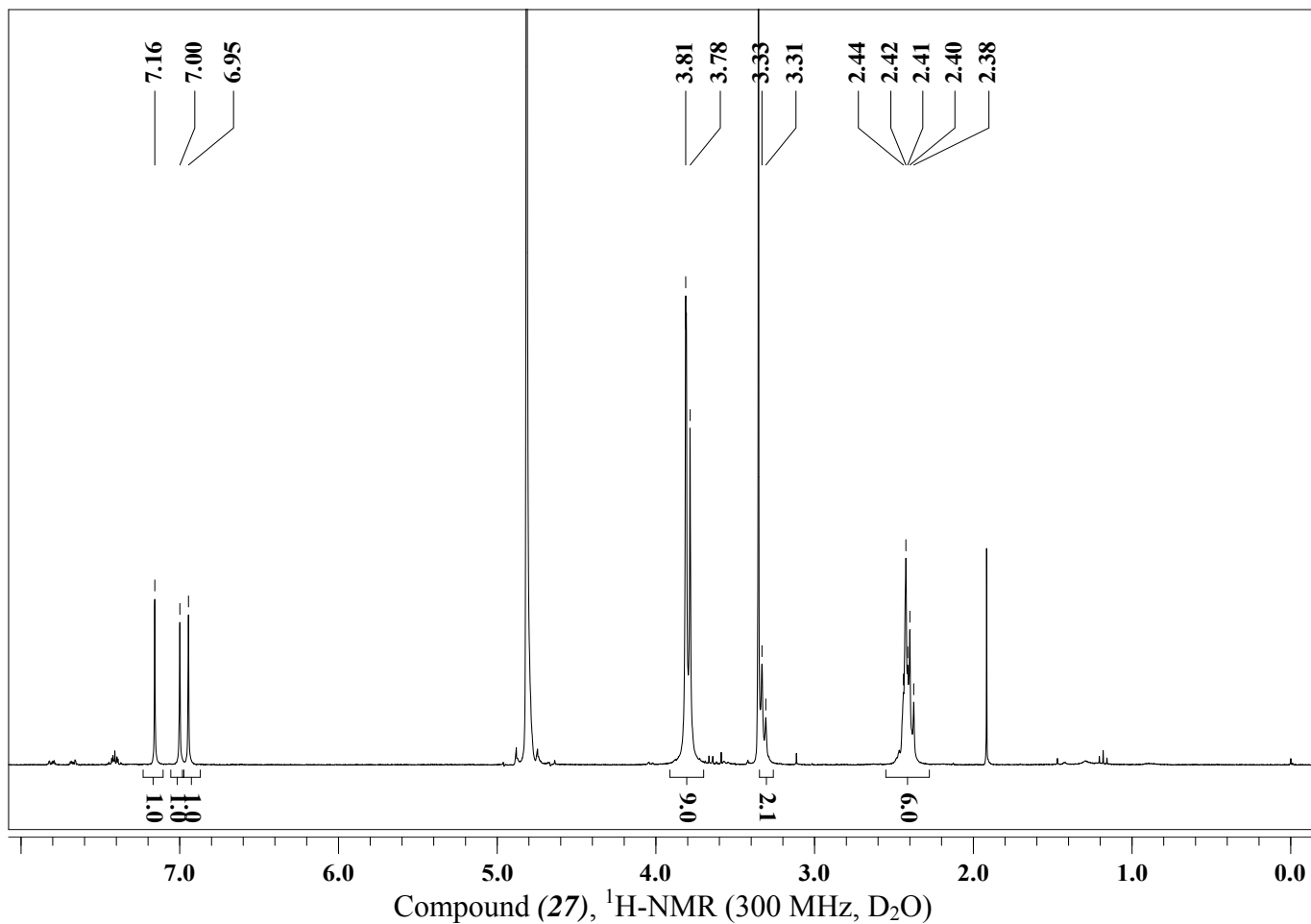
Comment: comment



Compound (26), MS (ESI-TOF, pos. MeOH)

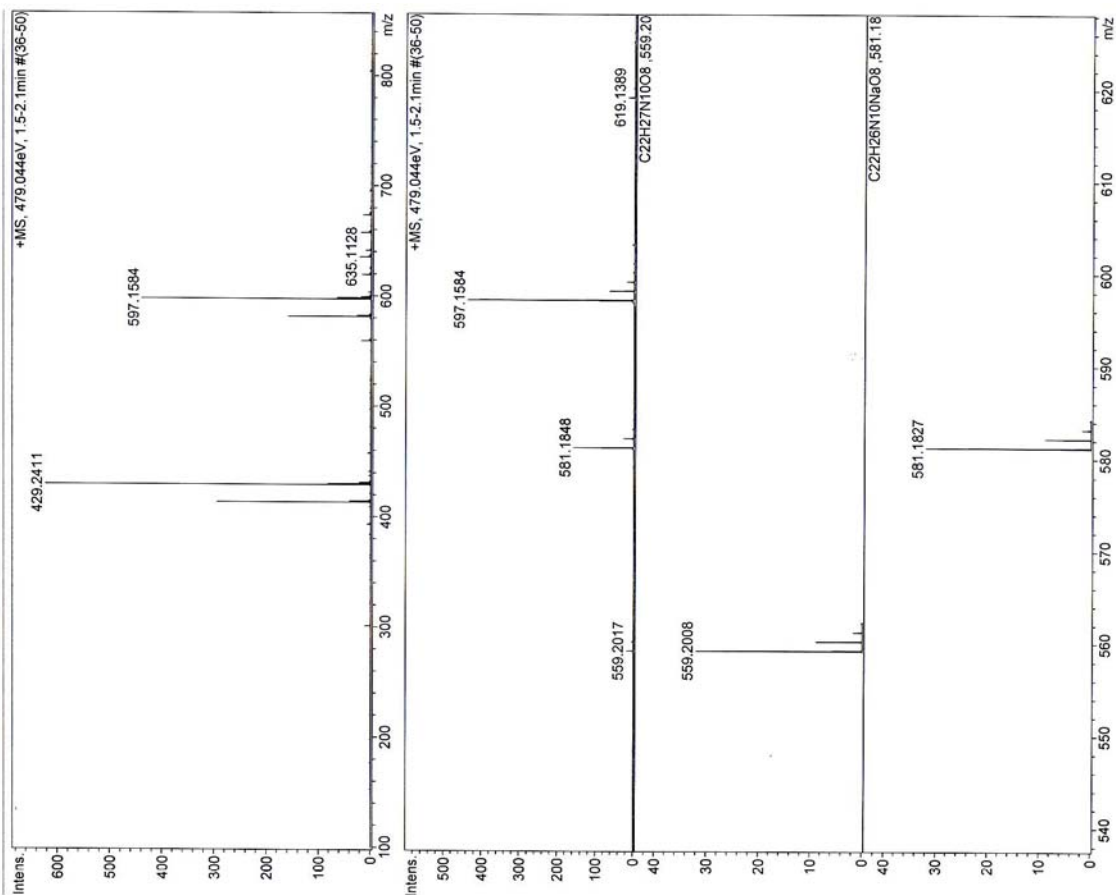


Compound (26), ¹³C-NMR (75 MHz, DMSO-*d*₆)

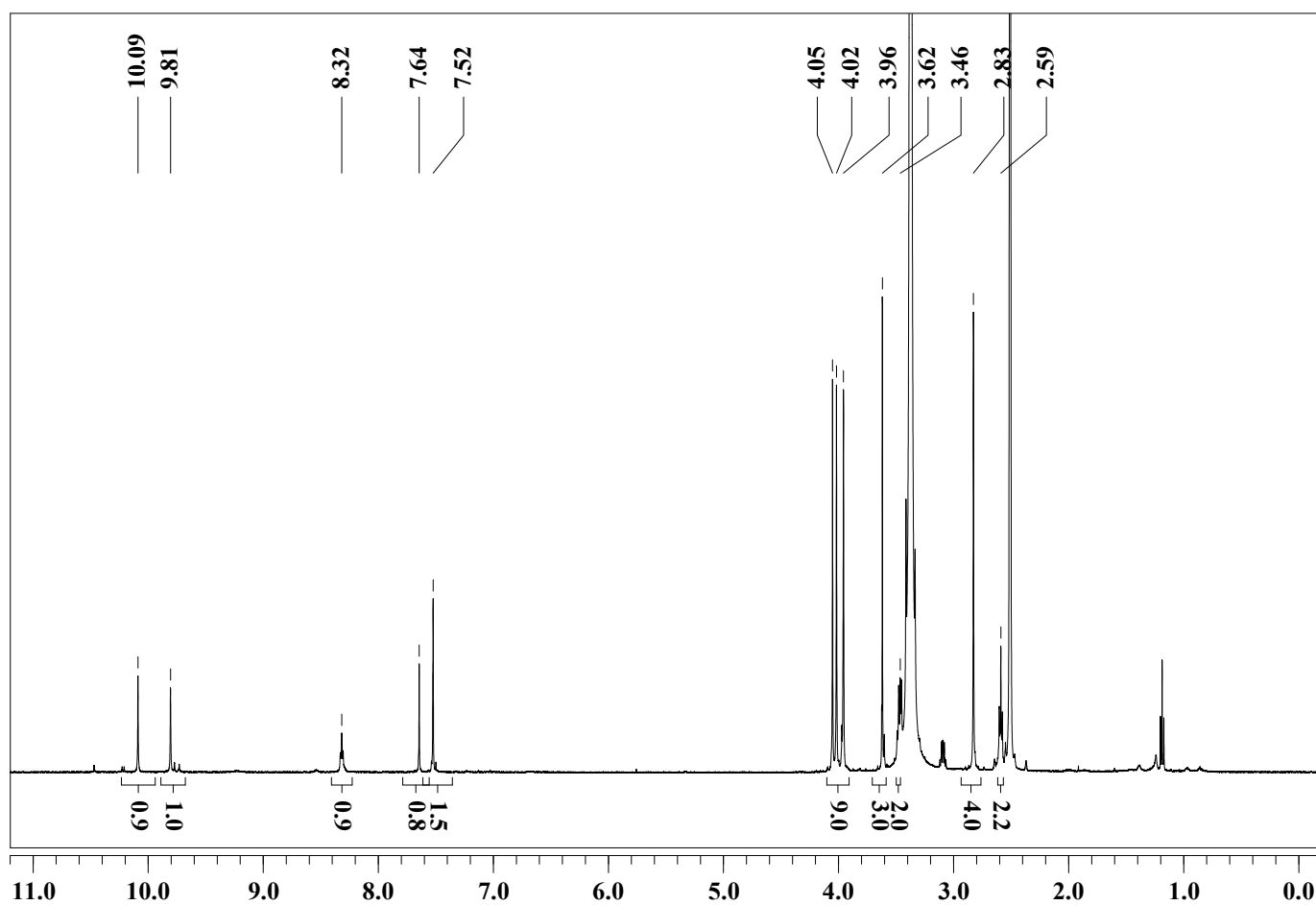


MS-Analyse: ESI-TOF

Analysis Name: E:\MS-Daten\HuWenbin\091019-P-H2O-091019-pos_01_16169.d\091019-P-H2O-091019-pos_01_16
Method: f88168name
Operator: Karow
Acquisition Date: 10/19/2009 2:48:13 PM
Instrument: Bruker BioTOF III
Comment: comment



Compound (27), MS (ESI-TOF, pos. CH₂Cl₂)

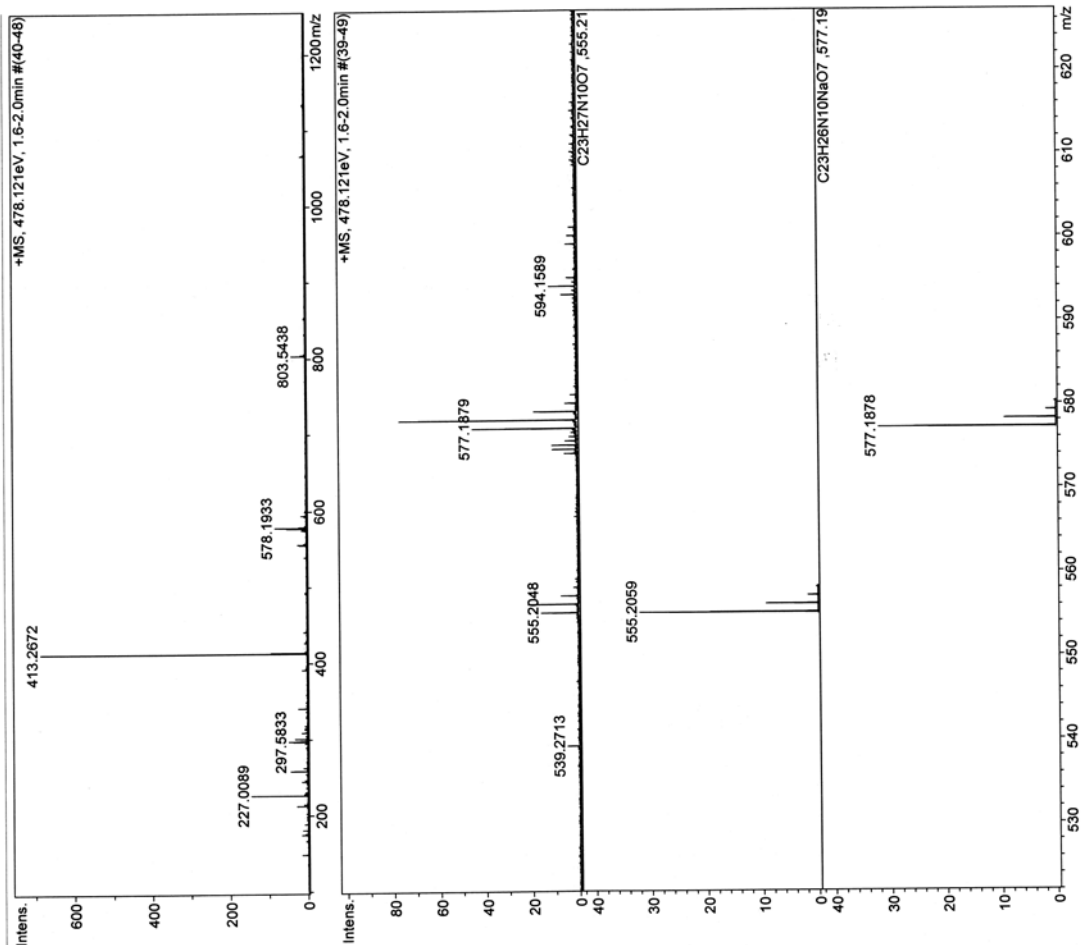


Compound (28), ¹H-NMR (300 MHz, DMSO-*d*₆)

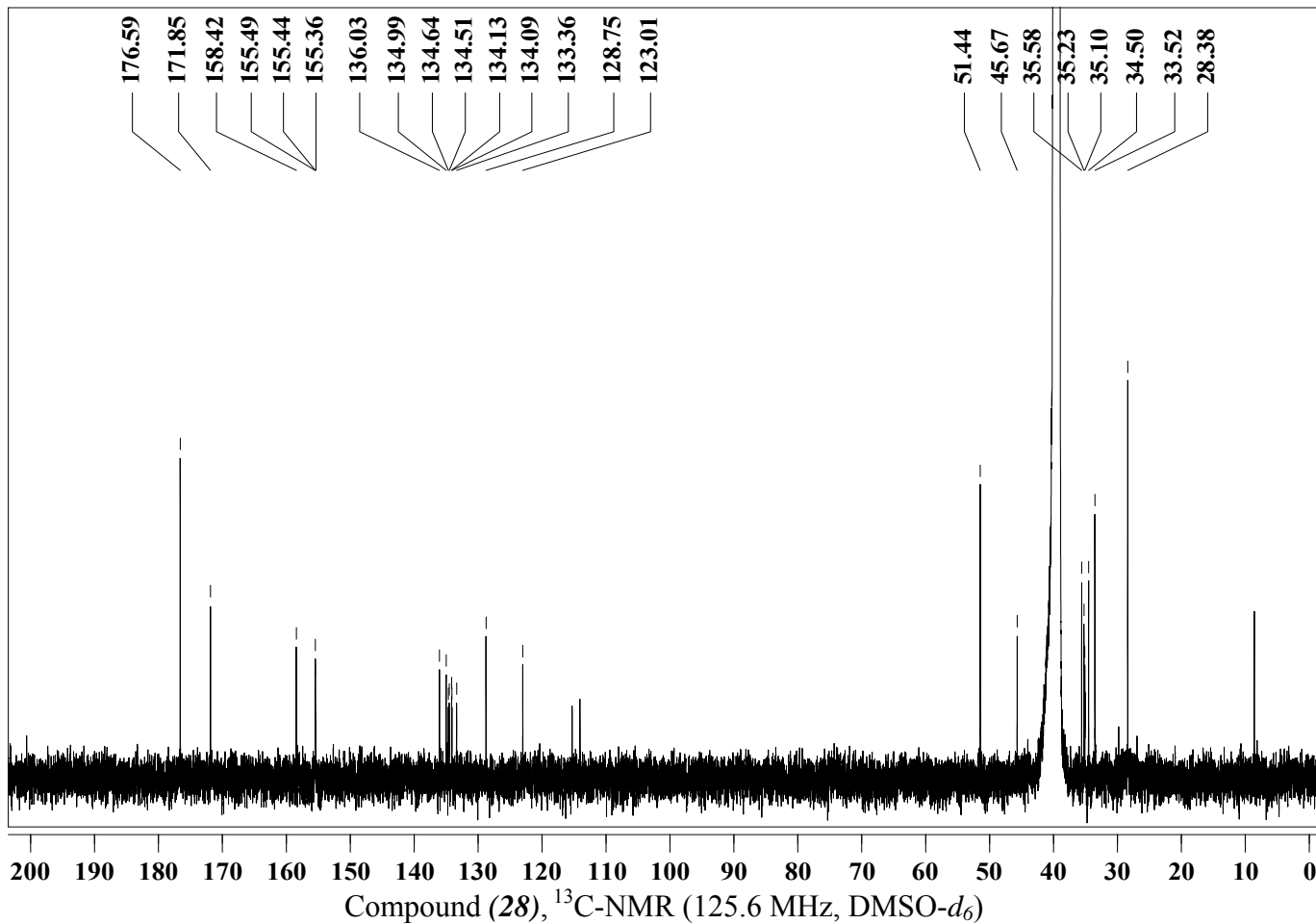
MS-Analyse: ESI-TOF

Analysis Name: E:\MS-Daten\HuWenbin\100618-R-1-100618-R-1-100618-pos_01_19398.d\100618-pos_01_19398.ser
Method: methodname
Acquisition Date: 6/18/2010 12:38:40 PM
Operator: Karow
Instrument: Bruker BioTOF III

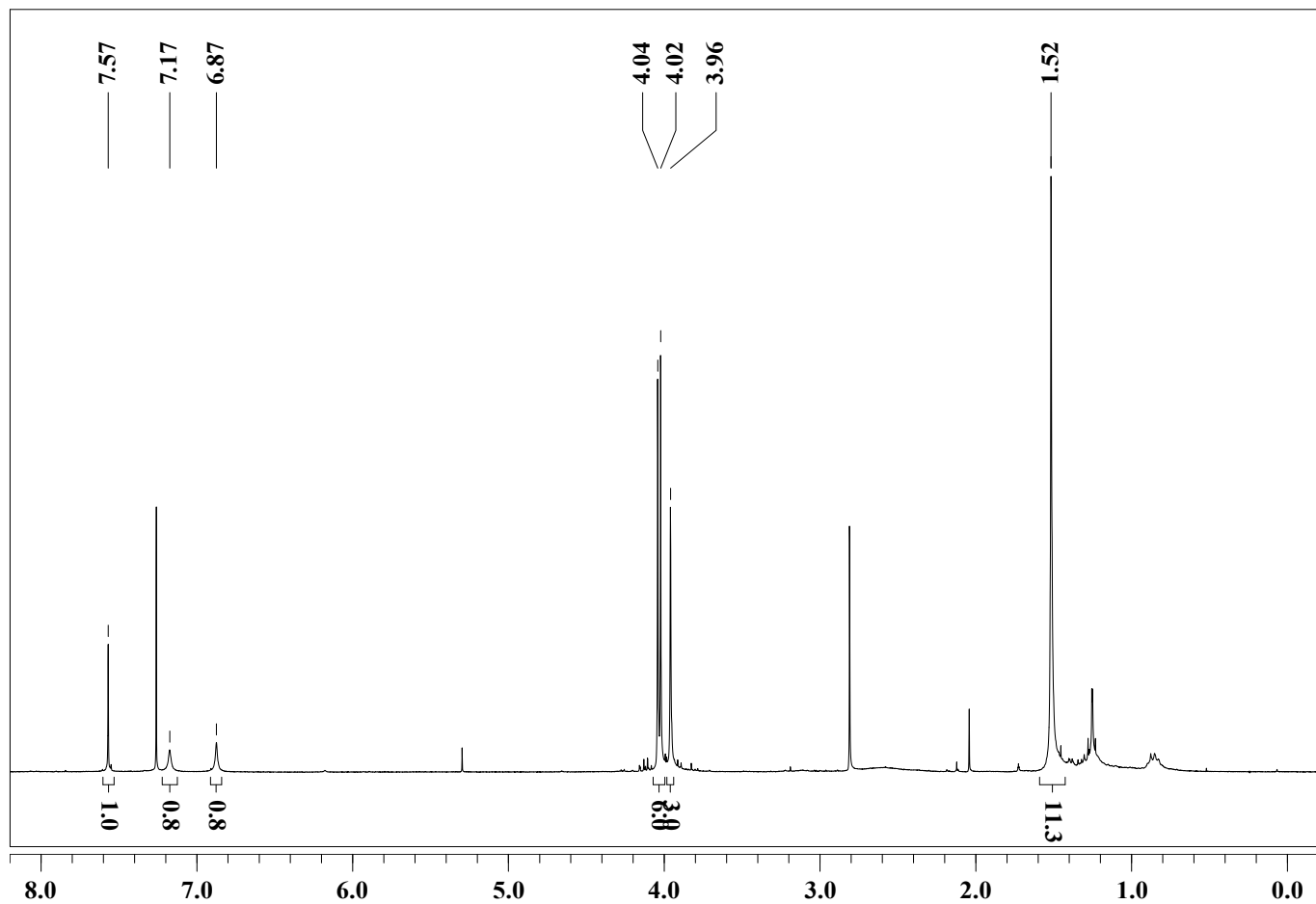
Comment: comment



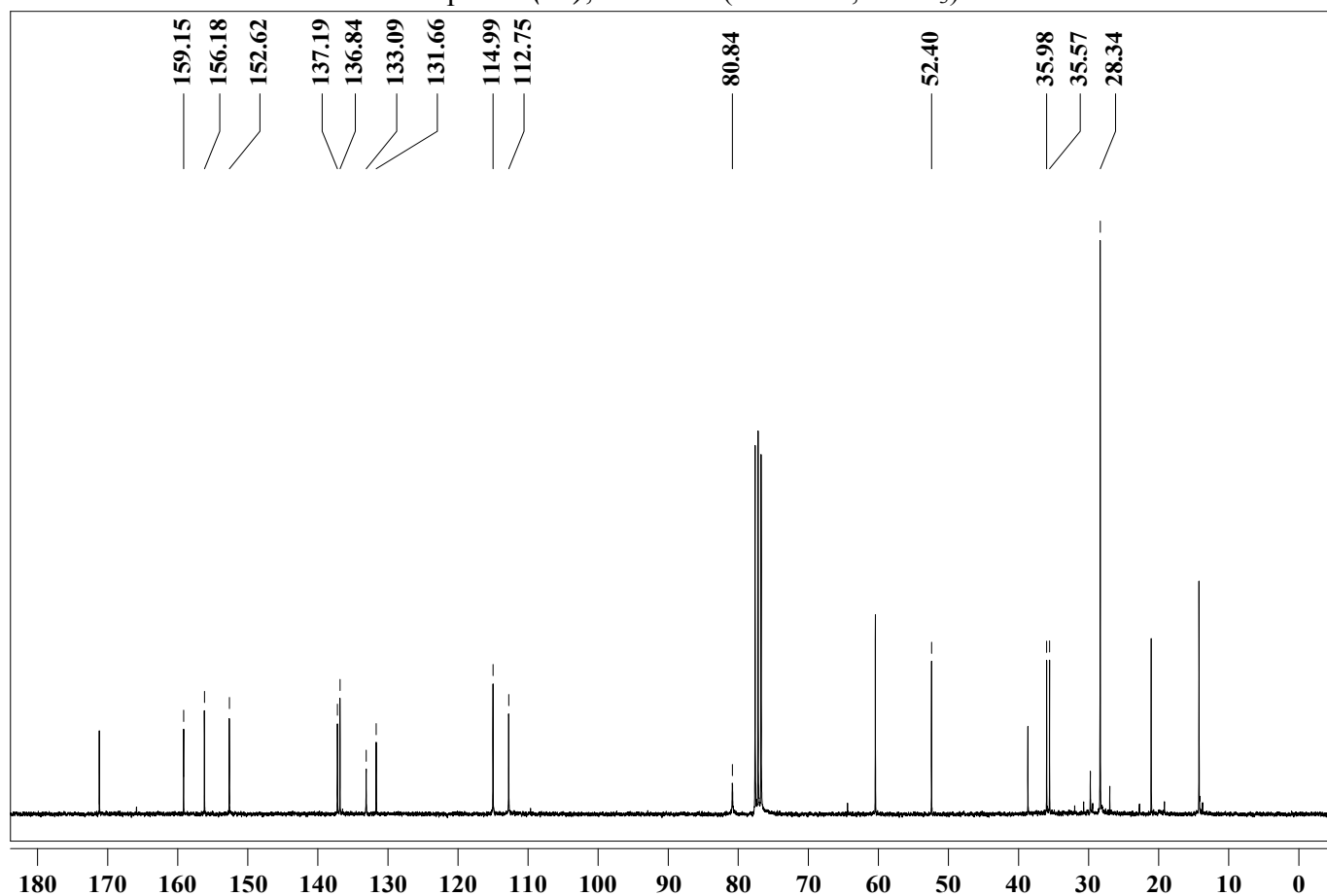
Compound (28), MS (ESI-TOF, pos. MeOH)



Compound (28), ¹³C-NMR (125.6 MHz, DMSO-d₆)



Compound (29), $^1\text{H-NMR}$ (300 MHz, CDCl_3)

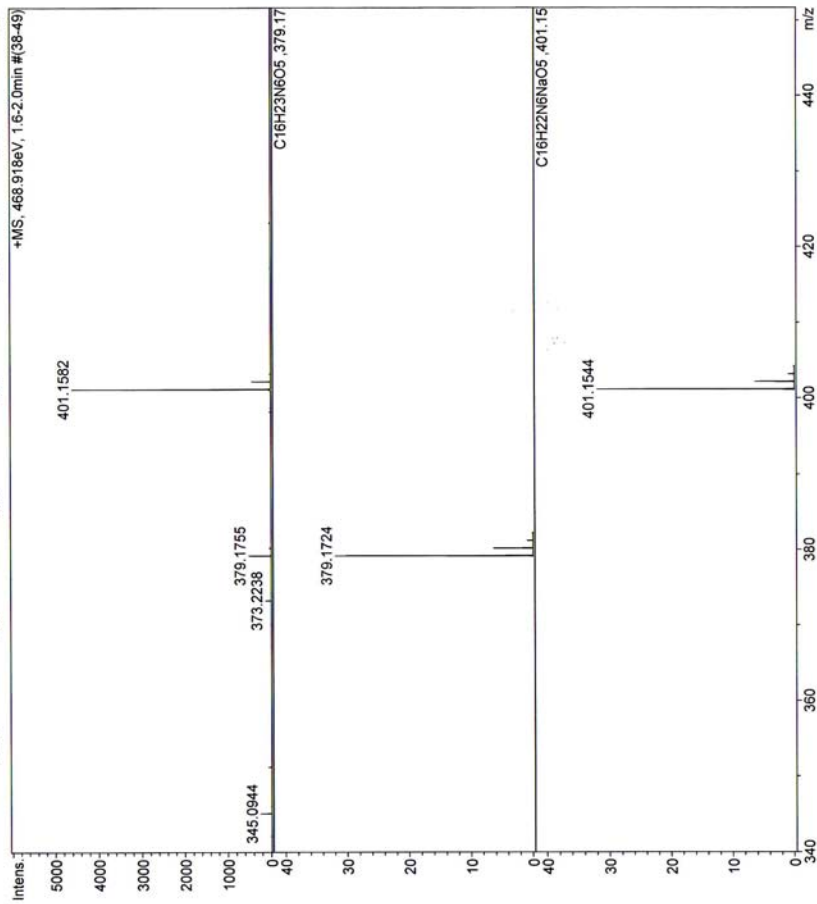
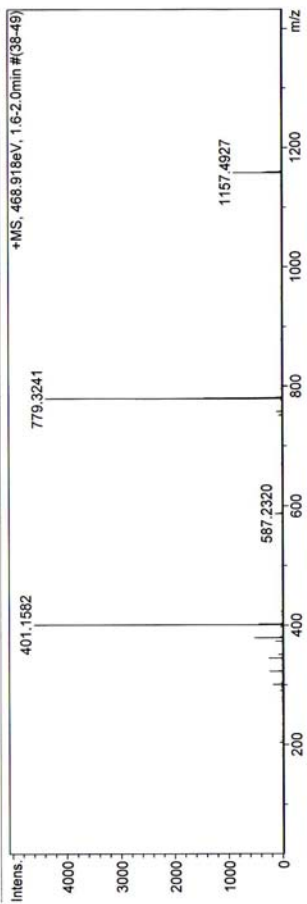


Compound (29), $^{13}\text{C-NMR}$ (75 MHz, CDCl_3)

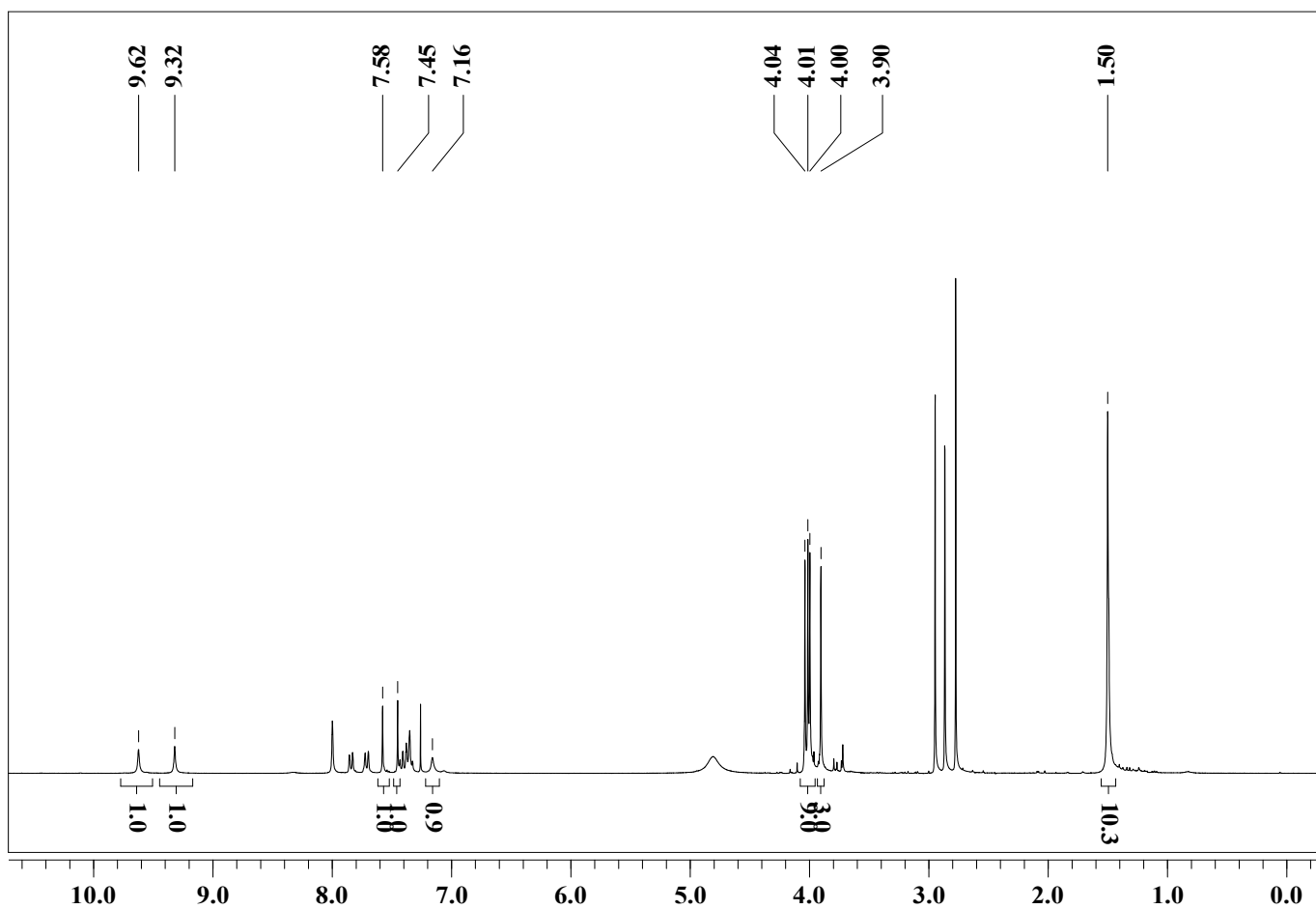
MS-Analyse: ESI-TOF

Analysis Name: E:\MS-Daten\HuWenbin\100927-S-3-100920-pos_01_20376-d\100927-S-3-100920-pos_01_20376.ser
Method: methodname
Operator: Karow
Acquisition Date: 9/27/2010 11:56:57 AM
Instrument: Bruker BioTOF III

Comment: comment



Compound (29), MS (ESI-TOF, pos. CH₂Cl₂)

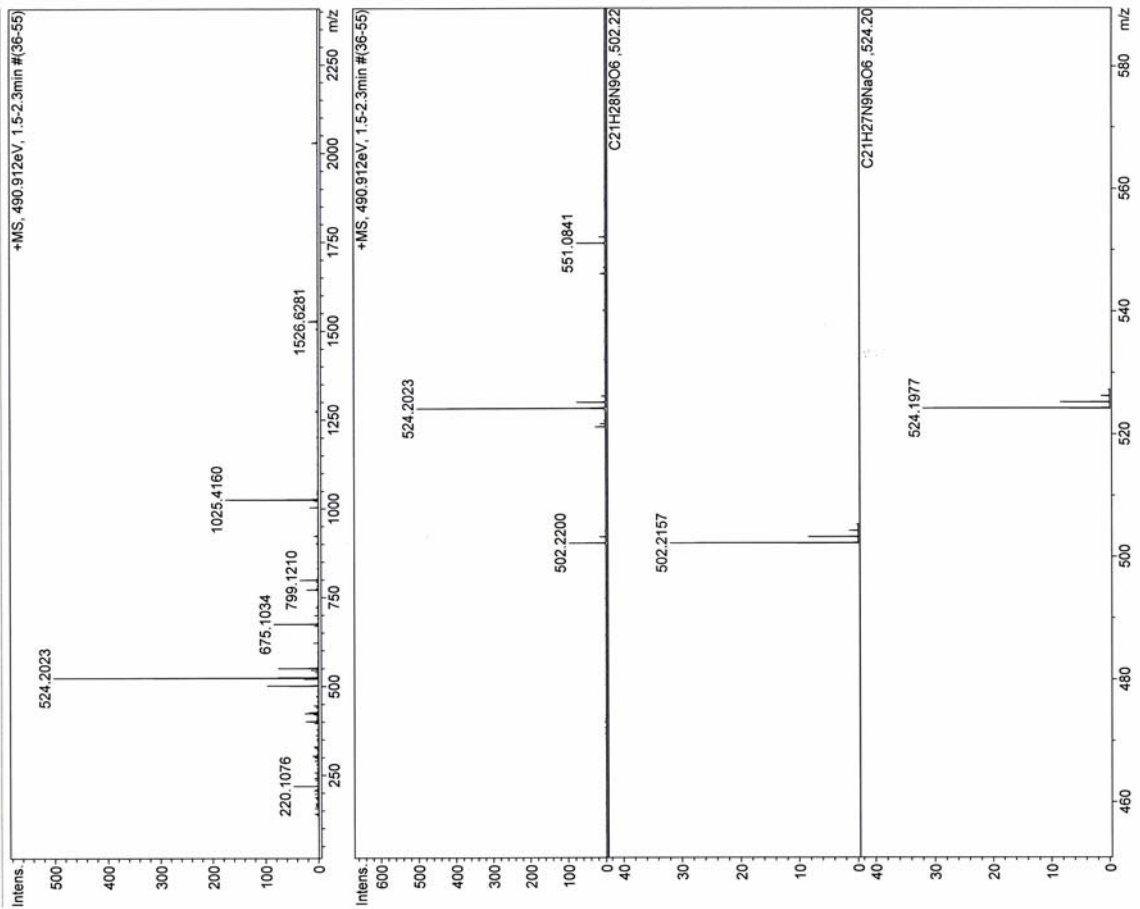


Compound (30), ¹H-NMR (300 MHz, CDCl₃)

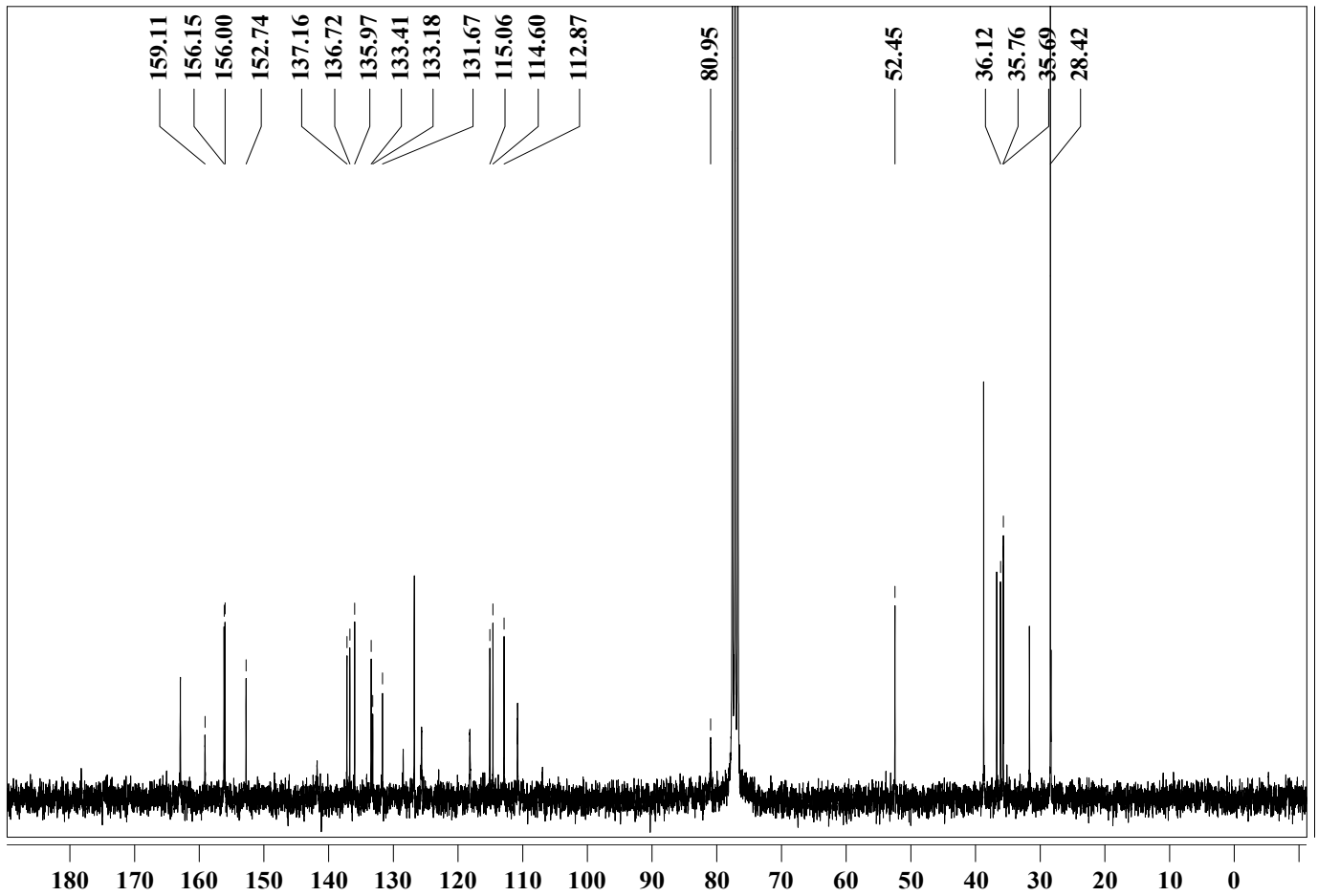
MS-Analyse: ESI-TOF

Analysis Name: E:\MS-Daten\Huwenbin\1010005-T-1010005-pos_01_20475.d\1010005-pos_01_20475.ser
 Method: Karow
 Acquisition Date: 10/05/2010 11:15:48 AM
 Instrument: Bruker BioTOF III

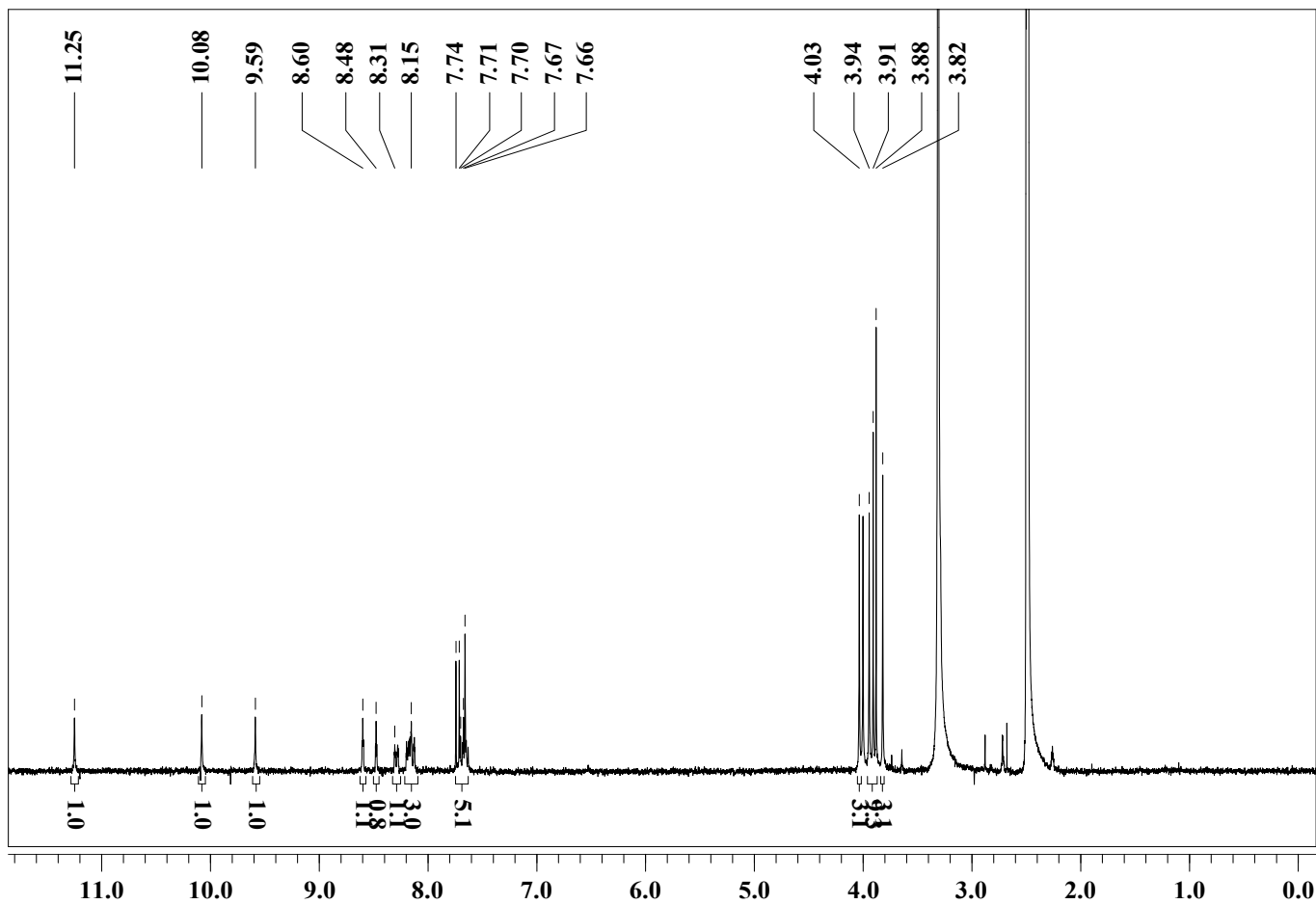
Comment:



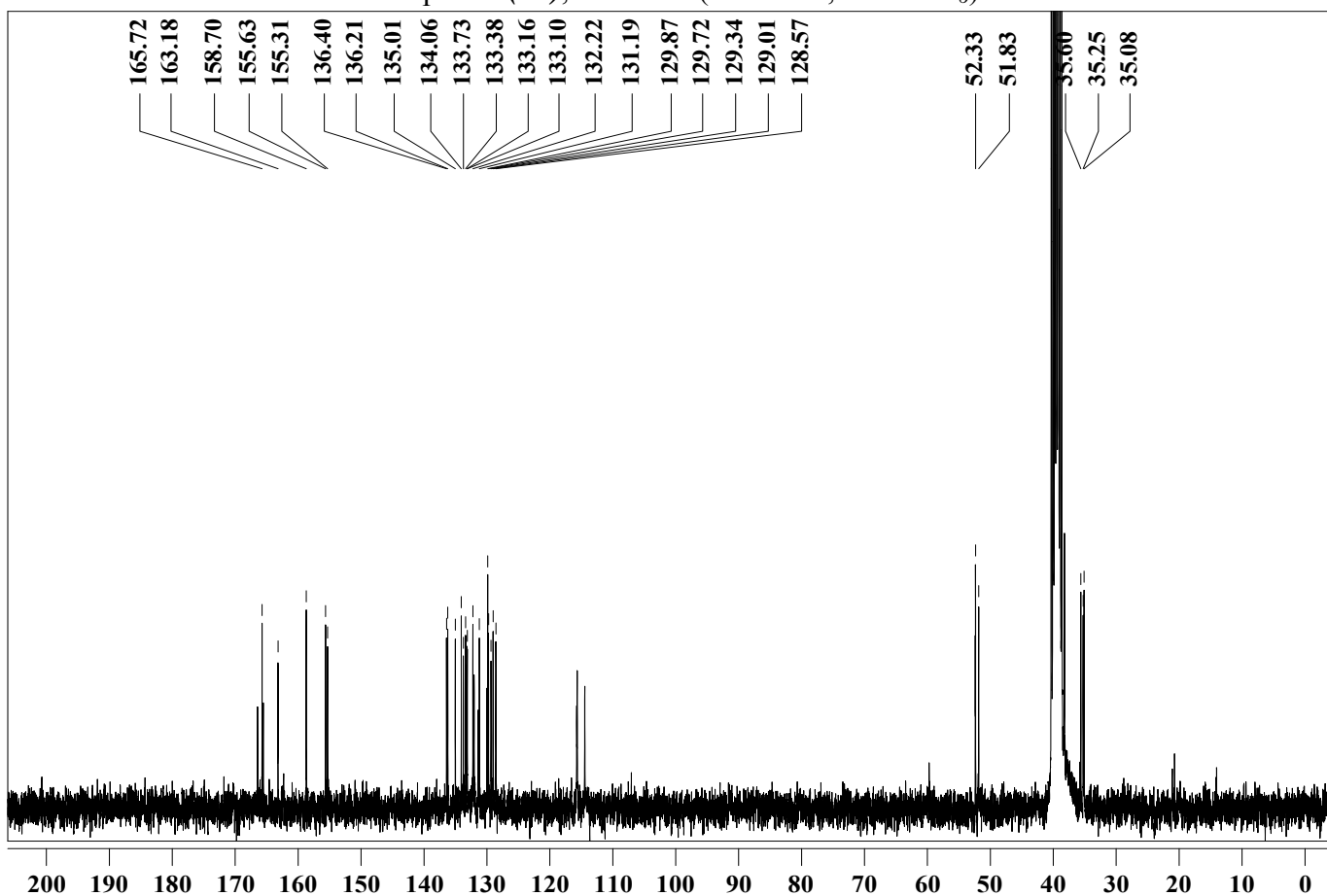
Compound (30), MS (ESI-TOF, pos. CH₂Cl₂)



Compound (30), ¹³C-NMR (75 MHz, CDCl₃)



Compound (**31**), $^1\text{H-NMR}$ (300 MHz, $\text{DMSO-}d_6$)

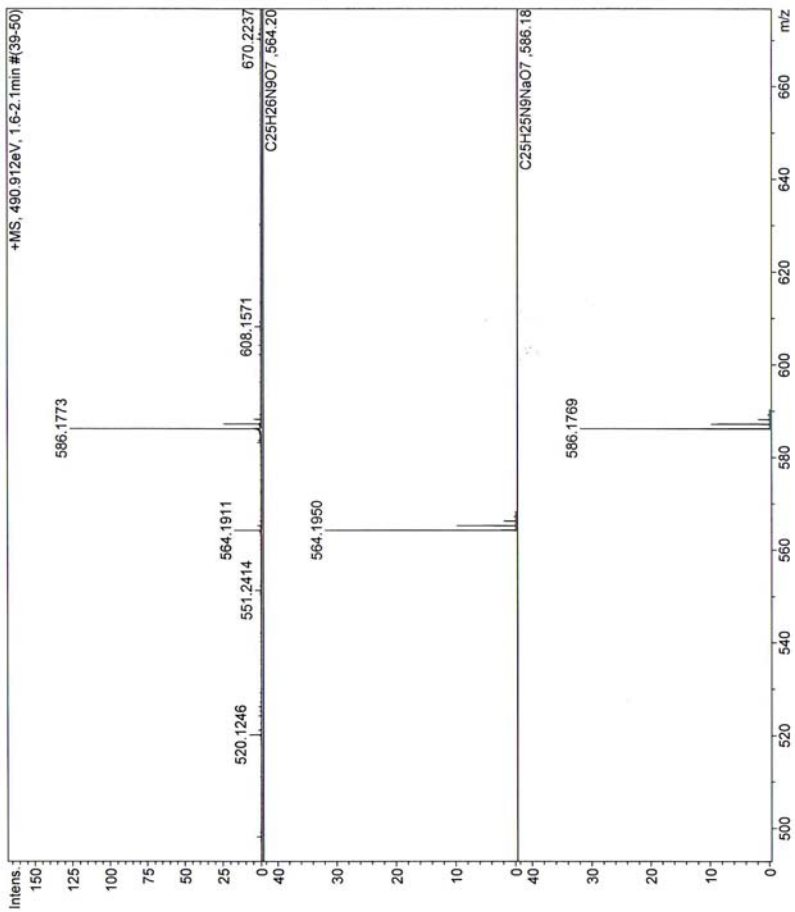
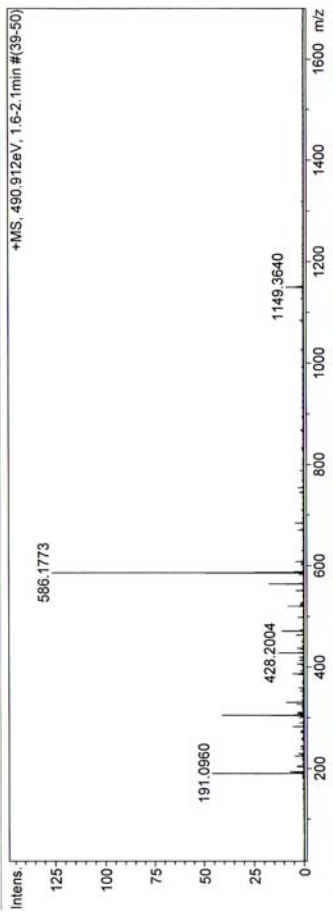


Compound (**31**), $^{13}\text{C-NMR}$ (75 MHz, $\text{DMSO-}d_6$)

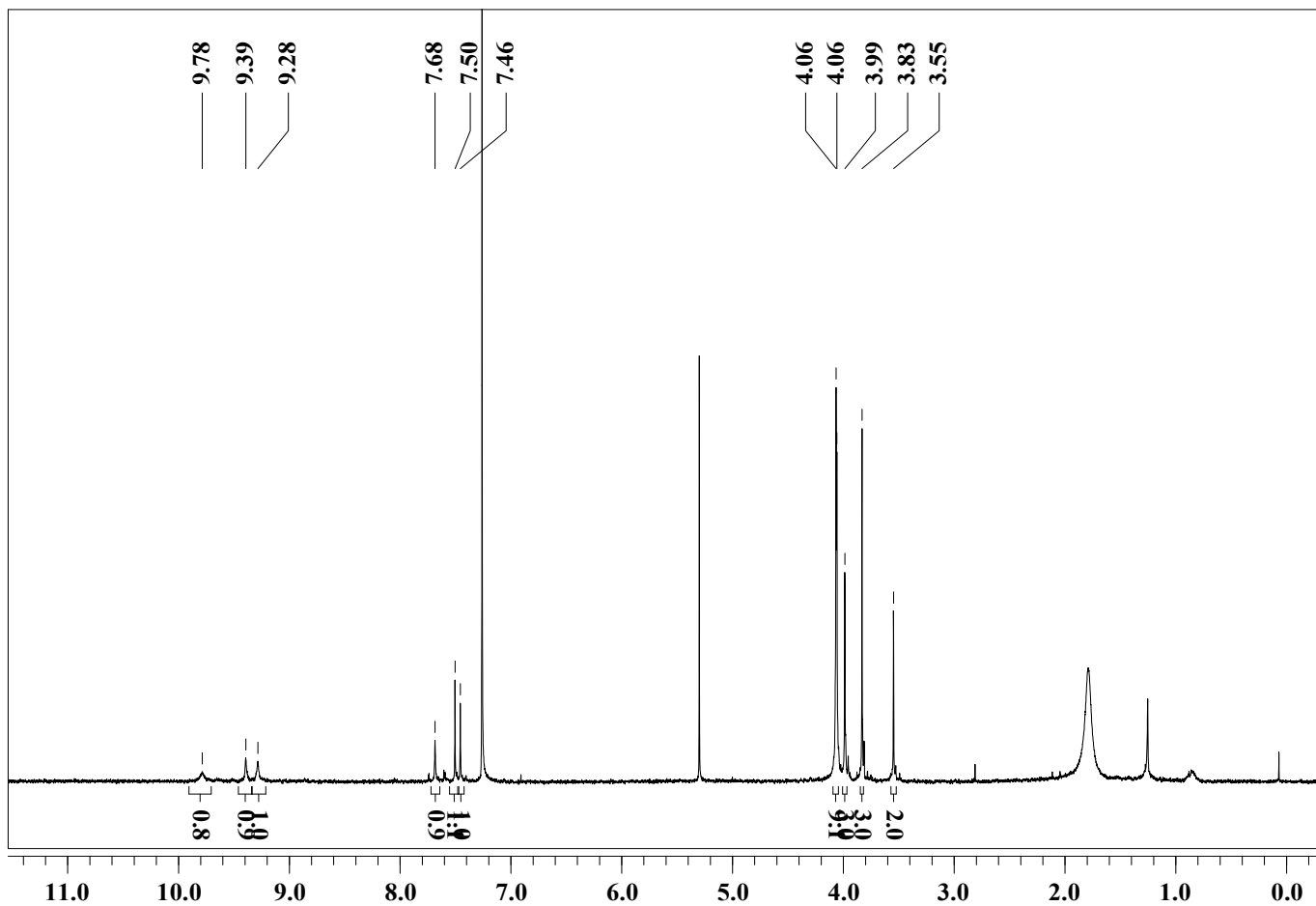
MS-Analyse: ESI-TOF

Analysis Name: E:\MS-Daten\HuWenbin\101025-U1-101022-pos_01_20869.ser
 Method: methodname Karow
 Acquisition Date: 10/25/2010 6:23:46 PM Instrument: Bruker BioTOF III

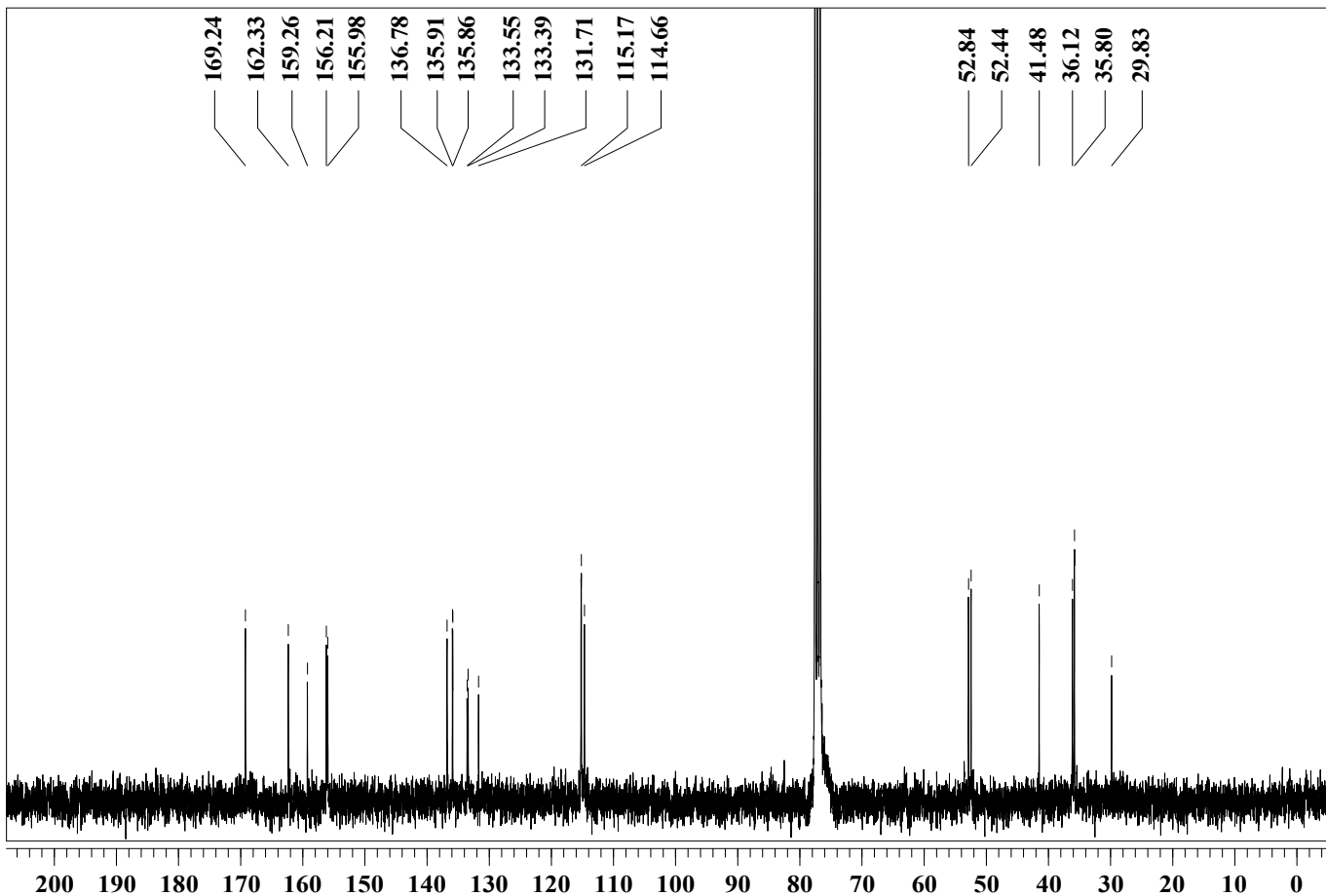
Comment: comment



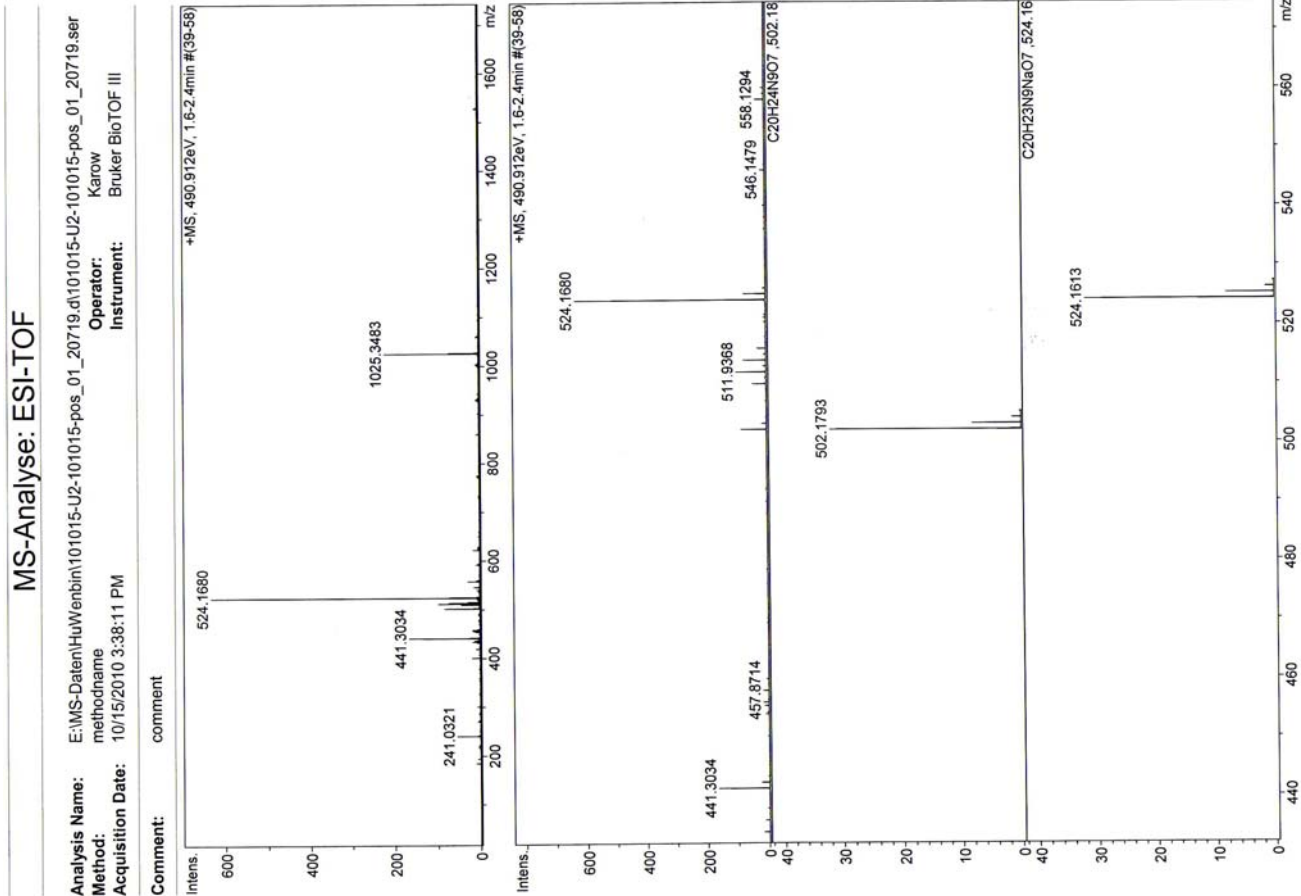
Compound (31), MS (ESI-TOF, pos. CH₂Cl₂)



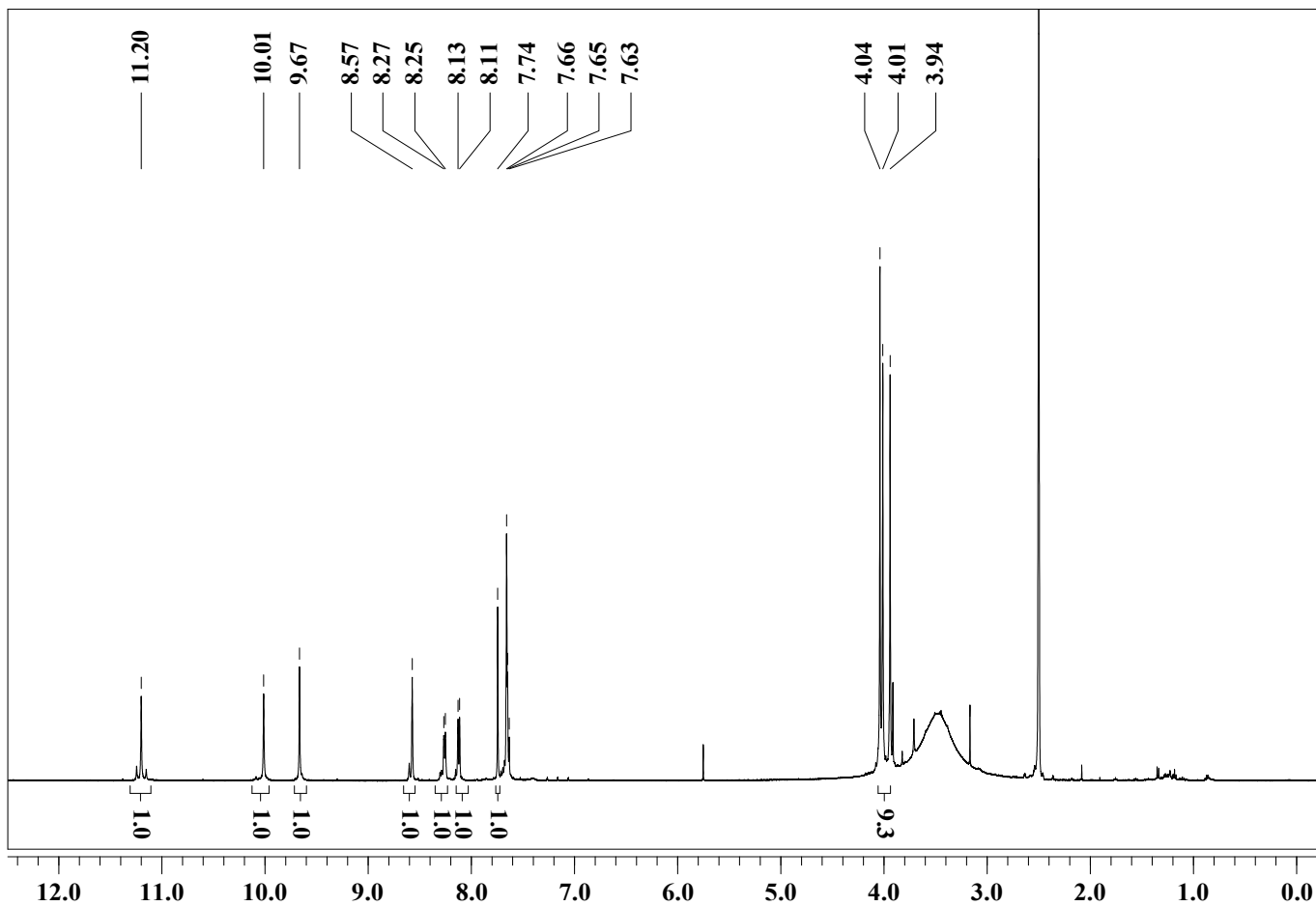
Compound (32), ¹H-NMR (300 MHz, CDCl₃)



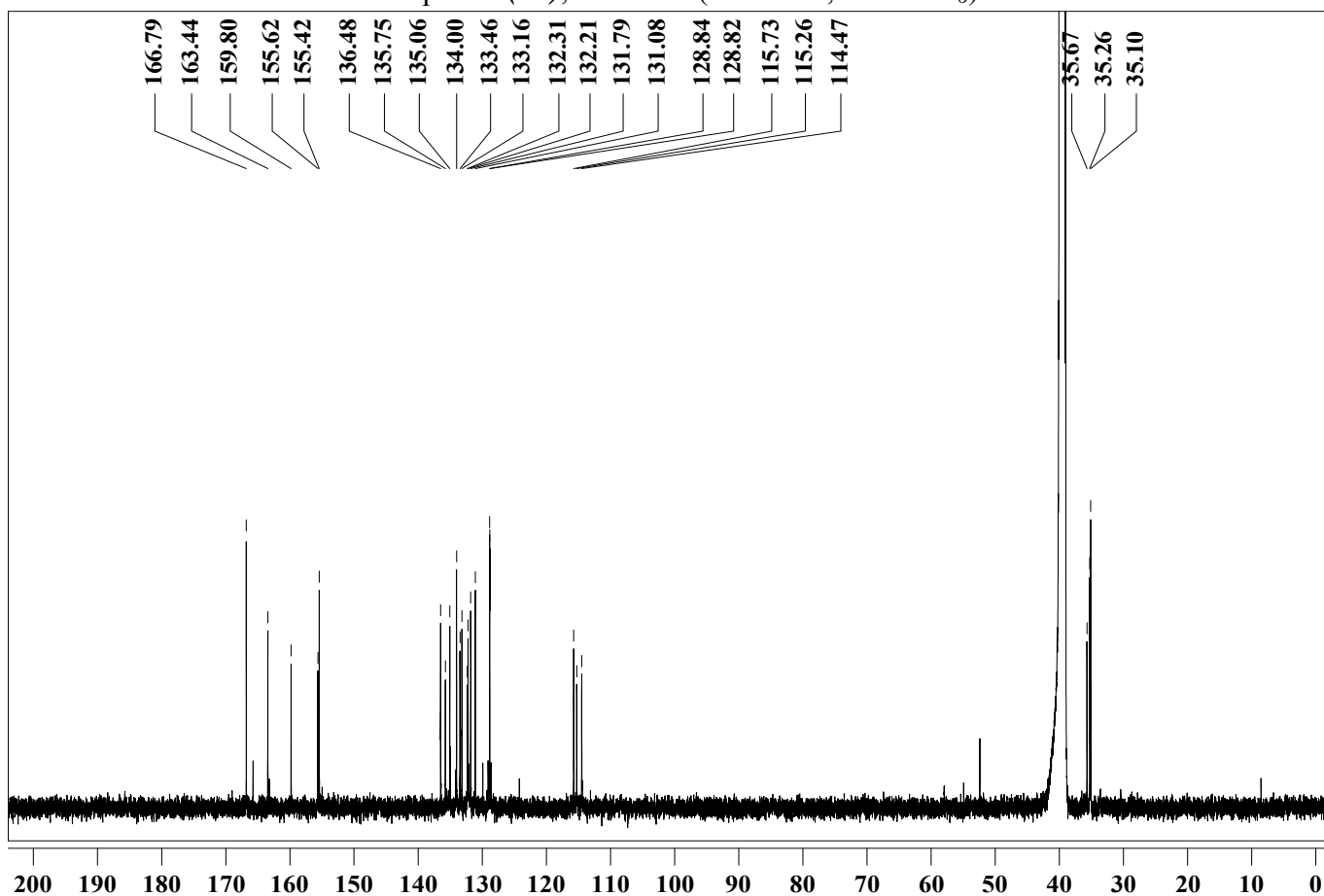
Compound (32), $^{13}\text{C-NMR}$ (75 MHz, CDCl_3)



Compound (32), MS (ESI-TOF, pos. CH_2Cl_2)



Compound (33), $^1\text{H-NMR}$ (300 MHz, $\text{DMSO-}d_6$)

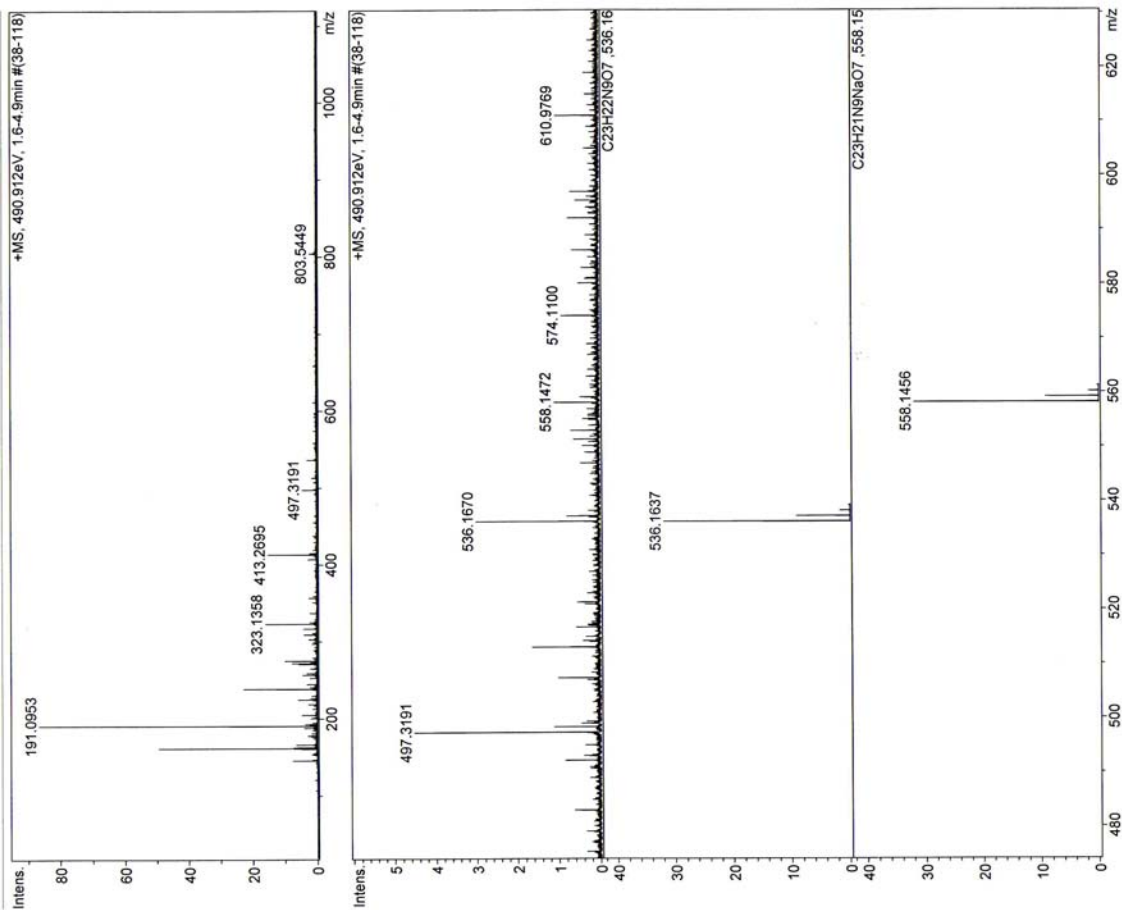


Compound (33), $^{13}\text{C-NMR}$ (125.6 MHz, $\text{DMSO-}d_6$)

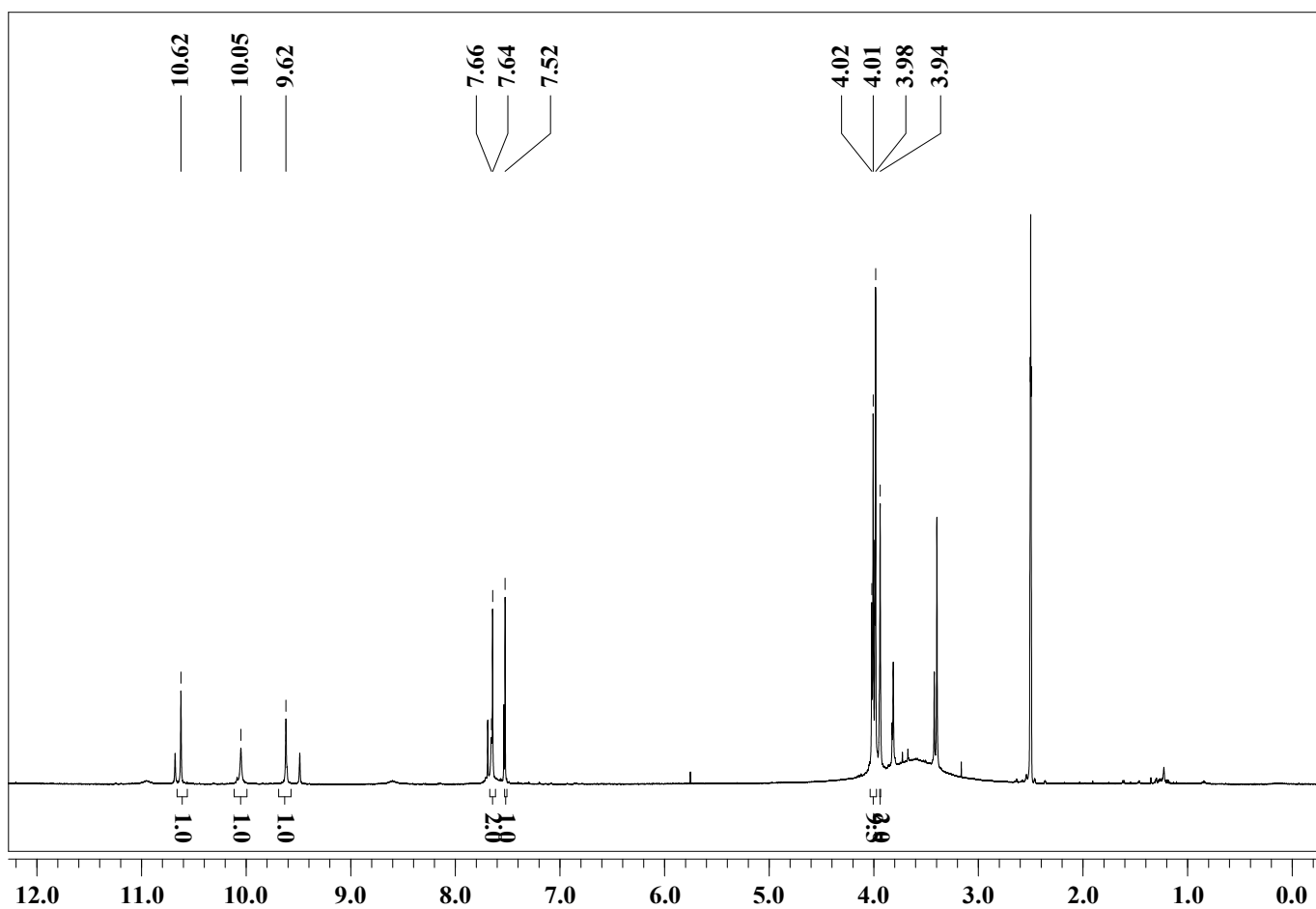
MS-Analyse: ESI-TOF

Analysis Name: E:\MS-Daten\HuWenbin\101029-V1-DMSO-101029-pos_01_20952.d\101029-V1-DMSO-101029-pos_
 Method: Bruker
 Acquisition Date: 10/29/2010 12:01:16 PM
 Operator: Karow
 Instrument: Bruker BioTOF III

Comment: comment



Compound (33), MS (ESI-TOF, pos. DMSO)

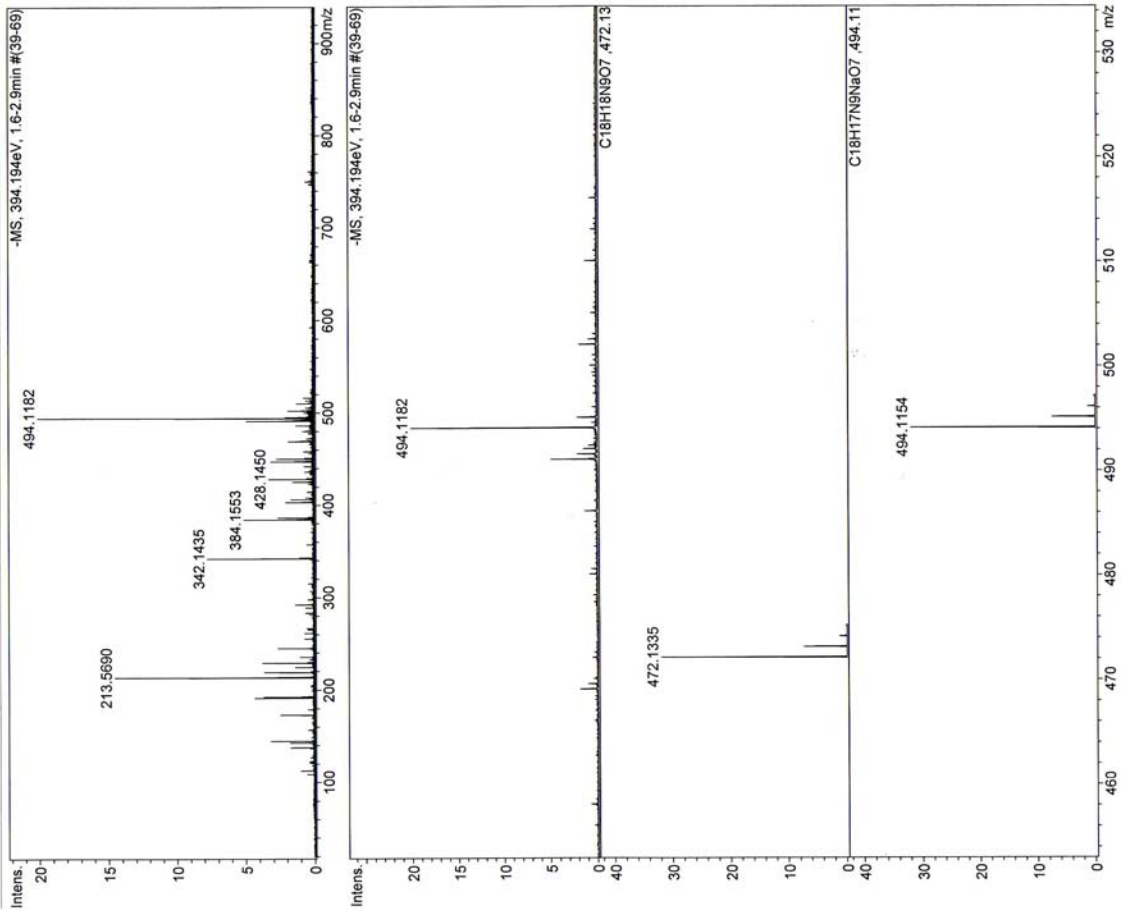


Compound (34), ¹H-NMR (125.6 MHz, DMSO-*d*₆)

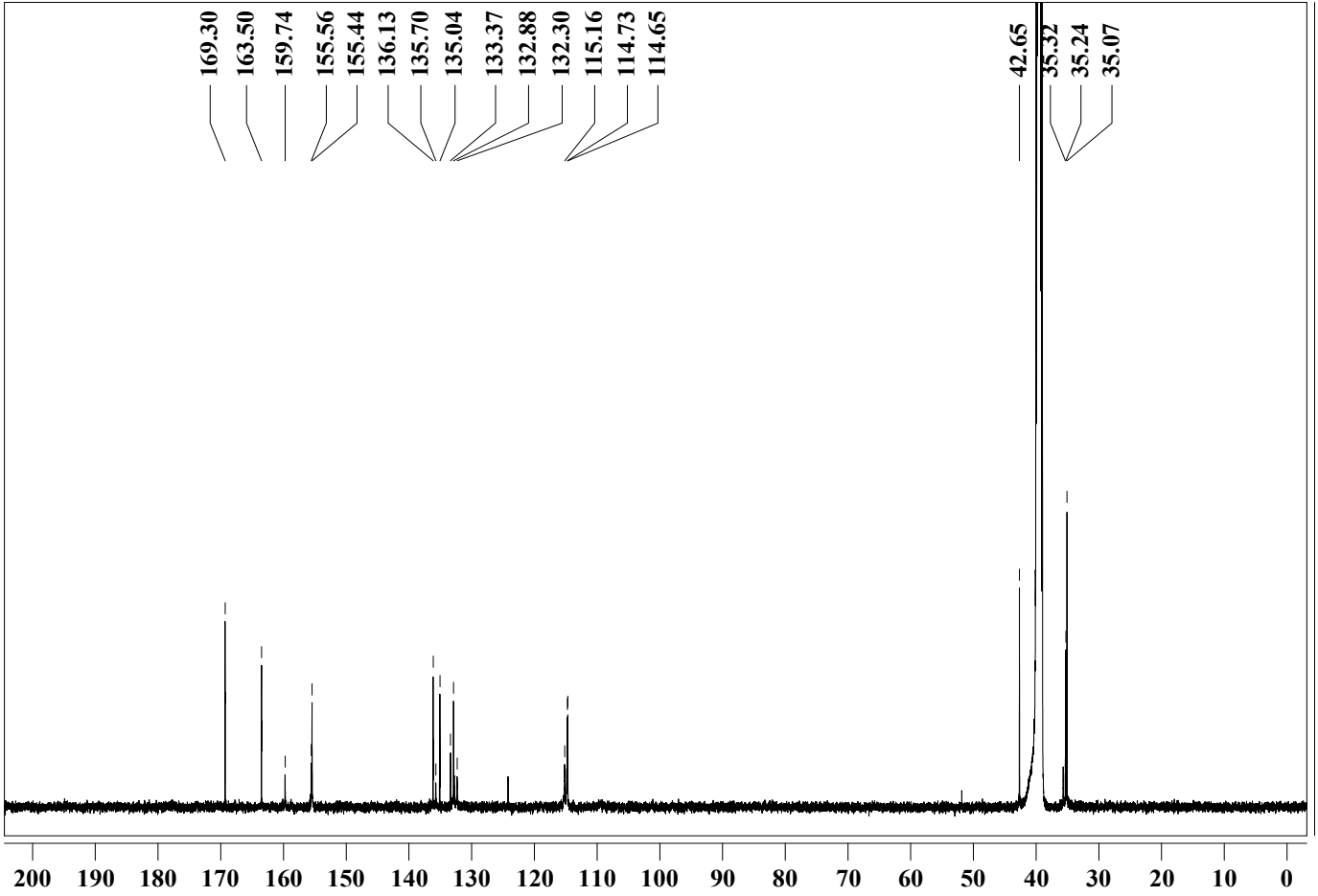
MS-Analyse: ESI-TOF

Analysis Name: E:\MS-Daten\HuWenbin\101029-V2-DMSO-101029-neg_01_20957.d\101029-V2-DMSO-101029-neg_01_20957.d
 Method: HESI-TOF
 Acquisition Date: 10/29/2010 12:34:18 PM
 Operator: Karow
 Instrument: Bruker BioTOF III

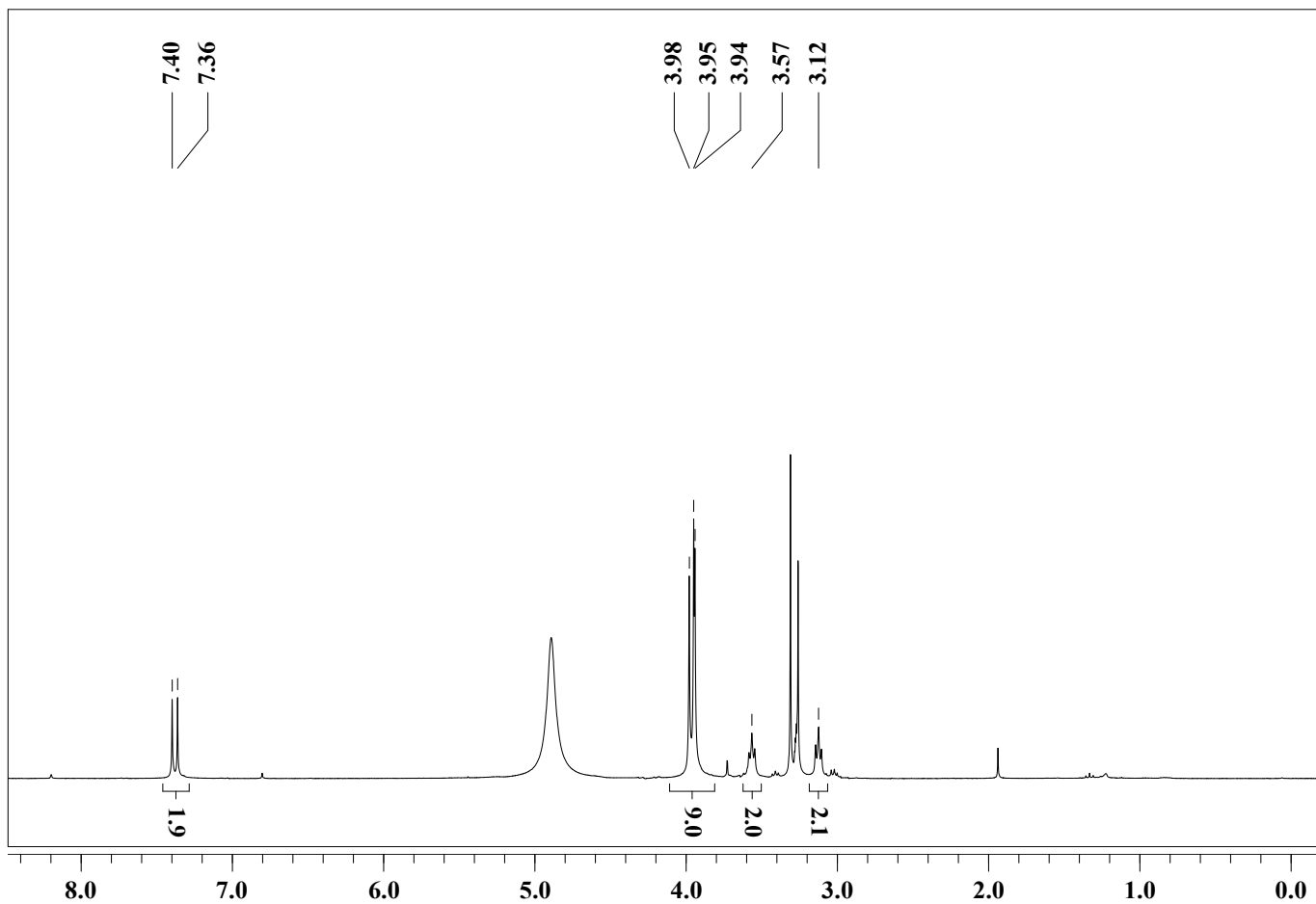
Comment: comment



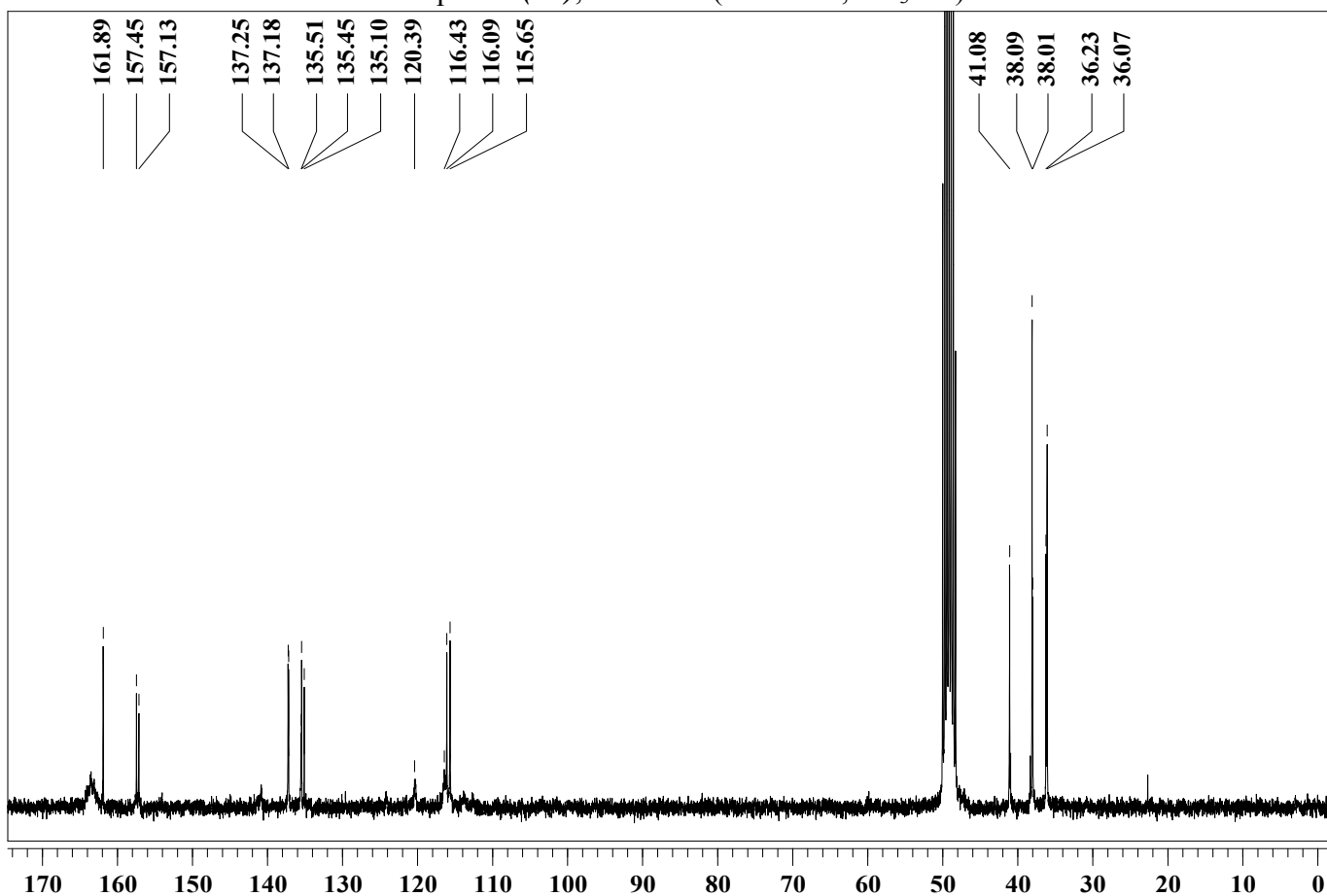
Compound (34), MS (ESI-TOF, pos. DMSO)



Compound (34), ¹³C-NMR (75 MHz, DMSO-d₆)



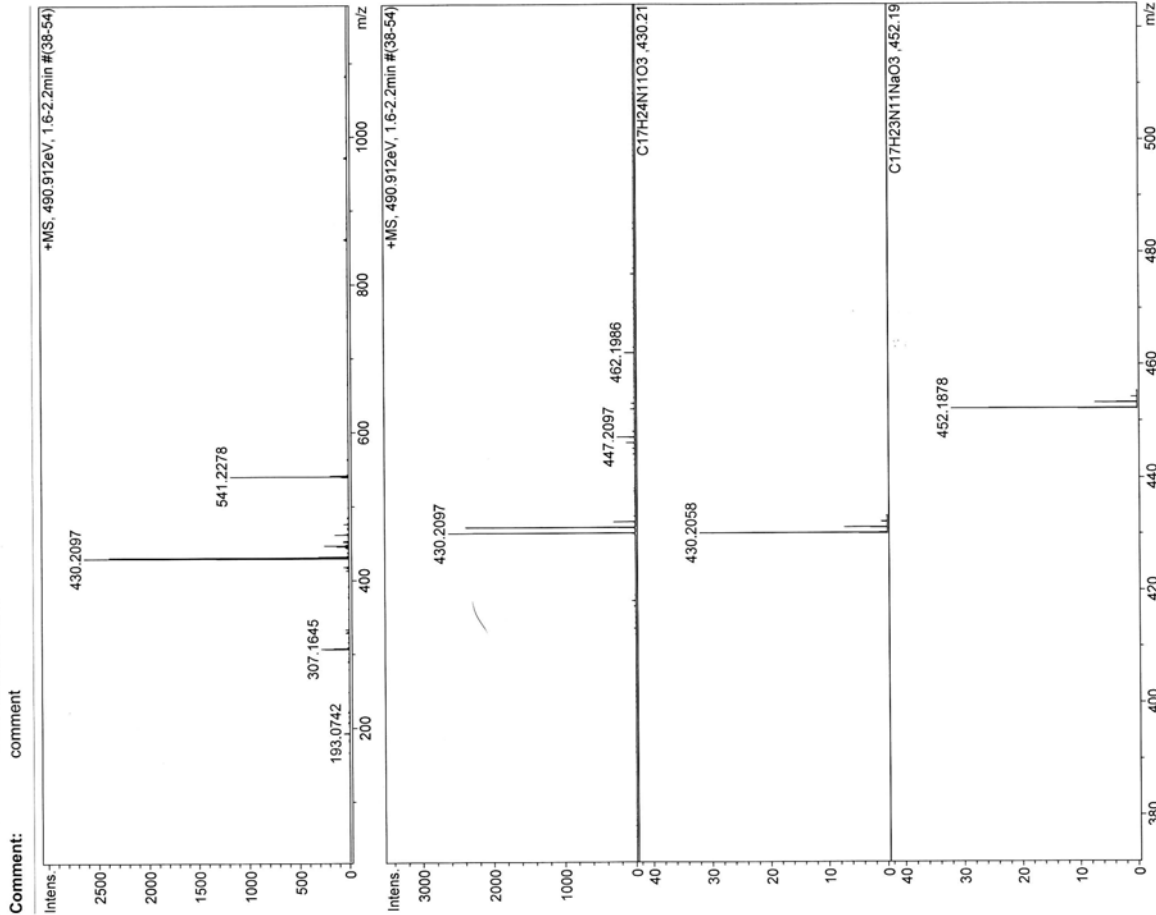
Compound (36), $^1\text{H-NMR}$ (300 MHz, CD_3OD)



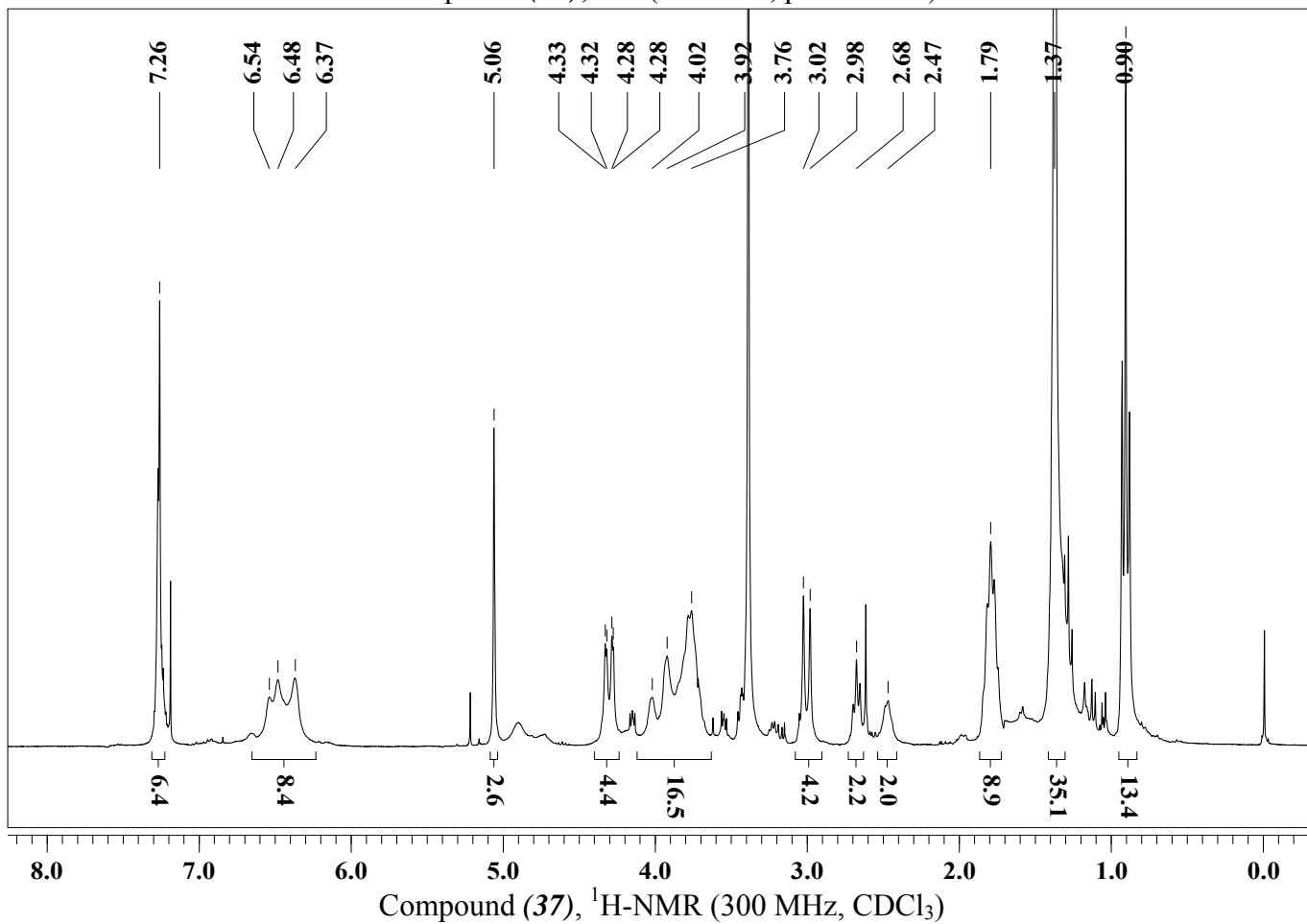
Compound (36), $^{13}\text{C-NMR}$ (75 MHz, CD_3OD)

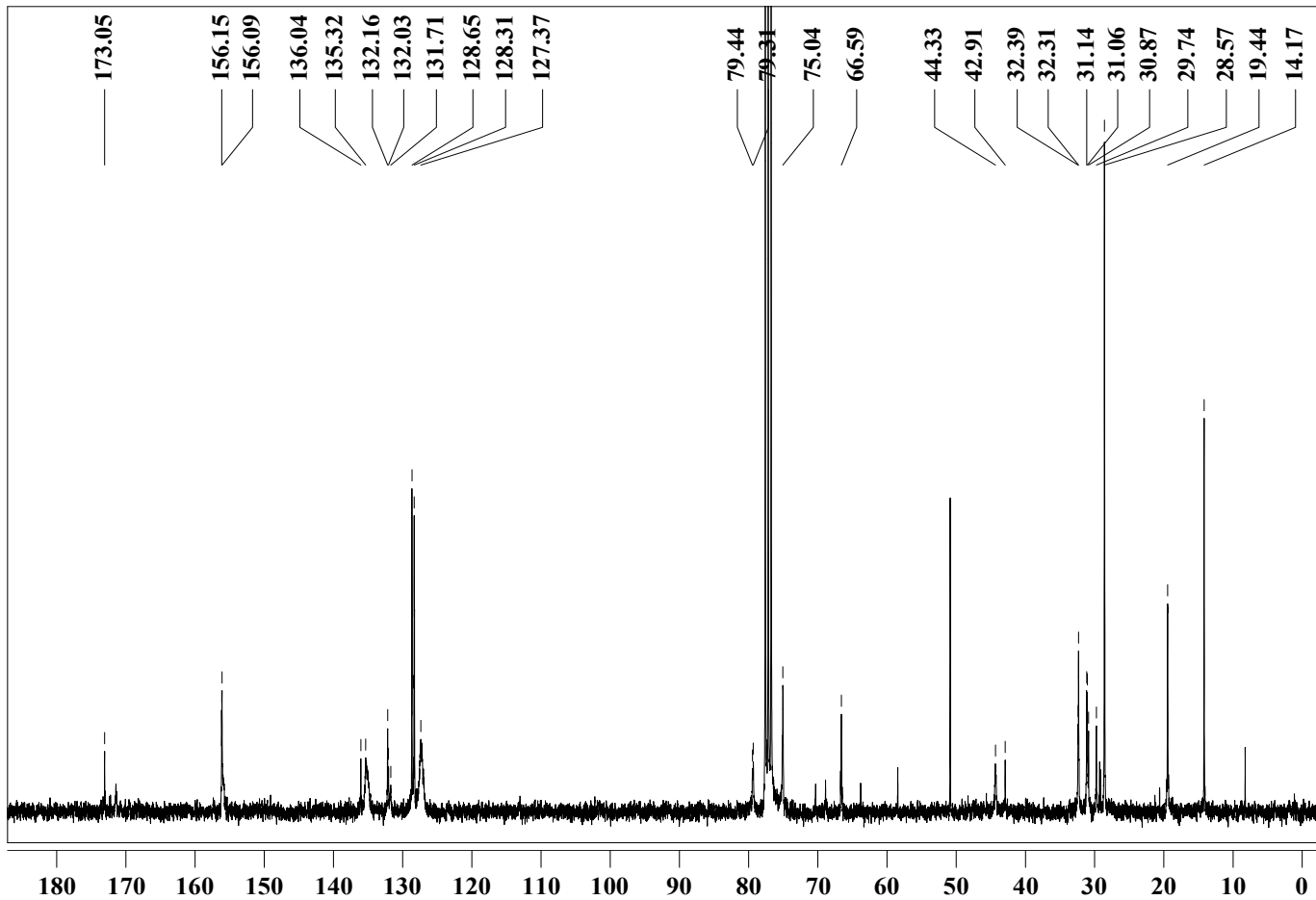
MS-Analyse: ESI-TOF

Analysis Name: E:\MS-Daten\HuWenbin\101202-Y2-101202-pos_01_21430.d\101202-Y2-101202-pos_01_21430.ser
Method: methodname
Acquisition Date: 12/2/2010 2:07:58 PM
Operator: Karow
Instrument: Bruker BioTOF III



Compound (36), MS (ESI-TOF, pos. MeOH)



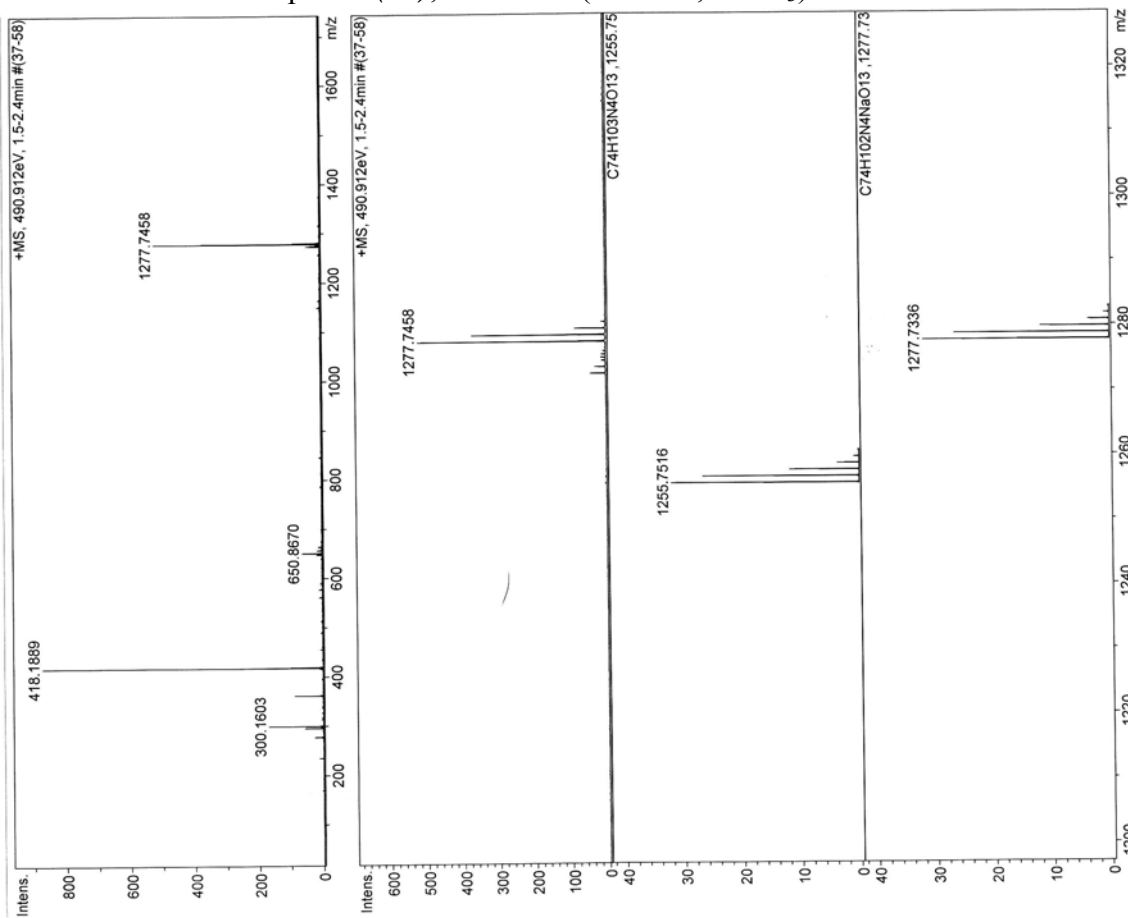


Compound (37), $^{13}\text{C-NMR}$ (75 MHz, CDCl_3)

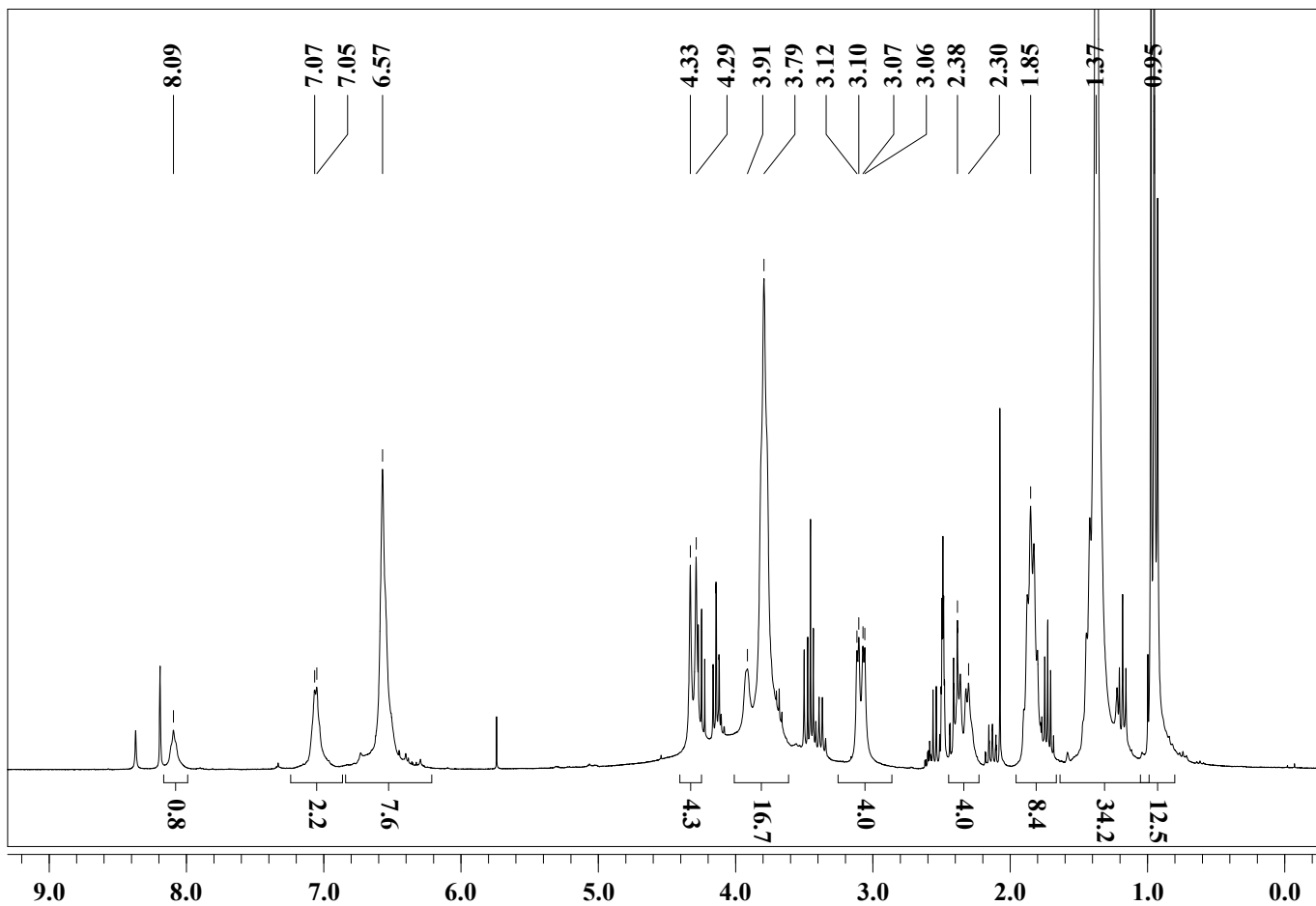
MS-Analyse: ESI-TOF

Analysis Name: E:\MS-Daten\HuWenbin\101201-Y6-4-101201-pos_01_21422.d\101201-Y6-4-101201-pos_01_21422.
 Method: Karow
 Acquisition Date: 12/1/2010 4:59:25 PM
 Instrument: Bruker BioTOF III

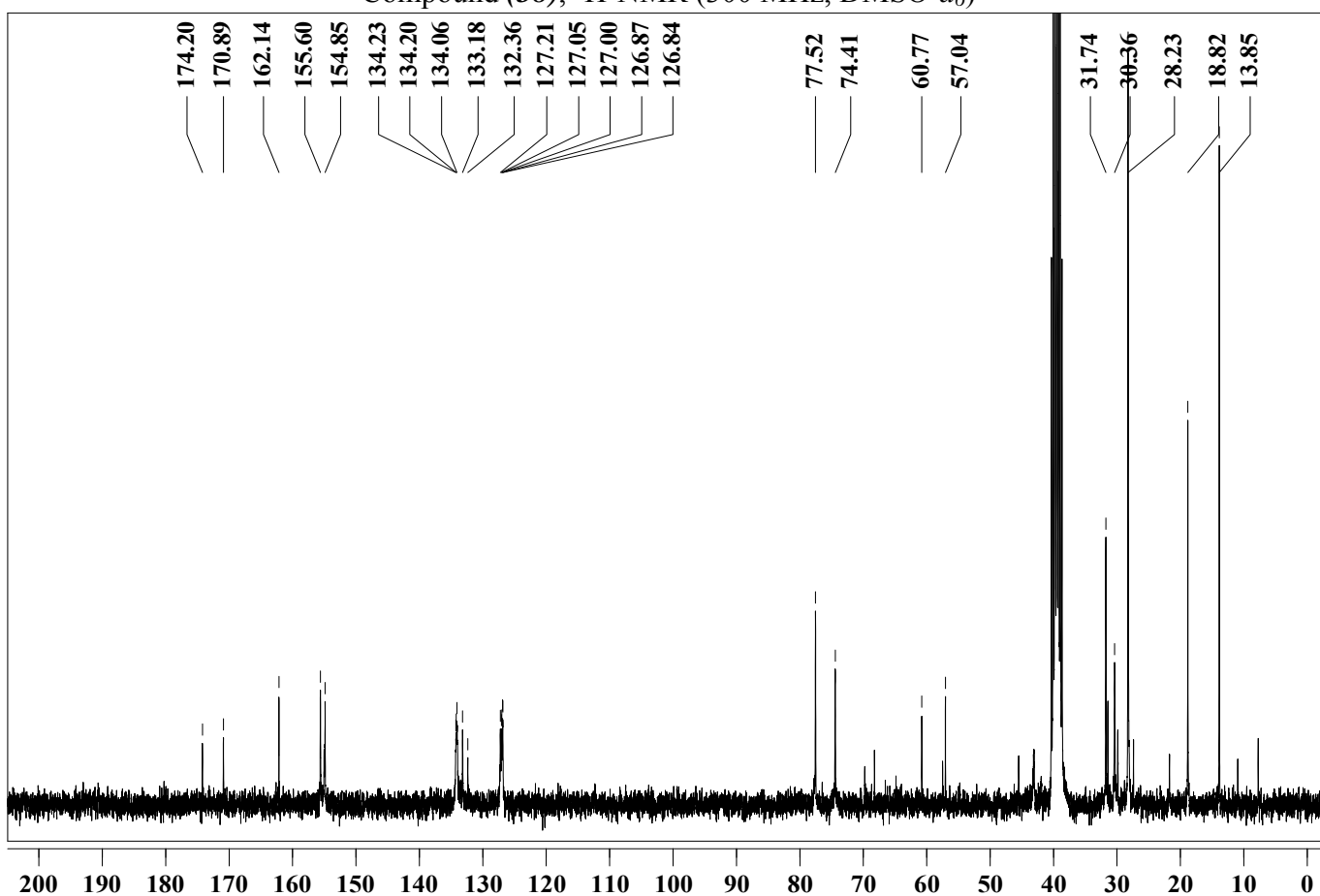
Comment: comment



Compound (37), MS (ESI-TOF, pos. CH_2Cl_2)



Compound (38), $^1\text{H-NMR}$ (300 MHz, $\text{DMSO-}d_6$)

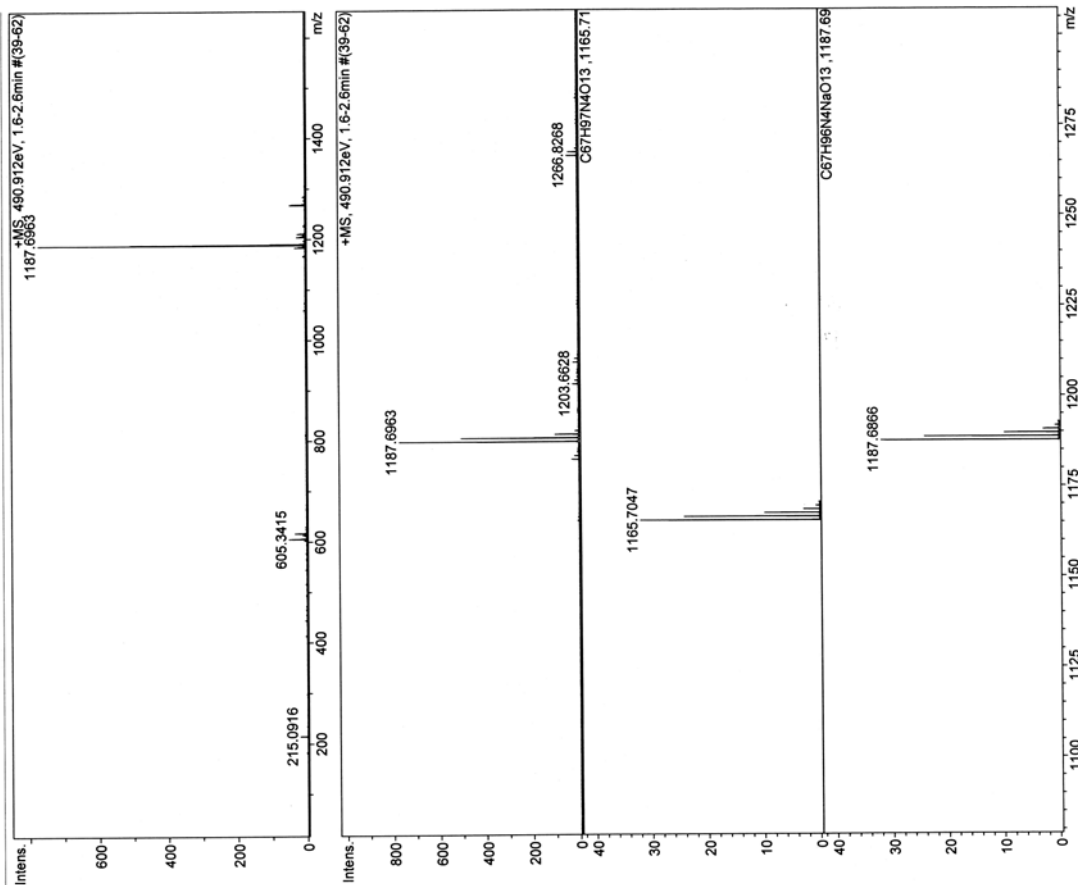


Compound (38), $^{13}\text{C-NMR}$ (75 MHz, $\text{DMSO-}d_6$)

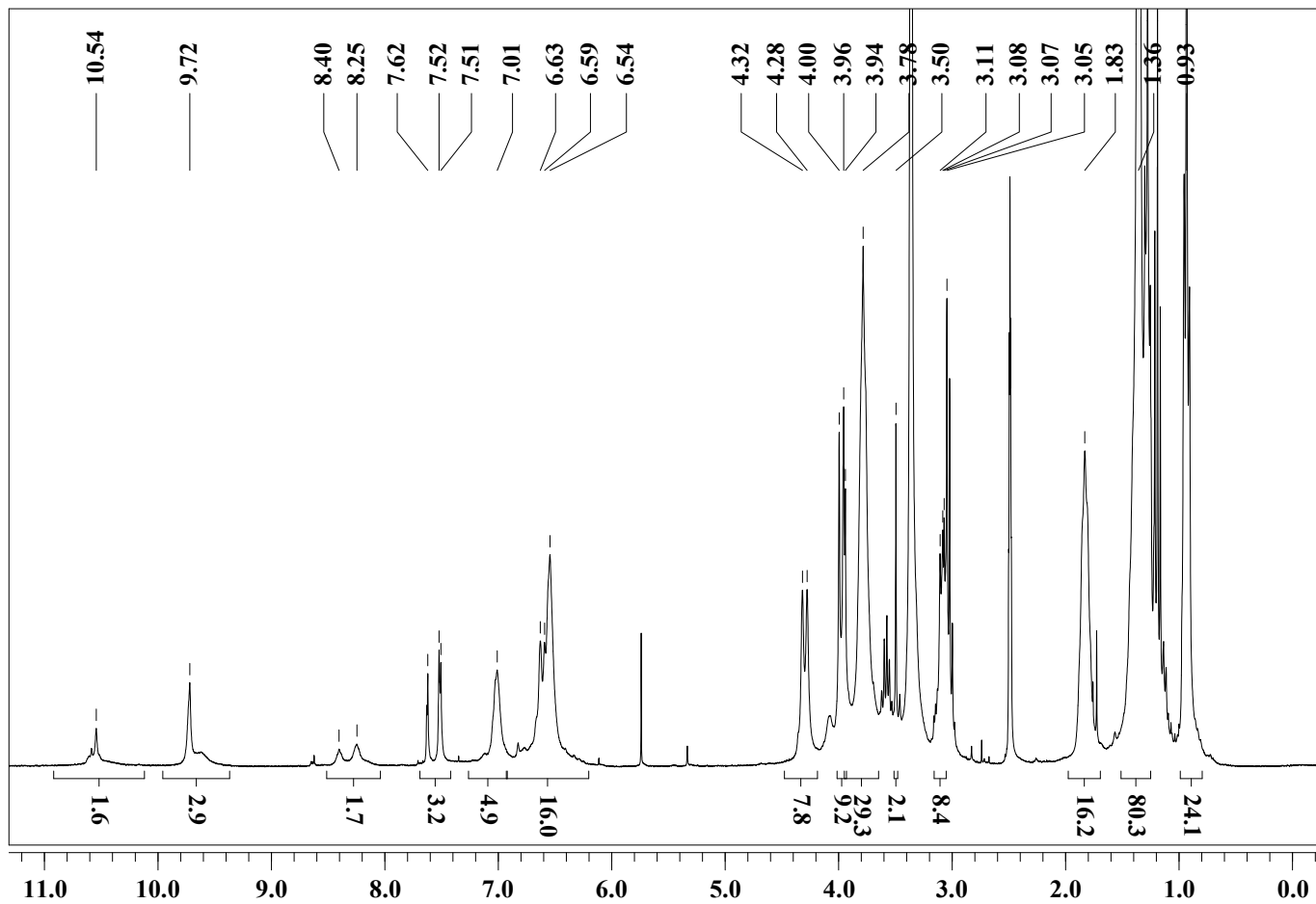
MS-Analyse: ESI-TOF

Analysis Name: E:\MS-Daten\HuWenbin\110117-Y5-1-110116-pos_01_21780.d\110117-Y5-1-110116-pos_01_21780.
Method: #methodname
Operator: Karow
Instrument: Bruker BioTOF III
Acquisition Date: 1/17/2011 12:16:10 PM

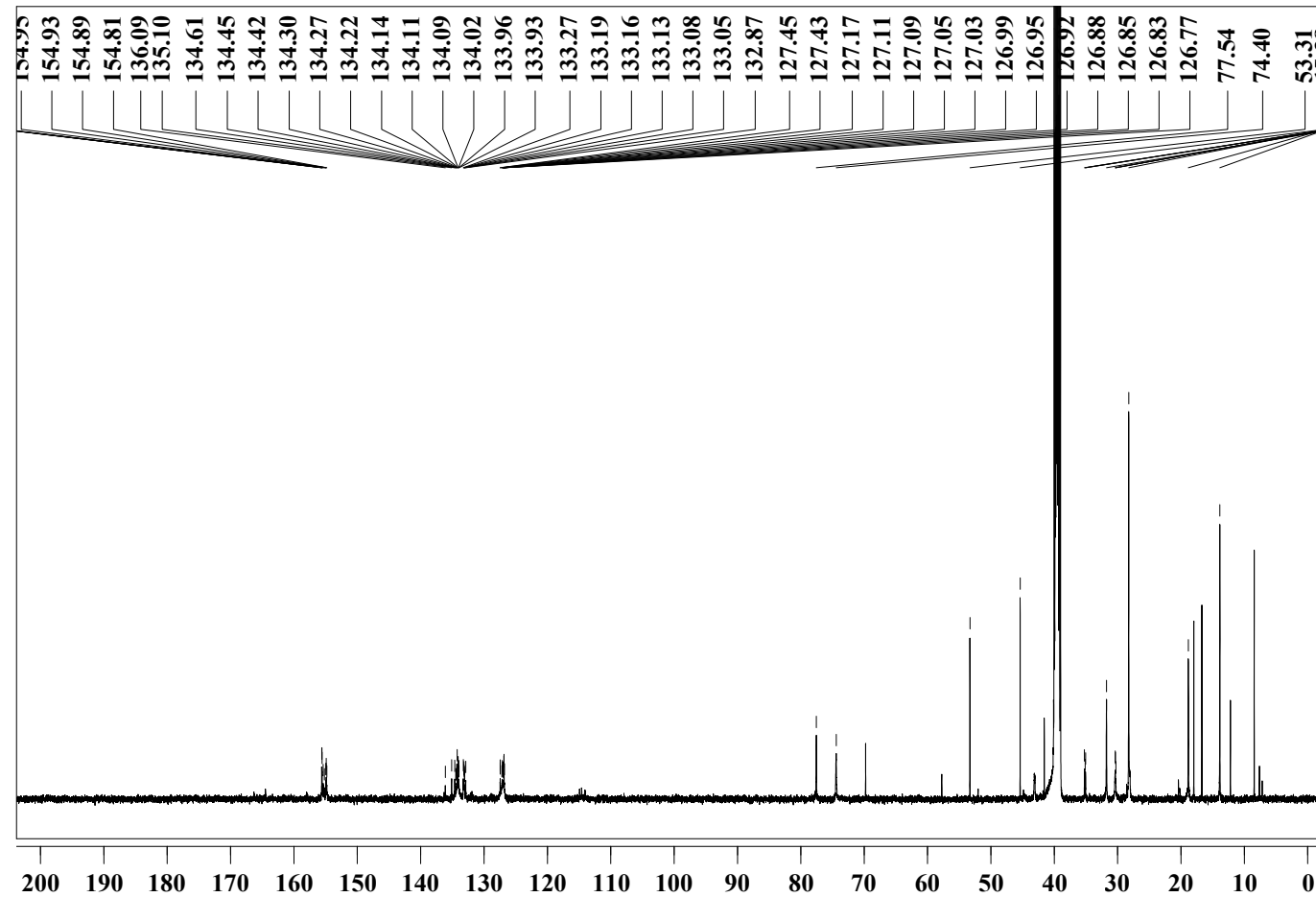
Comment: comment



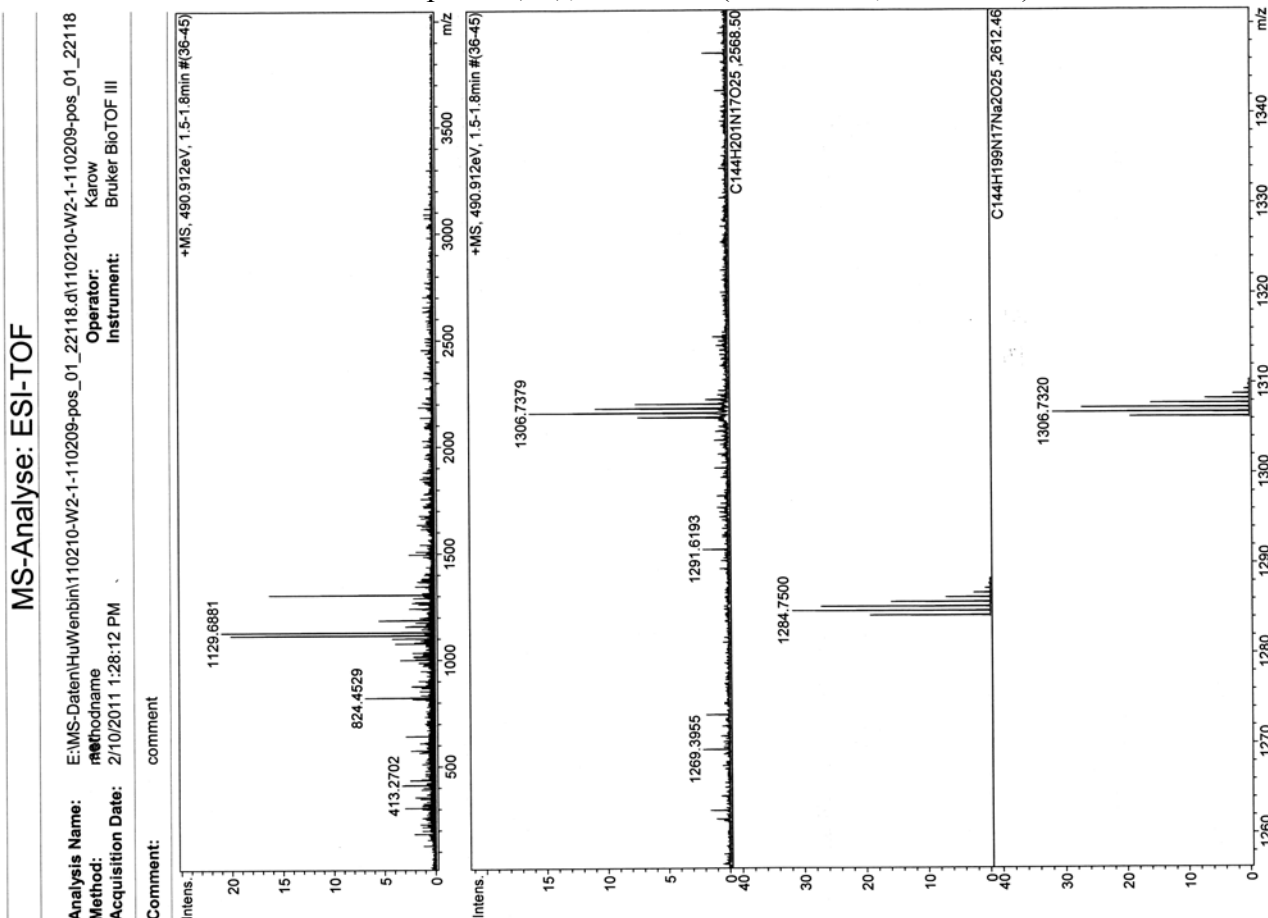
Compound (38), MS (ESI-TOF, pos. CH₂Cl₂)



Compound (39), ¹H-NMR (300 MHz, DMSO-*d*₆)



Compound (39), ^{13}C -NMR (125.6 MHz, $\text{DMSO-}d_6$)

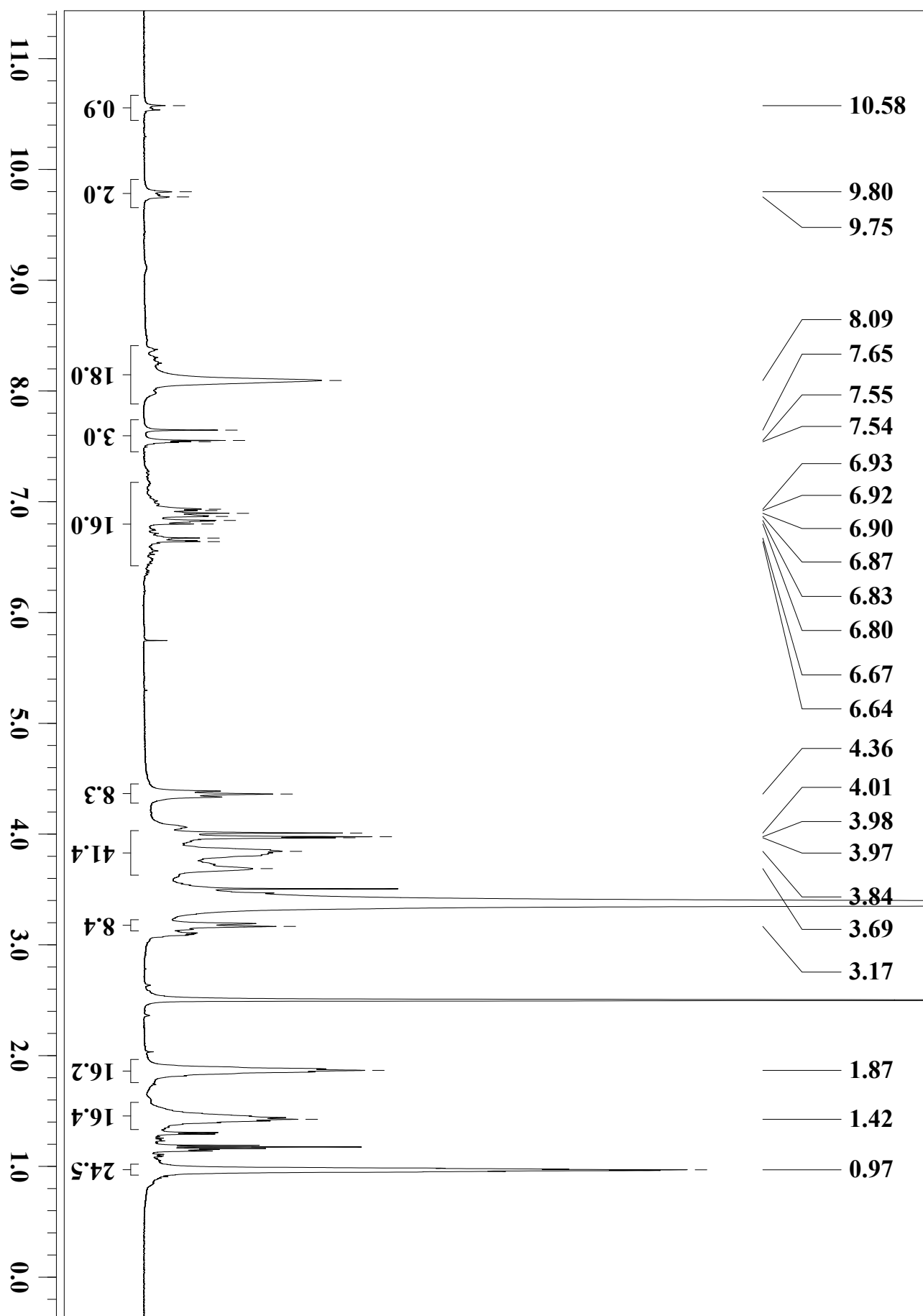


Compound (39), MS (ESI-TOF, pos. CH_2Cl_2)

MS-Analyse: ESI-TOF

Analysis Name: E:\MS-Daten\HuWenbin\110210-W2-1-110209-pos_01_22118.d\110210-W2-1-110209-pos_01_22118
 Method: r1methodname Karow
 Acquisition Date: 2/10/2011 1:28:12 PM Operator: Bruker BioTOF III
 Instrument: Bruker BioTOF III

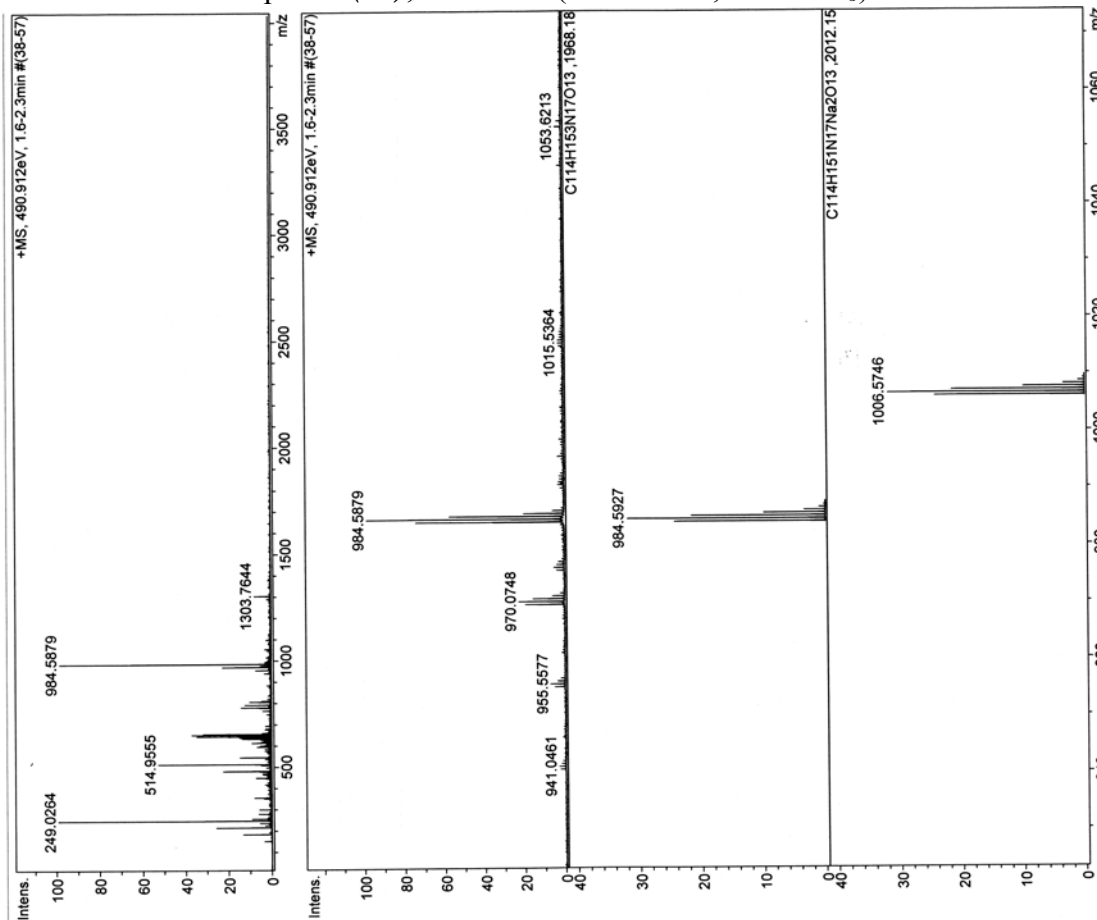
Comment: comment



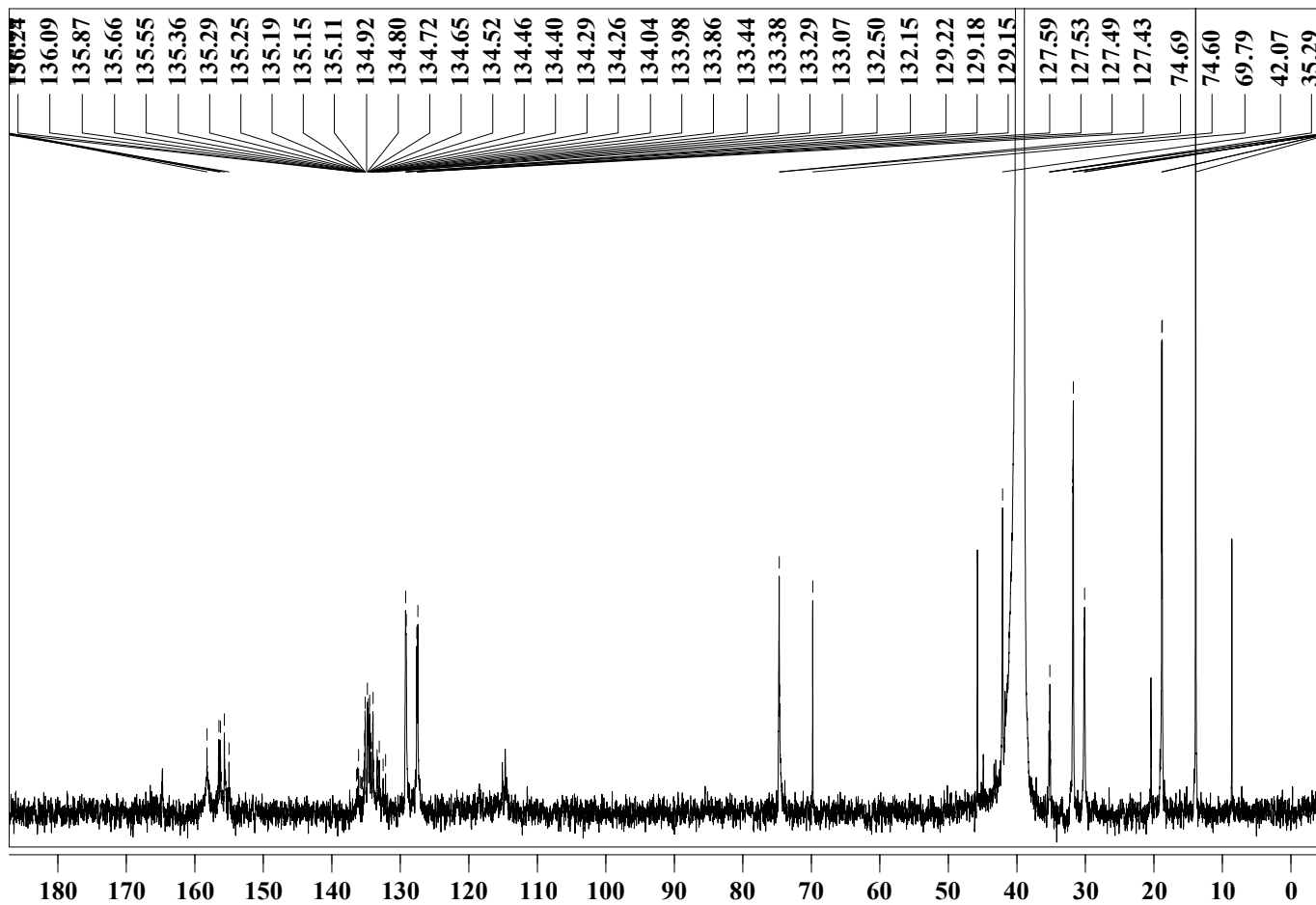
Compound (40), ¹H-NMR (500 MHz, DMSO-d₆)

MS-Analyse: ESI-TOF

Analysis Name: E:\MS-Daten\HuWenbin\110210-Z2-all-1-110209-pos_01_221119.d\110210-Z2-all-1-110209-pos_01_2
 Method: #Hoffmann Karow
 Operator: Karow
 Acquisition Date: 2/10/2011 1:34:22 PM Instrument: Bruker BioTOF III
 Comment: comment



Compound (40), MS (ESI-TOF, pos. CH₂Cl₂, free base)



Compound (40), ¹³C-NMR (125.6 MHz, DMSO-*d*₆)

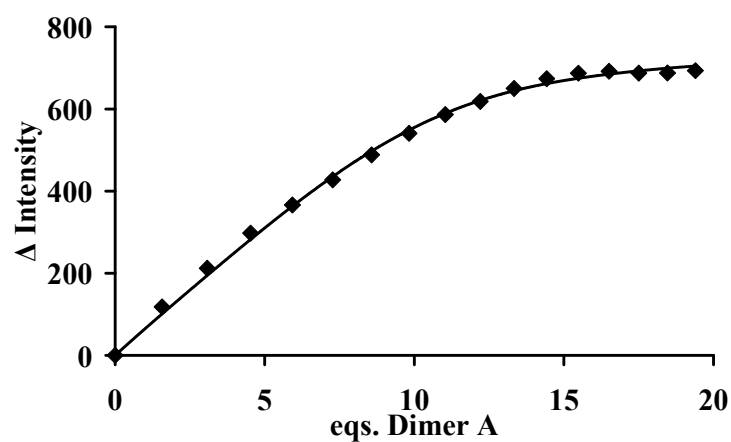
6.5 Data of Fluorescence Titration Experiments

No. 1

DNA: (dGdC)₁₀-(dGdC)₁₀ **ligand:** Dimer A
C_{FL-DNA}: 1.0×10⁻⁶ M **C_{ligand}:** 8.0×10⁻⁵ M
Buffer: 2 mM HEPES and 150 mM NaCl in water. pH=7.10

Addition ligand (μL)	Total volume (μL)	C _{FL-DNA} (mol/L)	C _{ligand} (mol/L)	ratio (C _{ligand} /C _{FL-DNA})	fluorescence emission	relative emission difference
0	500	1.00E-06	0.00E+00	0.00	949.593	0.000
10	510	1.00E-06	1.57E-06	1.57	831.428	118.165
20	520	1.00E-06	3.08E-06	3.08	737.502	212.091
30	530	1.00E-06	4.53E-06	4.53	651.990	297.603
40	540	1.00E-06	5.93E-06	5.93	583.291	366.302
50	550	1.00E-06	7.27E-06	7.27	522.218	427.375
60	560	1.00E-06	8.57E-06	8.57	461.330	488.263
70	570	1.00E-06	9.82E-06	9.82	408.851	540.742
80	580	1.00E-06	1.10E-05	11.03	363.267	586.326
90	590	1.00E-06	1.22E-05	12.20	331.192	618.401
100	600	1.00E-06	1.33E-05	13.33	299.662	649.931
110	610	1.00E-06	1.44E-05	14.43	275.918	673.675
120	620	1.00E-06	1.55E-05	15.48	262.613	686.980
130	630	1.00E-06	1.65E-05	16.51	257.894	691.699
140	640	1.00E-06	1.75E-05	17.50	262.355	687.238
150	650	1.00E-06	1.85E-05	18.46	262.054	687.539
160	660	1.00E-06	1.94E-05	19.39	256.188	693.405

The graphical representation of the titration curve:



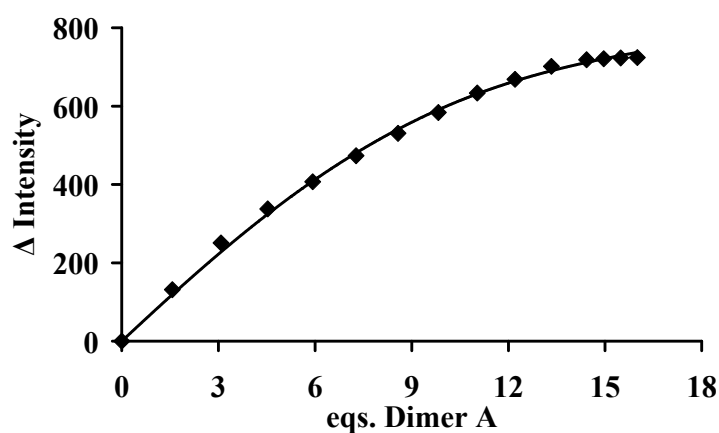
K_a(M⁻¹): 1.4×10⁶ **Statistical error:** 23%
Stoichiometry: 11:1 (ligand : DNA duplex)

No. 2

DNA: (dAdT)₁₀-(dAdT)₁₀ **ligand:** Dimer A
C_{FI-DNA}: 1.0×10⁻⁶ M **C_{ligand}:** 8.0×10⁻⁵ M
Buffer: 2 mM HEPES and 150 mM NaCl in water. pH=7.10

Addition ligand (μL)	Total volume (μL)	C _{FI-DNA} (mol/L)	C _{ligand} (mol/L)	ratio (C _{ligand} /C _{FI-DNA})	fluorescence emission	relative emission difference
0	500	1.00E-06	0.00E+00	0.00	925.456	0.000
10	510	1.00E-06	1.57E-06	1.57	794.207	131.249
20	520	1.00E-06	3.08E-06	3.08	674.742	250.714
30	530	1.00E-06	4.53E-06	4.53	587.920	337.536
40	540	1.00E-06	5.93E-06	5.93	518.475	406.981
50	550	1.00E-06	7.27E-06	7.27	452.032	473.424
60	560	1.00E-06	8.57E-06	8.57	394.860	530.596
70	570	1.00E-06	9.82E-06	9.82	341.693	583.763
80	580	1.00E-06	1.10E-05	11.03	292.004	633.452
90	590	1.00E-06	1.22E-05	12.20	256.903	668.553
100	600	1.00E-06	1.33E-05	13.33	223.876	701.580
110	610	1.00E-06	1.44E-05	14.43	206.986	718.470
115	615	1.00E-06	1.50E-05	14.96	204.389	721.067
120	620	1.00E-06	1.55E-05	15.48	202.434	723.022
125	625	1.00E-06	1.60E-05	16.00	201.526	723.930

The graphical representation of the titration curve:



K_a(M⁻¹): 5.6×10⁵ **Statistical error:** 24%
Stoichiometry: 10:1 (ligand : DNA duplex)

No. 3

RNA: A₂₀ - U₂₀

ligand: Dimer A

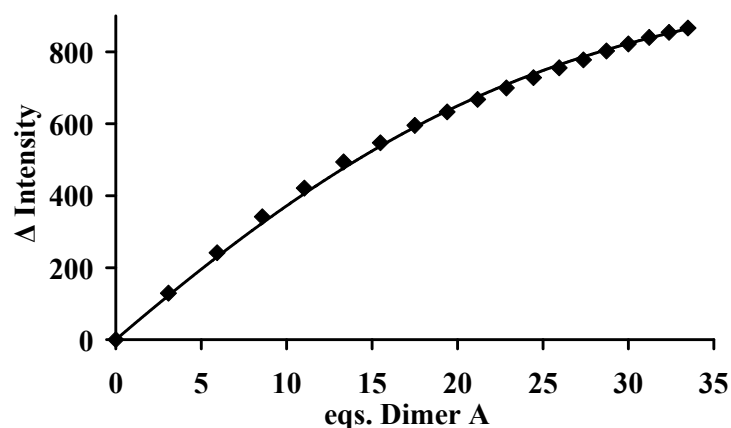
C_{FI-RNA}: 1.0×10⁻⁶ M

C_{ligand}: 8.0×10⁻⁵ M

Buffer: 2 mM HEPES and 150 mM NaCl in water. pH=7.10

Addition ligand (μL)	Total volume (μL)	C _{FI-RNA} (mol/L)	C _{ligand} (mol/L)	ratio (C _{ligand} /C _{FI-RNA})	fluorescence emission	relative emission difference
0	500	1.00E-06	0.00E+00	0.00	958.694	0.000
20	520	1.00E-06	3.08E-06	3.08	829.468	129.226
40	540	1.00E-06	5.93E-06	5.93	717.284	241.410
60	560	1.00E-06	8.57E-06	8.57	617.211	341.483
80	580	1.00E-06	1.10E-05	11.03	537.631	421.063
100	600	1.00E-06	1.33E-05	13.33	464.814	493.880
120	620	1.00E-06	1.55E-05	15.48	411.713	546.981
140	640	1.00E-06	1.75E-05	17.50	363.283	595.411
160	660	1.00E-06	1.94E-05	19.39	325.696	632.998
180	680	1.00E-06	2.12E-05	21.18	291.066	667.628
200	700	1.00E-06	2.29E-05	22.86	259.087	699.607
220	720	1.00E-06	2.44E-05	24.44	230.478	728.216
240	740	1.00E-06	2.59E-05	25.95	203.367	755.327
260	760	1.00E-06	2.74E-05	27.37	181.231	777.463
280	780	1.00E-06	2.87E-05	28.72	156.363	802.331
300	800	1.00E-06	3.00E-05	30.00	136.883	821.811
320	820	1.00E-06	3.12E-05	31.22	118.741	839.953
340	840	1.00E-06	3.24E-05	32.38	104.630	854.064
360	860	1.00E-06	3.35E-05	33.49	92.595	866.099

The graphical representation of the titration curve:



K_a (M⁻¹): 1.7×10⁵

Statistical error: 22%

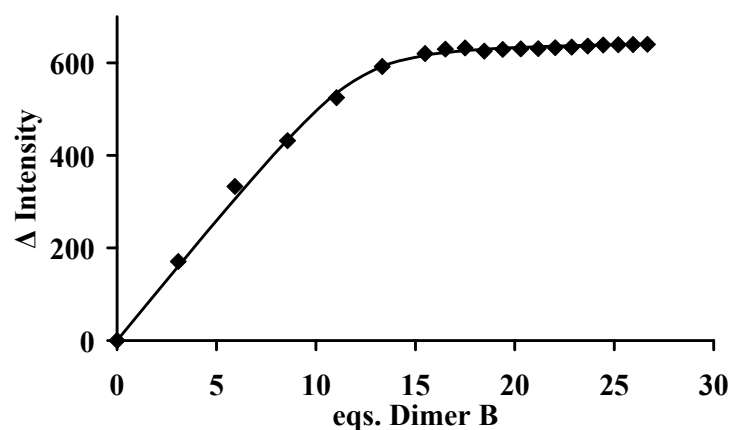
Stoichiometry: 23:1 (ligand : RNA duplex)

No. 4

DNA: (dGdC)₁₀-(dGdC)₁₀ **ligand:** Dimer B
C_{FI-DNA}: 1.0×10⁻⁶ M **C_{ligand}:** 8.0×10⁻⁵ M
Buffer: 2 mM HEPES and 150 mM NaCl in water. pH=7.10

Addition ligand (μL)	Total volume (μL)	C_{FI-DNA} (mol/L)	C_{ligand} (mol/L)	ratio (C_{ligand}/C_{FI-DNA})	fluorescence emission	relative emission difference
0	500	1.00E-06	0.00E+00	0.00	949.710	0.000
20	520	1.00E-06	3.08E-06	3.08	778.854	170.856
40	540	1.00E-06	5.93E-06	5.93	616.658	333.052
60	560	1.00E-06	8.57E-06	8.57	517.894	431.816
80	580	1.00E-06	1.10E-05	11.03	424.846	524.864
100	600	1.00E-06	1.33E-05	13.33	357.429	592.281
120	620	1.00E-06	1.55E-05	15.48	329.447	620.263
130	630	1.00E-06	1.65E-05	16.51	320.008	629.702
140	640	1.00E-06	1.75E-05	17.50	317.345	632.365
150	650	1.00E-06	1.85E-05	18.46	324.119	625.591
160	660	1.00E-06	1.94E-05	19.39	320.564	629.146
170	670	1.00E-06	2.03E-05	20.30	319.457	630.253
180	680	1.00E-06	2.12E-05	21.18	318.920	630.790
190	690	1.00E-06	2.20E-05	22.03	316.749	632.961
200	700	1.00E-06	2.29E-05	22.86	315.587	634.123
210	710	1.00E-06	2.37E-05	23.66	313.229	636.481
220	720	1.00E-06	2.44E-05	24.44	311.044	638.666
230	730	1.00E-06	2.52E-05	25.21	310.403	639.307
240	740	1.00E-06	2.59E-05	25.95	310.022	639.688
250	750	1.00E-06	2.67E-05	26.67	309.447	640.263

The graphical representation of the titration curve:



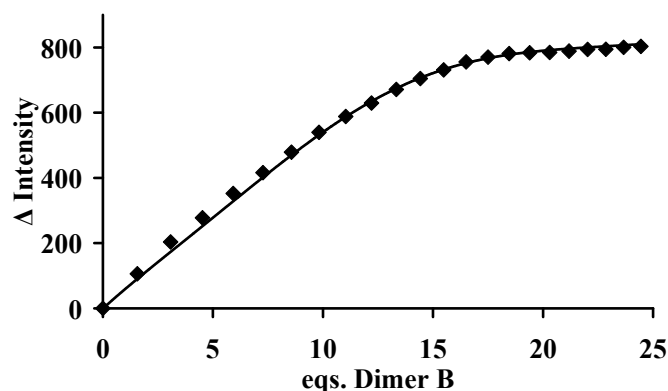
K_a (M⁻¹): 4.7×10⁶ **Statistical error:** 22%
Stoichiometry: 12:1 (ligand : DNA duplex)

No. 5

DNA: (dAdT)₁₀-(dAdT)₁₀ **ligand:** Dimer B
C_{FI-DNA}: 1.0×10⁻⁶ M **C_{ligand}:** 8.0×10⁻⁵ M
Buffer: 2 mM HEPES and 150 mM NaCl in water. pH=7.10

Addition ligand (μL)	Total volume (μL)	C _{FI-DNA} (mol/L)	C _{ligand} (mol/L)	ratio (C _{ligand} /C _{FI-DNA})	fluorescence emission	relative emission difference
0	500	1.00E-06	0.00E+00	0.00	971.039	0.000
10	510	1.00E-06	1.57E-06	1.57	865.253	105.786
20	520	1.00E-06	3.08E-06	3.08	767.641	203.398
30	530	1.00E-06	4.53E-06	4.53	693.458	277.581
40	540	1.00E-06	5.93E-06	5.93	618.422	352.617
50	550	1.00E-06	7.27E-06	7.27	555.051	415.988
60	560	1.00E-06	8.57E-06	8.57	491.890	479.149
70	570	1.00E-06	9.82E-06	9.82	431.115	539.924
80	580	1.00E-06	1.10E-05	11.03	382.591	588.448
90	590	1.00E-06	1.22E-05	12.20	341.238	629.801
100	600	1.00E-06	1.33E-05	13.33	299.599	671.440
110	610	1.00E-06	1.44E-05	14.43	266.419	704.620
120	620	1.00E-06	1.55E-05	15.48	239.771	731.268
130	630	1.00E-06	1.65E-05	16.51	215.138	755.901
140	640	1.00E-06	1.75E-05	17.50	200.450	770.589
150	650	1.00E-06	1.85E-05	18.46	189.764	781.275
160	660	1.00E-06	1.94E-05	19.39	187.012	784.027
170	670	1.00E-06	2.03E-05	20.30	186.284	784.755
180	680	1.00E-06	2.12E-05	21.18	182.127	788.912
190	690	1.00E-06	2.20E-05	22.03	176.928	794.111
200	700	1.00E-06	2.29E-05	22.86	176.477	794.562
210	710	1.00E-06	2.37E-05	23.66	170.802	800.237
220	720	1.00E-06	2.44E-05	24.44	167.719	803.320

The graphical representation of the titration curve:



K_a (M⁻¹): 2.3×10⁶ **Statistical error:** 24%

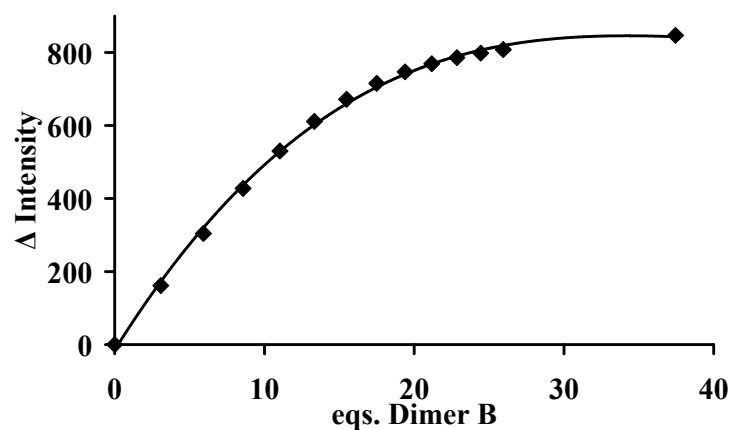
Stoichiometry: 14:1 (ligand : DNA duplex)

No. 6

RNA: A₂₀ - U₂₀ ligand: Dimer B
 C_{FI-RNA}: 1.0×10⁻⁶ M C_{ligand}: 8.0×10⁻⁵ M
 Buffer: 2 mM HEPES and 150 mM NaCl in water. pH=7.10

Addition ligand (μL)	Total volume (μL)	C _{FI-RNA} (mol/L)	C _{ligand} (mol/L)	ratio (C _{ligand} /C _{FI-RNA})	fluorescence emission	relative emission difference
0	500	1.00E-06	0.00E+00	0.00	972.917	0.000
20	520	1.00E-06	3.08E-06	3.08	819.784	153.133
40	540	1.00E-06	5.93E-06	5.93	670.850	302.067
60	560	1.00E-06	8.57E-06	8.57	540.366	432.551
80	580	1.00E-06	1.10E-05	11.03	446.862	526.055
100	600	1.00E-06	1.33E-05	13.33	360.843	612.074
120	620	1.00E-06	1.55E-05	15.48	302.185	670.732
140	640	1.00E-06	1.75E-05	17.50	262.228	710.689
160	660	1.00E-06	1.94E-05	19.39	231.650	741.267
180	680	1.00E-06	2.12E-05	21.18	201.064	771.853
200	700	1.00E-06	2.29E-05	22.86	181.781	791.136
220	720	1.00E-06	2.44E-05	24.44	168.780	804.137
240	740	1.00E-06	2.59E-05	25.95	156.866	816.051
440	940	1.00E-06	3.74E-05	37.45	134.000	838.917

The graphical representation of the titration curve:



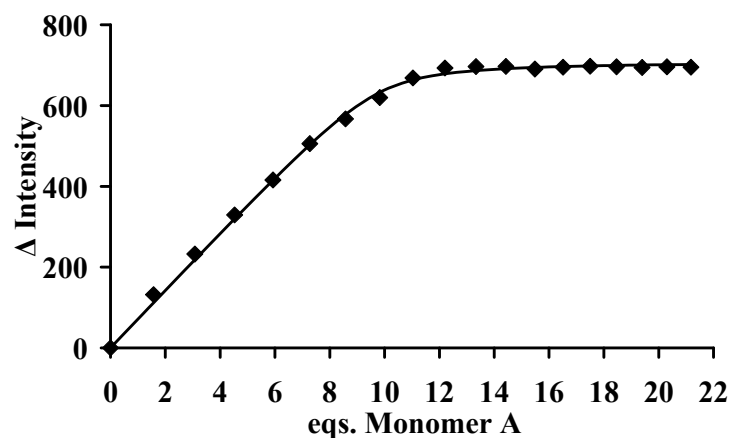
K_a (M⁻¹): 7.8×10⁵ Statistical error: 8%
 Stoichiometry: 15:1 (ligand : RNA duplex)

No. 7

DNA: (dGdC)₁₀-(dGdC)₁₀ **ligand:** Monomer A
C_{FI-DNA}: 1.0×10⁻⁶ M **C_{ligand}:** 8.0×10⁻⁵ M
Buffer: 2 mM HEPES and 150 mM NaCl in water. pH=7.10

Addition ligand (μL)	Total volume (μL)	C _{FI-DNA} (mol/L)	C _{ligand} (mol/L)	ratio (C _{ligand} /C _{FI-DNA})	fluorescence emission	relative emission difference
0	500	1.00E-06	0.00E+00	0.00	946.783	0.000
10	510	1.00E-06	1.57E-06	1.57	814.736	132.047
20	520	1.00E-06	3.08E-06	3.08	714.245	232.538
30	530	1.00E-06	4.53E-06	4.53	617.485	329.298
40	540	1.00E-06	5.93E-06	5.93	530.833	415.950
50	550	1.00E-06	7.27E-06	7.27	440.949	505.834
60	560	1.00E-06	8.57E-06	8.57	379.707	567.076
70	570	1.00E-06	9.82E-06	9.82	326.911	619.872
80	580	1.00E-06	1.10E-05	11.03	278.120	668.663
90	590	1.00E-06	1.22E-05	12.20	253.654	693.129
100	600	1.00E-06	1.33E-05	13.33	250.177	696.606
110	610	1.00E-06	1.44E-05	14.43	249.707	697.076
120	620	1.00E-06	1.55E-05	15.48	256.094	690.689
130	630	1.00E-06	1.65E-05	16.51	251.687	695.096
140	640	1.00E-06	1.75E-05	17.50	249.429	697.354
150	650	1.00E-06	1.85E-05	18.46	250.551	696.232
160	660	1.00E-06	1.94E-05	19.39	252.372	694.411
170	670	1.00E-06	2.03E-05	20.30	250.749	696.034
180	680	1.00E-06	2.12E-05	21.18	251.621	695.162

The graphical representation of the titration curve:



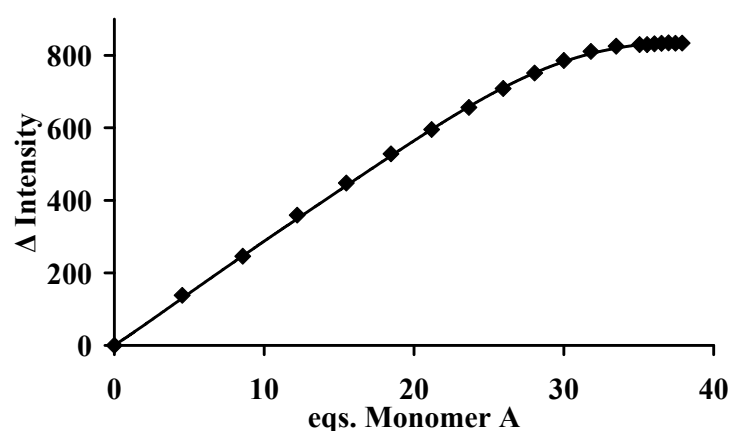
K_a (M⁻¹): 7.7×10⁶ **Statistical error:** 25%
Stoichiometry: 10:1 (ligand : DNA duplex)

No. 8

DNA: (dAdT)₁₀-(dAdT)₁₀ **ligand:** Monomer A
C_{FI-DNA}: 1.0×10⁻⁶ M **C_{ligand}:** 8.0×10⁻⁵ M
Buffer: 2 mM HEPES and 150 mM NaCl in water. pH=7.10

Addition ligand (μL)	Total volume (μL)	C_{FI-DNA} (mol/L)	C_{ligand} (mol/L)	ratio (C_{ligand}/C_{FI-DNA})	fluorescence emission	relative emission difference
0	500	1.00E-06	0.00E+00	0.00	975.099	0.000
30	530	1.00E-06	4.53E-06	4.53	837.054	138.045
60	560	1.00E-06	8.57E-06	8.57	729.216	245.883
90	590	1.00E-06	1.22E-05	12.20	615.945	359.154
120	620	1.00E-06	1.55E-05	15.48	527.273	447.826
150	650	1.00E-06	1.85E-05	18.46	446.865	528.234
180	680	1.00E-06	2.12E-05	21.18	379.797	595.302
210	710	1.00E-06	2.37E-05	23.66	318.825	656.274
240	740	1.00E-06	2.59E-05	25.95	266.625	708.474
270	770	1.00E-06	2.81E-05	28.05	223.813	751.286
300	800	1.00E-06	3.00E-05	30.00	189.313	785.786
330	830	1.00E-06	3.18E-05	31.81	164.178	810.921
360	860	1.00E-06	3.35E-05	33.49	149.853	825.246
390	890	1.00E-06	3.51E-05	35.06	145.363	829.736
400	900	1.00E-06	3.56E-05	35.56	145.389	829.710
410	910	1.00E-06	3.60E-05	36.04	143.221	831.878
420	920	1.00E-06	3.65E-05	36.52	141.815	833.284
430	930	1.00E-06	3.70E-05	36.99	140.727	834.372
440	940	1.00E-06	3.74E-05	37.45	141.689	833.410
450	950	1.00E-06	3.79E-05	37.89	141.185	833.914
460	960	1.00E-06	3.83E-05	38.33	142.059	833.040

The graphical representation of the titration curve:



K_a (M⁻¹): 2.9×10⁶ **Statistical error:** 20%

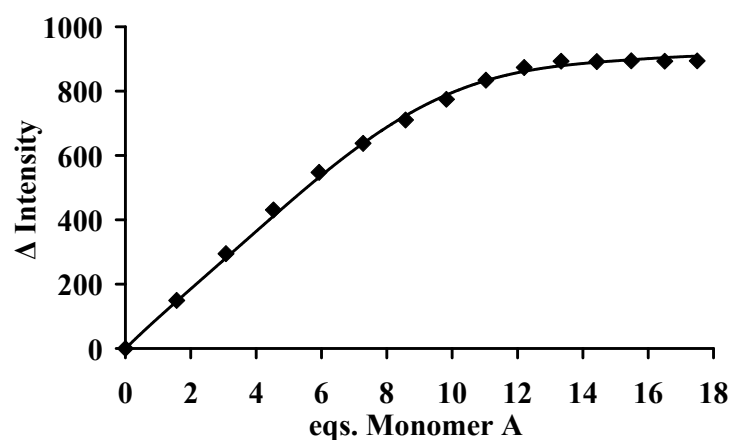
Stoichiometry: 30:1 (ligand : DNA duplex)

No. 9

RNA: A₂₀ - U₂₀ ligand: Monomer A
 C_{FI-RNA}: 1.0×10⁻⁶ M C_{ligand}: 8.0×10⁻⁵ M
 Buffer: 2 mM HEPES and 150 mM NaCl in water. pH=7.10

Addition ligand (μL)	Total volume (μL)	C _{FI-RNA} (mol/L)	C _{ligand} (mol/L)	ratio (C _{ligand} /C _{FI-RNA})	fluorescence emission	relative emission difference
0	500	1.00E-06	0.00E+00	0.00	990.965	0.000
10	510	1.00E-06	1.57E-06	1.57	841.446	149.519
20	520	1.00E-06	3.08E-06	3.08	696.212	294.753
30	530	1.00E-06	4.53E-06	4.53	560.258	430.707
40	540	1.00E-06	5.93E-06	5.93	443.353	547.612
50	550	1.00E-06	7.27E-06	7.27	353.329	637.636
60	560	1.00E-06	8.57E-06	8.57	280.664	710.301
70	570	1.00E-06	9.82E-06	9.82	216.196	774.769
80	580	1.00E-06	1.10E-05	11.03	156.910	834.055
90	590	1.00E-06	1.22E-05	12.20	117.296	873.669
100	600	1.00E-06	1.33E-05	13.33	97.756	893.209
110	610	1.00E-06	1.44E-05	14.43	98.893	892.072
120	620	1.00E-06	1.55E-05	15.48	96.666	894.300
130	630	1.00E-06	1.65E-05	16.51	97.800	893.165
140	640	1.00E-06	1.75E-05	17.50	96.779	894.186

The graphical representation of the titration curve:



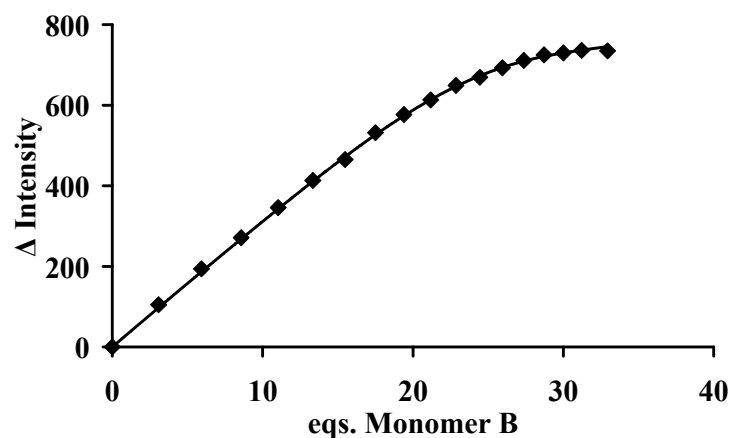
K_a (M⁻¹): 3.1×10⁶ Statistical error: 24%
 Stoichiometry: 10:1 (ligand : RNA duplex)

No. 10

DNA: (dGdC)₁₀-(dGdC)₁₀ **ligand:** Monomer B
C_{FI-DNA}: 1.0×10⁻⁶ M **C_{ligand}:** 8.0×10⁻⁵ M
Buffer: 2 mM HEPES and 150 mM NaCl in water. pH=7.10

Addition ligand (μL)	Total volume (μL)	C _{FI-DNA} (mol/L)	C _{ligand} (mol/L)	ratio (C _{ligand} /C _{FI-DNA})	fluorescence emission	relative emission difference
0	500	1.00E-06	0.00E+00	0.00	971.194	0.000
20	520	1.00E-06	3.08E-06	3.08	866.438	104.756
40	540	1.00E-06	5.93E-06	5.93	777.464	193.730
60	560	1.00E-06	8.57E-06	8.57	700.128	271.066
80	580	1.00E-06	1.10E-05	11.03	625.464	345.730
100	600	1.00E-06	1.33E-05	13.33	557.955	413.239
120	620	1.00E-06	1.55E-05	15.48	506.162	465.032
140	640	1.00E-06	1.75E-05	17.50	439.298	531.896
160	660	1.00E-06	1.94E-05	19.39	394.260	576.934
180	680	1.00E-06	2.12E-05	21.18	357.982	613.212
200	700	1.00E-06	2.29E-05	22.86	322.142	649.052
220	720	1.00E-06	2.44E-05	24.44	301.887	669.307
240	740	1.00E-06	2.59E-05	25.95	278.301	692.893
260	760	1.00E-06	2.74E-05	27.37	259.983	711.211
280	780	1.00E-06	2.87E-05	28.72	246.148	725.046
300	800	1.00E-06	3.00E-05	30.00	241.306	729.888
320	820	1.00E-06	3.12E-05	31.22	235.147	736.047
350	850	1.00E-06	3.29E-05	32.94	236.417	734.777

The graphical representation of the titration curve:



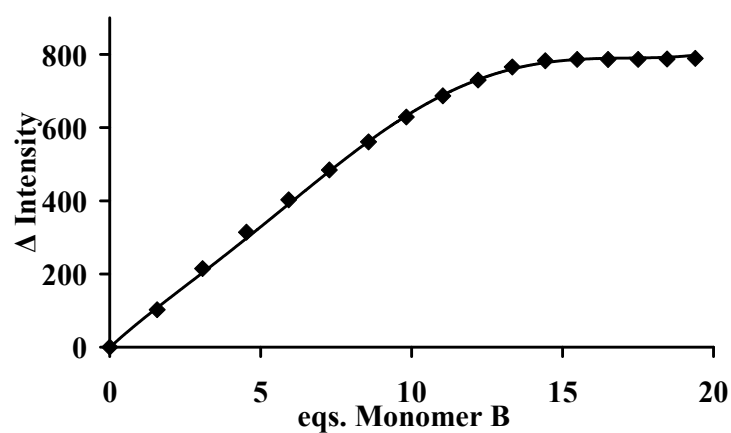
K_a (M⁻¹): 1.4×10⁶ **Statistical error:** 24%
Stoichiometry: 18:1 (ligand : DNA duplex)

No. 11

DNA: (dAdT)₁₀-(dAdT)₁₀ **ligand:** Monomer B
C_{FI-DNA}: 1.0×10⁻⁶ M **C_{ligand}:** 8.0×10⁻⁵ M
Buffer: 2 mM HEPES and 150 mM NaCl in water. pH=7.10

Addition ligand (μL)	Total volume (μL)	C _{FI-DNA} (mol/L)	C _{ligand} (mol/L)	ratio (C _{ligand} /C _{FI-DNA})	fluorescence emission	relative emission difference
0	500	1.00E-06	0.00E+00	0.00	955.704	0.000
10	510	1.00E-06	1.57E-06	1.57	853.336	102.368
20	520	1.00E-06	3.08E-06	3.08	740.908	214.796
30	530	1.00E-06	4.53E-06	4.53	641.592	314.112
40	540	1.00E-06	5.93E-06	5.93	553.095	402.609
50	550	1.00E-06	7.27E-06	7.27	471.362	484.342
60	560	1.00E-06	8.57E-06	8.57	394.624	561.080
70	570	1.00E-06	9.82E-06	9.82	326.730	628.974
80	580	1.00E-06	1.10E-05	11.03	268.800	686.904
90	590	1.00E-06	1.22E-05	12.20	225.635	730.069
100	600	1.00E-06	1.33E-05	13.33	189.943	765.761
110	610	1.00E-06	1.44E-05	14.43	172.917	782.787
120	620	1.00E-06	1.55E-05	15.48	169.347	786.357
130	630	1.00E-06	1.65E-05	16.51	169.501	786.203
140	640	1.00E-06	1.75E-05	17.50	169.240	786.464
150	650	1.00E-06	1.85E-05	18.46	168.360	787.344
160	660	1.00E-06	1.94E-05	19.39	166.567	789.137

The graphical representation of the titration curve:



K_a (M⁻¹): 7.3×10⁶ **Statistical error:** 23%

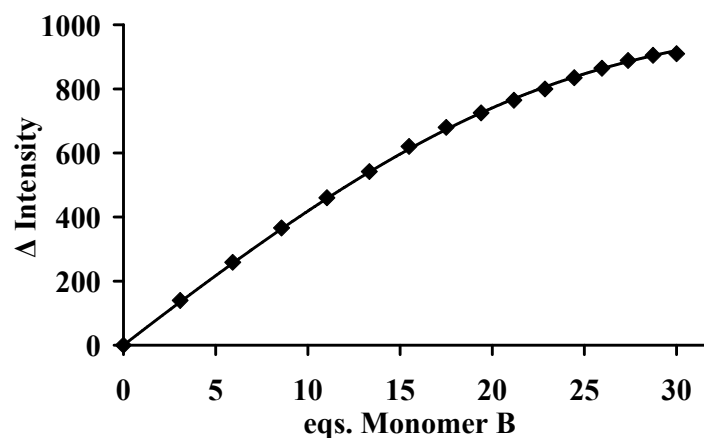
Stoichiometry: 12:1 (ligand : DNA duplex)

No. 12

RNA: A₂₀ - U₂₀ **ligand:** Monomer B
C_{FI-RNA}: 1.0×10⁻⁶ M **C_{ligand}:** 8.0×10⁻⁵ M
Buffer: 2 mM HEPES and 150 mM NaCl in water. pH=7.10

Addition ligand (μL)	Total volume (μL)	C _{FI-RNA} (mol/L)	C _{ligand} (mol/L)	ratio (C _{ligand} /C _{FI-RNA})	fluorescence emission	relative emission difference
0	500	1.00E-06	0.00E+00	0.00	990.261	0.000
20	520	1.00E-06	3.08E-06	3.08	850.433	139.828
40	540	1.00E-06	5.93E-06	5.93	731.555	258.706
60	560	1.00E-06	8.57E-06	8.57	624.199	366.062
80	580	1.00E-06	1.10E-05	11.03	530.081	460.180
100	600	1.00E-06	1.33E-05	13.33	448.252	542.009
120	620	1.00E-06	1.55E-05	15.48	369.936	620.325
140	640	1.00E-06	1.75E-05	17.50	310.435	679.826
160	660	1.00E-06	1.94E-05	19.39	265.009	725.252
180	680	1.00E-06	2.12E-05	21.18	225.636	764.625
200	700	1.00E-06	2.29E-05	22.86	190.482	799.779
220	720	1.00E-06	2.44E-05	24.44	155.389	834.872
240	740	1.00E-06	2.59E-05	25.95	125.593	864.668
260	760	1.00E-06	2.74E-05	27.37	101.429	888.832
280	780	1.00E-06	2.87E-05	28.72	85.465	904.796
300	800	1.00E-06	3.00E-05	30.00	80.380	909.881

The graphical representation of the titration curve:



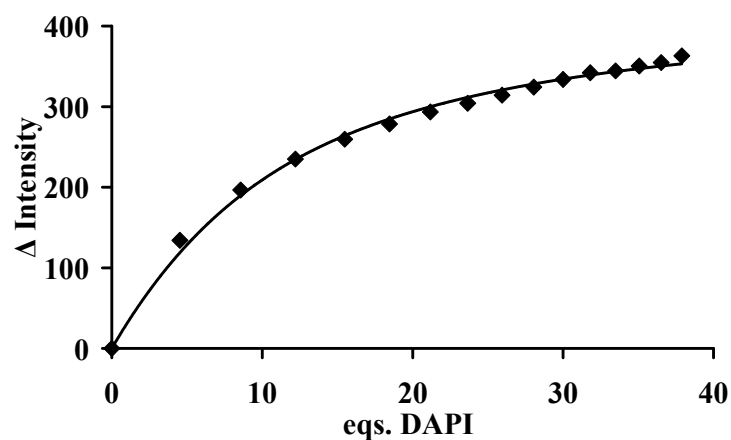
K_a (M⁻¹): 3.5×10⁵ **Statistical error:** 18%
Stoichiometry: 23:1 (ligand : RNA duplex)

No. 13

DNA: (dAdT)₁₀-(dAdT)₁₀ **ligand:** DAPI
C_{FI-DNA}: 1.0×10⁻⁶ M **C_{ligand}:** 8.0×10⁻⁵ M
Buffer: 2 mM HEPES and 150 mM NaCl in water. pH=7.10

Addition ligand (μL)	Total volume (μL)	C _{FI-DNA} (mol/L)	C _{ligand} (mol/L)	ratio (C _{ligand} /C _{FI-DNA})	fluorescence emission	relative emission difference
0	500	1.00E-06	0.00E+00	0.00	961.732	0.000
30	530	1.00E-06	4.53E-06	4.53	827.569	134.163
60	560	1.00E-06	8.57E-06	8.57	765.166	196.566
90	590	1.00E-06	1.22E-05	12.20	726.731	235.001
120	620	1.00E-06	1.55E-05	15.48	702.082	259.650
150	650	1.00E-06	1.85E-05	18.46	683.181	278.551
180	680	1.00E-06	2.12E-05	21.18	668.295	293.437
210	710	1.00E-06	2.37E-05	23.66	657.486	304.246
240	740	1.00E-06	2.59E-05	25.95	647.424	314.308
270	770	1.00E-06	2.81E-05	28.05	637.434	324.298
300	800	1.00E-06	3.00E-05	30.00	627.880	333.852
330	830	1.00E-06	3.18E-05	31.81	619.633	342.099
360	860	1.00E-06	3.35E-05	33.49	617.277	344.455
390	890	1.00E-06	3.51E-05	35.06	611.276	350.456
420	920	1.00E-06	3.65E-05	36.52	606.931	354.801
450	950	1.00E-06	3.79E-05	37.89	598.620	363.112

The graphical representation of the titration curve:



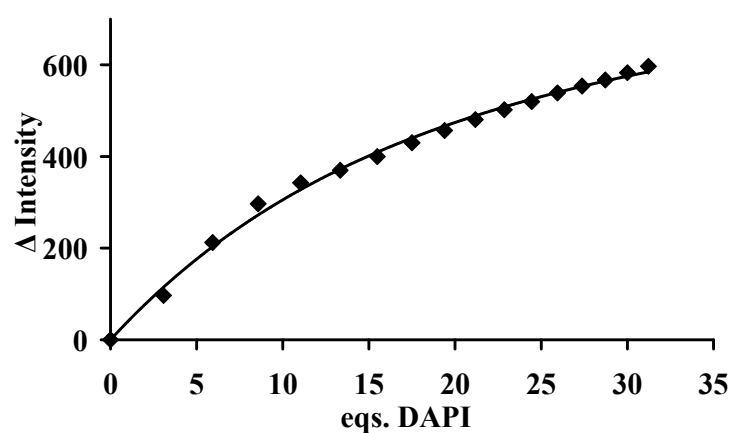
K_a (M⁻¹): 1.3×10⁵ **Statistical error:** 8%
Stoichiometry: 6:1 (ligand : DNA duplex)

No. 14

DNA: (dGdC)₁₀-(dGdC)₁₀ **ligand:** DAPI
C_{FI-DNA}: 1.0×10⁻⁶ M **C_{ligand}:** 8.0×10⁻⁵ M
Buffer: 2 mM HEPES and 150 mM NaCl in water. pH=7.10

Addition ligand (μL)	Total volume (μL)	C _{FI-DNA} (mol/L)	C _{ligand} (mol/L)	ratio (C _{ligand} /C _{FI-DNA})	fluorescence emission	relative emission difference
0	500	1.00E-06	0.00E+00	0.00	971.995	0.000
20	520	1.00E-06	3.08E-06	3.08	875.248	96.747
40	540	1.00E-06	5.93E-06	5.93	759.842	212.153
60	560	1.00E-06	8.57E-06	8.57	675.297	296.698
80	580	1.00E-06	1.10E-05	11.03	629.443	342.552
100	600	1.00E-06	1.33E-05	13.33	602.010	369.985
120	620	1.00E-06	1.55E-05	15.48	572.139	399.856
140	640	1.00E-06	1.75E-05	17.50	541.918	430.077
160	660	1.00E-06	1.94E-05	19.39	515.188	456.807
180	680	1.00E-06	2.12E-05	21.18	491.459	480.536
200	700	1.00E-06	2.29E-05	22.86	469.924	502.071
220	720	1.00E-06	2.44E-05	24.44	452.059	519.936
240	740	1.00E-06	2.59E-05	25.95	433.206	538.789
260	760	1.00E-06	2.74E-05	27.37	418.240	553.755
280	780	1.00E-06	2.87E-05	28.72	404.873	567.122
300	800	1.00E-06	3.00E-05	30.00	388.897	583.098
320	820	1.00E-06	3.12E-05	31.22	374.986	597.009

The graphical representation of the titration curve:



K_a (M⁻¹): 6.4×10⁴ **Statistical error:** 10%

Stoichiometry: 7:1 (ligand : DNA duplex)

No. 15

DNA: 12bp

ligand:Dimer A

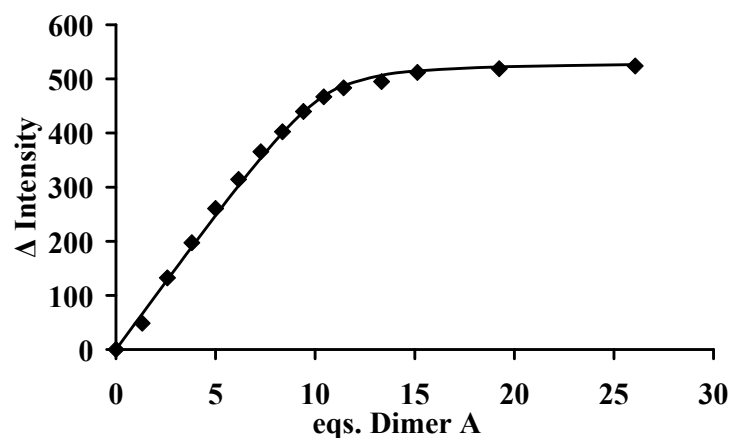
C_{FI-DNA}: 1.0×10^{-6} M

C_{ligand}: 8.0×10^{-5} M

Buffer: 2 mM HEPES and 150 mM NaCl in water. pH=7.10

Addition ligand (μ L)	Total volume (μ L)	C _{FI-DNA} (mol/L)	C _{ligand} (mol/L)	ratio (C _{ligand} /C _{FI-DNA})	fluorescence emission	relative emission difference
0	600	1.00E-06	0.00E+00	0.00	655.304	0.000
10	610	1.00E-06	1.31E-06	1.31	606.718	48.586
20	620	1.00E-06	2.58E-06	2.58	523.006	132.298
30	630	1.00E-06	3.81E-06	3.81	458.052	197.252
40	640	1.00E-06	5.00E-06	5.00	394.692	260.612
50	650	1.00E-06	6.15E-06	6.15	340.985	314.319
60	660	1.00E-06	7.27E-06	7.27	289.865	365.439
70	670	1.00E-06	8.36E-06	8.36	252.903	402.401
80	680	1.00E-06	9.41E-06	9.41	215.504	439.800
90	690	1.00E-06	1.04E-05	10.43	188.365	466.939
100	700	1.00E-06	1.14E-05	11.43	171.676	483.628
120	720	1.00E-06	1.33E-05	13.33	160.222	495.082
140	740	1.00E-06	1.51E-05	15.14	143.268	512.036
190	790	1.00E-06	1.92E-05	19.24	136.412	518.892
290	890	1.00E-06	2.61E-05	26.07	131.366	523.938

The graphical representation of the titration curve:



K_a (M⁻¹): 5.7×10^6 **Statistical error:** 31%

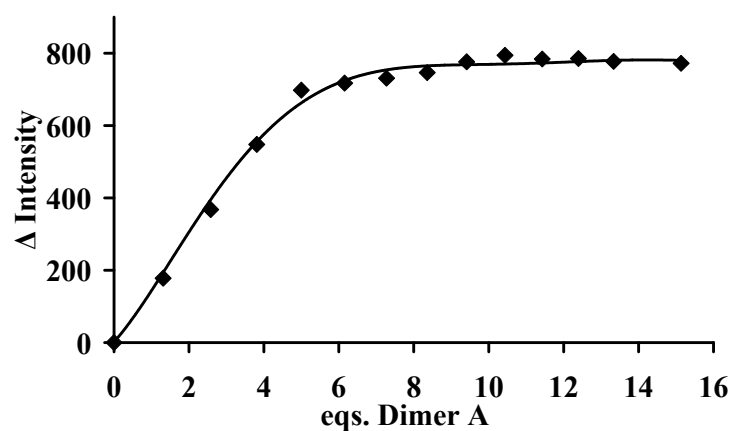
Stoichiometry: 10:1 (ligand : DNA duplex)

No. 16

DNA: dG₁₂ - dC₁₂ **ligand:** Dimer A
C_{FI-DNA}: 1.0×10⁻⁶ M **C_{ligand}:** 8.0×10⁻⁵ M
Buffer: 2 mM HEPES and 150 mM NaCl in water. pH=7.10

Addition ligand (μL)	Total volume (μL)	C _{FI-DNA} (mol/L)	C _{ligand} (mol/L)	ratio (C _{ligand} /C _{FI-DNA})	fluorescence emission	relative emission difference
0	600	1.00E-06	0.00E+00	0.00	954.423	0.000
10	610	1.00E-06	1.31E-06	1.31	776.482	177.941
20	620	1.00E-06	2.58E-06	2.58	586.611	367.812
30	630	1.00E-06	3.81E-06	3.81	406.507	547.916
40	640	1.00E-06	5.00E-06	5.00	256.409	698.014
50	650	1.00E-06	6.15E-06	6.15	237.001	717.422
60	660	1.00E-06	7.27E-06	7.27	223.390	731.033
70	670	1.00E-06	8.36E-06	8.36	207.867	746.556
80	680	1.00E-06	9.41E-06	9.41	178.098	776.325
90	690	1.00E-06	1.04E-05	10.43	160.259	794.164
100	700	1.00E-06	1.14E-05	11.43	170.186	784.237
110	710	1.00E-06	1.24E-05	12.39	169.011	785.412
120	720	1.00E-06	1.33E-05	13.33	176.853	777.570
140	740	1.00E-06	1.51E-05	15.14	182.285	772.138

The graphical representation of the titration curve:



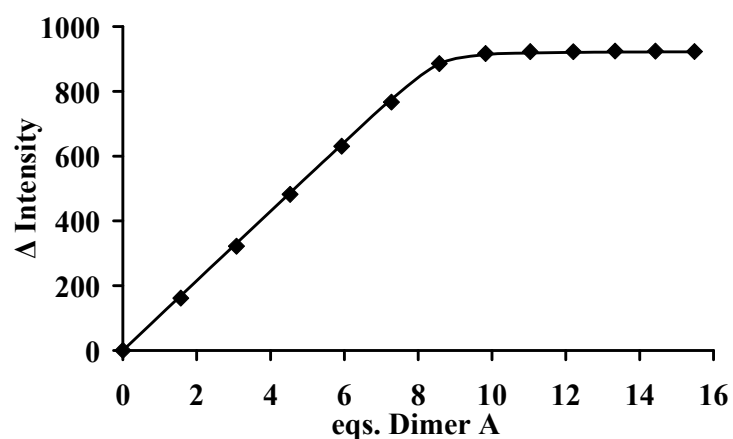
K_a (M⁻¹): 7.3×10⁶ **Statistical error:** 30%
Stoichiometry: 5:1 (ligand : DNA duplex)

No. 17

DNA: dA₁₂ - dT₁₂ **ligand:** Dimer A
C_{FI-DNA}: 1.0×10⁻⁶ M **C_{ligand}:** 8.0×10⁻⁵ M
Buffer: 2 mM HEPES and 150 mM NaCl in water. pH=7.10

Addition ligand (μL)	Total volume (μL)	C _{FI-DNA} (mol/L)	C _{ligand} (mol/L)	ratio (C _{ligand} /C _{FI-DNA})	fluorescence emission	relative emission difference
0	500	1.00E-06	0.00E+00	0.00	974.076	0.000
10	510	1.00E-06	1.57E-06	1.57	812.433	161.643
20	520	1.00E-06	3.08E-06	3.08	652.077	321.999
30	530	1.00E-06	4.53E-06	4.53	492.002	482.074
40	540	1.00E-06	5.93E-06	5.93	343.562	630.514
50	550	1.00E-06	7.27E-06	7.27	207.209	766.867
60	560	1.00E-06	8.57E-06	8.57	88.262	885.815
70	570	1.00E-06	9.82E-06	9.82	57.280	916.796
80	580	1.00E-06	1.10E-05	11.03	51.379	922.697
90	590	1.00E-06	1.22E-05	12.20	51.686	922.391
100	600	1.00E-06	1.33E-05	13.33	49.591	924.485
110	610	1.00E-06	1.44E-05	14.43	49.667	924.409
120	620	1.00E-06	1.55E-05	15.48	51.027	923.049

The graphical representation of the titration curve:



K_a (M⁻¹): 5.9×10⁷ **Statistical error:** 32%
Stoichiometry: 9:1 (ligand : DNA duplex)

No. 18

RNA: A₁₂ - U₁₂

ligand: Dimer A

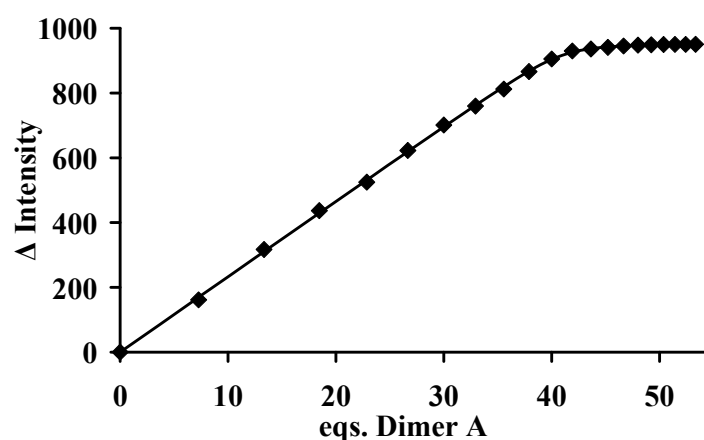
C_{FI-RNA}: 1.0×10⁻⁶ M

C_{ligand}: 8.0×10⁻⁵ M

Buffer: 2 mM HEPES and 150 mM NaCl in water. pH=7.10

Addition ligand (μL)	Total volume (μL)	C _{FI-RNA} (mol/L)	C _{ligand} (mol/L)	ratio (C _{ligand} /C _{FI-RNA})	fluorescence emission	relative emission difference
0	500	1.00E-06	0.00E+00	0.00	990.392	0.000
50	550	1.00E-06	7.27E-06	7.27	829.021	161.371
100	600	1.00E-06	1.33E-05	13.33	673.483	316.909
150	650	1.00E-06	1.85E-05	18.46	553.519	436.873
200	700	1.00E-06	2.29E-05	22.86	465.485	524.907
250	750	1.00E-06	2.67E-05	26.67	367.562	622.830
300	800	1.00E-06	3.00E-05	30.00	289.238	701.154
350	850	1.00E-06	3.29E-05	32.94	230.708	759.684
400	900	1.00E-06	3.56E-05	35.56	177.903	812.489
450	950	1.00E-06	3.79E-05	37.89	124.019	866.373
500	1000	1.00E-06	4.00E-05	40.00	85.176	905.216
550	1050	1.00E-06	4.19E-05	41.90	60.406	929.986
600	1100	1.00E-06	4.36E-05	43.64	54.223	936.169
650	1150	1.00E-06	4.52E-05	45.22	49.260	941.132
700	1200	1.00E-06	4.67E-05	46.67	45.092	945.300
750	1250	1.00E-06	4.80E-05	48.00	42.585	947.808
800	1300	1.00E-06	4.92E-05	49.23	41.328	949.064
850	1350	1.00E-06	5.04E-05	50.37	40.496	949.897
900	1400	1.00E-06	5.14E-05	51.43	40.133	950.259
950	1450	1.00E-06	5.24E-05	52.41	40.106	950.286
1000	1500	1.00E-06	5.33E-05	53.33	39.868	950.524

The graphical representation of the titration curve:



K_a (M⁻¹): 1.4×10⁷ Statistical error: 22%

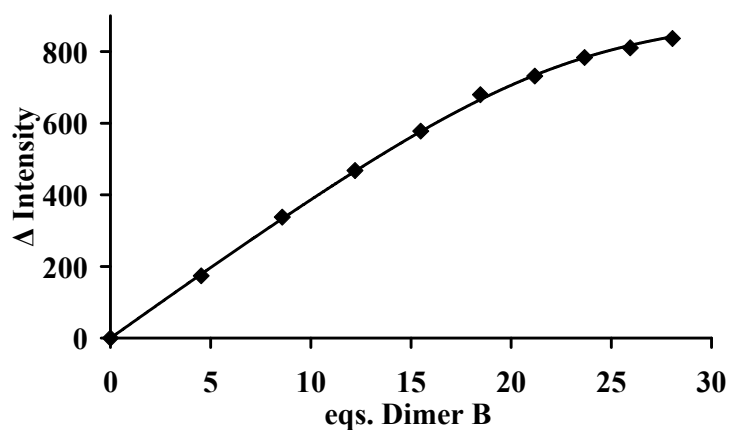
Stoichiometry: 41:1 (ligand : RNA duplex)

No. 19

DNA: 12bp
ligand: Dimer B
 $C_{\text{Fl-DNA}}$: 1.0×10^{-6} M
 C_{ligand} : 8.0×10^{-5} M
Buffer: 2 mM HEPES and 150 mM NaCl in water. pH=7.10

Addition ligand (μL)	Total volume (μL)	$C_{\text{Fl-DNA}}$ (mol/L)	C_{ligand} (mol/L)	ratio ($C_{\text{ligand}}/C_{\text{Fl-DNA}}$)	fluorescence emission	relative emission difference
0	500	1.00E-06	0.00E+00	0.00	993.386	0.000
30	530	1.00E-06	4.53E-06	4.53	819.469	173.917
60	560	1.00E-06	8.57E-06	8.57	655.619	337.767
90	590	1.00E-06	1.22E-05	12.20	525.585	467.801
120	620	1.00E-06	1.55E-05	15.48	415.356	578.030
150	650	1.00E-06	1.85E-05	18.46	313.734	679.652
180	680	1.00E-06	2.12E-05	21.18	261.756	731.630
210	710	1.00E-06	2.37E-05	23.66	210.000	783.386
240	740	1.00E-06	2.59E-05	25.95	182.942	810.444
270	770	1.00E-06	2.81E-05	28.05	156.889	836.497

The graphical representation of the titration curve:



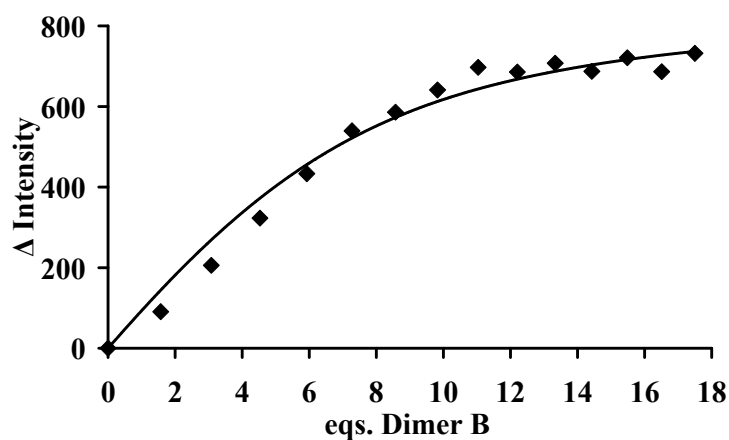
K_a (M^{-1}): 9.0×10^5 **Statistical error:** 31%
Stoichiometry: 23:1 (ligand : DNA duplex)

No. 20

DNA: dG₁₂ - dC₁₂ **ligand:** Dimer B
C_{FI-DNA}: 1.0×10⁻⁶ M **C_{ligand}:** 8.0×10⁻⁵ M
Buffer: 2 mM HEPES and 150 mM NaCl in water. pH=7.10

Addition ligand (μL)	Total volume (μL)	C _{FI-DNA} (mol/L)	C _{ligand} (mol/L)	ratio (C _{ligand} /C _{FI-DNA})	fluorescence emission	relative emission difference
0	500	1.00E-06	0.00E+00	0.00	965.612	0.000
10	510	1.00E-06	1.57E-06	1.57	874.984	90.628
20	520	1.00E-06	3.08E-06	3.08	759.987	205.625
30	530	1.00E-06	4.53E-06	4.53	642.687	322.925
40	540	1.00E-06	5.93E-06	5.93	532.342	433.270
50	550	1.00E-06	7.27E-06	7.27	426.087	539.525
60	560	1.00E-06	8.57E-06	8.57	379.592	586.020
70	570	1.00E-06	9.82E-06	9.82	324.709	640.903
80	580	1.00E-06	1.10E-05	11.03	268.498	697.114
90	590	1.00E-06	1.22E-05	12.20	280.086	685.526
100	600	1.00E-06	1.33E-05	13.33	258.116	707.496
110	610	1.00E-06	1.44E-05	14.43	278.379	687.233
120	620	1.00E-06	1.55E-05	15.48	244.575	721.037
130	630	1.00E-06	1.65E-05	16.51	279.222	686.390
140	640	1.00E-06	1.75E-05	17.50	233.615	731.997

The graphical representation of the titration curve:



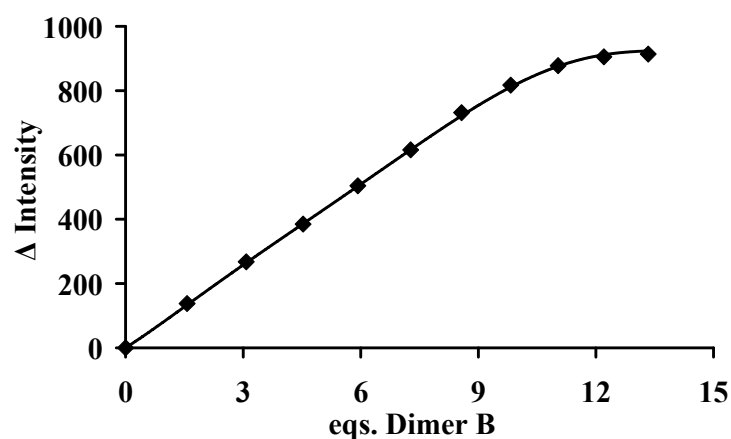
K_a (M⁻¹): 5.0×10⁵ **Statistical error:** 39%
Stoichiometry: 7:1 (ligand : DNA duplex)

No. 21

DNA: dA₁₂ - dT₁₂ **ligand:** Dimer B
C_{FI-DNA}: 1.0×10⁻⁶ M **C_{ligand}:** 8.0×10⁻⁵ M
Buffer: 2 mM HEPES and 150 mM NaCl in water. pH=7.10

Addition ligand (μL)	Total volume (μL)	C _{FI-DNA} (mol/L)	C _{ligand} (mol/L)	ratio (C _{ligand} /C _{FI-DNA})	fluorescence emission	relative emission difference
0	500	1.00E-06	0.00E+00	0.00	962.251	0.000
10	510	1.00E-06	1.57E-06	1.57	824.662	137.589
20	520	1.00E-06	3.08E-06	3.08	694.820	267.431
30	530	1.00E-06	4.53E-06	4.53	577.412	384.839
40	540	1.00E-06	5.93E-06	5.93	458.328	503.923
50	550	1.00E-06	7.27E-06	7.27	346.368	615.883
60	560	1.00E-06	8.57E-06	8.57	230.712	731.539
70	570	1.00E-06	9.82E-06	9.82	145.046	817.205
80	580	1.00E-06	1.10E-05	11.03	84.452	877.799
90	590	1.00E-06	1.22E-05	12.20	56.905	905.346
100	600	1.00E-06	1.33E-05	13.33	48.556	913.695

The graphical representation of the titration curve:



K_a (M⁻¹): 1.4×10⁷ **Statistical error:** 32%
Stoichiometry: 11:1 (ligand : DNA duplex)

No. 22

RNA: A₁₂ - U₁₂

ligand: Dimer B

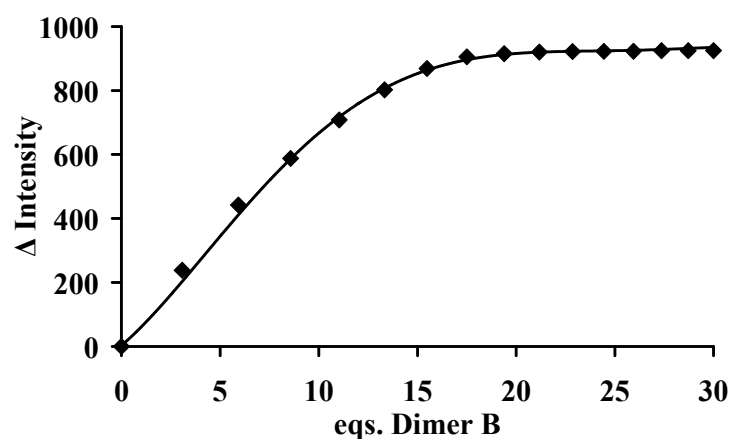
C_{FI-RNA}: 1.0×10⁻⁶ M

C_{ligand}: 8.0×10⁻⁵ M

Buffer: 2 mM HEPES and 150 mM NaCl in water. pH=7.10

Addition ligand (μL)	Total volume (μL)	C _{FI-RNA} (mol/L)	C _{ligand} (mol/L)	ratio (C _{ligand} /C _{FI-RNA})	fluorescence emission	relative emission difference
0	500	1.00E-06	0.00E+00	0.00	967.153	0.000
20	520	1.00E-06	3.08E-06	3.08	728.904	238.249
40	540	1.00E-06	5.93E-06	5.93	524.965	442.188
60	560	1.00E-06	8.57E-06	8.57	379.322	587.831
80	580	1.00E-06	1.10E-05	11.03	258.929	708.224
100	600	1.00E-06	1.33E-05	13.33	164.929	802.224
120	620	1.00E-06	1.55E-05	15.48	98.002	869.152
140	640	1.00E-06	1.75E-05	17.50	61.615	905.538
160	660	1.00E-06	1.94E-05	19.39	51.720	915.433
180	680	1.00E-06	2.12E-05	21.18	46.840	920.313
200	700	1.00E-06	2.29E-05	22.86	45.187	921.966
220	720	1.00E-06	2.44E-05	24.44	44.435	922.718
240	740	1.00E-06	2.59E-05	25.95	44.369	922.784
260	760	1.00E-06	2.74E-05	27.37	42.534	924.619
280	780	1.00E-06	2.87E-05	28.72	42.354	924.799
300	800	1.00E-06	3.00E-05	30.00	42.265	924.888

The graphical representation of the titration curve:



K_a (M⁻¹): 3.2×10⁶

Statistical error: 24%

Stoichiometry: 13:1 (ligand : RNA duplex)

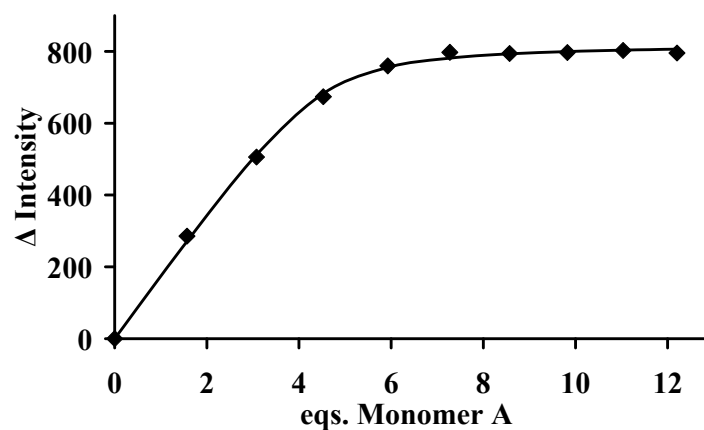
No. 23

DNA: 12bp
C_{FI-DNA}: 1.0×10^{-6} M
Buffer: 2 mM HEPES and 150 mM NaCl in water. pH=7.10

ligand: Monomer A
C_{ligand}: 8.0×10^{-5} M

Addition ligand (μ L)	Total volume (μ L)	C _{FI-DNA} (mol/L)	C _{ligand} (mol/L)	ratio (C _{ligand} /C _{FI-DNA})	fluorescence emission	relative emission difference
0	500	1.00E-06	0.00E+00	0.00	985.099	0.000
10	510	1.00E-06	1.57E-06	1.57	699.322	285.777
20	520	1.00E-06	3.08E-06	3.08	479.238	505.861
30	530	1.00E-06	4.53E-06	4.53	311.182	673.917
40	540	1.00E-06	5.93E-06	5.93	225.161	759.938
50	550	1.00E-06	7.27E-06	7.27	187.505	797.594
60	560	1.00E-06	8.57E-06	8.57	190.787	794.312
70	570	1.00E-06	9.82E-06	9.82	188.019	797.080
80	580	1.00E-06	1.10E-05	11.03	182.124	802.975
90	590	1.00E-06	1.22E-05	12.20	189.448	795.651

The graphical representation of the titration curve:



K_a (M⁻¹): 6.3×10^6 **Statistical error:** 19%
Stoichiometry: 4:1 (ligand : DNA duplex)

No. 24

DNA: dG₁₂ - dC₁₂

ligand: Monomer A

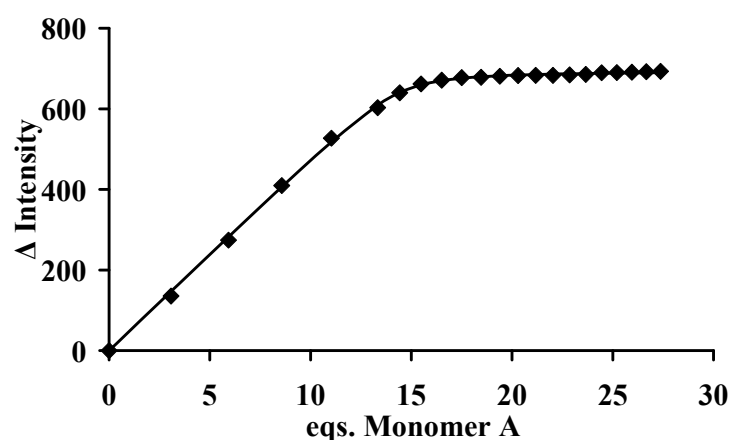
C_{FL-DNA}: 1.0×10⁻⁶ M

C_{ligand}: 8.0×10⁻⁵ M

Buffer: 2 mM HEPES and 150 mM NaCl in water. pH=7.10

Addition ligand (μL)	Total volume (μL)	C _{FL-DNA} (mol/L)	C _{ligand} (mol/L)	ratio (C _{ligand} /C _{FL-DNA})	fluorescence emission	relative emission difference
0	500	1.00E-06	0.00E+00	0.00	925.198	0.000
20	520	1.00E-06	3.08E-06	3.08	789.670	135.528
40	540	1.00E-06	5.93E-06	5.93	650.964	274.234
60	560	1.00E-06	8.57E-06	8.57	515.556	409.642
80	580	1.00E-06	1.10E-05	11.03	397.976	527.222
100	600	1.00E-06	1.33E-05	13.33	322.161	603.037
110	610	1.00E-06	1.44E-05	14.43	285.308	639.890
120	620	1.00E-06	1.55E-05	15.48	263.301	661.897
130	630	1.00E-06	1.65E-05	16.51	254.056	671.142
140	640	1.00E-06	1.75E-05	17.50	247.701	677.497
150	650	1.00E-06	1.85E-05	18.46	246.782	678.416
160	660	1.00E-06	1.94E-05	19.39	244.249	680.949
170	670	1.00E-06	2.03E-05	20.30	242.472	682.726
180	680	1.00E-06	2.12E-05	21.18	242.098	683.100
190	690	1.00E-06	2.20E-05	22.03	242.038	683.160
200	700	1.00E-06	2.29E-05	22.86	240.973	684.225
210	710	1.00E-06	2.37E-05	23.66	239.670	685.528
220	720	1.00E-06	2.44E-05	24.44	235.588	689.610
230	730	1.00E-06	2.52E-05	25.21	235.181	690.017
240	740	1.00E-06	2.59E-05	25.95	234.229	690.969
250	750	1.00E-06	2.67E-05	26.67	233.020	692.178
260	760	1.00E-06	2.74E-05	27.37	232.119	693.079

The graphical representation of the titration curve:



K_a (M⁻¹): 1.0×10⁷ Statistical error: 15%

Stoichiometry: 14:1 (ligand : DNA duplex)

No. 25

DNA: dA₁₂ - dT₁₂

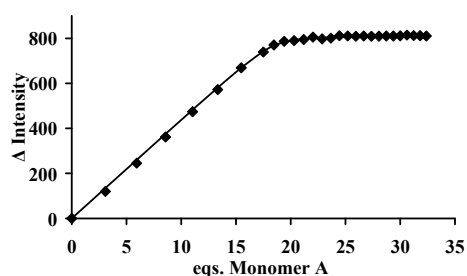
ligand: Monomer A

C_{FI-DNA}: 1.0×10⁻⁶ M

C_{ligand}: 8.0×10⁻⁵ M

Buffer: 2 mM HEPES and 150 mM NaCl in water. pH=7.10

Addition ligand (μL)	Total volume (μL)	C _{FI-DNA} (mol/L)	C _{ligand} (mol/L)	ratio (C _{ligand} /C _{FI-DNA})	fluorescence emission	relative emission difference
0	500	1.00E-06	0.00E+00	0.00	908.497	0.000
20	520	1.00E-06	3.08E-06	3.08	788.643	119.854
40	540	1.00E-06	5.93E-06	5.93	663.141	245.356
60	560	1.00E-06	8.57E-06	8.57	546.477	362.020
80	580	1.00E-06	1.10E-05	11.03	434.517	473.980
100	600	1.00E-06	1.33E-05	13.33	336.194	572.303
120	620	1.00E-06	1.55E-05	15.48	239.764	668.733
140	640	1.00E-06	1.75E-05	17.50	169.526	738.971
150	650	1.00E-06	1.85E-05	18.46	138.114	770.383
160	660	1.00E-06	1.94E-05	19.39	122.026	786.471
170	670	1.00E-06	2.03E-05	20.30	118.493	790.004
180	680	1.00E-06	2.12E-05	21.18	113.922	794.575
190	690	1.00E-06	2.20E-05	22.03	103.352	805.145
200	700	1.00E-06	2.29E-05	22.86	111.101	797.396
210	710	1.00E-06	2.37E-05	23.66	107.721	800.776
220	720	1.00E-06	2.44E-05	24.44	97.238	811.259
230	730	1.00E-06	2.52E-05	25.21	97.917	810.580
240	740	1.00E-06	2.59E-05	25.95	99.426	809.071
250	750	1.00E-06	2.67E-05	26.67	98.254	810.243
260	760	1.00E-06	2.74E-05	27.37	99.136	809.361
270	770	1.00E-06	2.81E-05	28.05	99.034	809.463
280	780	1.00E-06	2.87E-05	28.72	98.384	810.113
290	790	1.00E-06	2.94E-05	29.37	97.997	810.501
300	800	1.00E-06	3.00E-05	30.00	97.715	810.782
310	810	1.00E-06	3.06E-05	30.62	94.295	814.202
320	820	1.00E-06	3.12E-05	31.22	96.485	812.012
330	830	1.00E-06	3.18E-05	31.81	96.872	811.625
340	840	1.00E-06	3.24E-05	32.38	98.323	810.174
350	850	1.00E-06	3.29E-05	32.94	98.147	810.350



K_a (M⁻¹): 1.5×10⁷

Statistical error: 20%

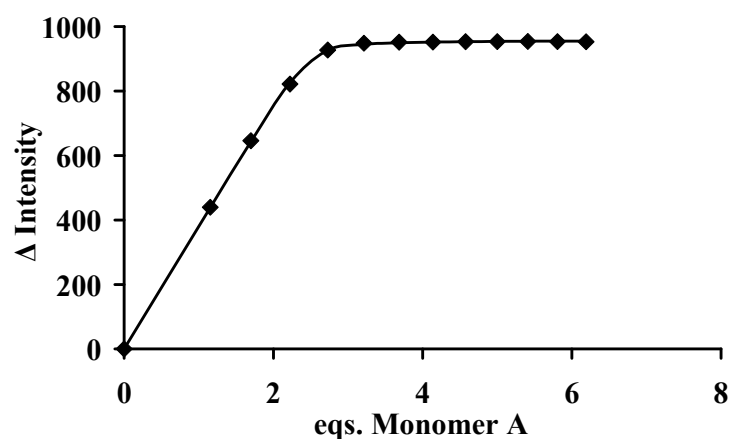
Stoichiometry: 18:1 (ligand : DNA duplex)

No. 26

RNA: A₁₂ - U₁₂ **ligand:** Monomer A
C_{FI-RNA}: 1.0×10⁻⁶ M **C_{ligand}:** 3.0×10⁻⁵ M
Buffer: 2 mM HEPES and 150 mM NaCl in water. pH=7.10

Addition ligand (μL)	Total volume (μL)	C_{FI-RNA} (mol/L)	C_{ligand} (mol/L)	ratio (C_{ligand}/C_{FI-RNA})	fluorescence emission	relative emission difference
0	500	1.00E-06	0.00E+00	0.00	990.043	0.000
20	520	1.00E-06	1.15E-06	1.15	550.600	439.443
30	530	1.00E-06	1.70E-06	1.70	344.020	646.023
40	540	1.00E-06	2.22E-06	2.22	168.313	821.730
50	550	1.00E-06	2.73E-06	2.73	62.711	927.332
60	560	1.00E-06	3.21E-06	3.21	41.609	948.434
70	570	1.00E-06	3.68E-06	3.68	38.353	951.690
80	580	1.00E-06	4.14E-06	4.14	38.028	952.015
90	590	1.00E-06	4.58E-06	4.58	36.817	953.226
100	600	1.00E-06	5.00E-06	5.00	36.625	953.418
110	610	1.00E-06	5.41E-06	5.41	36.042	954.002
120	620	1.00E-06	5.81E-06	5.81	36.660	953.383
130	630	1.00E-06	6.19E-06	6.19	37.149	952.894

The graphical representation of the titration curve:



K_a (M⁻¹): 9.5×10⁷ **Statistical error:** 10%
Stoichiometry: 3:1 (ligand : RNA duplex)

No. 27

DNA: 12bp

ligand: Monomer B

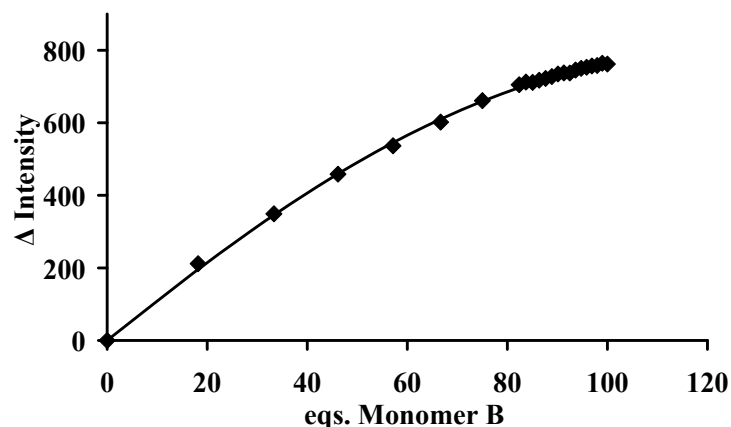
$C_{\text{FI-DNA}}: 1.0 \times 10^{-6} \text{ M}$

$C_{\text{ligand}}: 2.0 \times 10^{-4} \text{ M}$

Buffer: 2 mM HEPES and 150 mM NaCl in water. pH=7.10

Addition ligand (μL)	Total volume (μL)	$C_{\text{FI-DNA}}$ (mol/L)	C_{ligand} (mol/L)	ratio ($C_{\text{ligand}}/C_{\text{FI-DNA}}$)	fluorescence emission	relative emission difference
0	500	1.00E-06	0.00E+00	0.00	973.432	0.000
50	550	1.00E-06	1.82E-05	18.18	761.589	211.843
100	600	1.00E-06	3.33E-05	33.33	624.288	349.144
150	650	1.00E-06	4.62E-05	46.15	515.081	458.351
200	700	1.00E-06	5.71E-05	57.14	436.762	536.670
250	750	1.00E-06	6.67E-05	66.67	371.481	601.951
300	800	1.00E-06	7.50E-05	75.00	312.425	661.007
350	850	1.00E-06	8.24E-05	82.35	268.365	705.067
360	860	1.00E-06	8.37E-05	83.72	261.259	712.173
370	870	1.00E-06	8.51E-05	85.06	261.970	711.462
380	880	1.00E-06	8.64E-05	86.36	255.968	717.464
390	890	1.00E-06	8.76E-05	87.64	251.192	722.240
400	900	1.00E-06	8.89E-05	88.89	245.855	727.577
410	910	1.00E-06	9.01E-05	90.11	238.934	734.498
420	920	1.00E-06	9.13E-05	91.30	236.088	737.344
430	930	1.00E-06	9.25E-05	92.47	236.111	737.321
440	940	1.00E-06	9.36E-05	93.62	228.254	745.178
450	950	1.00E-06	9.47E-05	94.74	223.387	750.045
470	970	1.00E-06	9.69E-05	96.91	216.858	756.574
480	980	1.00E-06	9.80E-05	97.96	215.503	757.929
490	990	1.00E-06	9.90E-05	98.99	209.337	764.095
500	1000	1.00E-06	1.00E-04	100.00	211.468	761.964

The graphical representation of the titration curve:



$K_a (M^{-1}): 7.4 \times 10^4$

Statistical error: 24%

Stoichiometry: 78:1 (ligand : DNA duplex)

No. 28

DNA: dG₁₂ - dC₁₂

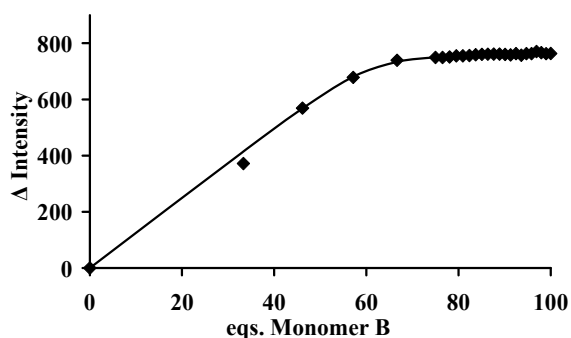
ligand: Monomer B

C_{FI-DNA}: 1.0×10⁻⁶ M

C_{ligand}: 2.0×10⁻⁴ M

Buffer: 2 mM HEPES and 150 mM NaCl in water. pH=7.10

Addition ligand (μL)	Total volume (μL)	C _{FI-DNA} (mol/L)	C _{ligand} (mol/L)	ratio (C _{ligand} /C _{FI-DNA})	fluorescence emission	relative emission difference
0	500	1.00E-06	0.00E+00	0.00	966.924	0.000
100	600	1.00E-06	3.33E-05	33.33	595.020	371.904
150	650	1.00E-06	4.62E-05	46.15	397.774	569.150
200	700	1.00E-06	5.71E-05	57.14	288.558	678.366
250	750	1.00E-06	6.67E-05	66.67	227.560	739.364
300	800	1.00E-06	7.50E-05	75.00	217.558	749.366
310	810	1.00E-06	7.65E-05	76.54	217.758	749.166
320	820	1.00E-06	7.80E-05	78.05	215.895	751.029
330	830	1.00E-06	7.95E-05	79.52	212.124	754.800
340	840	1.00E-06	8.10E-05	80.95	211.883	755.041
350	850	1.00E-06	8.24E-05	82.35	210.790	756.134
360	860	1.00E-06	8.37E-05	83.72	208.105	758.819
370	870	1.00E-06	8.51E-05	85.06	206.506	760.418
380	880	1.00E-06	8.64E-05	86.36	205.921	761.003
390	890	1.00E-06	8.76E-05	87.64	205.884	761.040
400	900	1.00E-06	8.89E-05	88.89	205.842	761.082
410	910	1.00E-06	9.01E-05	90.11	207.037	759.887
420	920	1.00E-06	9.13E-05	91.30	208.410	758.514
430	930	1.00E-06	9.25E-05	92.47	204.173	762.751
440	940	1.00E-06	9.36E-05	93.62	209.494	757.430
450	950	1.00E-06	9.47E-05	94.74	204.110	762.814
460	960	1.00E-06	9.58E-05	95.83	204.173	762.751
470	970	1.00E-06	9.69E-05	96.91	196.429	770.495
480	980	1.00E-06	9.80E-05	97.96	200.558	766.366
490	990	1.00E-06	9.90E-05	98.99	204.286	762.638
500	1000	1.00E-06	1.00E-04	100.00	203.544	763.380



K_a (M⁻¹): 2.3×10⁶

Statistical error: 35%

Stoichiometry: 61:1 (ligand : DNA duplex)

No. 29

DNA: dA₁₂ - dT₁₂

ligand: Monomer B

C_{FI-DNA}: 1.0×10⁻⁶ M

C_{ligand}: 2.0×10⁻⁴ M

Buffer: 2 mM HEPES and 150 mM NaCl in water. pH=7.10

Addition ligand (μL)	Total volume (μL)	C _{FI-DNA} (mol/L)	C _{ligand} (mol/L)	ratio (C _{ligand} /C _{FI-DNA})	fluorescence emission	relative emission difference
0	500	1.00E-06	0.00E+00	0.00	995.614	0.000
50	500	1.00E-06	2.00E-05	20.00	764.818	230.796
100	600	1.00E-06	3.33E-05	33.33	606.873	388.741
150	650	1.00E-06	4.62E-05	46.15	453.895	541.719
200	700	1.00E-06	5.71E-05	57.14	326.412	669.202
250	750	1.00E-06	6.67E-05	66.67	239.462	756.152
260	760	1.00E-06	6.84E-05	68.42	228.106	767.508
270	770	1.00E-06	7.01E-05	70.13	217.244	778.370
280	780	1.00E-06	7.18E-05	71.79	208.150	787.464
290	790	1.00E-06	7.34E-05	73.42	199.596	796.018
300	800	1.00E-06	7.50E-05	75.00	190.042	805.572
310	810	1.00E-06	7.65E-05	76.54	182.788	812.826
320	820	1.00E-06	7.80E-05	78.05	171.815	823.799
330	830	1.00E-06	7.95E-05	79.52	163.862	831.752
340	840	1.00E-06	8.10E-05	80.95	155.950	839.664
350	850	1.00E-06	8.24E-05	82.35	148.730	846.884
360	860	1.00E-06	8.37E-05	83.72	141.277	854.337
370	870	1.00E-06	8.51E-05	85.06	130.416	865.198
380	880	1.00E-06	8.64E-05	86.36	123.049	872.565
390	890	1.00E-06	8.76E-05	87.64	116.545	879.069
400	900	1.00E-06	8.89E-05	88.89	108.489	887.125

The graphical representation of the titration curve:



K_a (M⁻¹): 1.3×10⁴

Statistical error: 28%

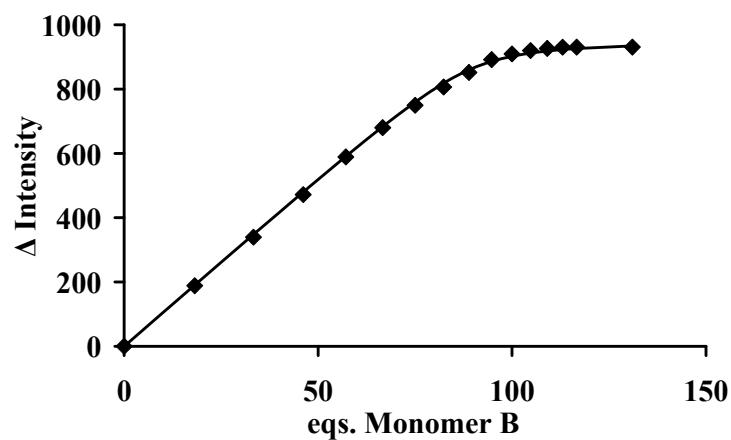
Stoichiometry: 67:1 (ligand : DNA duplex)

No. 30

RNA: A₁₂ - U₁₂ ligand: Monomer B
 C_{FI-RNA}: 1.0×10⁻⁶ M C_{ligand}: 2.0×10⁻⁴ M
 Buffer: 2 mM HEPES and 150 mM NaCl in water. pH=7.10

Addition ligand (μL)	Total volume (μL)	C _{FI-RNA} (mol/L)	C _{ligand} (mol/L)	ratio (C _{ligand} /C _{FI-RNA})	fluorescence emission	relative emission difference
0	500	1.00E-06	0.00E+00	0.00	965.792	0.000
50	550	1.00E-06	1.82E-05	18.18	777.454	188.338
100	600	1.00E-06	3.33E-05	33.33	626.285	339.507
150	650	1.00E-06	4.62E-05	46.15	494.046	471.746
200	700	1.00E-06	5.71E-05	57.14	376.835	588.957
250	750	1.00E-06	6.67E-05	66.67	285.638	680.154
300	800	1.00E-06	7.50E-05	75.00	216.190	749.602
350	850	1.00E-06	8.24E-05	82.35	159.159	806.633
400	900	1.00E-06	8.89E-05	88.89	113.996	851.796
450	950	1.00E-06	9.47E-05	94.74	73.991	891.801
500	1000	1.00E-06	1.00E-04	100.00	56.335	909.457
550	1050	1.00E-06	1.05E-04	104.76	45.890	919.902
600	1100	1.00E-06	1.09E-04	109.09	39.150	926.642
650	1150	1.00E-06	1.13E-04	113.04	35.356	930.436
700	1200	1.00E-06	1.17E-04	116.67	35.254	930.538
950	1450	1.00E-06	1.31E-04	131.03	35.056	930.736

The graphical representation of the titration curve:



K_a (M⁻¹): 1.2×10⁶ Statistical error: 25%

Stoichiometry: 90:1 (ligand : RNA duplex)

No. 31

DNA: 12bp

ligand: Dimer A

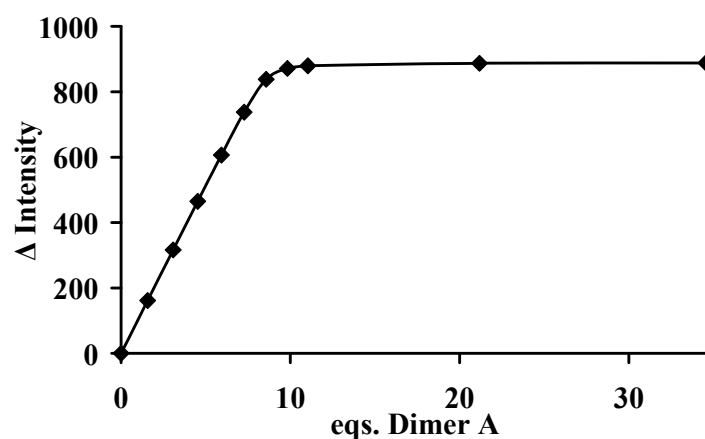
$C_{\text{Fl-DNA}}: 1.0 \times 10^{-6} \text{ M}$

$C_{\text{ligand}}: 8.0 \times 10^{-5} \text{ M}$

Buffer: 2 mM HEPES and 150 mM NaCl in water:MeOH=1:1. pH=7.10

Addition ligand (μL)	Total volume (μL)	$C_{\text{Fl-DNA}}$ (mol/L)	C_{ligand} (mol/L)	ratio ($C_{\text{ligand}}/C_{\text{Fl-DNA}}$)	fluorescence emission	relative emission difference
0	500	1.00E-06	0.00E+00	0.00	921.506	0.000
10	510	1.00E-06	1.57E-06	1.57	761.361	160.145
20	520	1.00E-06	3.08E-06	3.08	598.650	322.856
30	530	1.00E-06	4.53E-06	4.53	456.943	464.563
40	540	1.00E-06	5.93E-06	5.93	315.409	606.097
50	550	1.00E-06	7.27E-06	7.27	185.170	736.336
60	560	1.00E-06	8.57E-06	8.57	86.044	835.462
70	570	1.00E-06	9.82E-06	9.82	47.018	874.488
80	580	1.00E-06	1.10E-05	11.03	39.077	882.429
180	680	1.00E-06	2.12E-05	21.18	34.492	887.014
380	880	1.00E-06	3.45E-05	34.55	37.343	884.163

The graphical representation of the titration curve:



$K_a (M^{-1}): 3.5 \times 10^7$

Statistical error: 15%

Stoichiometry: 9:1 (ligand : DNA duplex)

No. 32

DNA: dG₁₂ - dC₁₂

ligand: Dimer A

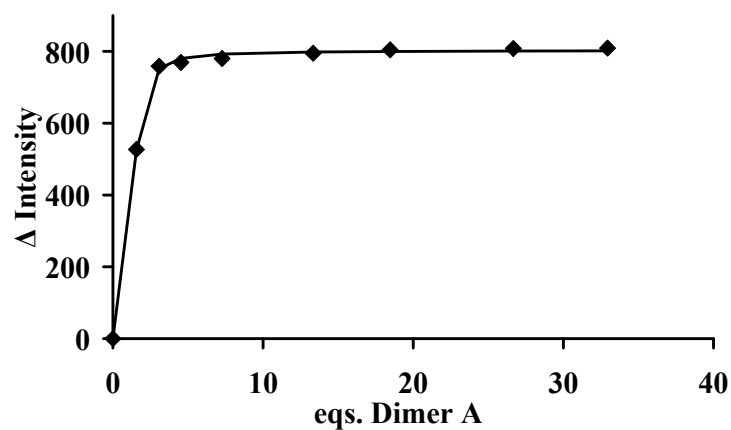
C_{FI-DNA}: 1.0×10⁻⁶ M

C_{ligand}: 8.0×10⁻⁵ M

Buffer: 2 mM HEPES and 150 mM NaCl in water:MeOH=1:1. pH=7.10

Addition ligand (μL)	Total volume (μL)	C _{FI-DNA} (mol/L)	C _{ligand} (mol/L)	ratio (C _{ligand} /C _{FI-DNA})	fluorescence emission	relative emission difference
0	500	1.00E-06	0.00E+00	0.00	942.958	0.000
10	510	1.00E-06	1.57E-06	1.57	415.784	527.174
20	520	1.00E-06	3.08E-06	3.08	184.274	758.684
30	530	1.00E-06	4.53E-06	4.53	173.644	769.314
50	550	1.00E-06	7.27E-06	7.27	162.660	780.298
100	600	1.00E-06	1.33E-05	13.33	147.895	795.063
150	650	1.00E-06	1.85E-05	18.46	138.573	804.385
250	750	1.00E-06	2.67E-05	26.67	134.797	808.161
350	850	1.00E-06	3.29E-05	32.94	133.638	809.320

The graphical representation of the titration curve:



K_a (M⁻¹): 1.5×10⁷ **Statistical error:** 17%
Stoichiometry: 4:1 (ligand : DNA duplex)

No. 33

DNA: dA₁₂ - dT₁₂

ligand: Dimer A

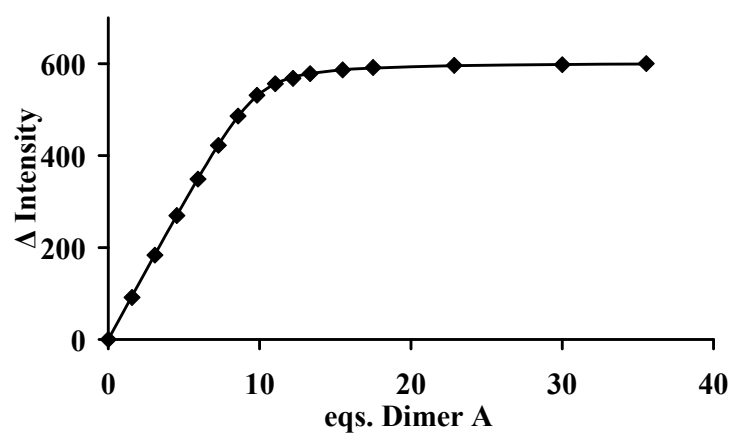
C_{FI-DNA}: 1.0×10⁻⁶ M

C_{ligand}: 8.0×10⁻⁵ M

Buffer: 2 mM HEPES and 150 mM NaCl in water:MeOH=1:1. pH=7.10

Addition ligand (μL)	Total volume (μL)	C _{FI-DNA} (mol/L)	C _{ligand} (mol/L)	ratio (C _{ligand} /C _{FI-DNA})	fluorescence emission	relative emission difference
0	500	1.00E-06	0.00E+00	0.00	642.419	0.000
10	510	1.00E-06	1.57E-06	1.57	550.903	91.516
20	520	1.00E-06	3.08E-06	3.08	458.856	183.563
30	530	1.00E-06	4.53E-06	4.53	372.752	269.667
40	540	1.00E-06	5.93E-06	5.93	293.381	349.038
50	550	1.00E-06	7.27E-06	7.27	219.934	422.485
60	560	1.00E-06	8.57E-06	8.57	156.191	486.228
70	570	1.00E-06	9.82E-06	9.82	111.028	531.391
80	580	1.00E-06	1.10E-05	11.03	85.822	556.597
90	590	1.00E-06	1.22E-05	12.20	74.087	568.332
100	600	1.00E-06	1.33E-05	13.33	63.872	578.547
120	620	1.00E-06	1.55E-05	15.48	55.839	586.580
140	640	1.00E-06	1.75E-05	17.50	50.535	591.885
200	700	1.00E-06	2.29E-05	22.86	45.975	596.444
300	800	1.00E-06	3.00E-05	30.00	44.304	598.115
400	900	1.00E-06	3.56E-05	35.56	41.971	600.448

The graphical representation of the titration curve:



K_a (M⁻¹): 5.9×10⁶ Statistical error: 4%

Stoichiometry: 10:1 (ligand : DNA duplex)

No. 34

RNA: A₁₂ - U₁₂

ligand: Dimer A

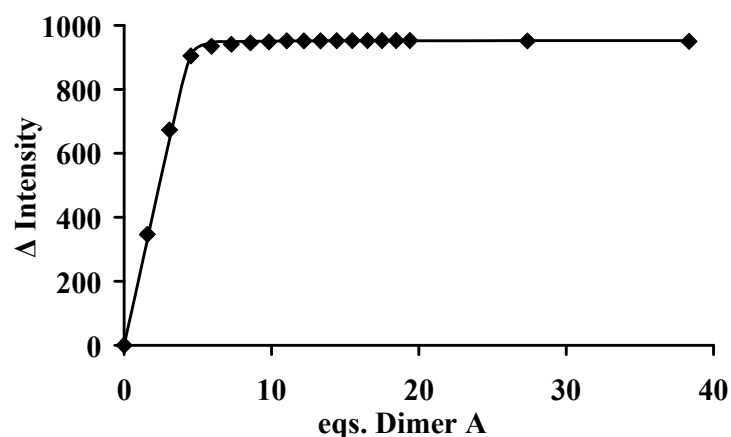
C_{FI-RNA}: 1.0×10⁻⁶ M

C_{ligand}: 8.0×10⁻⁵ M

Buffer: 2 mM HEPES and 150 mM NaCl in water:MeOH=1:1. pH=7.10

Addition ligand (μL)	Total volume (μL)	C_{FI-RNA} (mol/L)	C_{ligand} (mol/L)	ratio (C_{ligand}/C_{FI-RNA})	fluorescence emission	relative emission difference
0	500	1.00E-06	0.00E+00	0.00	987.605	0.000
10	510	1.00E-06	1.57E-06	1.57	640.782	346.823
20	520	1.00E-06	3.08E-06	3.08	314.397	673.208
30	530	1.00E-06	4.53E-06	4.53	82.842	904.763
40	540	1.00E-06	5.93E-06	5.93	52.749	934.856
50	550	1.00E-06	7.27E-06	7.27	46.569	941.036
60	560	1.00E-06	8.57E-06	8.57	42.079	945.526
70	570	1.00E-06	9.82E-06	9.82	39.146	948.460
80	580	1.00E-06	1.10E-05	11.03	35.697	951.908
90	590	1.00E-06	1.22E-05	12.20	35.870	951.735
100	600	1.00E-06	1.33E-05	13.33	35.661	951.945
110	610	1.00E-06	1.44E-05	14.43	35.186	952.419
120	620	1.00E-06	1.55E-05	15.48	35.078	952.527
130	630	1.00E-06	1.65E-05	16.51	35.093	952.512
140	640	1.00E-06	1.75E-05	17.50	34.923	952.682
150	650	1.00E-06	1.85E-05	18.46	34.806	952.799
160	660	1.00E-06	1.94E-05	19.39	34.796	952.809
260	760	1.00E-06	2.74E-05	27.37	36.069	951.536
460	960	1.00E-06	3.83E-05	38.33	37.326	950.279

The graphical representation of the titration curve:



K_a (M⁻¹): 9.0×10⁷ **Statistical error:** 44%

Stoichiometry: 5:1 (ligand : RNA duplex)

No. 35

DNA: 12bp

ligand:Dimer B

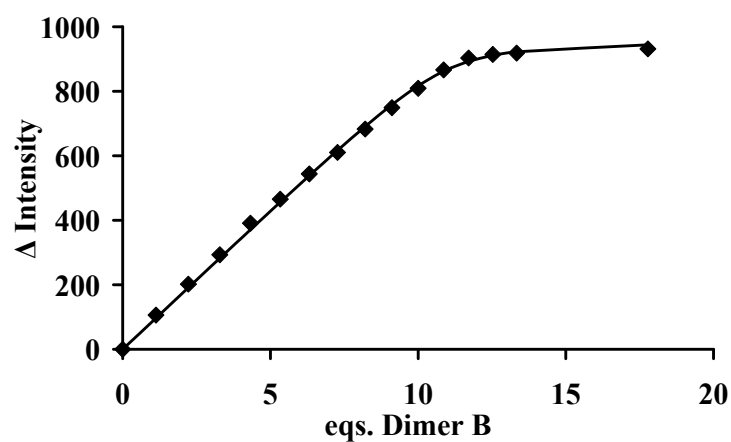
C_{FI-DNA}: 1.0×10^{-6} M

C_{ligand}: 8.0×10^{-5} M

Buffer: 2 mM HEPES and 150 mM NaCl in water:MeOH=1:1. pH=7.10

Addition ligand (μL)	Total volume (μL)	C _{FI-DNA} (mol/L)	C _{ligand} (mol/L)	ratio (C _{ligand} /C _{FI-DNA})	fluorescence emission	relative emission difference
0	700	1.00E-06	0.00E+00	0.00	990.402	0.000
10	710	1.00E-06	1.13E-06	1.13	884.177	106.225
20	720	1.00E-06	2.22E-06	2.22	788.420	201.982
30	730	1.00E-06	3.29E-06	3.29	697.102	293.300
40	740	1.00E-06	4.32E-06	4.32	599.476	390.926
50	750	1.00E-06	5.33E-06	5.33	524.655	465.747
60	760	1.00E-06	6.32E-06	6.32	446.420	543.982
70	770	1.00E-06	7.27E-06	7.27	379.815	610.587
80	780	1.00E-06	8.21E-06	8.21	307.211	683.191
90	790	1.00E-06	9.11E-06	9.11	241.044	749.358
100	800	1.00E-06	1.00E-05	10.00	181.034	809.368
110	810	1.00E-06	1.09E-05	10.86	123.950	866.452
120	820	1.00E-06	1.17E-05	11.71	86.992	903.410
130	830	1.00E-06	1.25E-05	12.53	76.031	914.371
140	840	1.00E-06	1.33E-05	13.33	71.863	918.539
200	900	1.00E-06	1.78E-05	17.78	58.687	931.715

The graphical representation of the titration curve:



K_a (M⁻¹): 9.1×10^6

Statistical error: 31%

Stoichiometry: 11:1 (ligand : DNA duplex)

No.36

DNA: dG₁₂ - dC₁₂

ligand: Dimer B

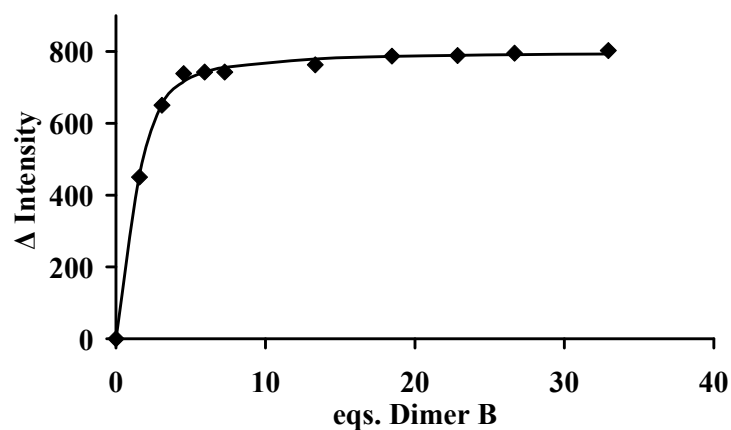
C_{FI-DNA}: 1.0×10⁻⁶ M

C_{ligand}: 8.0×10⁻⁵ M

Buffer: 2 mM HEPES and 150 mM NaCl in water:MeOH=1:1. pH=7.10

Addition ligand (μL)	Total volume (μL)	C_{FI-DNA} (mol/L)	C_{ligand} (mol/L)	ratio (C_{ligand}/C_{FI-DNA})	fluorescence emission	relative emission difference
0	500	1.00E-06	0.00E+00	0.00	971.136	0.000
10	510	1.00E-06	1.57E-06	1.57	520.990	450.146
20	520	1.00E-06	3.08E-06	3.08	320.757	650.379
30	530	1.00E-06	4.53E-06	4.53	232.646	738.490
40	540	1.00E-06	5.93E-06	5.93	228.492	742.644
50	550	1.00E-06	7.27E-06	7.27	228.449	742.687
100	600	1.00E-06	1.33E-05	13.33	208.234	762.902
150	650	1.00E-06	1.85E-05	18.46	183.976	787.160
200	700	1.00E-06	2.29E-05	22.86	182.528	788.608
250	750	1.00E-06	2.67E-05	26.67	176.003	795.133
350	850	1.00E-06	3.29E-05	32.94	168.733	802.403
450	950	1.00E-06	3.79E-05	37.89	92.000	879.136

The graphical representation of the titration curve:



K_a (M⁻¹): 3.1×10⁶

Statistical error: 9%

Stoichiometry: 4:1 (ligand : DNA duplex)

No. 37

DNA: dA₁₂ - dT₁₂

ligand: Dimer B

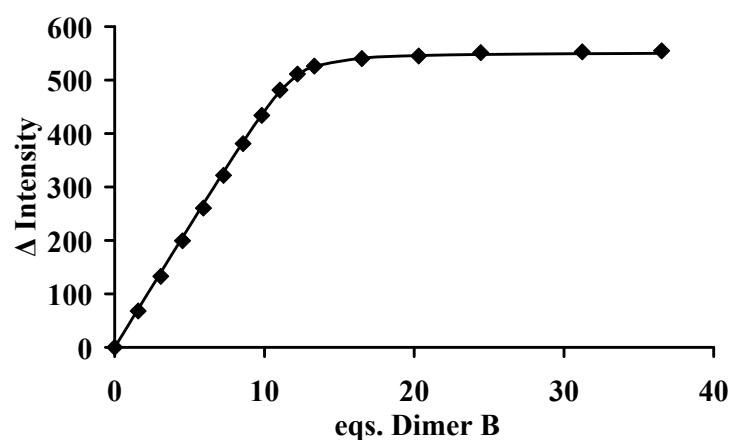
C_{FI-DNA}: 1.0×10⁻⁶ M

C_{ligand}: 8.0×10⁻⁵ M

Buffer: 2 mM HEPES and 150 mM NaCl in water:MeOH=1:1. pH=7.10

Addition ligand (μL)	Total volume (μL)	C _{FI-DNA} (mol/L)	C _{ligand} (mol/L)	ratio (C _{ligand} /C _{FI-DNA})	fluorescence emission	relative emission difference
0	500	1.00E-06	0.00E+00	0.00	601.653	0.000
10	510	1.00E-06	1.57E-06	1.57	533.641	68.012
20	520	1.00E-06	3.08E-06	3.08	468.894	132.759
30	530	1.00E-06	4.53E-06	4.53	402.270	199.383
40	540	1.00E-06	5.93E-06	5.93	341.023	260.630
50	550	1.00E-06	7.27E-06	7.27	279.913	321.740
60	560	1.00E-06	8.57E-06	8.57	220.484	381.169
70	570	1.00E-06	9.82E-06	9.82	167.673	433.980
80	580	1.00E-06	1.10E-05	11.03	120.300	481.353
90	590	1.00E-06	1.22E-05	12.20	90.251	511.402
100	600	1.00E-06	1.33E-05	13.33	75.511	526.142
130	630	1.00E-06	1.65E-05	16.51	61.430	540.223
170	670	1.00E-06	2.03E-05	20.30	56.605	545.048
220	720	1.00E-06	2.44E-05	24.44	50.291	551.362
320	820	1.00E-06	3.12E-05	31.22	48.852	552.801
420	920	1.00E-06	3.65E-05	36.52	46.946	554.707

The graphical representation of the titration curve:



K_a (M⁻¹): 1.0×10⁷

Statistical error: 18%

Stoichiometry: 12:1 (ligand : DNA duplex)

No. 38

RNA: A₁₂ - U₁₂

ligand: Dimer B

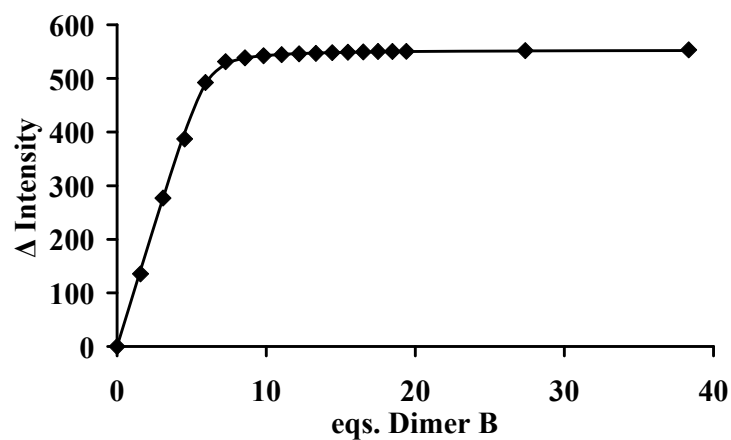
C_{FI-RNA}: 1.0×10⁻⁶ M

C_{ligand}: 8.0×10⁻⁵ M

Buffer: 2 mM HEPES and 150 mM NaCl in water:MeOH=1:1. pH=7.10

Addition ligand (μL)	Total volume (μL)	C _{FI-RNA} (mol/L)	C _{ligand} (mol/L)	ratio (C _{ligand} /C _{FI-RNA})	fluorescence emission	relative emission difference
0	500	1.00E-06	0.00E+00	0.00	571.400	0.000
10	510	1.00E-06	1.57E-06	1.57	435.928	135.472
20	520	1.00E-06	3.08E-06	3.08	294.467	276.933
30	530	1.00E-06	4.53E-06	4.53	184.184	387.216
40	540	1.00E-06	5.93E-06	5.93	78.894	492.506
50	550	1.00E-06	7.27E-06	7.27	40.107	531.293
60	560	1.00E-06	8.57E-06	8.57	32.903	538.497
70	570	1.00E-06	9.82E-06	9.82	29.098	542.302
80	580	1.00E-06	1.10E-05	11.03	27.076	544.324
90	590	1.00E-06	1.22E-05	12.20	25.457	545.943
100	600	1.00E-06	1.33E-05	13.33	24.583	546.817
110	610	1.00E-06	1.44E-05	14.43	23.277	548.123
120	620	1.00E-06	1.55E-05	15.48	22.480	548.920
130	630	1.00E-06	1.65E-05	16.51	21.992	549.408
140	640	1.00E-06	1.75E-05	17.50	21.092	550.308
150	650	1.00E-06	1.85E-05	18.46	21.019	550.381
160	660	1.00E-06	1.94E-05	19.39	20.919	550.481
260	760	1.00E-06	2.74E-05	27.37	19.462	551.938
460	960	1.00E-06	3.83E-05	38.33	18.132	553.268

The graphical representation of the titration curve:



K_a (M⁻¹): 1.2×10⁷ Statistical error: 11%

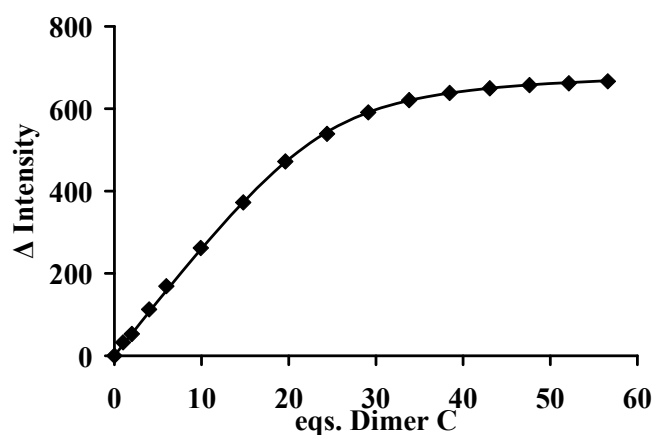
Stoichiometry: 6:1 (ligand : RNA duplex)

No. 39

DNA: (dGdC)₁₀-(dGdC)₁₀ **ligand:** Dimer C
C_{FI-DNA}: 1.0×10⁻⁶ M **C_{ligand}:** 1.0×10⁻³ M
Buffer: 2 mM HEPES and 150 mM NaCl in water. pH=7.10

Addition ligand (μL)	Total volume (μL)	C _{FI-DNA} (mol/L)	C _{ligand} (mol/L)	ratio (C _{ligand} /C _{FI-DNA})	fluorescence emission	relative emission difference
0	500	1,00E-06	0,00E+00	0,00	941,984	0,000
0,5	500,5	1,00E-06	9,99E-07	1,00	909,391	32,593
1	501	1,00E-06	2,00E-06	2,00	888,886	53,098
2	502	1,00E-06	3,98E-06	3,98	829,280	112,704
3	503	1,00E-06	5,96E-06	5,96	773,019	168,965
5	505	1,00E-06	9,90E-06	9,90	680,197	261,787
7,5	507,5	1,00E-06	1,48E-05	14,78	569,613	372,371
10	510	1,00E-06	1,96E-05	19,61	469,962	472,022
12,5	512,5	1,00E-06	2,44E-05	24,39	402,901	539,083
15	515	1,00E-06	2,91E-05	29,13	350,799	591,185
17,5	517,5	1,00E-06	3,38E-05	33,82	321,183	620,801
20	520	1,00E-06	3,85E-05	38,46	303,755	638,229
22,5	522,5	1,00E-06	4,31E-05	43,06	292,366	649,618
25	525	1,00E-06	4,76E-05	47,62	284,672	657,312
27,5	527,5	1,00E-06	5,21E-05	52,13	280,287	661,697
30	530	1,00E-06	5,66E-05	56,60	275,396	666,588

The graphical representation of the titration curve:



K_a (M⁻¹): 6.4×10⁵ **Statistical error:** 7%

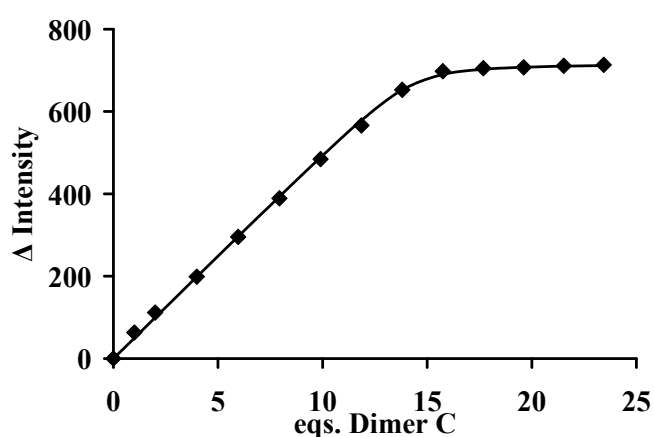
Stoichiometry: 24:1 (ligand : DNA duplex)

No. 40

DNA: (dAdT)₁₀-(dAdT)₁₀ **ligand:** Dimer C
C_{FI-DNA}: 1.0×10⁻⁶ M **C_{ligand}:** 1.0×10⁻³ M
Buffer: 2 mM HEPES and 150 mM NaCl in water. pH=7.10

Addition ligand (μL)	Total volume (μL)	C _{FI-DNA} (mol/L)	C _{ligand} (mol/L)	ratio (C _{ligand} /C _{FI-DNA})	fluorescence emission	relative emission difference
0	500	1,00E-06	0,00E+00	0,00	958,483	0,000
0,5	500,5	1,00E-06	9,99E-07	1,00	895,226	63,257
1	501	1,00E-06	2,00E-06	2,00	846,628	111,855
2	502	1,00E-06	3,98E-06	3,98	759,608	198,875
3	503	1,00E-06	5,96E-06	5,96	662,939	295,544
4	504	1,00E-06	7,94E-06	7,94	569,301	389,182
5	505	1,00E-06	9,90E-06	9,90	474,045	484,438
6	506	1,00E-06	1,19E-05	11,86	392,419	566,064
7	507	1,00E-06	1,38E-05	13,81	305,811	652,672
8	508	1,00E-06	1,57E-05	15,75	260,859	697,624
9	509	1,00E-06	1,77E-05	17,68	253,294	705,189
10	510	1,00E-06	1,96E-05	19,61	251,317	707,166
11	511	1,00E-06	2,15E-05	21,53	247,511	710,972
12	512	1,00E-06	2,34E-05	23,44	245,246	713,237

The graphical representation of the titration curve:



K_a (M⁻¹): 1.2×10⁷ **Statistical error:** 38%
Stoichiometry: 14:1 (ligand : DNA duplex)

No. 41

DNA: dG₂₀ – dC₂₀

ligand: Dimer C

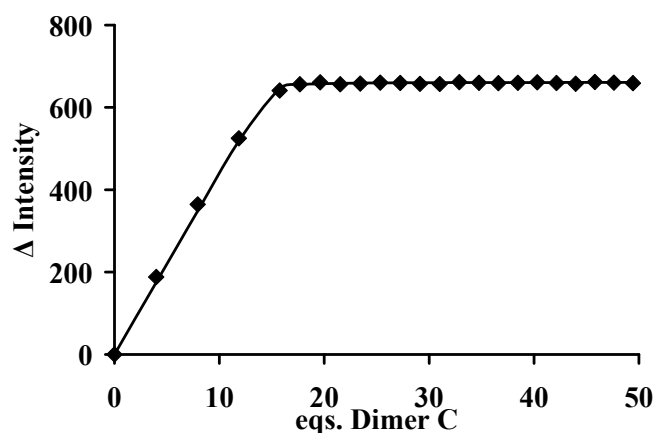
C_{FI-DNA}: 1.0×10⁻⁶ M

C_{ligand}: 1.0×10⁻³ M

Buffer: 2 mM HEPES and 150 mM NaCl in water. pH=7.10

Addition ligand (μL)	Total volume (μL)	C _{FI-DNA} (mol/L)	C _{ligand} (mol/L)	ratio (C _{ligand} /C _{FI-DNA})	fluorescence emission	relative emission difference
0	500	1,00E-06	0,00E+00	0,00	915,958	0,000
2	502	1,00E-06	3,98E-06	3,98	727,691	188,267
4	504	1,00E-06	7,94E-06	7,94	551,551	364,407
6	506	1,00E-06	1,19E-05	11,86	391,042	524,916
8	508	1,00E-06	1,57E-05	15,75	275,093	640,865
9	509	1,00E-06	1,77E-05	17,68	259,845	656,113
10	510	1,00E-06	1,96E-05	19,61	254,962	660,996
11	511	1,00E-06	2,15E-05	21,53	259,774	656,184
12	512	1,00E-06	2,34E-05	23,44	258,026	657,932
13	513	1,00E-06	2,53E-05	25,34	255,832	660,126
14	514	1,00E-06	2,72E-05	27,24	256,478	659,480
15	515	1,00E-06	2,91E-05	29,13	258,763	657,195
16	516	1,00E-06	3,10E-05	31,01	259,201	656,757
17	517	1,00E-06	3,29E-05	32,88	254,710	661,248
18	518	1,00E-06	3,47E-05	34,75	256,168	659,790
19	519	1,00E-06	3,66E-05	36,61	257,085	658,873
20	520	1,00E-06	3,85E-05	38,46	256,151	659,807
21	521	1,00E-06	4,03E-05	40,31	254,894	661,064
22	522	1,00E-06	4,21E-05	42,15	256,690	659,268
23	523	1,00E-06	4,40E-05	43,98	258,456	657,502
24	524	1,00E-06	4,58E-05	45,80	254,213	661,745
25	525	1,00E-06	4,76E-05	47,62	255,758	660,200
26	526	1,00E-06	4,94E-05	49,43	257,028	658,930

The graphical representation of the titration curve:



K_a (M⁻¹): 3.7×10⁷

Statistical error: 36%

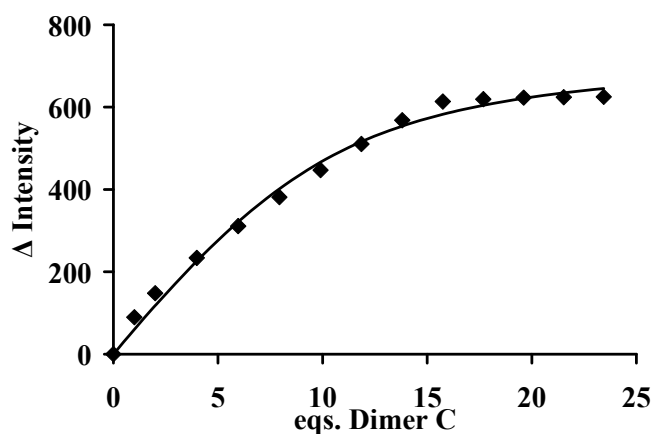
Stoichiometry: 15:1 (ligand : DNA duplex)

No. 42

DNA: dA₂₀ – dT₂₀ **ligand:** Dimer C
C_{FI-DNA}: 1.0×10⁻⁶ M **C_{ligand}:** 1.0×10⁻³ M
Buffer: 2 mM HEPES and 150 mM NaCl in water. pH=7.10

Addition ligand (μL)	Total volume (μL)	C _{FI-DNA} (mol/L)	C _{ligand} (mol/L)	ratio (C _{ligand} /C _{FI-DNA})	fluorescence emission	relative emission difference
0	500	1,00E-06	0,00E+00	0,00	930,973	0,000
0,5	500,5	1,00E-06	9,99E-07	1,00	841,182	89,791
1	501	1,00E-06	2,00E-06	2,00	782,963	148,010
2	502	1,00E-06	3,98E-06	3,98	697,248	233,725
3	503	1,00E-06	5,96E-06	5,96	619,976	310,997
4	504	1,00E-06	7,94E-06	7,94	549,519	381,454
5	505	1,00E-06	9,90E-06	9,90	483,944	447,029
6	506	1,00E-06	1,19E-05	11,86	420,489	510,484
7	507	1,00E-06	1,38E-05	13,81	362,890	568,083
8	508	1,00E-06	1,57E-05	15,75	317,535	613,438
9	509	1,00E-06	1,77E-05	17,68	311,759	619,214
10	510	1,00E-06	1,96E-05	19,61	308,075	622,898
11	511	1,00E-06	2,15E-05	21,53	306,880	624,093
12	512	1,00E-06	2,34E-05	23,44	305,993	624,980

The graphical representation of the titration curve:



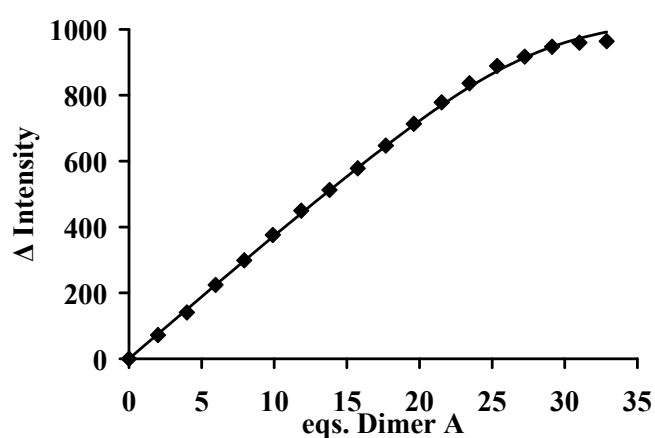
K_a (M⁻¹): 4.8×10⁵ **Statistical error:** 30%
Stoichiometry: 10:1 (ligand : DNA duplex)

No. 43

DNA: dG₂₀ – dC₂₀ **ligand:** Dimer A
C_{FI-DNA}: 1.0×10⁻⁶ M **C_{ligand}:** 1.0×10⁻³ M
Buffer: 2 mM HEPES and 150 mM NaCl in water. pH=7.10

Addition ligand (μL)	Total volume (μL)	C _{FI-DNA} (mol/L)	C _{ligand} (mol/L)	ratio (C _{ligand} /C _{FI-DNA})	fluorescence emission	relative emission difference
0	500	1,00E-06	0,00E+00	0,00	922,915	0,000
1	501	1,00E-06	2,00E-06	2,00	850,863	72,052
2	502	1,00E-06	3,98E-06	3,98	782,334	140,581
3	503	1,00E-06	5,96E-06	5,96	698,580	224,335
4	504	1,00E-06	7,94E-06	7,94	624,102	298,813
5	505	1,00E-06	9,90E-06	9,90	547,250	375,665
6	506	1,00E-06	1,19E-05	11,86	473,250	449,665
7	507	1,00E-06	1,38E-05	13,81	410,381	512,534
8	508	1,00E-06	1,57E-05	15,75	344,697	578,218
9	509	1,00E-06	1,77E-05	17,68	275,626	647,289
10	510	1,00E-06	1,96E-05	19,61	209,654	713,261
11	511	1,00E-06	2,15E-05	21,53	144,537	778,378
12	512	1,00E-06	2,34E-05	23,44	86,501	836,414
13	513	1,00E-06	2,53E-05	25,34	33,939	888,977
14	514	1,00E-06	2,72E-05	27,24	5,760	917,155
15	515	1,00E-06	2,91E-05	29,13	-24,320	947,235
16	516	1,00E-06	3,10E-05	31,01	-36,809	959,724
17	517	1,00E-06	3,29E-05	32,88	-41,192	964,107

The graphical representation of the titration curve:



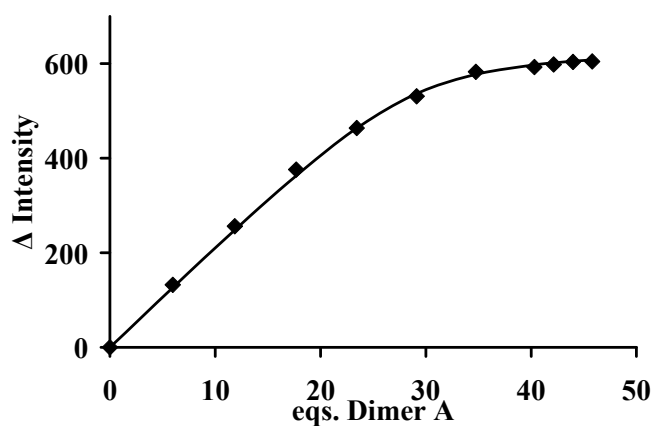
K_a (M⁻¹): 1.5×10⁶ **Statistical error:** 29%
Stoichiometry: 28:1 (ligand : DNA duplex)

No. 44

DNA: dA₂₀ – dT₂₀ **ligand:** Dimer A
C_{FI-DNA}: 1.0×10⁻⁶ M **C_{ligand}:** 1.0×10⁻³ M
Buffer: 2 mM HEPES and 150 mM NaCl in water. pH=7.10

Addition ligand (μL)	Total volume (μL)	C_{FI-DNA} (mol/L)	C_{ligand} (mol/L)	ratio (C_{ligand}/C_{FI-DNA})	fluorescence emission	relative emission difference
0	500	1,00E-06	0,00E+00	0,00	942,711	0,000
3	503	1,00E-06	5,96E-06	5,96	810,444	132,267
6	506	1,00E-06	1,19E-05	11,86	686,535	256,176
9	509	1,00E-06	1,77E-05	17,68	566,693	376,018
12	512	1,00E-06	2,34E-05	23,44	478,960	463,751
15	515	1,00E-06	2,91E-05	29,13	411,811	530,900
18	518	1,00E-06	3,47E-05	34,75	359,993	582,718
21	521	1,00E-06	4,03E-05	40,31	350,031	592,680
22	522	1,00E-06	4,21E-05	42,15	344,547	598,164
23	523	1,00E-06	4,40E-05	43,98	339,170	603,541
24	524	1,00E-06	4,58E-05	45,80	338,140	604,571

The graphical representation of the titration curve:



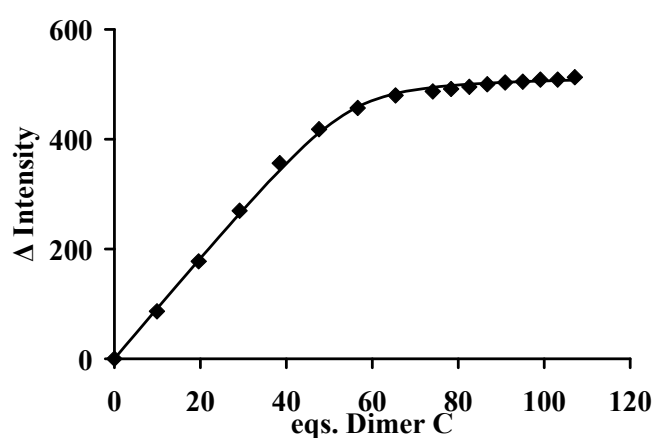
K_a (M⁻¹): 1.1×10⁶ **Statistical error:** 27%
Stoichiometry: 29:1 (ligand : DNA duplex)

No. 45

DNA: (dGdC)₁₀-(dGdC)₁₀ **ligand:** Dimer C
C_{FI-DNA}: 1.0×10⁻⁶ M **C_{ligand}:** 1.0×10⁻³ M
Buffer: 20 mM sodium phosphate in water. pH=7.0

Addition ligand (μL)	Total volume (μL)	C _{FI-DNA} (mol/L)	C _{ligand} (mol/L)	ratio (C _{ligand} /C _{FI-DNA})	fluorescence emission	relative emission difference
0	500	1,00E-06	0,00E+00	0,00	939,491	0,000
5	505	1,00E-06	9,90E-06	9,90	853,061	86,430
10	510	1,00E-06	1,96E-05	19,61	762,060	177,431
15	515	1,00E-06	2,91E-05	29,13	669,814	269,677
20	520	1,00E-06	3,85E-05	38,46	583,142	356,349
25	525	1,00E-06	4,76E-05	47,62	521,369	418,122
30	530	1,00E-06	5,66E-05	56,60	482,640	456,851
35	535	1,00E-06	6,54E-05	65,42	459,709	479,782
40	540	1,00E-06	7,41E-05	74,07	452,516	486,975
42,5	542,5	1,00E-06	7,83E-05	78,34	448,074	491,417
45	545	1,00E-06	8,26E-05	82,57	444,155	495,336
47,5	547,5	1,00E-06	8,68E-05	86,76	439,513	499,978
50	550	1,00E-06	9,09E-05	90,91	436,254	503,237
52,5	552,5	1,00E-06	9,50E-05	95,02	434,729	504,762
55	555	1,00E-06	9,91E-05	99,10	431,043	508,448
57,5	557,5	1,00E-06	1,03E-04	103,14	430,981	508,510
60	560	1,00E-06	1,07E-04	107,14	426,651	512,840

The graphical representation of the titration curve:

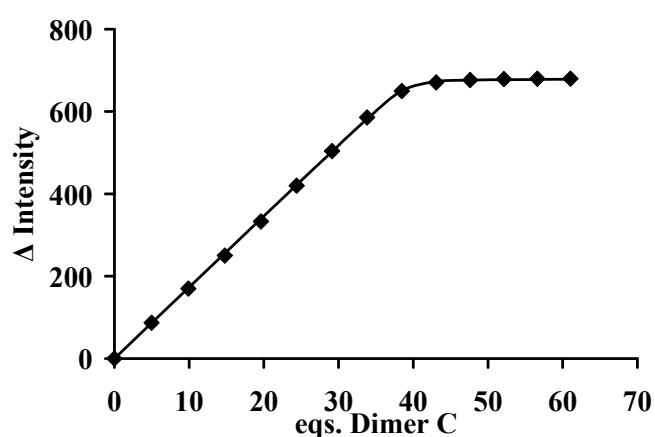


K_a (M⁻¹): 1.0×10⁶ **Statistical error:** 21%
Stoichiometry: 55:1 (ligand : DNA duplex)

DNA: (dAdT)₁₀-(dAdT)₁₀ **ligand:** Dimer C
C_{FI-DNA}: 1.0×10⁻⁶ M **C_{ligand}:** 1.0×10⁻³ M
Buffer: 20 mM sodium phosphate in water. pH=7.0

Addition ligand (μL)	Total volume (μL)	C _{FI-DNA} (mol/L)	C _{ligand} (mol/L)	ratio (C _{ligand} /C _{FI-DNA})	fluorescence emission	relative emission difference
0	500	1,00E-06	0,00E+00	0,00	950,256	0,000
2,5	502,5	1,00E-06	4,98E-06	4,98	863,299	86,957
5	505	1,00E-06	9,90E-06	9,90	780,418	169,838
7,5	507,5	1,00E-06	1,48E-05	14,78	700,261	249,995
10	510	1,00E-06	1,96E-05	19,61	617,382	332,874
12,5	512,5	1,00E-06	2,44E-05	24,39	530,579	419,677
15	515	1,00E-06	2,91E-05	29,13	446,275	503,981
17,5	517,5	1,00E-06	3,38E-05	33,82	364,694	585,562
20	520	1,00E-06	3,85E-05	38,46	300,578	649,678
22,5	522,5	1,00E-06	4,31E-05	43,06	279,761	670,495
25	525	1,00E-06	4,76E-05	47,62	273,907	676,349
27,5	527,5	1,00E-06	5,21E-05	52,13	271,502	678,754
30	530	1,00E-06	5,66E-05	56,60	270,629	679,627
32,5	532,5	1,00E-06	6,10E-05	61,03	270,577	679,679

The graphical representation of the titration curve:



K_a (M⁻¹): 2.3×10⁷ **Statistical error:** 36%
Stoichiometry: 39:1 (ligand : DNA duplex)

No. 47

DNA: dG₂₀ – dC₂₀

ligand: Dimer C

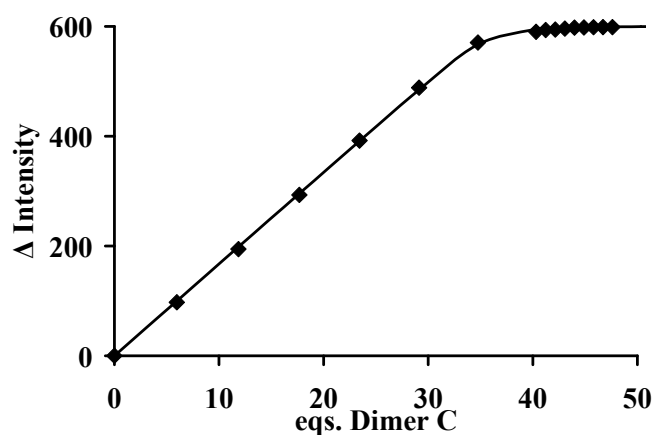
C_{FI-DNA}: 1.0×10⁻⁶ M

C_{ligand}: 1.0×10⁻³ M

Buffer: 20 mM sodium phosphate in water. pH=7.0

Addition ligand (μL)	Total volume (μL)	C _{FI-DNA} (mol/L)	C _{ligand} (mol/L)	ratio (C _{ligand} /C _{FI-DNA})	fluorescence emission	relative emission difference
0	500	1,00E-06	0,00E+00	0,00	899,617	0,000
3	503	1,00E-06	5,96E-06	5,96	802,254	97,363
6	506	1,00E-06	1,19E-05	11,86	705,420	194,197
9	509	1,00E-06	1,77E-05	17,68	606,690	292,927
12	512	1,00E-06	2,34E-05	23,44	507,604	392,013
15	515	1,00E-06	2,91E-05	29,13	411,284	488,333
18	518	1,00E-06	3,47E-05	34,75	329,164	570,453
21	521	1,00E-06	4,03E-05	40,31	309,410	590,207
21,5	521,5	1,00E-06	4,12E-05	41,23	306,236	593,381
22	522	1,00E-06	4,21E-05	42,15	305,409	594,208
22,5	522,5	1,00E-06	4,31E-05	43,06	303,777	595,840
23	523	1,00E-06	4,40E-05	43,98	301,990	597,627
23,5	523,5	1,00E-06	4,49E-05	44,89	301,788	597,829
24	524	1,00E-06	4,58E-05	45,80	301,195	598,422
24,5	524,5	1,00E-06	4,67E-05	46,71	301,013	598,604
25	525	1,00E-06	4,76E-05	47,62	300,996	598,621
25,5	525,5	1,00E-06	4,85E-05	48,53	299,015	600,602
26	526	1,00E-06	4,94E-05	49,43	298,165	601,452
26.5	527	1,00E-06	5,03E-05	50,33	297,889	601,728
27	527	1,00E-06	5,12E-05	51,23	297,025	602,592

The graphical representation of the titration curve:



K_a (M⁻¹): 1.8×10⁷

Statistical error: 29%

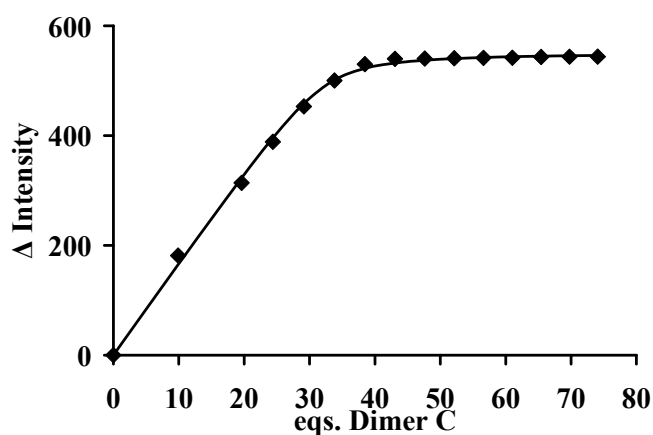
Stoichiometry: 36:1 (ligand : DNA duplex)

No. 48

DNA: dA₂₀ – dT₂₀ **ligand:** Dimer C
C_{FI-DNA}: 1.0×10⁻⁶ M **C_{ligand}:** 1.0×10⁻³ M
Buffer: 20 mM sodium phosphate in water. pH=7.0

Addition ligand (μL)	Total volume (μL)	C _{FI-DNA} (mol/L)	C _{ligand} (mol/L)	ratio (C _{ligand} /C _{FI-DNA})	fluorescence emission	relative emission difference
0	500	1,00E-06	0,00E+00	0,00	956,611	0,000
5	505	1,00E-06	9,90E-06	9,90	775,239	181,372
10	510	1,00E-06	1,96E-05	19,61	642,802	313,809
12,5	512,5	1,00E-06	2,44E-05	24,39	568,077	388,534
15	515	1,00E-06	2,91E-05	29,13	503,647	452,964
17,5	517,5	1,00E-06	3,38E-05	33,82	456,350	500,261
20	520	1,00E-06	3,85E-05	38,46	426,613	529,998
22,5	522,5	1,00E-06	4,31E-05	43,06	416,946	539,665
25	525	1,00E-06	4,76E-05	47,62	416,411	540,200
27,5	527,5	1,00E-06	5,21E-05	52,13	415,822	540,789
30	530	1,00E-06	5,66E-05	56,60	415,066	541,545
32,5	532,5	1,00E-06	6,10E-05	61,03	414,826	541,785
35	535	1,00E-06	6,54E-05	65,42	413,456	543,155
37,5	537,5	1,00E-06	6,98E-05	69,77	413,023	543,588
40	540	1,00E-06	7,41E-05	74,07	412,889	543,722

The graphical representation of the titration curve:



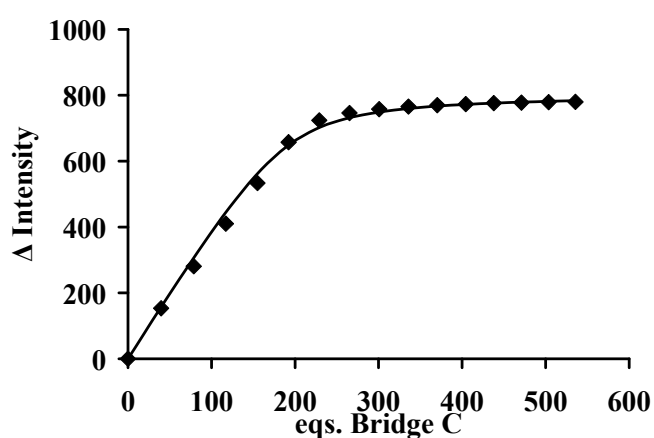
K_a (M⁻¹): 2.3×10⁶ **Statistical error:** 24%
Stoichiometry: 33:1 (ligand : DNA duplex)

No. 49

DNA: (dGdC)₁₀-(dGdC)₁₀ **ligand:** Bridge C
C_{FI-DNA}: 1.0×10⁻⁶ M **C_{ligand}:** 1.0×10⁻³ M
Buffer: 2 mM HEPES and 150 mM NaCl in water. pH=7.10

Addition ligand (μL)	Total volume (μL)	C _{FI-DNA} (mol/L)	C _{ligand} (mol/L)	ratio (C _{ligand} /C _{FI-DNA})	fluorescence emission	relative emission difference
0	500	1,00E-06	0,00E+00	0,00	977,227	0,000
4	504	1,00E-06	3,97E-05	39,68	823,880	153,347
8	508	1,00E-06	7,87E-05	78,74	696,288	280,939
12	512	1,00E-06	1,17E-04	117,19	567,138	410,089
16	516	1,00E-06	1,55E-04	155,04	443,959	533,268
20	520	1,00E-06	1,92E-04	192,31	319,858	657,369
24	524	1,00E-06	2,29E-04	229,01	253,281	723,946
28	528	1,00E-06	2,65E-04	265,15	231,255	745,972
32	532	1,00E-06	3,01E-04	300,75	219,604	757,623
36	536	1,00E-06	3,36E-04	335,82	211,642	765,585
40	540	1,00E-06	3,70E-04	370,37	207,310	769,917
44	544	1,00E-06	4,04E-04	404,41	204,162	773,065
48	548	1,00E-06	4,38E-04	437,96	200,964	776,263
52	552	1,00E-06	4,71E-04	471,01	199,607	777,620
56	556	1,00E-06	5,04E-04	503,60	198,205	779,022
60	560	1,00E-06	5,36E-04	535,71	197,545	779,682

The graphical representation of the titration curve:



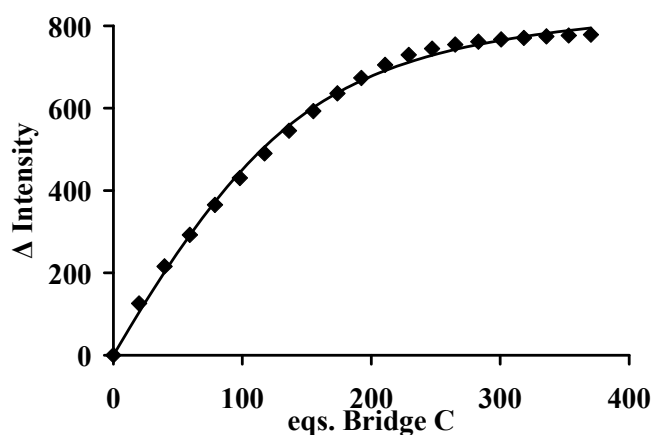
K_a (M⁻¹): 1.1×10⁵ **Statistical error:** 23%
Stoichiometry: 192:1 (ligand : DNA duplex)

No. 50

DNA: (dAdT)₁₀-(dAdT)₁₀ **ligand:** Bridge C
C_{FI-DNA}: 1.0×10⁻⁶ M **C_{ligand}:** 1.0×10⁻³ M
Buffer: 2 mM HEPES and 150 mM NaCl in water. pH=7.10

Addition ligand (μL)	Total volume (μL)	C _{FI-DNA} (mol/L)	C _{ligand} (mol/L)	ratio (C _{ligand} /C _{FI-DNA})	fluorescence emission	relative emission difference
0	500	1,00E-06	0,00E+00	0,00	974,078	0,000
2	502	1,00E-06	1,99E-05	19,92	848,392	125,686
4	504	1,00E-06	3,97E-05	39,68	758,247	215,831
6	506	1,00E-06	5,93E-05	59,29	681,675	292,403
8	508	1,00E-06	7,87E-05	78,74	608,944	365,134
10	510	1,00E-06	9,80E-05	98,04	543,547	430,531
12	512	1,00E-06	1,17E-04	117,19	483,850	490,228
14	514	1,00E-06	1,36E-04	136,19	428,770	545,308
16	516	1,00E-06	1,55E-04	155,04	381,154	592,924
18	518	1,00E-06	1,74E-04	173,75	338,076	636,002
20	520	1,00E-06	1,92E-04	192,31	300,678	673,400
22	522	1,00E-06	2,11E-04	210,73	269,031	705,047
24	524	1,00E-06	2,29E-04	229,01	244,634	729,444
26	526	1,00E-06	2,47E-04	247,15	229,413	744,665
28	528	1,00E-06	2,65E-04	265,15	219,604	754,474
30	530	1,00E-06	2,83E-04	283,02	212,639	761,439
32	532	1,00E-06	3,01E-04	300,75	207,230	766,848
34	534	1,00E-06	3,18E-04	318,35	203,408	770,670
36	536	1,00E-06	3,36E-04	335,82	199,628	774,450
38	538	1,00E-06	3,53E-04	353,16	197,564	776,514
40	540	1,00E-06	3,70E-04	370,37	195,611	778,467

The graphical representation of the titration curve:



K_a (M⁻¹): 3.3×10⁴ **Statistical error:** 10%

Stoichiometry: 136:1 (ligand : DNA duplex)

No. 51

DNA: dA₂₀ – dT₂₀

ligand: Bridge C

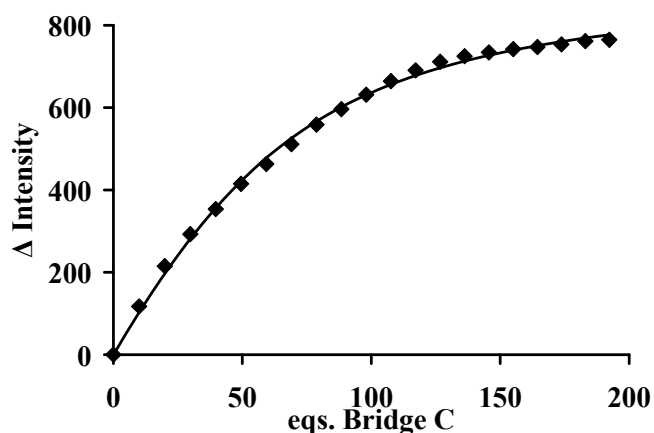
C_{FI-DNA}: 1.0×10⁻⁶ M

C_{ligand}: 1.0×10⁻³ M

Buffer: 2 mM HEPES and 150 mM NaCl in water. pH=7.10

Addition ligand (μL)	Total volume (μL)	C_{FI-DNA} (mol/L)	C_{ligand} (mol/L)	ratio (C_{ligand}/C_{FI-DNA})	fluorescence emission	relative emission difference
0	500	1,00E-06	0,00E+00	0,00	979,989	0,000
1	501	1,00E-06	9,98E-06	9,98	862,642	117,347
2	502	1,00E-06	1,99E-05	19,92	765,093	214,896
3	503	1,00E-06	2,98E-05	29,82	687,395	292,594
4	504	1,00E-06	3,97E-05	39,68	626,406	353,583
5	505	1,00E-06	4,95E-05	49,50	565,118	414,871
6	506	1,00E-06	5,93E-05	59,29	516,967	463,022
7	507	1,00E-06	6,90E-05	69,03	468,876	511,113
8	508	1,00E-06	7,87E-05	78,74	421,313	558,676
9	509	1,00E-06	8,84E-05	88,41	383,594	596,395
10	510	1,00E-06	9,80E-05	98,04	348,515	631,474
11	511	1,00E-06	1,08E-04	107,63	315,701	664,288
12	512	1,00E-06	1,17E-04	117,19	289,539	690,450
13	513	1,00E-06	1,27E-04	126,71	268,614	711,375
14	514	1,00E-06	1,36E-04	136,19	255,163	724,826
15	515	1,00E-06	1,46E-04	145,63	245,978	734,011
16	516	1,00E-06	1,55E-04	155,04	238,075	741,914
17	517	1,00E-06	1,64E-04	164,41	232,880	747,109
18	518	1,00E-06	1,74E-04	173,75	226,340	753,649
19	519	1,00E-06	1,83E-04	183,04	218,450	761,539
20	520	1,00E-06	1,92E-04	192,31	215,257	764,732

The graphical representation of the titration curve:



K_a (M⁻¹): 3.8×10⁴ **Statistical error:** 7%

Stoichiometry: 60:1 (ligand : DNA duplex)

Abbreviations

A	adenine
Å	Ångstrom
abs.	absolute
Arg	arginine
Bn	benzyl
Boc	<i>tert</i> -butyloxycarbonyl
Boc ₂ O	di- <i>tert</i> -butyldicarbonate
C	cytosine
CD	circular dichroism
DAPI	4',6-diamidino-2-phenylindole
DCC	<i>N,N'</i> -dicyclohexylcarbodiimide
DCM	dichloromethane
DIEA	<i>N,N</i> -diisopropylethylamine
DMAP	4-(<i>N,N</i> -dimethylamino)pyridine
DMF	<i>N,N</i> -dimethylformamide
DMSO	dimethyl sulfoxide
DNA	deoxyribonucleic acid
EDC	1-ethyl-3-(3-dimethylaminopropyl) carbodiimide hydrochloride
eq.	equivalent
ESI	electrospray ionization
Et ₃ N	triethylamine
EtBr	ethidium bromide
G	guanine
HATU	2-(7-aza-1 <i>H</i> -benzotriazole-1-yl)-1,1,3,3-tetramethyluronium hexafluorophosphate
HBTU	O-benzotriazole- <i>N,N,N',N'</i> -tetramethyl-uronium-hexafluoro-phosphate

HCTU	2-(6-chloro-1 <i>H</i> -benzotriazole-1-yl)-1,1,3,3-tetramethylaminium hexafluorophosphate
Hepes	4-(2-hydroxyethyl)-1-piperazineethanesulfonic acid
His	histidine
HOBt	hydroxybenzotriazole
Hz	Hertz
ICD	induced circular dichroism
ITC	isothermal titration calorimetry
M	moles per liter
mM	millimoles per liter
μM	micromoles per liter
Me	methyl
neg.	negative
nm	nanometer
NMR	nuclear magnetic resonance
PNA	peptide nucleic acid
pos.	positive
ppm	parts per million
R _f	retention value
RNA	ribonucleic acid
r.t.	room temperature
T	thymine
TFA	trifluoroacetic acid
THF	tetrahydrofuran
U	uracil
UV	ultraviolet
Vis	visible
Z	benzyloxycarbonyl

References

- [1] F. Crick, *Nature* **1970**, 227, 561-563.
- [2] D. S. Latchman, *Int. J. Biochem. Cell Biol.* **1997**, 29, 1305–1312.
- [3] R. G. Roeder, *Trends Biochem. Sci.* **1996**, 21, 327–335.
- [4] P. Blancafort, *Mol. Pharmacol.* **2004**, 66, 1361–1371.
- [5] D. Kletsas, *Exp. Opin. Invest. Drugs* **1999**, 8, 737-746.
- [6] P. A. Morcos, *Biochem. Biophys. Res. Commun.* **2007**, 358, 521–527.
- [7] K. V. Morris, *RNA and the Regulation of Gene Expression: A Hidden Layer of Complexity*, Caister Academic Press, La Jolla, USA, **2008**.
- [8] C. R. Dass, *Mol. Cancer Ther.* **2008**, 7, 243–251.
- [9] O. Bagasra, K. R. Prilliman, *J. Mol. Histol.* **2004**, 5, 545–553.
- [10] D. P. Bartel, *Cell* **2009**, 136, 215–233.
- [11] L. Stryer, J. M. Berg, J. L. Tymoczko, *Biochemistry*, W. H. Freeman, New York, **2007**.
- [12] J. D. Watson, F. H. Crick, *Nature* **1953**, 171, 737-738.
- [13] K. Hoogsteen, *Acta Crystallogr.* **1959**, 12, 822-823.
- [14] Y. K. Cheng, *J. Am. Chem. Soc.* **1992**, 114, 4465–4474.
- [15] F. Crick, *J. Mol. Biol.* **1966**, 19, 548–555.
- [16] E. Christophe, *Top Curr. Chem.* **2005**, 253, 109–148.
- [17] M. D. Frank-Kamenetskii, *Annu. Rev. Biochem.* **1995**, 64, 65-95.
- [18] P. P. Chan, P. M. Glazer, *J. Mol. Med.* **1997**, 75, 267–282.
- [19] A. Sen, A. Gräslund, *Biophysical Chemistry* **2000**, 88, 69-80.
- [20] W. Saenger, *Principles of Nucleic Acid Structure*, Springer-Verlag, New York, **1983**.
- [21] J. Feigon, A. H. J. Wang, G. A. van der Marel, J. H. van Boom, A. Rich, *Nucleic Acids Res.* **1984**, 12, 1243-1263.
- [22] P. W. Davis, K. Hall, P. Cruz, I. Tinoco, T. Neilson, *Nucleic Acids Res.* **1986**, 14, 1279-1291.
- [23] H. P. M. de Leeuw, C. A. G. Haasnoot, C. Altona, *Isr. J. Chem.* **1980**, 20, 108-126.
- [24] J. Fohrer, M. Henning, T. Carlomagno, *J. Mol. Biol.* **2006**, 356, 280-287.
- [25] I. Fierro-Monti, M. B. Mathews, *Trends. Biomol. Sc.* **2000**, 25, 241-246.
- [26] R. F. Gesteland, T. R. Cech, J. F. Atkins, *The RNA World*, Cold Spring Harbour Laboratory Press, Cold Spring Harbour, New York, **1998**.
- [27] M. Oivanen, S. Kuusela, H. Lonnberg, *Chem. Rev.* **1998**, 98, 961-990.
- [28] G. J. Quigley, A. Rich, *Science* **1976**, 194, 796-806.
- [29] B. Basham, G. P. Schroth, P. S. Ho, *Proc. Natl. Acad. Sci. U.S.A.* **1995**, 92, 6464–6468.
- [30] M. McCall, T. Brown, O. Kennard, *J. Mol. Biol.* **1985**, 183, 385-396.
- [31] M. Nowotny, G. A. Gaidamakov, R. J. Crouch, W. Yang, *Cell* **2005**, 121, 1005-1016.
- [32] R. Wing, H. Drew, T. Takano, C. Broka, S. Tanaka, K. Itakura, R. E. Dickerson, *Nature* **1980**, 287, 755-758.
- [33] R. E. Dickerson, H. R. Drew, B. N. Conner, R. M. Wing, A. V. Fratini, M. L. Kopka, *Science* **1982**, 216, 475-485.
- [34] R. R. Sinden, *DNA structure and function* (1st ed.), Academic Press, **1994**.

- [35] A. Rich, A. Norheim, A. H. J. Wang, *Annual Review of Biochemistry* **1984**, *53*, 791–846.
- [36] P. S. Ho, *Proc. Natl. Acad. Sci. U.S.A.* **1994**, *91*, 9549–9553.
- [37] H. Ihmels, C. Schmuck, in *Highlights in Bioorganic Chemistry* (Eds.: Wennemers. H, Schmuck C), Wiley-VCH, **2004**.
- [38] T. Yoshiyuki, *Nucleic Acid Research* **1999**, *27*, 949-955.
- [39] S. Premilat, G. Albiser, *Eur. Biophys. J.* **1999**, *28*, 574-582.
- [40] S. Premilat, G. Albiser, *Eur. Biophys. J.* **2001**, *30*, 404-410.
- [41] C. M. Hillary, *Nature* **1987**, *330*, 221-226.
- [42] H. S. Park, S. Arnottf, R. Chandrasekaran, R. P. Millane, *J. Mol. Biol.* **1987**, *197*, 513-523.
- [43] D. L. Nelson, *Lehninger Principles of Biochemistry*, W. H. Freeman, **2004**.
- [44] P. J. Mitchell, R. Tjian, *Science* **1989**, *245*, 371–378.
- [45] M. Ptashne, A. Gann, *Nature* **1997**, *386*, 569–577.
- [46] R. Wintjens, M. Rooman, *Journal of molecular biology* **1996**, *262*, 294–313.
- [47] C. Vinson, M. Myakishev, A. Acharya, A. A. Mir, J. R. Moll, M. Bonovich, *Molecular and cellular biology* **2002**, *22*, 6321–6335.
- [48] J. H. Laity, B. M. Lee, P. E. Wright, *Current opinion in structural biology* **2001**, *11*, 39–46.
- [49] J. M. Wong, E. Bateman, *Nucleic Acids Res.* **1994**, *22*, 1890-1896.
- [50] H. A. Nash, K. Mizuuchi, P. A. Rice, S. W. Yang, *Cell* **1996**, *87*, 1295-1306.
- [51] J. R. Huth, C. A. Bewley, M. S. Nissen, J. N. Evans, R. Reeves, *Nat. Struct. Biol.* **1997**, *4*, 957–965.
- [52] C. A. Bewley, A. M. Gronenborn, G. M. Clore, *Annu. Rev. Biophys. Biomol. Struct.* **1998**, *27*, 105–131.
- [53] C. G. Lobe, *Current topics in developmental biology* **1992**, *27*, 351–383.
- [54] D. Lemons, W. McGinnis, *Science* **2006**, *313*, 1918–1922.
- [55] G. Evan, E. Harrington, A. Fanidi, H. Land, B. Amati, M. Bennett, *Philos. Trans. R. Soc. Lond., B. Biol. Sci.* **1994**, 269–275.
- [56] T. A. Libermann, L. F. Zerbini, *Curr. Gene Ther.* **2006**, *6*, 17–33.
- [57] J. P. Overington, B. Al-Lazikani, A. L. Hopkins, *Nature reviews: Drug discovery* **2006**, *5*, 993–996.
- [58] W. D. Wilson, *Nucleic acids in chemistry and biology*, Oxford University Press, Oxford, **1996**.
- [59] J. A. Mountzouris, L. H. Hurley, *Bioorganic chemistry: nucleic acids*, Oxford University Press, New York, **1996**.
- [60] L. S. Lerman, *J. Mol. Biol.* **1961**, *3*, 18-30.
- [61] C. H. Takimoto, E. Calvo, in *Cancer Management: A Multidisciplinary Approach* (Eds: R. Pazdur, L. D. Wagman, K. A. Camphausen, W. J. Hoskins), New York, Cmp United Business Media, **2008**.
- [62] D. Debnath, K. G. Suresh, M. Maiti, *J. Biomol. Struct. Dyn.* **1991**, *9*, 61-79.
- [63] E. Nordmeier, *J. Phys. Chem.* **1992**, *96*, 6045–6055.
- [64] L. S. Lermann, *J. Mol. Biol.* **1961**, *3*, 18-30.
- [65] L. S. Lermann, *Proc. Natl. Acad. Sci. U.S.A.* **1963**, *49*, 94-102.
- [66] E. Westhof, S. T. Rao, M. Sundaralingam, *Journal of Molecular Biology* **1980**, *142*,

- 331-361.
- [67] T. D. Stephens, *Biochemical Pharmacology* **2000**, *59*, 1489-1499.
- [68] A. D. Marco, M. Gaetani, B. Scarpinato, *Cancer Chemother Rep.* **1969**, *53*, 33-37.
- [69] C. Tan, H. Tasaka, K. P. Yu, M. L. Murphy, D. A. Karnofsky, *Cancer* **1967**, *20*, 333-353.
- [70] E. Habib, M. Mishrif, *J. Egypt Natl. Canc. Inst.* **2005**, *17*, 308-311.
- [71] J. B. Chaires, *Archives of Biochemistry and Biophysics* **2006**, *453*, 26-31.
- [72] M. J. Waring, *Annu. Rev. Biochem.* **1981**, *50*, 159-192.
- [73] J. S. Ren, J. B. Chaires, *Biochemistry* **1999**, *38*, 16067-16075.
- [74] C. J. Roche, J. A. Thompson, D. M. Crothers, *Biochemistry* **1994**, *33*, 926-935.
- [75] C. Bailly, D. Suh, M. J. Waring, J. B. Chaires, *Biochemistry* **1998**, *37*, 1033-1045.
- [76] P. B. Dervan, *Science* **1986**, *232*, 464-471.
- [77] S. Neidle, *Nat. Prod. Rep.* **2001**, *18*, 291-309.
- [78] C. Carlsson, A. Larsson, M. Jonsson, B. Albinsson, B. Norden, *Phys. Chem.* **1994**, *98*, 10313-10321.
- [79] L. G. Lee, C.H. Chen, L. A. Chiu, *Cytometry* **1986**, *7*, 508-517.
- [80] J. Nygren, N. Svanvik, M. Kubista, *Biopolymers* **1998**, *46*, 39-51.
- [81] W. C. Tse, D. L. Boger, *Acc. Chem. Res.* **2004**, *37*, 61-69.
- [82] B. P. Reddy, S. M. Sondhi, J. W. Lown, *Therap.* **1999**, *84*, 1-111.
- [83] D. E. Wemmer, *Annu. Rev. Biophys. Biomol. Struct.* **2000**, *29*, 439-461.
- [84] R. R. Sauers, *Bioorg. Med. Chem. Lett.* **1995**, *5*, 2573-2576.
- [85] D. Chang, S. Cheng, *Int. J. Biol. Mol.* **1996**, *19*, 279-289.
- [86] C. Bailly, J. B. Chaires, *Bioconjugate Chem.* **1998**, *9*, 513-538.
- [87] A. Lauria, A. Montalbano, P. Barraja, G. Dattolo, A. A. Almerico, *Current Medicinal Chemistry* **2007**, *14*, 2136-2160.
- [88] C. J. Suckling, *Expert Opinion on Therapeutic Patents* **2004**, *14*, 1693-1724.
- [89] P. B. Dervan, *Bioorganic & Medicinal Chemistry* **2001**, *9*, 2215-2235.
- [90] R. E. Dickerson, in *Oxford Handbook of Nucleic Acid Structure*, eds.: S. Neidle, Oxford University Press, Oxford, **1999**.
- [91] H. M. Berman, W. K. Olson, D. L. Beveridge, J. Westbrook, A. Gelbin, T. Demeny, S-H. Hsieh, A. R. Srinivasan, B. Schneider, *Biophys. J.* **1992**, *63*, 751-759.
- [92] D. Goodsell, R. E. Dickerson, *J. Med. Chem.* **1986**, *29*, 727-733.
- [93] X. Shui, C. C. Sines, L. McFail-Isom, D. VanDerveer, L. D. Williams, *Biochemistry* **1998**, *37*, 16877-16887.
- [94] T. K. Chiu, M. Kaczor-Grzeskowiak, R. E. Dickerson, *J. Mol. Biol.* **1999**, *292*, 589-608.
- [95] P. L. Privalov, *J. Mol. Biol.* **2007**, *365*, 1-9.
- [96] M. L. Kopka, C. Yoon, D. Goodsell, P. Pjura, R. E. Dickerson, *J. Mol. Biol.* **1985**, *183*, 553-563.
- [97] H. Drew, R. Roberts, *J. Mol. Biol.* **1981**, *49*, 761-789.
- [98] M. Coll, C. A. Frederick, A. H. J. Wang, A. Rich, *Proc. Natl. Acad. Sci. U.S.A.* **1987**, *84*, 8385-8389.
- [99] J. W. Lown, *J. Mol. Recognit.* **1994**, *7*, 79-88.
- [100] J. W. Lown, K. Krowicki, U. G. Bhat, A. Skorobogaty, B. Ward, J. C. Dabrowiak, *Biochemistry* **1986**, *25*, 7408-7416.

- [101] K. Krowicki, J. C. Dabrowiak, J. W. Lown, *Biochemistry* **1987**, *26*, 5590-5595.
- [102] J. G. Pelton, D. E. Wemmer, *Proc. Natl. Acad. Sci. U.S.A.* **1989**, *86*, 5723-5727.
- [103] J. G. Pelton, D. E. Wemmer, *J. Am. Chem. Soc.* **1990**, *112*, 1393-1399.
- [104] X. Chen, B. Ramakrishnan, S. T. Rao, M. Sundaralingam, *Nat. Struct. Biol.* **1994**, *1*, 169-175.
- [105] M. L. Kopka, C. Yoon, D. Goodsell, P. Pjura, R. E. Dickerson, *Proc. Natl. Acad. Sci. U.S.A.* **1985**, *82*, 1376-1380.
- [106] S. White, J. W. Szewczyk, J. M. Turner, E. E. Baird, P. B. Dervan, *Nature* **1998**, *391*, 468-471.
- [107] R. Rohs, et. al., *Annu. Rev. Biochem.* **2010**, *79*, 233-269.
- [108] P. Weiner, et. al., *Proc. Natl. Acad. Sci. U.S.A.* **1982**, *79*, 3754-3758.
- [109] N. Seeman, J. Rosenberg, A. Rich, *Proc. Natl. Acad. Sci. U.S.A.* **1976**, *73*, 804-808.
- [110] R. J. Roberts, *Nucleic Acids Res.* **1981**, *9*, 75-98.
- [111] H. O. Smith, *Science* **1979**, *205*, 455-462.
- [112] N. P. Pavletich, C. O. Pabo, *Science* **1991**, *252*, 809-817.
- [113] S. S. Krishna, I. Majumdar, N. V. Grishin, *Nucleic Acids Res.* **2003**, *31*, 532-550.
- [114] B. Alberts, A. Johnson, J. Lewis, M. Raff, K. Roberts, P. Walter, *Molecular Biology of the Cell*, Fourth Edition, New York, Garland Science, **2002**.
- [115] R. Brennan, B. Matthews, *J. Biol. Chem.* **1989**, *264*, 1903-1906.
- [116] M. Ptashne, *Nature* **1967**, *214*, 232-234.
- [117] S. K. Kim, B. Nordén, *FEBS Lett.* **1993**, *315*, 61-64.
- [118] E. Tuite, B. Nordén, *J. Am. Chem. Soc.* **1994**, *116*, 7548-7556.
- [119] D. P. Arya, B. Willis, *J. Am. Chem. Soc.* **2003**, *125*, 12398-12399.
- [120] R. Zadnard, T. Schrader, *Angew. Chem. Int. Ed.* **2006**, *45*, 2703-2706.
- [121] J. W. Steed, J. L. Atwood, *Supramolecular Chemistry*, 2nd Edition, John Wiley & Sons, Ltd., **2009**.
- [122] H. J. Schneider, A. Yatsimirsky, *Principles and Methods in Supramolecular Chemistry*, John Wiley & Sons, Ltd., **2000**.
- [123] G. V. Oshovsky, D. N. Reinhoudt, W. Verboom, *Angewandte Chemie International Edition* **2007**, *46*, 2366-2393.
- [124] C. D. Gutsche, *Calixarenes*, Cambridge: Royal Society of Chemistry, **1989**.
- [125] R. Ludwig, *Microchim Acta* **2005**, *152*, 1-19.
- [126] Z. Asfari, V. Böhmer, J. Harrowfield, J. Vicens, *Calixarenes 2001*, Kluwer Academic Publishers, Dordrecht, **2001**.
- [127] J. Vicens, V. Bohmer, *Calixarenes, a Versatile Class of Macrocyclic Compounds*, Springer, **1991**.
- [128] L. Baldini, A. Casnati, F. Sansone, R. Ungaro, *Chem. Soc. Rev.* **2007**, *36*, 254-266.
- [129] A. Casnati, F. Sansone, R. Ungaro, *Acc. Chem. Res.* **2003**, *36*, 246-254.
- [130] N. Cheriaa, et. al., *J.N.B.T.*, **2005**, *2*, 3-9.
- [131] C. J. Breitkreuz, R. Zadnard, T. Schrader, *Supramolecular Chemistry* **2008**, *20*, 109-115.
- [132] C. Gutsche, *Calixarenes, Monographs in Supramolecular Chemistry*, the Royal Society of Chemistry, Cambridge, **1989**.
- [133] C. D. Gutsche, *Calixarenes Revisited*, Stoddart, Royal Society of Chemistry: Cambridge, **1998**.

- [134] C. D. Gutsche, M. Iqbal, *Org. Synth. Coll. Vol.* **1993**, *8*, 75-77.
- [135] S. H. Munch, C. D. Gutsche, *Org. Synth. Coll. Vol.* **1993**, *8*, 80-81.
- [136] C. D. Gutsche, B. Dhawan, M. Leonis, D. Stewart, *Org. Synth. Coll. Vol.* **1993**, *8*, 77-79.
- [137] F. Ullmann, K. Brittner, *Chem. Ber.* **1909**, *42*, 2539-2548.
- [138] C. D. Gutsche, *Acc. Chem. Res.* **1983**, *16*, 161-170.
- [139] C. D. Gutsche, D. E. Johnston, D. R. Stewart, *J. Org. Chem.* **1999**, *64*, 3747- 3750.
- [140] M. Tashiro, G. Fukata, S. Mataka, K. Oe, *Org. Prep. Proced. Int.* **1975**, *7*, 231-234.
- [141] C. D. Gutsche, B. Dhawan, J. A. Levine, K.H. No, L. J. Bauer, *Tetrahedron* **1983**, *39*, 409-426.
- [142] L. C. Groenen, B. H. Ruël, A. Casnati, P. Timmerman, W. Verboom, S. Harkema, A. Pochini, R. Ungaro, D. N. Reinhoudt, *Tetrahedron Letters* **1991**, *32*, 2675-2678.
- [143] V. S. Talanov, H. S. Hwang, R. A. Bartsch, *J. Chem. Soc., Perkin Trans. 2* **2001**, *66*, 1103-1108.
- [144] W. Verboom, S. Datta, Z. Asfari, S. Harkema, D N. Reinhoudt, *J. Org. Chem.* **1992**, *57*, 5394-5398.
- [145] S. Shinkai, K. Araki, T. Tsubaki, T. Arimura, O. Manabe, *J. Chem. Soc. Perkin Trans. I* **1987**, 2297-2300.
- [146] S. Shinkai, T. Tsubaki, T. Sone, O. Manabe, *Tetrahedron Lett.* **1985**, *26*, 3343-3344.
- [147] M. Almi, A. Arduini, A. Casnati, A. Pochini, R. Ungaro, *Tetrahedron* **1989**, *45*, 2177-2182.
- [148] C. D. Gutsche, I. Alam, *Tetrahedron* **1988**, *44*, 4689-4694.
- [149] A. Ikeda, S. Sbinkai, *J. Am. Chem. Soc.* **1994**, *116*, 3102-3110.
- [150] T. Arimura, T. Nagasaki, S. Shinkai, T. Matsuda, *J. Org. Chem.* **1989**, *54*, 3766-3768.
- [151] K. Niikura, E. Anslyn, *J. Chem. Soc. Perkin Trans. 2* **1999**, 2769-2775.
- [152] S. Shinkai, H. Kawabata, T. Matsuda, H. Kawaguchi, O. Manage, *Bull. Chem. Soc. Jpn.* **1990**, *63*, 1272-1274.
- [153] G. R. Newkome, Y. Hu, M. J. Saunders, F.R. Fronczek, *Tetrahedron Lett.* **1991**, *32*, 1133-1136.
- [154] A. Marra, M-C. Scherrmann, A. Dondoni, A. Casnati, P. Minari, R. Ungaro, *Angew. Chem. Intl. Ed.* **1994**, *33*, 2479-2481.
- [155] Y. Shi, Y. Z. Zhang, *J. Chem. Soc. Chem. Commun.* **1994**, 375-376.
- [156] G. Gansey, F. J. Steemers, W. Verboom, D .N. Reinhoudt, *Synthesis* **1997**, *38*, 643-646.
- [157] R. Zadnard, T. Schrader, T. Grawe, A. Kraft, *Org. Lett.* **2002**, *4*, 1687-1690.
- [158] C. A. Miller, R. A. Batey, *Organic Letters* **2004**, *6*, 699-702.
- [159] F. Sansone, M. Dudič, G. Donofrio, C. Rivetti, L. Baldini, A. Casnati, S. Cellai, R. Ungaro, *J. Am. Chem. Soc.* **2006**, *128*, 14528-14536.
- [160] C. J. Blecking, W. Hu, R. Zadnard, A. Dasgupta, T. Schrader, *Synthesis* **2011**, *8*, 1193-1204.
- [161] G. T. Hermanson, *Bioconjugate Techniques*, Academic Press, **1996**.
- [162] N. Isaacs, *Physical Organic Chemistry*, 2 edition, Prentice Hall, **1996**.
- [163] E. Atherton, R. C. Sheppard, *Solid Phase peptide synthesis: a practical approach*, Oxford, England, **1989**.

- [164] D. Jaramillo, Q. Liu, J. Aldrich-Wright, Y. Tor, *J. Org. Chem.* **2004**, *69*, 8151-8153.
- [165] E. E. Baird, P. B. Dervan, *J. Am. Chem. Soc.* **1996**, *118*, 6141-6146.
- [166] N. R. Wurtz, J. M. Turner, E. E. Baird, P. B. Dervan, *Org. Lett.* **2001**, *3*, 1201-1203.
- [167] E. Nishiwaki, S. Tanaka, H. Lee, M. Shibuya, *Heterocycles* **1988**, *27*, 1945-1952.
- [168] N. Sewald, H. D. Jakubke, *Peptides: Chemistry and Biology*, Wiley-VCH Verlag GmbH & Co. KGaA, **2002**.
- [169] M. Mrksich, M. E. Parks, P. B. Dervan, *J. Am. Chem. Soc.* **1994**, *116*, 7983-7988.
- [170] I. Abdelmoty, F. Albericio, L. A. Carpino, B. M. Foxman, S. A. Kates, *Lett. Pept. Sci.* **1994**, *1*, 57-67.
- [171] R. Knorr, A. Trzeciak, W. Bannwarth, D. Gillessen, *Tetrahedron Lett.* **1989**, *30*, 1927-1930.
- [172] A. DiFoena, P. Rovero, *Racemization studies on a novel Cl-HOBt-based coupling reagents*, presented at the European Peptide Symposium, August **2002**.
- [173] P. G. M. Wuts, T. W. Greene, *Greene's Protective Groups in Organic Synthesis*, 4th Edition, **2006**.
- [174] M. J. Earle, et. al., *Synlett.* **1990**, *10*, 621-623.
- [175] A. B. Hamlet, T. Durst, *Can. J. Chem.* **1983**, *61*, 411-415.
- [176] A. Chen, et. al., *Tetrahedron Lett.* **2001**, *42*, 1251-1254.
- [177] D. Suh, J. B. Chaires, *Bioorganic & Medicinal Chemistry* **1995**, *3*, 723-728.
- [178] V. A. Bloomfield, D. M. Crothers, J. L. Tinoco, *Physical Chemistry of Nucleic Acids*, Harper & Row, New York, **1974**.
- [179] E. C. Long, J. K. Barton, *Acct. Chem. Res.* **1990**, *23*, 271-273.
- [180] W. D. Wilson, R. L. Jones, *Intercalation Chem.*, Academic Press, New York, **1982**.
- [181] G. Dougherty, J. R. Pilbrow, *Int. J. Biochem.* **1984**, *16*, 1179-1192.
- [182] D. R. Hare, et. al., *J. Mol. Biol.* **1983**, *171*, 319-336.
- [183] D. J. Patel, S. A. Kozlowski, L. A. Marky, C. Broka, J. A. Rice, K. Itakura, K. J. Breslauer, *Biochemistry* **1982**, *21*, 428-436.
- [184] J. Ott, F. Eckstein, *Biochemistry* **1985**, *24*, 2530-2535.
- [185] D. Reha, et. al., *J. Am. Chem. Soc.* **2002**, *124*, 3366-3376.
- [186] A. D. Richards, A. Rodger, *Chem. Soc. Rev.* **2007**, *36*, 471-483.
- [187] J. Olmsted, D. R. Kearns, *Biochemistry* **1977**, *16*, 3647-3654.
- [188] J. B. LePecq, C. Paoletti, *J. Mol. Biol.* **1967**, *27*, 87-106.
- [189] A. J. Geall, I. S. Blagbrough, *Journal of Pharmaceutical and Biomedical Analysis* **2000**, *22*, 849-859.
- [190] H. S. Basu, H. C. A. Schwietert, B. G. Feuerstein, L. J. Marton, *Biochem. J.* **1990**, *269*, 329-334.
- [191] A. Rodger, B. Nordén, *Circular Dichroism and Linear Dichroism*, Oxford University Press, **1997**.
- [192] N. Berova, K. Nakanishi, R. W. Woody, *Circular Dichroism: Principle and Applications*, Second Edition, John Wiley & Sons, Inc., **2000**.
- [193] B. Nordén, *Journal of Molecular Recognition* **1994**, *7*, 141-156.
- [194] J. Kypr, et. al., *Nucleic Acids Research* **2009**, *37*, 61713-61725.
- [195] F. A. Tanious, J. M. Veal, H. Buczak, L. S. Ratmeyer, W. D. Wilson, *Biochemistry* **1992**, *31*, 3103-3112.
- [196] M. L. Barcellona, G. Cardiel, E. Gratton, *Biochem. Biophys. Res. Commun.* **1990**,

- 170, 270-280.
- [197] M. Kubista, et. al., *Biochemistry* **1987**, 26, 4545-4553.
- [198] J. Kapuscinski, *J. Histochem. Cytochem.* **1990**, 38, 1323-1329.
- [199] D. Vlieghe, J. Sponer, L. V. Meervelt, *Biochemistry* **1999**, 38, 16443-16451.
- [200] S. Eriksson, et. al., *Biochemistry* **1993**, 32, 2987-2998.
- [201] E. N. Zaitsev, S. C. Kowalczykowski, *Nucleic Acids Research* **1998**, 26, 650-654.
- [202] K. Hirose, in *Analytical Methods in Supramolecular Chemistry*, C. A. Schalley, Wiley-VCH, Weinheim, **2005**.
- [203] K. Hirose, *Journal of Inclusion Phenomena and Macrocyclic Chemistry* **2001**, 39, 193-209.
- [204] P. Job, *Compt. Rend.* **1925**, 180, 928-930.
- [205] H. J. Schneider, R. Kramer, S. Simova, U. Schneider, *J. Am. Chem. Soc.* **1988**, 110, 6442-6448.
- [206] E. J. Billo, *Excel for Chemists: A Comprehensive Guide*, Wiley-VCH Verlag GmbH, **1997**.
- [207] A. Czarny, D. W. Boykin, A. A. Wood, C. M. Nunn, S. Neidle, M. Zhao, W. D. Wilson, *J. Am. Chem. Soc.* **1995**, 117, 4716-4717.
- [208] J. B. Chaires, *Annu. Rev. Biophys.* **2008**, 37, 135-151.
- [209] M. Egli, et. al., *Current Protocols in Nucleic Acid Chemistry*, online ISSN: 1934-9289.
- [210] J. Puglisi, I. Tinoco, *Methods in Enzymology* **1989**, 180.
- [211] R. Thomas, *Gene* **1993**, 135, 77-79.
- [212] C. Escude, J. Sun, *Top Curr. Chem.* **2005**, 253, 109-148.
- [213] Y. Lee, J. Kim, T. Cho, R. Song, S. K. Kim, *J. Am. Chem. Soc.* **2003**, 125, 8106-8107.
- [214] S. Kumar, L. Xue, D. P. Arya, *J. Am. Chem. Soc.* **2011**, 133, 7361-7375.
- [215] L. Nekludova, C. O. Pabo, *Proc. Natl. Acad. Sci. U.S.A.* **1994**, 91, 6948-6952.
- [216] K. M. Weeks, D. M. Crothers, *Science* **1993**, 261, 1574-1577.
- [217] H. R. Neenhold, T. M. Rana, *Biochemistry* **1995**, 34, 6303-6309.
- [218] K. M. Weeks, D. M. Crothers, *Cell* **1991**, 66, 577-588.
- [219] L. Nekludova, C. O. Pabo, *Proc. Natl. Acad. Sci. U.S.A.* **1994**, 91, 6948-6952.
- [220] K. M. Weeks, D. M. Crothers, *Science* **1993**, 261, 1574-1577.
- [221] H. R. Neenhold, T. M. Rana, *Biochemistry* **1995**, 34, 6303-6309.
- [222] K. M. Weeks, D. M. Crothers, *Cell* **1991**, 66, 577-588.
- [223] P. Zhou, G. Wagner, *J. Biomol. NMR.* **2010**, 46, 23-31.
- [224] D. D. Perrin, W. L. F. Armatego, *Purification of Laboratory Chemicals*, 3rd. ed., Pergamon Press, New York, **1988**.
- [225] H. G. O. Becker, W. Berger, G. Domschke, E. Fanghänel, J. Faust, M. Fischer, F. Gentz, K. Gewald, R. Gluch, R. Mayer, K. Müller, D. Pavel, H. Schmidt, K. Schollberg, K. Schwetlick, E. Seiler, G. Zeppenfeld, *Organikum*, 20. Aufl., J. A. Barth Verlag, Heidelberg, Leipzig, **1996**.
- [226] W. C. Still, M. Kahn, A. Mitra, *J. Org. Chem.* **1978**, 43, 2923-2925.
- [227] H. E. Gottlieb, V. Kotyar, A. Nudelman, *J. Org. Chem.* **1997**, 62, 7512-7515.
- [228] D. R. Evans, M. Huang, J. C. Fettinger, T. L. Williams, *Inorg. Chem.* **2002**, 41, 5986-6000.

Curriculum Vitae

Personal Data

Name: Wenbin Hu

Nationality: People's Republic of China

Sex: Male

Birth Place: Beijing

Birthday: 23/01/1981

Marital Status: Single

E-mail: Wenbin.Hu@hotmail.com



Education Background

2007 — 2011 Degree of Doctor of Philosophy (Dr. rer. nat.)

Department of Organic Chemistry

University of Duisburg-Essen, Germany

Research Supervisor: Prof. Dr. Thomas Schrader

2005 — 2007 Degree of Master of Science

Department of Biochemistry and Organic Chemistry

Uppsala University, Sweden

Research Supervisor: Prof. Lars Baltzer

1999 — 2003 Degree of Bachelor of Science

School of Pharmaceutical Science

Health Science Center of Peking University, People's Republic of China

Research Supervisor: Prof. Fenglan Wu, Prof. Tiemin Ai

List of Publications

- 1 Wenbin Hu[§], Caroline Blecking[§], Marijeta Kralj, Lidija Šuman, Ivo Piantanida, Thomas Schrader.
Dimeric Calixarenes – A New Family of Major Groove Binders.
Chemistry – A European Journal, Accepted.
- 2 C. J. Blecking, W. Hu, R. Zadnurd, A. Dasgupta, T. Schrader.
A Modular Synthetic Route to Dimeric Calixarenes: A New Family of DNA Major Groove Binders.
Synthesis **2011**, 8, 1193-1204.

Conferences

- 1 **7th SUPRAPHONE MEETING 2010, Bonn, Germany**
Towards Sequence-Selective DNA Recognition with Designed Major Groove Binders
(oral presentation)